CHARACTERISING THE THERAPEUTIC POTENTIAL OF PEPITEM IN AGE-RELATED BONE LOSS, SKELETAL REMODELLING AND REPAIR

by

JONATHAN WILLIAM LEWIS

A thesis submitted to the University of Birmingham for the degree of

DOCTOR OF PHILOSOPHY

Institute of Inflammation and Ageing

College of Medical and Dental Sciences

University of Birmingham

December 2021

ABSTRACT

Bone is a constantly active organ, undergoing osteoclast-led bone resorption and osteoblast-induced bone formation. In homeostatic conditions, levels of resorption and formation are equivalent, ensuring there is no net change in bone mass. However, in osteoporosis there is an imbalance, leading to increased resorption compared to formation, ultimately increasing the risk of fracture. Currently, the main treatments include parathyroid hormone (targeting osteoblasts) and bisphosphonates (targeting osteoclasts), however there are issues with non-responders, patient compliance and side-effects. Therefore, there is a need for new therapeutics to boost bone growth, preventing initial bone loss and quickening fracture repair. We have previously identified a novel, endogenous peptide known as PEPITEM which, through the release of S1P, has anti-inflammatory actions.

In this thesis, we aimed to explore the response of bone to PEPITEM, looking at homeostatic bone, diseased bone and the direct action on osteoblasts and osteoclasts. We hypothesised that PEPITEM would act directly on bone, decreasing osteoclastogenesis and resorption, and enhancing osteogenesis and mineralisation.

We found increased tibiae and vertebrae trabecular parameters in murine bone following daily treatment with PEPITEM, indicating improved bone growth. The bioactivity of PEPITEM was maintained in disease: using ovariectomised mice as a model of rapid bone loss, PEPITEM therapy protected from bone loss. Overall, these data suggest a role for PEPITEM as pro-anabolic agent with therapeutic potential.

In vitro, we observed murine and human osteoblasts increased their anabolic potential in response to PEPITEM treatment, leading to enhanced alkaline

phosphatase activity and mineral production. Whilst there was no direct effect of PEPITEM on cultured osteoclasts, the number of osteoclasts on the bone surface decreased in PEPITEM treated mice, and osteoclastogenesis was reduced *in vitro* by molecules released from osteoblasts treated with PEPITEM. This indicates the ability for PEPITEM to induce crosstalk between osteoblasts and osteoclasts, leading to dual actions of decreased resorption and increased formation on the bone.

The molecular mechanism responsible for eliciting the bioactivity of PEPITEM in osteoblasts was also investigated, revealing a possible role for sphingosine-1-phosphate (S1P). S1P treatment increased osteogenesis and decreased osteoclastogenesis in human cells *in vitro,* but conversely had the inverse effects on murine cells (decreased osteoblast mineralisation and increased osteoclast numbers). Additionally, we identified for the first-time that the expression of cadherin-15 protein in osteoblasts localised at sites of adherens junctions. Protein expression was maintained in calvarial osteoblasts following knockdown of gene expression using siRNA, revealing high levels of protein storage and recycling. By contrast, siRNA knockdown of cadherin-15 in human osteoblasts led to decreased osteogenic potential of osteoblasts, suggesting an essential role in osteogenesis.

In conclusion, we have identified a novel, endogenous peptide which has dual action on osteoblasts and osteoclasts *in vivo* and *in vitro,* leading to increased bone growth in health and disease. PEPITEM therefore has potential to be used as a therapeutic in musculoskeletal diseases involving bone loss to induce bone repair processes. However, further work is required to understand the mechanism that controls its bioactivity.

ACKNOWLEDGEMENTS

Firstly, I would like to thank Versus Arthritis, the Medical Research Council, and the Centre of Musculoskeletal Ageing Research for funding and providing the support needed to complete this PhD.

An extra special thank you must go to my supervisor, Dr Helen McGettrick, for keeping me on track throughout the past 3 years. Your organisation, experimental suggestions and countless readthroughs of thesis drafts have got me to where I am today. I would also like to thank my second supervisors: Dr Amy Naylor for introducing me into the world of bone, and Professor James Edwards for providing invaluable insight into bone biology.

To every member of the RRG and LTG, I would like to thank you all for your support, questions, and suggestions. In particular, thanks must go to Laurence Hill for his continuous jokes to lighten the mood, Jenefa Begum for all the GIFs and Georgiana Neag for all the support in experimental planning, sense checking and providing someone to chat to when were both in at 3am. In addition, thank you Julia Manning for allowing me to talk rubbish at you for three years and never complaining, you have made my time in the lab very enjoyable.

Thank you also to my patient research partner, Elspeth Insch. Your experimental suggestions, help with explaining convoluted topics and general good humour has been greatly appreciated.

To my family: Caroline, Biff, Kathryn, Mum and Dad. Thank you for everything you have done for me. Your support and encouragement have pushed me to where I am today, and I will forever be so grateful.

Lastly, I would like to thank my amazing fiancée, Marianne. There are countless things I need to thank you for, but I don't have the page count to write another thesis. You have seen me through from start to finish and I will never be able to repay the love and support you have given me. Thank you.

Table of Contents

Table of Figures

Table of Tables

Abbreviations

AdipoR1	Adiponectin Receptor 1
AdipoR2	Adiponectin Receptor 2
ADSC	Adiponectin Derived Stem Cell
AIA	Antigen Induced Arthritis
ALP	Alkaline Phosphatase
APC	Adenomatous polyposis coli
ATP	Adenosine Triphosphate
Atp6v1c1	ATPase H+ Transporting V1 Subunit C1
Bcl2	B-cell lymphoma 2
Bglap	Bone Gamma-Carboxyglutamate Protein
BMAT	Bone Marrow Adipose Tisse
BMD	Bone Mineral Density
BMM	Bone Marrow Monocyte
BMP	Bone morphogenetic protein
BMSC	Bone Marrow Stem Cell
BFR/BS	Bone formation rate/ Bone surface
CaSR	Calcium-sensing receptor
C.Ob	Calvarial Osteoblasts
Col(x)	Collagen type X
CSF-1	Colony stimulating factor 1
Ctsk	Cathepsin K
CTX-1	Type I Collagen Cross-Linked C-Telopeptide
diH_2O	De-Ionised Water
DMP1	Dentin matrix acidic phosphoprotein 1
DMSO	Dimethyl sulfoxide
DSPP	Dentin sialophosphoprotein
E2	Oestradiol
EO	Endochondral ossification
EOD	Every other day
EphA4	Ephrin type-A receptor 4
ERα	Oestrogen receptor alpha
FBS	Foetal bovine serum
Fgf23	Fibroblast growth factor-23
Foxc1	Forkhead box C1
Foxo	Forkhead box O
GFP	Green fluorescent protein
HIF	Hypoxia-inducible factor
H.Ob	Human Osteoblasts
HMW	High Molecular Weight
IBSP	Integrin binding sialoprotein
IFA	Incomplete Freunds Adjuvant

IL	Interleukin
IO	Intramembranous ossification
IP	Intraperitoneal
KO	Knockout
KDM	Lysine Specific Histone Methylase
LMW	Low Molecular Weight
LPS	Lipopolysaccharide
Lrp	Lipoprotein receptor related protein
mBSA	Methylated Bovine Serum Albumin
m-CSF	Macrophage colony-stimulating factor
MEM	Minimum Essential Medium
MEPE	Matrix extracellular phosphoglycoprotein
Mineral apposition rate	MAR
Mineral formation rate	MS/BS
MITF	Melanocyte Inducing Transcription Factor
MMP	Matrix metalloproteinase
MMW	Medium Molecular Weight
mRNA	Messenger RNA
MSC	Mesenchymal Stem Cell
MW	Molecular Weight
NICD	Notch intracellular domain
nTx	Cross-linked N-telopeptide of type I collagen
OA	Osteoarthritis
OI	Osteogenesis Imperfecta
OPG	Osteoprotegerin
OPN	Osteopontin
OVX	Ovariectomy
P1NP	Total procollagen type 1 N-terminal propeptide
PBMC	Peripheral Blood Monocytic Cell
PBS	Phosphate Buffered Saline
PEPITEM	Peptide Inhibitor of Transendothelial Migration
PPi	Pyrophosphate
PTH	Parathyroid Hormone
RA	Rheumatoid Arthritis
RANKL	Receptor activator of nuclear factor-κB ligand
RFP	Red fluorescent protein
RNA	Ribonucleic acid
ROI	Regions of Interest
ROR2	Receptor Tyrosine Kinase Like Orphan Receptor 2
RUNX2	Runt-related transcription factor 2
S1P	Sphingosine-1-Phosphate
S1PR	S1P receptor
SAMP6	Senescence-accelerated mouse strain P6
SC	Subcutaneous
SCPP	Secretory calcium-binding phosphoprotein
Shh	Sonic Hedgehog

SIBLING	small integrin-binding ligand N-linked glycoproteins
SOX	SRY-box transcription factor
Sp7	Specificity protein-7
SPARC	Secreted Protein Acidic and Cysteine Rich
SPARCL	SPARC-like protein 1
SPHK	Sphingosine Kinase
SPNS	spinster homolog
SPP1	Secreted phosphoprotein 1
SR	Strontium ranelate
TGF	Transforming growth factor
TNF	Tumour Necrosis Factor
TRAP	Tartrate Resistant Acidic Phosphatase
TROPOS	Treatment of Peripheral Osteoporosis
Twist1	Twist-related protein 1
VEGF	Vascular Endothelial Growth Factor
WAT	White Adipose Tissue
Wnt	Wingless and Int-1
WT	Wild Type
YWHAZ	Tyrosine 3-Monooxygenase/Tryptophan 5-Monooxygenase Activation Protein Zeta

Publications arising from this work

1. **Lewis, J. W**., Edwards, J. R., Naylor, A. J., & McGettrick, H. M. (2021). Adiponectin signalling in bone homeostasis, with age and in disease. Bone research, 9(1), 1. https://doi.org/10.1038/s41413-020-00122-0
2. Manning JE*, **Lewis JW***, Marsh LJ, McGettrick HM. Insights Into Leukocyte Trafficking in Inflammatory Arthritis - Imaging the Joint. Front Cell Dev Biol. 2021 Mar 9;9:635102. https://doi.org/10.3389/fcell.2021.635102. *Joint first authors
3. Hopkin, S. J.*, **Lewis, J. W.***, Krautter, F., Chimen, M., & McGettrick, H. M. (2019). Triggering the Resolution of Immune Mediated Inflammatory Diseases: Can Targeting Leukocyte Migration Be the Answer?. Frontiers in pharmacology, 10, 184. https://doi.org/10.3389/fphar.2019.00184 *Joint first authors
4. Fenton, C. G., Webster, J. M., Martin, C. S., Fareed, S., Wehmeyer, C., Mackie, H., Jones, R., Seabright, A. P., **Lewis, J. W.**, Lai, Y. C., Goodyear, C. S., Jones, S. W., Cooper, M. S., Lavery, G. G., Langen, R., Raza, K., & Hardy, R. S. (2019). Therapeutic glucocorticoids prevent bone loss but drive muscle wasting when administered in chronic polyarthritis. Arthritis research & therapy, 21(1), 182. https://doi.org/10.1186/s13075-019-1962-3

List of presentations

1. European Workshop for Rheumatology Research **(Leuven, Belgium)** 2020
   "New therapeutic avenues in bone repair: Harnessing a novel endogenous molecule to boost bone growth and prevent bone loss"
   Oral Presentation
2. 5th Joint Conference of the Bone Research Society (BRS) and British Orthopaedic Research Society (BORS) **(Cardiff, UK)** 2019
   "New therapeutic avenues in bone repair: harnessing a novel endogenous molecule to boost bone and prevent bone loss in inflammatory disease"
   Selected Poster presentation and Poster Pitch
3. UK Cell Adhesion Society **(Birmingham, UK)** 2019
   "New therapeutic avenues in bone repair: Harnessing a novel endogenous molecule to boost bone growth and prevent bone loss in inflammatory disease"
   Selected poster presentation
4. University of Birmingham RPC **(Birmingham, UK)** 2019
   "Agent X: The creator of Bone"
   Selected poster presentation
5. CMAR Annual meeting **(Birmingham, UK)** 2019
   "Agent X: The creator of Bone"
   Poster presentation

1 Introduction

Part of this chapter (section 1.8 – Adiponectin in Bone) is based on Lewis et al, 2019, for which I carried out the literature review, wrote the text and created the figures. Co-authors Edwards, Naylor and McGettrick made corrections and minor revisions. The full review can be found in Appendix 9-22.

1.1 The Evolution and Function of Bone

Bone is a highly dynamic organ, with significant roles in human physiology. Understanding the origin of bone and its key functions allows us to manipulate this knowledge to ensure bone can be maintained.

1.1.1 Evolution of Bone

Over $1.5x10^9$ years ago, movement of the tectonic plates led to the release of significant amounts of calcium carbonate ($CaCO_3$) in to the ocean, sparking the development of mineralised tissues such as bone.[1] The first of these calcified tissues to develop occurred as tooth like structures in conodonts,[2] however whether these were present for feeding or protection is unknown.[2] Next to develop, was a rigid outer skeleton used as a protection mechanism and to extend limb length, however this led to significant mobility and growth issues.[3] As a result, an internal skeleton evolved. Internalisation of bone allowed for the development of a musculoskeletal system, extending the capability for movement.[4] Bone originally consisted of calcium carbonate, however this has since changed to calcium phosphate (Hydroxyapatite: $3Ca_3[PO_4]_2Ca[OH]_2$).[5] Many reasons have been postulated for this evolutionary change, with the most compelling being protecting bone from the increase in blood pH which occurs following anaerobic exercise.[6] Bone is a highly vascularised organ, thus greatly susceptible to changes in the circulatory system. For example, blood calcium levels in rainbow trout (which contain calcium carbonate bones) increased 70% following high intensity exercise, resulting in acute vascular hypercalcemia.[7] Implants of calcium carbonate or hydroxyapatite into such trout, followed by a change in serum pH from 7.8 to 7.1, led to a serum calcium concentration increase of 48% in calcium carbonate implanted trout, whereas only a 3% increase in hydroxyapatite

implanted animals.[7] This change in believed to have occurred in early Palaeozoic protochordates, whose highly active lifestyle required increased anaerobic capacity to generate adenosine triphosphate (ATP).[8] The evolution of bone can also be followed by exploring changes and preservation in genes. There are 5 key genes identified for bone development known as small integrin-binding ligand N-linked glycoproteins (SIBLINGs), which include dentin sialophosphoprotein (DSPP), dentin matrix acidic phosphoprotein 1 (DMP1), Integrin binding sialoprotein (IBSP), matrix extracellular phosphoglycoprotein (MEPE) and secreted phosphoprotein 1 (SPP1). All these genes contain a Ser-Xaa-Glu motif, Glu-Asp clusters, and an Arg-Gly-Asp motif, which binds the osteoblast and osteoclast integrin motif. In addition, they can also bind calcium following their phosphorylation.[9] All 5 genes are found on a 375kb region on 4q21 and were developed following duplication of the secretory calcium-binding phosphoprotein (SCPP) gene. Around 531mya, a similar time to when conodonts first developed bone, the secreted protein acidic and cysteine rich (SPARC) gene duplicated to form the SPARC-like protein 1 gene (SPARCL).[9] At the 5' region of SPARCL, the SCPP genes arose allowing the production of bone in both Actinopterygians (e.g trout/ fugu) and Sarcoptrygians (Amphibians/mammals).[10] While the above shows the key changes that occurred in the original formation of bone, recent evidence has suggested bone continues to evolve to current conditions. Comparisons of bone from Pecos Indians from the 14th century bones with post-mortem bones in the 20th century showed the older bones had smaller haversian canal area.[11] This may be explained due to the loss of an active lifestyle in the current populations, though equally may be a result of the younger age of the Pecos Indian population due to their mean age at death being ~40 years-old.[11] This may

also explain the lack of evidence showing intercostal bone loss with ageing in Pecos Indian bones, since this often does not occur till later in life.[11] Overall, bone is continuously evolving and understanding the changes may allow the development of novel therapeutics to maintain bone throughout life.

1.1.2 Function of Bone

Since the first development of bone, its function has grown significantly. There are now 206 bones in the human body, each with their own functions to ensure homeostasis and survival are maintained.[12] These functions can be broken down into mineral storage, protection, locomotion and haematopoiesis in the bone marrow (not discussed below).

1.1.2.1 Mineral storage

Human bone is essential for ensuring serum mineral content is maintained. This is of particular importance for calcium and phosphate which constitute 50% of bone areas and 75% of bone mass in the form of hydroxyapatite.[13] In fact, 99% of whole body calcium[14,15] and 90% of phosphate[15] are stored in the bone at any one time. Calcium is the 5th most abundant element in the human body, however it only has a serum concentration of 8-10mg/dL.[14] This serum concentration must be maintained to ensure it can continue to mediate muscle contraction,[16] hormone production,[17] neurotransmission[18] and blood clotting.[19] Key determinants on calcium homeostasis are parathyroid hormone (PTH) and calcitonin (discussed in section 1.6), which alter bone breakdown to increase calcium release and thus increase serum calcium. Radiocalcium was first used to identify the role of PTH in calcium homeostasis, where thyroidectomy in dogs led to a significant reduction in calcium observed in the bone and serum.[20]

Phosphate makes up 1% of the total body weight and is involved in metabolisms and energy production,[21,22] cell signalling pathways[23,24] and maintaining cell structure.[25] Bone can therefore be used as a phosphate storage reservoir. Like calcium, phosphate homeostasis is controlled by parathyroid hormone, with additional control by FGF23.[26]

Carbonate (70-80%) and 30-50% of sodium and magnesium are also stored in the bone, where they are adsorbed to the crystal structures. Diets containing high magnesium levels increased magnesium in bone ash, whereas the reverse was seen in low magnesium diets.[27] Likewise, induction of alkalosis in dogs significantly increased levels of tibial sodium and carbonate, which was reversed in acidosis,[28] indicating high levels of storage capacity.

Overall, bone is an essential reservoir for these minerals, ensuring that serum levels can be maintained, and homeostasis can be achieved.

1.1.2.2 **Protection**

A major function for bones is protection, including the roles of ribs, protecting the lungs and heart; spine, protecting the spinal cord and major blood vessels; skull, protecting the brain; pelvis, protecting the reproductive organs.

These protective functions can be seen with evolution, where the key hypothesis for the development of spine occurred for protection against predators.[29] Alternatively, the vital role for ribs in protecting internal organs can be seen following motor vehicle crashes. Trauma patients with rib injuries had a significantly higher death odds ratio than patients without rib injuries.[29] The skull is also shown evolutionary to evolve for protection, with skull shape significantly changing in

carnivores, particularly in those that practice polygyny, where they must defend and compete with force.[30] Similar is also seen in the frog species, where hyper ossification has evolved independently at least 30 times, showing its role in protection.[31] In addition, hyper ossification is particularly observed in frogs that undertake phragmotic behaviour (use their heads to protect themselves), which further indicates a role in protecting vital organs.[31] In humans, early homins display an orthognathic face in addition to more robust mandibular corpus and maxilla compared to non-human primates.[31] This is believed to develop for protection from fights, with the face being the central target. In present day, 83% of fractures resulting from interpersonal violence occur on the face[31] and two thirds of assaults result in damage to the face.[32] However, there is an alternative theory to the evolution of the face focussing on bite force as opposed to protection. For example, frog skulls change depending on a diet of vertebrates against invertebrates.[31] Likewise, it is believed that when humans began eating harder, more difficult to crush items of food, their skull began to change.[33] However, this does not provide an explanation for the sexual dimorphisms seen between male and females, which is present in nearly all species (excluding cheetahs, where locomotion is their main evolutionary push).[34,35]

1.1.2.3 **Locomotion**

A major driver to progress from an external skeleton to an internal skeleton was to aid range of movement and general locomotion. This is evident in cheetahs, which are the only carnivore without sexual dimorphism in their bones, allowing fast sprinting to catch prey in both males and females.[35] Locomotion induced changes are also present between Bonobos and Chimpanzees, where the former spend more

time airborne, moving from tree to tree and the latter more time moving up and down trees.[36] Bonobos therefore have a smaller chest, scapular and pelvis, making them smaller but less powerful.[36] In addition, they have a curve to their proximal and middle phalanges, allowing easier swinging from trees.[36] Likewise, differences between apes and humans are evident, allowing humans to move via bipedalism, which is 75% less costly in ml of O2 kg^{-1} m^{-1} than quadrupedal.[37] This in part is due to the development of longer tibias and femurs, which were first observed in early humans and are not seen in non-human primates.[38] Humans are also the only primate which are able to endurance run, which evolved due to hunting for protein rich resources.[39] Each step in running puts 3-4 times the body weight in the legs,[40] therefore humans have evolved to resist these impacts through an increase in the size of the iliac pillar[41] and articular surface area.[42] Arms have also evolved to increase throwing potential, which again occurred due to the need to hunt. In humans, humeral torsion is 10-20% lower than in chimps, allowing increased movement of the arm.[43] Additionally, in the throwing arm of pitchers[44] and handball players,[45] humeral torsion is significantly lower than their contralateral non-throwing arm, showing how bone is constantly changing to improve locomotion.

Loss of bone therefore calls into question all of the above roles, having detrimental impact on people who are affected. Understanding how bone is formed, maintained, and lost in diseases is therefore essential to ensure bone can be protected and continue to perform these major functions.

1.2 Formation of Bone

During week 7 of human embryogenesis, ossification (the generation of bone) begins,[46] continuing until peak bone mass is produced at 12-15 years-old.[47]

However, bone growth and the mechanisms involved in maintenance continue well into life, ensuring damages large (fractures) or small (micro-fractures) are fixed and homeostasis is maintained. During development, ossification can be split into intramembranous or endochondral ossification. Understanding the mechanisms via which ossification occurs not only provides possible mechanisms inducing bone loss (genetic and non-hereditary), but also provides targets for novel therapeutics to treat disease impacting bone.

1.2.1 Intramembranous ossification

Intramembranous ossification (IO) causes the formation of flat bones, such as the mandible and the skull.[48] IO works through direct bone formation, where the recruitment of bone forming osteoblast precursors and mature osteoblasts release collagen and mineral (see section 1.3.1) causing the production of mineralised bone (for in-depth review see [49]).

In the first stages of development, an ossification centre is formed by recruitment of mesenchymal stem cells and osteoblast precursors from the mesoderm. In ephrin type-A receptor 4 (EphA4) knockout (KO) or twist-related protein 1 (Twist1) homozygous mice, where neural crest and mesoderm boundaries are lost causing altered mesodermal cell development, there is reduced fusion of the skull, as observed with alizarin red staining.[50] Furthermore, mutant forkhead box C1 (Foxc1) KO mice (congenital hydrocephalus) died due to skeletal abnormalities, resultant from decreased osteoprogenitor proliferation.[51] Following osteoblast recruitment and initial osteogenesis and matrix production, osteoblasts continue to produce mineralised collagen to increase bone strength and cortical bone thickness.[49] In humans, mutations in Twist1 (Saethre-Chotzen syndrome) results in

decreased fusion of frontal and parietal bone due to lack of intramembranous ossification.[52] Further research is required to breakdown the stages of intramembranous ossification, leading to increased knowledge of osteoblast formation which can be used for future disease treatments.

1.2.2 Endochondral ossification

Endochondral ossification (EO) is more common, leading to the creation of long bones, such as the tibia and femur. Additionally, EO is the primary method of fracture response throughout life.[53–55] Therefore, understanding the direct stages of endochondral ossification can provide insight in to how to boost bone growth following fracture using therapeutics.

EO begins by the recruitment of chondrocytes to the area of bone formation, which leads to the production of cartilage and the formation of a bone template. Neural-crest specific inactivation of SRY-box transcription factor (Sox) 9, a major chondrocyte inducing transcription factor, resulted in complete absence of endochondral malleus and incus bones, but had no effect on intramembranous bones.[56] Following initial recruitment, chondrocytes undergo hypertrophy, increasing chondrocyte numbers and altering their phenotype. Sox5 and Sox6 KO mice display delayed chondrocyte hypertrophy, leading to defective growth plates in long bones and decreased bone formation.[57] Similar long bone skeletal abnormalities are also observed in runt-related transcription factor (Runx2) dominant negative mice and mice overexpressing Runx2. In overexpressing mice, premature chondrocyte maturation resulted in altered EO,[58] whilst lack of chondrocyte hypertrophy in mutant Runx2 mice delayed EO.[59,60]

Once chondrocyte hypertrophy has occurred, osteoblasts are recruited to initiate matrix deposition and mineralisation of cartilage. In mice expressing collagen type X alpha 1 (Col10a1) induced red fluorescent protein (RFP) (chondrocyte-specific) and Col1a2 induced green fluorescent protein (GFP) (osteoblast-specific), all cells in the osteogenic region of bones expressed RFP and GFP, thus showing expression of both Col1 and Col10, indicating chondrocyte to osteoblasts differentiation.[61]

Blood vessel infiltration also occurs in bone, bringing additional osteogenic precursors.[62,63] This vasculature invasion and the generation of essential H-vessels ($CD31^{high}$/$endomucin^{high}$) allows increased osteoblast and osteoblast-precursor migration into the bone, causing enhanced bone growth.[64]

In fibrodysplasia ossificans progressive, mutations in bone morphogenetic protein (BMP) type 1 receptor have been identified leading to increased EO in sites outside the skeleton, this EO needs to be targeted to reduce bone production.[65] In contrast, fracture recovery requires increased levels of EO to boost bone growth, thus mechanisms to boost EO are needed to enhance the fracture response.[53,54,66]

1.3 Bone remodelling

Following the generation of bone, it enters a remodelling cycle to ensure structure and strength are maintained. Bone remodelling revolves around osteoblast induced bone formation, osteoclast led bone resorption and detection of changes by osteocytes. Small imbalances in this cycle can result in pathological bone conditions. Therefore, understanding the cellular mechanisms of the remodelling cycle enables

the development of novel treatments to stabilise bone remodelling in disease conditions.

1.3.1 Osteoblasts

Osteoblasts are pro-anabolic cells, which are solely responsible for the generation of new bone. Commitment to the osteoblast lineage requires mesenchymal stem cell (MSC) differentiation into pre-osteoblasts, preventing differentiation into chondrocytes, adipocytes, fibroblasts or myocytes.[67,68] Following osteoblast commitment, pre-osteoblasts differentiate into pro-osteoblasts, where they progress through 3 stages of differentiation to become mature cells. First cells become highly proliferative and express osteopontin (SPP1),[69–71] before exiting the cell cycle and expressing alkaline phosphatase (ALP) and Col1a1.[69–71] This leads to the ability to generate matrix.[69–71] Mature osteoblasts are mononuclear, cuboidal cells,[72] which are found directly adjacent on the bone surface.[73] The different stages of differentiation are dependent on multiple signalling pathways (explored in section 1.4).

Osteoblasts were first identified to be involved in bone remodelling using incisors absent (iu), toothless (tl) and osteopetrosis (op) rat models which have a high bone volume.[74] Mutant rats had increased messenger ribonucleic acid (mRNA) levels of *Alp* and *Spp1* in the calvaria, contributing to the accumulation of bone.[75] To enable bone growth and repair, osteoblasts produce mineral (hydroxyapatite) and collagen, which combine to form a matrix of calcified fibrils and subsequently bone (Figure 1.1).[76,77] Type I collagen is produced by osteoblasts as a trimer, made up of two α1 chains and one α2 chain.[67,78–80] Due to its essential nature in generating bone, KO of either chain is embryonically lethal,[81] however Col1a1 mutations are

present in osteogenesis imperfecta, where brittle bone is produced as a result of abnormal collagen fibrils.[82,83] In addition, the Col1a1 promoter is often used to create osteoblast-specific Cre-recombinase mice,[84] showing its specificity and essential nature in osteoblast maturation. In order to solidify collagen fibrils, hydroxyapatite (Section 1.1.1) is produced and released from osteoblasts, which incorporates into the fibrils to provide support.[78,85] Hydroxyapatite is produced by combining calcium with inorganic phosphate (Figure 1.1).[86] A key enzyme involved in the production of inorganic phosphate is ALP, which hydrolyses P-O bonds in esters and leads to the release of free phosphate.[87–90]

R-OP +H2O > ALP> R-OH + P

ALP knockout mice develop severe skeletal defects, due to weakness of the bone fibrils.[87] In addition, ALP is used as a direct marker of osteoblast activity, with ALP activity increasing following osteoblast differentiation.[91–95] If treatments have the ability to boost both ALP activity and Col1a1 production in osteoblast, bone matrix development could be enhanced to induce the production of new bone in disease.

1.3.2 **Osteoclasts**

In order to facilitate bone remodelling and ensure old/damaged bone is removed, osteoclasts are recruited to resorb bone. Osteoclasts are multinucleated cells,[96] which can be derived from the bone marrow or circulating monocyte precursors.[97] Differentiation into osteoclasts and away from macrophages or dendritic cells involves stimulation with receptor activator of nuclear factor κ B ligand (RANKL, see 1.4.2.1),[98–100] or TNF. There is also evidence of specific osteoclast precursor cells, however these have only been identified in murine studies thus far.[101] However,

osteoclasts require constant replenishment due to a lifespan of ~10 days.[102] Therefore osteoclast progenitors continuously circulate in the bloodstream ready to be recruited to the bone.[100,103]

Bone resorption occurs through the formation of resorption pits,[104,105] which are sealed spaces between the osteoclast and bone, enabling localised release of bone resorption molecules (Figure 1.2). Formation of resorption pit requires binding of integrins to the bone.[106] Immunofluorescence for $\alpha_5\beta_3$ revealed high expression in human osteoclasts, which upon activation localised to the ruffled border.[107] Inhibiting $\alpha_5\beta_3$ binding using Echistatin significantly decreased resorption pit sizes and actin ring generation in human osteoclast like cells cultured on dentine, without altering cell number.[106] Integrins are also involved in outside-in signalling of osteoclasts, where KO of downstream signalling molecule Src in osteoclasts decreases osteoclast spreading on vitronectin (an $\alpha_5\beta_3$ stimulator) coated plates.[108] Understanding how osteoclast adhesion receptors function may provide potential targets for disease with pathological osteoclasts.

Once osteoclasts have bound to the bone and formed a resorption pit, multiple bone resorbing molecules are released, including matrix metalloproteinases (MMP), cathepsins and acidic H^+ ions. RANKL treatment of osteoclasts leads to an increase in ATPase H+ transporting v1 subunit c1 (*Atp6v1c1*) mRNA and protein expression in murine bone marrow macrophages.[109] Furthermore, addition of Atp6v1c1 interfering RNA decreased the acidity of osteoclast conditioned media, thus decreasing resorption.[109] In a similar pattern, osteoclasts increase mRNA expression of cathepsin K (Ctsk) following RANKL treatment.[110] Reduction of Ctsk activity using Odanacatib and L-873724 leads to decreased resorption when treating rabbit

osteoclasts on bovine bone.[111] Osteoclasts also have high expression of MMPs, with MMP9, 10, 12 and 14 mRNA found in murine and rabbit osteoclasts (in-situ hybridisation (ISH) and polymerase chain reaction (PCR)).[112] Blocking such MMP's using a molecular inhibitor leads to decreased resorption pit formation.[112] Understanding how osteoclasts resorb bone provides possible targets to reduce bone resorption in pathological conditions.

1.3.3 **Osteocytes**

Osteoblasts have two options following their attraction to the bone surface. They either continue to produce bone until they apoptose (at around 30 days)[102] or they become entrapped in the bone by new mineral, resulting in their differentiation into osteocytes.[113,114] Due to the unique environment inside the bone, isolating and generating osteocytes *in vitro* is difficult.[115] Therefore, understanding the differentiation of osteocytes and their function inside the bone is not fully understood. Nonetheless podoplanin,[116] DMP1,[117] fibroblast growth factor-23 (FGF23)[117] and sclerostin[118–121] all increase during osteoblast to osteocyte differentiation, with podoplanin particularly important in dendrite formation.[116] Investigating the microstructure of new-born rabbit tibiae during development found osteocytes consistently maintain contact with adjacent cells.[122] Furthermore, imaging cortical bone sections found the connections between osteocytes contain gap junctions, enabling fast movement of molecules between cells.[123] For example, injection of a red tracer dye into rats revealed presence of the dye inside osteocyte lacunae after only 30 minutes.[124]

In diphtheria toxin induced osteocyte KO mice, there is a significant decrease in trabecular bone and an increase in micro-fractures, indicating osteocytes as a key

controller of bone remodelling.[125] Using the tail suspension unloading model, osteocyte KO mice were protected from bone loss, showing a role in mechanosensory bone regulation.[125] Many signalling molecules are believed to be involved in osteocyte signalling to other bone cells. In DMP-cre mice directed at RANKL to produce osteocyte specific RANKL KO, mice become highly osteopetrotic.[126] In addition, the sclerostin gene *Sost* is highly expressed in osteocytes, with prevalence increasing in HYP osteopetrotic mice.[120] Lastly, *in vitro* culture of embryonic chick osteocytes with rat long bone osteoblasts induces the release of NO_2, with further induction under mechanical pressure.[127] These data indicate osteocytes are a highly responsive sensory cell, with a key role in controlling bone remodelling. Therefore, altering osteocyte signalling or uncovering the mechanisms by which osteocytes control bone growth may enable new avenues to explore in altering bone remodelling in disease.

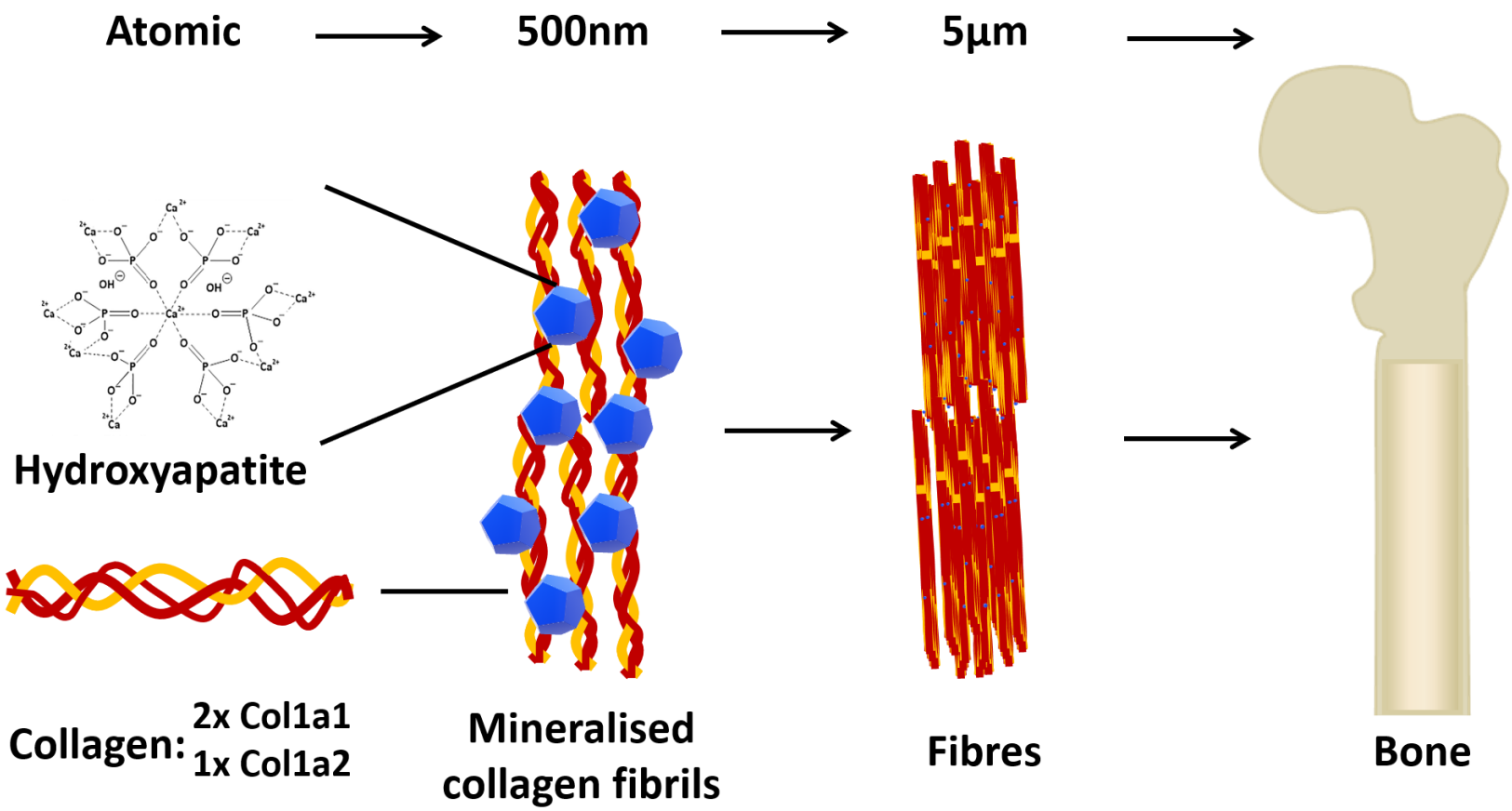

Figure 1.1. Bone is made from hydroxyapatite and collagen, which create fibrils, fibres and ultimately bone.

Osteoblasts produce hydroxyapatite, made from phosphate and calcium, and collagen, in the forms of Col1a1 and Col1a2. Collagen fibrils intertwine and combine with hydroxyapatite crystals to create mineralised fibrils. These fibrils combine further to generate fibres and eventually bone.

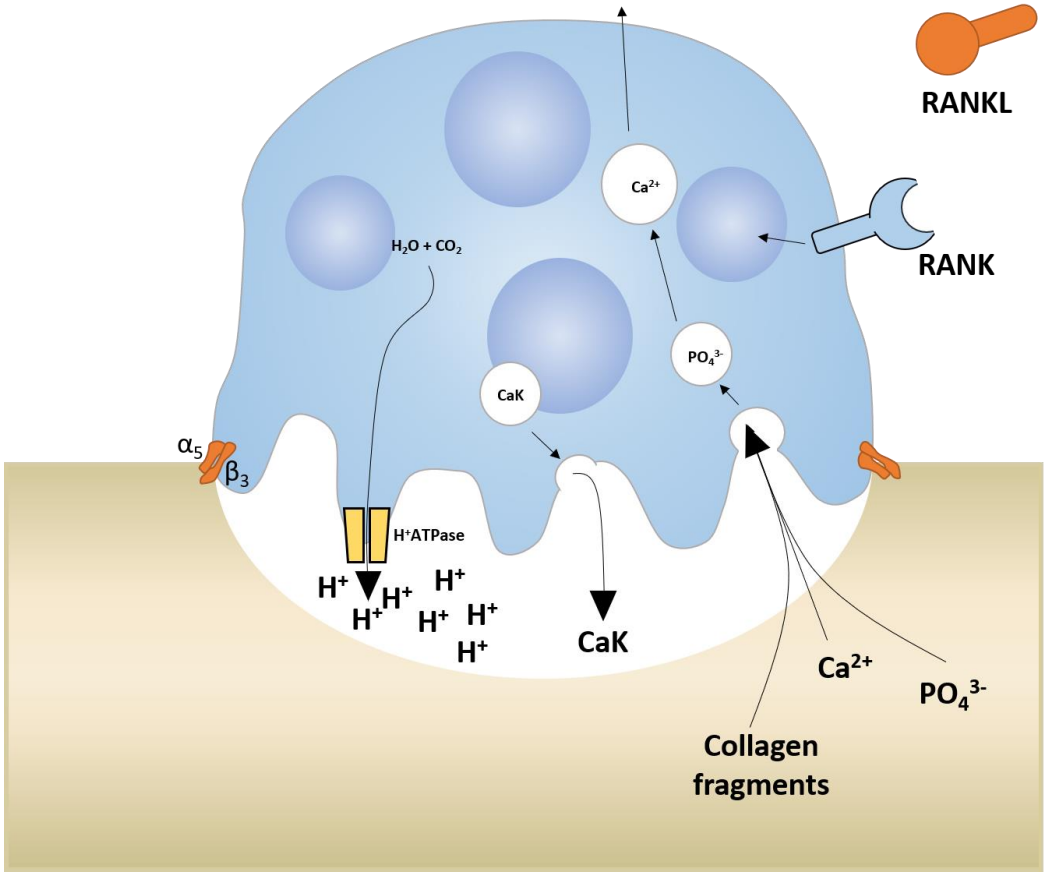

Figure 1.2. Mechanisms involved in osteoclast bone resorption

Osteoclasts are stimulated by binding of RANKL, released by stromal and immune cells, to RANK. This induces differentiation into mature osteoblasts, which bind to bone using integrin α5β3 and form resorption pits. Release of H^+ ions and cathepsin K causes the breakdown of bone into collagen fragments, calcium, and phosphate, which are taken up by the osteoclasts and released into the periphery.

1.4 Signalling pathways

Understanding the signalling involved in the differentiation and function of bone cells enables the targeting of specific molecules to boost or inhibit cell function in disease. Here we outline the key signalling pathways for osteoblasts and osteoclasts.

1.4.1 Osteoblasts

Tightly controlled osteoblast signalling pathways are essential for co-ordinated differentiation, proliferation, and survival, in addition to amplifying hydroxyapatite and collagen formation. Signalling can be induced through many factors from circulating molecular signals to external stimuli such as sheer stress, gravity, and compression. Activated osteoblast pathways include Wingless-related integration site (Wnt), Bmp and Runx2, all of which are essential in ensuring complete osteoblast differentiation.

1.4.1.1 Wnt

Wnt signalling is split into canonical (β-catenin dependent; Figure 1.3) and non-canonical pathways.[128] Non-canonical signalling through Wnt3a[129] and Wnt4[130] in ST2 cells and C2C12 cells led to increased mineralisation. In contrast, inhibition of ROCK1 and 2 or heterozygous Vangl2 mutations reduced the planal cell polarity pathway in osteoblasts, causing decreased mineralisation.[131,132] Knock out of Wnt signalling molecules *in vivo* have also shown essential roles in bone remodelling. Most Wnt knock outs are embryonically lethal due to their other essential roles in embryogenesis.[133–136] however, *in vivo* knock out of Wnt16,[137] Wnt10b[138] and Wnt7b[139] have all lead to decreased bone mass and ossification, thus showing an essential role for Wnt signalling in bone growth and homeostasis. However, further

research is required to fully understand the role on non-canonical signalling pathways in osteoblasts.

The canonical pathway has been more extensively researched and targeting different members of the pathway have been shown to alter osteoblast signalling. Gain-in-function mutations in the lipoprotein receptor related protein (Lrp) were observed in a single patient with extremely high bone mass.[140] This mutation was later confirmed using murine models[141] and protects mice from ovariectomy (OVX) and unloading induced osteoporosis.[142] Interestingly the opposite occurs in the human disease osteoporosis psuedoglioma, where loss-of-function mutations in LRP5 decreased bone mass.[143,144] Further down the pathway, increased β-catenin signalling through osteoblast specific KO of adenomatous polyposis coli (APC)[145] or significant decreases using β-catenin KO[145,146] led to significantly increased and decreased trabecular bone mineralisation respectively. These data indicate a pro-anabolic phenotype of Wnt signalling on bone growth and remodelling.

Targetting dickkopf Wnt signalling pathway inhibitor 1 (Dkk1), a natural inhibitor of canonical Wnt signalling by blocking LRP6 signalling, led to a reduced bone mass.[147] Similarly, mutations in Wnt inhibiting sclerostin are present in sclerostiosis[148,149] and van buchems disease,[150] where bone growth occurs at a pathological rate. This has led to the development of treatments for osteoporosis that focus on inhibiting sclerostin signalling (see section 1.6). Overall Wnt signalling is pro-anabolic, thus enhancing signalling through therapeutics would lead to bone growth and possible repair.

1.4.1.2 **Notch**

Notch signalling is a contact dependent pathway between Notch 1/2 on the target cell and Jag1/2 or DLL1/3/4 on the signalling cell.[151] Binding to Notch initiates cleavage of the Notch intracellular domain (NICD) by Adam10/Tace and γ secretase, leading to translocation to the nucleus and removal of a corepressor to initiate transcription (Figure 1.3).[151] However, the role of Notch signalling in osteoblasts is controversial.

Whilst 8-week-old Notch1/2 KO mice initially displayed significantly increased trabecular bone mass, they lacked mesenchymal stem cells and thus osteoprogenitors, leading to decreased trabecular bone volume by 24-weeks.[152] At 26 weeks, notch KO mice have nearly 10% of WT mineralised bone mass.[152] Additionally, overexpression of NICD on the 2.3kb Col1a1 promoter enhanced differentiation of osteoblasts, which was reversed when NICD was expressed on the 3.6kb promoter, leading to osteopenia.[152] Using GFP tagged Col1a1 promoters, pre-osteoblasts expressed higher levels of the 3.6kb Col1a1,[153] thus the timing of notch signalling may alter the osteoblastic response. Due to notch signalling being universal and the range of osteoblast responses to signalling, therapeutics have yet to be developed to target it in bone. Resveratrol has been shown to enhance notch signalling in multiple cell types and caused enhanced differentiation when added to osteoblastic MC3T3-E1 cells.[154] In addition, resveratrol increased bone mass in obese males when given daily for 16 weeks.[155] Due to its short-half life, it is believed resveratrol causes intermittent activation,[156,157] thus providing a possible mechanism of targeting notch signalling in osteoblasts to promote bone growth.

1.4.1.3 **BMP**

Part of the transforming growth factor β (TGF-β) superfamily, bone morphogenetic protein (BMP) signalling is another major osteoblast pathway. BMP has increased specificity towards the bone than Wnt/Notch,[158] indicating less off-target effects if targeted in disease. Binding of BMP to a BMP receptor dimer causes phosphorylation of the receptor, activation of P38 and Smad pathways, and downstream signalling.[159]

Direct addition of BMP to C2C12 cells increased expression of osteoblast differentiation genes *Runx2*,[51,160] osterix (*Sp7*)[161] and *Id1*,[51] and led to increased osteoblastogenesis and decreased adipogenesis.[51,160,161] In addition, BMP2 increased LRP5 expression in 2T3 and MC3T3 cells, promoting Wnt signalling.[162] *In vivo,* osteopenic mice are protected from bone loss following recombinant BMP2 injection.[163] Enhanced release of truncated BMPR-1β via the Col1a1 promoter, thus inhibiting BMP signalling, decreased bone formation in WT mice.[153] Similar findings are observed in osteoblast specific Col1a1-cre mice targeting Smad4 which reduces osteoblast *Runx2, Alp* and *Col1a1* gene expression.[164] Endogenous inhibitors, noggin and gremlin also point towards the role of BMP signalling in osteoblasts. Retroviral expression of noggin in U-33 cells led to decreased *Runx2* expression,[165] whilst expression of noggin on the osteocalcin promoter decreased trabecular bone volume.[153] Further, gremlin overexpression on an osteocalcin (Bglap) promoter inhibited osteogenesis of bone marrow stromal cells, decreasing the number of osteoblasts present on the bone and bone formation.[166] Interestingly, BMP signalling induced expression of gremlin and noggin, thus providing negative feedback mechanisms.[167,168] Due to the pro-osteogenic potential of BMP signalling, members

of the pathway can be targeted in therapeutics to induce bone growth. For example, recombinant human BMP2, BMP7 and BMP4 have been used in clinical trials, boosting bone growth following thoracolumbar burst or tibial fractures.[169–171] However, there were only small changes when compared to controls.

1.4.1.4 Hedgehog signalling

More recently, hedgehog signalling has been indicated to be involved in osteoblast differentiation. When recombinant sonic hedgehog (Shh) is added to K5483 pre-osteoblasts, increased ALP activity was observed.[172] Similarly, the amino terminal end of Shh caused an increase in ALP activity in C3H10T1/2 and MC3T3 cells.[173] However, more research is needed to fully understand the specific signalling of Shh and other hedgehog proteins.

1.4.1.5 Transcription Factors in osteoblast differentiation

Following activation of the above signalling pathways, transcription factors specific to stimulate osteoblast differentiation are initiated.

Sp7 is a key transcription factor in osteoblast differentiation.[174] Retroviral induced Sp7 expression in bone marrow-derived mesenchymal stromal cells (BMSCs) significantly increased ALP activity and cell proliferation.[175] Sp7 KO mice die in utero with their bones completely absent of mineralisation.[174] In addition, Col1a1 levels are significantly reduced in Sp7 KO bone regions, whilst chondrocyte markers Sox9 and Col2a1 are increased, indicating a lack of osteoblast differentiation.[174] Overexpression of Sp7 in BMSCs followed by their injection into mice with calvarial defects enhanced defect healing, showing a pro-anabolic phenotype.[176] However, when Sp7 is consistently overexpressed in late stage

osteoblasts using to 2.3kb Col1a1 promoter, osteoblast specific genes are downregulated, indicating a need for differentiation stage specific expression.[177]

Runx2 is another osteoblast inducing transcription factor. Interestingly, in Sp7 KO mice Runx2 is still expressed, whereas Sp7 is not present in Runx2 KO, suggesting a need for Runx2 earlier in the osteoblast differentiation pathway.[174] In addition, Runx2 KO calvarial osteoblasts spontaneously differentiate into adipocytes and chondrocytes.[178] Runx2 KO mice are embryonically lethal, lacking all mineralisation,[179] whereas Col2a1 overexpression of Runx2 leads to increased mineralisation throughout the skeleton.[180] However, when Runx2 is only knocked out in late stage osteoblasts (2.3kb Col1a1 driven), mice are born indistinguishable from WT, but develop a severe bone loss phenotype in early adolescence.[181] These data indicate that whilst Runx2 is essential for initial osteoblast development, it is also required to ensure bone maintenance can occur. However, Runx2 expression oscillates throughout the cell cycle, with higher expression G1 phase and lower in S phase.[182] Using adenovirus induced continuous Runx2 expression throughout the cell cycle, MC3T3 proliferation decreased.[182] Therefore, targeting Runx2 directly may be difficult in enhancing osteoblast differentiation in disease, due to the need for timing specific expression.

1.4.2 **Osteoclasts**

Osteoclastogenesis and osteoclast activation involves different, novel pathways compared to osteoblast (Figure 1.4), thus providing a range of new targets to altered bone growth.

1.4.2.1 **RANK**

The RANK-RANKL interaction is the main signal to initiate osteoclastogenesis in macrophages and subsequent osteoclast precursors. RANK is expressed by macrophages once they commit to the osteoclast lineage with HL60 cells increasing in RANK expression after treatment with 1,25D, but not following granulitic differentiation with dimethyl sulfoxide (DMSO).[183] RANKL is expressed on multiple cell types, such a osteoblasts,[184] lymphocytes,[185] and fibroblasts[186] all of which can cause osteoclastogenesis when co-cultured with macrophages *in* vitro. The essential nature of RANK-RANKL interactions can be seen using RANK mutant[187] or KO[98] mice, where an osteoporotic phenotype develops due to an inability to form osteoclasts.

Knocking out RANK downstream signalling molecule TRAF6 in bone marrow cells inhibited RANKL induced osteoclastogenesis and osteoclast activation,[188] which resulted in mice gaining a high bone mass and increased trabecular bone.[189] RANKL treatment of monocytes increased phosphorylation of AKT and ERK1/2, and differentiation into osteoclasts was lost when treating cells with inhibitors for PI3K, P38 and ERK.[190] However, differentiation can be restored using retroviral overexpression of c-fos, indicating it as a key transcription factor.[191] Similarly, fos KO mice are osteopetrotic[192,193] with significantly decreased tartrate-resistant acid phosphatase (TRAP) positive osteoclasts present on the bone.[192]

Natural inhibitors of RANK signalling exist, the most prominent being osteoprotegerin (OPG). Crystallisation has revealed a similar structure of OPG to RANK, indicating it works as a decoy receptor, binding RANKL with 500 times more affinity than RANK.[194] In transgenic OPG overexpressing mice, monocyte-

macrophage numbers are normal, however osteoclasts are significantly decreased leading to increased bone mass.[195] Likewise, the isolation of splenocytes form these mice have decreased differentiation, which is also seen with direct addition of OPG to osteoclastogenic media.[195] In fact, mice are protected from OVX induced bone loss following injection of OPG.[195] In contrast, OPG KO mice have significantly decreased trabecular and cortical bone due to enhanced osteoclastogenesis.[196,197] In light of this, molecules targeting RANK-RANKL signalling have been developed, such as denosumab (see section 1.6).

Protein levels of the Pu.1 transcription factor are increased during the differentiation of bone marrow monocytes (BMM) into osteoclasts.[198] Furthermore, total Pu.1 KO, osteoclast specific Pu.1 knockout using the cathepsin K promoter, or molecular inhibition (CC-4047) of Pu.1 leads to a high bone phenotype due to loss of bone resorption.[198–200] These data point to the essential nature of Pu.1 in osteoclast differentiation.

Overall, understanding the signalling pathways that control osteoblast and osteoclast differentiation and survival may allow the development of new therapies which restore the balance of resorption and formation often lost in disease.

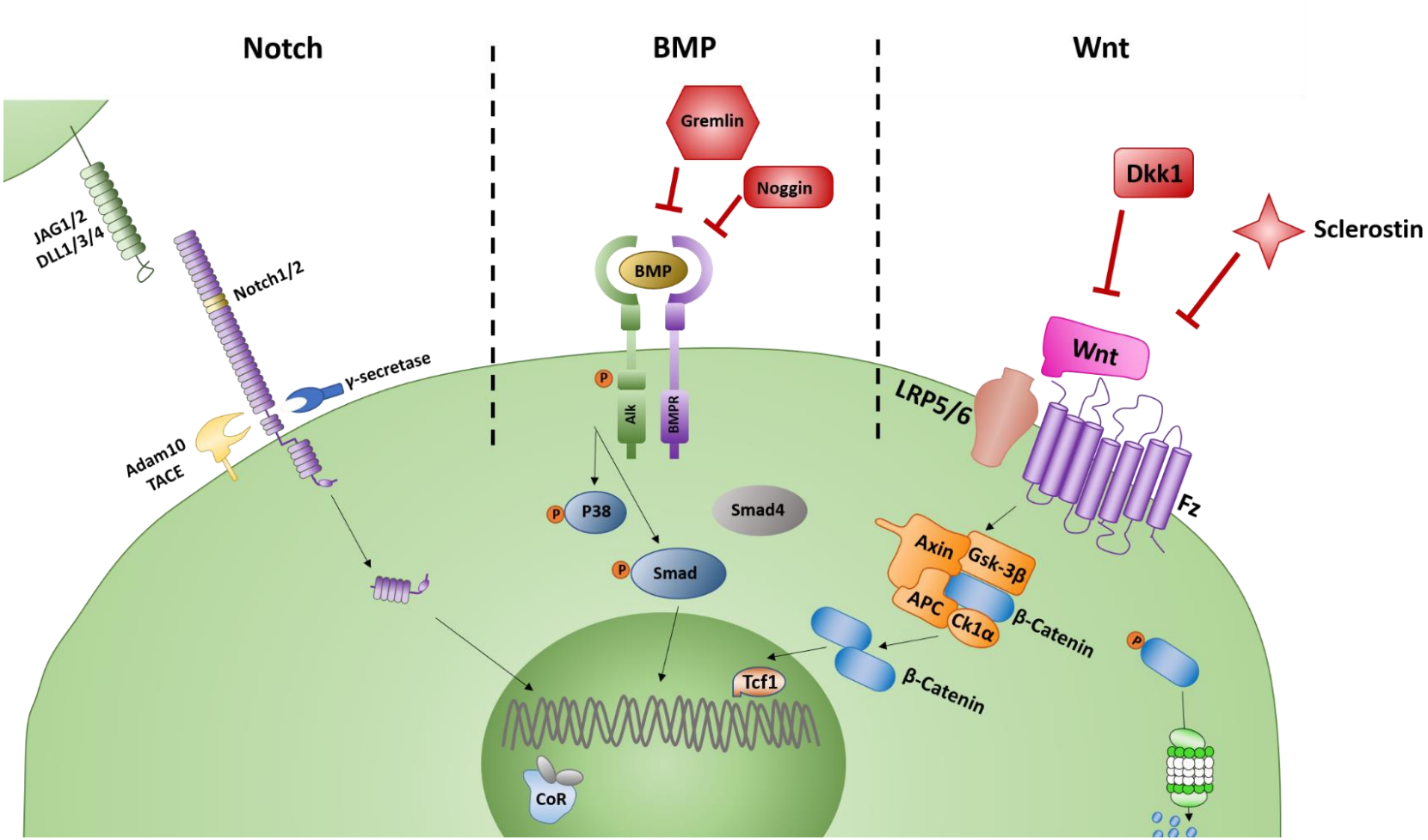

Figure 1.3. Osteoblast signalling pathways

Osteoblast signalling can be broken down into three main pathways. Wnt signalling through the canonical pathway induces the release of β-catenin and induction of osteoblast signalling. Molecules that inhibit this pathway include sclerostin and Dkk1. BMP signalling induces a unique smad led pathway, where stimulation increases osteoblast differentiation. Lasty, Notch binding to receptors on adjacent cells results in cleavage of the NICD, which induces osteoblast signalling and thus differentiation.

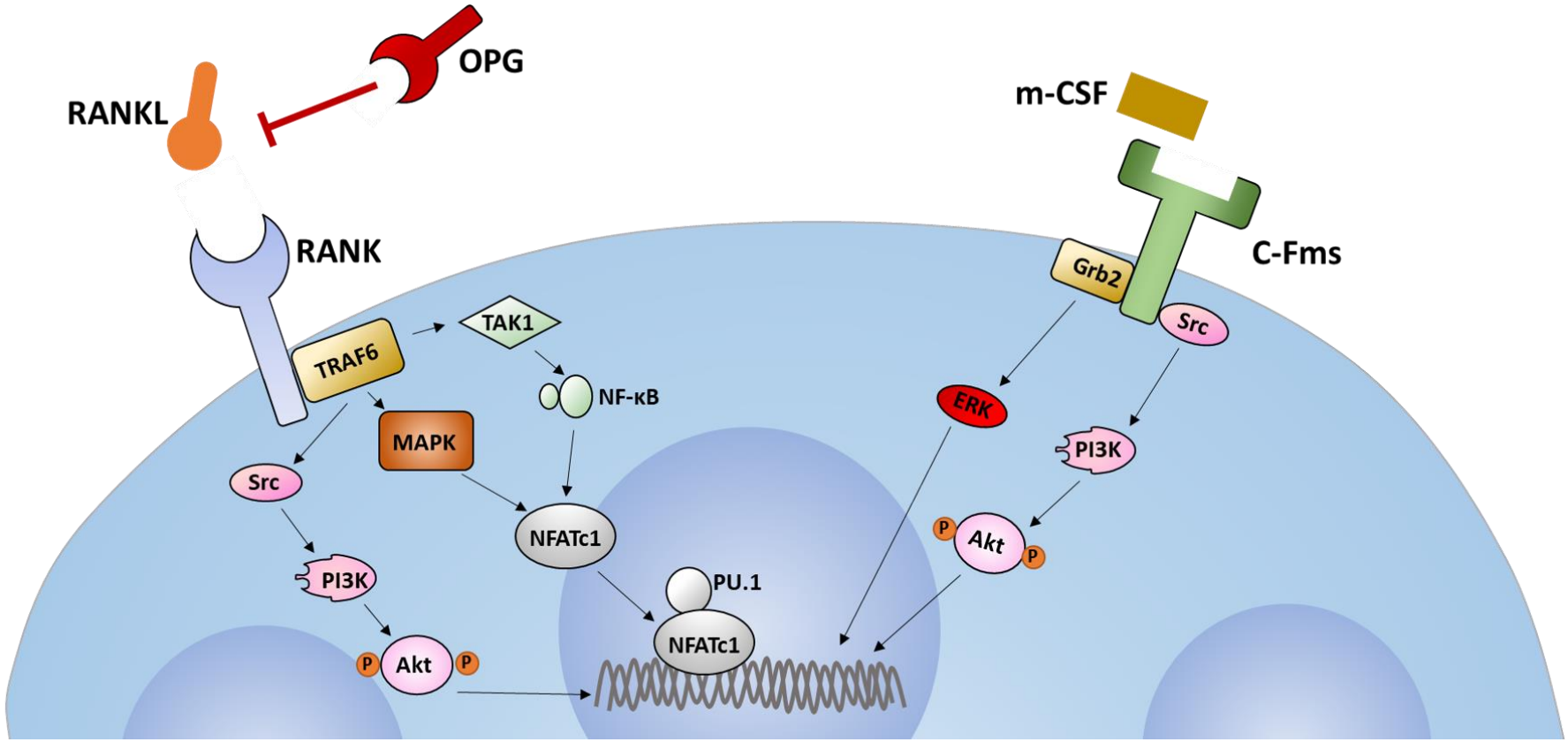

Figure 1.4. Osteoclast signalling pathways

Osteoclastogenesis is induced through multiple pathways, however the most common involves signalling between RANK and RANKL. First, monocyte to macrophage differentiation is initiated through binding of m-CSF to its receptor, leading to upregulation of RANK expression. RANKL is expressed and released on many cells (osteoblasts, endothelium, T cells, B cells) and binds to RANK, resulting in stimulation of the Akt and MAPK pathways and induction of osteoclastogenesis. RANKL can be targeted by OPG, a natural complementary inhibitor with significantly higher affinity for RANKL. Binding of OPG to RANKL results in decreased osteoclastogenesis and thus resorption.

1.5 Diseases of Bone

A delicate balance between bone resorption and formation is essential in ensuring healthy bone is maintained. For this reason, slight alterations in the degree of resorption or formation lead to pathological bone remodelling that are detrimental to quality of life, and in some cases lead to secondary issues that increase the likelihood of death.[201–203] Bone pathologies can take many forms from genetic disorders, such as osteogenesis imperfecta[82], to diseases that occur naturally as a result of aging such as osteoporosis.[204] Additionally, issues with healthy bone can occur following traumas and excess use, leading to fractures,[205] where likelihood of fracture is increased as a result of pre-existing bone diseases that cause weaker more brittle bone.[206] As outlined below, treatments to these diseases are available, however complications often occur. Exploring novel therapeutics is therefore essential to treat bone pathologies.

1.5.1 Osteoporosis

Osteoporosis is the most common cause of bone loss, affecting over 20% of European women and 6% of European men aged 50 - 84,[204] with increased prevalence in Caucasians and the elderly.[207] The increased fragility caused by osteoporosis costs the UK £4.4 billion annually, with hip fractures alone taking up 1.3 million beds. Osteoporosis can be split into primary and secondary osteoporosis based on onset due to normal ageing or disease respectively.[208] Primary osteoporosis is then further split into type 1 (post-menopausal) or type 2 (ageing/ senile osteoporosis), predominantly resulting from alterations in osteoclasts and osteoblasts repectively.[208]

1.5.1.1 **Type 1 osteoporosis**

Menopause results in a significant decline in oestrogen levels in females,[209] leading to a destructive bone phenotype of thinner, less dense trabecular and cortical bone. On a cellular level, oestrogen signalling is detrimental to osteoclast activity and boosts osteoblast activity, thus loss of oestrogen in type 1 osteoporosis results in increased osteoclast resorption activity, and therefore enhanced bone destruction. In a large cross-sectional study, a significant decrease in bone mineral density (BMD) was observed between the onset of menopause (early peri-menopause) and once menopausal changes have occurred (late peri-menopause), regardless of ethnic background.[210] Furthermore, cortical porosity and trabecular bone volume (BV/TV) decreased at a faster rate in post-menopausal women compared to pre-menopause or peri-menopause when measured 12 months apart.[211] OVX is the gold standard for modelling *in vivo* menopausal osteoporosis on bone.[212] OVX significantly reduced trabecular bone volume and trabecular number, whilst increased trabecular separation and trabecular thickness in mice from a range of backgrounds.[213,214] Similar reductions have also been observed in rats[215–217] as well as cynomolgus monkeys post-OVX.[218,219] Due to the similar phenotype to human menopausal osteoporosis and the fast onset, OVX can be used to test therapeutic potential of compounds on osteoporosis in mice. However, as rodents do not go through menopause naturally, OVX is an artificial method and sudden loss of oestrogen may alter the course of the disease. In addition, in-depth analysis of cortical bone changes is difficult due to the lack of haversian cannels in mice.

The effects of oestrogen on bone have been shown to be pro-anabolic, decreasing osteoclast activity and increasing osteoclast apoptosis, whilst in turn

increasing osteoblast activity (Figure 1.5). *In vivo* injection of 17β-estradiol benzoate (E2), the major oestrogen secreted by the premenopausal ovary, into female mice significantly decreased the number of osteoclasts observed attached to the metaphysis region of tibias, with a concomitant increase in osteoclasts in the bone-marrow space,[220] leading to disrupted osteoclast activity and thus decreased resorption*. In vitro,* E2 treatment directly on osteoclasts decreased osteoclastogenesis in human[221] and murine osteoclasts,[222] reducing osteoclast resorption.[223]

The majority of oestrogen's effects on bone are resultant from interactions with other bone cells. Loss of oestrogen increased RANKL gene and protein expression in bone lining cells, which returned to baseline levels following E2 treatment.[224] Post-OVX, Fas ligand (FasL) gene and protein expression are significantly decreased on mature osteoblasts *in vivo* and bone marrow osteoblast precursors *ex vivo*,[225,226] whilst the reverse is observed in E2 treated cells.[225] These results indicate a direct pro-apoptotic role of oestrogen on osteoclasts, dampening resorption to match levels of formation.

Another role for oestrogen in controlling osteoclast function occurs through regulating immune cell phenotypes. In nude mice, lacking a thymus and thus T-cells, bone damage does not occur following induction of OVX.[220,227] T cells isolated from post-OVX mice increased tumour necrosis factor α (TNFα) secretion compared to sham operated controls.[228] Direct *in vitro* treatment of osteoclasts with TNFα increased resorption potential,[229] and TNF receptor 1 knock out mice are resistant to OVX induced bone damage,[230] showing TNF and T cells are essential in the development of OVX bone disease. Monocytes are also believed to have a similar

role, with monocytes isolated from post-menopausal osteoporotic women secreting higher interleukin 1 (IL-1) expression compared to patients receiving oestrogen replacement therapy.[231] Overexpression of IL-1 receptor 1 on monocytic cells led to increased osteoclastogenesis *in vitro*,[232] which was also observed in monocytic cells treated directly with IL-1.[231]

Osteoblast activity is enhanced by oestrogen treatment, with increased osteoblasts expression of pro-survival gene B-cell lymphoma 2 (Bcl2) in oestrogen treated mice, leading to decreased apoptosis *ex vivo*.[233]

Due to the anti-catabolic, pro-anabolic effects of oestrogen, loss during menopause results in an increased osteoclast response, ultimately leading to enhanced resorption and bone damage (Figure 1.5).

1.5.1.2 **Age-related (type 2) osteoporosis**

Type 2 osteoporosis, otherwise known as senile osteoporosis, occurs in both males and females naturally with ageing, often due to cellular ageing (senescence) rather than environmental changes. Bone mass in humans peaks at 15-20 years and then slowly declines,[234,235] with age-related bone loss becoming more prominent during the 50's,[236] and lower BMD recorded in 50, 60 and 70-year-old males when followed up 10 years later.[237] Female participants BMD decreased by a similar degree; however, all participants had gone through menopause by time of follow-up.[237] Studying type 2 osteoporosis in females is extremely difficult due to menopause confounding the effects of age on the bone. While no accelerated models of senile osteoporosis are routinely used in mice, natural ageing follows similar mechanisms to human ageing. C57Bl/6 mice display bone loss during ageing,

with bone density and elasticity also decreasing in parallel.[238,239] Hormonal changes occur in senile osteoporosis, however to a much lesser extent than type 1. Oestradiol has been found to positively correlate with BMD in human males,[240] thus decreases in oestradiol that occur with ageing may impact bone formation similar to type 1 osteoporosis. Additionally, increases in PTH occur with age due to decreased vitamin D levels and thus lower calcium absorption from the gut.[241] Whilst PTH provides a positive effect on osteoblast activity and bone strength in the short run, prolonged high PTH exposure, such as during human hyperparathyroidism, leads to decreased bone strength and more osteoporotic bone.[242]

In contrast to the primary changes that occur in type 1 osteoporosis, type 2 pathogenesis is mostly osteoblast driven, with decreased osteoblast differentiation and proliferation, and increased apoptosis (Figure 1.6). Mature osteoblasts isolated from aged mice (18 months) have significantly lower gene expression of Wnt5a and Wnt7b (drivers of osteoblast differentiation) than 6 week old mice.[243] In addition, Wnt-10b overexpressing mice have increased bone mass over controls, which was maintained until 28 months.[138] These data indicate a loss of Wnt signalling with ageing decreases osteoblast differentiation and activity. Similarly, osteoblast differentiation genes (*RUNX2, BGLAP* and *SPP1*) were all expressed at lower levels in the bones of older humans compared to young bone,[244] indicating osteoblast differentiation was decreased in aged bone. In regards to apoptosis, male C57Bl/6 mice show increased gene expression of forkhead box O (*FOXO*) controlled genes in calvarial isolated osteoblasts of aged mice.[245] FOXO is increased in these cells as a result of increased H_2O_2,[245] a product of oxidative stress. Over time, oxidative stress increases in osteoblasts,[245] thus in aged mice leading to enhanced cell death and

therefore decreased osteoblast activity. If cells don't undergo cell death, they can instead become senescent.[246] Senescent osteoblasts are a key driver to senile osteoporosis as observed in WT C57Bl/6 mice injected with senescence accelerated mouse strain P6 bone marrow cells.[247] An osteoporotic phenotype is observed in these mice with decreased bone volume density.[247] A senescent phenotype also occurs in osteoblasts at late stages of passage *in vitro,* where they begin to express lower levels of *Alp* and *Col1a1* mRNA.[248] In addition, MSCs obtained at age 59 to 75 produced fewer osteoblasts and cell cycle arrest occurred after half the number of cycles compared MSCs obtained from 0 to 18-year-olds.[249] A key inducer of this cell senescence is shortening of telomeres. In Terc KO and Wrn Terc double KO mice,[250,251] where telomeres cannot be repaired leading to early senescence, bone became osteoporotic at an earlier age despite having little impact on initial bone development. Another mechanism of cell senescence is caused by increased DNA damage or lack of repair. In osteoblasts isolated from 24 month and 6 week old mice, DNA damage markers are increased in the aged,[252] leading to increased senescence. Furthermore, ERCC1-XPF KO BMSCs (where DNA damage cannot be repaired) proliferation is reduced and senescence increased.[253] Senescent cells also increase expression of IL6, TNFα and RANKL,[253] suggesting the senescent phenotype may be pro-resorptive, however little research has been done in this area. Overall, type 1 and type 2 osteoporosis significantly alter quality of life, have a large impact on the economy and can lead to death. Effective and novel treatments are therefore required to decrease the impact of such diseases.

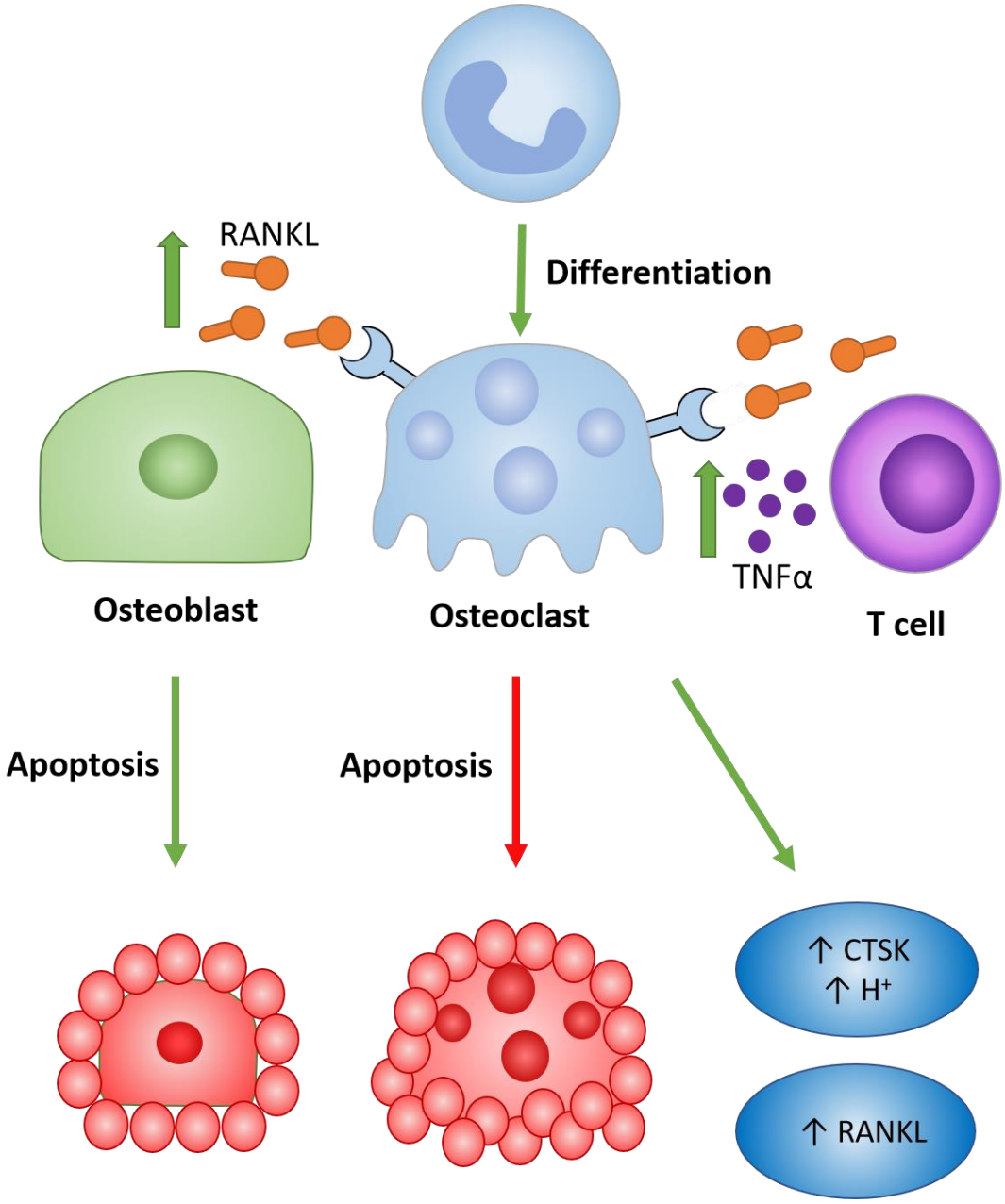

Figure 1.5. Osteoclast changes in post-menopausal osteoporosis

In post-menopausal osteoporosis, osteoclast differentiation is significantly enhanced. Increased release of RANKL and TNF from osteoblasts and T cells induces osteoclastogenesis and release of CTSK and H^+ ions. In addition, loss of oestrogen causes increased osteoblast apoptosis. Similarly, to senile osteoporosis, this imbalance leads to net bone loss, and thus phenotypic disease.

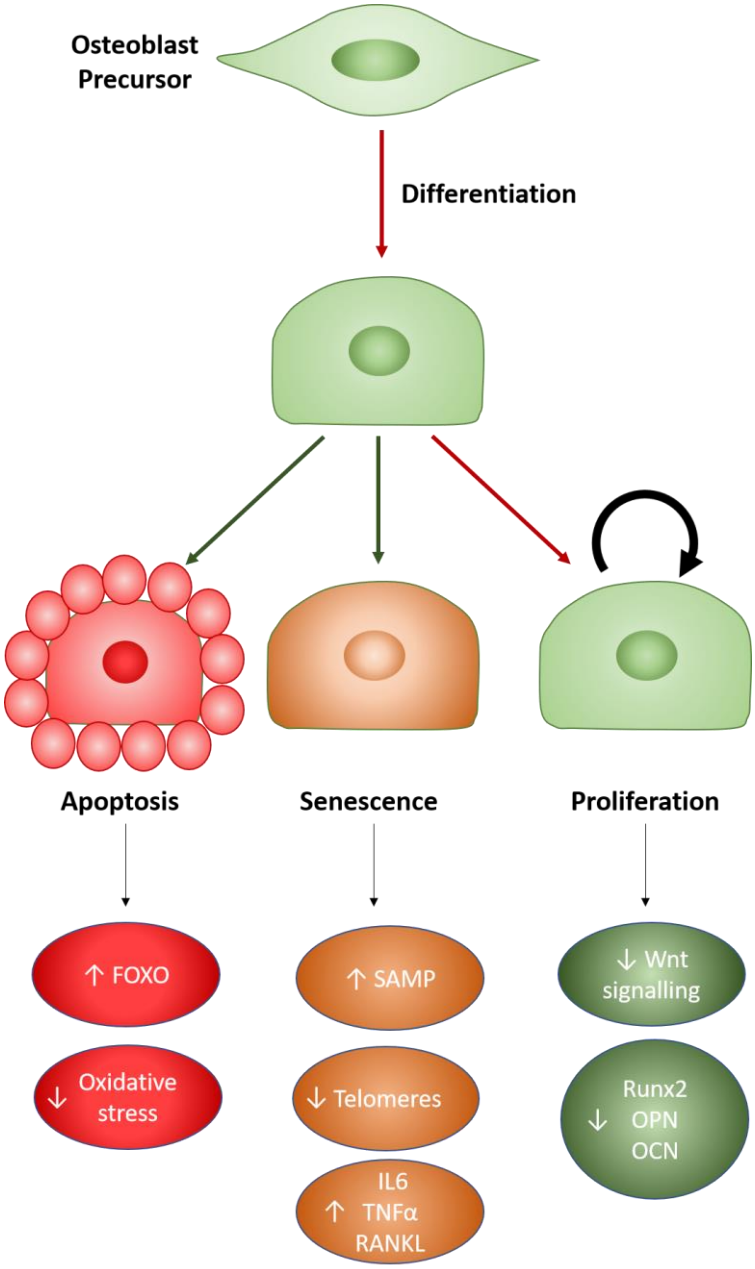

Figure 1.6. Osteoblast changes in osteoporosis

Senile osteoporosis is mainly resultant from decreased osteoblast activity. During ageing, osteoclast proliferation and gene expression are reduced, and cellular apoptosis is increased. Alternatively, cells become senescent, increasing the release of inflammatory cytokines. Combined these changes results in decreased bone formation and enhanced resorption, leading to net bone loss and disease.

1.5.2 **Inflammatory bone loss**

Bone loss can also occur due to secondary effects on bone cells. A major inducer of this bone loss is inflammation, which promotes an anti-anabolic, pro-catabolic environment. Inflammatory bone loss occurs in many conditions, including rheumatoid arthritis, osteoarthritis and spondyloarthropathies.[254–258] The main inducers of inflammatory bone loss are cytokines, including IL1α,[259,260] IL6,[261,262] MCSF and TNF.[263,264] Together they promote the activation and differentiation of osteoclasts and inhibit osteogenesis and mineral production.[259–264] Specifically in rheumatoid arthritis, autoantibodies have been shown to enhance osteoclastogenesis, promoting localised bone resorption.[265] Cells involved in inflammation also directly increase osteoclast activation, such as T cells and B cells, which both express RANKL, inducing osteoclastogenesis.[266–268] Overall, inflammation leads to net bone loss, promoting secondary complications in bone. Resolution of inflammation does not restore bone growth, leading to long-term complications in bone. Therefore, therapeutics are required which can restore bone following inflammatory bone loss.

Inflammation is also prevalent in ageing (known as inflammaging). This is demonstrated by significant increases in cytokine levels, such as IL6, and increases in serum CRP.[269] Inflammaging may drive the development of senile osteoporosis. This is through the same mechanisms as above driving the pro-catabolic environment[269] and additional mechanisms depleting skeletal stem cells.[270] In murine models of inflammaging, pharmacologically inhibiting systemic inflammation restores osteogenic function and progenitor populations.[270] Thus, targeting inflammation and bone in ageing may slow or inhibit the development of osteoporosis.

1.5.3 **Bone fractures**

The main issue with osteoporosis is the increased likelihood of fracture. Post-menopausal women and aged male and females are significantly more likely to fracture,[271,272] due to weakened bone. However, fractures induced by trauma are also prevalent in the general population regardless of age, impeding quality of life.[205] Fractures can also be induced by the build-up of microfractures over time, ultimately leading to a stress fracture.[273,274] Irrespective of the cause, fracture healing occurs via either a direct pathway, which is less common and only occurs after open reduction and internal fixation, or a more standard secondary pathway.[55] Due to its increased prevalence, here I will focus on the secondary process for fracture healing. In all cases, secondary healing follows the pathway of: generation of a hematoma; inflammatory cell infiltration; fibrovascular phase; bone formation (often endochondral); remodelling (Figure 1.7).[275]

1.5.3.1 **Hematoma**

The first stage following fracture involves generating a fibrin rich clot around the vessels ensuring excess blood loss does not occur.[55] However, leakage allows the generation of a haematoma which provides a scaffold for the onset of bone growth and the healing process.[276] Extraction and analysis of RNA from cells present in a human hematoma post-fracture found increased expression of *Spp1* and *Runx2* and angiogenic vascular endothelial growth factor (VEGF), providing an environment for osteoblast maturation and vascular growth.[277] In osteotomised sheep, removal of the hematoma 4 days after osteotomy led to reduced formation of woven bone, but the formation of larger hematoma present at day 14 than controls.[278] This is

suggestive that hematomas are an essential prerequisite to bone regrowth and must occur before the damage can be fixed.

1.5.3.2 **Inflammatory cell infiltration**

Following formation of a hematoma, multiple inflammatory cell populations migrate into the fracture site, providing signals to aid repair. Macrophages are an essential cell, with peak cell numbers and activity occurring within a week of osteotomy in mice.[279] Deletion of macrophages either pre[280] or post[280] osteotomy (in either the inflammatory or anabolic phase) leads to a reduction or complete loss in callus formation. Little research shows exactly why this occurs; however some evidence suggests a role for macrophages in inducing osteoblast differentiation through cytokine release.[281] The key cytokine in this process is TNFα, with levels of TNFα peaking 1-3 days post osteotomy.[281,282] TNFα receptor KO mice have an initial delay in fracture repair at day 7 and 14, however by day 21 levels are restored.[283] This change is matched by a decrease in chondrocyte apoptosis at day 7, however apoptosis levels are found higher at days 14 and 21.[283] This suggests loss of TNFα delays chondrocyte apoptosis, stopping bone development. Another function of TNFα is through attraction of MSCs, leading to osteoblast differentiation and increased bone formation.[284] TNFα is also involved in the later remodelling stage, by boosting osteoclast differentiation and activation through increasing monocyte differentiation and RANKL expression, restoring levels of resorption.[285,286] T and B cells are also involved in the initial fracture repair process. CD3+ cells increased in the bone marrow of C57Bl/6 mice following fracture, shifting towards a CD4 phenotype.[287] B cells also increased, with fluorescent staining showing a distribution of B cells throughout the callus after fracture.[287] T and B cells also express OPG, [287] ultimately

providing the driving force to shift bone remodelling towards formation, initiating the main repair process.

1.5.3.3 **Vascular regrowth**

As discussed above, the formation of a hematoma and infiltration of immune cells initiates the regrowth of blood vessels (angiogenesis) and the formation of new blood vessels (vasculogenesis). This regrowth is essential to remove the hypoxic environment which develops in the fracture site, in addition to providing a supply of osteoblasts and chondrocytes to initiate bone regrowth. VEGF is essential during this process, with levels peaking at day 10 in osteotomised mice.[288] VEGF is involved in increasing endothelial CD31 (PECAM) expression, which in turn increases angiogenesis.[288] In osteotomised mice treated with a soluble VEGF receptor, levels of fracture repair, CD31 expression and angiogenesis are significantly reduced.[288] Addition of VEGF to these mice can counteract the suppression and restore vessel growth.[288] A key driver of this angiogenesis is hypoxia, which develops as a result of lack of blood flow into the fracture site. Hypoxia causes an increase in hypoxia-inducible factor 1-alpha (HIF1α) transcription and activation, allowing translocation into the nucleus and subsequent transcription of essential factors such as VEGF.[289] In addition to a direct effect on angiogenesis, VEGF has also been shown to act directly on osteoblasts and osteocytes, increasing their proliferation and survival.[290]

1.5.3.4 **Bone formation and remodelling**

Following the invasion of vasculature, bone formation can begin. While fracture bone repair can follow either intramembranous or endochondral bone formation, the majority of cases follow the latter pathway. Many anabolic factors are essential here, particularly BMP2. In BMP2 KO mice ($BMP2^{c/c}$Prk1-cre), fracture

healing does not occur despite normal bone growth being observed during development.[291] This suggests BMP2 has a more significant role in bone repair compared to bone development.

Due to lack of lack of effective, economically viable treatments, fracture in otherwise healthy individuals is often left to heal without pharmacological intervention. In addition, confounding factors such as age and BMI, where bone remodelling/formation mechanisms are supressed, require treatment.

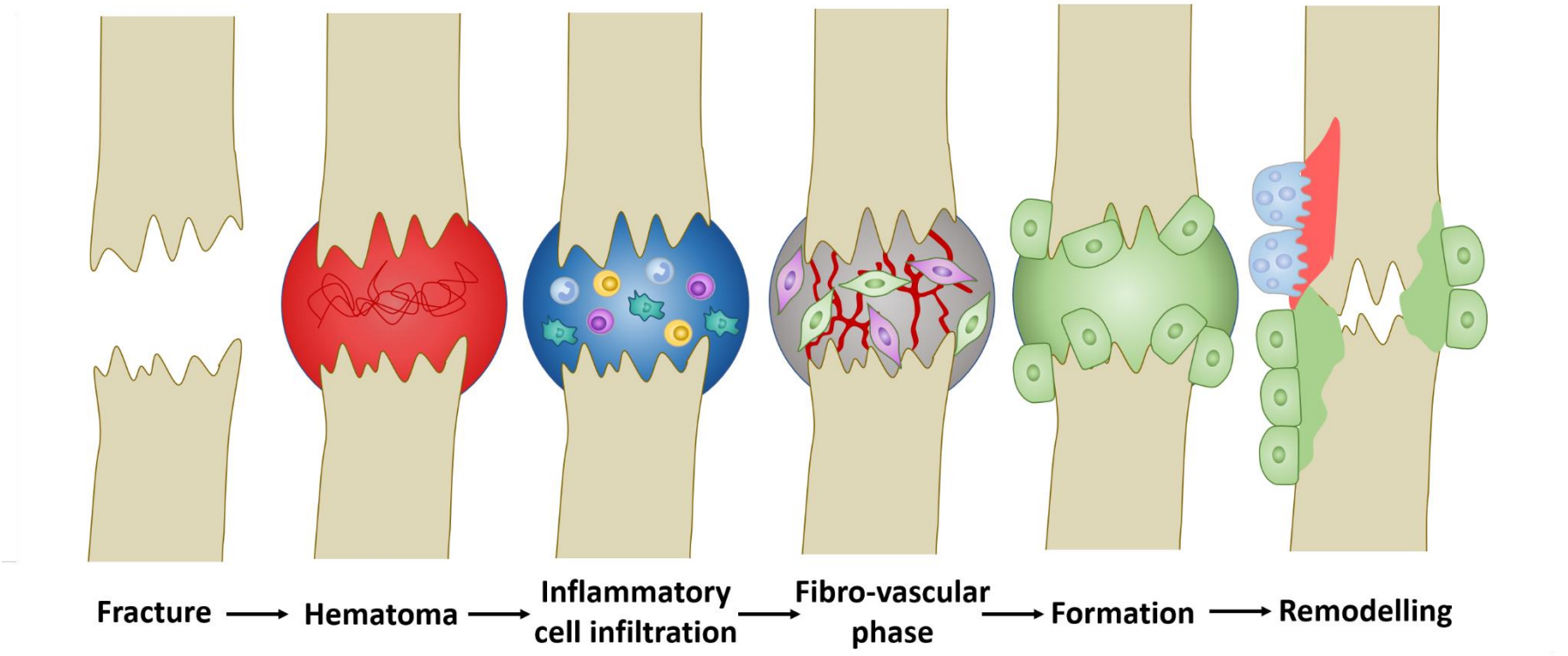

Figure 1.7. Fracture time course response
Response of bone to fracture can be separated into 5 key stages. Initially a hematoma occurs, leading to the attraction and migration of immune cells, in addition to essential metabolites required for repair. The induction of immune cell infiltration leads to the inflammatory phase, where the inflammatory environment causes degradation of necrotic tissues. This provides space for the invasion of vasculature and stromal cells, which begin repairing the bone. Differentiation of cells into mature osteoblasts allows the deposition of new mineral which can repair the bone. Bone then re-enters the remodelling pathway to maintain bone strength and prevent future fractures.

1.6 Disease treatments

Diseases which induce loss of bone lead to an increased incidence of fracture and are detrimental to patients' lives. Following a hip fracture in patients over the age of 50, 40% cannot walk independently a year later and 80% of patients have issues completing daily tasks (e.g. housework).[292,293] Consequentially, risk of mortality increases 3-fold in over 65s following a hip fracture,[294] with particular concern in over 75 year-olds with co-morbidities.[293] Therefore, there is need for treatments which reduce bone loss or increase bone growth, in doing so decreasing the primary cause of fracture or quickening fracture recovery times. Here we will explore treatments that act directly on cells of the bone (osteoclasts, osteoblasts, osteocytes, or their precursors). Therapies which do not act directly on the bone, such as selective oestrogen receptor modulators/ hormone replacement therapy used in menopausal osteoporosis (see [295–297]) or mechanical treatments which result in rigid fixation of fractures (see [298–300]) will not be discussed.

1.6.1 Bisphosphonates

Bisphosphonates are the most common treatment to reduce bone loss and are the gold standard treatment for all forms of osteoporosis.[301] In their simplest form bisphosphates share a similar structure to inorganic pyrophosphates (PPi). PPi's are chemically made up from two-phosphate ions linked by esterification.[302] In comparison, bisphosphonates are phosphate ions linked by a central nonhydrolyzable carbon which allows for expansion of the molecule through additional bonds (termed R1 and R2).[303,304] Substitution of R1 and R2 groups changes bisphosphonate efficacy, with R1 often displaying a hydroxyl compound and R2 controlling the bisphosphonate potency and response.[303,304] Due to its similar

structure to PPi, all bisphosphonates can bind to hydroxyapatite crystals and localise to bone.[302] Administration of ^{14}C-alendronate into rats, dogs and horses showed peak concentration (up to 60% of the absorbed dose) in the bone after 1 hour, with only 5% found in non-calcified tissues.[304–306] Despite a low initial bioavailability (between 0.7% and 2% in all species),[307,308] once incorporated into the bone the bisphosphonate's half-life is maintained until that bone is resorbed and thus can extend for 10 years.[309] Of note, bisphosphonate incorporation is higher in bone with a faster turnover rate.[305,310] Injection of fluorescent tagged resendronate[310] or ^{14}C alendronate[305] showed increased binding to joints and trabecular bone in comparison to cortical bone 1 day after injection into young mice, however incorporation was decreased in senescent mice due to lower rates of bone turnover.[305]

During normal resorption, osteoclast binding, resorption pit formation and release of HCL lowers the pH at the bone surface, causing dissociation of bisphosphonates. A reduction in pH from 7 to 3.5 reduces bisphosphonate binding to bone by 50%.[311] Free bisphosphonates are then endocytosed by osteoclasts and acidification of the vesicles results in their release into the osteoclast cytoplasm.[312] This mechanism of action depends highly on the type of bisphosphonate taken, split into non-nitrogen containing and nitrogen containing bisphosphates depending on the R2 group. Non-nitrogen containing R2 groups were the first to be derived, such as etidronate.[302] After release into the cytoplasm, non-nitrogen containing bisphosphonates incorporate into ATP like molecules using the aminoacyltransferase system.[313,314] For example, medronate incorporates with AMP to form APPCH2P rather than pure ATP.[315] This ATP is non-hydrolysable, building up inside the osteoclasts, becoming cytotoxic and resulting in osteoclast apoptosis.[302] However,

osteoclast apoptosis could be rescued by treatment with RANKL or TNFa, due to an increase in Bcl2 expression.[316] Treatment of OVX rats with etidronate[317–319] or clodrinate[318,319] significantly increased trabecular bone parameters to protect from bone loss. However, clinical trials of osteoporosis patients treated with etidronate are not always as positive. Whilst some studies found increased BMD and bone volume following treatment,[320,321] reductions in fracture risk are only short term (<2 years)[321] or not observed at all.[320,321]

The more potent forms of bisphosphonates are nitrogen containing, which are 1000x more potent.[322,323] In an extensive review of bisphosphonate trials, Ballantyre *et al* showed non-nitrogen containing bisphosphonates Etidronate and Tiludronate have a relative potency of 1 and 50 respectively, compared to a relative potency of over 1000 of nitrogen containing Ibandronate, Pamidronate and Zoledronate.[324] As indicated, nitrogen-containing bisphosphates all contain nitrogen within their R2 group. The addition of nitrogen into the bisphosphonate causes an alteration mechanism of osteoclast inhibition, without impacting their ability to bind to bone and be resorbed by osteoclasts. Rather than altering ATP metabolism, nitrogen containing bisphosphonates alter the mevalonate pathway, inhibiting the formation of geranylpyrophosphate (GPP) and farnesylpyrophosphate (FPP).[325,326] Treatment of macrophage-like J774 cells with zoledronic acid increased the levels of GTP-bound Rac, Cdc42 and Rho, a response that is also seen after treatment with prenylation inhibitors GGTI-298 and mevastatin.[327] Further analysis using a tagged prenylation precursor [^{14}C]mevalonolactone found risendronate treated J774 cells lacked ^{14}C labelled Rac and Cdc42, indicating a loss of prenylation.[327] This loss of prenylation caused increased phospho-p38 and thus increased activation, leading to higher

Caspase3/7 activity in cell lysate.[327] Altering GTPase signalling in osteoclasts causes changes in cytoskeleton rearrangement, border ruffling, trafficking and apoptosis, significantly impairing osteoclast resorption activity.[327] Electron microscopy of tibiae from adult rats treated with PTH and alendronate found that whilst osteoclast still bound to bones, they completely lacked a ruffled border.[327] In addition, as opposed to non-nitrogen containing bisphosphonates, inhibiting caspases still caused decreased in osteoclast activity.[328]

There have been many trials involving nitrogen containing bisphosphonates showing anti-resorptive protection on the bone, with over 50% reduction in vertebral fractures and 20-30% decrease in non-vertebral fracture after 1 year of treatment and continuing until at least 3 years following treatment.[329–333] Similar findings have also been observed in Cochrane reviews on bisphosphonate treatment for post-menopausal osteoporosis,[334] and steroid-induced osteoporosis.[335] In fact, treatment of osteoporosis patients with bisphosphonates decreases mortality by 30%.[336] However, the bone formation rate (BFR) decreased after 3 months of bisphosphonate treatment, questioning its long-term efficacy.[337,338] When bisphosphonates have been stopped after 3-5 years, reductions in fracture incidence are maintained,[339] however discontinuation of alendronate by osteoporotic women after 5 years showed small but significant decreases in BMD.[339] Bisphosphonates have also been used in osteogenesis imperfecta where a 2-3 year treatment regime causes an increase in cortical thickness by 88% and trabecular bone volume by almost 50%.[340] Similarly, bisphosphonate trials have taken place aboard the international space station, finding a 50% reduction in bone loss in astronauts who take the therapy regardless of additional exercise routines.[341]

However, possible side-effects of bisphosphates reduce the desire for long-term treatment. Oral bisphosphonates require daily intake and the patient must be upright for at least 30 minutes post ingestion, causing significant disruption to patients' lives.[342] In addition, absorption was 4-5x higher in healthy volunteers when they were in a fasted state, therefore fasting must occur for 2 hours before ingestion.[343,344] This causes 20% of patients to discontinue bisphosphate treatment, even if the treatment is effective.[342] Intravenous (IV) bisphosphates are also used, however flu symptoms were reported in 30% of patients.[333] More importantly, side-effects can include atrial fibrillation and musculoskeletal pain.[333] One in 10,000-100,000 patients also get osteonecrosis of the jaw and/or microfractures,[313] leading to an increase in subtrochanteric fractures.[345] This is due to "frozen bone", where lack of osteoclast induced resorption causes an inability to remove and repair microfractures.[346] Whilst bisphosphonates are positive in enabling bone resorption to decrease in disease, enabling homeostatic bone turnover is necessary to ensure long-term treatment is possible.

1.6.2 **Denosumab**

Specific osteoclast activation, differentiation and signalling pathways have also been targeted by novel therapeutics. Denosumab is a monoclonal antibody produced with high specificity against RANKL,[347] approved for use in the UK in postmenopausal osteoporosis.[348] By removing binding sites for RANK on osteoclast precursors, osteoclastogenesis no longer occurs and bone resorption is decreased.[349] Addition of denosumab to RAW624.7 osteoclasts *in vitro* decreased the number and size of TRAP+ osteoclasts following stimulation with recombinant RANKL.[350] Three-week denosumab treatment of young 6-8 week human-RANKL

overexpressing mice significantly decreased the number of TRAP+ stained osteoclasts on the bone surface, leading to increased trabecular bone volume.[347] In addition, denosumab treatment of ovariectomised cynomolgus monkeys protected them from vertebral bone loss, significantly increasing trabecular bone volume and bone strength.[351] Similarly, treatment of postmenopausal women (60-90 years old) with denosumab decreased fracture risk short-term[349] and increased bone mineral density, even after 8 years of treatment.[352] Due to its similarity in inhibiting osteoclast activity, denosumab treatment comes with many of the same side effects as bisphosphonates, such as frozen bone.[353,354] However, due to denosumab's short half-life compared to bisphosphonates, the side effects are believed to be decreased, with patients being more adherent and compliant to denosumab,[355] particularly since it can be given once every 6 months versus biweekly alendronate tablets.[356] Denosumab is therefore a highly potential treatment for post-menopausal osteoporosis, though its effect in senile osteoporosis has yet to be fully investigated and due to its lack of impact on osteoblast signalling, results might be limited.

1.6.3 **Calcitonin**

Calcitonin, a 32 amino acid hormone released from parafollicular C cells, can be used as a therapy to target osteoclasts. In normal conditions, calcitonin binds to its receptor on osteoclasts, leading to activation of the cAMP/PLC pathway, and causing subsequent inhibition of osteoclast activity.[357] Calcitonin receptor KO mice significantly decrease binding of ^{125}I-salmon calcitonin to osteoclasts, reversing the effects of calcitonin treatment.[358] Calcitonin used for treatments is made as an analogue of salmon calcitonin due to an increase in potency of 40-50 times compared to human calcitonin, in addition to a longer duration of action.[359] Treating

in vitro RAW264.7 cells with salmon calcitonin enhanced cAMP activity,[360] which *in vivo* protected rats and ewes from OVX induced bone loss.[361–363] Treatment of post-menopausal women with salmon calcitonin significantly decreased serum C-terminal telopeptide 1 (CTX-1) levels after 3 months,[359] indicating decreased bone resorption. Lower resorption led to increased BMD measurements after 1-3 years of treatment.[364] An advantage of salmon calcitonin treatment is it can be given as a nasal spray, reducing the nausea, flushing and vomiting occurrence opposed to when it is given via intramuscular or subcutaneous injections.[365] However, it has been observed that 40-70% of patients develop antibodies against the calcitonin, although whether these antibodies have negative outcomes has yet to be observed.[366] Furthermore, 10% of all patients discontinue the drug due to side effects, which include an increase in cancer by 2-4%,[364,367] leading to approval for treatment being removed.[367]

1.6.4 **Cathepsin K and V-ATPase inhibitors**

Downstream mechanisms of osteoclast bone resorption can also be targeted for therapeutic use. This includes inhibiting the actions of cathepsin K or reducing the ability of osteoclasts to cause acidification at the bone by inhibiting V-ATPase. Treatment of adult OVX rhesus monkeys with Odanacatib, a cathepsin K inhibitor, significantly increased hip bone mass and cortical thickness.[368] Similar results have also been seen in human clinical trials, where post-menopausal bone loss is decreased.[369–371] However, multiple clinical trials using cathepsin K inhibitors have been halted or stopped due to off target side effects including an increase in risk of cardiovascular diseases such as stroke, or dermatological issues.[372] Targeting V-ATPase has recently been found as a potential treatment for bone loss, but has not

yet entered clinical trials. Regardless, selective V-ATPase inhibitors, SB 242784[373,374] and FR167356,[373] were effective at inhibiting OVX induced bone loss and increasing BMD in rats compared to untreated controls.[373,374]

1.6.5 Sclerostin inhibitors

Alternatively, recent advances have occurred in boosting osteoblast matrix mineralisation, hoping to counteract the increased resorption. The most promising of which is Romosozumab, a monoclonal antibody against sclerostin (see section 1.4.1.1). In ovariectomised cynomolgus monkeys, treatment with romosozumab for 12 months significantly increased bone mass, and trabecular bone volume in both the vertebrae and the femur.[375] In addition, treatment of postmenopausal women for 12 months significantly decreased incidence of vertebral fractures,[376,377] with trials also showing increased BMD in the lumber vertebrae, hip and femoral neck.[377] However, an increase in adverse cardiovascular events following romosozumab treatment has been observed, believed to be due to expression of sclerostin on aortic vascular smooth muscle.[378] Nonetheless, a recent exploration into the effect of anti-sclerostin antibodies directly on the cardiovascular system found no interactions took place in animal models.[379] More research therefore needs to be undertaken on potential side effects of sclerostin before it is used more readily as a bone loss treatment.

1.6.6 Strontium ranelate

Another promising pro-anabolic treatment is strontium ranelate (Sr). Treatment of primary calvarial osteoblasts with Sr significantly increased *Alp* and *Bglap* mRNA expression, in addition to bone nodule formation in a concentration dependent manner.[380] Similarly, treatment of spleen derived monocytes with Sr decreased

TRAP+ multinucleated osteoclast numbers, with an additional decreases in resorption.[380] Treatment of calvarial osteoblasts with Sr led to activation on the Akt signalling pathway, which is lost by addition of a calcium sensing receptor (CaSR) antagonist.[381] *In vivo* mice and rats receiving Sr increased trabecular bone mass and cortical thickness,[382,383] and in OVX led to a dose dependant decrease in bone loss.[384] In human postmenopausal osteoporosis patients over 50, treatment increased BMD after 5 years, however BMD decreased slightly if patients were switched to a placebo after 4 years.[385] Increases in BMD are observed in male osteoporosis patients after only 6 months,[386] however the treatment of peripheral osteoporosis (TROPOS) trial found these increases could be maintained for 10 years.[387] Ultimately, a Cochrane review found treatment with Sr for osteoporosis decreased vertebral and non-vertebral fractures.[388] However, due to strontium having a higher atomic number than calcium and strontium replacing 1.6% of the bone calcium over 3 years of treatment, BMD measurements are often overestimated.[389] In fact, for every 1% of Sr in bone, BMD readings are overestimated by 10%.[390] Furthermore, long term trials have had no placebo group due to ethical issues, and the patients would have been more likely to continue if it had previously shown positive effect, thus results might be inflated. In addition, treatment has shown correlation with increased cardiovascular risks as a side effect.[388]

1.6.7 **PTH**

The last osteoblast targeting drug is PTH, known therapeutically as teriparatide. Released by the parathyroid gland, PTH is an 84 amino acid peptide which is increased naturally in response to low serum calcium levels. *In vitro*, treatment of human and murine osteoblasts with recombinant PTH increased their mineralisation

and proliferation, whilst decreasing apoptosis.[92,93,391–394] This translates to increased mineral production in mice, particularly when given in daily injections.[395–398] However, continuous PTH infusion does the opposite, resulting in decreased bone and increased bone resorption.[396–398] This is also the case in rats, mice and cynomolgus monkeys subjected to OVX, where daily, but not continuous PTH administration reduces bone loss.[399–402] In osteoporotic post-menopausal women, trabecular bone volume and BMD increased with 21 months of teriparatide treatment leading to a decrease in vertebral fracture risks by up to 65%.[403] However, 10% of patients developed hypercalcemia, leading to cramps, dizziness,[403–405] and some trials found an increased risk of osteosarcoma.[404] Therefore, long term studies have yet to be carried out. However, promising results have occurred with short term (1 year) PTH treatment to boost bone growth followed by bisphosphonate treatment to stop further loss,[406,407] indicating the potential use for combined therapies in bone loss.

1.7 Novel molecules in bone homeostasis

Whilst many of the above treatments are effective at reducing bone loss in the short term, longer treatment regimens are less effective and increases the adverse side effects in the bone, including osteonecrosis of the jaw.[379] Therefore, novel mechanisms are being investigated to find new targets in which treatments can be evolved around.

1.8 Adiponectin in bone

Adiponectin is the most abundant circulating adipocyte-secreted adipokine found in blood serum (5–15 μg/mL).[408,409] The full-length protein (244 amino acids)[410] can be cleaved into smaller active components,[411] which circulate either as its globular domain[411] or as full-length homo-complexes referred to by their differing

molecular weights (MW): a trimer (low MW; LMW); a hexamer (medium MW; MMW) or an oligomer (high MW; HMW) (Figure 1.8).[412–414] At a cellular level, adipocytes within the bone marrow adipose tissue (BMAT) and white adipose tissue (WAT) produce all of these adiponectin isoforms.[415] For example, similar levels of adiponectin gene expression were observed in murine adipocytes isolated from WAT or BMAT.[415] Yet protein expression was reportedly lower in rat total BMAT lysates[416] and higher in adipocytes isolated from BMAT from rabbits and healthy 30-year old humans,[415] compared to WAT. As such, adipocytes from both tissues can contribute to the local levels of adiponectin within the bone (and bone marrow), as well as the circulating levels of adiponectin that are more commonly reported in studies. Indeed, BMAT levels positively correlate with total serum adiponectin levels in humans.[417] Whilst the relative contribution of each adipose tissue to the levels of adiponectin in the bone is unclear, and may change with age and disease (as discussed in the later sections), many studies speculate that due to its proximity, BMAT acts as the largest contributor of adiponectin to the local bone levels.

Adiponectin mediates its effects through adiponectin receptors 1 and 2 (AdipoR1 and AdipoR2)[418,419] leading to downstream signalling through several pathways including AMP kinase (AMPK), PI3K/protein kinase B, MAP kinase (MAPK), STAT3 (signalling transducer and activator of transcription 3) and ceramidase activation (Figure 1.8).[420–422] In addition to the classical adiponectin receptors, HMW and MMW adiponectin can also interact with T-cadherin (cadherin-13; CDH13).[423,424] However, AdipoR1 and R2 knockout mice have a near-complete lack of adiponectin signalling,[425] thus the functional relevance of T-cadherin in mediating the effects of adiponectin is currently unclear. Moreover, potential signalling mechanisms

downstream of adiponectin–T-cadherin interactions have not yet been fully explored. Crucially, evidence suggests that the individual adiponectin receptors have differing binding efficacies for the different isoforms of adiponectin; with a murine myocyte cell line demonstrating higher affinity of AdipoR1 for globular adiponectin, whilst AdipoR2 displays an intermediate affinity for all adiponectin isoforms.[418] Thus, it is likely that these differing protein–receptor interactions results in divergent cellular responses to adiponectin, even within the same cell. In addition, many studies explore serum levels rather than the tissue-level expression of adiponectin, and whilst the bone is well vascularised,[426] understanding the link between serum levels and local tissue effects has proved challenging.

1.8.1 Adiponectin receptor expression in cells of the bone

Within the bone, precursor bone cells, osteoblasts and osteoclasts have all been reported to express the adiponectin receptors, although conflicting findings exist that are important to consider when interpreting adiponectin-signalling responses from in vitro studies. For instance, AdipoR1 and R2 mRNA and protein are detectable in murine osteoblasts,[427] human osteoblast precursors (bone marrow stromal cell- BMSC and osteoblast-like cell lines)[428,429] and osteoclast precursors (human peripheral blood monocytes, PBMC).[430,431] In all cases, adiponectin receptor 1 was detected at significantly higher levels (up to 100-fold) than adiponectin receptor 2. Indeed in some studies expression of AdipoR2 was below the limits of detection—e.g. no AdipoR2 protein was detected in healthy human tibial osteoblasts[91] nor gene expression observed in the MC3T3 murine osteoblast precursor cell line.[432] The absence or lower expression of adiponectin receptor 2 on bone cells suggests that they preferentially respond to globular adiponectin, which

has a higher affinity for adiponectin receptor 1 than the other forms of adiponectin.[418] Moreover, the majority of in vitro osteoblast models display increased expression of AdipoR1, but not AdipoR2, following differentiation, including Saos-2[429] and C3H10T1/2,[428] a response not seen when MC3T3 were used.[427] In contrast, MC3T3 cells up-regulated AdipoR2 expression and down-regulated AdipoR1 expression upon differentiation.[427] This difference in the expression pattern by MC3T3 cells upon differentiation may help to explain some of the confounding results observed between studies exploring osteoblast response to adiponectin. By contrast, in vitro osteoclastogenesis does not appear to affect the expression of adiponectin receptors at either the mRNA or protein level.[431]

The expression of adiponectin receptors by the main precursors and mature bone cells demonstrates that all have the potential to interact with and respond to adiponectin during the different stages of bone homeostasis. However, key questions remain: What is the impact of adiponectin signalling on bone formation and turnover? How are these adiponectin-mediated effects influenced by bone damage, with age and by inflammatory diseases? Can a greater understanding of adiponectin regulation of bone homeostasis lead to novel strategies to repair injured and damaged bone?

1.8.2 **Impact of adiponectin on osteoblastogenesis and activity**

Bone marrow adipocytes continuously release adipokines into the bone niche, bathing all cells including osteoblast and osteoclast progenitors in adiponectin.[433,434] Indeed, the limited available data indicates that within the bone marrow niche adiponectin acts to promote osteoblastogenesis, whilst simultaneously inhibiting osteoclastogenesis (Table 1.1).[428,435–438] Addition of full-length[428,438] or

globular[439] adiponectin induces the expression of the osteogenic-related genes osteopontin[428] and alkaline phosphatase[428,438,439] in the murine mesenchymal progenitor cell line, C3H10T1/2,[428] the pre-osteoblast MC3T3-E1 murine cell-line,[438] and in human adipose-derived stem cells (ADSC) in vitro.[439] Moreover, BMSCs from 5 week old adiponectin knockout mice exhibited reduced gene expression of key osteoblast promoting lysine specific histone demethylases (KDM4B and KDM6B) when compared to wildtype mice infused with either globular or full-length adiponectin.[440] Absence of KDM4B and KDM6B reportedly increased gene expression of PPARG in human BMSC and thus switched the differentiation fate from osteogenic to adipogenic in vitro.[441] Indeed, the presence of fatty bone marrow in adiponectin KO mice was attributed to reduced KDM4B and KDM6B expression in BMSCs, triggering adipogenesis and ultimately causing a reduction in osteoblasts and increase in adipocytes on the trabecular surfaces.[440] Furthermore, siRNA knockdown of AdipoR1 in C3H10T1/2 cells significantly reduced adiponectin-induced osteoblast differentiation in vitro.[428] Supporting this, enhanced matrix mineralisation was observed in human ADSCs cultured in the presence of globular adiponectin compared to untreated controls.[439] Of note, one study disagrees with the above literature: Kajimura et al., demonstrated that 6 week old adiponectin knockout mice have increased bone mass and osteoblast numbers, suggesting adiponectin inhibits bone mass accrual in young mice.[437] However, no changes were observed in the gene expression of the osteoblast differentiation markers runx2 and osterix in 12-week-old bones from adiponectin knockout mice compared to the wildtype controls-suggesting that by this time point adiponectin was no longer able to limit bone formation.[437] Importantly the mineralisation capacity of cells from these bones was

not assessed. Bones from 10-day old adiponectin knockout mice exhibited increased cellular proliferation and reduced apoptosis.[437] Indeed, treating serum-starved wildtype calvarial osteoblasts with either full-length or global adiponectin reduced proliferation and increased apoptosis rate over 24 h.[437] Importantly, no changes in proliferation or apoptosis have been reported in the aforementioned studies, where various osteoblasts were cultured in the presence of serum.[428,438,439] Serum starvation, therefore, may account for the discrepancies in proliferation and apoptosis observed between these studies and Kajimura et al. Overall, adiponectin appears to have a predominantly positive role in boosting pre-osteoblast differentiation and mineralisation capacity, potentially protecting the bone by inducing formation and repair.

1.8.3 Impact of adiponectin on osteoclastogenesis and activity

By contrast, few groups have analysed the effect of adiponectin on osteoclastogenesis to date (Table 1.1). Addition of full-length adiponectin significantly inhibited the ability of human mononuclear cells and murine macrophage progenitors to differentiate into mature osteoclasts when cultured in vitro in the presence of osteoclastogenic stimulating factors [macrophage colony-stimulating factor and receptor activator of nuclear factor kappa-B ligand (RANKL)].[442] Similarly, globular adiponectin blocked RANKL-induced osteoclastogenesis of the murine monocyte cell line RAW264.7.[442] Importantly these studies indicate that adiponectin reduces the ability of osteoclast precursors to mature. Akin to data on osteoblast precursors, global adiponectin treatment reduced the proliferation rate of RAW264.7 osteoclast precursors and increased their apoptosis through APPL1-mediated down-regulation of Akt1 activity.[442] As such it is unclear whether adiponectin mediates a direct effect

on osteoclastogenesis or an indirect effect by reducing overall precursor numbers. Additional studies are urgently required to reproduce these findings and clarify the supposed anti-osteoclastogenic role of adiponectin.

1.8.4 **Regulator of osteoblast and osteoclast progenitor migration**

Osteoblast progenitors must exit the bone marrow niche to migrate towards the sites of resorption and/or damage (Figure 1.9).[443] Indeed fate mapping experiments have revealed that 70% of the osteoblasts found replenishing the endosteal surface during homeostasis originated from the bone marrow-derived osteoblast precursors.[444] In addition, YFP-positive osteoblast precursors migrated from the neighbouring bone marrow to the site of calvarial microfracture, accounting for the majority of the cells at the site of injury after 7 days when compared to the bone resident pre- and mature osteoblast.[444] This process can be controlled by the CXCR4-CXCL12 axis, where high levels of CXCL12 attract CXCR4 expressing cells and retain them.[445] Globular adiponectin significantly reduces expression of CXCR4 mRNA in cultured murine BMSCs,[442] therefore reducing the attraction of these cells to CXCL12 in the bone marrow. Similarly, adiponectin-deficient mice have higher numbers of CXCL12 positive cells within the bone marrow compared to wildtype mice,[443] indicating that adiponectin regulates the exit of BMSCs from the bone marrow into the local bone environment where they can differentiate into osteoblasts.[444–446] In addition, globular adiponectin enhanced BMSC migration across a Matrigel-coated Boyden chamber over 16h in vitro, which was coupled with an increase in MMP9 mRNA expression.[443] Moreover, systemic globular adiponectin infusion increased serum CXCL12 levels and promoted nestin^{+} BMSC exit the bone marrow niche into the peripheral blood.[443] Furthermore, therapeutic infusion of

globular adiponectin significantly increased new bone formation at the site of calvarial injury, to a higher degree than seen in wildtype and adiponectin-deficient mice.[443] This was attributed to enhanced migration of osteoblasts from the periphery to the injury site following adiponectin treatment, resulting in increased bone regeneration. Collectively these studies indicate that adiponectin regulates the CXCR4–CXCL12 axis within the bone marrow niche, facilitating the migratory exit of bone progenitor cells from this niche into the periphery in health and in response to injury. Comparably, osteoclast precursors such as PBMCs, express CXCR4[447] and therefore osteoclast migration out the bone may mirror the mechanisms described for osteoblasts. Yet, few studies have examined the functional consequence of adiponectin on osteoclast migration, which are required to fully understand the overall impact of adiponectin on bone.

In addition to the CXCR4-CXCL12 axis, the bioactive lipid - sphingosine-1-phosphate (S1P) - has also been reported to influence the migration of osteoblast and osteoclast precursors (Figure 1.9).[448,449] Elevated levels of circulating S1P are observed in adiponectin-overexpressing transgenic mice.[421] However, very little is known about the possible consequence of adiponectin on S1P-regulated migration (explored in section 1.9).

1.8.5 **Role of adiponectin in the regulation of bone homeostasis**

1.8.5.1 **In health and ageing**

The actions of adiponectin in homeostatic bone turnover have been extensively explored in human and murine *in vivo* and in vitro studies in order to understand how it can be targeted in disease states. Of note, these studies

overwhelmingly focus on juvenile or adult models, where BMAT and WAT are fully developed, and can both contribute to bone adiponectin levels. No studies to date have examined the role of adiponectin in foetal and neonatal bone development.

Global overproduction of full-length adiponectin significantly increases trabecular bone mass and reduces bone resorption (as measured by plasma cross-linked N-telopeptides of type I collagen (nTx) levels) over a 2-week period in young 8 week old mice.[438] Similarly, higher bone mineral density (BMD) and reduced number of TRAP5b-positive osteoclasts were observed in aged (56 weeks) AdipoR1-overexpressing transgenic mice, but not in younger mice aged 8 or 32 weeks.[436] Likewise, AdipoR1-deficient mice have decreased trabecular bone volume, thickness, number and spacing, along with reduced osteoblast numbers.[450] Similarly, 36 week old adiponectin knockout mice also display severe low bone mass affecting all skeletal elements, yet this was linked to decreased number and proliferation ability of osteoblasts rather than effects on osteoclasts.[437] Interestingly osteoclast numbers were unaffected by loss of AdipoR1 in young mice aged 4 and 30 weeks.[450] Collectively, these studies suggest that age may significantly alter the effects of adiponectin on osteoclasts. Moreover, they suggest that adiponectin-signalling through AdipoR1 is critical for maintaining osteoblast survival and activity with age and may also regulate osteoclast apoptosis.

Mirroring the *in vivo* findings described above, bone explants from 3-day old wildtype mice implanted subcutaneously into the flank of adiponectin knockout mice had reduced trabecular volume and cortical bone parameters 2–4 weeks after implantation when compared to those implanted into wildtype mice,[442] indicating that systemic levels of adiponectin were sufficient to impact normal bone remodelling. In

vitro studies support these findings, with full-length adiponectin stimulating bone matrix deposition and hydroxyapatite formation by MC3T3-E1 cells, and reducing hydroxyapatite resorption by $CD14^+$ PBMC osteoclast precursors.[438] Collectively these data indicate that adiponectin promotes bone formation and limits bone resorption in healthy young and old mice, where exogenous adiponectin may serve to maintain bone mass during age-related bone loss. Moreover, therapeutically adjusting the circulating levels of adiponectin may result in beneficial effects on the bone, avoiding the need to develop drugs that specifically target the bone. Importantly, no studies have yet explored the role of adiponectin in the development and maturation of healthy human bones either *in vivo* or *ex vivo*.

Both BMAT and serum adiponectin increase significantly with age[451] and in osteoporosis[452,453] and are broadly thought to negatively correlate with BMD in humans. For example, post-menopausal women have higher serum adiponectin levels and reduced BMD compared to pre-menopausal women of the same age.[454] Interestingly, a lack of adiponectin protects young mice from ovariectomy-induced bone loss 10 weeks after surgery.[455] In contrast, sustained local release of low levels of therapeutic full-length adiponectin, from a hydroxyapatite-Matrigel implant, protected against ovariectomy-induced trabecular bone loss in the mandibles of rabbits.[456] These studies suggest that the absence or consistently maintained low levels of adiponectin protect against menopause (hormonal) induced bone loss, maintaining BMD. Indeed, this would mitigate against the elevated levels of adiponectin anticipated in response to the increased BMAT levels observed with age (as reviewed by [457]). This contrasts with healthy young bone (as discussed above), where higher levels of adiponectin are thought to promote bone formation

and limit bone loss to maintain BMD. The exact mechanisms regulating the differential effects of adiponectin with age/in post-menopausal state remains unclear and requires further investigation. One possible explanation is the ability of the oestrogen receptor (ERα) to influence the downstream signalling response from the adiponectin receptors — where the presence of ERα triggers the MAPK pathway, rather than activating AMPK as would normally occur (Figure 1.8).[458] Given these changes occur in the absence of oestrogen[458] as would be seen in post-menopausal women, it is unlikely that it is signalling through the Erα that is responsible for these changes, but rather highlights the possibility that ERα acts as a co-receptor for the adiponectin receptors to alter the downstream signalling that is observed in response to adiponectin. Importantly, murine ovariectomy increased ERα mRNA expression in multiple tissues,[459] and therefore is it likely that elevated ERα expression promotes adiponectin signalling through the MAPK pathway in these tissues and potentially contributes to menopause-induced bone loss.

Age-related decline in BMD is associated with increased susceptibility to microfractures in humans,[460] however very few studies have directly examined the effect of adiponectin on bone strength. High circulating levels of adiponectin negatively correlate with bone strength and reduced maximal load in middle-aged overweight men (mean ± S.D.—age 40 ± 11.5 years, BMI 25 ± 6.2).[461] By contrast, no link has been found between circulating adiponectin levels and the frequency of fracture in the men over the age of 70 with an average BMI ~26 in this correlative study.[462] These limited data appear to suggest that circulating levels of adiponectin influences bone strength and risk of fracture at least in overweight middle-aged men. However, more detailed longitudinal human studies, in which confounders such as

BMI are controlled for, are required to fully dissect the interaction of circulating adiponectin levels with BMD and fracture rates across different age groups.

Even fewer *in vivo* and in vitro studies exist that have directly assessed bone strength in response to adiponectin. Agreeing with the human data, adiponectin-overexpressing transgenic mice exhibited lower bone mass and lower strength at 2, 4[436] and 5[26] months compared to age matched wild-type controls. In addition, treating 3-D cultures of human osteoblasts and osteoclast precursors in mineral forming spheres (known as osteospheres) with an unknown adiponectin isoform significantly reduced their strength, as assessed using nano-indentation; indicating weaker, more breakable bone.[463] Mechanistic studies are required to elucidate how the ageing process alters adiponectin signalling within the bone, but also systemically, to modulate BMD and strength.

1.8.6 **Conclusion**

Under healthy conditions, adiponectin supports the proliferation, migration, mineralisation, and survival of osteoblasts, whilst concomitantly limiting proliferation, migration, and survival in osteoclasts. On balance, this allows adiponectin to promote bone formation and limit bone resorption. More detailed mechanistic studies are required to understand the interaction of the different adiponectin isoforms with each of the receptors, and the impact which oestrogen receptors and other unknown molecules have on downstream signalling and the functional consequences of these. These studies are critical to further our understanding of the beneficial and pathological roles of adiponectin for a specific context, and the efficacy of targeting adiponectin or it's signalling therapeutically to treat bone abnormalities and induce repair.

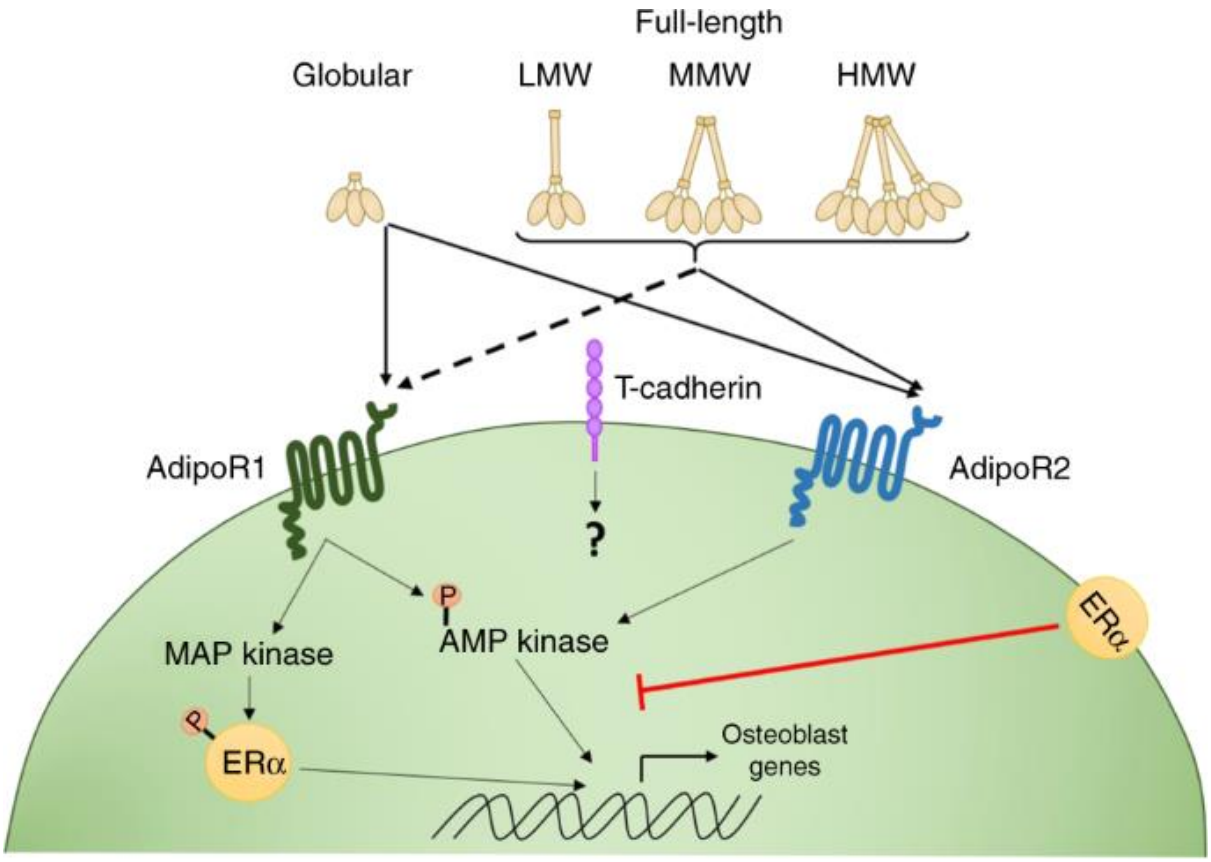

Figure 1.8. Adiponectin signalling

The full-length adiponectin protein can be cleaved into smaller active components, which circulate either as it's globular domain or as full-length homo-complexes—low molecular weight (LMW) trimers, medium molecular weight (MMW) hexamers or high molecular weight (HMW) oligomers.[412–414] Adiponectin can bind to two classical adiponectin receptors 1 and 2 (AdipoR1 and AdipoR2)[418,419] leading to downstream signalling through several pathways, primarily driving AMP kinase (AMPK) and to a lesser extent activating MAP kinase (MAPK).[420–422] Expression of the oestrogen receptor (ERα) appears to skew adiponectin receptor signalling to primarily trigger the MAPK pathway,[458] which in turn phosphorylates both ERα and transcription factor SP1, altering downstream signalling. AdipoR1 has a higher affinity for the globular domain of adiponectin, whilst AdipoR2 displays an intermediate affinity for all adiponectin isoforms.[425] In addition to the classical adiponectin receptors, HMW and MMW adiponectin can also interact with T-cadherin (cadherin-13; CDH13),[423,424] although the downstream signalling and functional outcomes from these interactions are currently unknown. This figure is reproduced from [464]

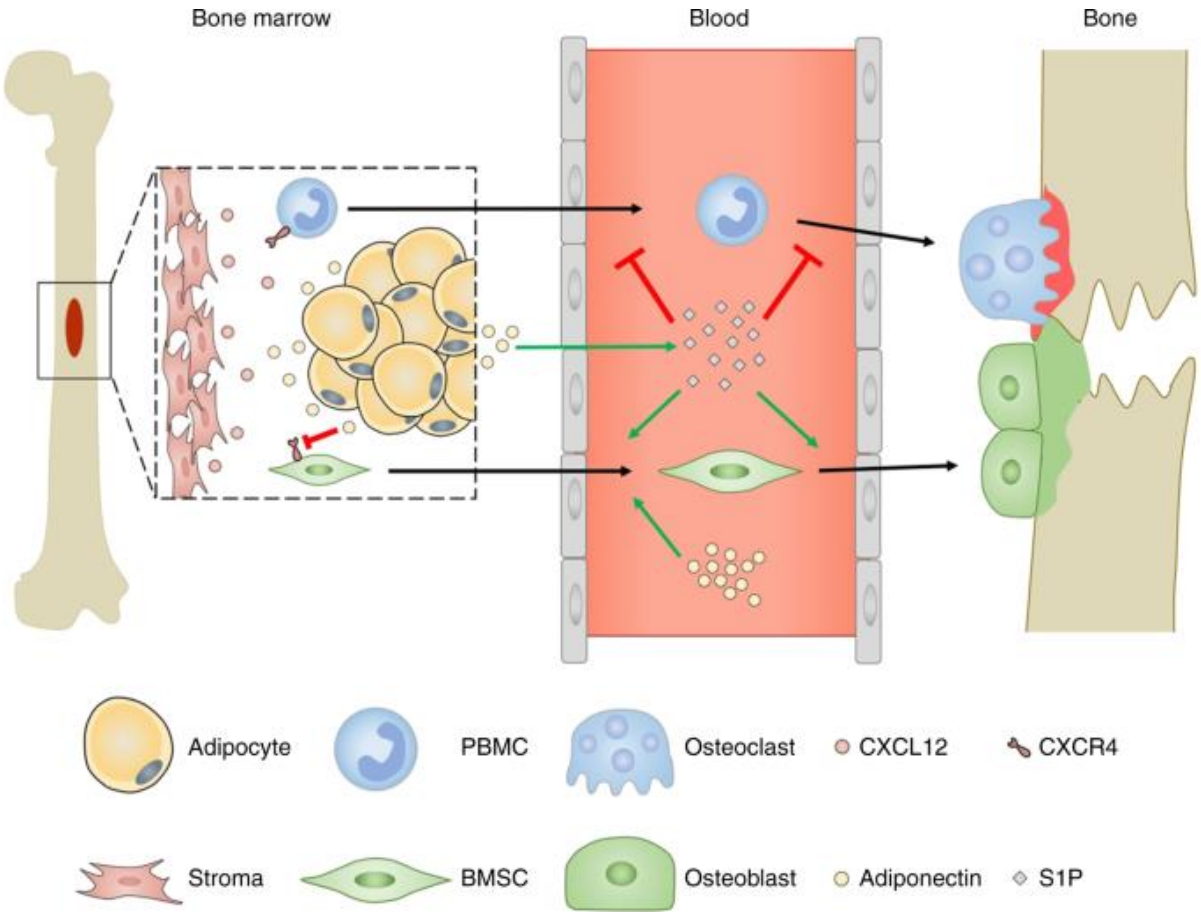

Figure 1.9. Adiponectin regulation of osteoblast and osteoclast migration.

Osteoblast progenitors must exit the bone marrow niche to migrate towards the sites of resorption and/or damage. In fate mapping experiments, YFP expressing bone marrow-derived osteoblast precursors migrated to the endosteal surface to replenish osteoblast populations in healthy conditions and also in response to calvarial microfracture.[444] Osteoblast and osteoclast progenitors express CXCR4 and migrate towards high levels of CXCL12 causing them to be retained in the bone marrow.[445] Adiponectin directly[443] and through increasing S1P in the serum,[421] leads to increased osteoblast progenitor migration into the circulation and to bone in health,[465] which is enhanced during injury.[444,466,467] In contrast, S1P chemorepels osteoclast progenitors and osteoclasts,[468] leading to decreased migration to damaged sites. This ultimately maintains the balance between resorption (red) and formation (green) to ensure structured bone repair. This figure is reproduced from [464]

Table 1.1. In vitro effects of adiponectin on bone cells.

Adiponectin Type	Species	Cell type	Effect	Ref
Full-length	Mouse	C3H10T1/2	↑ OPN mRNA ↑ ALP mRNA	[428]
	Mouse	MC3T3	↑ Mineralisation	[438]
	Mouse	RAW624	↓ Differentiation ↑ Apoptosis	[435]
	Human	Mononuclear osteoclast precursor	↓ Differentiation ↑ Apoptosis	[438]
	Mouse	$CD14^+$ PBMC	↓ Resorption	[438]
Globular	Human	Adipogenic stem cells	↑ RUNX2, OPN, ALP mRNA ↑ Mineralisation	[439]
	Mouse	RAW264.7	↓ Resorption ↓ Osteoclast number ↑ Apoptosis	[442]
All	Mouse	Adiponectin KO BMSC	↓ Adipogenic differentiation	[440]
	Mouse	AdipoR1 siRNA KD C3H10T1/2	↓ Osteoblast differentiation	[428]

AdipoR adiponectin receptor 1, *ALP* alkaline phosphatase, *BMSC* bone marrow stem cells, *KD* knock down, *KO* knockout, *OPN* osteopontin, *PBMC* peripheral blood monocytic cells, *RUNX2* RUNX family transcription factor 2, *siRNA* short interfering RNA. This table is reproduced from [464]

1.9 S1P in bone

Another novel molecule shown to be involved in bone homeostasis and in disease is S1P, which recently has been found to have significant involvement in both anabolism and catabolism of bone. Whilst the role of S1P in bone has been previously reviewed (see [448,449,469]), here I will briefly discuss the current research and provide additional up-to-date findings.

S1P in found in the serum at around 1nMol/ml in both men and women,[470] often found bound to albumin and lipids.[471] Previously, S1P has been shown to be involved in multiple pathways including vascular development,[472] leukocyte trafficking[473] and neurogenesis.[474] It is produced by initial breakdown of ceramide (sphingosine + long chain fatty acid) into sphingosine, which is then phosphorylated by either sphingosine kinase 1 or 2 (Sphk1 or Sphk2) to produce S1P.[475] S1P can then either be dephosphorylated (by S1P phosphatase), irreversibly broken down (by S1P lyase) or released from the cell through spinster homolog 2 (Spns2).[476] Once in the periphery, S1P acts on one of 5 G-protein coupled receptors (GPCR, previously referred to as EDG1, 3, 5 & 8) to induce its downstream signalling.[477–480]

S1P receptors 1, 2, 3, 4 and 5 ($S1PR_{1-5}$) have been found by PCR to be expressed in murine and human osteoblasts, osteoclasts and their precursors,[358,481–486] and therefore each cell has potential to respond to S1P. In addition, S1P is found in the cell lysate and conditioned media from primary human and murine osteoblasts.[487] BMMs also have high expression of Sphk1, which increases further after stimulation with RANKL, leading to increased intracellular S1P after 60

minutes.[488] Therefore S1P is highly prevalent in the bone environment and may be involved in bone homeostasis.

1.9.1 S1P on osteoblasts

Initial studies on S1P investigated its role in osteoblast proliferation. Using primary rat calvarial osteoblasts and osteoblasts derived from human periodontal explants, treatment with S1P increased [H^3]-thymidine incorporation and thus proliferation.[489,481]

Differentiation of MSCs into osteoblasts can also be controlled by S1P. C3H10T1/2 differentiation into adipocytes decreased expression of *S1pr1* and *S1pr2*.[490] However pre-treatment of these cells with S1P (1μM) decreased gene expression of adipogenic markers *Pparγ/Fabp4* and increased *Alp* and *Bglap*.[490] Furthermore, treatment of human MSCs with an S1PR1/3 antagonist (VPC23019) decreased mineralisation, suggesting the pro-osteoblast role of S1P is through S1PR1.[491] In addition, treatment of C2C12 MSCs with S1P in concentrations ranging from 0.01μM to 0.1μM for 7 days significantly increased ALP staining and *Alp/Bglap* mRNA.[492] Acting directly on human osteoblasts, 200nM treatment for 3 weeks increased ALP levels.[481] Furthermore, 3 days treatment of both SaOS-2 and MC3T3 cells with 1μM of S1P led to increased ALP levels.[493]

Human bone marrow MSC's also increased migration across a filter in response to an S1P agonist (VPC24191).[448] Migration was stopped by S1PR1 antagonist (W123) and S1PR2 antagonist (JTE-013), thus showing a role for S1P in osteoblast migration to the bone.[448]

The majority of studies therefore point to a pro-anabolic, pro-migratory action of S1P on osteoblasts, indicating a possible use as an anabolic agent in bone diseases.

1.9.2 **S1P on osteoclasts**

As previously mentioned, osteoblast signalling can directly link to osteoclastogenesis. Treatment of primary calvarial osteoblasts with 1μM of S1P led to increased RANKL expression, thus inducing higher osteoclast activation.[358]

S1P also directly acts on osteoclasts and their precursors. Interestingly, treatment of RAW624.7 and BMM with S1P increases their migration.[483,484] However, this migration peaks at 10^{-9} M and migration is inhibited in higher concentrations.[484] Treating cells with *S1pr2* siRNA allowed migration to continue in the higher S1P concentrations, indicating that S1PR2 is chemorepulsive.[484] This is confirmed further in S1PR2 KO BMM which have increased migration and migration velocity across a Boyden chamber in response to S1P and C5a.[484] *S1PR2* is also decreased in monocytes after treatment with vitamin D, increasing their motility and velocity towards S1P.[494] In contrast, S1PR1 is involved in the chemoattraction of osteoclasts towards S1P in lower concentration. Using the S1PR1 agonist SEW2871 *in vivo*, two-photon microscopy showed increased motility.[495] Additionally, S1PR1 osteoclast conditional KO mice develop an osteoporotic phenotype, with increased TRAP+ cells found on trabecular surfaces.[483] In turn, this leads to decreased trabecular bone volume, trabecular thickness and trabecular number.[483]

S1P also impacts osteoclastogenesis directly. Whilst extracellular S1P had no effect on TRAP+ cell number *in vitro*, *Sphk1* siRNA increased TRAP+ MNCs.[488] This suggests that intracellular, but not extracellular S1P disrupts osteoclastogenesis.

Overall, S1P may have a pro-anabolic, anti-catabolic effect on the bone, promoting bone growth, indicating it could be used as a target for future therapeutics to boost bone formation.

1.10 PEPITEM

As demonstrated in the above sections (Sections 1.8 & 1.9), there is growing evidence to suggest adiponectin and S1P have a major role in bone homeostasis and in disease. Interestingly, a novel endogenous peptide has been identified which links both S1P and adiponectin into the same pathway.[473] Mass spectrometry analysis of B cell conditioned media identified a unique 14 amino acid peptide, which was only found in serum of B cells following culture with adiponectin.[473] This peptide, when added directly to endothelium *in vitro*, reduced the transmigration of lymphocytes, an effect which was lost when S1PR antagonists or Sphk1 inhibitors are used.[473] Therefore this peptide was given the name PEPtide Inhibitor of TransEndothelial Migration (PEPITEM; Figure 1.10).[473] Due to the inhibition of transmigration by PEPITEM, it has a range of anti-inflammatory actions in disease. For example, therapeutic PEPITEM treatment in murine collagen induced arthritis[496] or lupus nephritis[497] results in decreased inflammation, protecting from disease. Interestingly, the bones from PEPITEM treated collagen induced arthritic mice were completely protected from bone loss, indicating possibly direct actions of PEPITEM on bone.[496]

When compared to a library of protein sequences, PEPITEM had complete sequence identity to amino acids 28-41 of the ubiquitously expressed 254 amino-acid protein 14-3-3ζδ.[473] Transcribed from the tyrosine 3-monooxygenase/tryptophan 5-monooxygenase activation protein zeta (YWHAZ) gene, 14-3-3ζδ is a member of a family of 7 14-3-3 proteins denoted β, γ, ε, η, σ, τ and ζδ.[498,499] 14-3-3s are known to have a role in a variety of cell signalling pathways including cell-cycle control,[500] response to DNA damage,[501] protein trafficking[500] and metabolism.[502] In-fact, 14-3-3 proteins have been proposed to engage ~0.6% of the human genome and therefore have a role in many signalling pathways and cellular processes.[499]

Included in the roles of 14-3-3s is an impact on bone development and remodelling. Using short hairpin RNA (shRNA) specific for 14-3-3β, leading to a 60% decrease in protein expression, human MSCs significantly increased mineral production, with no effect on cell proliferation or apoptosis.[503] This was due to an absence of Receptor Tyrosine Kinase Like Orphan Receptor 2 (ROR2) homodimerization.[503] Disruption of (ROR2) leads to significant abnormalities with the skeleton due to its role in committing MSCs to the osteoblastic lineage.[12] Furthermore, calvarial bones from mice infected with 14-3-3β shRNA had reduced bone area and a 50% decrease in osteoblast number.[503] Overall, these studies demonstrated an inhibitory effect of 14-3-3β on bone growth and osteoblast mineralisation. In a similar fashion, 14-3-3ε has been indicated to induce degradation of cartilage.[12] Proteomic analysis of the medium from compressed murine osteoblasts revealed an upregulation of 14-3-3ε, which correlated with MMP-3 and MMP-13 expression in chondrocytes.[504] Such increase in MMP expression was attenuated with the use of a 14-3-3ε blocking antibody.[504] In addition, treatment of

murine chondrocytes and human OA chondrocytes with 14-3-3ε significantly upregulated mRNA expression of MMP-3 and MMP-13.[504] Further investigations into this response found CD13 KO chondrocytes do not respond to 14-3-3ε and labelled 14-3-3ε could bind to the surface of mouse chondrocytes, a response which was attenuated with pre-treatment using a CD13 blocking antibody.[12] Therefore, 14-3-3 proteins released from osteoblasts plays a role in bone development and destruction.

Most interestingly, the PEPITEM precursor protein, 14-3-3ζ ,has also been shown to impact bone development. Immunoprecipitation experiments found 14-3-3ζ binds to microphthalmia-associated transcription factor (MITF).[505] In immature primary osteoclasts, immunofluorescent staining found that the 14-3-3ζ – MITF interaction occurs in the cytoplasm.[505] When RANKL and colony stimulating factor 1 (CSF-1) were added *in vitro*, partial nuclear localisation of MITF occurred, leading to osteoclastogenesis.[505] However, overexpression of 14-3-3ζ removed the nuclear localisation and led to a reduction of cathepsin K and TRAP mRNA measured by qRT-PCR.[505] Thus, 14-3-3ζ may play a role in inhibiting osteoclast precursor maturation.

Osteoblasts also express 14-3-3ζ, with 14-3-3ζ found in the vesicles[506] and exosomes[507] released from human BMSC derived osteoblasts[506] and osteoblasts isolated from subchondral tissue.[507] Interestingly, co-immunoprecipitation assays using a yeast two-hybrid system showed a complex formed between 14-3-3ζ (as-well as 14-3-3 τ) and 3BP2 (3 binding-protein 2).[508] Usually 3BP2 induces an increase in NFAT activity, however transfection of Jurkat cells with a 14-3-3τ plasmid abrogated this increase.[508] In osteoblasts, 3BP2 mutations result in decreased mineralisation and *Alp* expression by calvarial osteoblasts.[509] Therefore, 14-3-3 induced decrease

in 3BP2 may alter downstream osteoblast signalling and therefore increase osteoblast differentiation and activity. Directly, novel miRNAs, miR-451[510] and miR-22[511], have been identified to decrease during osteoblast differentiation, with inhibition resulting in increased ALP activity and mineralisation.[510] Interestingly, addition of an miR-451 and miR-22 inhibitors resulted in a reduction of YWHAZ expression, thus implicating YWHAZ in osteoblast differentiation.[510] Silencing YWHAZ expression led to a reduction in ALP activity and mineralisation, with western blots displaying lower *RUNX2, ALP* and *COL1A1* expression.[510] Interestingly, injection of OVX mice with a miR-451 inhibitor over a 6-week period moderately stopped the decrease in BV/TV and trabecular number usually observed, while increasing femoral strength and stiffness.[510] In addition to the roles of the 14-3-3 proteins above, changes in 14-3-3 expression have been shown in diseases affecting bone, with RA patients displaying 14-3-3η and 14-3-3γ in the synovium correlating with expression of MMPs.

Overall, with S1P, adiponectin and 14-3-3 proteins all showing positive results to boost bone growth in a range of conditions, there is a distinct possibility that PEPITEM may be able to control these processes and have a role in bone growth in health and disease.

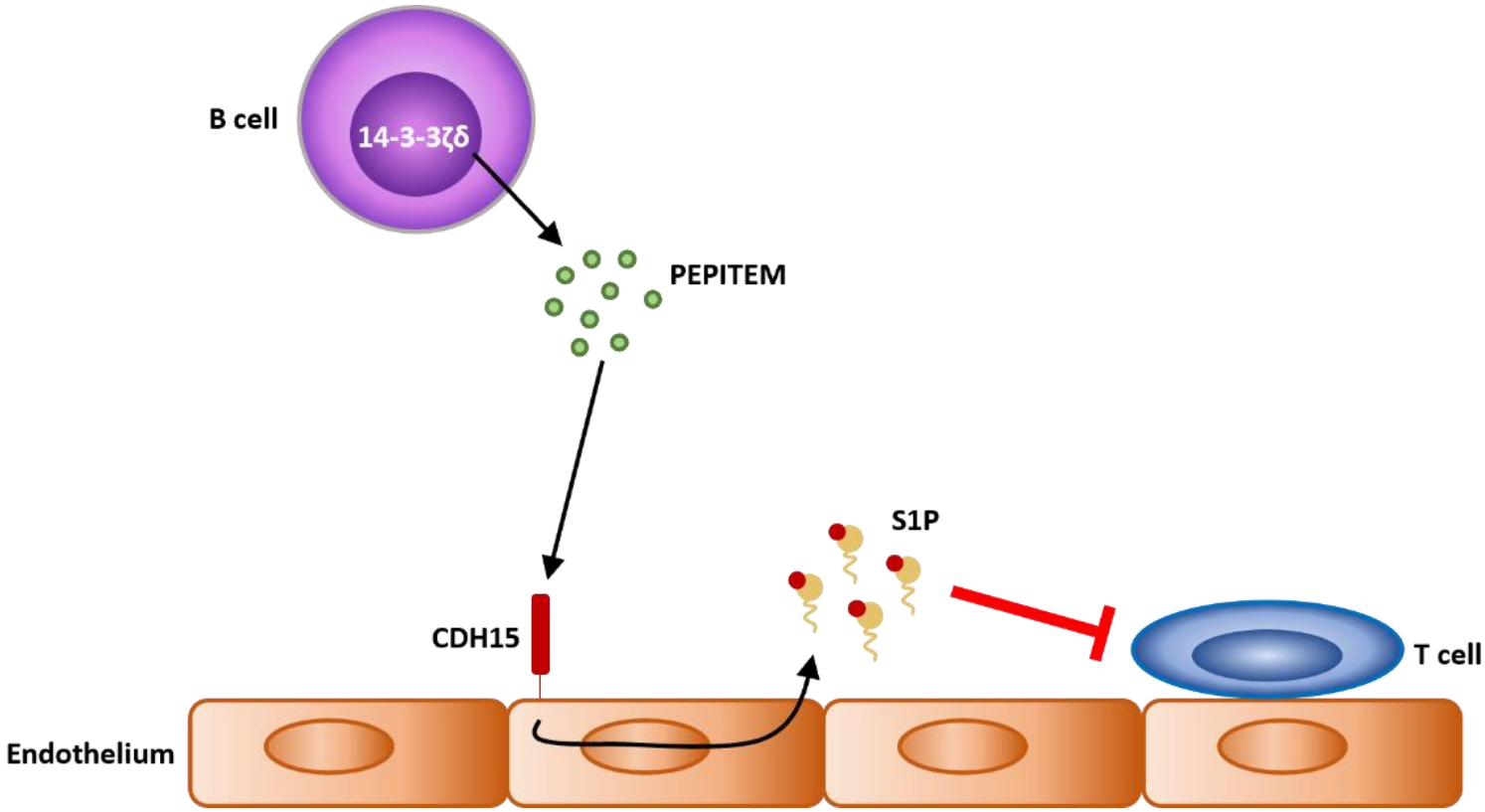

Figure 1.10. The PEPITEM signalling pathway.

PEPITEM is a novel endogenous molecule which has recently been discovered to be involved in inhibition of leukocyte transmigration. B cells are the only know PEPITEM releasing cell, promoting PEPITEM release through the breakdown of ubiquitously expressed 254 amino-acid protein 14-3-3ζδ. PEPITEM then signals through Cadherin15 (CDH15) expressed on endothelium to promote the release of Sphingosine-1-phosphate (S1P). S1P subsequently inhibits T cell transmigration through endothelium by binding the S1P receptors expressed on T cells, promoting the resolution of inflammation.

1.11 Aims and Objectives

As demonstrated above, PEPITEM pathway proteins have a large influence on bone production and resorption. In addition, treatment of arthritic mice with PEPITEM reduces bone damage. Therefore, we sought to explore the direct response of bone in health and disease to PEPITEM, with the global aim of characterising the response of bone to PEPITEM.

Therefore, we sought to test the following hypotheses that:

(i) PEPITEM induces a pro-anabolic phenotype on healthy bone

(ii) Molecules involved in PEPITEM signalling, S1P and cadherin-15, are also involved in the bone homeostasis.

(iii) PEPITEM is able to protect bone from disease induced changes.

Therefore, the project had the following aims:

1. To assess the response of the bone to PEPITEM treatment in healthy, homeostatic mice.

2. To explore the response of osteoblasts and osteoclasts to direct treatment with PEPITEM and S1P *in vitro*.

3. To characterise the pathway by which PEPITEM mediates its bioactivity.

4. To investigate the response of diseased bone (e.g. osteoporosis) to PEPITEM treatment.

2 Methods

2.1 Mice

All animal experiments were run in accordance with Home Office regulations and the University of Birmingham animal welfare and ethical review body (PPL - PE5985209, PP0156739, PP5475067). C57 Black 6 (C57Bl/6) mice were purchased from Charles River Laboratories (Kent, UK), Janvier (Aged C57BL/6JRj, Mayenne, France) or bred at the University of Birmingham in the Biomedical Service Unit (BMSU, Birmingham, UK). All mice were housed in specific pathogen-free conditions.

2.1.1 Measuring bone turnover in homeostatic conditions

Resting 8-week-old, male, C57Bl/6J wild type (WT) mice were given daily intra-peritoneal (IP) injections of 300µg PEPITEM (sequence: SVTEQGAELSNEER-PEG(352)-Amide; Alta Bioscience; Redditch, UK or Cambridge Research Biochemicals Limited; Cambridge, UK) or an equivalent volume of phosphate-buffered saline (PBS; cat: BR0014; Oxoid, Basingstoke, UK) for two weeks. *In vivo* PEPITEM concentrations and regime were previously used in inflammatory studies to promote positive results (unpublished data). Alternatively, mice were given bi-weekly subcutaneous (SC) injections of 400µg PEPITEM enclosed in a liposome (kindly produced and provided by Marie-Christine Jones, University of Birmingham) or equivalent volumes of empty liposome controls. Six and two days prior to termination, mice were given IP injections of 20mg/kg of calcein (cat: C0875; Sigma-Aldrich, Gillingham, UK).[512] Mice were culled by schedule 1 cervical dislocation or via cardiac puncture. Limbs and spine were dissected and cleaned of muscle and fat before fixation in 10% buffered formaldehyde (cat: HT5011; Sigma-Aldrich,) overnight.[513] Bones were then transferred into 70% ethanol (cat: 20821; VWR, Leicestershire, UK)

and stored between 2-8°C until analysis. Blood was spun at 10,000g for 10 minutes, the serum collected and stored at -80°C.

2.1.2 Ovariectomy induced bone damage

Ovariectomy (OVX) surgical procedures were performed by University of Birmingham BMSU staff. Female, 12-week-old C57Bl/6 mice were given 7 days to acclimatise to BMSU housing conditions, after which OVX was induced via ligation at the distal uterine horn to remove the ovaries.[213] For baseline control measurements mice were taken at 0, 1, 2 and 4 weeks post-OVX. Alternatively, mice were given daily IP injections with 300µg PEPITEM or an equivalent volume of PBS, starting 2 weeks post-OVX and continuing for 14 days. After 14 days, mice were culled via cardiac puncture and tissue was collected and processed as described in section 2.1.1.

2.2 *Ex vivo* micro-CT analysis of bone

2.2.1 Imaging

Hind limbs, front limbs and spines were transferred into 5ml polypropylene tubes (cat: 89497; VWR) or tightly sealed straws depending on the size of the sample and covered in ethanol (cat: 20821; VWR). Polystyrene and straws were used to keep samples in a vertical position and to reduce sample movement during scanning. Samples were placed vertically into the Skyscan 1172 micro-CT scanner (Bruker; Kontich, Belgium) and fixed in place with dental wax. Images were taken every 0.45° with an X-ray voltage of 60kV, current of 167µA through a 0.5mm aluminium filter at a resolution of 2000x1200 pixels.[512,514,515] Images were saved as .Tiff files ready for reconstruction.

2.2.2 **Image reconstruction**

Images were reconstructed using NRecon 1.6.1.5 (Bruker). Initially the misalignment that occurred during sample scanning was calculated and automatic compensation was applied by NRecon to account for this misalignment.[516] However, if a misalignment was larger than ±2.5 pixels, samples were rescanned to ensure accurate reconstruction occurred. In order to eliminate the beam hardening induced cupping effects, where the image appears brighter around the edge due to hardening of the X-ray once it hits the surface of bone, a beam hardening correction of 20% was applied using the inbuilt setting in NRecon. Ring artefact correction was set to 4 to reduce distortions produced during scanning. In order to create cross sectional images of scanned samples, micro-CT images were reconstructed using the Feldkamp algorithm.[517] Spinal scans were additionally processed by opening cross-sectional images in DataViewer (Bruker), which were converted to a 3D image in order to generate coronal views of the sections and saved as a dataset of .bmp files (Figure 2.1C).[518] Tibiae were already scanned in the ideal analysis orientation so were analysed without rotation.

Cross-sectional images of the whole bone could then be used to calculate trabecular and cortical parameters and generate 3D images of scanned samples using the CTan v1.12 software (Computed Tomography Analyser; Bruker).[519] By comparing the image created by CTan and the original CT image, a global threshold was manually set to differentiate “real” bone from background noise. From the cross-sectional images, regions of interest (ROI) were drawn around either cortical (encompassing the perimeter of the bone and the inside of the outside ring) or trabecular bone (drawn just inside the cortical bone) (Figure 2.1, ROI = Pink). The

bottom of the growth plate where trabecular bone begins was used as the reference point to begin creating ROI. For tibia trabecular bone analysis, ROI were drawn around trabecular bone from section 1-100 (Figure 2.1A), whereas spinal trabecular bone was analysed for 14 sections due a thinner area of trabecular bone (Figure 2.1D). For cortical bone, two ROIs were analysed at the point where the trabecular bone was no longer present at section 250 through to section 350: one ROI encompassed the whole bone to determine bone diameter and the other was created around cortical bone only to calculate cortical thickness (Figure 2.1B). Analysis was then performed by first applying “despeckle” to remove all white speckles smaller than 10 voxels to reduce background noise in CTan v1.12,[520] then using 3D or 2D analysis, trabecular or cortical parameters were calculated respectively (Table 2.1).

2.2.3 **Generation of a 3D mesh**

Using a marching cube algorithm 33,[521] cross-sectional reconstructed images were converted to a 3D model in CTan v1.12 and saved as a polygon file (.PLY). These 3D meshes were made up of polygons generated from ROI described in Section 2.2.2. Meshes were then analysed in MeshLab 1.3.2[522] (ISTI-CNR, Italy) by applying the following parameters: smooth rendering to increase the likeness to the original shape; ambient occlusion per face to generate soft shadows on the bone; and a quadratic edge collapse decimation of 0.2% to simplify the image by reducing the number of vertices in the mesh, in doing so making the analysis and imaging of the mesh clearer. Snapshots of 3D models were taken and saved as .JPG.

Table 2.1. Parameters analysed from Micro-CT

Parameter	Unit
Trabecular bone volume (BV/TV)	%
Trabecular number	1/µm
Trabecular separation	µm
Trabecular thickness	µm
Cortical area	μm^2
Total bone area	μm^2
Cross sectional thickness	µm

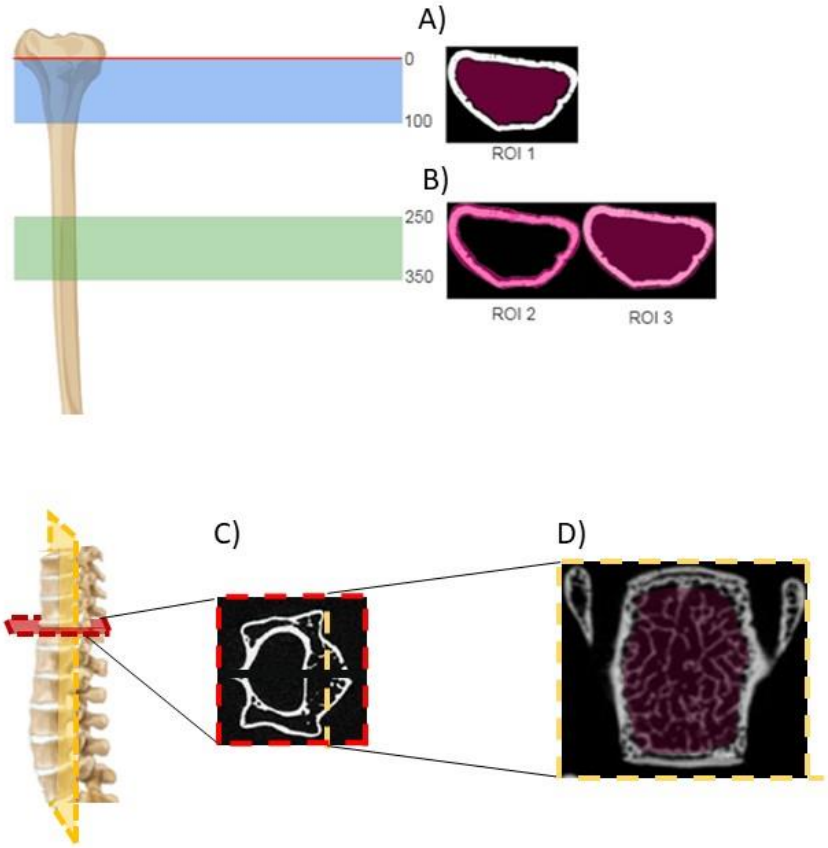

Figure 2.1. Representative diagram of the ROIs drawn for analysing trabecular and cortical bone.

A. For analysis of trabecular bone, regions of interest were drawn around the trabecular bone for 100 slices below the tibia growth plate (ROI 1). **B.** Analysis of cortical bone required two ROIs, which began 250 slices below the growth plate and continued for 100 slices. ROI 2 encapsulated the cortical bone and excluded the trabecular bone. ROI 3 surrounded the cortical bone and included the trabecular bone. **C-D.** Vertebral trabecular analysis was performed by first creating cross-sectional images through the spine (**C,** red), which were converted to coronal cross-sectional images (**D,** yellow). Trabecular bone was then analysed for 14 slices.

2.3 Mechanical testing of mouse femurs

Femurs were cleaned of all muscle using forceps and tested to the point of failure in the 3-point bending test as previously described.[512] Using the ElectroForce® BioDynamic® 5500 (Bose, ElectroForce Systems Group, Minnesota, USA), femurs were placed on their lateral surface on two plates 8mm apart so both the distal femur and trochanter major were balanced (Figure 2.2). A 22N load cell was placed under the bone and used to measure force applied. The load head was set to descend at 1 mm/minute, and force and displacement data were recorded into an excel spreadsheet with 100 data points comprising of time, displacement, and force (N) measured every second. These data were plotted as displacements (mm) against force (N), which were used to calculate:

stiffness (N/mm; gradient of the rising portion);

load to failure (N; maximum load supported by the bone);

load to fracture (N; force when the bone no longer bends and snaps);

work required to fracture (Nmm; determined from the area under the curve until fracture)

2.4 Measuring serum P1NP

Serum was analysed for RatLaps™ total procollagen type-1 N terminal propeptide (P1NP, cat: AC-33F1; immunodiagnosticsystems (IDS), Boldon, UK) by a competitive ELISA as per the manufacturer's instructions. All reagents were purchased from IDS.

For analysis of P1NP serum concentration,[216] 50µl of calibrators, controls or samples diluted 1:9 in sample diluent (cat: AC-3309) were added individually to the desired well of 96 wells plates (cat: AC-3302W). All samples were run in duplicate. All wells were incubated with 50µl of P1NP biotinylated (cat: AC-3303), which were left at room temperature for 1 hour. Wells were washed, followed by incubations with an enzyme conjugate (cat: AC-3304), and then TMB substrate (AC-TMB) for 30 minutes each at room temperature. After 30 minutes, the reaction was stopped using HCL (cat: AC-STOP) and read on the Synergy HT (BioTek, Swindon, UK) at 405nm.

Analysis was done in Prism 8 (GraphPad Software Inc, California, USA). A 4-parameter logistical curve fit was applied to the data, calculating a = Minimum value, b = Hills slope of curve c = Point of inflection and d = Maximum value, which could be used to calculate concentrations using the equation $X = c(\frac{a-d}{y-d} - 1)^{\frac{1}{b}}$. P1NP serum concentration was then calculated, with P1NP values corrected for the initial dilution factor.

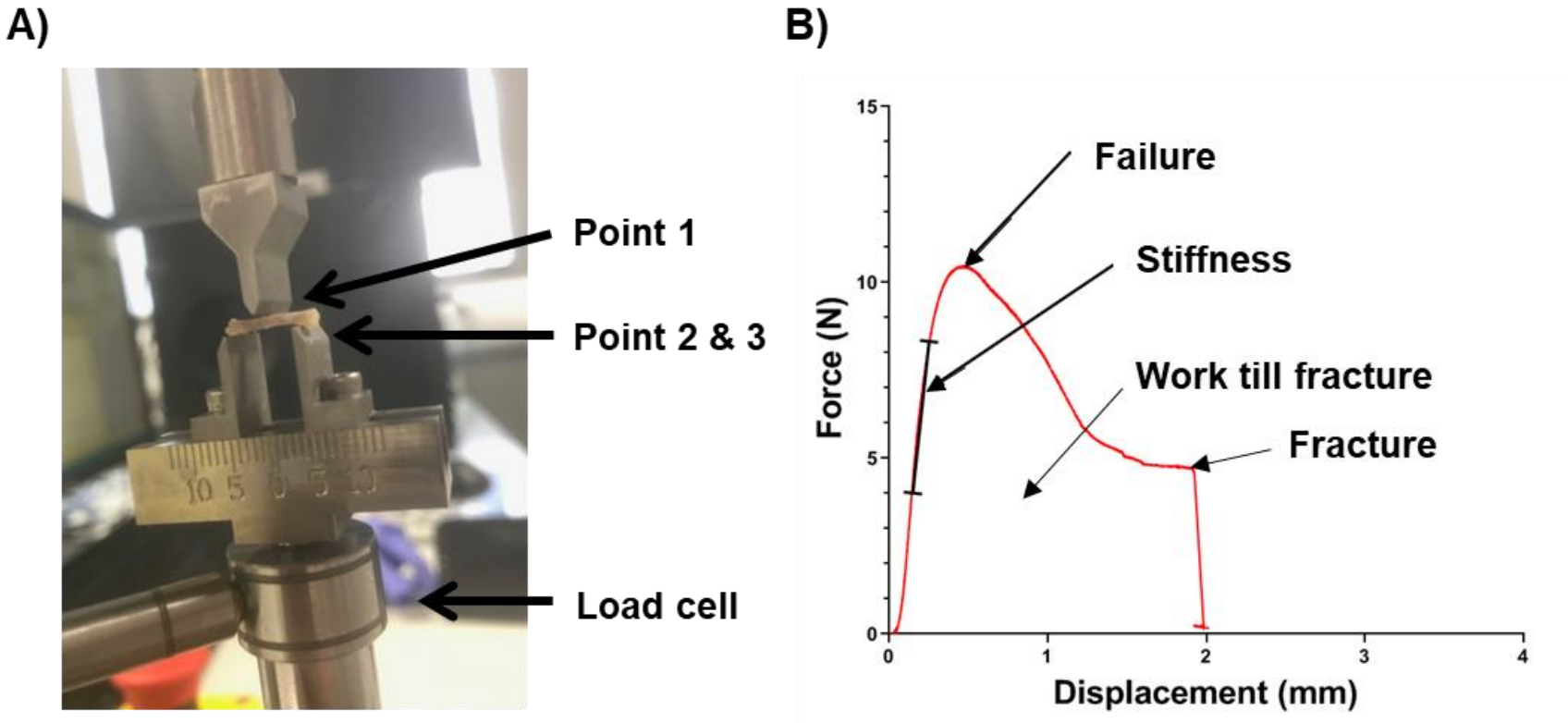

Figure 2.2. Method of mechanically testing femurs.

A. Representative photograph of femurs on the ElectroForce® BioDynamic® 5500. Femurs were placed on their lateral surface with the distal femur and trochanter major balanced on **Point 2 and 3**, 8mm apart. The **load cell** recorded the force applied on the bone by **Point 1**. **B**. Representative plot of displacement of point 1 and the force applied recorded by the load cell were plotted and used to calculate stiffness (N; gradient of the rising portion), load to failure (N/mm; maximum load supported by the bone), load to fracture (N; force when the bone no longer bends and snaps) and work required to fracture (N.mm; determined from the area under the curve until fracture).

2.6 Sectioning of murine tibiae

Following micro-CT analysis, one tibia per mouse was decalcified for 4 weeks with 10% w/v ethylenediaminetetraacetic acid (EDTA; cat: T4174; Sigma-Aldrich) diluted in ultra-pure water and buffered to a pH of 7.4 using NaOH (cat: 221465; Sigma-Aldrich) or HCL (cat: 320331; Sigma-Aldrich).[523] Decalcified bone were then dehydrated using rising concentration of ethanol (70%, 95%, 95%, 100%, 100%, 100%), with tissue remaining in each concentration for 1 hour. Dehydrated tissue was subsequently placed in xylene (cat: X/0250/17; Fisher Scientific, Loughborough, UK) for 2 hours, with a change in xylene halfway, to remove any remaining ethanol and fat. Bones were placed in melted paraffin at 58°C - 60°C for an hour to allow infiltration into the tissue. To embed the bone, a coating of paraffin was placed on the bottom of a cassette (cat: 3802276; Leica, Milton Keynes, UK) and the tibia was placed flat against the paraffin layer and surrounded in paraffin. Paraffin was then allowed to harden before sectioning. To section, tibiae embedded in paraffin blocks were cooled on ice for 10 minutes before being placed inside the cassette holder of a HistoCore MULTICUT Semi-Automated Rotary Microtome (cat:149MULTI0C1; Leica). Using Feather R35 microtome blades (cat: JDA-0300-00A, Cell Path, Newtown, Mid Wales) blocks were trimmed by 20µm per section until the bone was reached, at which point the microtome was changed to section at 6µm per section. Sections were then transferred into a water bath set at 37°C (cat: HI1210, Leica) and captured by an X-tra ADHESIVE slide (cat: 3800050; Leica). Slides were baked in a high-capacity section dryer (cat: JAX-0400-00A; Cell Path) set at 60°C for at least 1 hour to bake the sections onto the slide and stored until staining. Alternatively,

decalcified bones were sent to the Royal Orthopaedic Hospital (ROH) Birmingham to be paraffin embedded and sectioned (10 sections per bone starting at the midpoint).

2.7 Tartrate-Resistant Acidic Phosphatase (TRAP) staining

In order to analyse the number of osteoclasts in each section, tartrate-resistant acidic phosphatase (TRAP) staining was performed.[524] TRAP basic incubation medium was first made up by adding sodium acetate anhydrous (0.11mM, cat: 10236; VWR), L+ Tartaric acid (0.074mM, cat: 137855000; Fisher Scientific) and glacial acetic acid (2%, cat: 1005706; Sigma-Aldrich) to deionised water (diH2O). TRAP staining solution was then made: 98% (V/V) TRAP basic incubation mix; 1.6M Fast Red Violet LB salt (cat:F3381; Sigma-Aldrich); and 2% (V/V) of Naphthol AS-MX phosphate substrate mix (58mM Naphthol AS-MX (cat: N4875; Sigma-Aldrich) in 2-ethoxyethanol (cat: 16100; Alfa Aesar, Lancashire, UK)). TRAP staining solution was heated to 37°C on the digital orbital shaker (Heathrow Scientific; Illinois, USA).

Slides were deparaffinised using Xylene (cat: 28975.325; VWR), followed by rehydration in decreasing concentrations of ethanol (100%, 90%, 80%, 70%; cat: 20821; VWR) and finished with two washes with de-ionised water (di$H_2$0). Deparaffinised slides were submerged in the TRAP staining solution for 30 minutes at 37°C and stained slides were mounted using immu-mount (cat: 1900331; Fisher Scientific) and covered with a coverslip. Slides were imaged using the slide scanner axioscan Z1 (ZEISS, Cambridge, UK) and stored as .Zen files.

For analysis of whole hind limb sections, Zen Blue software (ZEISS) was used to break whole leg scans into regions of 20µm by 20µm, which were saved as images (JPEG) and opened on ImageJ (National institute of health (NIH); Maryland,

USA). Images were colour separated in ImageJ using CIELAB colour space (L*A*B*), where L* (lightness) and B* (blue/yellow) were set as 0 to remove colours that are not red. A threshold was then manually set on A* (green/magenta) so that the image only showed pink osteoclasts. Osteoclasts were counted per region using ImageJ count maxima tool, where maxima were defined according to noise tolerance to neighbouring squares and given as total number of osteoclasts per section. Manual counting and automated counting showed no differences in number of osteoclasts observed (Figure 2.3).

For analysis of tibias, samples were manually counted by drawing a ROI around the diaphysis, which was measured and exported to ImageJ. Osteoclasts were counted manually using the ImageJ cell counter plugin, normalised to the area of the ROI, and presented as osteoclasts/mm^2.

2.8 Calcein analysis

Calcein labelling analysis was performed at the University of Sheffield by the Skelet.AL team (Sheffield, UK). One tibia from each mouse was decalcified and embedded in plastic. Sections of 8µm were cut at 3 depths 30µm apart in each tibia, which were then imaged. Imaging was performed using “Osteomeasure” (Osteometrics, Georgia, USA), taking measurements at the endocortical bone surface at magnification 20X. Six fields of view were taken along both the medial and lateral surfaces starting 0.33mm from the growth plate, totalling a distance of 3.6mm.[525,526] Measurements taken were double-labelled surface/bone surface, mineral apposition rate (MAR) by $\frac{Ir.l.Th}{Ir.l.T}$ and bone formation rate/bone surface (BFR/BS) by $MAR \times \frac{(\frac{MS}{BS})}{100}$.

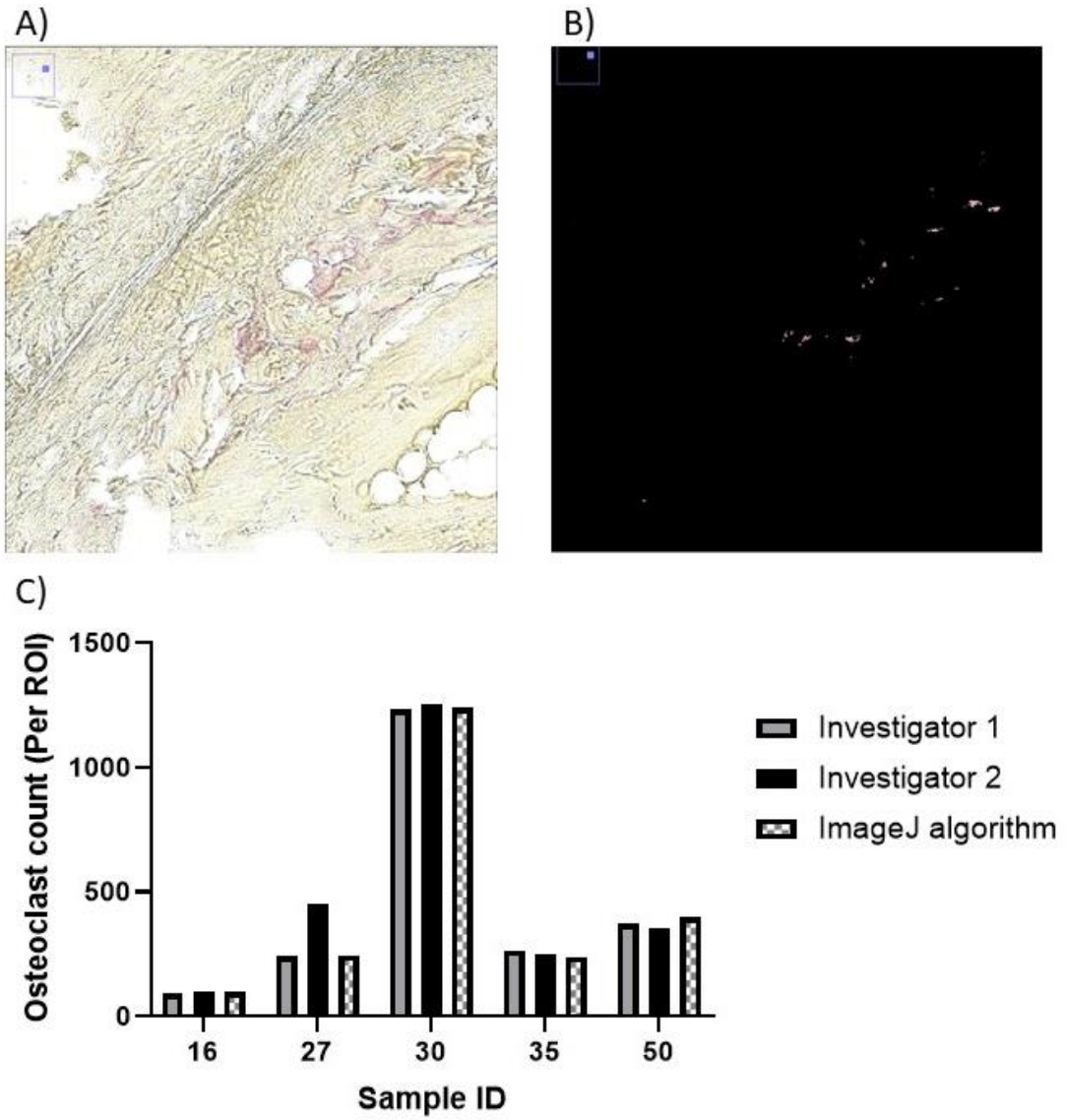

Figure 2.3. Automated counting of osteoclasts

Whole limb sections were stained for osteoclasts (pink) using TRAP and imaged on the slide scanner. **A.** Images were split into smaller sections and opened in ImageJ **B.** Colour threshold was manually changed to remove all background noise and select only pink colouring. Pixels were counted using the Find Maxima setting, excluding maxima which are not different from surrounding maxima. **C.** Sections were counted by two independent researchers and using the ImageJ algorithm.

2.9 Generation of recombinant S1P

Shingosine-1-Phosphate was purchased from Cayman Chemicals (Michigan, USA) and made up following published protocols.[527,528] S1P was dissolved in methanol:water (95:5) to create a solution at 0.5mg/ml and heated to methanol's boiling point (45°C - 65°C). The S1P-methanol solution was then sonicated until S1P was fully suspended. Solution was aliquoted into 2.0 mL Screw-Thread glass vials (cat: 24620, Restek, Bucks, UK) with 20µg (40µl) per vessel. Methanol was evaporated from the tubes using a stream of liquid nitrogen and the vessel was heated to 50°C to generate a thin film of S1P around the edge of the vial. Vials were stored at -20°C until use. When ready, 4mg/ml BSA in water was added to the vials to generate an S1P solution at 125uM, which was stored at 4°C for a maximum of two months.

2.10 Cell culture

Murine (primary and cell line) and human osteoblasts were cultured in differing culture medias.

Table 2.2. Murine basal media

Reagent	Concentration	Company	Cat number
α-MEM[1]	90%	Sigma-Aldrich	M8042
L-Glutamine	2 mM	Sigma-Aldrich	G1146
Penicillin	100 U/ml	Sigma-Aldrich	G1146
Streptomycin	100 µl/ml	Sigma-Aldrich	G1146
Fetal bovine serum	10%	Biosera[2]	FB1001

[1]MEM: Minimum Essential Medium Eagle. [2]Biosera, East Sussex, UK

Table 2.3. Murine osteoblastogenic media

Reagent	Concentration	Company	Cat number
Basal Media	100%	Table 2.2	-
β- Glycerol phosphate	10 mM	Sigma-Aldrich	G9422
L- Ascorbic acid	50 µg/ml	Sigma-Aldrich	A5960

Table 2.4. Murine osteoclastogenic media

Reagent	Concentration	Company	Cat number
Basal Media	100%	Table 2.2	-
RANKL[1]	50ng/ml	Abcam[3] (Cambridge, UK)	ab129136
mCSF[2]	50 ng/ml	R&D Systems[4] (Abingdon, UK)	416-ML

[1]RANKL: Receptor Activator of Nuclear Factor-κB Ligand. [2]mCSF: macrophage colony-stimulating factor. [3]Abcam, Cambridge, UK. [4]R&D Systems, Abingdon, UK.

Table 2.5. Human basal osteoblast media

Reagent	Concentration	Company	Cat number
DMEM[1]	89%	Sigma-Aldrich	D6546
Fetal Bovine Serum	10%	Biosera	FB1001
L-Glutamine	2 mM	Sigma-Aldrich	G1146
Penicillin	100 U/ml	Sigma-Aldrich	G1146
Streptomycin	100 µl/ml	Sigma-Aldrich	G1146
Non-essential Amino Acid Solution	1%	Sigma-Aldrich	M7145
β- Glycerol phosphate	2mM	Sigma-Aldrich	G9422
L-Ascorbic acid	50 µg/ml	Sigma-Aldrich	A5960

[1]DMEM: Dulbecco's Modified Eagle Medium

2.10.1 Isolation of murine calvaria osteoblasts

Calvarial osteoblasts (C.Ob) were isolated following previously established method.[529,530] Day 3-5 C56Bl/6 WT mouse pups were culled via decapitation and heads were washed briefly in 70% ethanol and kept hydrated in αMEM media supplemented with 2mM L-Glutamine, 100U/ml Penicillin and 100µg/ml Streptomycin. Skin was removed from calvaria using forceps, and the calvaria was dissected out and cleaned of any contaminating tissue. Calvaria where digested 4 times in different conditions by shaking and the media collected after each condition (excluding digestion 1) and pooled. The first 2 washes were in αMEM + 1mg/ml of collagenase d (cat: COLLD-RO; Merck, Feltham, UK) at 37°C for 10 minutes followed by 30 minutes. Wash 3 was in αMEM + 5µM EDTA for 10min at 37°C and wash 4 in αMEM + 1mg/ml collagenase d for 30min at 37°C.

Collected cells were then counted using a haemocytometer. Cells were then diluted in murine basal media (Table 2.2) to $1x10^6$ cells/ml and split among culture flasks with additional murine basal media. After 24 hours, media was changed to remove non-adhesive and contaminated cells. Primary calvarial osteoblasts were then utilised at P1 or frozen down for analysis later (Section 2.10.4).

2.10.2 Isolation of Human Osteoblasts

Human osteoblasts (H.Ob) were isolated following protocols established in Davies et al.[531] Knee and Hip joints from OA joint replacement patients were collected from the Royal Orthopaedic Hospital (NRES 16/SS/0172). Alternatively, bone samples collected from healthy or osteoporotic patients following fractures that require surgery at the Queen Elizabeth Hospital (Birmingham, UK) were provided by the Human Biomaterials Resource centre (University of Birmingham, Birmingham,

UK). Samples were kept in human basal osteoblast media (Table 2.5) and cleaned of cartilage and fat. Approximately 2mm bone sections were cut from the joints and washed in human osteoblast media to remove fat. Bone chips were placed in T75 flasks in 10ml of human osteoblast media, replacing media every 2-3 days. Cellular outgrowth occurs between 10-14 days, after which chips were placed in new flasks to capture any further outgrowth. At 90% confluence, cells were trypsinised (Section 2.10.3) and used or split 1 in 2 for further culture.

2.10.3 Detachment of cells

Cells were detached using 2X Trypsin-EDTA (1g/L porcine trypsin and 400mg/L EDTA, cat: T4717; Sigma-Aldrich) diluted in PBS and incubated at 37°C for ~5 minutes. Trypsin was neutralised using basal media (murine or human depending on cells) in a ratio of 2:1 media to trypsin, and cells were pelleted by centrifugation at 300g for 4 minutes. Cells were resuspended in 1ml basal media, counted using a haemocytometer and diluted to a desired concentration in basal media prior to seeding for experimental use or split 1 in 4 for expansion.

2.10.4 Freezing and storage of cells

In order to freeze cells for long term storage, once trypsinised all media was removed and cells were resuspended in a freezing solution of 10% dimethyl sulfoxide (DMSO, cat: D2650; Sigma-Aldrich), FBS (40%, Biosera) and basal media (50%, human or murine) to a dilution of $1x10^6$ cell/ml. Using Cryo.s™ Cryovial (cat: 122280; Greiner Bio-one, Kremsmünster, Austria), 1ml of cell suspension was added and cryovials were transferred into a Freezing container Nalgene® (cat: C1562, Sigma-Aldrich) and placed in a -80°C freezer for a minimum of 2 hours to allow freezing at -

1°C/minute. Once frozen, cryovials were transferred to liquid nitrogen for long term storage.

2.10.5 Induction of myocyte differentiation

The immortalised murine myoblast C2C12 (cat: CRL-1772™, ATCC, Virginia, USA) was cultured in DMEM (cat: D6429, Sigma-Aldrich) supplemented with L-Glutamine (2mM), Penicillin (100U/ml) and Streptomycin (100µl/ml) (cat: G1146, Sigma-Aldrich). Cells ($5x10^4$ cells/well) were seeded into a 48 well plate and allowed to settle for 24 hours. Differentiation was induced using DMEM supplemented with 2% Horse serum (cat: H1138, Sigma-Aldrich) for 8 days, with media changed every other day. After 8 days mRNA (Section 2.13) or protein (Section 2.16) were isolated or cells were stained for immunofluorescence (Section 2.17) or flow cytometry (Section 2.18).

2.10.6 Induction of osteoblast mineralisation

The spontaneously immortalised passage 6 (P6) murine MC3T3-E1 cell line (cat: CRL-2593; ATCC) and stromal P1 murine ST2 cell line (kindly provided by Professor James Edwards, University of Oxford, UK) were brought up from liquid nitrogen by thawing cells in murine basal media, centrifuging to remove DMSO and cultured until 80% confluence.

MC3T3-E1, C.Ob, ST2 or H.Ob ($8x10^3$ cells/well) were seeded into a 48 well plate and treated with basal (human or murine) or osteoblastogenic media (Table 2.3) with or without 10ng/ml *in vitro* non-pegylated PEPITEM (Alta Bioscience) or 1µM sphingosine-1-phosphate (S1P, cat: S9666; Sigma-Aldrich). Concentrations of S1P and PEPITEM were determined by previously published protocols[449,482,483,486,488]

or by running concentration gradient studies and adjusting for the lowest functioning concentration. Cells were cultured for up to 21 days at 37°C in 5% CO2, with the media and treatment changed every other day. Mineralisation was assessed using an alizarin red staining quantification assay and alkaline phosphatase assay (see below).

2.10.7 **Alizarin red mineralisation assay**

Alizarin red analysis was performed following the manufacturer's instructions (cat: SC8678; Caltag+Medsystems, Buckingham, UK). Briefly, cells were washed twice in PBS and fixed in 4% paraformaldehyde (cat: HT501128; Sigma-Aldrich) for 15 minutes at room temperature. Cells were washed a further 3 times in diH_2O and stained with 40mM of Alizarin red S for 35 minutes at room temperature with gentle shaking on a digital orbital shaker (Heathrow Scientific). Following staining, excess dye was removed by washing the wells at least 5 times with diH_2O until the water was clear. Cells were imaged using the Cytation 5 microscope (Biotek) run through Gen5 software (Biotek), taking multiple images at 4x magnification to encompass the whole well. Images were then stitched together within Gen5 to form one complete image per well.

Alizarin red stain was quantified by dye extraction as per manufacturer's instructions (cat: SC8678; Caltag+Medsystems). Cells were treated with 10% acetic acid for 30 minutes at room temperature with gentle shaking on a digital orbital shaker and then collected in a 1.5ml centrifuge tube (Corning CoStar, Flintshire, UK) using a cell scraper (cat: 83.1830; Sarstedt, Nümbrecht, Germany). Cells were then vortexed, heated to 85°C for 10 minutes in a Sub Aqua Pro water bath (cat: SAP26; Grant, Cambridge, UK) and cooled on ice for 5 minutes. Tubes were then centrifuged

at 20,000g for 15 minutes, the supernatant collected and then neutralised to with 10% ammonium hydroxide (pH 4.1-4.5). Neutralised supernatants were transferred to a 96 well plate, and absorbance at 405nm was read by a Synergy HT plate reader. Each sample was run in technical replicates, which were used to calculate a mean. A standard curve was produced by measuring the absorbance of Alizarin red standard from a concentration of 0 to 2mM. Using the equation of the standard curve, the concentration of Alizarin red was calculated. Data were expressed as concentration (mM) of Alizarin red in each well as a percentage of untreated control.

2.10.8 **Alkaline Phosphatase assay**

To measure alkaline phosphatase activity, osteoblasts were washed in PBS before being lysed in 100µl of RIPA buffer (cat: R0278; Sigma-Aldrich) for 30 minutes on ice.[189,532] Cells were harvested using a cell scraper and transferred into an Eppendorf before being vortexed and centrifuged at 13,000g for 10 minutes. A 1:4 ratio of cell lysate to alkaline phosphatase yellow (pNPP) liquid substrate for ELISA (cat: P7998; Sigma-Aldrich) were added to a 96 well plate.[189] The plate was wrapped in foil and incubated for 45 minutes at 37°C in an incubated shaker (SciQuip, Shropshire, UK) before being quantified using a Synergy HT plate reader with absorbance set at 405nm. Data are expressed as percentage of control (%) or absorbance at 405nm.

2.11 Osteoclast culture and analysis

2.11.1 Isolation of bone marrow osteoclast precursors and induction of osteoclastogenesis

Eight-week-old C57Bl/6 mice were culled by Schedule 1, and hind limbs were removed and cleaned of muscle and fat. Small cuts (~1mm) were made at both ends of the tibias and femurs before they were placed in 200µl pipette tips inside an Eppendorf Safe-Lock Tubes 1.5ml (cat: 0030 120.086; Eppendorf, Hamburg, Germany). Murine basal media (Table 2.2) was added to each Eppendorf before centrifugation at 10,000g for 15 seconds to spinout the bone marrow from the inside of the bones. A 25G needle was used to break up the resulting pellet, which was then suspended in 10ml of murine basal media, filtered through a 70µm pore (cat: 542070; Greiner Bio-one) and counted using a haemocytometer.[533] On an Osteoassay plate (cat: CLS3987; Corning),[534] $1x10^6$ cells were cultured in 500µl of murine basal media for 72 hours, to allow mononuclear cells to adhere before media was changed.

Once 80-90% confluence had been reached, media was changed to murine osteoclastogenic media (Table 2.4) with or without 10ng/ml of *in vitro* PEPITEM. Media was replaced every 3 days, with differentiation occurring around day 7 seen by presence of large multi-nucleated cells.

2.11.2 RAW264.7 osteoclast differentiation

The murine macrophage-like cell line RAW264.7 (cat: ATCC TIB-71; ATCC, Manassas, Virginia) was cultured in basal media and plated in a 48 well plate at a cell density of $8x10^3$ cells per well. Media was then switched to basal media supplemented with 10ng/ml RANKL (cat: ab129136; Abcam) to induce

osteoclastogenesis. Media was replaced every 3 days, with cells also treated with or without 10ng/ml PEPITEM (cat: 416-ML; R&D Systems), 1μM S1P or Zoledronic acid hydrate (1μM, cat: Z5744; Cambridge Biosciences). After 5 days in culture large multinucleated cells were observed.

2.11.3 Isolation of human monocytes and induction of osteoclastogenesis

Human PBMCs were isolated from blood of donors collected in EDTA coated vacutainers. Blood was layered onto a density gradient of H1119 (cat: 11191, Sigma-Aldrich) and H1077 (cat: 10771, Sigma-Aldrich) and tubes were centrifuged at 800g for 30 minutes with no break or acceleration to separate red blood cells, PBMCs, granulocytes and plasma. The PBMC layer was collected and washed in MACs buffer. Monocytes were negatively selected from PBMCs using the EasySep™ Human Monocyte Isolation Kit (cat: 19359, Stem Cell, Cambridge, UK). Briefly, PBMCs were diluted to a concentration of 5 x 10^7 cells/mL and monocyte isolation cocktail (50 μL/mL) and platelet removal cocktail (50 μL/mL) were added for 5 minutes at room temperature. Magnetic beads (50 μL/mL) were added to the sample and incubated for 10 minutes before the samples were toped up to 5ml using MACs buffer. Tubes were placed into the EasySep 'The Big Easy' magnet (cat: 18001, Stem Cell) for 5 minutes before the non-stuck cells were collected ready for culturing.

For osteoclast differentiation,[535] Monocytes were plated at 1x10^6/ml in a variety of well plates and cultured overnight in human osteoclast differentiation media containing 50ng/ml m-CSF (cat: 216-MC-025, R&D systems). Half the media was replaced after 24 hours with human osteoclast differentiation media containing 25ng/ml m-CSF and 50 ng/ml RANKL (cat: 390-TN-010, R&D systems) to create a final concentration of 25ng/ml. Cells were cultured for 8 days with media replaced

every 3 days. In addition, PEPITEM (10ng/ml), Zoledronic acid (1μM) or S1P (1μM) were added at each media change.

2.11.4 **TRAP staining of osteoclasts in culture**

After onset of osteoclast differentiation, cells were fixed in 10% paraformaldehyde for 15 minutes at room temperature. Meanwhile, TRAP staining solution was made up as in Section 2.5.[536] Once fixed, paraformaldehyde was replaced by staining solution, and plates were left at 37°C for 30 minutes, after which the TRAP solution was removed, wells were washed with PBS and left topped up with PBS. Whole wells were imaged using the Cytation5 microscope, with images at 4x taken in rows across the whole well, which were stitched together to form one image. Images were opened in ImageJ and manually counted to calculate osteoclasts/mm^2.

2.11.5 **Analysis of hydroxyapatite pits**

In wells used to analyse resorption by osteoclasts, 10% hydrogen peroxidase (H_2O_2, cat: H1009; Sigma-Aldrich) was added for 5 minutes to remove all attached cells.[537] Peroxidase was washed off with PBS, which was also removed and wells allowed to air dry. Once dry, wells were imaged as described in Section 2.11.4 to generate images of whole wells. Images were then opened in ImageJ and colour threshold was manually changed to distinguish and select resorbed from intact hydroxyapatite. These areas were measured using the measurement tool and presented as area of OsteoAssay™ plate resorbed as a percentage of total well coverage.

2.11.6 Dentine assay for osteoclast resorption

To investigate human osteoclast resorption, cells were cultured on dentine provided by Dr James Edwards (University of Oxford, Oxford, UK). Monocytes were isolated as in Section 2.11.3 and plated at 2 x 10^5 cells/well in a 96 well plate contraining small dentine disks. Cells were differentiated (Section 2.11.3) for a total of 21 days with media changed every 3rd day. In addition, PEPITEM (10ng/ml) or S1P (1µM) were added at each media change. After 21 days, dentine disks were then treated with 1M NH_4OH (cat: 205840010; Thermo Scientific Acros, Belgium) overnight, washed in distilled water and sonicated. Disks were then air dried and 0.5% Toluidine Blue in 0.5% Boric acid (pH 7.4) was added for 2 minutes to stain resorption pits. Dentine was then washed with distilled water, air dried and mounted onto slides using DPX mountant for histology (cat: 06522, Sigma-Aldrich) and a coverslip was added. Slides were imaged using the slide scanner axioscan Z1 with a Z stack to ensure all the dentine was in focus and saved as Zen files. Analysis was performed by creating a manual mask over the stained resorption pits and percentage of the total dentine disk resorbed by the osteoclasts was calculated.

2.11.7 Resazurin proliferation assay

RAW264.7 cell proliferation was analysed using resazurin.[538] Cells were plated and cultured for 5 days (Section 2.11.2). On day 5, known densities of RAW264.7 cells were plated into 48 well plates in cell densities varying from 0 - 2 x 10^6 to generate standards. Resazurin sodium salt (cat: R7017; Sigma-Aldrich) was diluted 10X in media and 100µl was added to each well and left for 4 hours, at which point media was transferred into a 96 well plate in duplicate and read on a Synergy HT plate reader at a wavelength of 570nm. A standard curve was generated using the

known cell number reads and used to calculate the number of cells present in each treatment group, and thus the level of proliferation.

2.12 Short interfering RNA knockdown of Cadherin-15

Calvarial and human osteoblasts were plated as in Section 2.10 and allowed to reach 80% confluence. For siRNA knockdown, first Opti-MEM (cat: 31985062, ThermoFisher) was mixed with Lipofectamine RNAiMAX reagent (cat: 13778030, Invitrogen, Hertford, UK) in a ratio of 50:3. In addition, Opti-MEM was combined with a mix of 4 relevant siRNAs or an siRNA control (Table 2.6, Qiagen, Manchester, UK) in a ratio of 50:1. Diluted siRNA and diluted Lipofectamine were then mixed 1:1 and incubated at room temperature for 5 minutes. The siRNA-Lipid complex was added to each well of a 48 well plate to a final concentration of 2.5pmol of each siRNA/well and incubated for 6 hours, before media was replaced with basal osteoblast media without antibiotics. Cells were cultured for up to 4 days with some wells supplemented on day 1 and day 3 with 10ng/ml PEPITEM. Cells were then analysed by qPCR or protein expression via western blot and flow cytometry.

2.13 RNA Extraction and cDNA conversion from cultured cells

RNA extraction from calvarial osteoblasts, human osteoblasts, human osteoclasts and RAW264.7 cells was performed using the RNeasy kit (cat: 74104; Qiagen) following the manufacturer's instructions. RLT buffer supplemented with 1% β-mercaptoethanol (cat:M6256; Sigma-Aldrich) was added to wells for 10 minutes before they were scraped, and pellets were broken up using a 19G needle. Samples were vortexed to further break up the cell suspension, before being centrifuged at 18,000g for 1 minute at room temperature (these centrifuge conditions were used for all future spins). Ethanol (70%) was added to each sample and cells were transferred

to RNA easy spin columns and spun for 2 minutes before addition of RW1 buffer was added to the top of the column and spun again. DNase incubation mix (1 part DNase to 7 parts Buffer RDD (cat: 79254; Qiagen)) was added to samples for 15 minutes. RW1 was again added, samples spun for 1 minute, washed with 500µl of RPE and spun for a further minute. Ethanol (80%) was added to each column and were spun for 2 minutes, columns were transferred to a new collection tube and spun dry for a further 5 minutes or until ethanol could no longer be detected. RNAse free water (cat: 129112; Qiagen) was then added to the top of the filter and run through twice, each time spinning for 2 minutes. Samples were then analysed on the Nanodrop 2000 (cat: ND2000CLAPTOP; ThermoFisher) to record the amount of RNA collected and the mRNA quality (260/280). A 260/280 ratio of 2±0.15 was deemed acceptable for cDNA conversion. Samples were then stored in the -80°C until cDNA conversion.

mRNA from each sample was converted to cDNA using a high capacity cDNA reverse transcription kit as per the manufacturer's instructions (cat: LT-02241; Applied Biosystems, Cheshire, UK). A master mix was made up containing 1x RT buffer, 1x dNTP mix, 1x random primers and 50 units random primers. mRNA (500ng) was added to 5.8 µl of master mix and nuclease free water (cat: 129114, Qiagen) was used to bring the total volume to 20µl. Using the mastercycler nexus GSX1 (Eppendorf), samples were heated to 25°C for 10 minutes, 37°C for 120 minutes and then 85°C for 5 minutes before being held at 4°C. Following conversion to cDNA, samples were stored at -20°C until required for polymerase chain reaction (PCR) analysis.

2.13.1 **PCR analysis**

cDNA from Section 2.13 was diluted 1:3 in nuclease free water. Gene specific Applied Biosystems Assay on Demand TaqMan primers (Table 2.7) were diluted 1:10 in master mix (cat: 4369016; Applied Biosystems). Using a E1-Clip Tip Electronic Pipette (ThermoFisher), 2.3 µl of cDNA and 2.7 µl of the primer/master mix solution was added to each well of a 384 LightCycler® 480 Multiwell Plate (cat: 04729749001; Roche, Hertfordshire, UK). Three technical repeats were conducted for each sample. The plate was sealed with a MicroAmp™ Optical Adhesive Film (cat: 4311971; Applied Biosystems) and centrifuged at 300g for 2 minutes at 20°C.

The quantitative PCR was run on the LightCycler® 480 11/96 (Roche diagnostics, Burgess Hill, UK). Samples were initially heated to 50°C at a ramp rate of 4.8°C/s and held for 2 minutes, followed by heating to 95°C at the same ramp rate and holding for 10 minutes for initial denature. Repeated cycles of heating to 95°C with a ramp rate of 4.8°C/s for 15 seconds, followed by cooling to 60°C with a ramp rate of 2.5°C/s for 1 minute was performed for a total of 40 cycles.

A mean of the three technical repeats was calculated to provide the average CT value. Any values greater than 1SD different from the other two values, or >35 cycles were omitted from the average; if the other two repeats were not within 1.5 cycles that sample was disregarded. The ΔCt value was calculated by subtracting the Ct value for the housekeeping gene from the Ct value for the gene in question, $2^{-\Delta CT}$ was plotted graphically. Alternatively, ΔΔCt was calculated by comparing the ΔCt value from control samples and experimental samples and presented as $2^{-\Delta\Delta CT}$.

Table 2.6. SiRNAs used to target human and murine CDH15.

Flexitube Gene solution GS1013 for CDH15 (Human)
SI04348393 (FlexiTube siRNA)
SI04175829 (FlexiTube siRNA)
SI00341586 (FlexiTube siRNA)
SI00341572 (FlexiTube siRNA)
Flexitube Gene solution GS12555 for Cdh15 (Mouse)
SI00946708 (FlexiTube siRNA)
SI00946701 (FlexiTube siRNA)
SI00946694 (FlexiTube siRNA)
SI00946687 (FlexiTube siRNA)
Negative control siRNA
1027310

Table 2.7. Taqman primers used throughout this thesis

Gene name	Code
B2m	Mm00437762
Cdh15	Mm00483191
Runx2	Mm00501584
S1pr1	Mm00514644
S1pr4	Mm00468695
Sphk1	Mm00448841
Sphk2	Mm00445021
Spns2	Mm01249328
Acp5	Hs00356261
Alpl	Hs01029144
ATP6V0D2	Hs01084784
B2M	Hs99999907
Bglap	Hs01587814
Cdh15	Hs00170504
Ctsk	Hs00166156
E-selectin	Hs00950401
Msr1	Hs00911250
PECAM-1	Hs00169777
Runx2	Hs00231692
S1pr1	Hs00173499
S1pr4	Hs02330084
Sp7	Hs01866874
Sphk1	Hs01116530
Sphk2	Hs01016543
Spp1	Hs00959010
vWF	Hs00169795
Ywhaz	Hs01122445

2.14 RNA sequencing

2.14.1 Performing RNA sequencing

Following isolation of RNA, samples were passed to the University of Birmingham Genomics Service (Birmingham, UK), where each of the following stages were performed. Samples had their RNA integrity number (RIN) calculated using the High Sensitivity RNA ScreenTape® (Agilent, California)[539]. RIN scores for each sample are shown in Figure 2.4. All samples had RIN scores >7, thus allowing library prep to occur.[540] Library prep was performed using the Lexogen QuantSeq 3' mRNA-Seq Library Prep Kit FWD for Illumina (Illumina, California). Samples that passed library prep (15/16) were pooled in equal volumes and quality checked by the Genomics service using the Agilent TapeStation DNA 1000 tape (Aligent) and DNA HS Qubit™ (Fisher Scientific). Sequencing was then performed using the NextSeq 500 (Illumina), where the run had a Yield (Gbp) of 44.86 and an average %Q30 of 90.13, indicating a successful run and analysis could be performed in house.[541,542]

2.14.2 RNA sequencing analysis

All scripts used for bulk sequencing analysis are shown in Appendix 9.1 - 9.3. Data generated were provided in .fastq format, where quality of each sample could be checked using FASTQC and MULTIQC packages in Rstudio (RStudio Public-benefit corporation).[543] Four reads were generated for each sample, which were combined and subsequently trimmed. Trimming was performed using BBMap to remove the polyA tail, low quality RNA (Using the Phred quality score algorithm) and contaminating adaptor regions.[544] FASTQC was performed to visualise the changes in RNA quality.

In order to align the genome, a genome index was created using a pre-assembled genome from ensembl.[545] The “Mus_musculus.GRCm39.104.gtf” genome and corresponding primary_assembly file were used to create the genome used for our analysis. Trimmed sequences were then aligned to the newly created genome using the STAR align package and the Encode standard settings.[546] MultiQC was performed on FastQC files generated from the aligned samples and each parameter was checked to ensure quality of pre-processing.

Feature counts were produced using the Subread package to generate a table of gene counts,[547,548] which could be analysed using DESeq2 to explore differentially expressed genes.

2.14.3 **Analysis of differentially expressed genes and pathways.**

Feature counts were loaded into R and analysed using DESeq2.[549] First counts per million (CPM) were calculated for each gene, and a threshold was generated to remove genes with a CPM value of <10. A DESeq dataset was generated using the filtered count data, accounting for batch within the design. Contrasting genes with a P value of <0.05 were generated from the dataset and a histogram was produced to explore the range of P values across the sample. Our data showed anti-conservative p-values, meaning subsequent analysis could continue. Differentially expressed genes were named using the ensemble database and analysed for Log_2 fold change.[545]

Differentially expressed upregulated or downregulated genes were separated and pathway analysis was performed using gseGO or enrichGO to identify key pathways, which were visualised using a range of plots.[550] Alternatively all differentially expressed gene pathways (upregulated and downregulated combined) were analysed

using gseKEGG.[550] Differentially regulated pathways could be explored using a range of plots and visualised using pathview.[551]

2.15 Analysis of single-cell sequencing data sets

Barcode, Gene and Matrix files for data sets GSE147174[552] (script in 9.4) and GSE128423[553] (Script in 9.5) were downloaded from GEO Accession viewer and analysed using the Seurat package in R.[554–557] Seurat objects were created for each repeat run and merged to create a singular large Seurat object. For GSE147174 each run represented a different time-point as opposed to individual repeats, so the SplitObject parameter was used to ensure samples could be analysed as one dataset, but also as individual timepoints. Seurat objects were processed to remove cells with RNA counts of <200 and >6000, and mitochondrial counts of <5. Data were normalised and variable features were found between each cell. Samples were plotted using a PCA and clusters were generated using a resolution of 0.5. Clusters were visualised using a TSNE plot and differences between the clusters were identified using the FindAllMarkers setting in Seurat. The top differentially regulated genes from each cluster were used to manually identify the cell types in each cluster, which were renamed. Samples were then split into subsets to look at the cells of interest (GSE128423 – osteoblasts (Figure 9.1), GSE147174 – monocytes, macrophages, and osteoclasts), from which clusters could again be generated and named to identify differing maturation stages of cells. Gene expression changes in each cluster of the newly generated subsets could be visualised using violin plots, feature plots and dot plots.

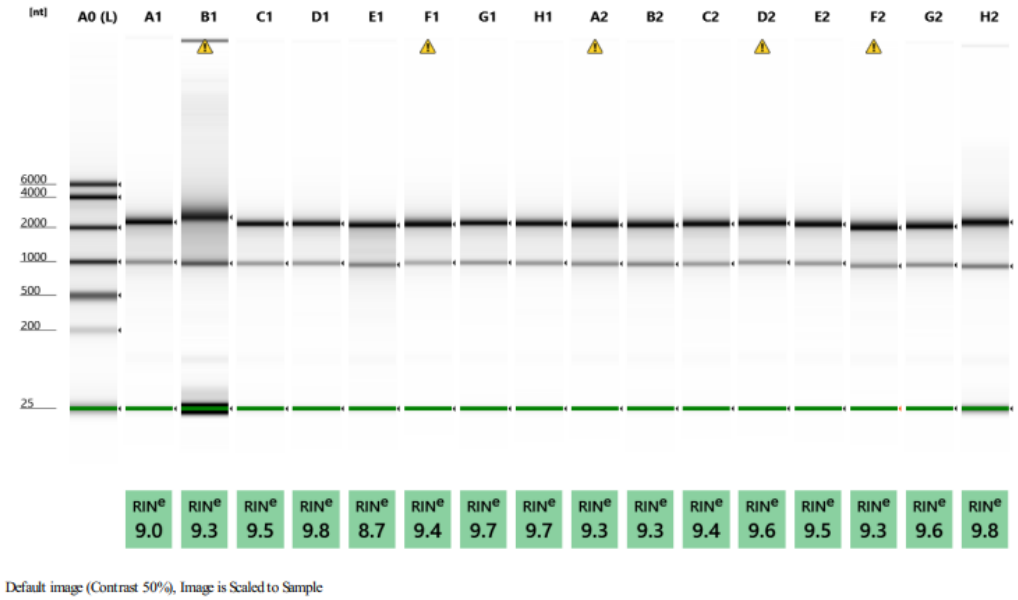

Figure 2.4. RIN scores calculated for each RNA sample.

Following RNA isolation, samples were analysed for RIN score using the High Sensitivity RNA ScreenTape® to ensure all samples had a RIN >7.

2.16 Western Blot

Protein isolation from cells was performed using RIPA buffer (cat: R0278; Sigma-Aldrich) containing 1X PhosStop (cat: 4906845001; Merck) and 1X cOmplete™ Mini Protease Inhibitor Cocktail (cat: 11836153001; Merck). First, cells were washed with ice-cold PBS and RIPA buffer was added to the well. Cells were scraped and transferred into an Eppendorf and kept under constant agitation for 30 minutes on ice, before being centrifuged at 12,000g for 20 minutes. Supernatants were transferred into a fresh tube and stored at -80°C until needed.

Protein quantification was performed using the Peirce BSA Protein Assay (cat: 23225; ThermoScientific). Briefly, BSA standards were made up into concentrations from 0µg/ml to 2000µg/ml by dilution in RIPA buffer. 25µl of samples or standards were added to a 96 well plate in duplicate. Working reagent was produced by mixing 50 parts of BCA Reagent A with 1 part of BCA Reagent B, and 200µl was added to each well. Plates were kept in foil for 30 minutes at 37°C and then read on the Synergy HT plate reader using wavelength 562nm. The blank (0µg/ml) read was subtracted from all other reads before analysis of protein concentration. Standards were plotted and a standard curve was created to allow quantification of protein concentration in the samples.

Samples (20µg protein/sample) or PageRuler Plus Prestained Protein Ladder (cat: 26620; ThermoScientific) were mixed 1:1 with 2x Laemmli sample buffer (cat: 1610757; BioRad, Watford, UK) and heated to 95°C on the Eppendorf ThermoMixer C (cat: EP5382000015; Eppendorf) for 5 minutes, before being spun briefly to remove condensation. Criterion 10% Tris-HCL protein gels (cat: 3450009; BioRad) were then prepared by adding Tris/Glycine running buffer to a Criterion™ Cell buffer

tank (cat: 1656001; BioRad) and filling in the tank till all the wells were submerged. The comb was then removed, and the ladder (5µl) and samples were loaded into adjacent wells. Proteins were separated using a 100V current PowerPac Basic Power supply (cat: 1645050; BioRad) for 90 minutes. Following protein separation, the gel was transferred onto a PVDF membrane using the Trans Blot Turbo Midi 0.2mm (cat: 170415; BioRad). The gel was opened and laid flat on top of the membrane. The second half of the membrane was then placed on top, and the gel was flattened gently using a roller. The gel-membrane sandwich was then placed into the Trans-Blot Turbo transfer system (cat: 1704150, BioRad) and run using the MIDI gel settings for 7 minutes to transfer the protein.

To stain the membranes, first membranes were blocked with 5% milk diluted in TBS-T for one hour under constant agitation. Membranes were then washed with TBS-T, and primary antibody (Table 2.8) diluted in 5% milk was added and kept overnight at 4°C. The next day, membranes were washed with TBS-T three times and a HRP conjugated antibody was added (Table 2.8). After 1 hour of incubation, membranes were washed with TBS-T and 4ml of Immobilon Western HRP substrate peroxide solution and Immobilon Western HRP substrate Luminol Reagent mixed 1:1 (cat: WBKLS0500; Millipore) was added for 1 minute. Membranes were imaged using the ChemiDOC MP Imaging system (BioRad) with images taken from an exposure of 0.1s to 30s and a brightfield image taken of the ladder. Membranes were then stripped for 1 hour using ReBlot Plus 1X mMild Antibody Stripping Solution (Sigma-Aldrich) diluted in PBS before staining could begin with any subsequent antibodies.

Images taken were quantified by comparison of band intensity of protein of interest and housekeeping protein using ImageJ.

2.17 Immunofluorescence staining of cells

In order to visualise cellular protein expression, cells were stained with immunofluorescent markers and imaged. To begin, cells were plated onto round (cat: DV40008; ThermoFisher, Loughborough, UK) or square (cat: 3800105; Leica) cover slips in 24 or 6 well plates respectively. When cells were ready to be imaged, they were washed with PBS before fixation in 10% buffered formaldehyde for 15 minutes at room temperature. Formaldehyde was then removed, and cells were washed twice with PBS. Primary antibodies were made up at in PBS at the concentrations shown in Table 2.9 and 100µl of antibody cocktail was added to the cover slips. Cells were left for 1 hour at room temperature to allow binding before washing with three times with PBS. Secondary antibodies and phalloidin were made up as in Table 2.9 and added to the cells for 40 minutes at room temperature in the dark. Antibodies were then removed, and cells were washed with PBS. All liquid was removed from slides and excess was dried gently using tissue. Prolong Gold Antifade Mountant with DAPI (cat: P36935; ThermoFisher) was added onto slides and the cover slips containing cells were placed face down onto the mounting media. Slides were left to dry in the dark overnight and then stored at -20°C for longer term storage.

To image the cells, slides were imaged using either the Zeiss LSM 780 (Zeiss) or the Leica SP8 AOBS-HyD CONFOCAL system (Leica) and stored as .Zen files.

Table 2.8. Western antibodies

Protein Target	Catalogue number	Company	Host	Dilution	Conjugate
Mouse/Human Cadherin-15	Ab129078	Abcam	Rabbit	1/1000	N/A
Mouse/Human B-actin	4967S	Cell signalling	Rabbit	1/1000	N/A
Anti-Rabbit secondary	7074S	Cell signalling	Mouse	1/10000	HRP

Table 2.9. Immunofluorescence antibodies

Antibody target	Catalogue number	Company	Concentration	Colour	Host
Cadherin-15	800516	Biotech	1:100	N/A	Rat
Talin-1	Ab71333	Abcam	1:100	N/A	Rabbit
Vinculin	700062	Invitrogen	1:100	N/A	Rabbit
Phalloidin	Ab176753	Abcam	1:1000	AF488	N/A
Anti-Rat	A11081	Life Technologies	1:100	AF546	Goat
Anti-Rabbit	A11043	Life Technologies	1:100	AF488	Goat
Anti-Rabbit	711-606-152	Jackson Immuno Research[1]	1:200	AF647	Donkey

[1]Jackson Immuno Research; Cambridgeshire, UK

2.18 Intracellular flow cytometry

To further analyse protein expression, intracellular staining was performed. First cells were trypsinised and spun at 300g for 4 minutes to remove all media. Cells were the stained with the Zombie Violet™ Fixable Viability Kit (cat: 423113; BioLegend, London, UK) using a 1/1000 dilution in PBS. Positive control cells had cell death induced by ethanol for 10 minutes, before being mixed with live control cells. Cells were then fixed and permed using the eBioscience™ Foxp3 / Transcription Factor Staining Buffer Set (cat: 00-5523-00; Invitrogen) as per the manufacturer's instructions. Briefly, the Fixation/Permeabilization concentrate was diluted 1:3 in Fixation/Permeabilization diluent and 1ml was added to the cells for 15 minutes. Samples were then washed twice with 1x Permeabilization Buffer diluted in diH_2O, spun at 300g for 4 minutes in between washes. Fixed and permeabilised cells were incubated with mouse M-cadherin/cadherin-15 antibody (cat: MAB7677; R&D systems) or Rat IgG2a kappa Isotype Control (cat: 14-4321-82; Invitrogen) diluted 1:100 in 1x Permeabilization Buffer for 30 minutes. Samples were then washed twice with 1x Permeabilization Buffer and stained with a PE Goat anti-Rat secondary (1:100, cat: A10545; Invitrogen) for 30 minutes. Samples were then washed a further 2 times, before resuspension in 200µL of 2% BSA in PBS and transferred into 12x75 mm polystyrene tubes (BD Biosciences, Berkshire, UK). Single fluorochrome stained controls were run on the 4-laser Fortessa X20 flow cytometer (BD Biosciences) and automatic compensation was applied using the FACSDiva software (BD Biosciences). Samples were then run and exported as .FSC files.

Analysis of flow cytometry data was performed using FlowJo (BD Biosciences). Cells were selected based on forward and side scatter and gating for live cells using

the positive control cells. Median fluorescent intensity (MFI) for PE-expression in each sample was analysed and presented as MFI of sample compared to isotype control.

2.19 Statistical analysis

Statistical analysis was performed on GraphPad Prism 8.0 (GraphPad, San Diego, USA). All data shown are means ± standard error of mean (SEM). Normality was first tested for via the Kolmogorov-Smirnov test. For *in vivo* experiments comparing independent data, unpaired student's t tests were performed, whilst paired samples were run by a paired t test. For multivariant analysis, a one-way or two-way ANOVA was used depending on the number of independent variables, followed by a post-hoc Bonferonni test. Significance levels were set at $P<0.05$, with only significant values represented by * on figures.

3 Investigating the Effect of PEPITEM on Healthy Bone

3.1 Introduction

Understanding the impact of potential therapeutics on healthy bone is essential in beginning to comprehend a drugs full function and its impact directly on the key bone cells, osteoblasts, and osteoclasts.

Currently approved therapeutics for bone loss, such as parathyroid hormone (PTH) and bisphosphonates boost bone growth in homeostatic mice.[328,395,558] In addition, key roles for boosting osteoblast mineral production (PTH)[95,392,559,560] or inhibiting osteoclastogenesis and resorption (bisphosphonates)[311,316,561] were revealed by *in vitro* studies. However, they also revealed that PTH treatment was highly dependent on dosing regime,[397,398] duration of treatment[393] and cell-cycle point of the cells.[559] In addition, the presence of osteoblasts coupled with PTH treatment *in vitro* led to a significant increase in osteoclast resorption potential.[562] Alternatively, homeostatic investigation also revealed the requirement for bisphosphonates to be taken in a fasted state,[343,344] leading to increased absorption, but decreased patient compliance. Thus, homeostatic testing not only reveals the direct actions of a therapeutic, but also explores treatment nuances and disadvantages.

Peptide inhibitor of transendothelial migration (PEPITEM) is a novel endogenous 14 amino acid peptide that has been shown to reduce bone damage in murine models of inflammatory arthritis,[473,496] however, whether this is due to altered bone remodelling directly or through reduced inflammation remains unknown.

Here we explore the effect of PEPITEM on bone formation and resorption *in vivo* and *in vitro* investigating direct effects on bone architecture, in addition to murine and human osteoblast and osteoclast activity.

3.2 Results

3.2.1 Investigating short term PEPITEM treatment on trabecular and cortical bone *in vivo.*

PEPITEM has previously been observed to decrease bone damage in a murine model of inflammatory arthritis.[496] In order to identify whether PEPITEM can influence bone remodelling in an inflammation independent manner, we explored homeostatic bone response to PEPITEM treatment *in vivo*. Mice were treated with PEPITEM or PBS control daily for 14 days before vertebrae and tibiae were analysed for trabecular and cortical bone parameters by µ-CT (Figure 3.1). To understand changes in bone formation, tibia trabecular bone was analysed, and an altered trabecular structure was observed in PEPITEM treated mice (Figure 3.2). After two weeks of treatment, tibia bone volume density (BV/TV) was significantly increased in mice treated with PEPITEM compared to PBS control mice (Figure 3.3A). PEPITEM treatment also significantly increased trabecular number and trabecular thickness, whilst it significantly decreased trabecular separation compared to controls (Figure 3.3B,C,D). A decrease in trabecular pattern factor, a parameter of bone structure that negatively correlates with bone strength,[563] was also observed in PEPITEM treated mice (Figure 3.3E), indicating more interconnected, stronger bone. Like trabecular bone, cortical bone was analysed by µ-CT analysis of tibiae (Figure 3.4). We observed no changes in any of the cortical parameters assessed (cortical area, cross-sectional thickness, and percentage of cortical bone) following PEPITEM treatment in comparison to PBS treated mice (Figure 3.5A-D).

Micro-CT analysis of vertebral trabecular parameters (Figure 3.6, Measured in L4-L6 vertebrae) mirrored those observed in the long bones, with significantly

increased BV/TV, trabecular number and trabecular thickness and decreased trabecular separation and trabecular pattern factor in PEPITEM treated mice compared to PBS controls (Figure 3.7A-E). This suggests that regardless of the bone location, PEPITEM is able to enhance trabecular bone growth or decrease bone resorption.

3.2.2 Dissecting the relationship between PEPITEM treatment and long bone strength

To analyse the functional effects of increased trabecular bone induced by PEPITEM, we performed 3-point-bend tests on femurs from the PEPITEM treated mice to interpret bone stiffness and strength. Generation of force profile traces allowed assessment of the stiffness of the bone, the force at which the bone starts to bend and fail, the total force/work the bone can sustain prior to fracture, and the force at which the bone fractures (Figure 3.8A). We observed a tendency for the stiffness of the bone to be increased in animals treated with PEPITEM, albeit with borderline significance (P=0.0510; Figure 3.8B). Nonetheless, fracture force was significantly elevated in PEPITEM treated mice compared to the control mice (Figure 3.8C). However, no changes were observed in work till fracture or fracture force (Figure 3.8D/E). These findings suggest PEPITEM was able to increase bone strength and stiffness possibly through increasing trabecular bone.

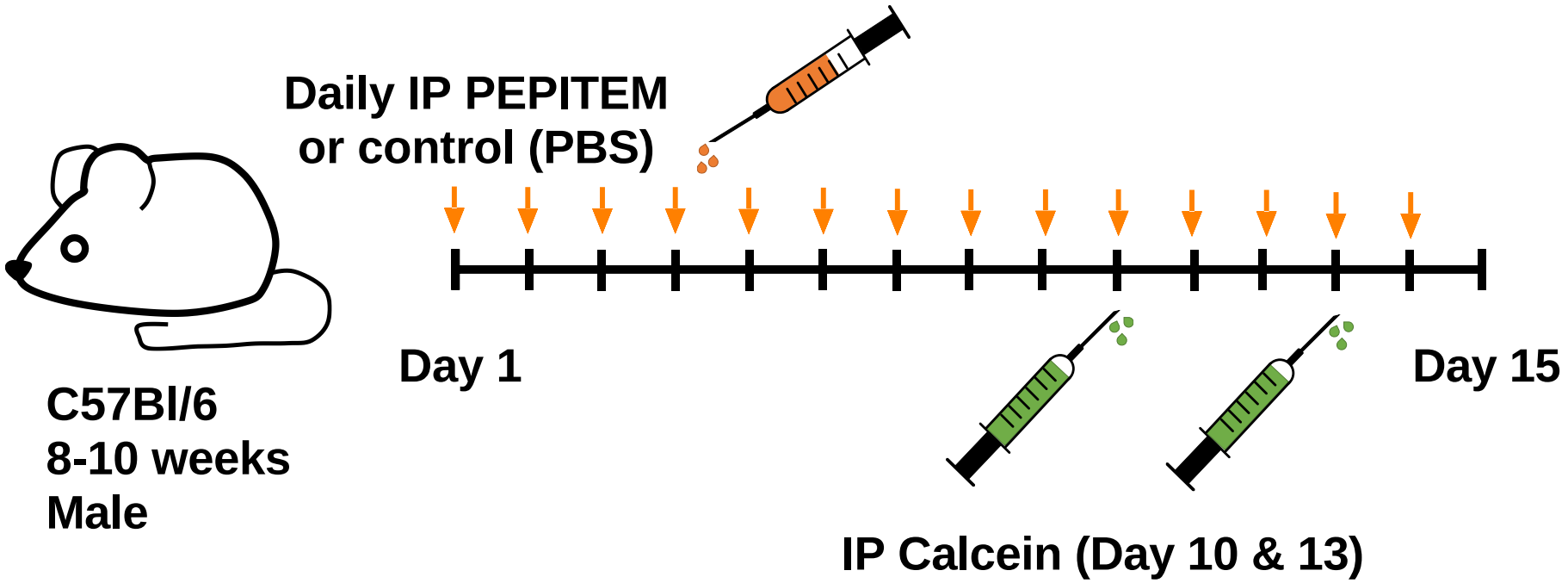

Figure 3.1. *In vivo* model to study PEPITEM's role on bone homeostasis.

WT mice were given daily IP PEPITEM (300µg) or control (PBS) for 14 days. IP calcein was given in combination with daily injections at 6 and 2 days prior to termination of the experiment. Fifteen days post the onset of daily injections, mice were culled, and tissue was collected for analysis.

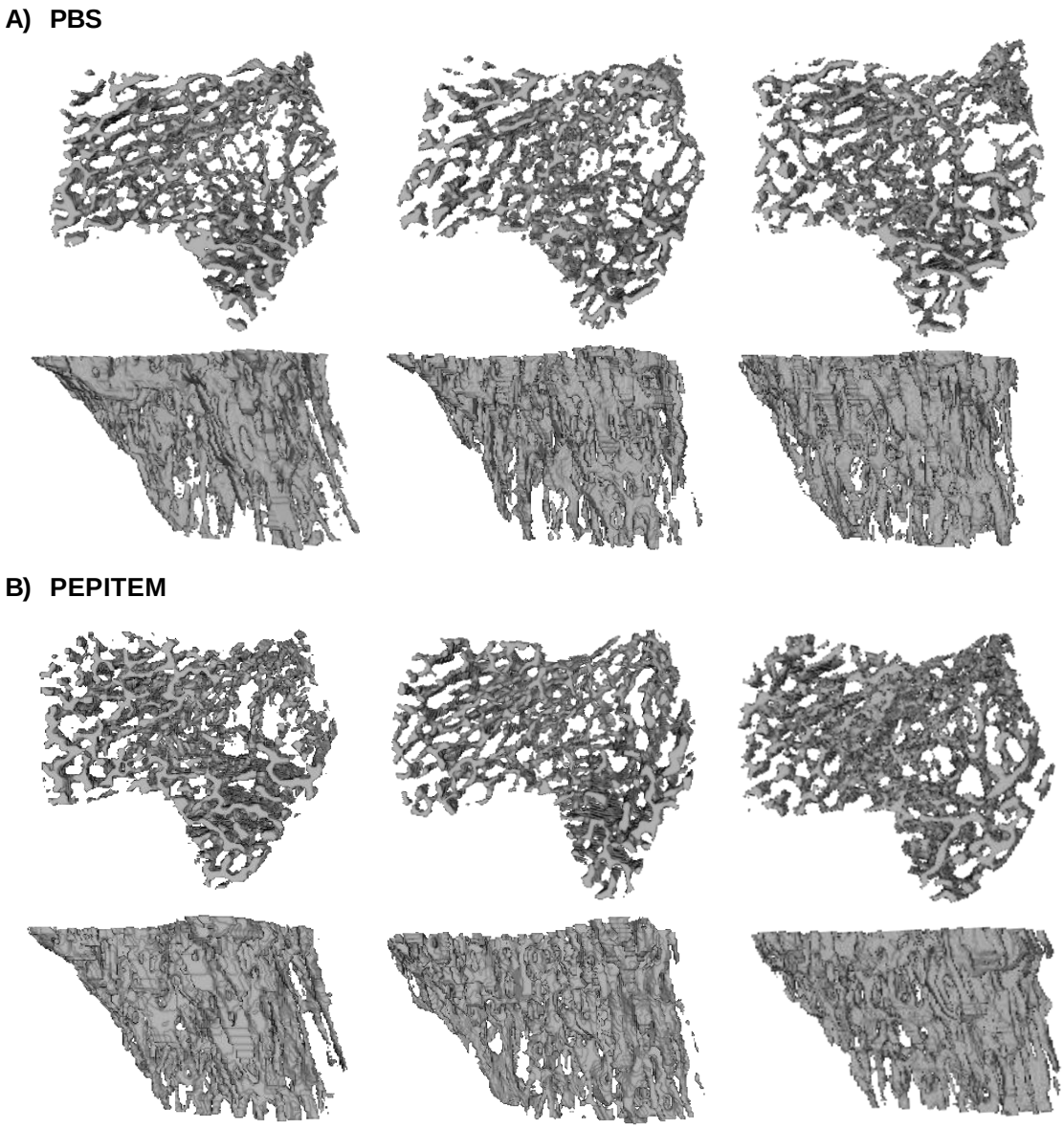

Figure 3.2. 3D models of tibial trabecular bone from PBS and PEPITEM treated mice.

WT mice were treated with PEPITEM (n=8), or PBS control (n=6) and 15 days post the onset of daily injections, mice were culled, and tibiae were dissected, fixed in paraformaldehyde, and scanned by µ-CT. 3D models of trabecular bone were generated and imaged on the transverse and coronal plane. **A-B.** Trabecular bone models from PBS control **(A)** and PEPITEM **(B)** treated mice. Images show trabecular architecture from 3 representative mice.

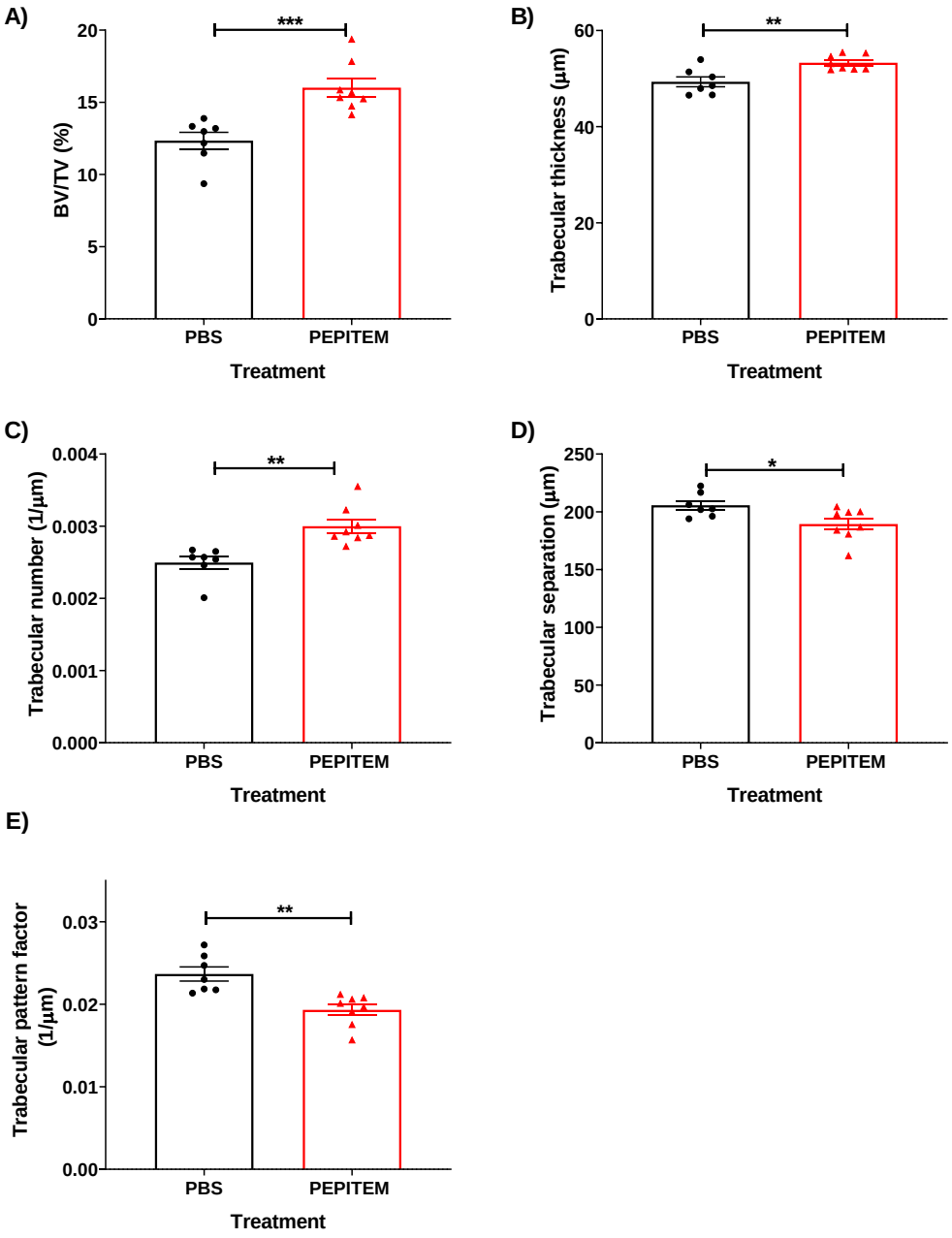

Figure 3.3. PEPITEM increased long bone trabecular bone parameters *in vivo.*

Mice were injected with PBS control (black, n=7) or PEPITEM (red, n=8) for 14 days. Tibiae scanned by µ-CT and regions of interest were drawn around trabecular bone in the metaphysis to analyse trabecular parameters. **A-E.** Trabecular bone was analysed for **A.** trabecular bone volume (BV/TV, %), **B.** trabecular thickness (µm), **C.** trabecular number (1/µm), **D.** trabecular separation (µm) and **E.** trabecular pattern factor (1/µm). Data are mean ± SEM for 3 independent experiments. * = P<0.05, ** = P<0.01 and ***=P<0.001 by student's t-test.

A) PBS

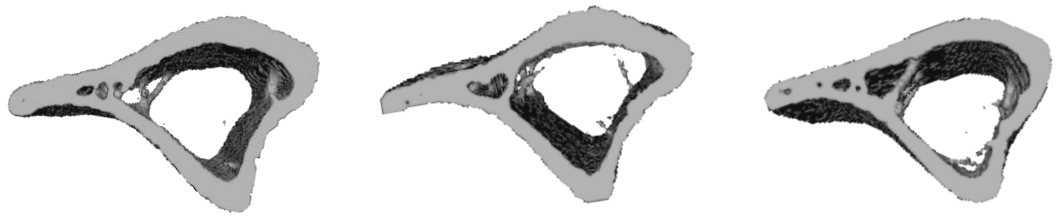

B) PEPITEM

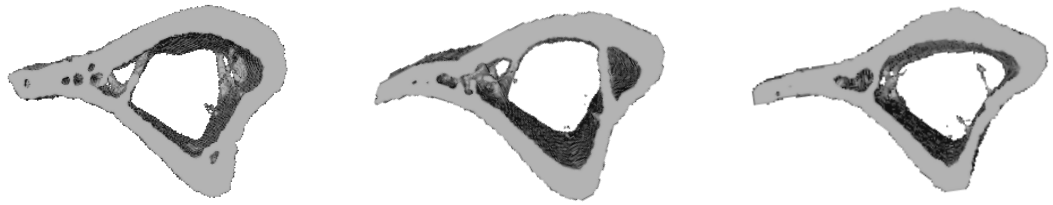

Figure 3.4. 3D models of tibial cortical bone from PBS and PEPITEM treated mice.

Mice were treated with daily IP PEPITEM (n=6) or PBS control (n=6) for 14 days. Fifteen days post the onset of daily injections, tibiae were scanned by µ-CT. 3D models of cortical bone were generated and imaged on the transverse plane. **A-B.** Cortical bone models from PBS control **(A)** and PEPITEM **(B)** treated mice. Images shown are from 3 representative mice per group.

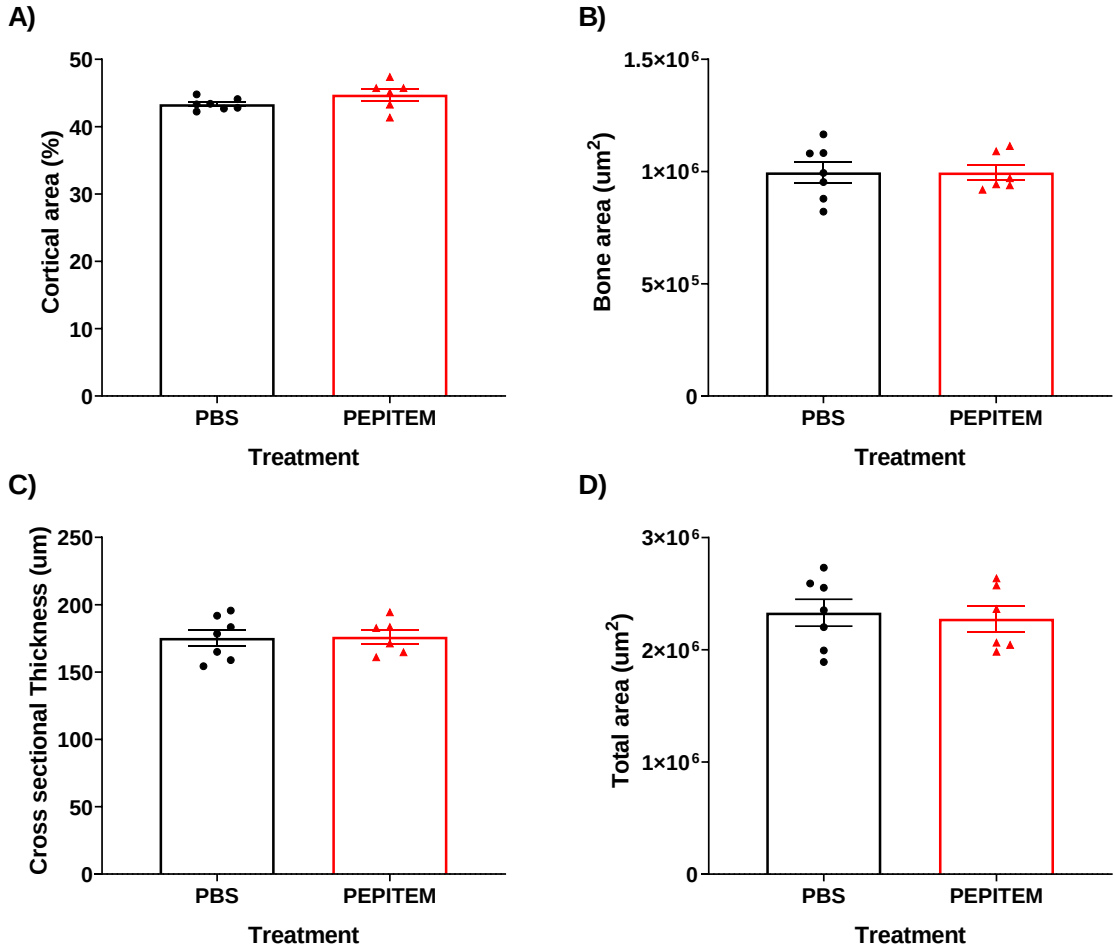

Figure 3.5. PEPITEM had no effect on long bone cortical bone over two weeks.

Mice were injected with PBS control (black, n=7) or PEPITEM (red, n=6) for 14 days. Tibiae scanned by µ-CT and regions of interest were drawn around epiphyseal cortical bone and analysed for cortical parameters. **A-D.** Cortical bone was analysed for **A.** percentage of cortical area (%), **B.** total bone area (µm^2), **C.** total cortical area (µm^2), and **D.** cortical thickness (µm). Data are mean ± SEM for 3 independent experiments.

A) PBS

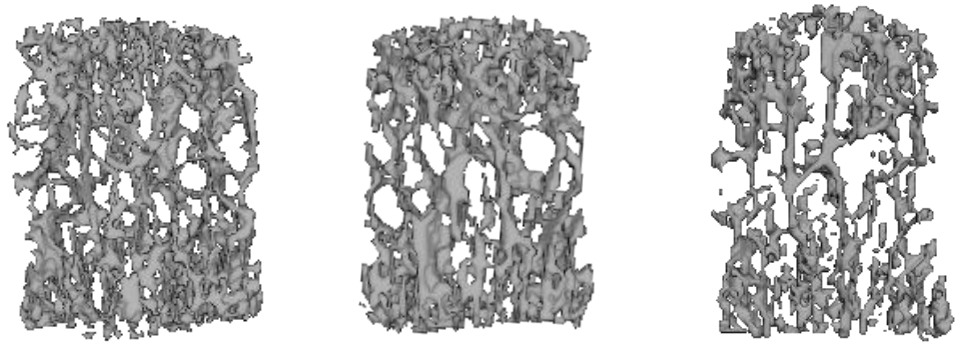

B) PEPITEM

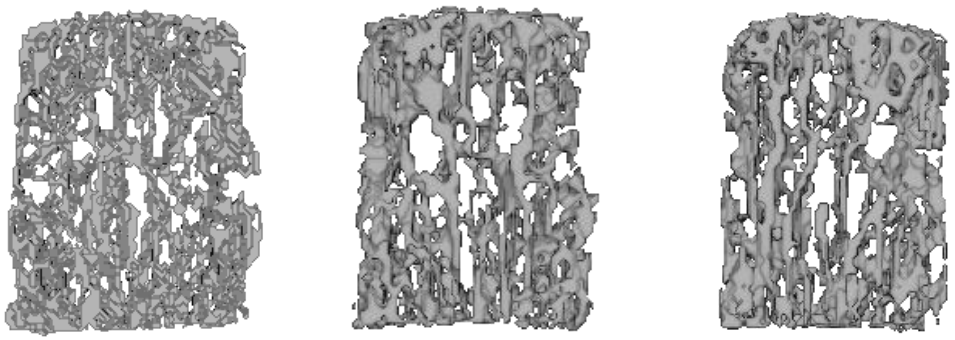

Figure 3.6. 3D models of vertebral trabecular bone from PBS and PEPITEM treated mice.

Mice were treated with PEPITEM (n=8) or PBS control (n=7) for 14 days. Vertebrae were dissected and scanned by µ-CT. 3D models of trabecular bone from vertebrae L4, L5 and L6 were generated and imaged on the coronal plane. **A-B.** Trabecular models of L4 vertebrae from PBS control **(A)** and PEPITEM **(B)** treated mice. Images are representative of 3 mice per group.

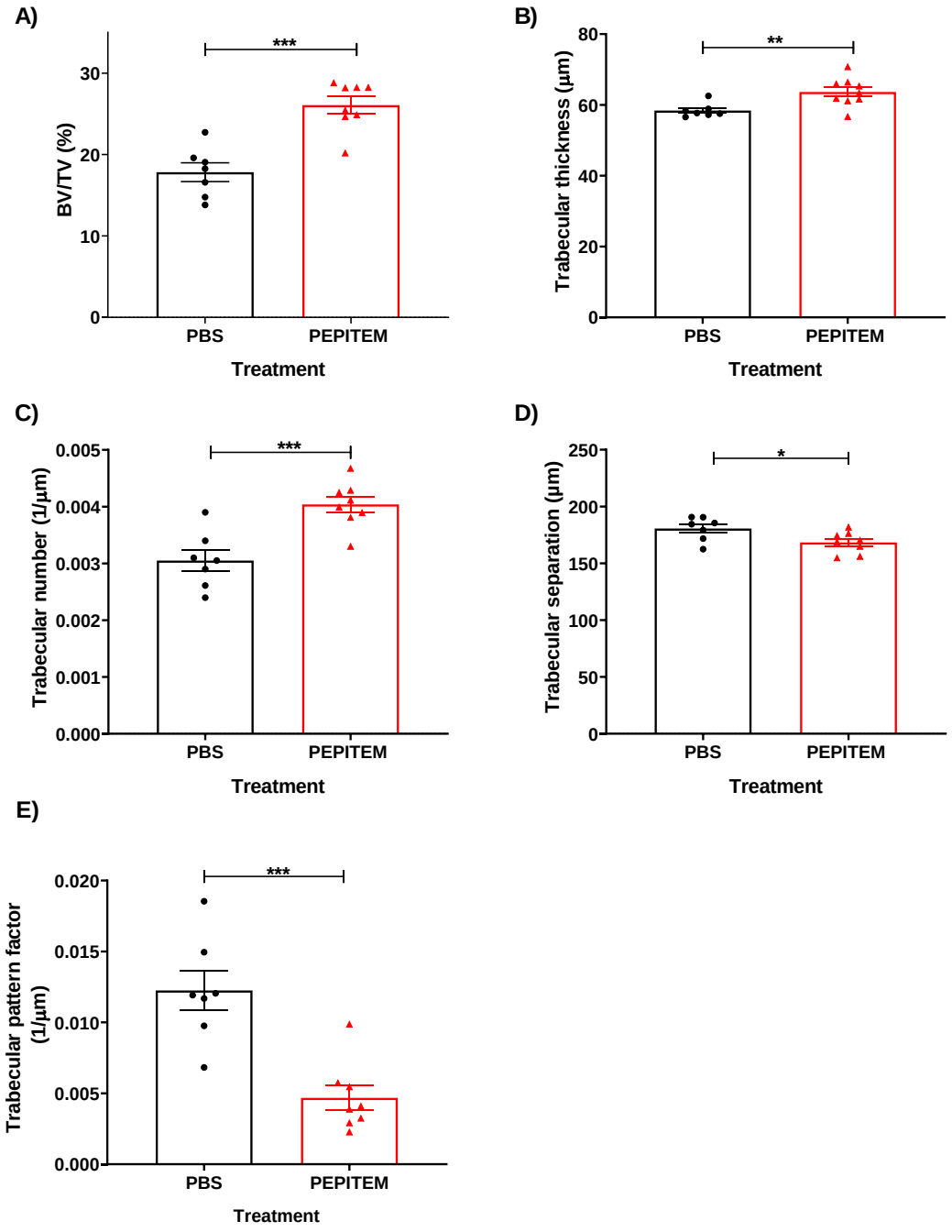

Figure 3.7. PEPITEM increased vertebral trabecular bone parameters *in vivo.*

Mice were injected with PBS control (back, n=7) or PEPITEM (red, n=8 for 14 days. Vertebrae were scanned by µ-CT and regions of interest were drawn around trabecular bone in vertebrae L4, L5 and L6 and analysed for trabecular parameters. **A-E.** Trabecular bone averages from L4, L5 and L6 were analysed for **A.** trabecular bone volume (BV/TV, %), **B.** trabecular thickness (µm), **C.** trabecular number (1/µm), **D.** trabecular separation (µm) and **E.** trabecular pattern factor (1/µm). Data are mean ± SEM for 3 independent experiments. * = P<0.05, ** = P<0.01 ***=P<0.001 by student's t-test.

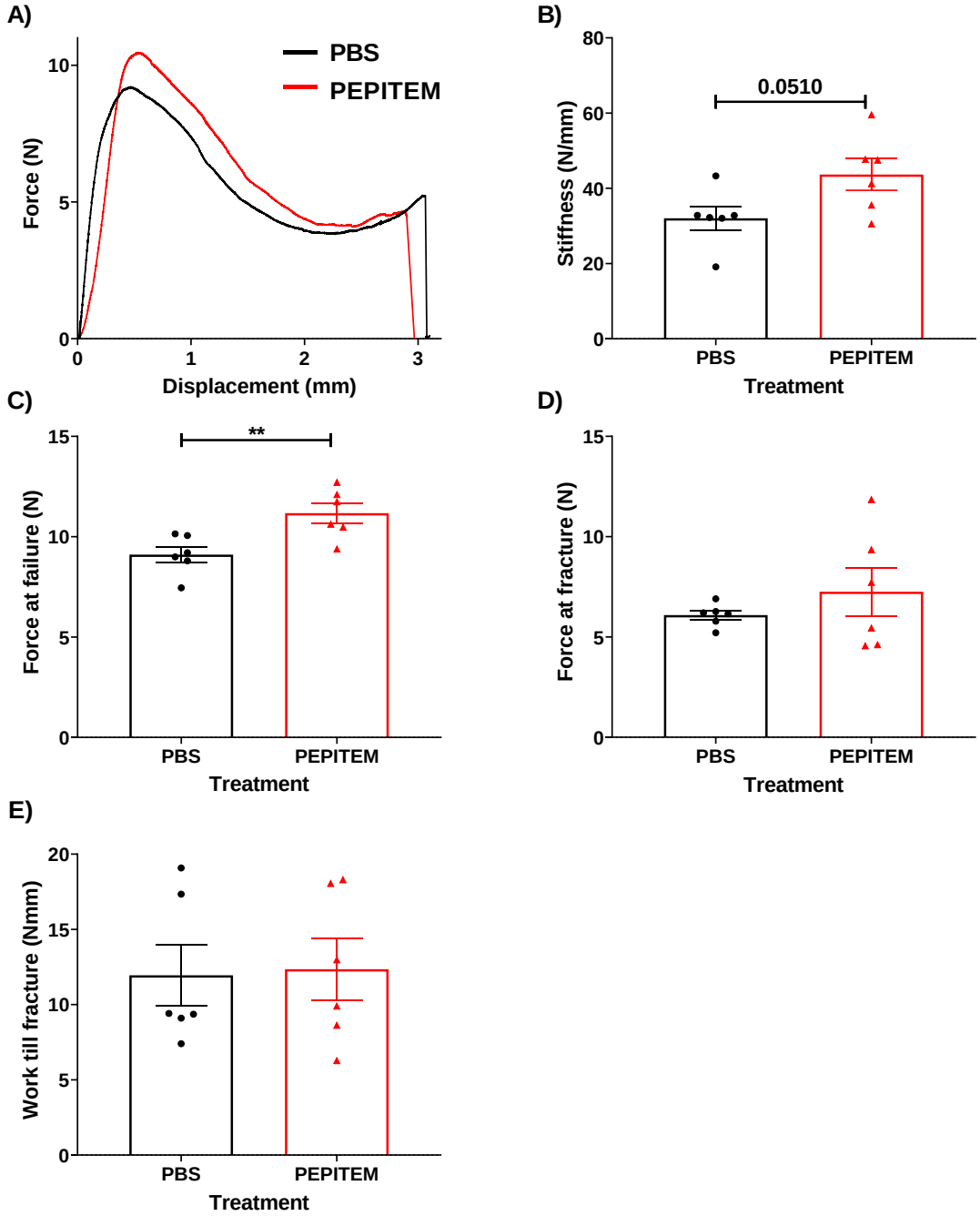

Figure 3.8. Changes in trabecular bone are paralleled by increased bone strength.

Mice were injected with PBS control (black, n=3) or PEPITEM (red, n=3) for 14 days. Femurs were tested by 3-point-bend. **A.** Representative graphs showing displacement of bone (mm) in relation to force applied (N) from PBS or PEPITEM treated mice from 1 femur per group. **B-E.** Force vs displacement plots were analysed for **B.** stiffness (N/mm), **C.** force at failure (N), **D.** force at fracture (N), and **E.** work till fracture (Nmm). Data are mean ± SEM for 1 independent experiment, 2 femurs per mouse. ** = P<0.01 by student's t-test.

3.2.3 Comparison of PEPITEM treatment regimens on trabecular bone response

Given that daily PEPITEM intraperitoneal (IP) injections led to significant increases in trabecular parameters, we explored using altered treatment regimens to better understand the efficacy of PEPITEM treatment. Mice were injected with 300µg I.P PEPITEM every other day (EOD) or subcutaneous (SC) twice weekly with a liposome enclosed PEPITEM (400µg) for a total of 14 days (Figure 3.9). Interestingly, treatment EOD led to no change in any of the trabecular parameters explored (Figure 3.10A-E). However, tibiae trabecular BV/TV significantly increased in mice treated with PEPITEM enclosed in a liposome compared to control liposomes (Figure 3.11A). This increase was matched by significant increases in trabecular number and decreases in trabecular pattern factor (Figure 3.11C/E). However, changes in trabecular thickness and trabecular separation were not significant compared to control (Figure 3.11B/D). Nonetheless, twice weekly treatment with PEPITEM in a liposome showed a similar percentage change in all trabecular parameters when compared to daily I.P PEPITEM injections (Figure 3.12A-E).

3.2.4 Investigating the effect of PEPITEM on bone mineral production

Increases in trabecular bone from PEPITEM treatment could be a result of enhanced osteoblast induced mineral deposition or decreased osteoclast driven resorption. To determine the cause, bone formation parameters were analysed. Mice treated with PEPITEM or PBS (Section 3.2.1) were IP injected with calcein 6 and 2 days prior to dissection (Figure 3.1). As calcein incorporates into newly remodelled bone, the calcein labels were used to calculate the amount of mineral produced normalised to the time between injections (distance between the calcein labels)

(Figure 3.13A). Mineral apposition rate (MAR) trended towards an increase in PEPITEM treated mice when compared to PBS control (Figure 3.13C). Bone formation rate (BFR/BS) and total length of double-labelled line spacing (d.LS/BS) were further analysed to identify normalised levels of bone formation and the amount of the bone perimeter forming bone, showing a slight increase in PEPITEM over PBS treated mice (Figure 3.13B/D). Overall, these data indicate a role for increased mineralisation in PEPITEM treated bones, enhancing trabecular bone growth. However, changes in delivery mechanisms following liposome delivery may alter PEPITEMs mechanism of action, promoting differing changes in bone which needs to be investigated further.

To further analyse this trend towards increased rate of mineral deposition in mice treated with PEPITEM, we isolated serum from the blood of WT mice treated with PEPITEM for 14 days and analysed bone production marker pro-collagen peptide (P1NP) concentration by a competitive ELISA. However, no changes in serum P1NP concentration were observed between PEPITEM and PBS treated mice (Figure 3.14A).

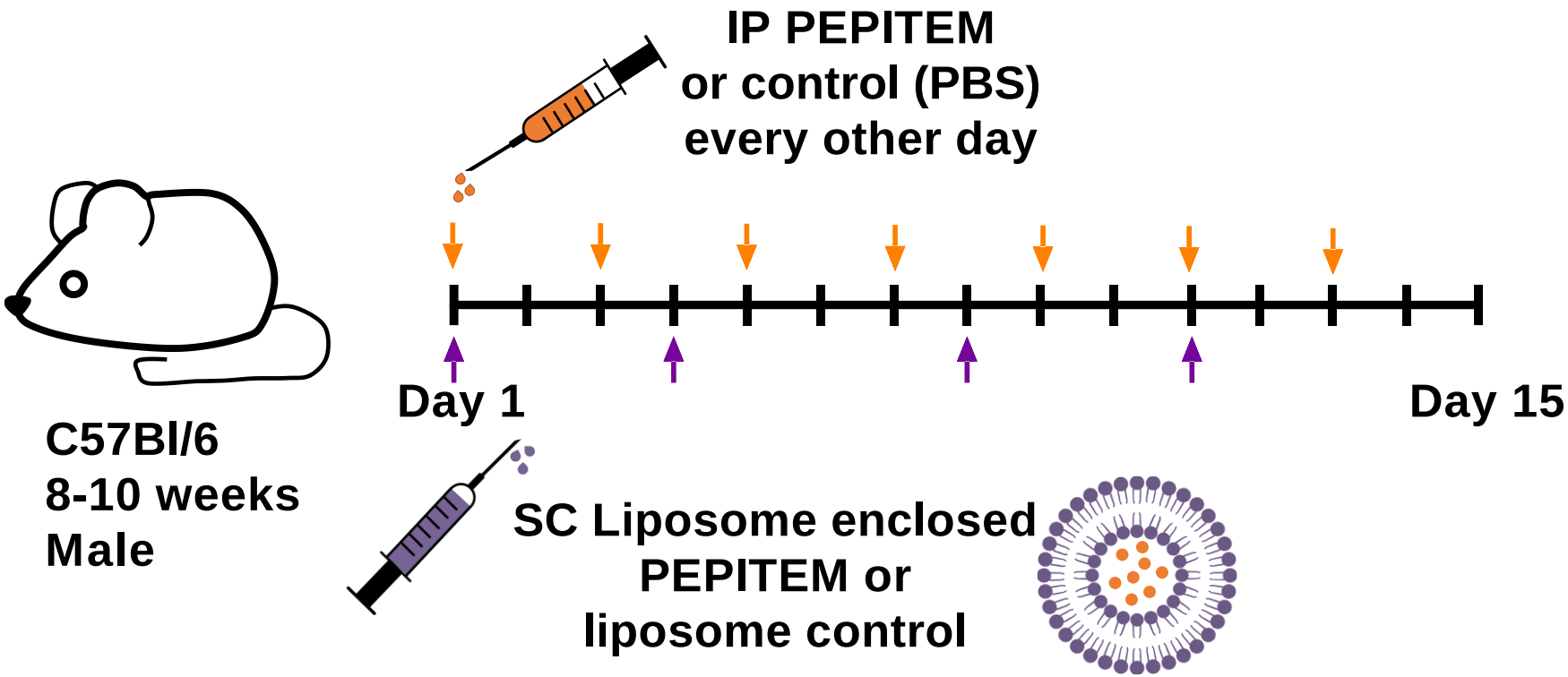

Figure 3.9. Treatment regimens to study PEPITEM action in bone.

Mice were given IP PEPITEM or control (PBS) every other day or SC PEPITEM enclosed in a liposome or control liposome twice weekly for 14 days. Fifteen days post the onset of injections, mice were culled, and tissue was collected for analysis.

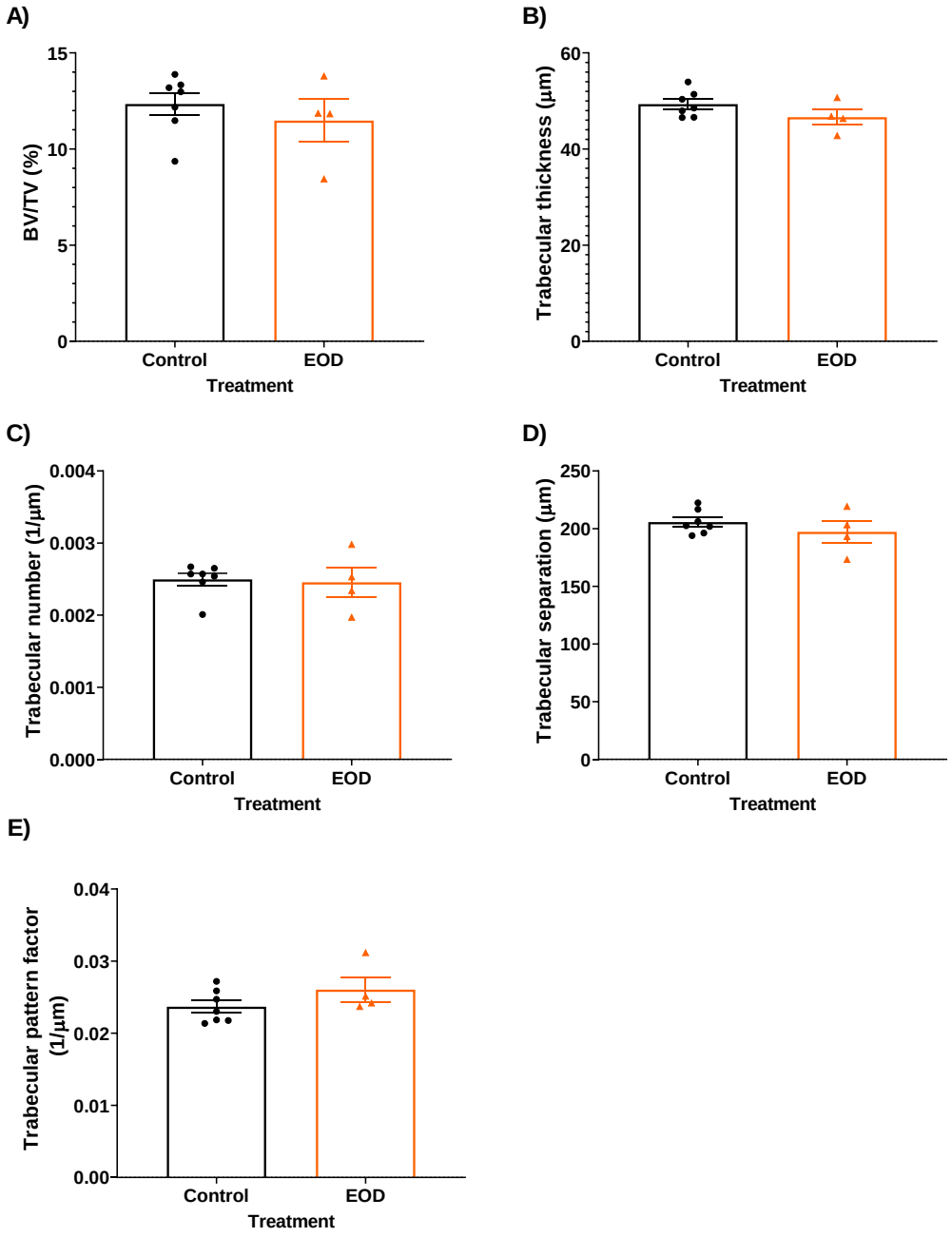

Figure 3.10. Tibiae trabecular bone was not increased by every other day PEPITEM treatment.

Mice were injected with PBS control (black, n=7) or PEPITEM every other day (EOD, orange, n=4) for 14 days. Tibiae were scanned by µ-CT and regions of interest were drawn around metaphyseal trabecular bone and analysed for trabecular parameters. **A-E.** Trabecular bone was analysed for **A.** trabecular bone volume (BV/TV, %), **B.** trabecular thickness (µm), **C.** trabecular number (1/µm), **D.** trabecular separation (µm) and **E.** trabecular pattern factor (1/µm). Data are mean ± SEM for 1 independent experiment.

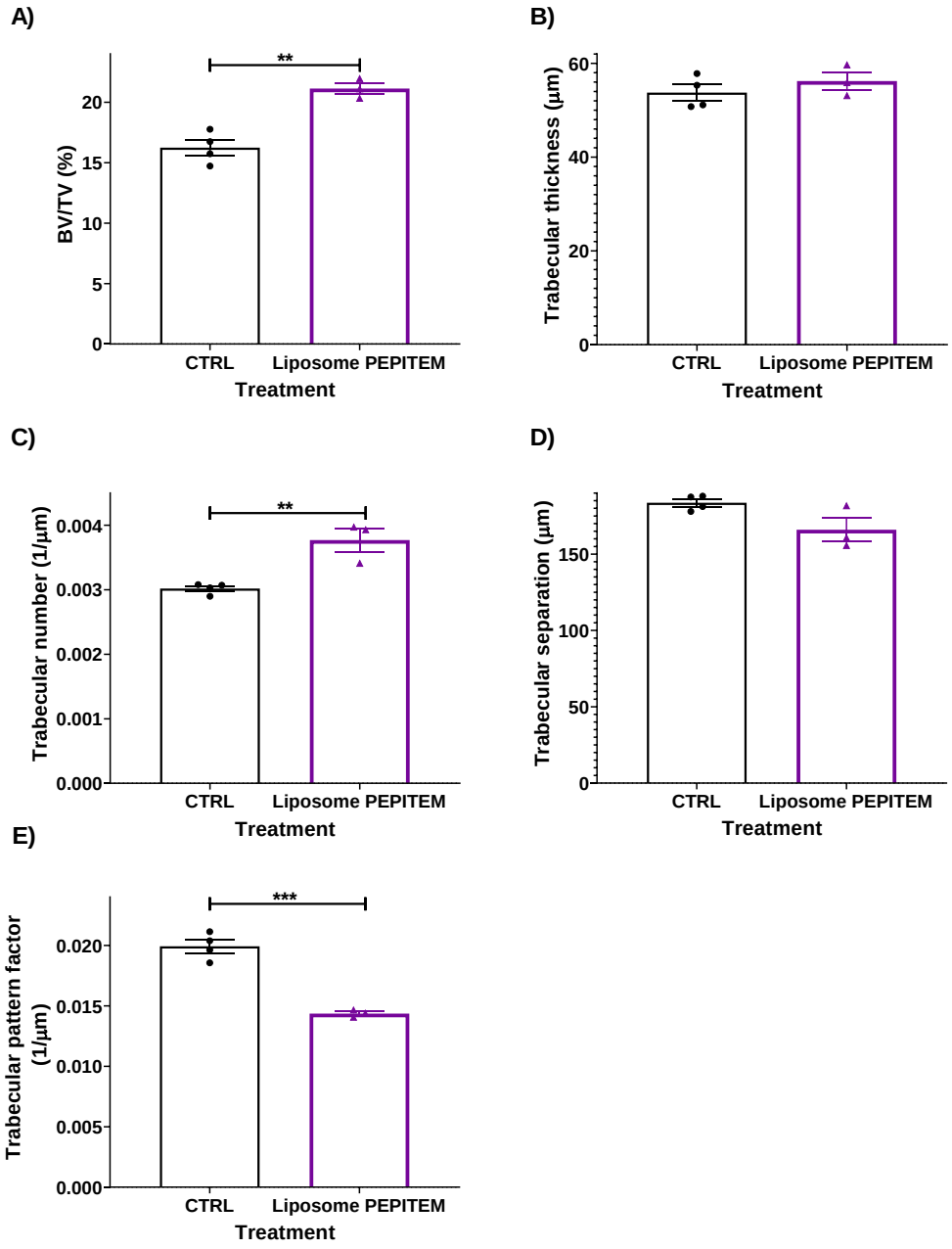

Figure 3.11. Liposome-PEPITEM increased trabecular bone parameters.

Mice were injected with control liposomes (black, n=4) or liposomes enclosing PEPITEM (purple, n=3) twice weekly for 14 days. Tibiae were scanned by µ-CT and regions of interest were drawn around metaphyseal trabecular bone and analysed for trabecular parameters. **A-E.** Trabecular bone was analysed for **A.** trabecular bone volume (BV/TV, %), **B.** trabecular thickness (µm), **C.** trabecular number (1/µm), **D.** trabecular separation (µm) and **E.** trabecular pattern factor (1/µm). Data are mean ± SEM for 1 independent experiment. ** = P<0.01 ***=P<0.001 by student's t-test.

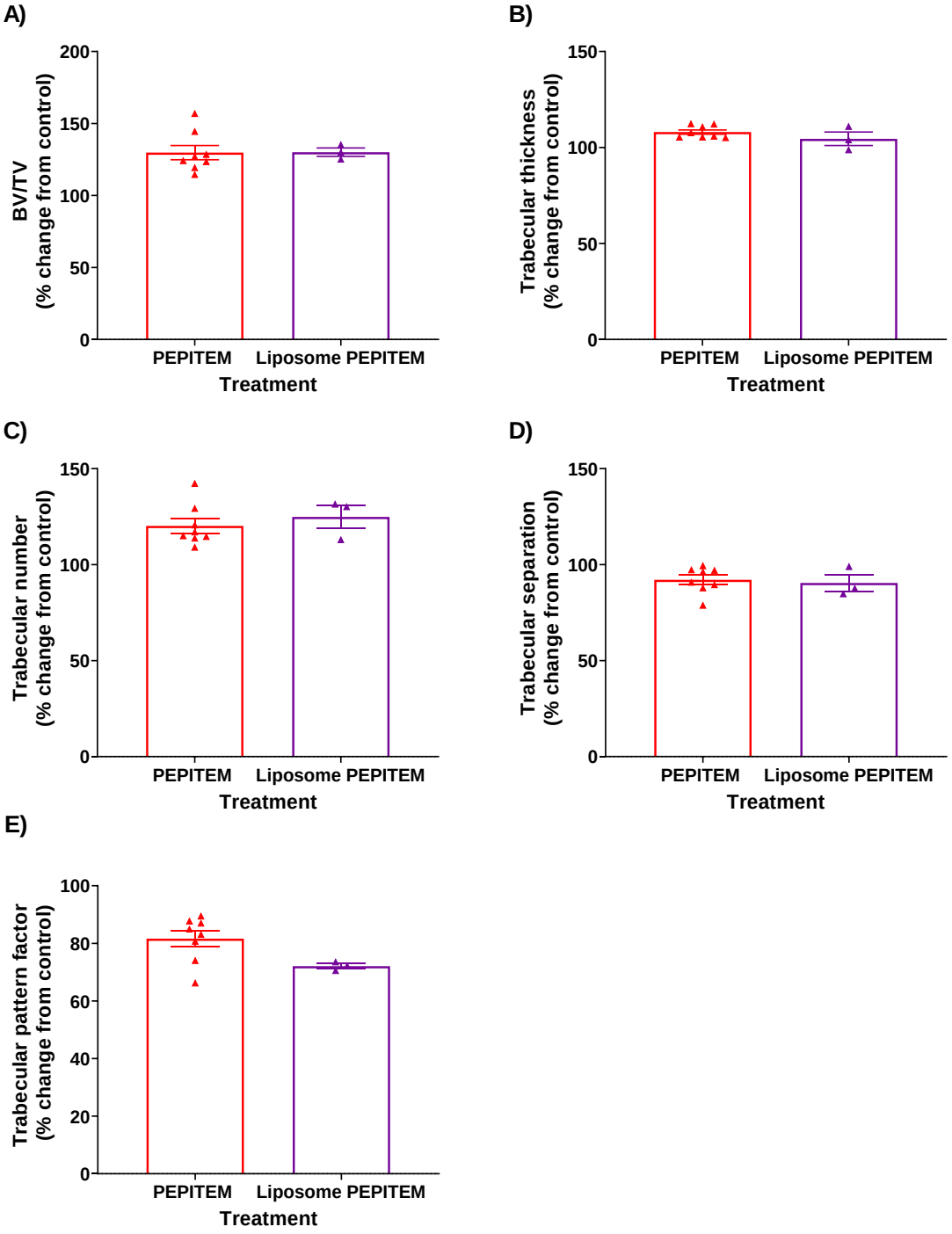

Figure 3.12. Trabecular changes by twice-weekly Liposome-PEPITEM match daily PEPITEM.

Mice were injected either daily with PBS control or PEPITEM or twice weekly with control liposomes or liposomes enclosing PEPITEM for 14 days. **A-E.** Tibiae were analysed and % change was calculated comparing PEPITEM treatment regime to the equivalent control for **A.** trabecular bone volume, **B.** trabecular thickness, **C.** trabecular number, **D.** trabecular separation and **E.** trabecular pattern factor. Data are mean ± SEM for n=8 (PEPITEM) or n=3 (liposome-PEPITEM).

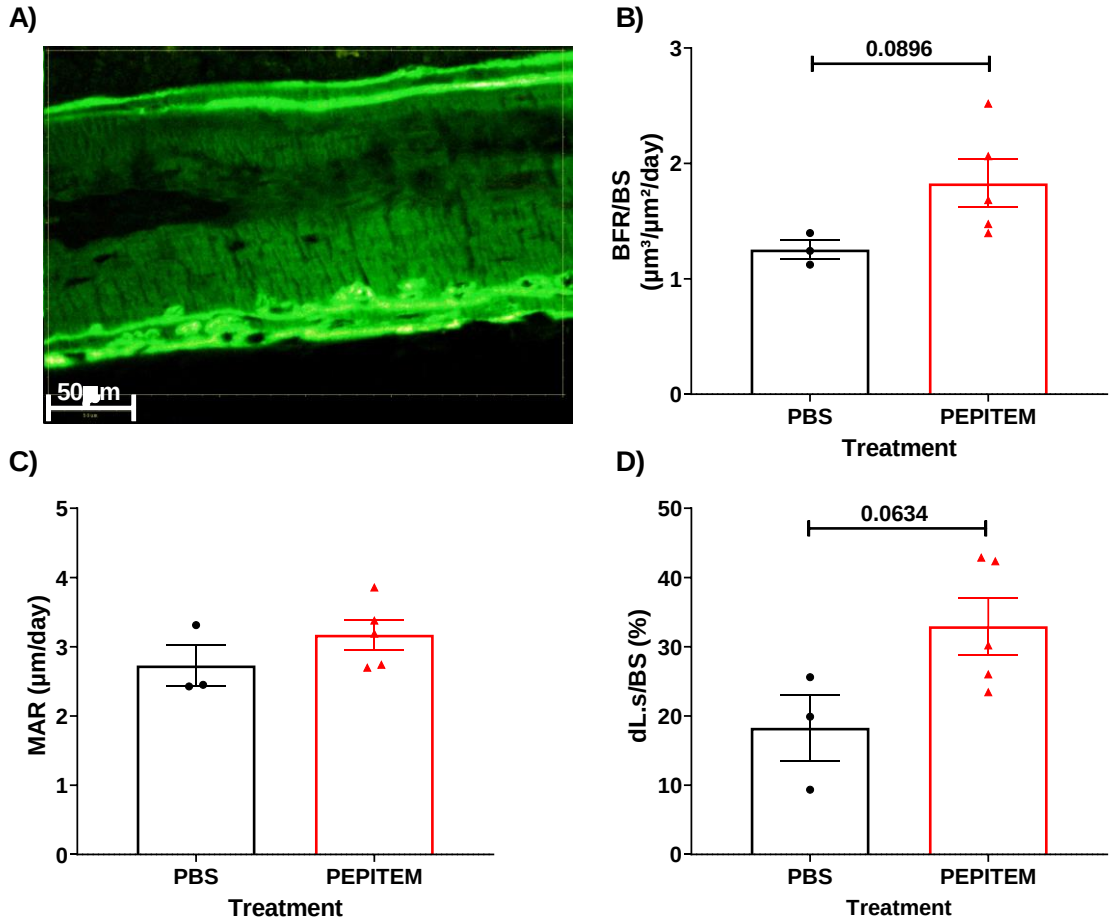

Figure 3.13. PEPITEM treatment trends towards increased bone mineral production.

Mice were injected with PBS control (black, n=3) or PEPITEM (red, n=5) for 14 days, with calcein injected 6 and 2 days prior to termination. Tibiae were plastic embedded, sectioned and imaged for calcein. **A.** Calcein imaging and analysis was performed using "Osteomeasure" to analyse rate of bone growth **B-D.** Calcein labelling was analysed for **B.** bone formation rate normalised to bone surface perimeter (BFR/BS, $\mu m^3/\mu m^2$/day), **C.** mineral apposition rate (MAR, µm/day) and **D.** length of double calcein labels normalised to total bone surface perimeter (dL.s/BS, %). Data are mean ± SEM for 2 independent experiments. Statistical analysis was performed by student's t-test. Scale bar = 50µm.

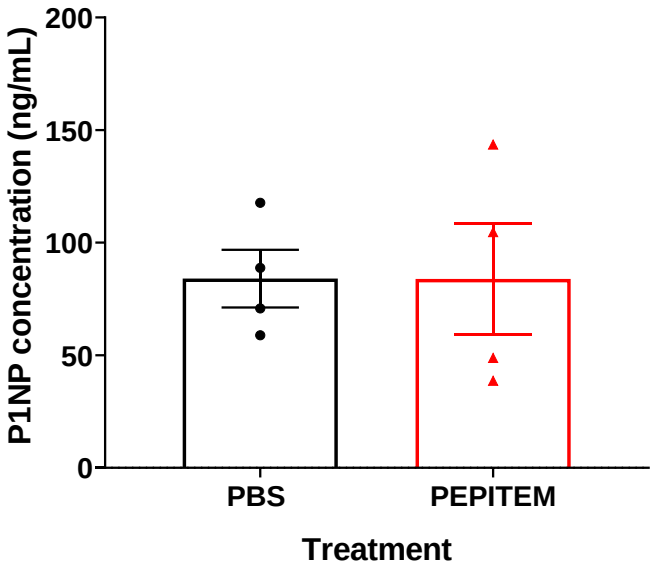

Figure 3.14. PEPITEM does not affect serum P1NP concentration.

Mice were injected with PBS control (black, n=4) or PEPITEM (red, n=4) for 14 days. Serum was isolated and analysed by competitive ELISA for total P1NP concentration. P1NP concentration in PBS and PEPITEM treated mice. Data are mean ± SEM for 1 independent experiment

3.2.5 **Analysis of osteoblast maturation *in vitro***

The above data indicates a possible role for enhanced mineralisation in response to PEPITEM. Mineralisation is controlled by the level of osteoblast activity, thus we analysed the responsiveness of cultured osteoblasts to PEPTIEM *in vitro*.

In order to investigate the effect of PEPITEM on osteoblasts, we first needed to understand the time course and changes osteoblasts undergo during their differentiation. The immortalised MC3T3-E1 (pre-osteoblast) cell line and primary calvarial osteoblasts (C.Ob) were differentiated into mature osteoblasts for up to 21 days and stained for mineralisation with alizarin red.[564] Staining was first observed 12 days after the onset of differentiation in both MC3T3-E1 cells and C.Ob, whilst no staining was detected at any time point in undifferentiated cells (Figure 3.15A,B). Extraction and quantification of alizarin red, as a direct measure of mineralisation production rates, showed a significant time-dependent increase in concentration from day 12 onwards in both cell types, which was maximal at day 16 for MC3T3-E1 cells (Figure 3.16A) and day 20 for C.Ob (Figure 3.16B). Another measure of osteoblast mineralisation capacity is alkaline phosphatase (ALP) activity,[565] a phosphate enabling enzyme essential for bone formation. ALP activity in C.Ob increased over time, with significant increases in ALP activity at both 4 and 8 days post onset of differentiation compared to control (Figure 3.16D), however MC3T3-E1 ALP activity was highly variable and thus as of yet inconclusive (Figure 3.16C). Calvarial osteoblasts and MC3T3-E1 cells maturation profiles match previously established timescales and thus these cultures can be used in future studies.[566,567]

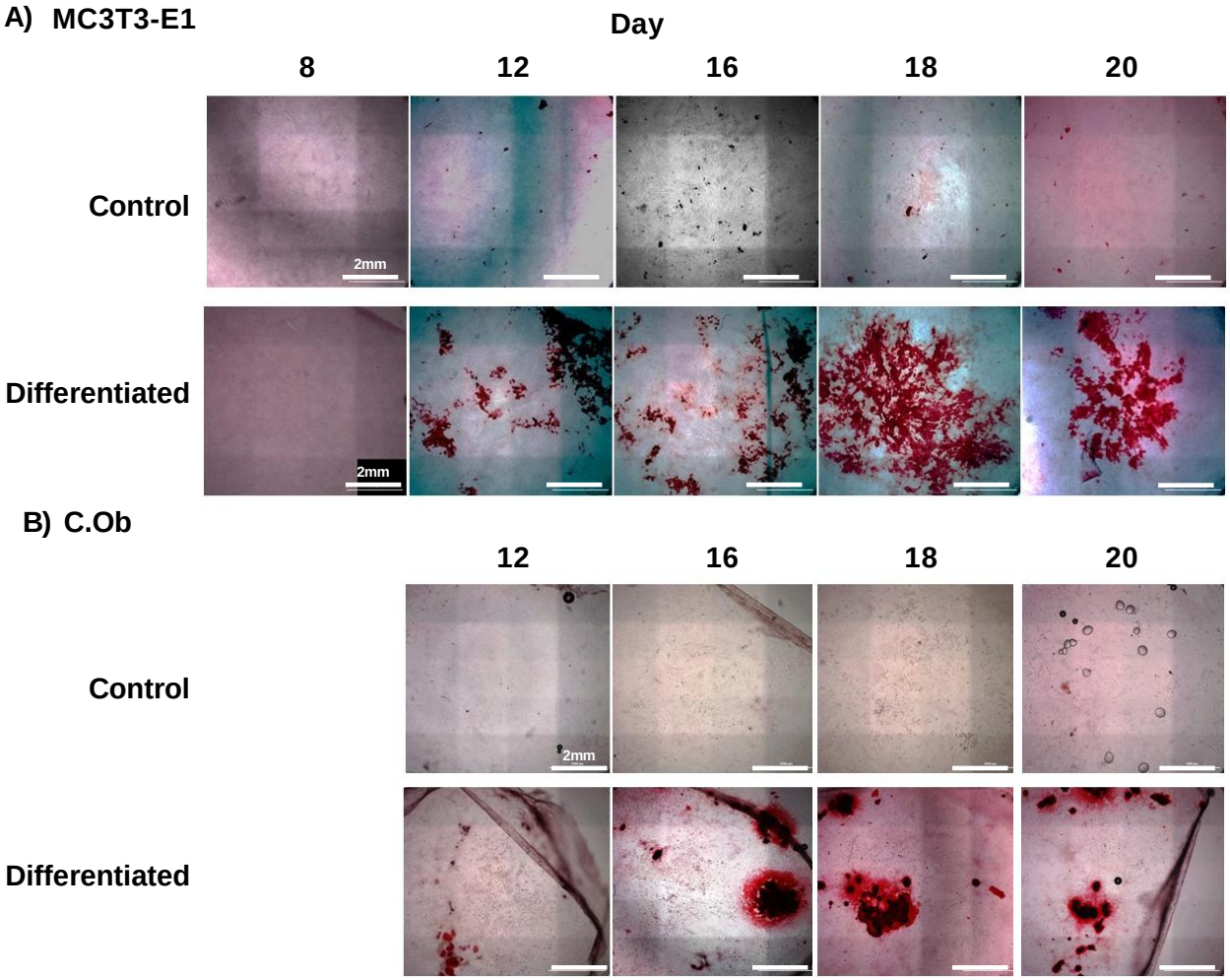

Figure 3.15. Investigating mineral production by osteoblasts *in vitro*.

MC3T3-E1 cells and C.Ob were cultured in control or osteogenic media for up to 20 days. **A-B.** Representative images of alizarin red stained control undifferentiated or differentiated MC3T3-E1 cells **(A)** or C.Ob **(B)** over time up to day 20. Scale bar = 2mm

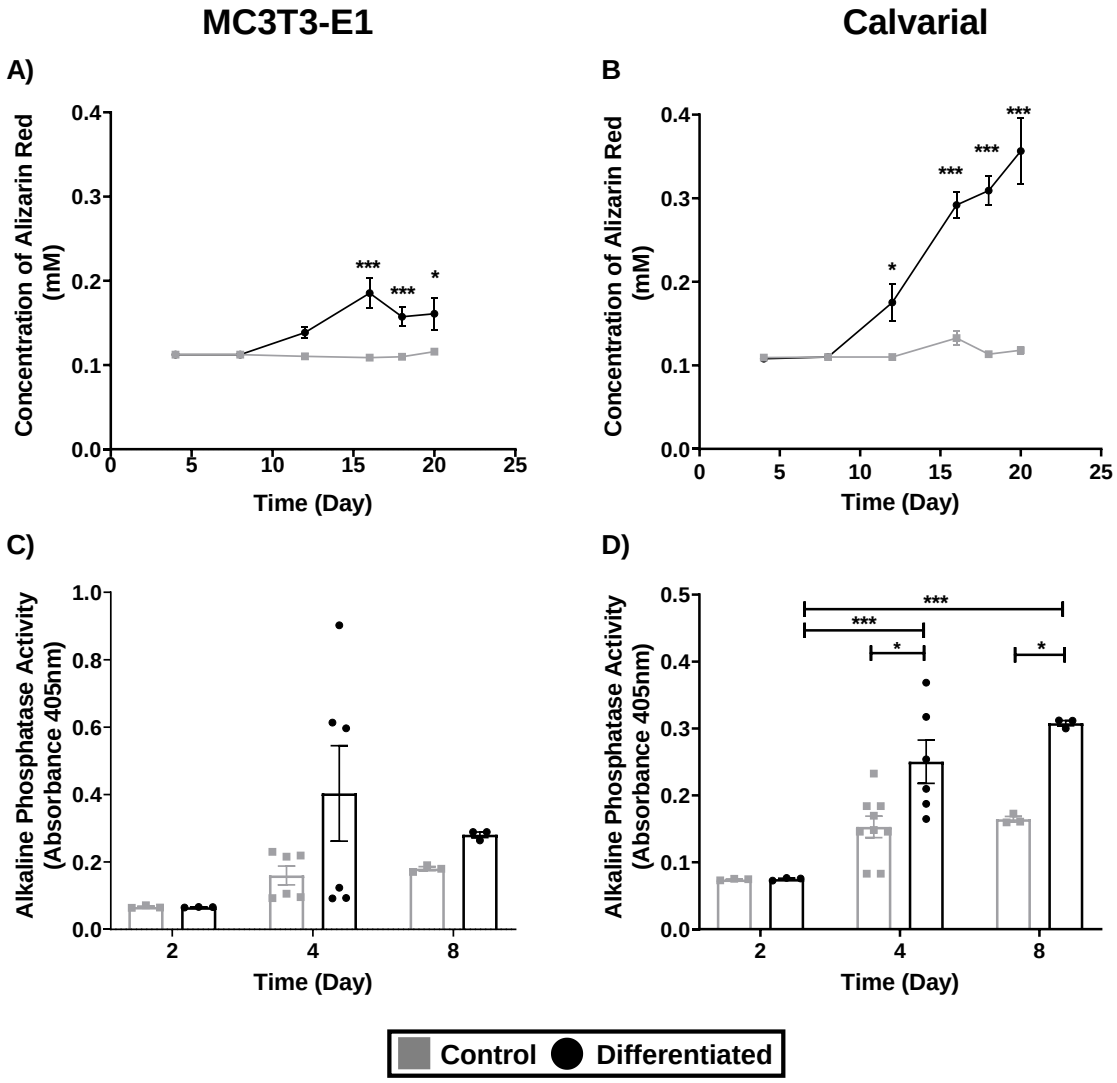

Figure 3.16. Effect of differentiation on MC3T3-E1 and C.Ob mineralisation.

MC3T3-E1 cells and C.Ob were cultured in control or osteogenic media for up to 20 days. **A-B.** Time course of mean alizarin red concentration (mM) extracted from MC3T3-E1 cells **(A)** or C.Ob **(B)** in control (undifferentiated, grey) and differentiated (black) conditions (n=4 for 4 independent experiments). ANOVA showed a significant effect of time and culture conditions on Alizarin Red concentration in both cell types, $p<0.001$. **C-D.** Time course of ALP activity in control and differentiated MC3T3-E1 cells **(C)** or C.Ob **(D)** measured by analysing the conversion of PNPP to p-nitrophenol by cell lysates (n > 3 for at least 3 independent experiments). ANOVA showed a significant effect of time and culture conditions on ALP activity in C.Ob, $p<0.001$. Data are mean ± SEM. * = $P<0.05$, ** = $P<0.01$ and ***=$P<0.001$ by Bonferroni multiple comparisons test comparing control to differentiated cells (A/B/D) or between the same conditions at different time-points (D).

3.2.6 PEPITEM induced changes in murine osteoblast mineralisation

Based on the initial experiments, we found the key timepoints of osteoblast differentiation to test ALP activity and alizarin red staining in response to treatment with PEPITEM. MC3T3-E1 cells and C.Ob were cultured in differentiation media and treated with 10ng/ml of PEPITEM every other day for up to 8 days.[473] PEPITEM significantly increased ALP activity at both 4 (Figure 3.17A) and 8 days (Figure 3.17B) post the onset of differentiation in C.Ob, but not MC3T3-E1 cells (Figure 3.17C,D), when compared to untreated controls. Since PEPITEM increased ALP activity, we explored whether PEPITEM was also able to increase mineral production by osteoblasts by staining cultures with alizarin red (Figure 3.18A,C,E). PEPITEM significantly increased the ability of MC3T3-E1 cells (Figure 3.18B) and C.Ob (Figure 3.18D,F) to produce mineral, as measured by alizarin red concentration, when compared to untreated osteoblasts at the same time point. Overall, PEPITEM increased osteoblast activity at both early (ALP activity) and late (alizarin red) time points in their mineralisation process.

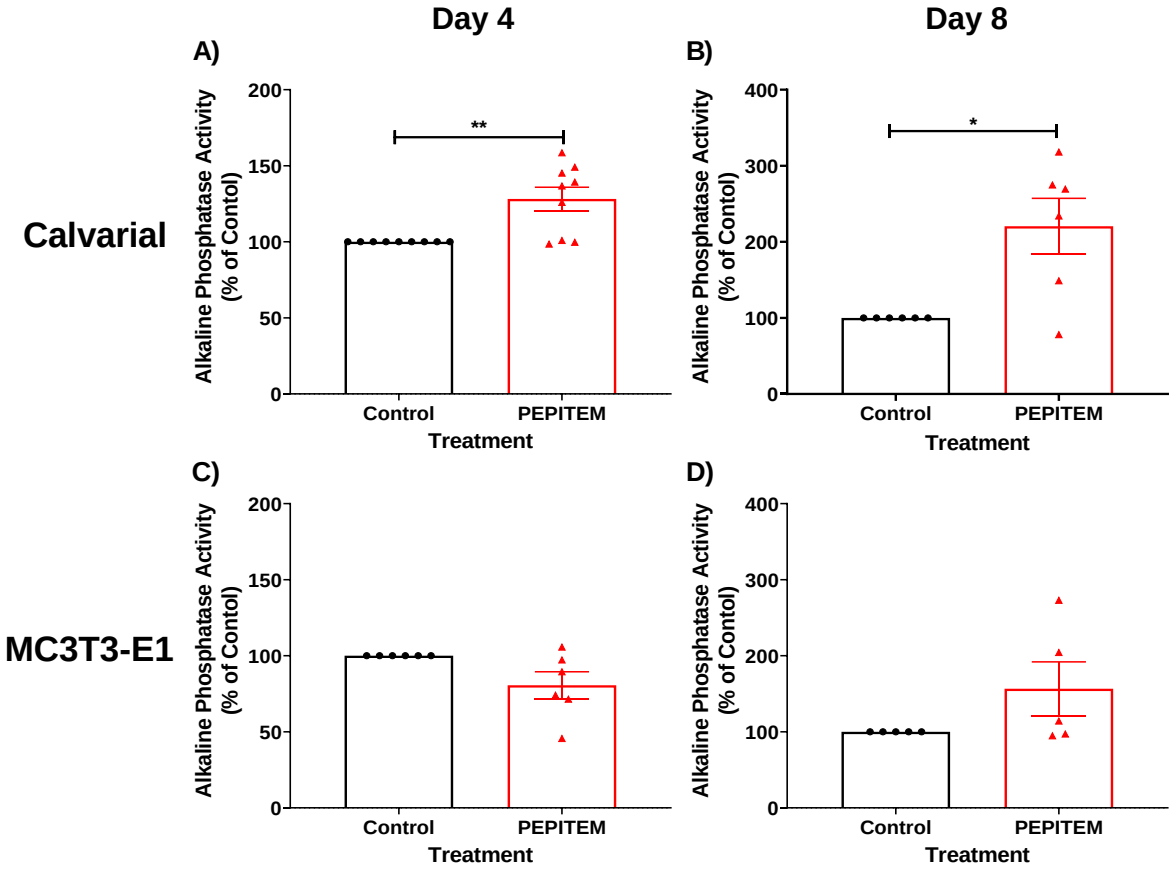

Figure 3.17. PEPITEM increased ALP activity in C.Ob but not MC3T3-E1 cells.

A-B. C.Ob and **C-D.** MC3T3-E1 cells were cultured in osteogenic media supplemented with control (untreated differentiation media, black) or PEPITEM (red) for 4 **(A, C)** or 8 **(B, D)** days following onset of differentiation. ALP activity was measured by analysing the conversion of PNPP to p-nitrophenol and data were normalised as a percentage of ALP activity in control conditions. Data are mean ± SEM, where A n=9, B/C n=6 and D n=5 independent experiments and where A and B contain the same donors. * = P< 0.05 and **=P<0.01 by paired t-test comparing PEPITEM to untreated control cultures.

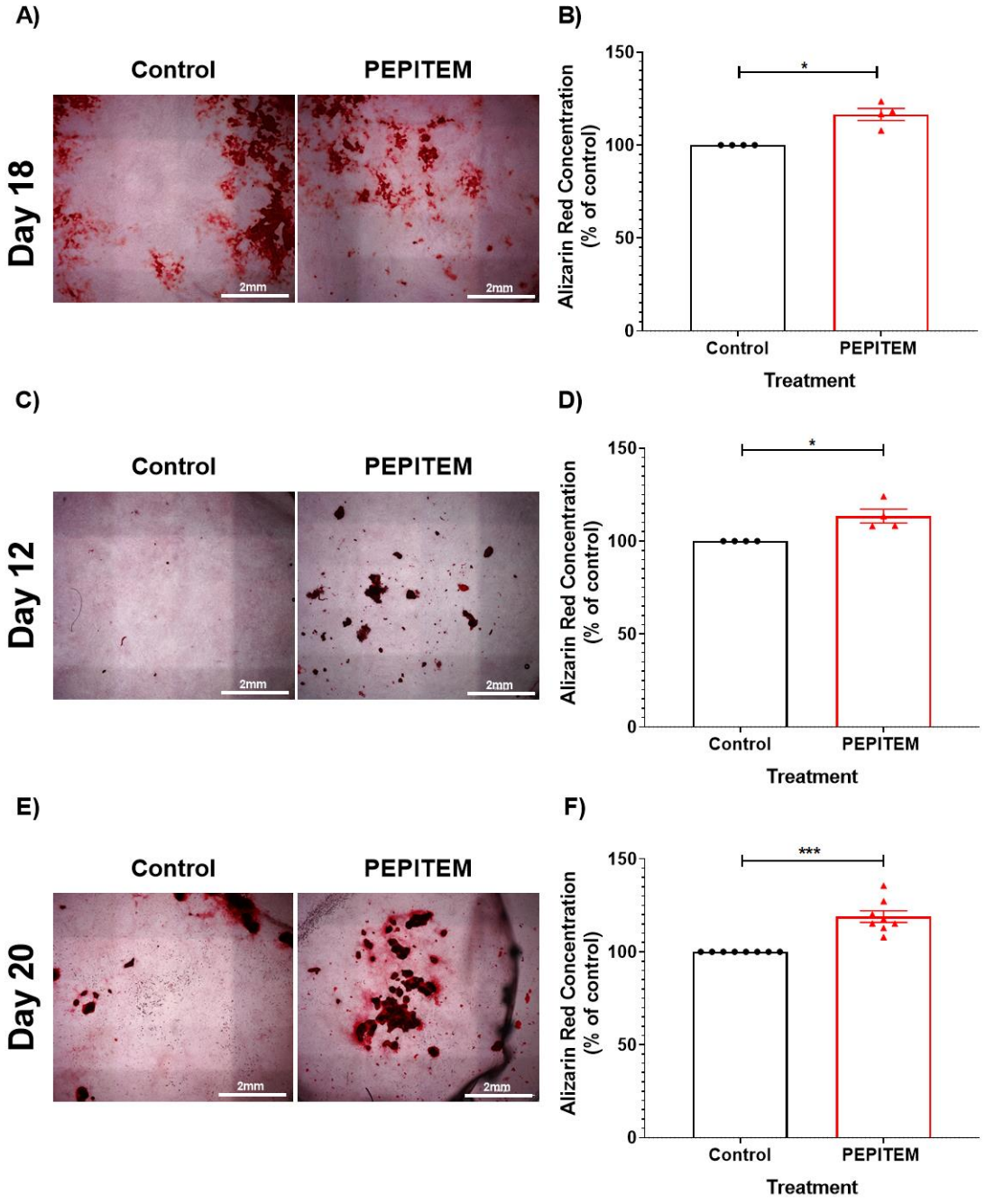

Figure 3.18. PEPITEM increased the mineralisation capacity of osteoblasts.

A-B. MC3T3-E1 cells and **C-F.** C.Ob were differentiated in the absence (control; black) and presence of PEPITEM (red) for up to 20 days. **A,C,E.** Representative images of alizarin red stained control or PEPITEM treated MC3T3-E1 cells **(A)** or C.Ob **(C,E)** from 18- (n=4) or 12- (n=4) and 20-days (n=8) post-differentiation respectively. Mean alizarin red concentration (mM) extracted from MC3T3-E1 cells **(B)** or C.Ob **(D,F)** at the above time-points (n=4 for 4 independent experiments) as a percentage of alizarin red concentration in control conditions. Data are mean ± SEM. * = P<0.05 by paired t-test comparing PEPITEM treated to untreated control cultures. Scale bar = 2mm

3.2.7 **PEPITEM induced increases in human osteoblast mineralisation**

Changes in murine osteoblasts are not always matched in human osteoblasts.[347,568] We therefore examined the effect of PEPITEM (10ng/ml) on human osteoblasts (H.Ob) isolated from the joints of patients with osteoarthritis (OA). Gene expression was analysed by qPCR to confirm osteoblast phenotype, showing significantly increased osteoblast genes *SP7* and *RUNX2* compared to non-matched MSC cells (Figure 3.19A-D). H.Ob were treated with PEPITEM for up to 8 days and ALP activity analysed. Significant increased ALP activity was observed at 4 days (Figure 3.20A), which increased further 8 days post differentiation (Figure 3.20B).

These results indicate an overall positive role of PEPITEM on increasing osteoblast activity, however further work is required to confirm these findings and investigate the mechanism of action.

3.2.8 **Investigating the effect of PEPITEM on bone resorption *in vivo***

Increases in osteoblast activity are usually matched by enhanced osteoclastogenesis to ensure balance is maintained, however this can often hamper efforts to boost bone growth and restore normal bone structure and strength.

For analysis of changes in osteoclasts *in vivo*, tibiae from PEPITEM and PBS treated mice were stained for tartrate resistant acidic phosphatase (TRAP) to identify and count osteoclasts (Figure 3.21A). PEPITEM treatment significantly decreased osteoclast numbers when normalised to total area analysed compared to PBS treated mice (Figure 3.21B). These data indicate PEPITEM may also mediate its effect by altering osteoclasts numbers, however this could be due to direct action on osteoclasts or occur indirectly through PEPITEM acting on osteoblasts of other cells.

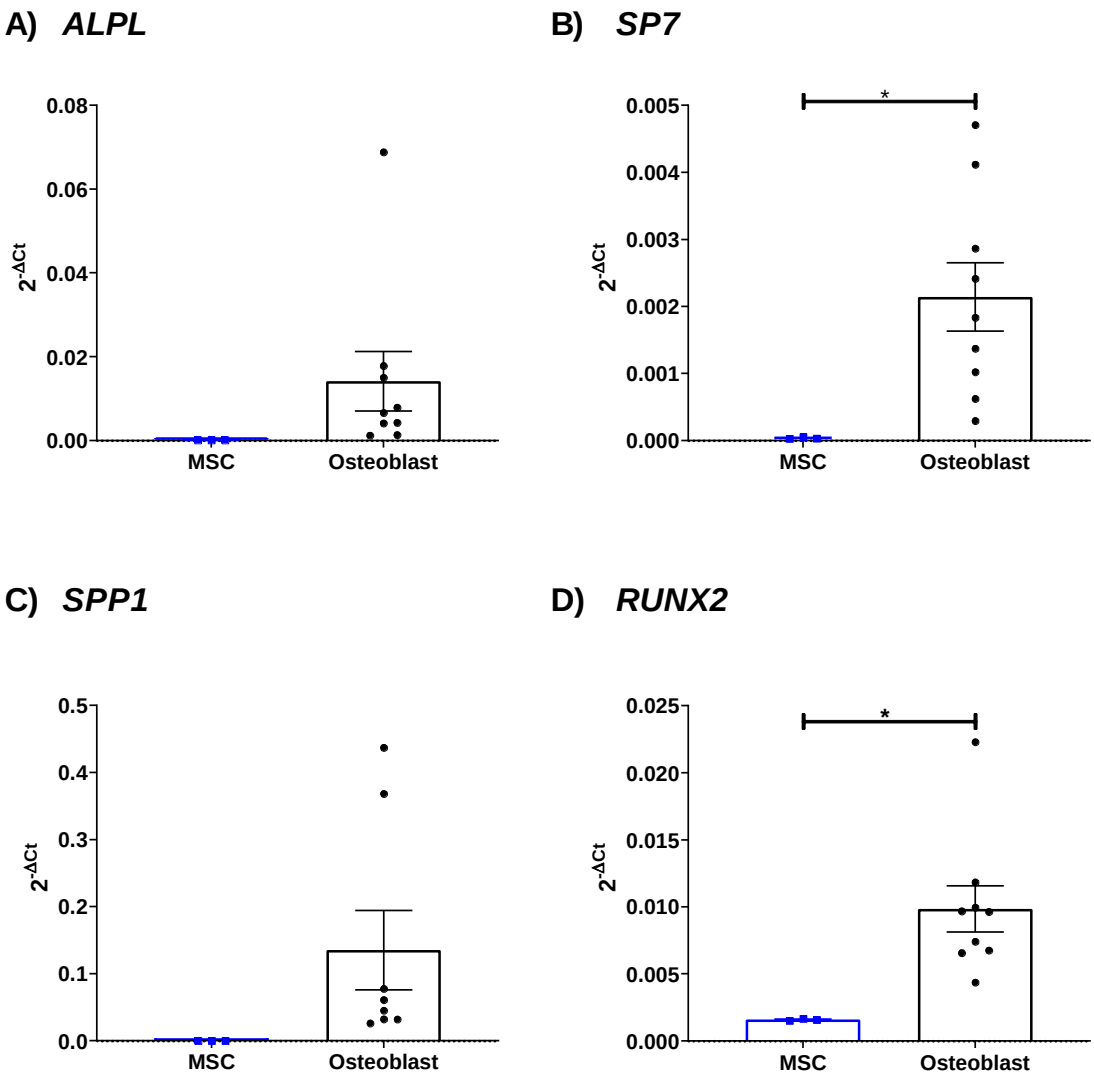

Figure 3.19. Trabecular bone outgrowth cells express osteoblast specific genes.

Osteoblasts were isolated from human bone samples by culturing trabecular bone chips in osteoblast specific media for up to 21 days to allow outgrowth of cells. **A-D.** RNA isolated from cultures (n=8 individual donors) were analysed by qPCR for expression of *ALPL* **(A)**, *SP7* **(B)**, *SPP1* **(C)** and *RUNX2* **(D)** compared to non-matched MSC controls (n=3). Data are mean ± SEM. Data are displayed as $2^{-\Delta Ct}$, where ΔCt is the relative expression compared to *B2m* housekeeping gene. *=P<0.05 by student's t-test.

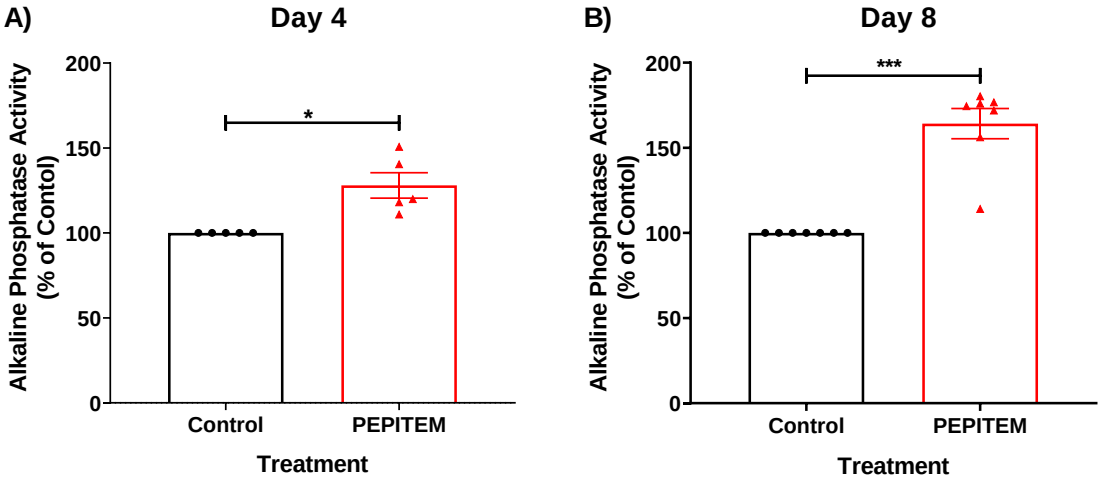

Figure 3.20. Human osteoblasts increase ALP activity in response to PEPITEM.

Human osteoblasts derived from the joints of OA patients were differentiated and treated with PEPITEM for up to 8 days. **A-B.** ALP activity was measured 4 **(A)** and 8 **(B)** days following differentiation by ELISA in control (untreated, black) and PEPITEM treated (red) cells and presented as percentage of untreated control. Data are mean ± SEM, where A n=5 and B n=7 independent experiments where A and B contain cells isolated from the same donors. * = P< 0.05 and *** = P< 0.001 by paired t-test comparing PEPITEM to untreated control cultures.

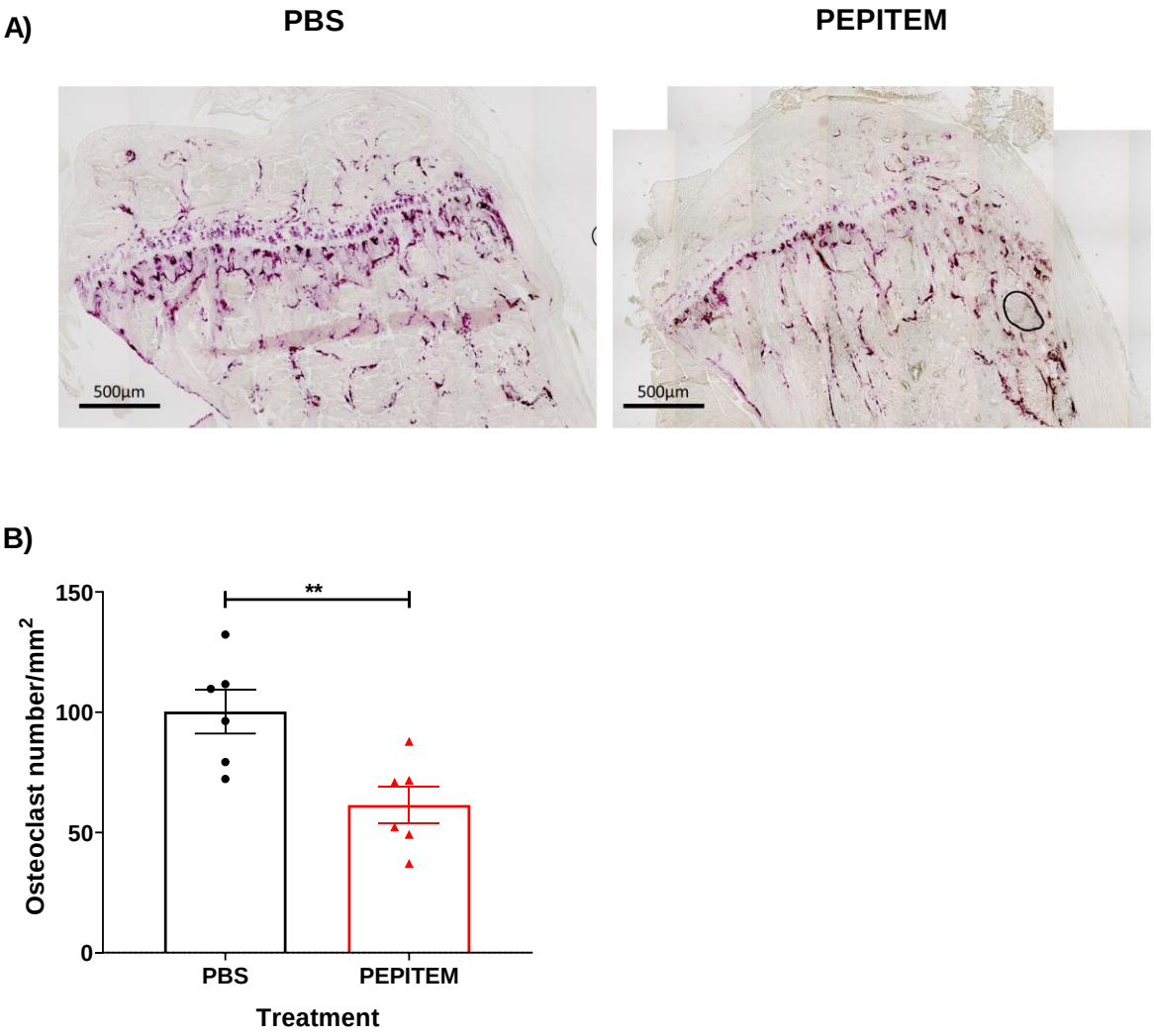

Figure 3.21. PEPITEM treatment decreased osteoclasts in trabecular bone.

Mice were treated with PBS control (black, n=6) or PEPITEM (red, n=6) for 14 days. Tibiae were paraffin embedded, sectioned, and stained for TRAP. **A.** Representative images (1 mouse per treatment group) of TRAP-stained sections from PBS or PEPITEM treated mice. **B.** Osteoclasts were quantified and normalised to the area of region of interest (Osteoclasts/mm^2). Data are mean ± SEM for 2 independent experiments. ** = $p<0.01$ by student's t test comparing PEPITEM to PBS control. Scale bars = 500µm.

3.2.9 Changes in osteoclastogenesis in response to PEPITEM treatment

To separate direct and indirect effects of PEPITEM on osteoclast, *in vitro* osteoclastogenesis and resorption assays were performed. The murine RAW264.7 macrophage cell line was differentiated into osteoclasts using RANKL and cultured in the presence of PEPITEM or known osteoclastogenesis inhibitor, zoledronic acid, as a positive control (Figure 3.22A). No difference was observed in the number of TRAP+ osteoclast per well when compared to PEPITEM or untreated control wells (Figure 3.23A/B). However, addition of zoledronic acid significantly decreased osteoclastogenesis, leading to decreased number of TRAP+ osteoclasts per well (Figure 3.23A/B). To confirm these results in human cells, human primary monocytes were isolated from whole blood and osteoclastogenesis was induced using m-CSF and RANKL (Figure 3.22B). Addition of RANKL to cultures led to osteoclastogenesis and thus an increase in the number of TRAP+ multinucleated cells per well (Figure 3.24A-C). Induction of osteoclastogenesis was confirmed by qPCR, where expression of osteoclast genes *ACP5, ATP6V1B1* and *CTSK* were all significantly increased in RANKL treated cells (Figure 3.25A-C), whereas there was no change in macrophage marker MSR-1 (Figure 3.25D). Addition of PEPITEM to the cultures did not change the number of TRAP+ multinucleated cells per well (Figure 3.26A/B). In contrast, addition of zoledronic acid completely inhibited osteoclastogenesis, causing a significant reduction in osteoclast numbers per well (Figure 3.26A/B). These data indicated PEPITEM is unable to act directly on osteoclasts *in vitro*.

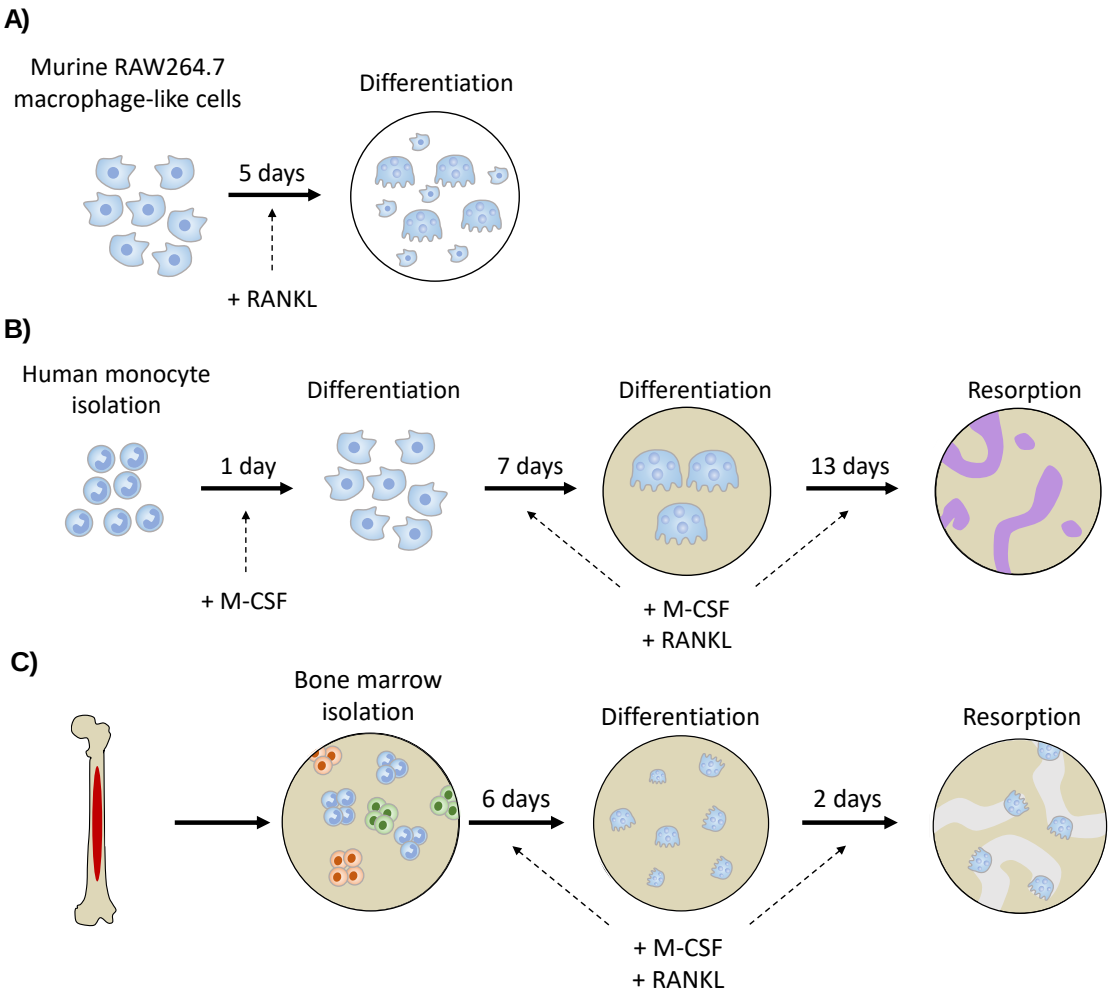

Figure 3.22. Methods for testing *in vitro* osteoclastogenesis and resorption in murine/human cells.

A. Schematic of the stages and timings of *in vitro* osteoclast differentiation of murine RAW264.7 macrophage-like cells. **B.** Schematic of induction of osteoclastogenesis in human primary monocytes and testing resorption on dentine discs (Purple = resorption). **C.** Schematic of induction of osteoclastogenesis of whole bone marrow cells into osteoclasts on Osteoassay plates, followed by allowing resorption.

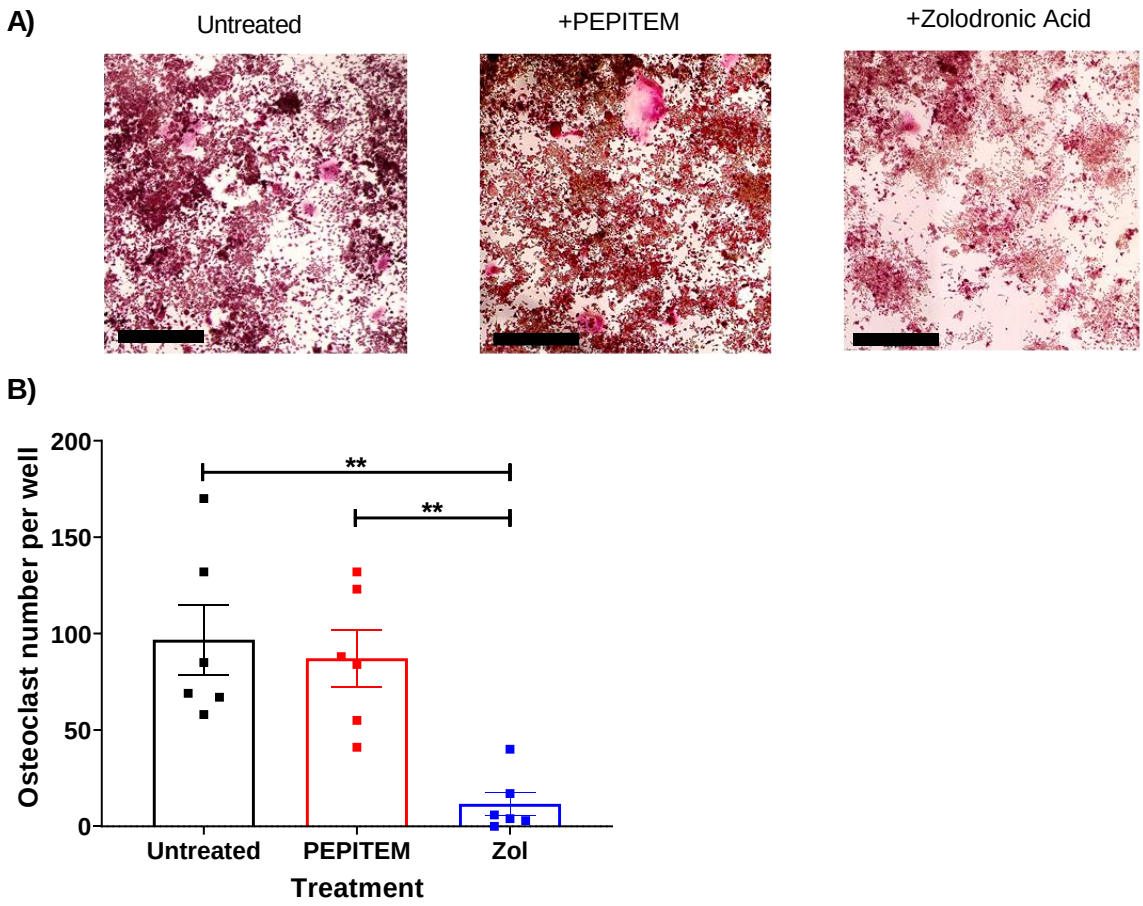

Figure 3.23. PEPITEM does not alter osteoclastogenesis of murine RAW264.7 macrophage-like cells.

Murine RAW264.7 macrophage-like cells were differentiated into osteoclasts by addition of RANKL to culture condition for 5 days. The number of TRAP+ multinucleated cells per well was analysed following culture alone (black, n=6), with PEPITEM (red, n=6) or with Zoledronic acid (blue, n=6). **A.** Representative images (one per treatment group) of untreated, PEPITEM treated or Zoledronic acid treated wells. **B.** Osteoclasts were counted in each condition and presented as number of osteoclasts per well. ANOVA showed a significant effect of treatment on osteoclast number, $p<0.01$. Data are mean ± SEM, where n=6 for 3 independent experiments. **=$P<0.01$ by Bonferroni multiple comparisons test. Scale bars = 500μm.

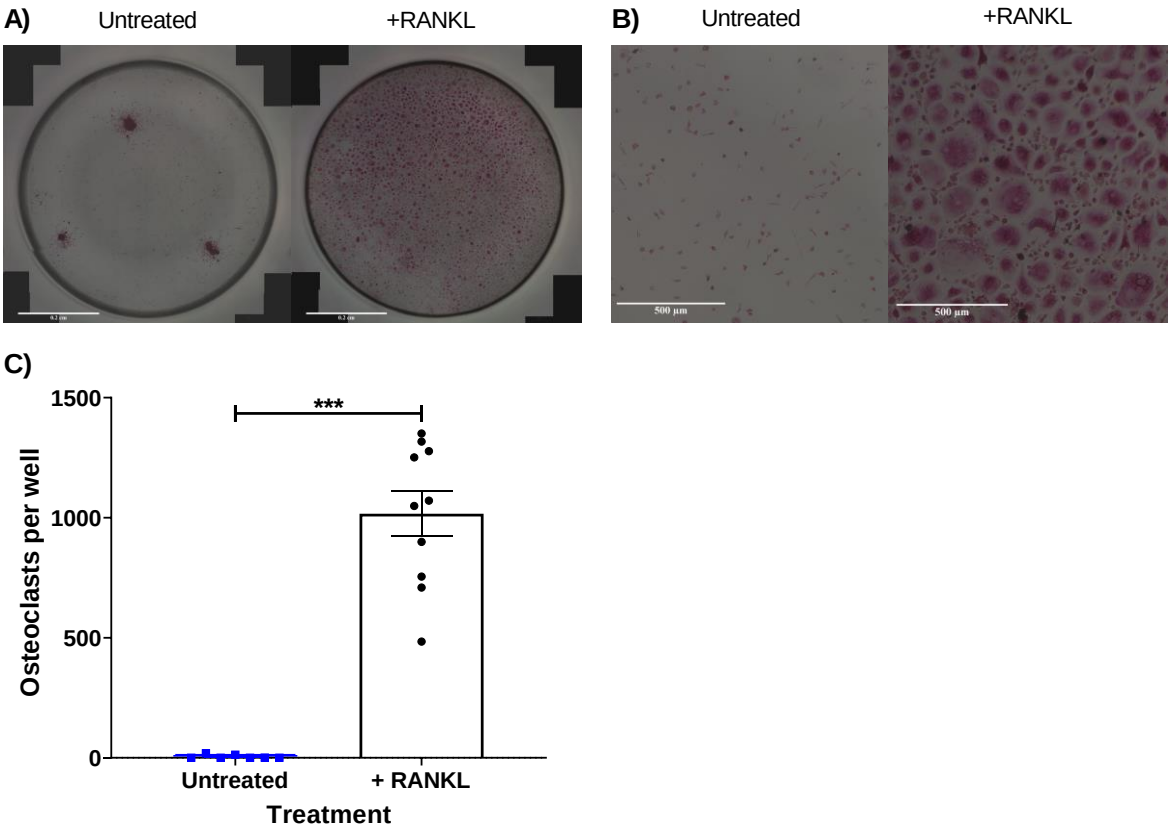

Figure 3.24. Addition of RANKL to human primary monocytes induced osteoclastogenesis.

Human monocytes were isolated from whole blood PBMCs and osteoclastogenesis was induced by addition of RANKL and m-CSF to cultures prior to staining with TRAP to detect TRAP+ multinucleated osteoclasts. **A-B.** Representative images (n=1 per treatment group) of TRAP stained RANKL treated or untreated cells following 8 days of culture at whole well level **(A)** or at 10x magnification **(B)**. **C.** Osteoclasts were quantified per well in untreated (blue, n=7) and RANKL treated (black, n=10) wells. Data are mean ± SEM. ***=P<0.001 by students t-test. Scale bars: A = 2mm, B = 500µm.

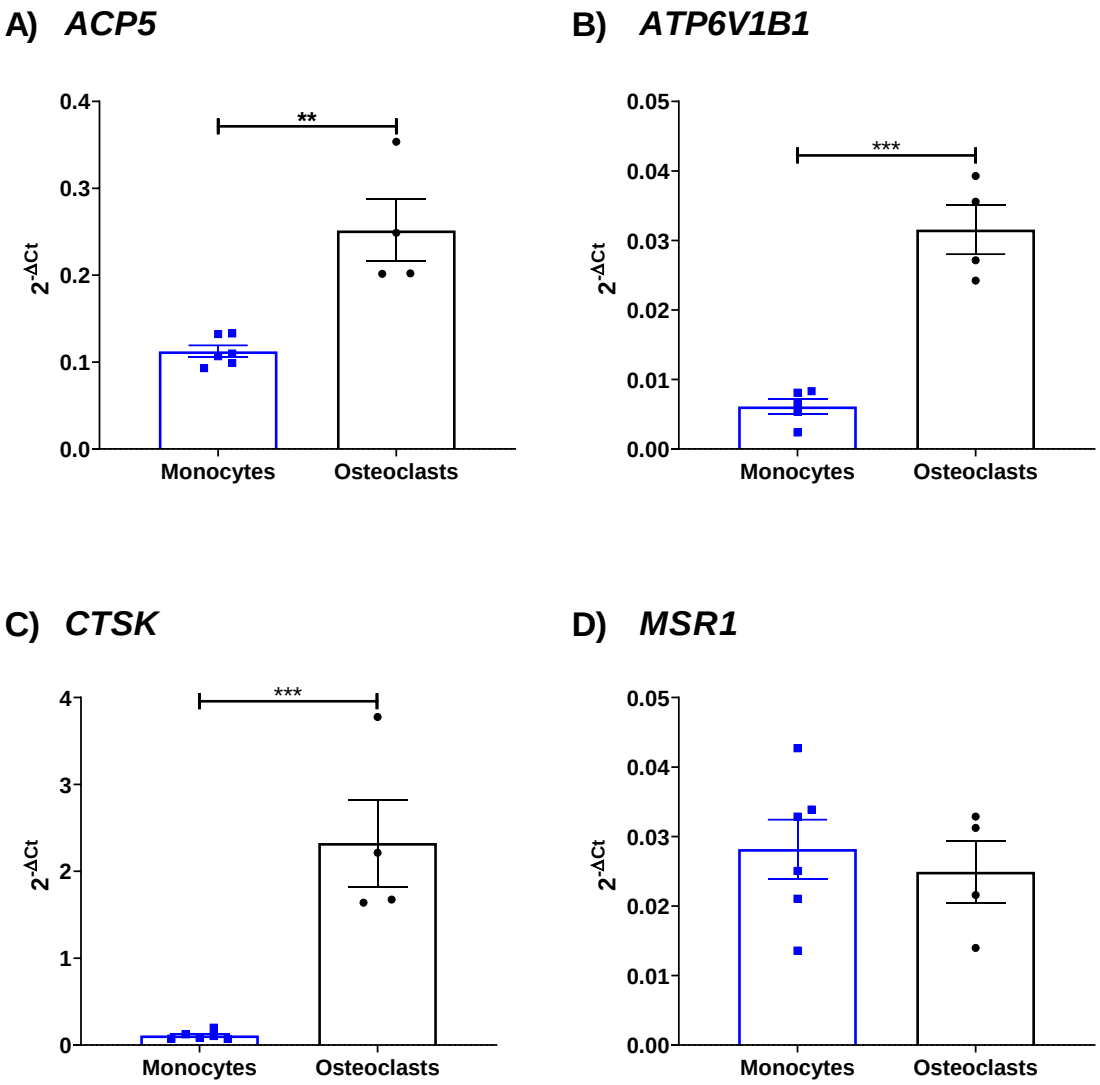

Figure 3.25 RANKL treated monocytes increase expression of osteoclast genes.

Human monocytes were isolated from whole blood PBMCs and osteoclastogenesis was induced by addition of RANKL and m-CSF to cultures. **A-D.** Gene expression *ACP5* **(A)**, *ATP6V1B1* **(B)**, *CTSK* **(C)** and *MSR1* **(D)** were analysed by qPCR for untreated monocytes (blue, n=6) and RANKL induced osteoclasts (black, n=4). Data are displayed as $2^{-\Delta Ct}$, where ΔCt is the relative expression compared to *B2m* housekeeping gene. Data are mean ± SEM. **=P<0.01 and ***=P<0.001 by students t-test.

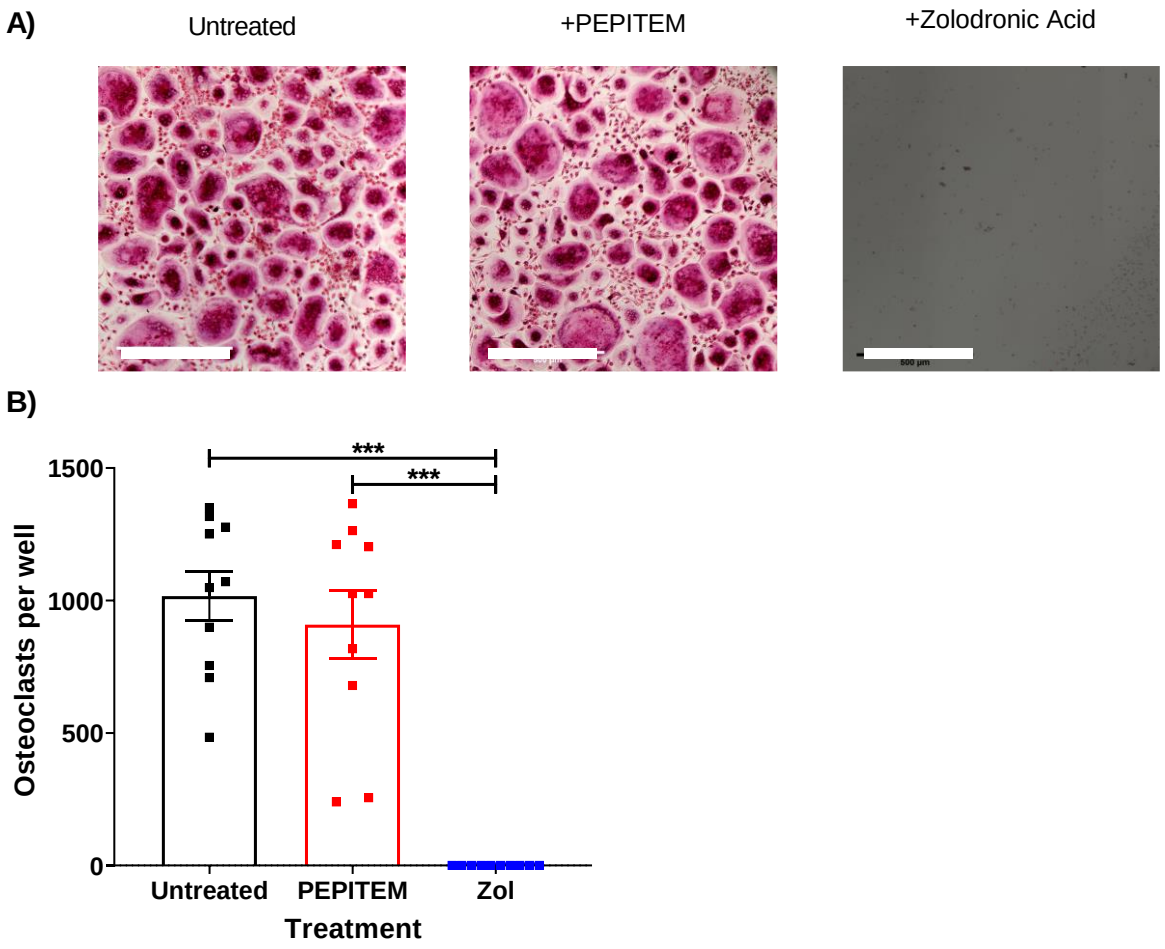

Figure 3.26. PEPITEM treatment does not alter osteoclastogenesis of human monocytes.

Human monocytes were treated with RANKL and m-CSF to induce osteoclastogenesis, which was analysed by TRAP staining **A.** Representative images (n=1 per treatment group) of TRAP+ osteoclasts following 8 days of culture alone (untreated, black, n=10), with PEPITEM (red, n=10) or with Zoledronic acid (blue, n=10). **B.** Osteoclasts were counted in each condition and presented as number of osteoclasts per well. ANOVA showed a significant effect of treatment on osteoclast number, $p<0.01$. Data are mean ± SEM, where n=10 for 3 independent experiments. ***=$P<0.001$ by Bonferroni multiple comparisons test. Scale bars = 500μm.

3.2.10 Investigating the effect of PEPITEM on osteoclast resorption capacity

Despite no differences being observed in osteoclastogenesis in response to PEPITEM treatment, there was the possibility that osteoclast resorption capacity was altered. Human osteoclast resorption potential was investigated by the culture of primary human monocytes on dentine, where resorption pits were stained and analysed following 21 days of culture with RANKL and m-CSF (Figure 3.22A/B). No differences in resorption by primary human monocytes were observed on dentine slices in response to PEPITEM treatment (Figure 3.27A-C). Murine osteoclast resorption potential was analysed by extraction and culture of whole bone marrow for 8 days with M-CSF and RANKL on Osteoassay™ plates (Figure 3.22C).[537] The percentage of the plate resorbed by osteoclasts was significantly decreased when comparing PEPITEM treated and zoledronic acid treated to untreated wells (Figure 3.28A/B).

These data indicate that PEPITEM may have no effect on osteoclastogenesis or osteoclasts when acting directly on the cells, however addition of other cells, such as the remainder of the bone marrow may result in secondary indirect effects on the osteoclasts.

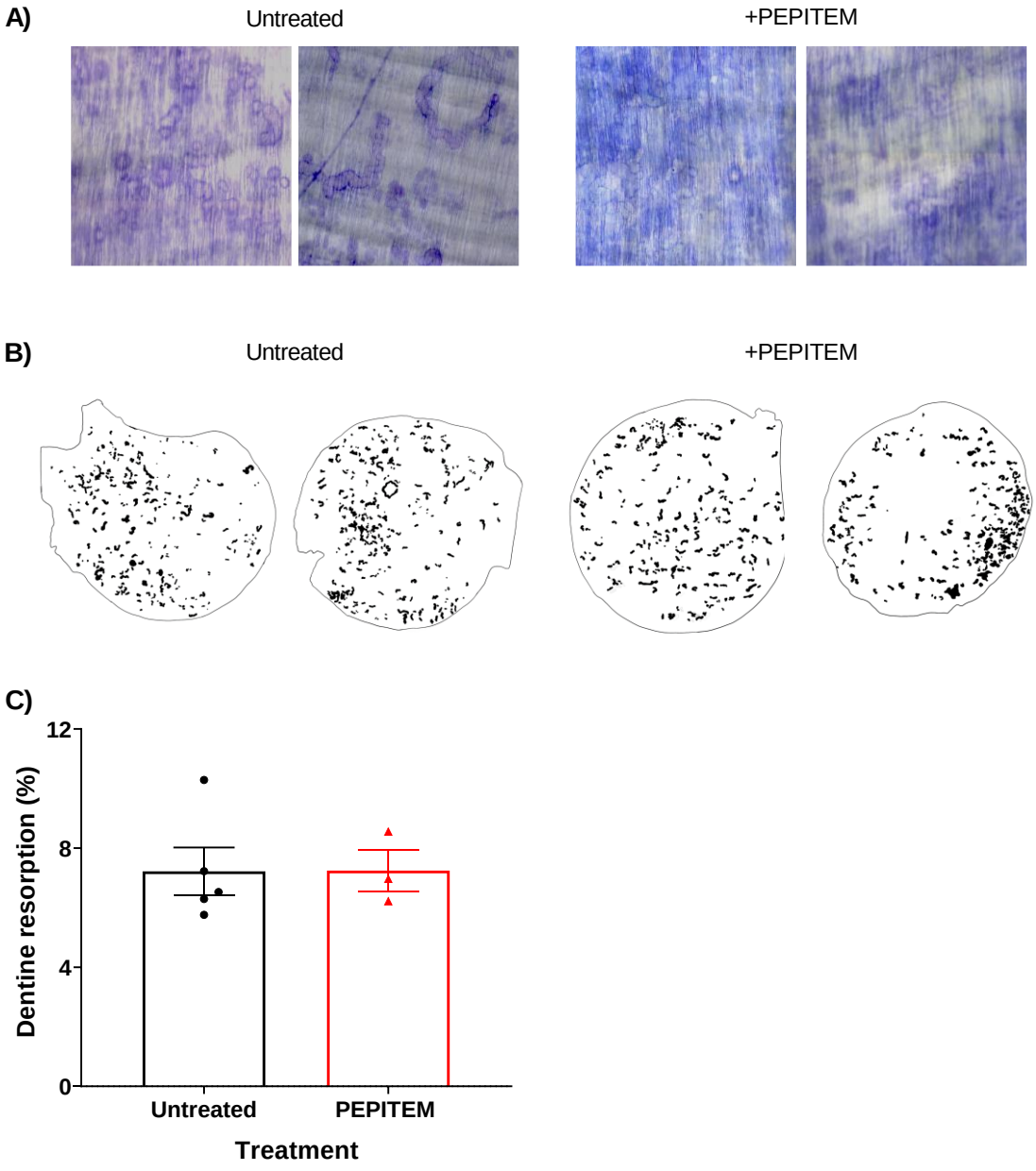

Figure 3.27. PEPITEM does not change human osteoclast resorption potential on dentine slices.

Human monocytes were isolated from whole blood PBMCs and osteoclastogenesis was induced on dentine slices by addition of RANKL and m-CSF to cultures. Cells were cultured for a total of 21 days alone (black, n=6) or in the presence of PEPITEM (red, n=3), after which cells were removed and dentine was stained for resorption. **A.** Representative images (n=1 per treatment group) of stained dentine slices. **B.** Representative images of masks generated to show areas resorbed by osteoclasts. **C.** The area resorbed was recorded in each condition and displayed as a percentage of total area. Scale bars = 500μm.

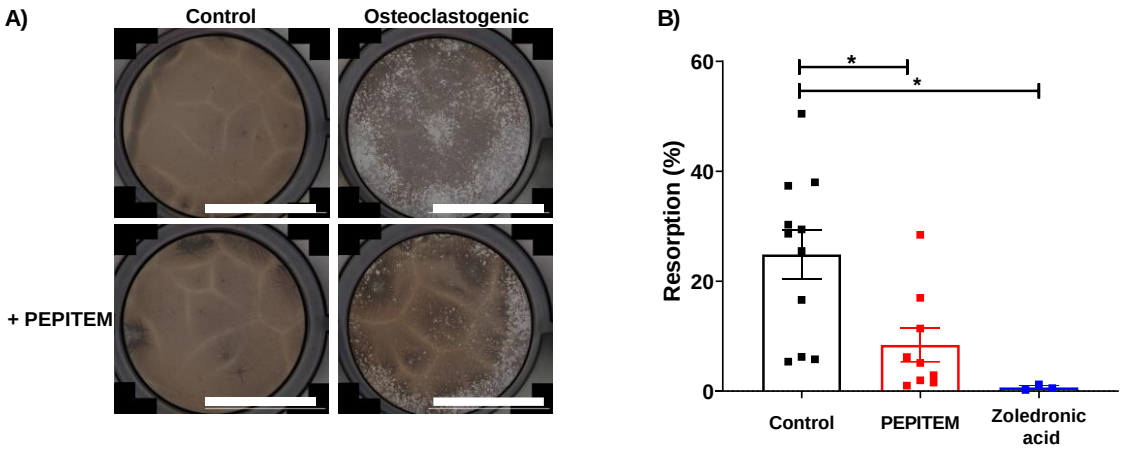

Figure 3.28. PEPITEM decreases osteoclast resorption on Osteoassay plates.

Whole bone marrow cells were differentiated and left to resorb on commercially available (Osteoassay) plates for 8 days alone (black, n=11) or in the presence of PEPITEM (red, n=9) or Zoledronic acid (blue, n=3). **A.** Representative images (n=1 per treatment group) of resorption on Osteoassay plates. **B.** Percentage of whole wells resorbed by osteoclasts in the above conditions on Osteoassay plates. ANOVA showed a significant effect of treatment on osteoclast resorption. Data are mean ± SEM, where n≥5 independent experiments. *=P<0.05 by Bonferroni multiple comparisons test. Scale bars = 1000μm.

3.3 Discussion

Here we explored the effect of a novel endogenous peptide, PEPITEM, on healthy homeostatic bone in an inflammation-independent manner. We observed a direct anabolic action of PEPITEM on tibial and vertebral trabecular bone over two-weeks when given as daily I.P injections or twice-weekly when enclosed in a liposome. However, this was performed with only a PBS control, thus results need to be viewed in caution until a scrambled control is run which can provide a peptide control. This translated at a physiological level to an increase in bone strength and stiffness in PEPITEM treated mice, despite no obvious change in cortical bone being observed. Investigations at the cellular level revealed that PEPITEM increased ALP activity when acting directly on primary murine and human osteoblasts, leading to an increase in mineralisation. Despite PEPITEM treatment *in vivo* decreasing osteoclast numbers on the bone surface, PEPITEM had no direct effect on murine macrophage-like RAW264.7 cell or human monocyte osteoclastogenesis or resorption. We therefore propose that PEPITEM is able to act directly on osteoblasts to enhance their mineralisation potential and indirectly on osteoclasts to decrease osteoclastogenesis. There are many soluble mediators that are involved in promoting or inhibiting osteoclastogenesis, including RANKL, OPG, TNF and S1P, all of which could be released in response to PEPITEM and thus need investigating.[194,195,488,569] Consequently, PEPITEM treatment results in an increase in trabecular bone growth and subsequent increase in bone strength in homeostatic bone, which should clinically translate to a decreased incidence of fractures that are commonly associated with musculoskeletal (MSK) disorders such as osteoporosis.

Preliminary data from our group has shown a significant reduction in bone damage following therapeutic administration of PEPITEM in mice with inflammatory arthritis.[496] However, the anti-inflammatory role of PEPITEM means it is impossible to dissect what represents a direct effect of PEPITEM on the bone or what improvements in bone damage are due to reduced inflammation.[473,497]. There is currently very little evidence reporting the direct influence of PEPITEM on bone to compare our results against. As such this discussion will focus on what evidence exists for a role of the parent protein in bone homeostasis and also how the bioactivity of PEPITEM compares with licenced pharmaceuticals currently in the clinical for MSK disorders.

3.3.1 Evidence of PEPITEMs actions in bone

The precursor to PEPITEM, 14-3-3ζδ, has been found to affect bone growth both *in vivo* and *in vitro*. In human foetal calvarial pre-osteoblasts, transfection with an miR-22 mimic led to a significant decrease in YWHAZ gene and protein expression.[511] In addition, there was decreased of alkaline phosphatase activity, mineralisation, and expression of osteoblast genes *Col1A1*, *RUNX2*, *ALP* and *BMP2* in the murine osteoblast cell line MC3T3-E1, human MSCs and human pre-osteoblasts.[511] Likewise, siRNA knockdown of *YWHAZ* in both murine and human cells caused a significant decrease in ALP activity and mineralisation, indicating a possible role of *YWHAZ*, and thus PEPITEM production in positively regulating osteoblast differentiation.[510,511] This is further supported by *in vivo* data, where reduced miR-22 expression in BALB/c mice (following treatment with an antagomir), leading to increased *YWHAZ* expression, significantly increased femoral trabecular number, femoral strength, and femoral stiffness.[511] Our data adds further weight to

these findings, where PEPITEM promotes bone growth and strength *in vivo* and enhances osteoblast ALP activity and mineralisation in human and murine pre-osteoblasts. Thus, indicating that the loss of YWHAZ leads to a decrease in homeostatic PEPITEM expression in the bone, leading to a decrease in osteoblastogenesis.

In contrast to our findings with PEPITEM, miR-22 inhibition and by extension increased YWHAZ expression had no impact on BV/TV or trabecular number.[511] Whilst the exact location and processing of YWHAZ required to generate PEPITEM is currently unclear, given the reduced response in this study, it is likely that some of these elements are not specifically regulated by miR-22. As such, direct treatment with PEPITEM may have bolstered the response due to an increased local concentration and being able to act directly on the bone without requiring further processing. Of note, YWHAZ/14-3-3ζδ have been shown to be involved in multiple other processes in cells and are found to be upregulated in many cancers.[570] Therefore, targeting the parent protein may lead to an increase in unwanted side effects within the bone, whilst treating with a PEPITEM-derivative may limit these off-target effects.

3.3.2 **Understanding the bioactivity of PEPITEM**

Of importance, our study focused on the effect of PEPITEM in 6-8 week mice, where there is net bone formation and thus bone is highly osteoblast driven.[571] Since *in vitro* we observed a greater effect of PEPITEM on osteoblasts it may indicate that the effect of PEPITEM would be reduced in older mice, where osteoblasts and osteoclast activity are finely balanced to maintain bone (as opposed to generating net growth). In addition, whilst we directly observed an increase in bone growth, there

was no change in bone growth serum marker P1NP. This may be partially due to the short time frame of experiment, or alternatively may point towards the mechanisms of PEPITEM, where bone may have high level of remodelling towards the start of treatment, but by the end changes are undetectable. Alternatively, there may be changes in both bone formation and resorption influencing bone growth, therefore measuring one alone would not provide a difference. Therefore, future studies should explore changes in both P1NP and resorption marker CTX-1 to understand the relationships between the two. Additionally, histomorphometry of osteoblasts on the bone surface, in addition to osteoclasts, may provide additional knowledge of the driving force behind the bone growth.

Additionally, there may be some differences between I.P injection of native PEPITEM and S.C injections of PEPITEM enclosed in a liposome. Whilst the size and composition of the liposomes meant uptake of liposomes by cells is a rare occurrence,[572–575] there will be some interactions with scavenging cells such as macrophages.[575] Changes in drug delivery would change PEPITEMs bioactivity, particularly in relation in osteoclasts, where PEPITEM had no effect when given to osteoclasts extracellularly, but intracellular uptake by scavenging receptors may alter osteoclast responses. More research is required to understand the changes in PEPITEM delivery in liposomes looking at more than prolonged release. Similarly, liposomes were given S.C as opposed to I.P, which would alter the distribution of PEPITEM around the body.[574] This was done to allow for prolonged release of PEPITEM as opposed to cellular scavenging, which is more common in other delivery mechanisms, but it may alter PEPITEMs effects, such as the changes observed in trabecular thickness, which needs to be explored in further detail. Serum

levels of PEPITEM over time following native or liposome injections are needed to understand the distribution of PEPITEM over time and the amount of PEPITEM that makes it into the blood to be transported around the body.

3.3.3 **Do the effects of PEPITEM match current therapeutics?**

The main currently licenced therapeutics that improve bone growth are PTH and bisphosphonates, targeting the osteoblasts to initiate mineralisation or decreasing osteoclastogenesis and increasing osteoclast apoptosis respectively. Regardless of mechanism, these treatments induce bone growth in homeostatic mice, which will be explored below.

The majority of studies looking a bone therapeutics use at least a 4-week time point for analysis, with very few using a 2-week treatment window as used in our study. Zweifler et al evaluated the response of WT mice to PTH by collating the results from multiple studies.[576] Whilst they did not look specifically at 2-weeks of treatment, they found a significant positive corelation in BV/TV when comparing control and PTH treated trabecular bone volume in mice treated for less than 4 weeks (linear regression slope of 1.347).[576] Whilst statistically significant at 4-weeks, the correlation was more apparent when examining 5-6-weeks - linear regression of 2.459.[576] Few studies have analysed the changes in trabecular bone following two-weeks of treatment.[577,578] WT mice treated for two-weeks with PTH had significantly increased trabecular thickness of 30%[577] and 25%[578] when compared to control animals in each study. These increases were higher than those we observed following PEPITEM treatment (8%). Importantly, we also observed a 20% increase in trabecular number, which was above the changes noted in the previous PTH studies: non-significant change[578] or an increase of 10%[577]. Nevertheless, these studies

explored changes in femoral bone as opposed to trabecular, which may alter trabecular changes. Overall, PEPITEM induced changes similar to treatment with PTH, however altered responses in trabecular thickness and trabecular number may indicate different mechanisms.

PTH induced vertebral trabecular bone changes were non-significant in one of the studies,[577] whereas the other showed a 10% increase,[578] similar to the 9% observed by PEPITEM. The differences between these individual studies on PTH may be explained by the slightly higher dose (40µg/kg[578] compared to 30µg/kg[577]) or only treating for 5 days/week[578] compared to every day.[577] Of relevance, PTH treatment regime and concentration has been refined over many years, whilst these are the first experiments exploring PEPITEM. Therefore, future experiments should examine a full dosing regimen to ascertain the optimal does to maximise PEPITEM response and minimise any off-target effects. Importantly, PEPITEM bioactivity appears to match the response of homeostatic bone to PTH, implying it is possibly suitable for therapeutic use.

Bisphosphonates also show similar patterns of bone responses to our PEPITEM treated mice, where 2-week treatment with zoledronic acid increased femoral trabecular thickness by 12%[579] - a similar percentage increase seen with PEPITEM. A variety of bisphosphates have been reported to induce substantial increases in trabecular number at 2-weeks (32%) and beyond [e.g. 3-weeks treatment with Clodronate (43%), Zoledronic acid (90%), Alendronate (157%) and or Pamidronate (49%)].[580] However, the latter study found no change in trabecular thickness.[580] Whilst PEPITEM does not induce a trabecular number increase to the same degree (20%) as bisphosphonates, the increase in trabecular thickness and trabecular

number may further indicate its dual effects on increasing osteoblasts (increased trabecular thickness as seen with PTH) and osteoclasts (increased trabecular number as seen with bisphosphonates). That said, future studies are required to investigate if the bioactivity of PEPITEM continues or improves over longer time points, and how it compares to the responses of bone following treatment with PTH and bisphosphonates in disease states.

3.3.4 **Comparing current therapeutics action at a cellular level**

Cellular responses to PEPITEM can also be used to begin to understand its mechanism of action and compare to current therapies. The effects of PTH on cultured osteoblasts is unclear with studies reporting increases,[92,393,581,582] decreases[393,581] and no change[92,393,581,583,584] in osteoblast activity and or mineralisation. Some studies have implicated exposure time,[393] differentiation state,[92,581] or species (mouse compared to rat)[581] as factors influencing the responsiveness of cells, however results still vary when similar regimens are followed.[393,583,584] Of relevance, continuous PTH treatment (replaced every 48 hours) for 9 days significantly inhibited ALP activity and mineralisation,[393] whereas continuous PEPITEM treatment showed the inverse response – promoting mineralisation.

Whilst we observed no difference when adding PEPITEM directly to monocytes, *in vivo* analysis revealed a decreased osteoclast number on the bone surface. In contrast, PTH treatment increased osteoclast numbers *in vivo*[585,586] by upregulating RANKL expression on the cells.[587–589] Therefore, PTH induced bone formation may be suppressed by the increased osteoclastogenesis, whilst the dual effect of PEPITEM on osteoblasts and osteoclasts may lead to more efficient bone

production. Bisphosphonates directly target osteoclastogenesis, leading to a significant decrease in osteoclast numbers and resorption.[580] However, as shown through both our study and other *in vitro* studies this can lead to a significant inhibition of osteoclastogenesis,[316,590] leading to damaged bone not being resorbed and the development of micro-fractures.[591–593] The reduced level of osteoclast resorption seen following PEPITEM treatment *in vivo*, would allow bone remodelling (resorption followed by formation) to still occur albeit at a diminished level, as opposed to completely suppressed resorption, leading to a build-up of bone without additional damage.

The location of osteoclast changes may also help understand the bioactivity of PEPITEM. The biggest change in osteoclast numbers, whilst not measured directly, appears to occur around the growth plate. Bone elongation around the growth plate stops following 12 weeks of age in mice, therefore older mice may show different responses due to the reduced number of osteoclasts already present. Measuring osteoclasts at differing locations around the bone would enable understanding of how PEPITEM may influence older mice, where osteoclast numbers are more evenly spread.

3.3.5 **Treatment induced cortical bone changes**

Some interesting differences were observed when comparing PEPITEM treatment to studies using PTH and bisphosphonates that may point towards differences in mechanism. Following PEPITEM treatment, we observed no difference in cortical bone parameters, which was also the case following 2-week treatment with zoledronic acid.[579] This could be expected due to the short-term treatment with PEPITEM (2-weeks). Cortical bone in both human and murine bone has been shown

to turn over 2-3 times slower than trabecular bone,[310,594] thus longer treatment regimens provide time for PEPITEM to increase cortical bone. This is the case with bisphosphonates, where cortical bone was observed to increase after 10-weeks of treatment,[595] but not 2-weeks.[579] Importantly, PTH treatment for two-weeks has been previously shown to increase cortical bone.[578] The potential differences in how these compounds influence cortical bone turnover and formation might provide novel insights into the molecular mechanism for the bioactivity of PEPITEM. In addition, longer PEPITEM treatment of WT mice may begin to show increases in cortical bone area and thickness, which were unable to be quantified in our study.

3.3.6 Difference in cell responses to PEPITEM

Of note, unlike the primary osteoblasts used in this study, MC3T3-E1 cell line did not show altered ALP levels in response to PEPITEM. It is well known that subclones of the MC3T3 line vary in their differentiation responses. For example, clone 4, 14 and 24 all show differing levels of ALP activity, mineral production, and response to PTH.[596] Furthermore, the MC3T3 line is calvarial in origin and non-tumorigenic, however differences between this line and primary calvarial osteoblasts have also been described.[596] Comparing transcripts from pre-differentiated and differentiated MC3T3 subclones 4 and 24, and primary calvarial osteoblasts revealed only the *Spp1* gene was upregulated by all 3 cell types, with each cell type displaying its own array of upregulated and downregulated genes.[596] Therefore, differences in responses between calvarial osteoblasts and MC3T3 cells could be expected. Large scale sequencing of the MC3T3 and calvarial osteoblasts to reveal whole genome expression changes may provide insight into why cells show differential responses. Following the better understanding of the molecular mechanisms regulating

PEPITEM bioactivity in the bone, further analysis of these factors could be explored to ascertain whether differences in these explain the functional differences between primary and immortalised MC3T3 osteoblasts.

3.3.7 **Conclusion**

In conclusion, we have shown PEPITEM can act directly on osteoblasts and indirectly on osteoclasts, leading to an increase in trabecular bone growth and in doing so increasing the strength and stiffness of the bone. Therefore, we accept our original hypothesis that PEPITEM induces a pro-anabolic and anti-catabolic phenotype on homeostatic bone.

We have yet to determine the signalling mechanism by which PEPITEM causes the increased osteoblast mineral production *in vitro* or osteoclastogenesis *in vivo*. Previously, the bioactivity of PEPITEM in endothelial cells was shown to be regulated by S1P and endothelial expression of cadherin-15.[473] Therefore, we next sought to understand if these same molecules were influential in the activity of PEPITEM in bone.

4 Investigating the Role of S1P in the Bioactivity of PEPITEM

4.1 Introduction

In the previous chapter, we clearly demonstrated a direct effect of PEPITEM on osteoblasts to induce an increase in mineral production. Similarly, indirect actions of PEPITEM on monocytes decreased osteoclastogenesis *in vivo* and in cultures where multiple cell populations were observed. However, we have yet to determine the mechanism of action downstream of PEPITEM that induces these cellular responses.

Several endogenous molecules influence bone growth through actions on osteoblasts and osteoclasts, including RANKL,[73,184,597,598] adiponectin,[464] PTH,[392] and S1P.[448,449,599] We have previously demonstrated that PEPITEM induces the release of S1P from endothelium.[473] Inhibition of S1P production using sphingosine kinase inhibitors or decreasing S1P release through siRNA knockdown of S1P transporter SPNS2 blocks the bioactivity of PEPITEM on T-cell trafficking, thus showing S1P's essential role in PEPITEM signalling.

Human (primary)[481,487] and murine (primary calvarial, MC3T3-E1)[487] osteoblasts can release S1P into their surrounding environment. In addition, osteoblasts and osteoclasts express an array of S1P receptors (S1PR1-4)[358,483,485,486] and both cell types have been shown to respond to S1P *in vivo* and *in vitro.*[481,486,488,493]

In this chapter, we aim to investigate the responses to osteoblasts and osteoclasts to S1P. We hypothesise that osteoblasts and osteoclasts will directly respond to S1P, leading to similar responses as seen with PEPITEM treatment.

4.2 Results

4.2.1 Osteoblasts produce an osteoclast inhibitory substance in response to PEPITEM.

Osteoblast-osteoclast coupling is highly prevalent in the bone, thus we explored if the changes observed in osteoclast numbers *in vivo* could result from the direct action of PEPITEM on osteoblasts. To assess this, we treated monocytes with conditioned media from primary human osteoblasts which were either undifferentiated, differentiated and differentiated treated with PEPITEM, and supplemented the media with m-CSF and RANKL to induce osteoclastogenesis. After 8 days, we observed a significant reduction in the number of osteoclasts in wells treated with conditioned media from PEPITEM treated osteoblasts compared to other conditioned media (Figure 4.1B). This indicates PEPITEM induces the production of a soluble mediator by osteoblasts which can interfere with osteoclastogenesis.

4.2.2 Osteoclasts express receptors to respond to S1P

Considering PEPITEM is known to induce S1P release from endothelial cells, we explored the responsiveness of osteoclasts to S1P to understand if S1P could be the soluble mediator. We first explored S1P receptor expression in osteoclasts using a published single cell dataset (GSE147174) of whole murine bone marrow treated with m-CSF and RANKL to induce osteoclastogenesis where samples were taken at baseline (day 0), day 1 and day 3. Four clusters of relevance were isolated from the combined dataset and identified as *s100a8*^{high} *S100a9*^{high} monocytes (Figure 4.2B/C), *Cd16*^{high} *F4/80*^{high} macrophages (Figure 4.2D/E), *Acp5*^{med} *Atp6c0d2*^{med} *Ctsk*^{med} *Mmp9*^{med} pre-osteoclasts (Figure 4.2F-I) and *Acp5*^{high} *Atp6c0d2*^{high} *Ctsk*^{high} *Mmp9*^{high}

osteoclasts (Figure 4.2F-I). Maturation stages were confirmed by splitting the clusters based on the number of days post RANKL treatment. At baseline (day 0) few pre-osteoclasts or osteoclasts were identified in the sample, whereas at day 1 the majority of cells were pre-osteoclasts, which changed to osteoclasts at day 3 (Figure 4.2A). Using these clusters, expression of S1P receptors were explored throughout osteoclastogenesis. *S1pr1* and *S1pr3* were not detected in any subset, whereas the percentage of cells expressing *S1pr2* increased throughout differentiation (Figure 4.3). In contrast, expression of *S1pr4* was only present in the monocyte cluster and lost during osteoclastogenesis (Figure 4.3). We next confirmed gene expression of two key S1P receptors in murine osteoclast precursors RAW264.7 cells by PCR. Interestingly, RAW264.7 cells expressed both *S1pr1* and *S1pr4*, however *S1pr4* was expressed at a significantly lower level (Figure 4.4). Expression was also confirmed in human primary monocytes and RANKL induced osteoclasts. Monocytes and osteoclasts both expressed *S1pr1* (Figure 4.5A) and *S1pr4* (Figure 4.5B), however whilst *S1pr1* expression was maintained through osteoclastogenesis (Figure 4.5A), there was a significant reduction in *S1pr4* expression (Figure 4.5B).

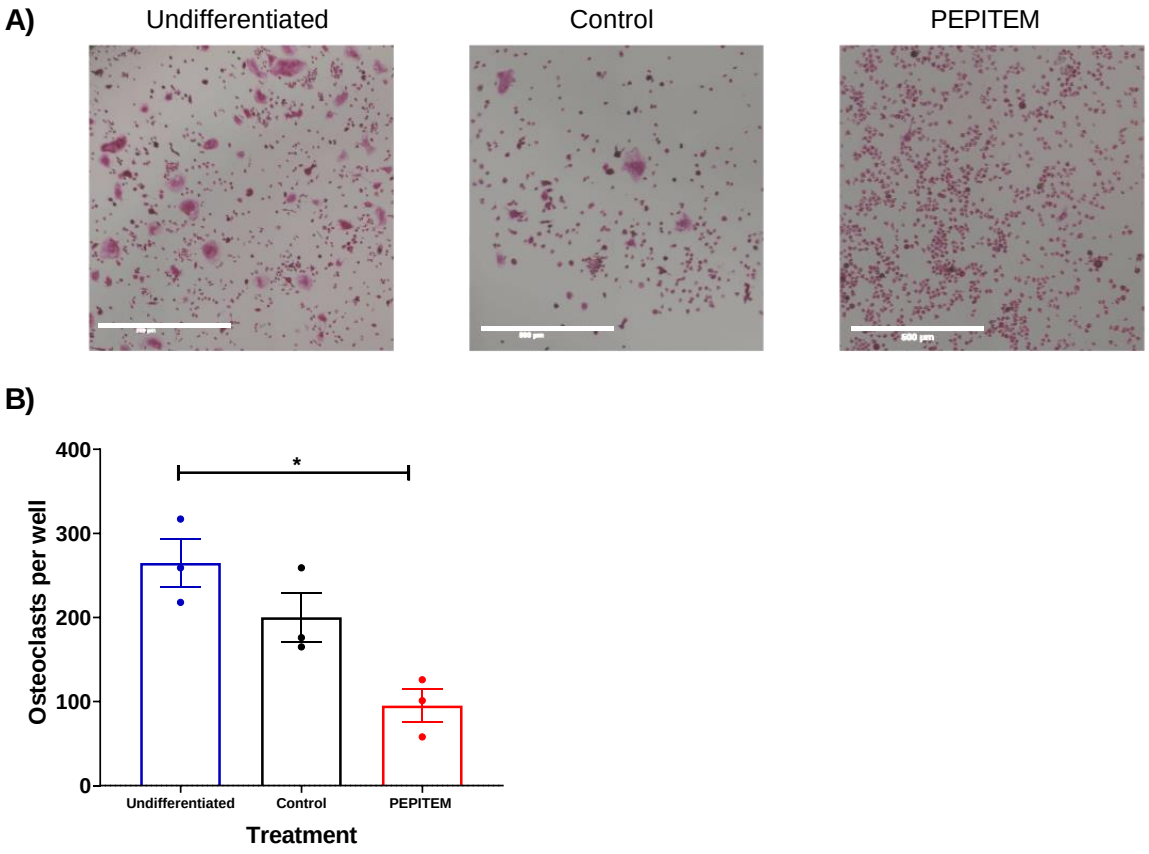

Figure 4.1 PEPITEM treated osteoblasts decrease osteoclastogenesis.

Primary human osteoblasts were cultured in basal media (undifferentiated), differentiation media (control) or differentiation media with PEPITEM for 8 days. Conditioned media was collected every third day, supplemented with m-CSF and RANKL and added to primary monocyte cultures. After 8 days in culture osteoclasts were fixed and stained for TRAP. **A**. Representative images of TRAP-stained cells from undifferentiated, control or PEPITEM treated conditioned media wells. **B**. Number of TRAP+ osteoclasts per well in each culture condition. ANOVA showed significant effect of culture conditions on osteoclastogenesis, $p<0.05$. Data are mean±SEM, with n=3 for 3 different donors. * = $p<0.001$ by Bonferroni's multiple comparisons test comparing different culture conditions. Scale bars = 500μm.

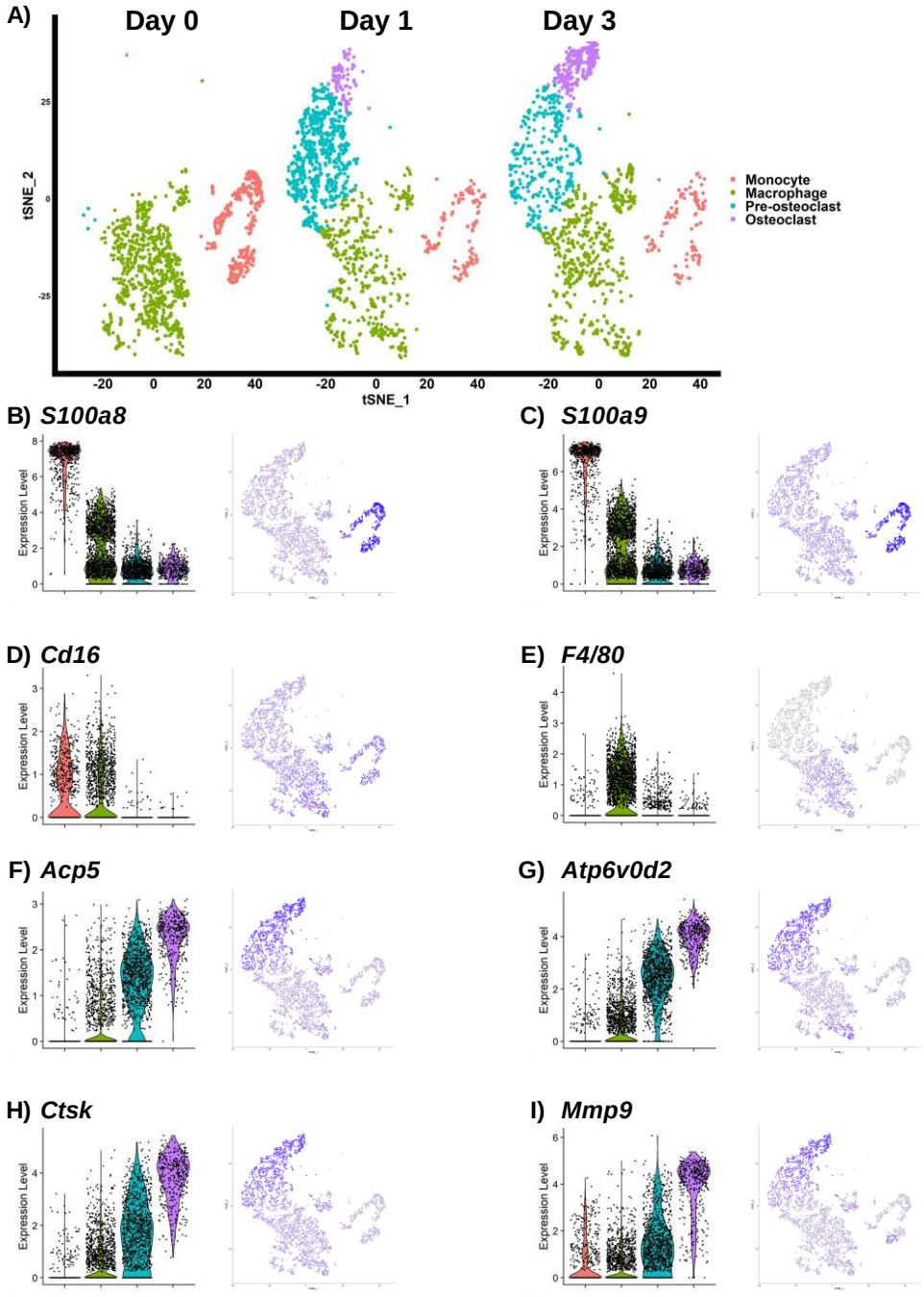

Figure 4.2. Single-cell analysis of RANKL treated murine bone marrow.

Cells involved in osteoclastogenesis were identified from pre-published dataset GSE147174 (single cell RNA sequencing of RANKL treated whole bone marrow) and clustered into four distinct groups using the Seurat software. **A.** Feature plot of clustered osteoclasts grouped by TSNE and separated by time since RANKL treatment (Day 0, Day 1, Day 3). **B-I.** Violin plots and feature plots of osteoblast genes *S100a8* **(B)**, *S100a9* **(C)**, *Cd16* **(D)**, *F4/80* **(E)**, *Acp5* **(F)**, *Atp6v0d2* **(G)**, *Ctsk* **(H)** and *Mmp9* **(I)**.

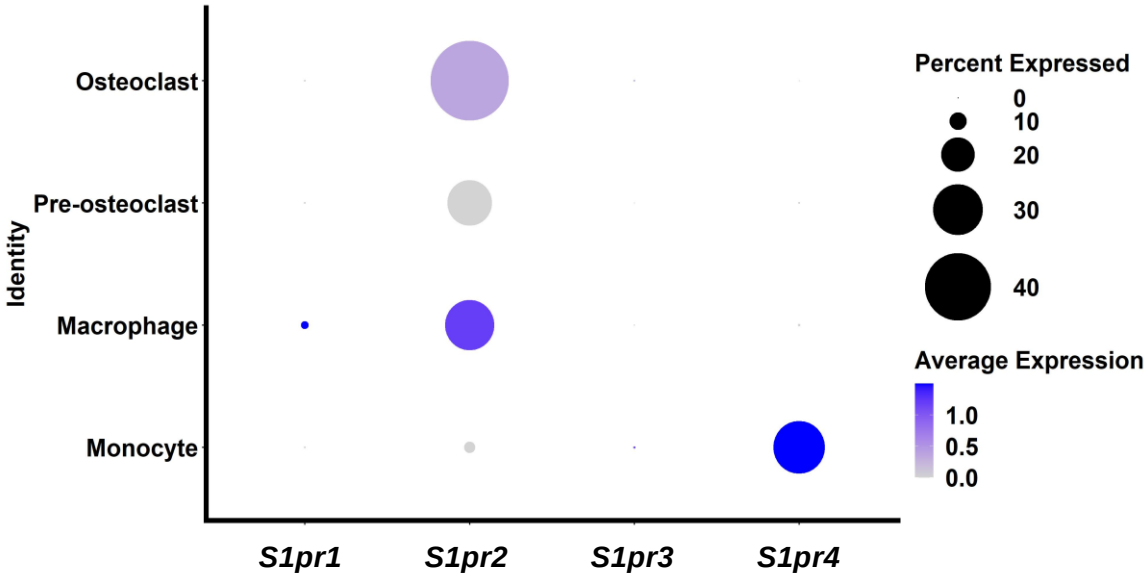

Figure 4.3. Osteoclasts express a range of S1P receptors.

Clustered monocytes, macrophages, pre-osteoclasts, and osteoclasts from single-cell dataset GSE147174 were analysed for gene expression of S1P receptors. Dotplot of expression of *S1pr1*, *S1pr2*, *S1pr3* and *S1pr4* in each cell subset. Circle size represents the percentage of cells expressing the gene, and colour indicates average expression value (blue to grey = high to low expression).

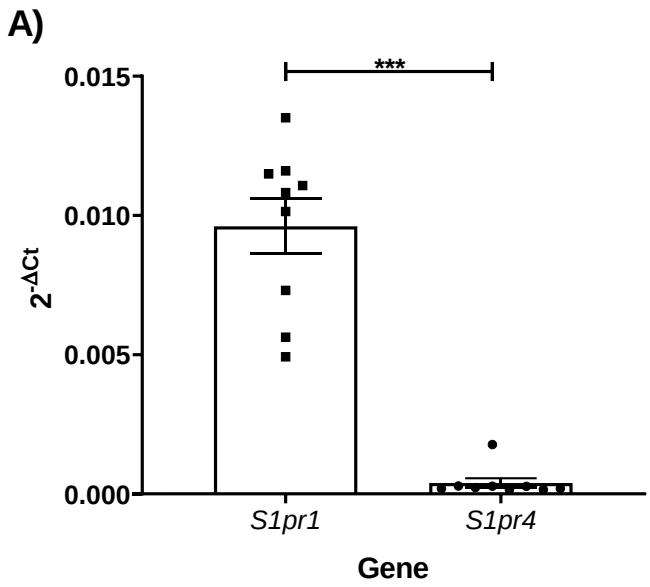

Figure 4.4 RAW264.7 cells express *S1pr1* and low *S1pr4.*

Murine macrophage-like RAW264.7 cells were cultured *in vitro for 3 days*, and RNA was isolated. RNA was analysed by qPCR for expression of *S1pr1 and S1pr4*. Data are displayed as $2^{-\Delta Ct}$, where ΔCt is the relative expression compared to *B2m* housekeeping gene. Data are mean ± SEM for n=9 and 3 independent experiments. ***=P<0.001 by student t-test.

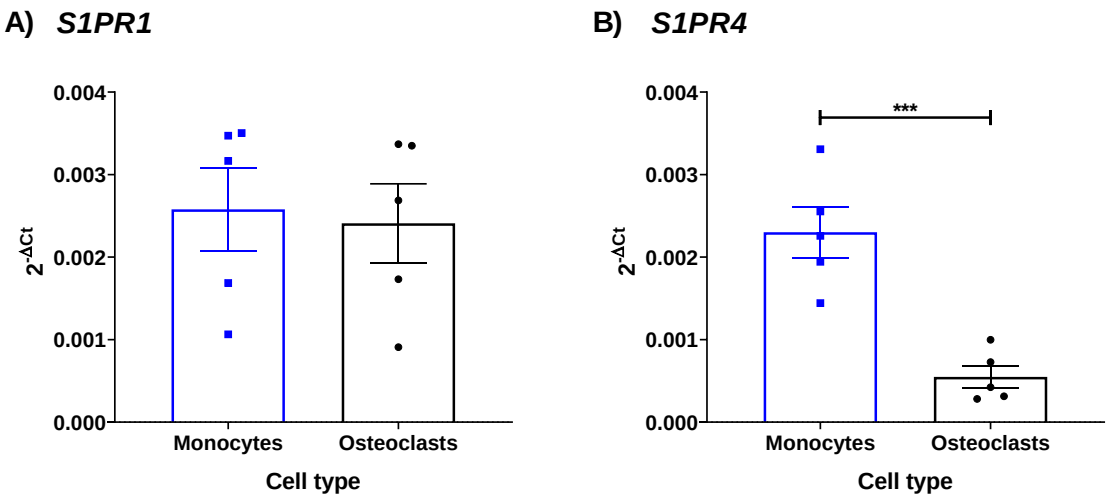

Figure 4.5. Human osteoclasts express S1P receptor genes.

Human primary monocytes were isolated from PBMCs and cultured for 8 days alone or with m-CSF and RANKL. mRNA was isolated on day 8 from undifferentiated monocytes (blue, n=5) or osteoclasts (black, n=5) and analysed for expression of **A.** *S1PR1* or **B.** *S1PR2*. Data are displayed as $2^{-\Delta Ct}$, where ΔCt is the relative expression compared to *B2M* housekeeping gene. Data are mean ± SEM for 5 independent donors. ***=P<0.001 by paired t-test comparing monocytes to osteoclasts.

4.2.3 Human osteoclastogenesis is disrupted by S1P signalling

Since osteoclasts and their precursors showed expression of S1P receptors, we next explored the cellular changes that occurred following S1P treatment. Osteoclastogenesis was induced in primary human monocytes by RANKL for 8 days and osteoclast numbers were assessed by TRAP staining. There was a significant reduction in the number of osteoclasts in S1P treated wells compared to untreated controls, however osteoclasts were still present in low numbers (Figure 4.6A/B). In contrast, zoledronic acid treated wells had a complete absence of osteoclasts (Figure 4.6A/B). Reduction in osteoclast number with S1P treatment was coupled to decreased resorption in cells cultured on dentine disks for 21 days (Figure 4.7A/B). The percentage of dentine resorbed in S1P treated wells was significantly decreased compared to untreated controls (Figure 4.7A/B), indicating an inhibitory effect of S1P on osteoclasts.

Exploring the changes in osteoclasts further, expression of major osteoclast genes were analysed in untreated and S1P treated wells 8 days after induction of osteoclastogenesis by RANKL. Osteoclast markers *ACP5* and *CTSK* were significantly decreased in S1P treated wells compared to control (Figure 4.8A/B). In contrast, macrophage marker *MSR1* significantly increased following S1P treatment (Figure 4.8C). These data indicate an inhibitory effect of S1P on human monocyte osteoclastogenesis, leading to the acquisition of a macrophage-like phenotype. Due to the morphology of S1P treated monocytes and the known ability for monocytes to differentiate into endothelial type cells, the expression of endothelial markers *VWF*, *PECAM1,* and *SELE* were also explored and compared to levels detected in human umbilical vein endothelial cells (HUVECs). All genes were significantly decreased in

monocytes, RANKL treated monocytes (osteoclasts), and RANKL and S1P treated monocytes when compared to HUVEC, however, no significant differences were observed between untreated osteoclasts and S1P treated cells (Figure 4.9A-C).

We also explored the response of murine RAW264.7 macrophage like cells to S1P. Interestingly, we observed a significant increase in TRAP+ osteoclasts in wells treated with S1P compared to untreated controls (Figure 4.10A/B) indicating increased osteoclastogenesis. To investigate this further we examined the proliferation of RAW264.7 cells left untreated, following RANKL treatment alone or in combination with PEPITEM or S1P. Known cell numbers (0 to 2 x 10^6 cells) were plated and resazurin, which undergoes a colour change when reduced, was added to determine the colour change that occurs with each cell number (Figure 4.11A). The control curve was used to calculate the number of cells following 5 days in culture of treated cells. Differentiation and PEPITEM treatment had no effect on RAW264.7 cell number over 5 days, however S1P treatment led to a significant increase in RAW264.7 cell number compared to untreated control cells, indicating increased proliferation in response to S1P (Figure 4.11B).

Overall, we have identified an inverse action of S1P on human and murine osteoclasts leading to decreased or increased osteoclastogenesis respectively.

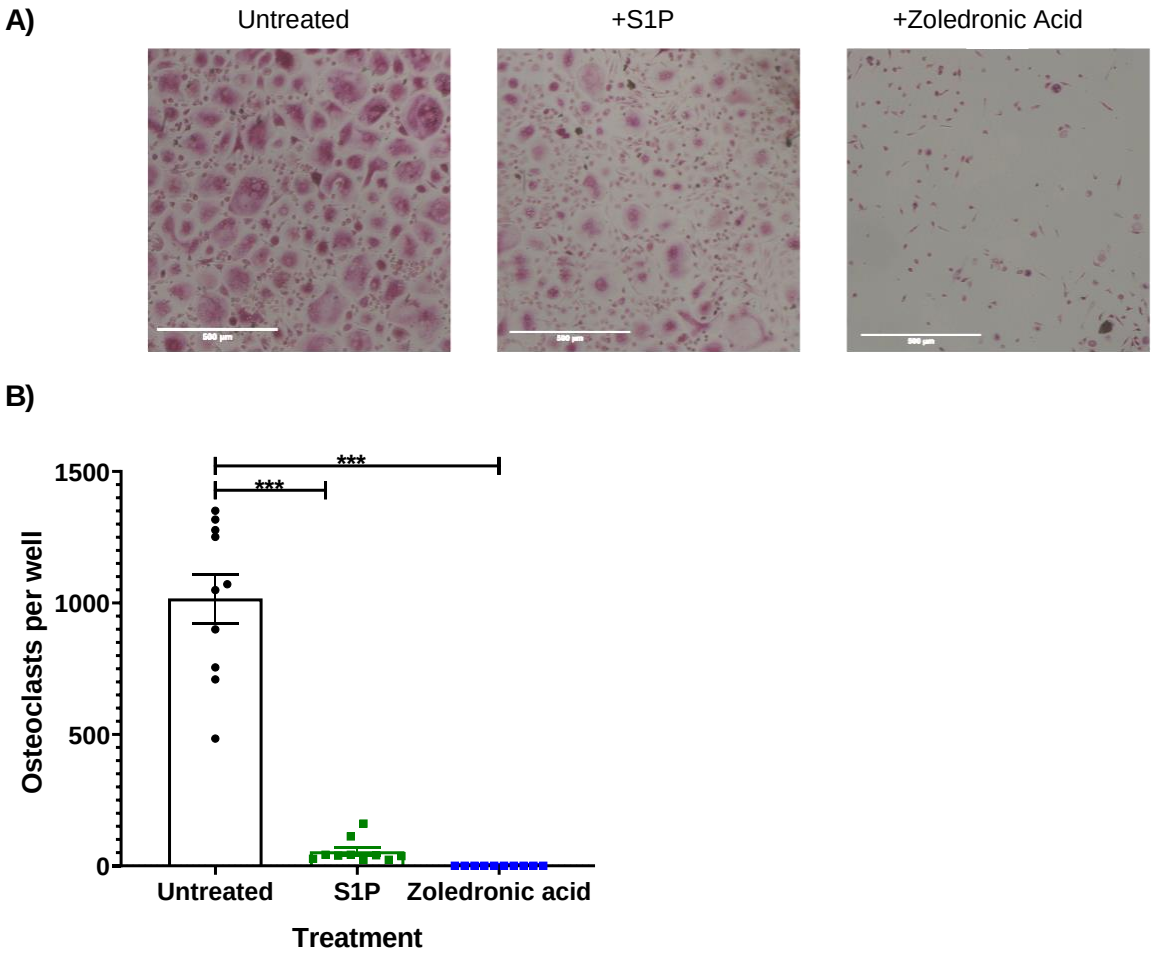

Figure 4.6. S1P reduced osteoclastogenesis of primary human monocytes.

Human PBMC isolated monocytes were treated with RANKL to induce osteoclastogenesis. Cells were either untreated (black, n=10) or treated with S1P (green, n=10) or Zoledronic acid (blue, n=10) and the resulting osteoclasts were stained for TRAP. **A.** Representative images of untreated, S1P treated or Zoledronic acid treated wells. **B.** Osteoclasts were counted in each condition and presented as number of osteoclasts per well. ANOVA showed a significant effect of treatment on osteoclast number, $p<0.01$. Data are mean ± SEM, where n=10 for 3 independent experiments. ***=$p<0.001$ by Bonferroni multiple comparisons test comparing treatment condition. Scale bars = 500µm.

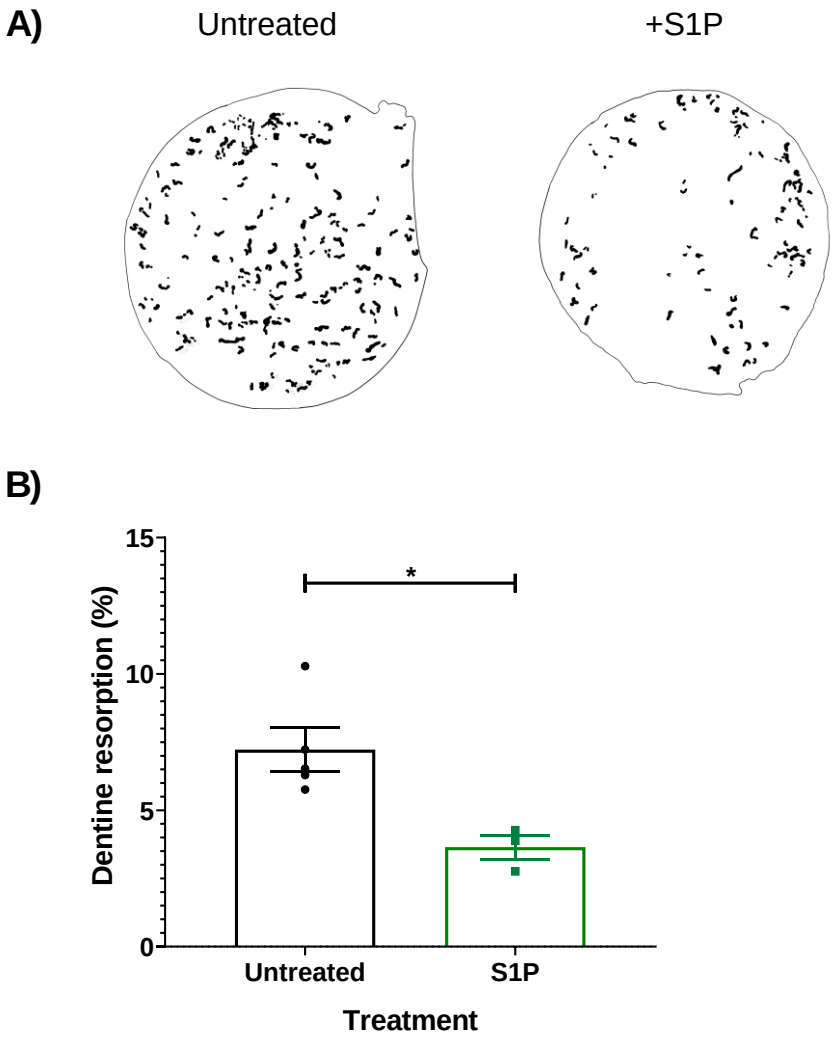

Figure 4.7. S1P reduced osteoclast resorption on dentine slices.

Human monocytes were isolated from whole blood PBMCs and osteoclastogenesis was induced on dentine slices by addition of RANKL and m-CSF to cultures. Cells were cultured for a total of 21 days alone (black, n=6) or in the presence of S1P (green, n=3), after which cells were removed and dentine was stained for resorption. **A.** Representative images of masks generated to show areas resorbed by osteoclasts. **B.** The area resorbed was recorded in each condition and displayed as a percentage of total area. Data are mean ± SEM from 3 independent donors. * = $p < 0.05$ by students t-test.

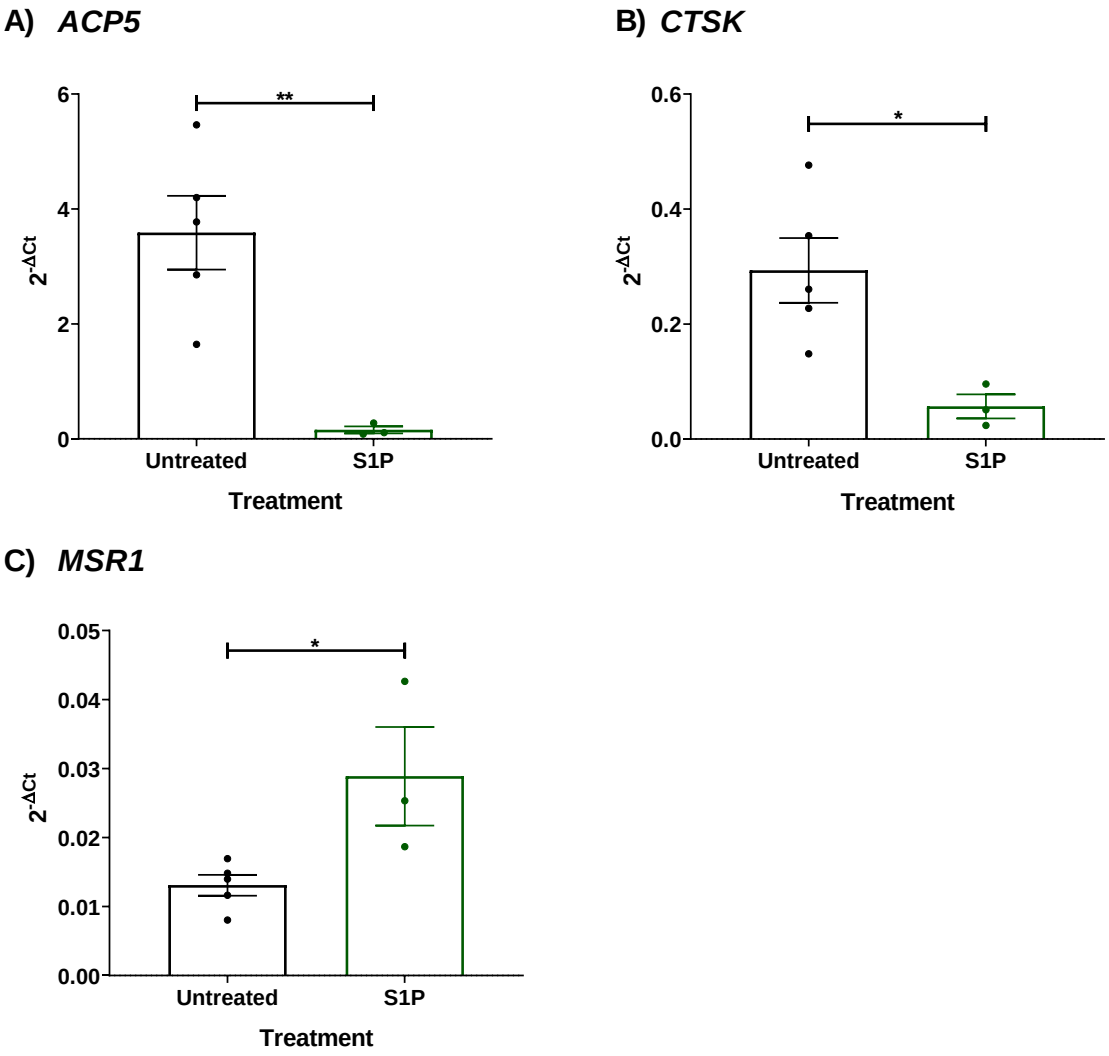

Figure 4.8. S1P treated osteoclasts decrease osteoclast related gene expression.

Human monocytes were isolated from whole blood PBMCs and osteoclastogenesis was induced by addition of RANKL and m-CSF to cultures. Cells were left untreated (black, n=5 independent donors) or treated with S1P (green, n=3 independent donors) for 8 days **A-C.** RNA expression of *ACP5* **(A)**, *CTSK* **(B)** and *MSR1* **(C)** were analysed by qPCR. Data are displayed as $2^{-\Delta Ct}$, where ΔCt is the relative expression compared to *B2M* housekeeping gene. Data are mean ± SEM. *=P<0.05, **=P<0.01 by student's t-test.

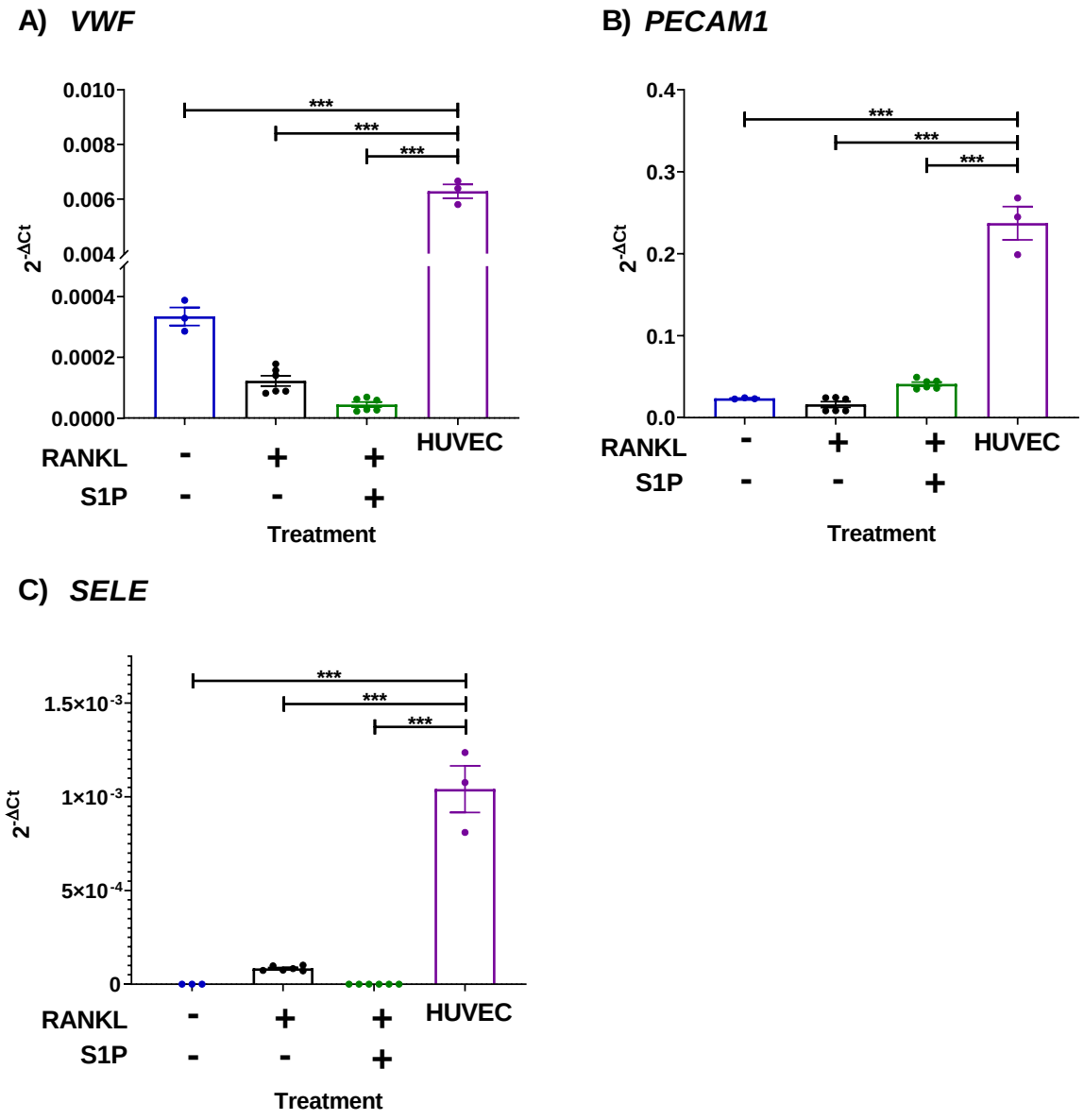

Figure 4.9. S1P treated osteoclasts do not express endothelial markers.

Human monocytes were isolated from whole blood PBMCs and cultured alone (blue, n=3) or osteoclastogenesis was induced by addition of RANKL and m-CSF to cultures. Differentiated cells were left untreated (black, n=6) or treated with S1P (green, n=6) for 8 days. Endothelial cells were isolated from umbilical cords (purple, n=3). **A-C.** RNA expression *VWF* **(A)**, *PECAM1* **(B)** and *SELE* **(C)** were analysed by RTPCR. Data are displayed as $2^{-\Delta Ct}$, where ΔCt is the relative expression compared to *B2M* housekeeping gene. ANOVA showed a significant effect of culture conditions on gene expression, p<0.01. Data are mean ± SEM. ***=P<0.001 by Bonferroni multiple comparisons test.

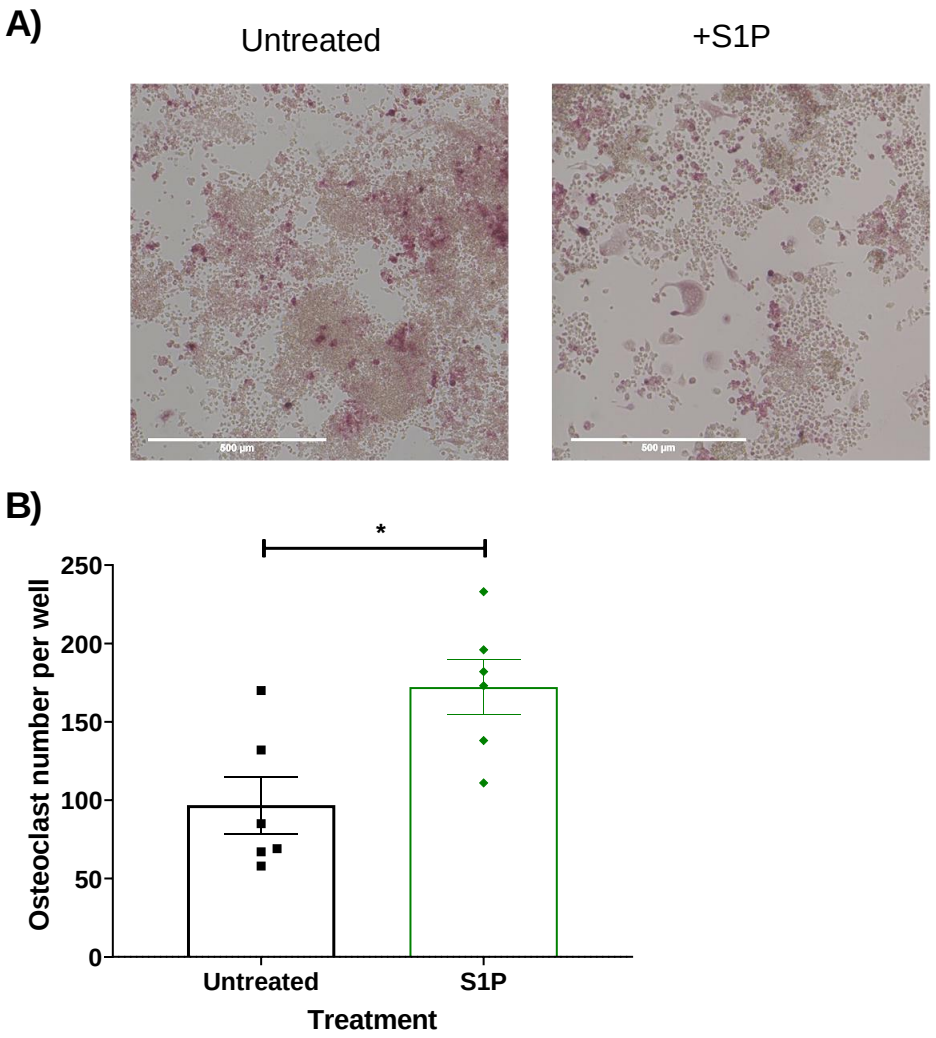

Figure 4.10. S1P increased osteoclastogenesis of murine RAW264.7 macrophage-like cells.

Murine RAW264.7 macrophage-like cells were differentiated into osteoclasts by addition of RANKL. TRAP staining following 5 days of culture allowed analysis of the number of TRAP+ multinucleated cells present in the wells following culture alone (black, n=6) or with S1P (green, n=6). **A.** Representative images of untreated or S1P treated wells. **B.** Osteoclasts were counted in each condition and presented as number of osteoclasts per well. Data are mean ± SEM for 3 independent experiments. *=P<0.05 by students t-test. Scale bars = 500µm.

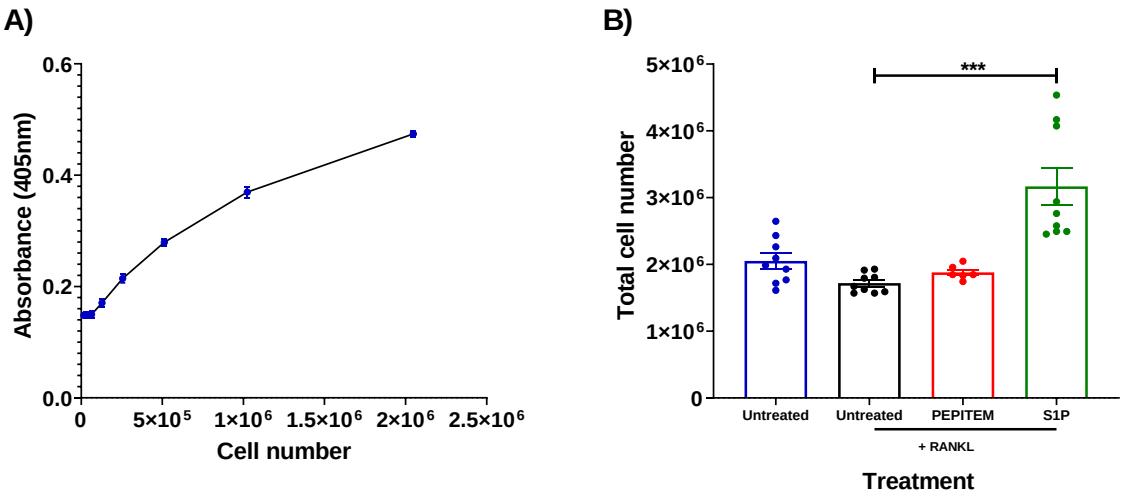

Figure 4.11. S1P increased the proliferation of RAW264.7 macrophage-like cells.

RAW264.7 cells were cultured alone (blue, n=9) or with RANKL to induce osteoclastogenesis. RANKL treated cells were left untreated (black, n=9) or treated with PEPITEM (red, n=5) or S1P (green, n=9). After five days in culture, cells were incubated with resazurin, and colour change was analysed using absorbance. **A.** Standard curve of known numbers of RAW264.7 cells and absorbance of resazurin measured. **B.** Cell numbers were analysed in each conditioned. ANOVA showed a significant effect of treatment on RAW264.7 cell number, $p<0.01$. Data are mean ± SEM. ***=$P<0.001$ by Bonferroni multiple comparisons test.

4.2.4 **Osteoblasts express S1P production genes.**

Osteoclasts and their precursor cells showed ability to respond to S1P, thus we explored the ability of osteoblasts to produce S1P to understand the cross-link between the signalling.

Using a published single cell RNAseq dataset containing stromal cells from the bone marrow of C57Bl6 mice,[553] we first analysed the expression of S1P-related genes in maturing osteoblasts. Firstly, we used cluster profiling and osteoblast-specific genes to identify any cells of osteoblast lineage. Osteoblast were first identified by expression of *Runx2* and *Sp7* (Figure 4.12A-C). Osteoblasts were further sub-divided into 3 main clusters: *Cxcl12*^{high} early osteoprogenitors (Figure 4.12D); *Alpl* ^{high} *Spp1*^{high} pre-osteoblasts (Figure 4.12E/F); *Bglap1*^{high} *Col1a1*^{high} *Col1a2*^{high} mature osteoblasts (Figure 4.12G-I). Using these subsets, changes in S1P production genes throughout differentiation were analysed. *Sphk1, Sphk2* and *Spns2* were all expressed to some degree in mature osteoblasts, however expression levels of *Sphk1* and *Sphk2* decreased with differentiation (Figure 4.13). In contrast, the percentage of cells expressing *Spns2* and average expression levels of *Spns2* increased with differentiation, with highest expression observed in mature osteoblasts (Figure 4.13). Confirming the RNAseq analysis we detected the sphingosine kinases in both primary murine and primary human osteoblasts by qPCR (Figure 4.14A/B & Figure 4.15). No differences were observed in kinase expression or *Spns2 expression* during calvarial osteoblast differentiation (Figure 4.14A/C). These data indicate an ability for osteoblast to release S1P as a paracrine signalling molecule for communication between osteoblasts and osteoclasts.

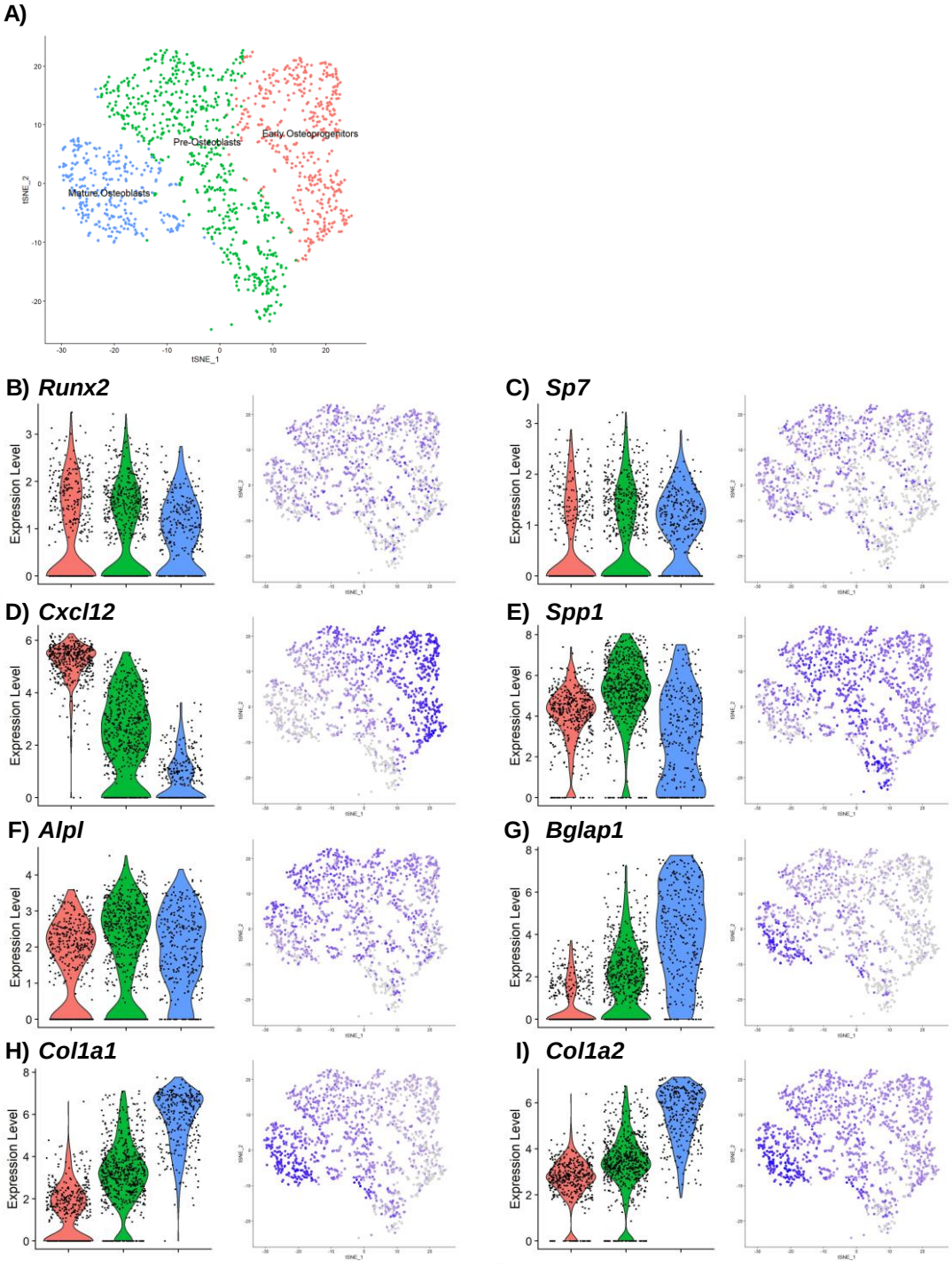

Figure 4.12. Exploration of osteoblast maturation in bone marrow stroma.

Osteoblasts were identified from pre-published dataset GSE128423 where single-cell RNA sequencing was performed on the stromal cells from murine bone marrow. Osteoblasts were clustered into three maturation stages using the Seurat software. **A.** Feature plot of clustered osteoblasts separated via TSNE. **B-I.** Violin plots and feature plots of osteoblast genes *Runx2* **(B)**, *Sp7* **(C)**, *Cxcl12* **(D)**, *Spp1* **(E)**, *Alpl* **(F)**, *Bglap* **(G)**, *Col1a1* **(H)** and *Col1a2* **(I)**.

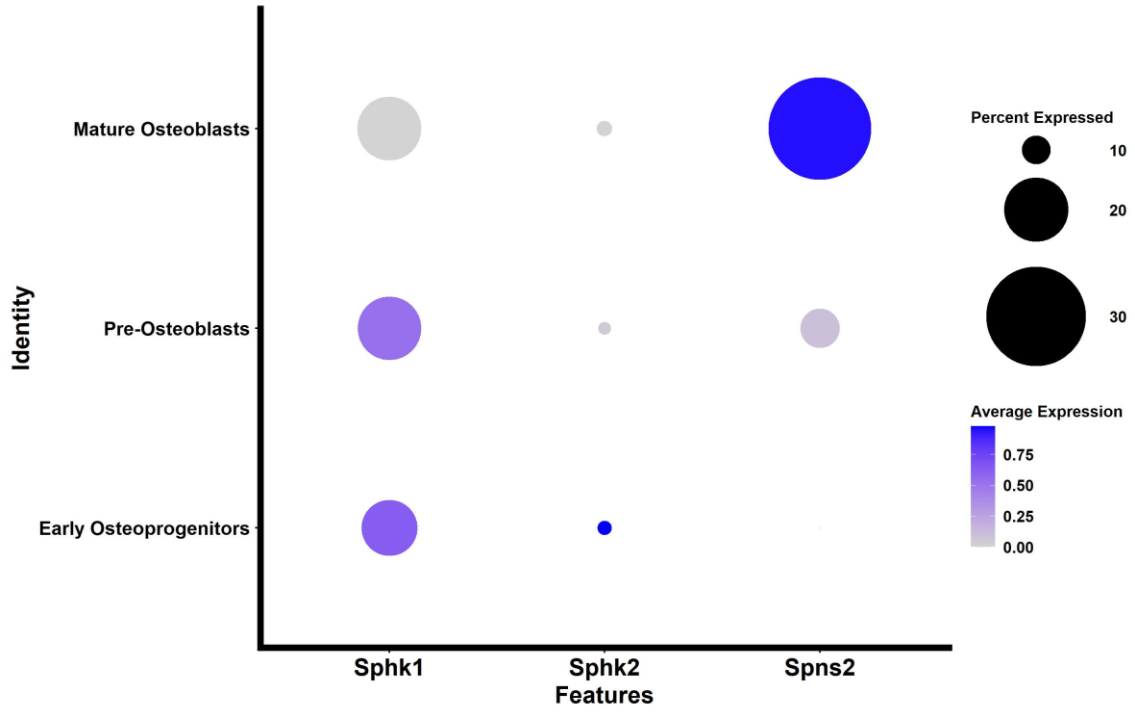

Figure 4.13. Genes involved in S1P production have altered expression throughout osteoblast maturation.

Clustered early osteoprogenitors, pre-osteoblasts and mature osteoblasts from dataset GSE128423 were analysed for expression of S1P production genes. A dotplot was created of expression of *Sphk1, Sphk2,* and *Spns2* in each osteoblast subset where circle size represents percentage of cells expressing the gene and colour indicates average expression value.

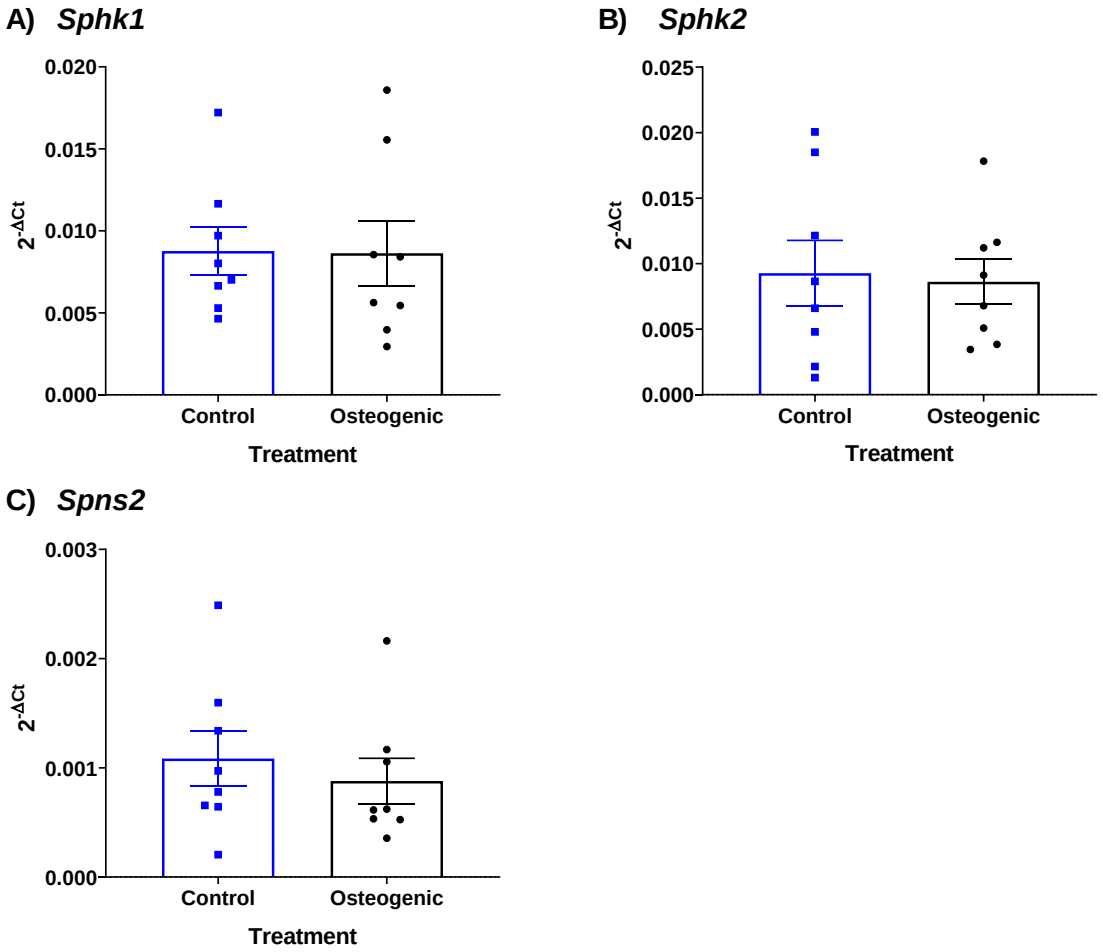

Figure 4.14. Calvarial osteoblasts express genes related to S1P production.

Calvarial osteoblasts were cultured in control (n=8) or osteogenic media (n=8) for 8 days. RNA was isolated and analysed for expression of *Sphk1* **(A)** *Sphk2* **(B)** *Spns2* **(C)** using RT-PCR. Data are displayed as $2^{-\Delta Ct}$, where ΔCt is the relative expression compared to *B2m* housekeeping gene. Data are mean ± SEM for 8 individual donors.

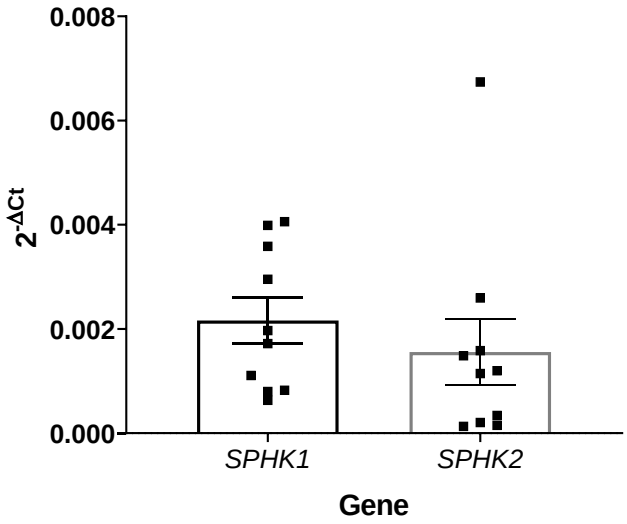

Figure 4.15. Human osteoblasts express S1P production genes.

RNA was isolated from human primary osteoblasts and analysed for expression of *SPHK1* and *SPHK2*. Data are displayed as $2^{-\Delta Ct}$, where ΔCt is the relative expression compared to *B2M* housekeeping gene. Data are mean ± SEM for n = 10 for 10 independent donors.

4.2.5 **S1P inhibits murine osteoblast osteogenesis.**

Since osteoblasts are shown to release S1P, it is possible S1P can function as an autocrine signalling molecule in response to S1P. Therefore, we next explored the ability for osteoblasts to respond to S1P. Exploring the murine bone marrow osteoblast maturation single cell data, only *S1pr1* and *S1pr3* were expressed in over 10 percent of cells at all stages of maturation, whilst *S1pr4* was not detected. In addition, the average expression levels of *S1pr1, S1pr2* and *S1pr3* decreased during maturation, with highest expression in the early osteoprogenitors (Figure 4.16). Expression of *S1pr1* was confirmed in murine calvarial osteoblasts and primary human osteoblasts, with no change observed following differentiation (Figure 4.17A & Figure 4.18). However, *S1pr4* was detected in both murine and human cells, but expression was significantly lower that *S1pr1* (Figure 4.18) and decreased further with differentiation (Figure 4.17B). Thus, indicating that osteoblasts have the ability to response to S1P.

Given the fact that S1P receptors are expressed on osteoblasts, we then explored the response of osteoblast directly to S1P. Differentiated primary calvarial osteoblasts, murine MC3T3-E1 cells and murine ST2 cells all showed decreased ALP activity following S1P treatment (1μm) for 8 days (Figure 4.19A-C). However, human primary osteoblasts increased ALP activity in response to S1P treatment (Figure 4.19D), indicating a different signalling mechanism in human and murine cells in response to S1P.

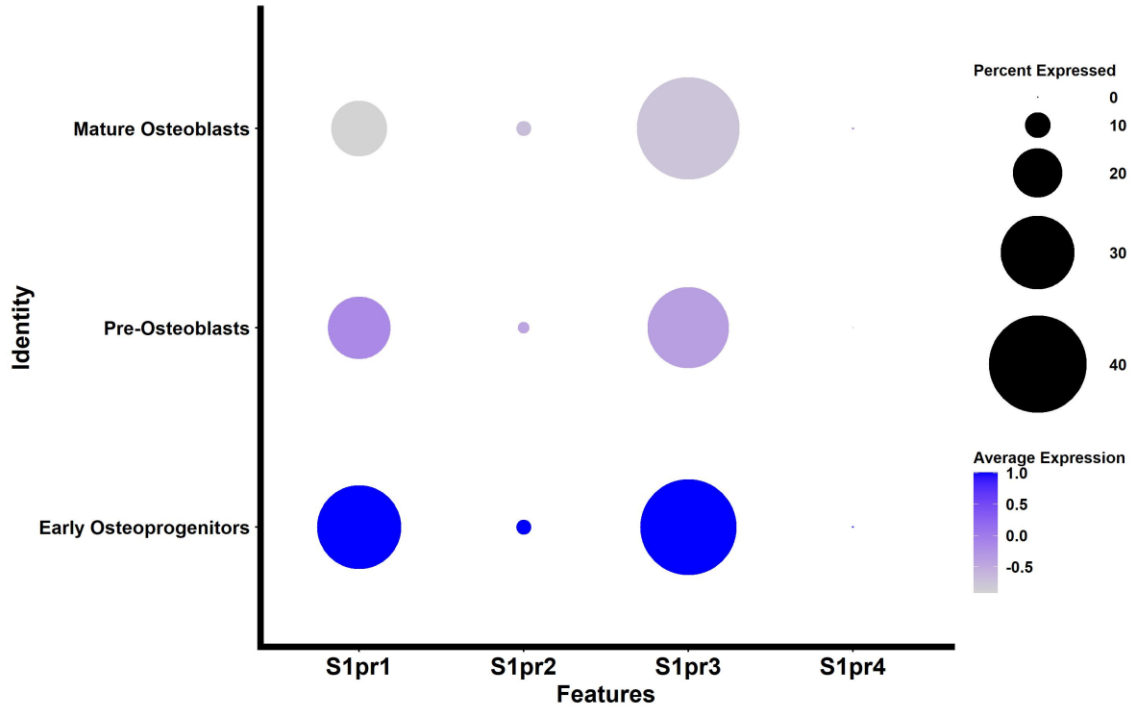

Figure 4.16. S1P receptor genes are decreased during osteoblast differentiation.

Clustered early osteoprogenitors, pre-osteoblasts and mature osteoblasts from dataset GSE128423 were analysed for expression of S1P receptor genes. Dotplot of expression of *S1pr1*, *S1pr2*, *S1pr3* and *S1pr4* in each osteoblast subset where circle size represents percentage of cells expressing the gene and colour indicates average expression value.

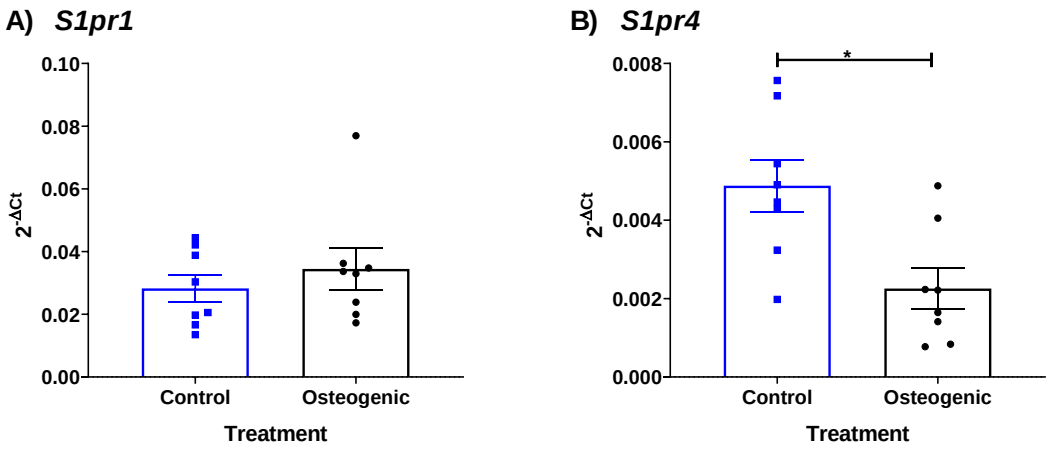

Figure 4.17. Calvarial osteoblasts express genes for S1P receptors.

Calvarial osteoblasts were cultured in control (blue, n=8) or osteogenic media (black, n=8) for 8 days. RNA was isolated and analysed for expression of *S1pr1* **(A)** and *S1pr4* **(B)** using RT-PCR. Data are displayed as $2^{-\Delta Ct}$, where ΔCt is the relative expression compared to *B2m* housekeeping gene. Data are mean ± SEM for 4 independent repeats. * = $p<0.05$ by paired t-test.

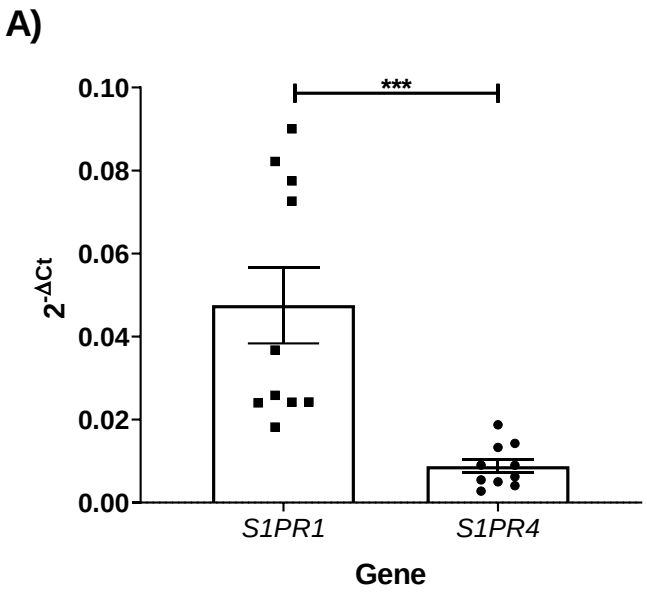

Figure 4.18. Human osteoblasts express S1P receptors

RNA was isolated from human primary osteoblasts and analysed for expression of *S1PR1* and *S1PR4*. Data are displayed as $2^{-\Delta Ct}$, where ΔCt is the relative expression compared to *B2M* housekeeping gene. Data are mean ± SEM for n = 10 for 10 independent donors. *** = p<0.001 by paired t-test.

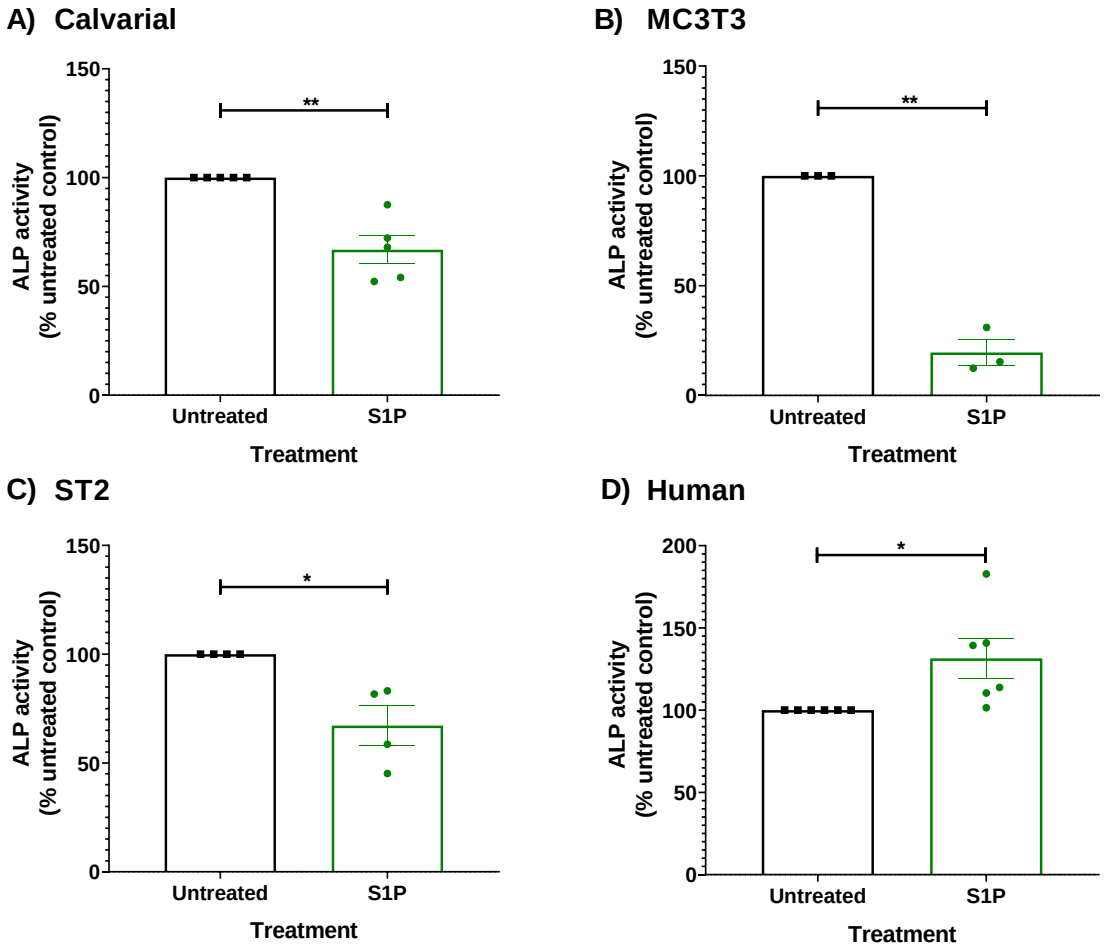

Figure 4.19. Murine and human osteoblasts respond differently to S1P treatment.

Primary calvarial osteoblasts **(A**, n=5**)**, murine MC3T3-E1 cells **(B**, n=3**)**, murine ST2 cells **(C,** n=4**)** and primary human osteoblasts **(D**, n=6**)** were cultured for 8 days in osteogenic media alone (untreated) or in media supplemented with S1P. ALP activity was analysed in each cell type and expressed as ALP activity as a percentage of untreated control. Data are mean ± SEM with each point representing an individual experiment/donor. * = $p<0.05$, ** = $p<0.01$ by paired t-test.

4.2.6 S1P induces an inflammatory osteoblast phenotype.

To explore the response of calvarial osteoblast further, we ran bulk RNA sequencing on primary calvarial osteoblast untreated or treated with S1P for 8 days. Following initial pre-processing of data, gene expression of untreated and S1P treated cells were compared using the DESeq2 package. Principle component analysis revealed that cells could be split independently into clusters of untreated or S1P treated cells (Figure 4.20A), which was also observed through the generation of a heatmap of differentially expressed genes between each sample (Figure 4.20B). Generation of an MA (ratio intensity) and volcano plot revealed a high number of differentially expressed genes when comparing untreated to S1P treated samples (Figure 4.21A/B). Differentially expressed genes were then analysed, with 1177 genes significantly upregulated by S1P and 1086 genes downregulated based on adjusted p value of <0.05. Exploring the top 50 upregulated (Table 4.1) and top 50 downregulated genes (Table 4.2) revealed that multiple genes from different pathways are altered by S1P treatment.

To explore this further, gene set enrichment analysis was performed to understand which pathways are upregulated and downregulated. Upregulated pathways include multiple immune functions (defence response to other organism – 208/1084 genes: immune effector process – 158/1084 genes), cytokine production (142/1084 genes) and blood vessel morphogenesis with a gene ratio of 95/1084 (Table 4.3). The connectivity of these pathways was then analysed by exploring the differentially expressed genes shared between the pathways which are displayed as an Emap and Cnet plots (Figure 4.22A/B), showing that a large number of differentially expressed genes are shared between the different pathways. Similar

analysis was performed on downregulated genes and thus pathways. Animal organ morphogenesis had the biggest significance with a gene ratio of 132/953, closely followed by downregulation of ossification (72/953) and muscle tissue development (65/953) (Table 4.4). Analysis again showed high levels of interconnectivity between pathways and differentially expressed genes (Figure 4.23). To confirm these pathways, data was also analysed for gene set enrichment using Kegg analysis looking at both upregulated and downregulated genes combined (Table 4.5). Pathways analysed again focussed on upregulation of immune signalling including NOD-like receptor signalling (Figure 4.24), TNF signalling (Figure 4.25) and cytokine-cytokine receptor interactions (Figure 4.26). In addition, genes involved in S1P synthesis and response were upregulated through S1P treatment (Figure 4.27). In contrast, downregulated pathways (Table 4.5) included aldosterone-regulated sodium reabsorption (Figure 4.28A), and protein digestion and absorption (Figure 4.28B), and in relation to osteoblasts specifically parathyroid hormone synthesis and action (Figure 4.29), and cardiac muscle contraction (Figure 4.30).

Overall, S1P treatment of calvarial osteoblasts leads to an upregulation of genes involved in inflammatory pathways and a downregulation of genes involved in osteogenesis. Thus, S1P treatment may lead to a decrease in murine osteoblast activity.

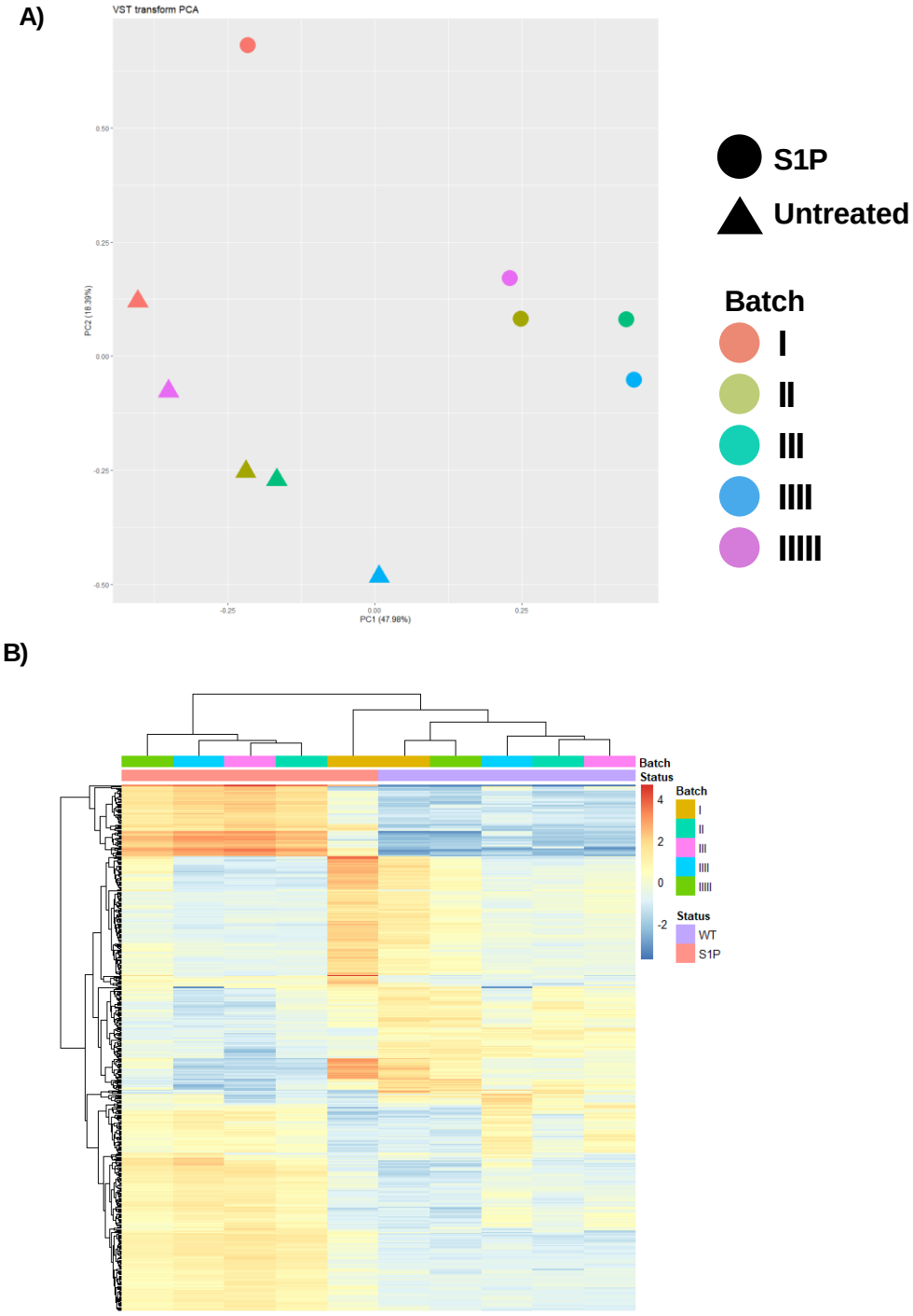

Figure 4.20. S1P treated calvarial osteoblasts have differential gene expression.

Primary calvarial osteoblasts were differentiated for 8 days alone or treated with S1P. RNA was isolated and bulk RNA sequencing was performed to analyse changes in gene expression. Following pre-processing, differential gene expression was analysed using DESeq. **A)** PCA plot of separation between untreated (triangle, n=5) and S1P treated cells (circle, n=5) where individual osteoblast donors are separated by colour. **B)** Gene expression between each sample was analysed by the generation of a heatmap. Closeness of samples are shown by hierarchal clustering.

A)

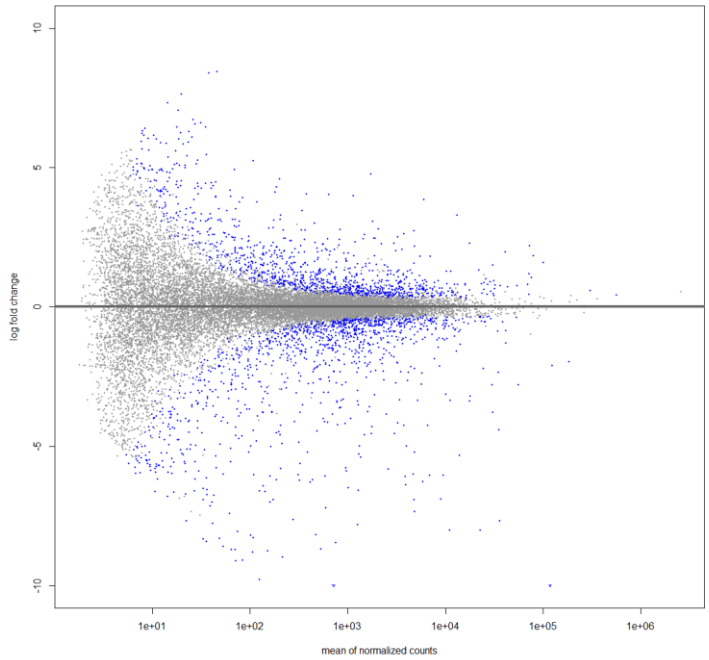

B)

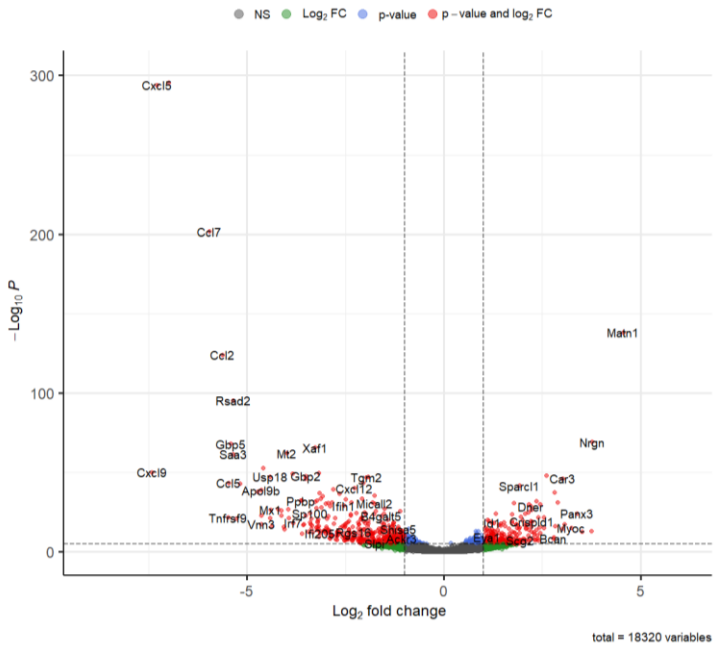

Figure 4.21. S1P treatment of calvarial osteoblasts leads to differential expression of many genes.

Primary calvarial osteoblasts were differentiated for 8 days alone or treated with S1P. RNA was isolated and bulk RNA sequencing was performed to analyse changes in gene expression. Following pre-processing, differential gene expression was analysed using DESeq. **A)** MAplot showing log fold change of gene compared to normalised counts between untreated and S1P treated cells. **B)** Volcano plot of differentially expressed genes following S1P treatment. Significantly different gene expression by both changes in p-value and log_2FC values are shown in red.

Table 4.1. Top 50 genes upregulated by S1P osteoblast treatment.

mgi_symbol	log2FoldChange	padj
Saa3	-11.165986	4.705571e-59
Cxcl9	-10.092511	1.252886e-47
Tnfrsf9	-9.783291	6.012397e-20
Vnn3	-9.110545	5.317250e-16
Cngb3	-9.082005	2.565976e-02
Il6	-8.982218	2.446915e-03
Oas1g	-8.794241	1.770779e-06
Gm4841	-8.747855	3.262248e-19
Nos2	-8.710692	3.488469e-02
Reg3g	-8.705452	3.502187e-02
Serpina3f	-8.689391	2.170454e-16
Serpina3i	-8.593489	3.941085e-13
Plac8	-8.464983	1.883700e-06
Klra2	-8.404900	1.793976e-11
Insyn2b	-8.330870	4.891610e-11
Saa2	-8.308341	4.730271e-02
H2-Q7	-8.278493	1.526926e-03
Ccl11	-8.184792	2.317529e-03
Cxcl10	-8.157905	1.727587e-07
H2-Q5	-8.056990	1.413748e-14
Lcn2	-8.015769	4.896502e-25
Ccl5	-8.000755	2.711945e-41
Zbp1	-7.816626	1.503289e-12
Olfr56	-7.760669	2.526845e-10
Cxcl5	-7.681087	9.276631e-291
H2-Q10	-7.663849	5.229646e-08
Ccl8	-7.619482	6.104404e-09
Csta2	-7.402981	2.217057e-14
Cxcl1	-7.340806	5.973054e-292
Serpina3g	-7.213172	1.667561e-09
Gbp4	-7.127687	1.933354e-08
Kng1	-7.005617	6.606419e-07
Piwil4	-6.992684	4.789533e-09
Iigp1	-6.920462	3.580754e-17
Acod1	-6.914355	1.988915e-21
Ifi206	-6.913371	1.925424e-07
Mmp3	-6.882703	1.163340e-40
Gm14275	-6.800392	4.272166e-05
9330175E14Rik	-6.746855	3.414242e-08
S100a8	-6.742094	9.085954e-09
Cxcl11	-6.714765	4.698238e-05
Ifi213	-6.646955	2.072781e-04
Ifi203-ps	-6.614694	3.218223e-04
Oas3	-6.614618	3.519812e-07
Cfb	-6.604360	1.456229e-19
Ifi208	-6.587561	2.778571e-06
Gm4951	-6.580509	4.068345e-08
Gbp6	-6.556774	3.402311e-02
Cxcl3	-6.504116	1.140059e-07
H2-Q4	-6.492687	2.422623e-21

mgi_symbol = official gene symbol for a mouse gene, padj = adjusted p value

Table 4.2. Top 50 genes downregulated by S1P osteoblast treatment.

mgi_symbol	log2FoldChange	padj
Bglap	8.450916	5.196237e-12
Bglap2	8.399249	2.174167e-11
Gm27204	7.647276	1.696990e-07
Slc35f3	7.330831	5.925292e-06
Gm2464	7.058485	1.347003e-06
Vwc2	6.734250	4.817388e-06
9030619P08Rik	6.609620	3.504287e-02
Scg2	6.573136	1.199215e-06
F630028O10Rik	6.466466	8.522951e-05
Col13a1	6.466443	1.369644e-05
Rab17	6.419738	1.920929e-03
D230022J07Rik	6.333275	2.739450e-03
AI646519	6.292998	1.875860e-05
Gm37363	6.265271	1.704811e-04
Gm49711	6.239761	3.918463e-03
Nsg2	6.168452	6.051182e-04
Cox8b	6.163432	1.340926e-02
Rasgrf1	6.091118	5.687441e-05
Sgca	6.051621	1.003655e-02
Calml3	6.045060	3.098723e-04
Gm13782	6.037366	8.670403e-05
Klhl40	5.942016	1.880108e-02
Asb10	5.921591	6.537838e-06
Cbfa2t3	5.902088	2.444132e-03
Efhc2	5.884944	2.502521e-03
Cidea	5.852008	5.546334e-05
Kcnh5	5.669345	3.135296e-02
Ifnlr1	5.632584	2.812776e-03
Bfsp2	5.616250	6.097698e-04
Fam107a	5.470832	7.135367e-07
Gm42770	5.428432	2.472220e-03
Slc35f2	5.376420	3.917066e-03
Gm17276	5.321359	1.746908e-02
Tnni2	5.266226	1.184101e-03
Myoc	5.252683	7.340402e-14
Gm7599	5.171434	5.340426e-03
Cntn2	5.166191	1.429705e-03
Abcg3	5.143873	1.787931e-03
Gm15998	5.143826	2.476797e-02
Exoc3l2	5.128258	4.066669e-02
Gpr34	5.109787	7.536152e-03
Zpld1	5.098094	8.760897e-05
Sfrp5	5.087934	2.854850e-03
Gm9768	5.068242	7.467892e-03
Gm46212	5.023364	4.722243e-02
Med9os	5.007241	2.359298e-03
Gng13	4.994971	4.768500e-02
Cd207	4.964837	4.040308e-02
Spock1	4.963678	1.945185e-02
Mal	4.952021	2.467044e-02

mgi_symbol = official gene symbol for a mouse gene, padj = adjusted p value

Table 4.3. S1P upregulated genes related to immune functions and chemotaxis

ID	Description	GeneRatio	p.adjust
GO:0098542	defense response to other organism	208/1084	1.153246e-50
GO:0002252	immune effector process	158/1084	4.800439e-34
GO:0001817	regulation of cytokine production	142/1084	7.099004e-30
GO:0048525	negative regulation of viral process	34/1084	6.447057e-13
GO:0048514	blood vessel morphogenesis	95/1084	5.354509e-12
GO:0008284	positive regulation of cell population proliferation	123/1084	2.018621e-11
GO:0052547	regulation of peptidase activity	70/1084	9.070391e-11
GO:0044092	negative regulation of molecular function	121/1084	1.129536e-09
GO:0051090	regulation of DNA-binding transcription factor activity	65/1084	3.027810e-08
GO:0010817	regulation of hormone levels	61/1084	4.398569e-08
GO:0048878	chemical homeostasis	118/1084	1.179664e-07
GO:0010876	lipid localization	60/1084	1.357466e-07
GO:0023061	signal release	63/1084	2.200315e-07
GO:0006692	prostanoid metabolic process	16/1084	1.652110e-06
GO:0006693	prostaglandin metabolic process	16/1084	1.652110e-06
GO:0046031	ADP metabolic process	22/1084	2.197233e-05
GO:0044706	multi-multicellular organism process	28/1084	2.816469e-05
GO:0030198	extracellular matrix organization	39/1084	1.830359e-04
GO:0043062	extracellular structure organization	39/1084	1.830359e-04
GO:0045229	external encapsulating structure organization	39/1084	1.830359e-04
GO:0071495	cellular response to endogenous stimulus	102/1084	1.928195e-04
GO:0051767	nitric-oxide synthase biosynthetic process	9/1084	3.824379e-04
GO:0051769	regulation of nitric-oxide synthase biosynthetic process	9/1084	3.824379e-04
GO:0035150	regulation of tube size	20/1084	5.854908e-04
GO:0035296	regulation of tube diameter	20/1084	5.854908e-04
GO:0019233	sensory perception of pain	19/1084	2.134188e-03
GO:0009628	response to abiotic stimulus	88/1084	3.390099e-03
GO:0048511	rhythmic process	33/1084	4.106284e-03
GO:0043900	regulation of multi-organism process	11/1084	4.964367e-03
GO:0010499	proteasomal ubiquitin-independent protein catabolic process	9/1084	7.981626e-03
GO:0032963	collagen metabolic process	18/1084	1.335023e-02
GO:2000241	regulation of reproductive process	23/1084	1.575777e-02
GO:0051260	protein homooligomerization	16/1084	2.788130e-02
GO:0110148	biomineralization	16/1084	3.661654e-02
GO:0048266	behavioral response to pain	5/1084	4.122756e-02
GO:0000028	ribosomal small subunit assembly	7/1084	4.791250e-02

Table shows GoID, go pathway description, number of genes upregulated in the pathway and adjusted p value.

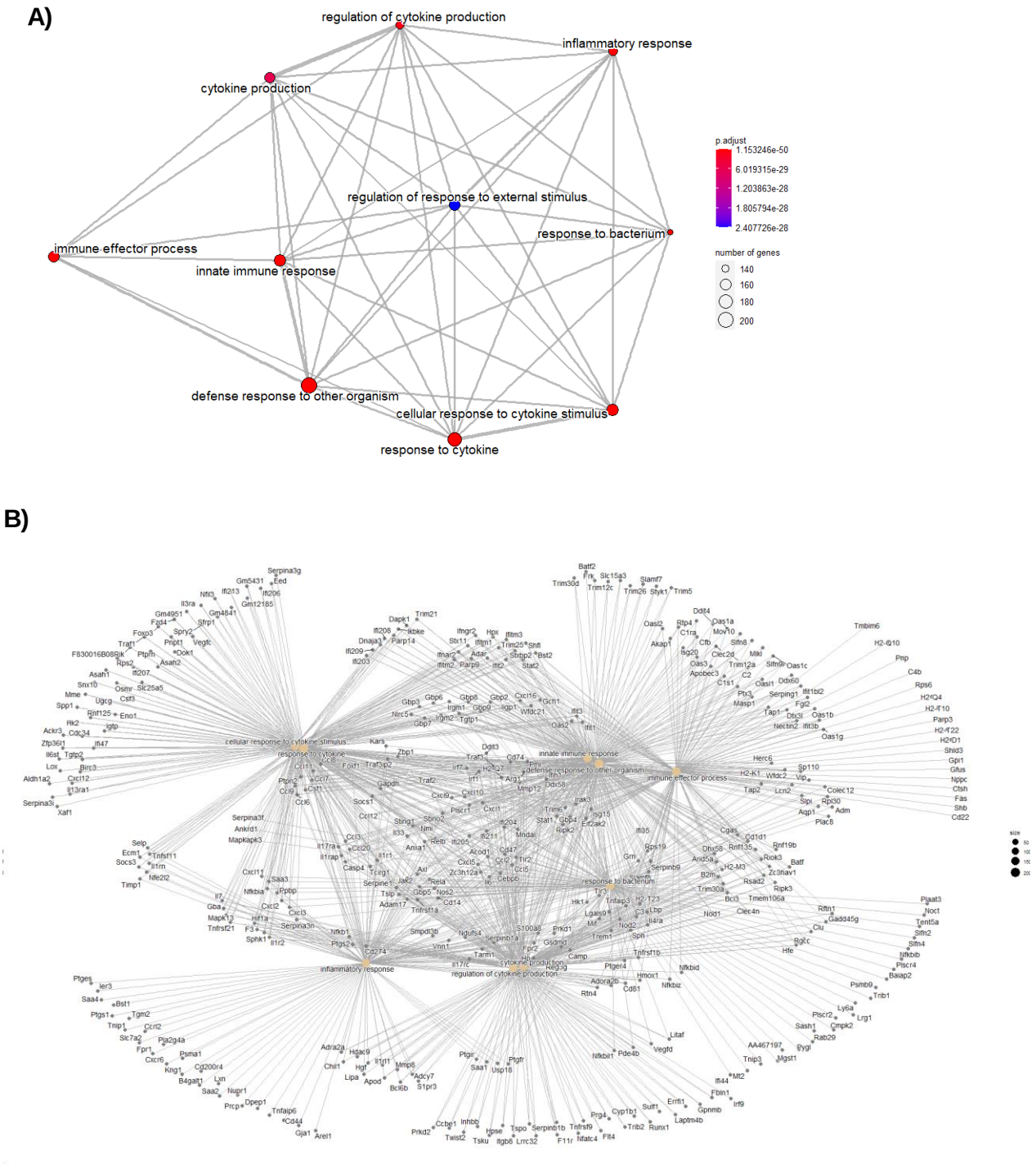

Figure 4.22. Connectivity of pathways upregulated by S1P.

Following analysis of differential gene expression, significantly different upregulated genes were isolated and pathway analysis was performed on the using clusterprofiler and gene set enrichment analysis. **A)** Emap plot of top 10 pathways upregulated by S1P, with how the pathways map onto each other shown by connection lines, adjusted p-value by colour and number of genes involved by size of circle. **B)** Connectivity of pathways was analysed further through generation of a cnet plot showing the top 10 upregulated pathways and the genes significantly upregulated in these pathways.

Table 4.4. S1P downregulated genes involved in ossification, morphogenesis, and muscle.

ID	Description	GeneRatio	p.adjust
GO:0009887	animal organ morphogenesis	132/953	5.507581e-13
GO:0001503	ossification	72/953	6.564003e-13
GO:0007167	enzyme linked receptor protein signaling pathway	107/953	1.515089e-09
GO:0110148	biomineralization	36/953	2.765147e-09
GO:0060537	muscle tissue development	65/953	4.569182e-09
GO:0030198	extracellular matrix organization	48/953	1.994191e-08
GO:0045229	external encapsulating structure organization	48/953	1.994191e-08
GO:0031589	cell-substrate adhesion	57/953	2.321275e-08
GO:0003012	muscle system process	53/953	4.310844e-06
GO:0009612	response to mechanical stimulus	24/953	5.346674e-05
GO:0040007	growth	95/953	4.903222e-04
GO:0042330	taxis	54/953	1.419105e-03
GO:1903034	regulation of response to wounding	22/953	1.983524e-03
GO:0071604	transforming growth factor beta production	9/953	2.033257e-03
GO:0045926	negative regulation of growth	32/953	4.084285e-03
GO:0048871	multicellular organismal homeostasis	45/953	9.004542e-03
GO:0002682	regulation of immune system process	83/953	9.009077e-03
GO:0044092	negative regulation of molecular function	75/953	1.153184e-02
GO:1990845	adaptive thermogenesis	21/953	1.307914e-02
GO:0000122	negative regulation of transcription by RNA polymerase II	80/953	1.398928e-02
GO:0010563	negative regulation of phosphorus metabolic process	45/953	1.623664e-02
GO:0045936	negative regulation of phosphate metabolic process	45/953	1.623664e-02
GO:0006812	cation transport	79/953	1.655558e-02
GO:0031529	ruffle organization	11/953	1.655558e-02
GO:0042100	B cell proliferation	11/953	1.655558e-02
GO:0051480	regulation of cytosolic calcium ion concentration	31/953	1.963326e-02
GO:0006954	inflammatory response	42/953	2.214485e-02
GO:0097194	execution phase of apoptosis	9/953	2.285601e-02
GO:0050999	regulation of nitric-oxide synthase activity	6/953	2.856960e-02
GO:0071402	cellular response to lipoprotein particle stimulus	7/953	3.078575e-02
GO:0080164	regulation of nitric oxide metabolic process	9/953	4.708722e-02
GO:0051606	detection of stimulus	17/953	4.981751e-02

Table shows GoID, go pathway description, number of genes upregulated in the pathway and adjusted p value.

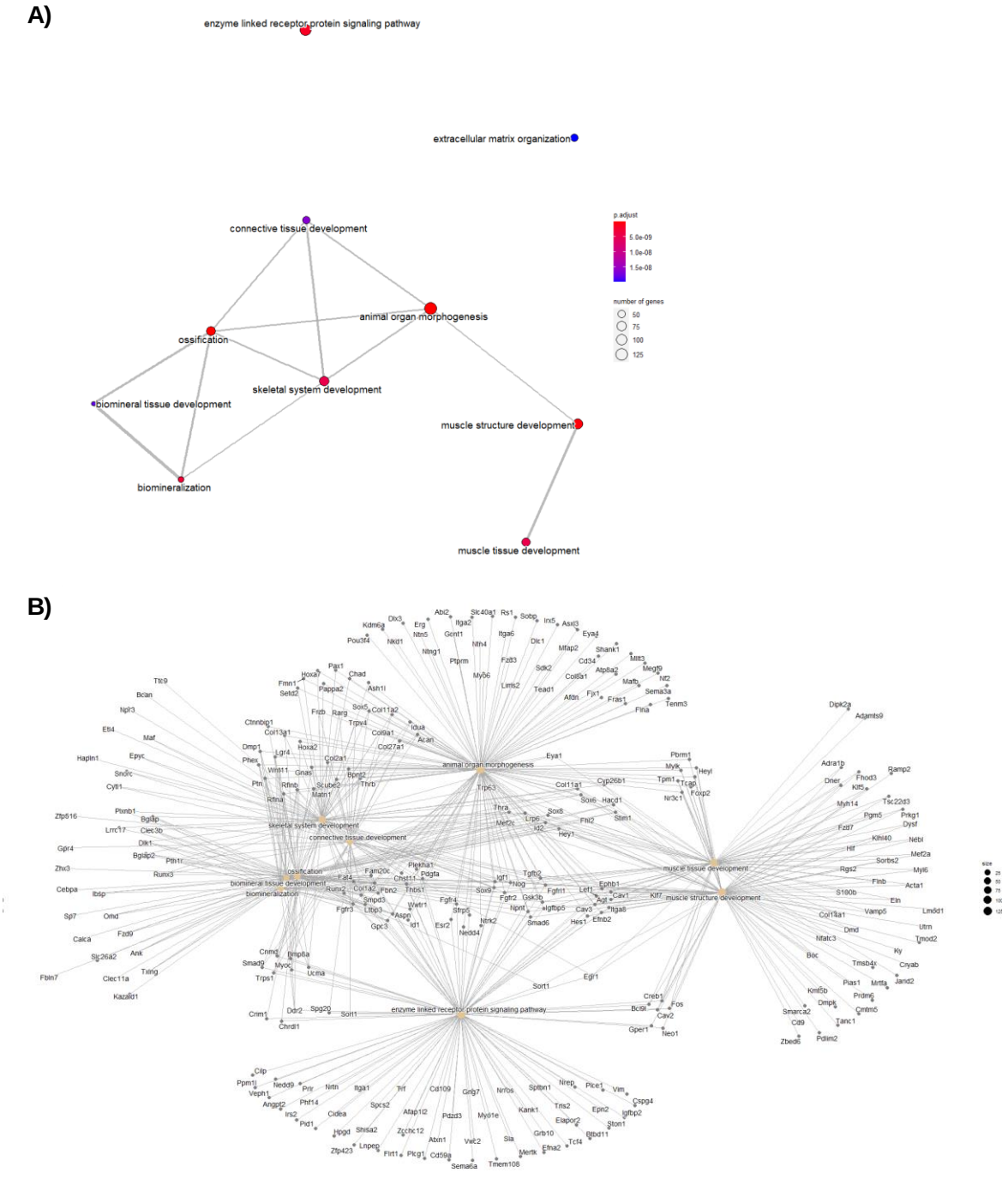

Figure 4.23. Connectivity of pathways downregulated by S1P.

Following analysis of differential gene expression, significantly different downregulated genes were isolated and pathway analysis was performed on the using clusterprofiler and gene set enrichment analysis. **A)** Emap plot of top 10 pathways downregulated by S1P, with how the pathways map onto each other shown by connection lines, adjusted p-value by colour and number of genes involved by size of circle. **B)** Connectivity of pathways was analysed further through generation of a cnetplot showing the top 10 downregulated pathways and the genes significantly downregulated in these pathways.

Table 4.5. List of pathways altered by S1P treatment.

ID	Description	NES	p.adjust
mmu04668	TNF signaling pathway	-2.202382	0.0001404100
mmu05164	Influenza A	-2.156983	0.0001374382
mmu04061	Viral protein interaction with cytokine and cytokine receptor	-2.137685	0.0001499925
mmu04621	NOD-like receptor signaling pathway	-2.135736	0.0001334223
mmu05169	Epstein-Barr virus infection	-2.046039	0.0001298533
mmu05323	Rheumatoid arthritis	-2.041436	0.0001483459
mmu04657	IL-17 signaling pathway	-2.035697	0.0001456028
mmu04940	Type I diabetes mellitus	-2.022586	0.0001616554
mmu05320	Autoimmune thyroid disease	-2.010949	0.0001616554
mmu05332	Graft-versus-host disease	-1.998545	0.0001647446
mmu05330	Allograft rejection	-1.994008	0.0001642845
mmu04060	Cytokine-cytokine receptor interaction	-1.993548	0.0001300221
mmu04620	Toll-like receptor signaling pathway	-1.984104	0.0001449485
mmu05162	Measles	-1.984037	0.0001397819
mmu04622	RIG-I-like receptor signaling pathway	-1.961541	0.0001535627
mmu05134	Legionellosis	-1.915462	0.0001525786
mmu05160	Hepatitis C	-1.913246	0.0001371178
mmu04612	Antigen processing and presentation	-1.901819	0.0001514693
mmu04623	Cytosolic DNA-sensing pathway	-1.880392	0.0001551590
mmu05168	Herpes simplex virus 1 infection	-1.875933	0.0001178550
mmu05171	Coronavirus disease - COVID-19	-1.844757	0.0001274372
mmu04062	Chemokine signaling pathway	-1.817834	0.0001322052
mmu04610	Complement and coagulation cascades	-1.806813	0.0001525786
mmu04064	NF-kappa B signaling pathway	-1.793073	0.0002859185
mmu05416	Viral myocarditis	-1.743611	0.0003051572
mmu05146	Amoebiasis	-1.728394	0.0005772839
mmu05203	Viral carcinogenesis	-1.721485	0.0001289491
mmu05417	Lipid and atherosclerosis	-1.719798	0.0001305313
mmu05167	Kaposi sarcoma-associated herpesvirus infection	-1.697495	0.0002616431
mmu05142	Chagas disease	-1.616116	0.0025688597
mmu04145	Phagosome	-1.615203	0.0010920011
mmu03010	Ribosome	-1.608468	0.0012243232
mmu05166	Human T-cell leukemia virus 1 infection	-1.604781	0.0002534854
mmu04218	Cellular senescence	-1.600629	0.0010604454
mmu05144	Malaria	-1.599182	0.0085809630
mmu05163	Human cytomegalovirus infection	-1.592027	0.0002534854
mmu05321	Inflammatory bowel disease	-1.580284	0.0093221678
mmu00983	Drug metabolism - other enzymes	-1.572212	0.0080953108
mmu05133	Pertussis	-1.570140	0.0058391975
mmu04217	Necroptosis	-1.565196	0.0024903154
mmu00053	Ascorbate and aldarate metabolism	-1.558627	0.0212110225
mmu04514	Cell adhesion molecules	-1.556270	0.0037741124
mmu05150	Staphylococcus aureus infection	-1.534636	0.0159280871
mmu05322	Systemic lupus erythematosus	-1.531286	0.0086030913
mmu00220	Arginine biosynthesis	-1.529166	0.0275680421
mmu05140	Leishmaniasis	-1.513426	0.0107056695
mmu05310	Asthma	-1.509092	0.0350626118
mmu04080	Neuroactive ligand-receptor interaction	-1.508138	0.0037234043
mmu00790	Folate biosynthesis	-1.497748	0.0335166724
mmu03050	Proteasome	-1.496395	0.0225343417
mmu05170	Human immunodeficiency virus 1 infection	-1.490735	0.0029658285
mmu01523	Antifolate resistance	-1.488566	0.0352312573
mmu00030	Pentose phosphate pathway	-1.483437	0.0339603796
mmu04630	JAK-STAT signaling pathway	-1.480497	0.0077476480
mmu00860	Porphyrin and chlorophyll metabolism	-1.469612	0.0420929063
mmu05152	Tuberculosis	-1.464074	0.0076654115
mmu00760	Nicotinate and nicotinamide metabolism	-1.447196	0.0464707761
mmu04144	Endocytosis	-1.433850	0.0037518759
mmu05165	Human papillomavirus infection	-1.413858	0.0030211480
mmu05145	Toxoplasmosis	-1.401805	0.0250351617
mmu05235	PD-L1 expression and PD-1 checkpoint pathway in cancer	-1.390023	0.0339860281
mmu04933	AGE-RAGE signaling pathway in diabetic complications	-1.387295	0.0289343684
mmu04936	Alcoholic liver disease	-1.355696	0.0356696738
mmu04934	Cushing syndrome	1.317505	0.0286885246
mmu05414	Dilated cardiomyopathy	1.343564	0.0441935484
mmu04512	ECM-receptor interaction	1.354363	0.0377419355
mmu04022	cGMP-PKG signaling pathway	1.400554	0.0103171571
mmu05032	Morphine addiction	1.411854	0.0282122048
mmu04725	Cholinergic synapse	1.425485	0.0175497806
mmu04260	Cardiac muscle contraction	1.440222	0.0204018547
mmu04713	Circadian entrainment	1.445516	0.0179429670
mmu04611	Platelet activation	1.447095	0.0100589664
mmu04928	Parathyroid hormone synthesis, secretion and action	1.448513	0.0134408602
mmu04925	Aldosterone synthesis and secretion	1.479592	0.0157202438
mmu04261	Adrenergic signaling in cardiomyocytes	1.482807	0.0048005908
mmu04921	Oxytocin signaling pathway	1.513590	0.0033149171
mmu04971	Gastric acid secretion	1.531478	0.0133531157
mmu04916	Melanogenesis	1.540235	0.0075065274
mmu04961	Endocrine and other factor-regulated calcium reabsorption	1.635540	0.0081944824
mmu04974	Protein digestion and absorption	1.700946	0.0018820577
mmu04960	Aldosterone-regulated sodium reabsorption	1.702246	0.0049133695

Table shows KEGGID, KEGG pathway description, normalised enrichment score and adjusted p value.

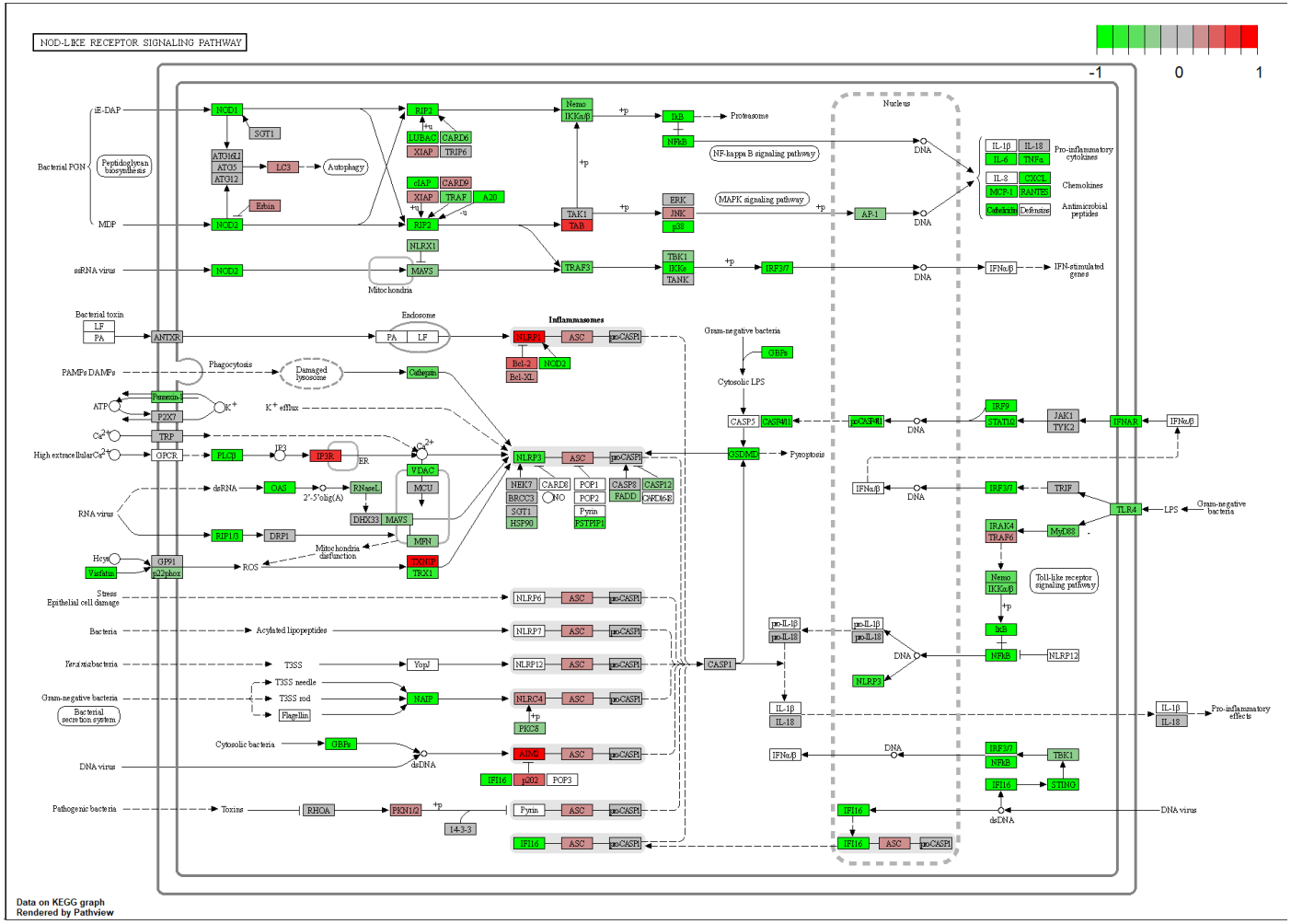

Figure 4.24. Genes involved in NOD-like receptor signalling are upregulated in osteoblasts with S1P treatment.

Significantly upregulated pathways from gseKEGG analysis were analysed using the pathview package. Upregulated genes are shown in green and downregulated in red.

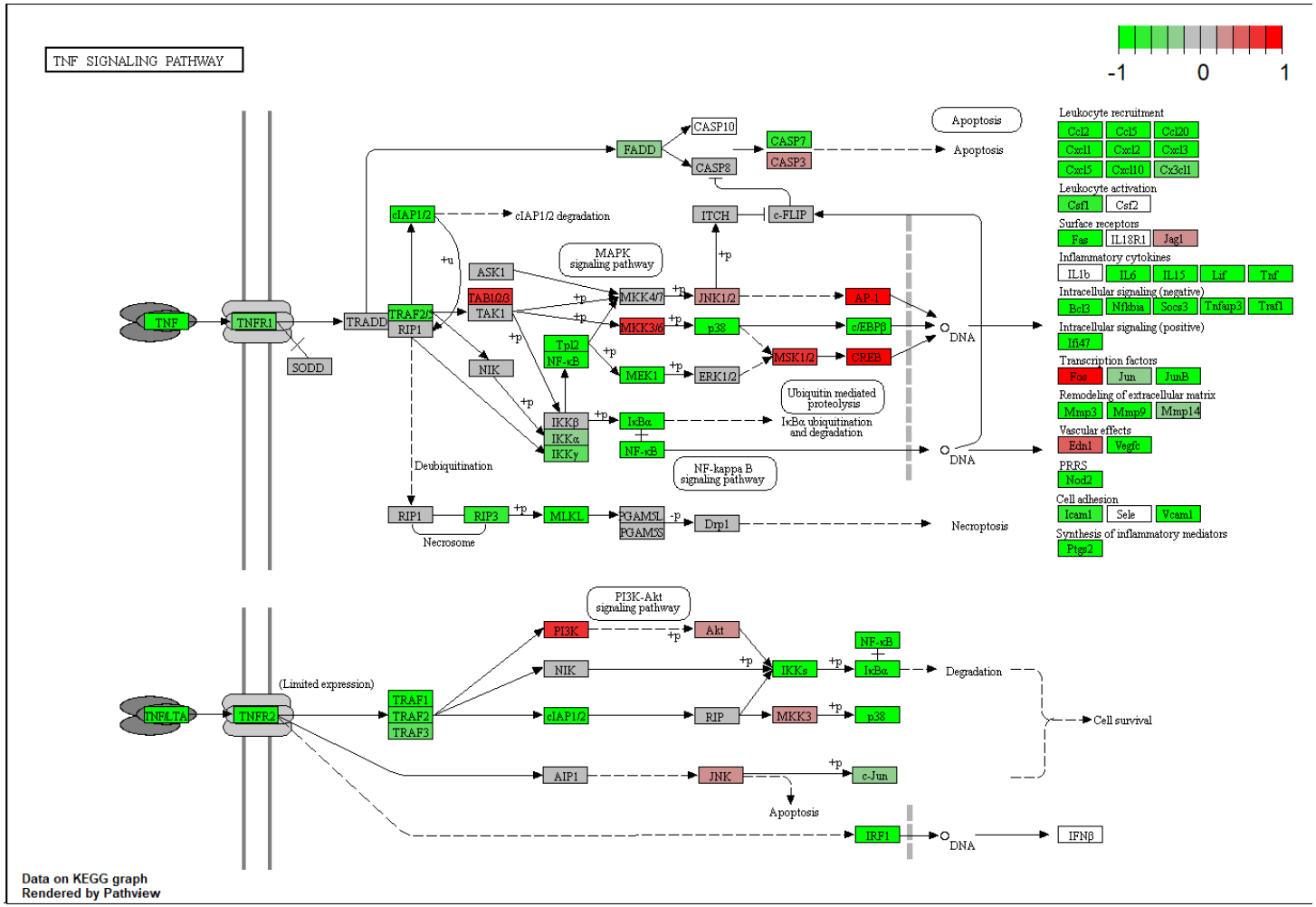

Figure 4.25. Genes involved in TNF signalling are upregulated in S1P treated osteoblasts.

Significantly upregulated pathways from gseKEGG analysis were analysed using the pathview package. Upregulated genes are shown in green and downregulated in red.

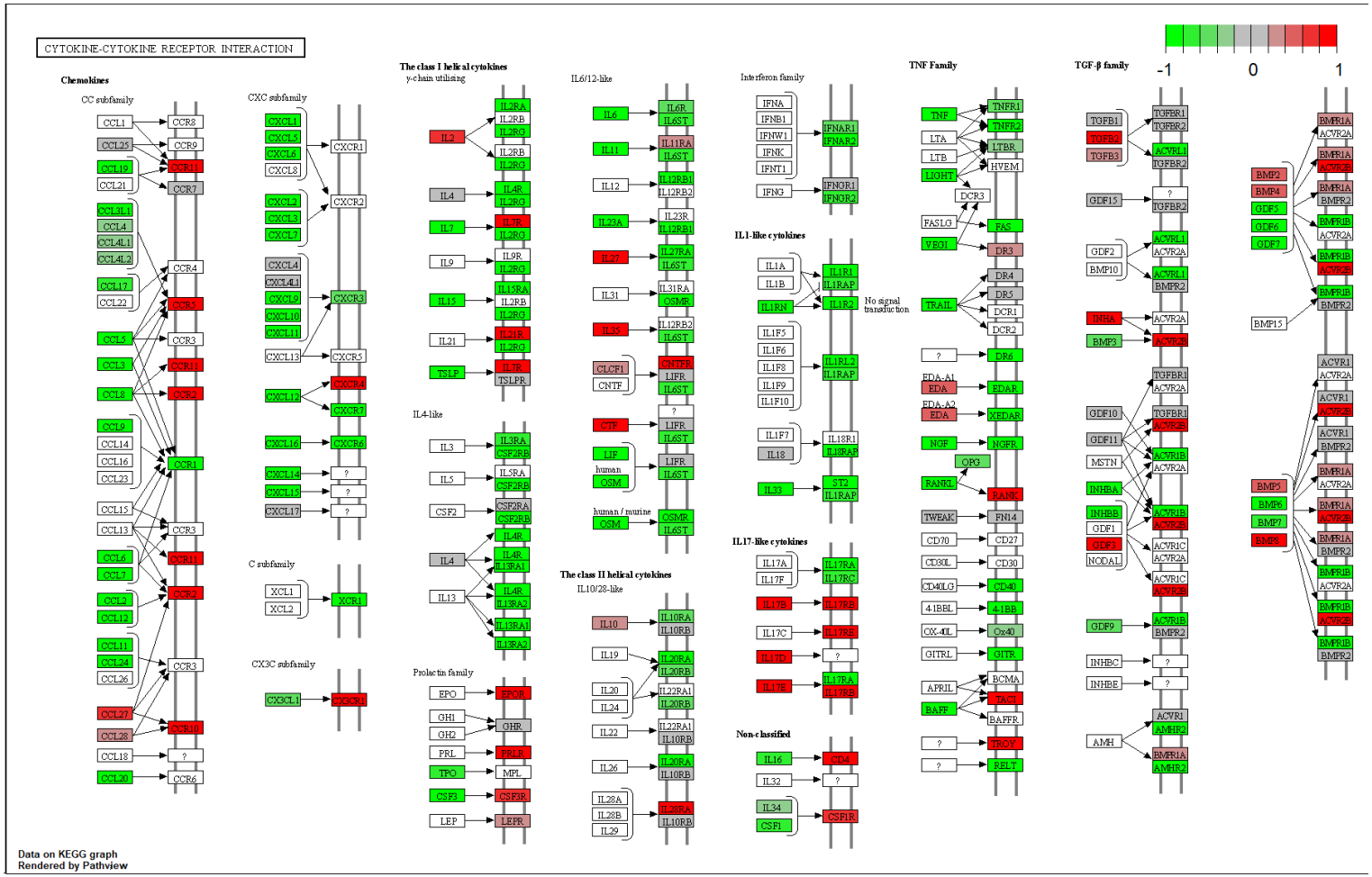

Figure 4.26. Genes involved in cytokine signalling are upregulated in S1P treated osteoblasts.

Significantly upregulated pathways from gseKEGG analysis were analysed using the pathview package. Upregulated genes are shown in green and downregulated in red.

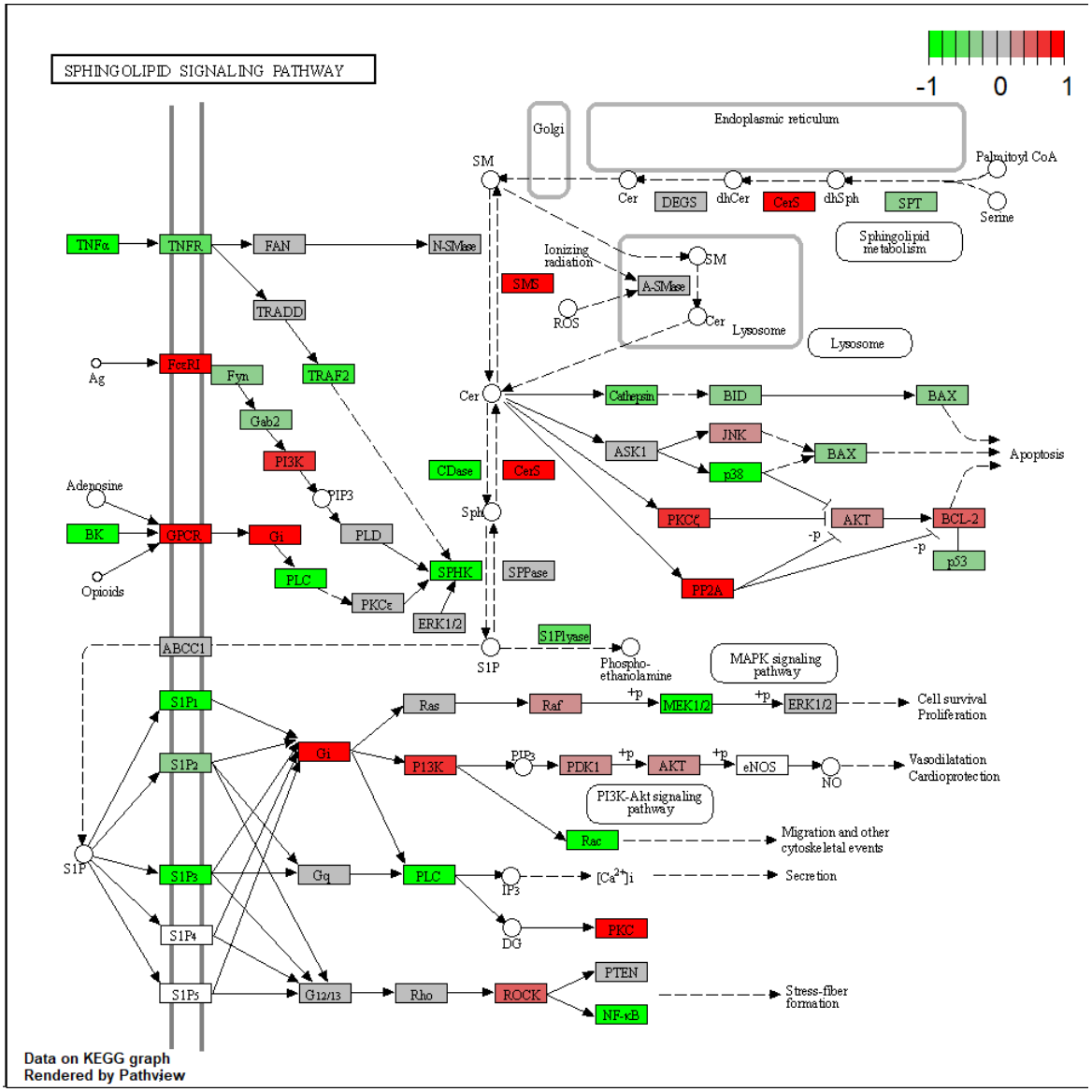

Figure 4.27. Genes involved in S1P signalling and production are upregulated by S1P treatment.

Significantly upregulated pathways from gseKEGG analysis were analysed using the pathview package. Upregulated genes are shown in green and downregulated in red.

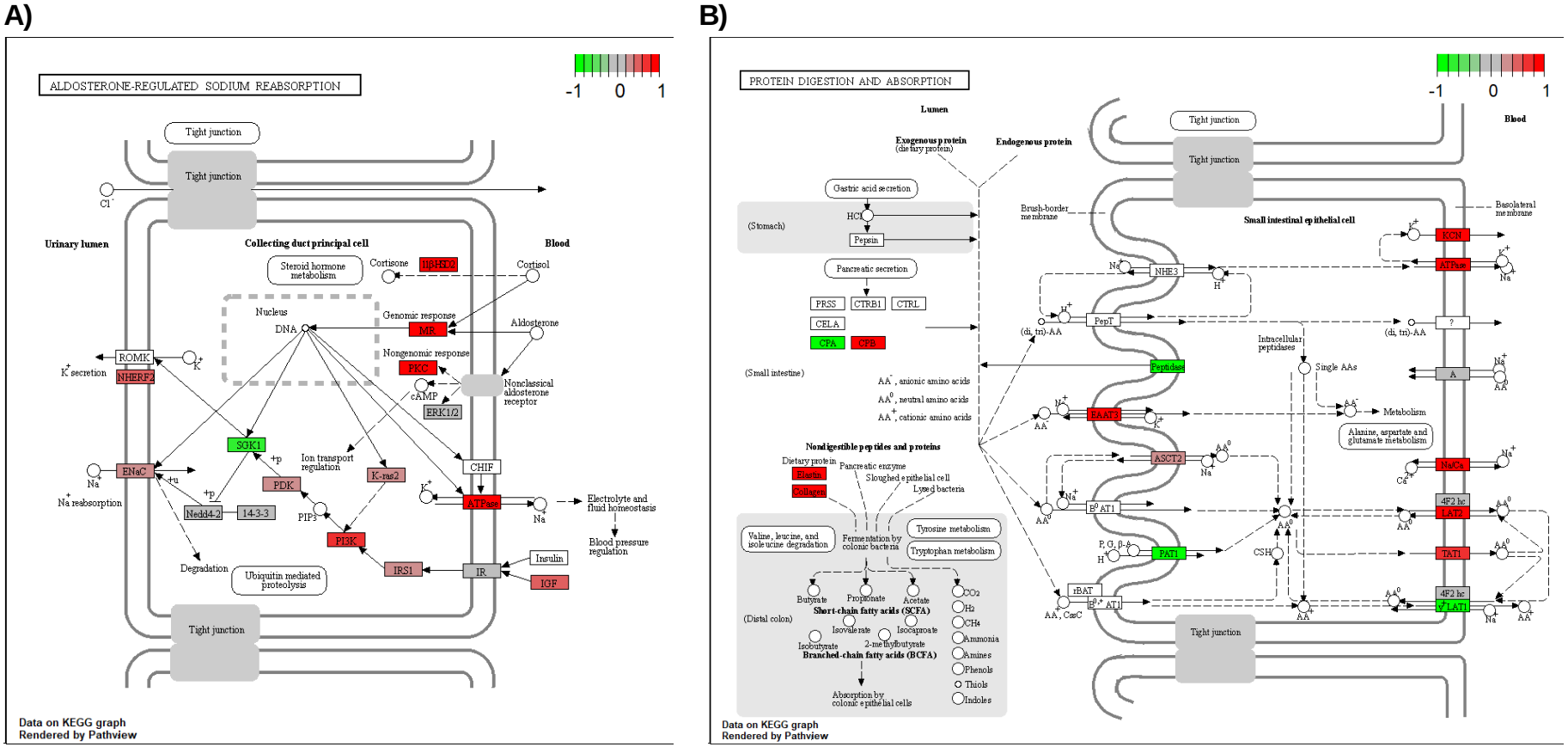

Figure 4.28. Genes involved in aldosterone-regulated sodium reabsorption and protein absorption are downregulated by S1P treatment.

Significantly upregulated pathways from gseKEGG analysis were analysed using the pathview package. **A.** Aldosterone-regulated sodium reabsorption. **B.** Protein digestion and reabsorption. Upregulated genes are shown in green and downregulated in red.

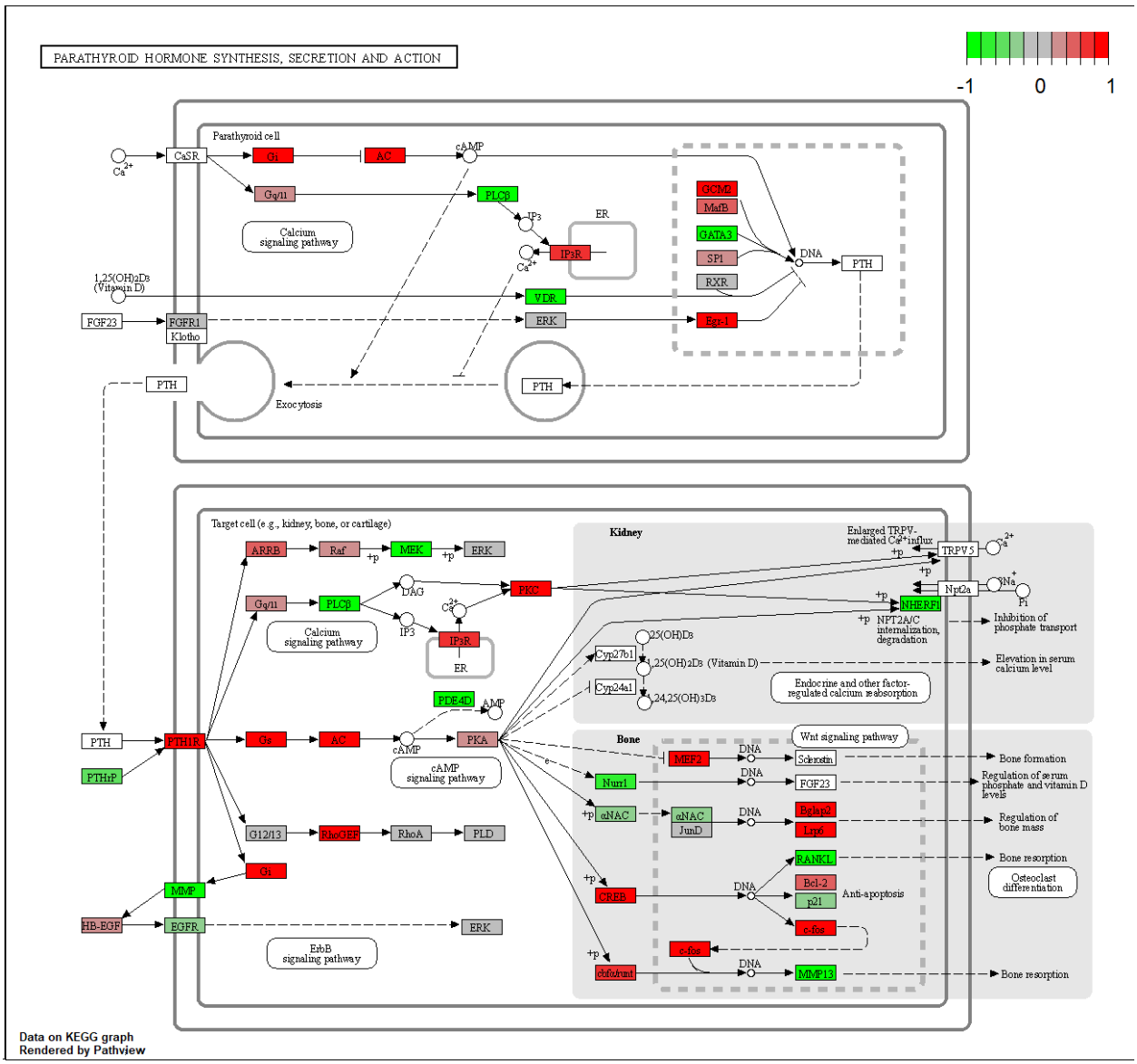

Figure 4.29. Genes involved in parathyroid hormone synthesis, secretion and action are downregulated by S1P treatment of osteoblasts.

Significantly upregulated pathways from gseKEGG analysis were analysed using the pathview package. Upregulated genes are shown in green and downregulated in red.

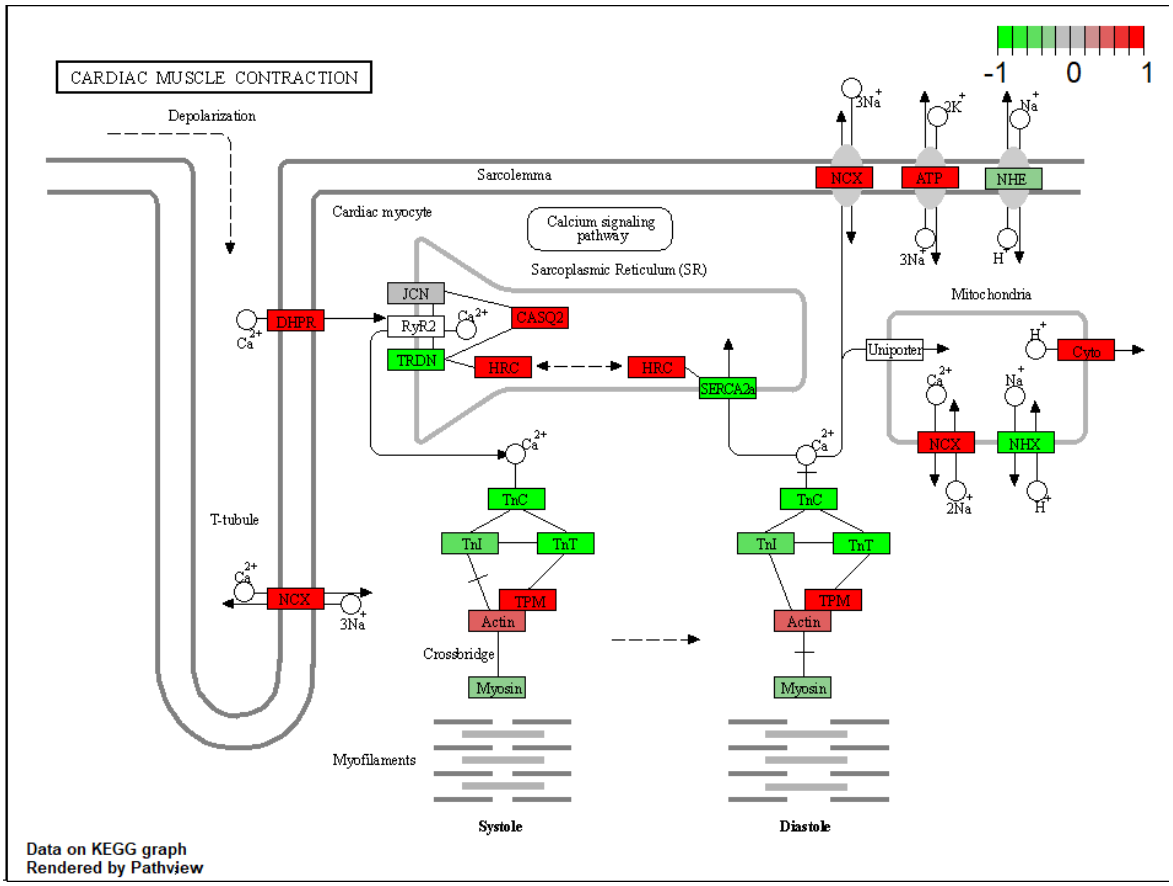

Figure 4.30. Genes involved in cardiac muscle contraction are downregulated by S1P treatment of osteoblasts.

Significantly upregulated pathways from gseKEGG analysis were analysed using the pathview package. Upregulated genes are shown in green and downregulated in red

4.3 Discussion

The ability for PEPITEM to regulate leukocyte trafficking is mediated through PEPITEM induced S1P release and the inhibitory actions of S1P.[473] Here we identify that osteoblasts secrete soluble mediators that inhibit osteoclastogenesis. Osteoblasts express the machinery to generate S1P, whilst osteoblasts and osteoclasts can respond to S1P in their local environment. We observed species specific responses to S1P, whereby S1P positively induced osteogenesis and inhibited osteoclastogenesis on human cells, but the inverse was observed when murine cells were treated with S1P. Thus, there is a need to explore the effect of S1P concentration and other soluble mediators to fully interpret how bones respond to PEPITEM.

4.3.1 S1P as a bone signalling molecule

Osteoblasts and osteoclasts have both previously been shown to produce and release S1P. *Ex vivo* staining of bone sections and culture of human osteoblast cell lines Ob-6 and hFOb showed expression of *Sphk1* and *Sphk2*[600] and release has been confirmed by measuring S1P in the media from murine MC3T3 cells, primary calvarial osteoblasts and primary human osteoblasts.[487] We also found this in our data, with *Sphk1, Sphk2* and *Spns2* expression detected in calvarial osteoblasts and human osteoblasts by qPCR and single cell sequencing analysis of murine bone marrow stromal cells. However, we did not measure S1P release directly at any stage in osteoblast media, therefore other soluble factors such as RANKL, OGP or mCSF may be the cross-signalling molecules. S1P treatment of osteoblasts has also been shown to stimulate S1P production in human osteoblasts following positive feedback,[481] thus high levels of S1P release may occur from low levels of stimulation.

S1P's role as a soluble mediator in bone biology further supported by the changes in the bone *in vivo* induced by S1P signalling. Osteoblast specific loss of S1P release led to a decrease in bone growth and osteogenesis,[601] suggesting S1P is essential in bone growth. This is proven further through S1P receptor studies. S1PR2[482] and S1PR3[358] knockout mice have decreased trabecular BV/TV and bone formation rates. In a similar fashion, use of an S1PR2 agonist led to an increase in trabecular bone growth.[485] Exploring changes in osteoclasts, S1PR3$^{-/-}$ mice demonstrated increased osteoclasts on the bone surface,[358] whilst S1PR1 knockout specifically in CD11b expressing cells increased bone volume.[483] These data indicate S1P can promote bone growth and control osteoclast generation and resorption. S1P inhibitory action on osteoclastogenesis

4.3.2 **S1P's inhibitory action on osteoclastogenesis**

Changes in osteoclastogenesis that occur following S1P treatment have scarcely been investigated. In fact, to our knowledge no other study has explored human monocyte to osteoclast differentiation in the presence of S1P. However, human monocytes have been shown to increase CD32 in response to S1P.[602] CD32 expression increases during monocyte to macrophage differentiation,[602] thus indicating increased macrophage differentiation. Our data supports this, with decreased osteoclastogenesis, yet increased expression of MSR-1, which is also increased in macrophages.[603] LPS induced human monocyte into dendritic cell differentiation is also altered by high concentrations of S1P (50μM), however these cells do become CD14 and CD64 negative, indicating the ability to progress past the macrophage stage of differentiation.[604] Importantly, this finding may be explained by the use of an inflammatory stimulus, which alters monocyte differentiation,[603] or a

largely inflated S1P concentration. Overall, these data indicate a pro-macrophage phenotype of S1P treated monocytes, supporting the hypothesis that S1P is able to inhibit osteoclast differentiation in human cells.

Only Ryu et al (2006) have looked at direct responses of murine bone marrow monocytes (BMM) and osteoclasts to S1P treatment during osteoclastogenesis. They found that higher BMM intracellular S1P concentration decreased osteoclastogenesis, however supplementation of external media with S1P in concentration range of 0.001μM to 1μM had no influence on osteoclastogenesis.[605] We did not look at S1P directly on BMM, however S1P treatment of RAW264.7 murine macrophage-like cells increased osteoclast numbers. This difference may be explained by their use of a 4-time higher concentration of RANKL during their differentiation protocol (200ng/ml), which has previously been shown to significantly increase osteoclast differentiation compared to standard levels (as used in our study) and may render S1P ineffective.[605,606]

Differences in murine cell responses to S1P may also be explained by S1P receptor expression. BMM decreased expression of *S1pr1* and increased *S1pr2* during osteoclast differentiation,[482,605] which is supported by our analysis of monocyte to osteoclast single cell data, showing similar gene expression changes with differentiation. In contrast, RAW264.7 cells do not change expression of *S1pr2* during differentiation,[482] which may alter the S1P signalling pathway. We also found RAW264.7 expression of *S1pr4*, which was not found in the BMM. However, this expression was very low and PCR analysis on BMM was only run for 25 cycles as opposed to the 35 cycles used in our study.[482] This would mean genes with lower mRNA expression are not amplified, but may still be expressed. Similarly, single cell

sequencing has difficulty detecting genes with low gene expression,[607] so S1P receptor genes may not be detected. Overall, differences in receptor expression in cell lines compared to primary murine cells may lead to differences in signalling (explored further later in the discussion) and thus response to S1P.

RAW264.7 cells have been shown to decrease apoptosis in response to S1P,[608] in addition to increasing ATP release.[600] A combination of decreased apoptosis and increased metabolic activity may explain the increase in RAW264.7 cell number in S1P treated wells. Increased seeding density of RAW264.7 cells increased the number of TRAP+ osteoclasts following RANKL induction.[609] Therefore, increased osteoclastogenesis may be a secondary effect to increased RAW264.7 number and not a direct effect on osteoclastogenesis. In order to explore S1P directly on osteoclasts, differentiation could be initiated without S1P, with supplementation of S1P occurring later. This would allow analysis of the direct effect of S1P on osteoclasts and allow further analysis of our hypothesis.

Overall, our data on human osteoclasts supports our hypothesis that S1P can decrease osteoclastogenesis directly. However, many more studies are required to analyse the specific signalling pathways involved and why the different murine cells act in inverse ways.

4.3.3 S1P promotion of osteogenesis

Our data on human osteoblasts response also supports our hypothesis, finding increased mineral production in response to S1P. These data supplement published data, with increases in ALP activity observed following 8 days of S1P treatment. Human osteoblasts have previously been shown to increase the

proliferation,[610] ALP activity[481] and mineral production[481] in response to S1P treatment. These data were produced using a range of human osteoblasts (NHOst cell line, human bone marrow MSC derived osteoblasts, primary osteoblasts derived from periodontal bone and primary osteoblasts from fracture patients) and using a range of S1P concentrations (200nM to 10μM), thus indicating a robust response of human osteoblasts to S1P.

The majority of published data shows a pro-anabolic impact of S1P on murine osteoblasts, which contradicts our findings from 3 different murine cell lines. However, it is important to note that osteoblast activity in response to S1P was only measured short term by ALP activity, therefore other functional assays are required to confirm results. Calvarial osteoblasts treated for 4 days with 2μM of S1P were reported to have increased ALP activity,[485] in addition to increased cellular viability when 0.1 - 1μM of S1P are used.[605] Whilst these contradict our data, it is important to note that osteoblasts were not treated with β-glycerophosphate or L-ascorbic acid in these studies, thus were in an immature state whereas we differentiated our cells for 8 days. This may indicate that S1P is able to promote bone when osteoblasts are in a pre-osteoblast state but is inhibitory when treating mature osteoblasts.

MC3T3 cells have also been shown to have positive responses to S1P, increasing ALP activity,[485,610] osteoblast gene expression (*Alpl, Opn, Opg* and *Runx2*)[485] and mineral production[485] following 0.1 - 1μM S1P treatment. Differences may again be explained by differentiation, with studies either not inducing differentiation,[610] or inducing differentiation with hydrocortisone.[485] It has previously been found that S1P interferes with cortisol signalling,[611] thus possibly changing the osteoblast differentiation. In addition, in mesangial cells, hydrocortisone

downregulates S1PR1 protein expression.[612] If a similar mechanism occurs in osteoblasts, this would potentially alter S1P signalling pathways. C2C12 cells, which we did explore, have also been shown to have increased ALP activity[613] and *Alpl* and *Runx2* mRNA,[492] however differentiation was either induced in the presence of hydrocortisone or BMP2. BMP2 osteogenesis, as compared to induction with β-glycerophosphate, leads to an increase in smad signalling.[614,615] S1P treatment of cells enhanced Smad1/5/8 phosphorylation,[492] thus working via a unique pathway to induce osteogenesis. Therefore, depending on the environment of osteoblast differentiation, S1P may induce distinct osteoblast responses.

It is also important to note that none of the studies give timing of S1P treatment, making it unclear if S1P was continuously added, added intermittently or only added at the start of the study, which may alter osteoblast responses. Overall, our mechanism of S1P treatment in murine osteoblasts indicates S1P may not be inducing autocrine signalling in osteoblasts in response to PEPITEM. However further research is required to understand the specific pathways activated in each cell type and in each culture condition leading to the range of responses observed.

4.3.4 **Novel osteoblast pathways altered by S1P signalling**

4.3.4.1 **S1P and chemotaxis**

Bulk RNA sequencing from S1P treated osteoblasts revealed some other interesting pathways S1P is involved in in osteoblasts. Multiple genes involved in cytokine release and chemotaxis are upregulated following S1P treatment. Involvement of S1P in chemotaxis of osteoblasts is not a new topic. Firstly, calvarial

osteoblasts display a positive chemotaxis towards S1P when placed in the upper well of a transwell.[605] In addition, S1P treatment of MC3T3-E1 cells increased their migration towards PDGF.[486] Our data indicates that *Pdgfra* is upregulated following S1P treatment, thus potentially explaining the increase in migration observed by Roelofsen *et al*. Similarly, we observe an increase in *Cxcl12* in S1P treated osteoblasts. CXCL12 is involved in the migration of osteoblast precursors,[616] thus increased CXCL12 release may create a gradient to the bone, promoting the migration of CXCR4 expressing pre-osteoblasts to the bone.[617] Increased chemotaxis to the bone would enable enhanced bone production in disease and promoting bone repair.

Osteoclast chemotaxis has been more fruitfully studied in response to S1P. In low S1P concentrations there was an increase in osteoclast chemotaxis reported in BMM, BM-MDM and RAW264.7 cells.[482,483,605] However increased S1P concentrations lead to chemorepulsion, decreasing migration compared to controls.[482,484] Therefore, it is possible that increased S1P release in response to PEPITEM could lead to decreased osteoclastogenesis in the bone not just due to decreased osteoclastogenesis, but also decreased osteoclast migration to the bone.

4.3.4.2 **S1P induced an inflammatory osteoblast phenotype**

Many pathways involved in inflammatory responses are also upregulated by S1P treatment, including cytokine release, TNF signalling and leukocyte recruitment. This has previously been found as MC3T3-E1 cells increase *IL1β* and *IL6* gene expression in response to S1P,[618,619] which was also seen in our calvarial osteoblasts. Interestingly, treatment of osteoblasts with inflammatory cytokines induced both pro-osteogenic and anti-osteogenic responses. Treatment of human

BMSC, murine BMSC or calvarial osteoblasts with IL6 potentiated osteogenesis,[261,620,621] however treatment of human and murine MSCs with TNFα or IL1β enhanced osteoblast differentiation.[622–625] This may indicate that changes in inflammation may cancel out any changes in osteoblastogenesis in response to S1P. This would mean the bioactivity of S1P would decrease in disease due to less responsive osteoblasts, however understanding the proportional changes and their functions are required to interpret the full impact.

Inflammation would also lead to an increase in leukocyte migration to the bone, which would increase bone damage and diseases such as rheumatoid arthritis.[626–629] However, S1P is involved in decreasing the migration of leukocytes across blood vasculature.[473] In addition, PEPITEM treatment of arthritic mice led to a decrease in inflammation and bone damage.[496] Alternatively, acute inflammation, which occurs during fracture, leads to clearance of necrotic tissue and the eventual recruitment of MSCs and osteoblasts,[277,278,286,630] thus S1P induced inflammation may aid repair in fracture.

Anti-anabolic S1P inflammatory changes may be outcompeted by positive actions, therefore leading increased bone growth.

4.3.4.3 **S1P and induction of angiogenesis**

Finally, angiogenesis related genes are also upregulated in response to S1P. S1P has previously been shown to influence osteoblast endothelial interactions, with osteosarcoma MG63 cell line increasing VEGF release in response to S1P.[631] In our calvarial osteoblasts, *Vegfa*, *Vegfc* and *Vegfd* are all upregulated by S1P treatment. Similarly, conditioned media from S1P treated osteoblasts have been shown to

increase the migration of endothelial cells and to increase the vascularisation of a chick embryo.[631] Angiogenesis is essential for bone repair due to providing key metabolites for osteoblast differentiation and also allowing the migration of osteoblasts into the bone. In diseases such as osteoporosis, angiogenesis is significantly reduced,[632,633] and restoration of vasculature in osteoporosis models using Zeb1-packaged liposomes protected mice from bone loss, showing its essential nature is maintaining bone.[617] Moreover, *CXCL9* has been shown to be an anti-angiogenic VEGF antagonising molecule released by osteoblasts[634,635] and *Cxcl9* was increased in expression in our S1P treated calvarial osteoblasts. Increased osteoblast induced angiogenesis in response to S1P may allow long-term pro-anabolic effects on the bone through an increase in vasculature.

4.3.5 Differences in murine and human cells in response to S1P

In both osteoblasts and osteoclasts, we observed different responses of cells to S1P, with increased osteoblastogenesis and decreased osteoclastogenesis in human cells and the inverse seen in murine cells.

Differences between human and murine osteoclastogenesis may be explained by altered expression of receptors. RAW264.7 cells expressed significantly lower levels of *S1pr4* compared to *S1pr1*, however human monocytes express similar levels of *S1PR1* and *S1PR4*. This may allow for increased co-signalling, in turn altering the responses to S1P. Signalling through S1PR1 has previously been shown to signal through $G_{i/o}$, whereas S1PR4 also signals through $G_{12/13}$,[477–480] thus different downstream signalling may occur altering the cellular responses to S1P.

This may not be the case in osteoblasts, where murine and human cells both express decreased S1PR4 compared to S1PR1. However, *S1PR1* and *S1PR3* decreased and *S1PR2* increased during maturation of human osteoblasts,[481] whereas calvarial osteoblasts increased *S1pr1* and *S1pr3* with differentiation.[358] Therefore, differences in receptor expression that occur with differentiation may lead to the changes in responses observed.

Interspecies differences are not a novel concept. It has been previously shown that osteoblasts from different species donors respond differently to differentiation when exposed to the same culture conditions.[636] In addition, specific osteoblast genes, such as osteocalcin, have differing gene locus organisation in human and murine cells.[568] This alters the response of human and murine osteoblasts to 1,25-$(OH)_2D_3$ where human, but not mouse, osteocalcin is upregulated.[568] It is therefore possible that S1P treatment differentially regulates genes between human and mouse cell due to a similar mechanism.

Here we have demonstrated a unique osteoblast regulation pathway through release S1P treatment, which alters osteogenesis and osteoclastogenesis. However, we have also identified a unique species difference in response to S1P, which requires further exploration before the therapeutic potential of S1P can be fully analysed. Nonetheless, S1P induction of human osteoblast differentiation and inhibition of osteoclastogenesis indicates a possible clinical benefit during bone diseases such as fracture and osteoporosis. To further these findings, exploration of S1P release in response to PEPITEM and understanding changes in other signalling molecules (RANKL, OPG, Wnt, TGFβ) would allow us to understand if S1P is the key inducer of PEPITEM signalling in bone.

5 Investigating the Role of Cadherin-15 in the Bioactivity of PEPITEM

5.1 Introduction

As demonstrated in the previous chapter, PEPITEM is able to act directly on osteoblasts and indirectly on osteoclasts to induce a pro-anabolic bone phenotype. We therefore aimed to identify the mechanisms by which PEPITEM could induce these cellular responses.

Previous work exploring the effect of PEPITEM on endothelial cells revealed a key mechanism responsible for mediating the actions of PEPITEM.[473] Following PEPITEM treatment of endothelial cells, PEPITEM-bound molecules were subjected to mass-spectrometry, which revealed cadherin-15 as a PEPITEM binding partner. In addition, siRNA knockdown of *CDH15* (the cadherin-15 gene) on endothelium abolished the immunomodulatory effect of PEPITEM on these cells, demonstrating that cadherin-15 was essential in the PEPITEM pathway on endothelial cells.[473]

There is very limited research into cadherin-15 expression on osteoblasts and osteoclasts and its role in cell function. However, other cadherin molecules such as N-cadherin (CDH2) and Ob-cadherin (CDH11) are expressed in murine and human osteoblasts and have osteogenic and adhesion properties.[637–639] It was therefore essential to characterise cadherin-15 expression and to identify whether the same pathway plays a role in PEPITEM bioactivity in the bone.

Here we investigate the response of osteoblasts and osteoclasts to PEPITEM, exploring the expression and function of cadherin-15. We hypothesise that PEPITEM bioactivity is mediated by cadherin-15 in osteoblasts.

5.2 Results

5.2.1 Osteoblasts, but not osteoclasts express cadherin-15

Currently, the only confirmed methodology understanding the cellular response to PEPITEM has come from the response of endothelial cells to PEPITEM in the immune cell trafficking pathway.[473] We sought to define the mechanism of action of PEPITEM in osteoblasts and osteoclasts, considering the lessons learnt from endothelial responses. In order to do this, we explored the expression of cadherin-15 protein and the *CDH15* gene in osteoblasts and osteoclasts.

Gene expression of *Cdh15* in primary calvarial osteoblasts was analysed by qPCR, revealing *Cdh15* was expressed, however expression was at significantly lower levels comparatively to the murine myocyte C2C12 cell line (Figure 5.1A). *CDH15* gene expression was also observed in human primary osteoblasts by qPCR (Figure 5.2B). Whilst this expression was relatively low, gene expression was completely absent in umbilical cord mesenchymal stem cells (UCMSC, Figure 5.1B), suggesting an increase in expression upon differentiation into osteoblasts. Interestingly, neither the murine RAW264.7 macrophage like cell line, or human primary peripheral monocytes or osteoclasts showed detectable expression of the cadherin-15 gene (data not shown). At a protein level, intracellular flow cytometry staining for cadherin-15 revealed protein expression in primary calvarial osteoblasts and C2C12 myocytes (Figure 5.2A/B). Moreover, when comparing the median fluorescent intensity between the calvarial osteoblasts and C2C12 muscle cells, no difference in protein expression was identified (Figure 5.2C). Protein expression was also confirmed by western blot analysis of the lysates of primary calvarial osteoblasts (Figure 5.2D) and primary human osteoblasts (Figure 5.2E).

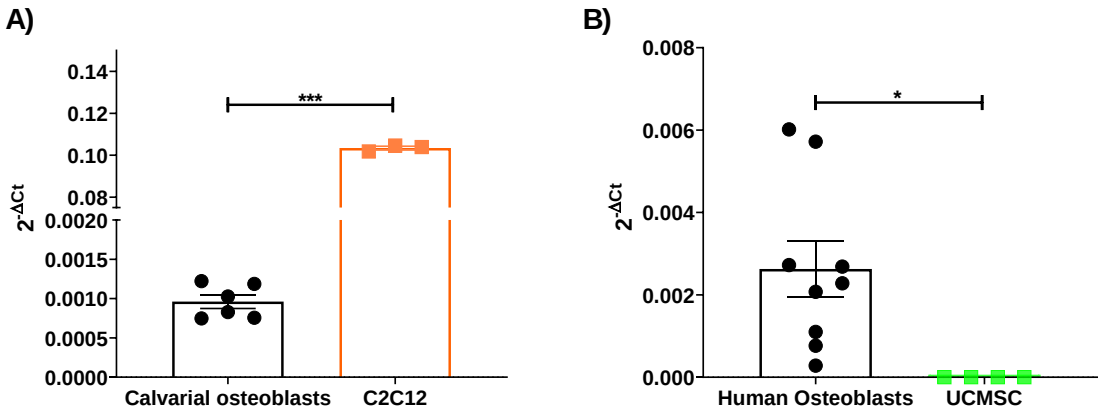

Figure 5.1. Osteoblasts express the cadherin-15 gene, but at lower levels than muscle cells.

Primary calvarial osteoblasts, the murine myoblast C2C12, primary human osteoblasts and umbilical cord mesenchymal stem cells (UCMSCs) were cultured *in vitro* and analysed for expression of the *Cdh15* gene using RTPCR. Data are displayed as $2^{-\Delta Ct}$ where ΔCt is the difference between *Cdh15* expression and *B2m* housekeeping gene **A.** Expression of *Cdh15* mRNA in calvarial osteoblasts (black, n=6 donors) and C2C12 (orange, n=3). **B.** Expression of *CDH15* mRNA in primary isolated human osteoblasts (black, n=9 for 9 individual donors) and non-matched UCMSCs (green, n=4). Data are mean ± SEM. * = P<0.05 and ***=P<0.001 by students t-test.

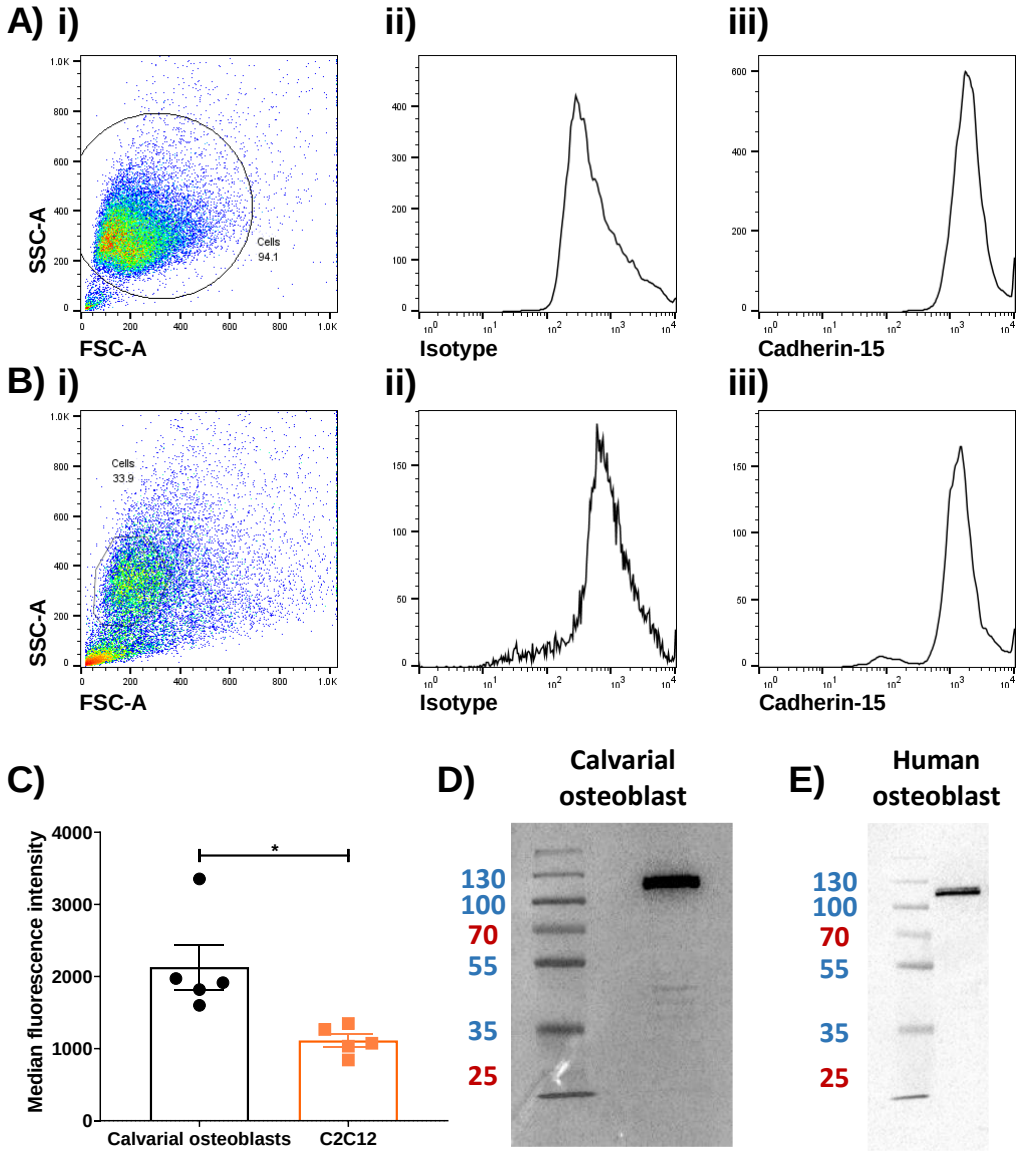

Figure 5.2. Osteoblasts express cadherin-15 at protein level.

Primary calvarial osteoblasts, the murine myoblast C2C12 and primary human osteoblasts were cultured *in vitro* to analyse cadherin-15 protein expression. **A-C.** Calvarial osteoblasts and C2C12 cells were stained for cadherin-15 by intracellular staining and analysed for cadherin-15 expression in comparison to an isotype control. **A-B.** Gating strategy of calvarial osteoblasts **(A)** and C2C12 **(B)** showing total cell populations **(i)**, isotype control **(ii)** and cadherin-15 **(iii)** representative of n=5 independent experiments **C.** Median fluorescence intensities were calculated for cadherin-15 expression in calvarial osteoblasts (n=3) and C2C12 cells (n=3). **D-E.** Cell lysates were isolated from calvarial osteoblasts **(D,** representative of 2 independent experiments**)** or primary human osteoblasts **(E,** representative of 2 independent experiments from 6 different donors**)** and analysed for total cadherin-15 content by western blot. Data are mean ± SEM. * = $p<0.05$ by student t-test.

5.2.2 **Osteoblasts express cadherin-15 in adherens junction clusters**

Protein expression was also confirmed in calvarial osteoblasts using immunofluorescent imaging of *in vitro* cell cultures (Figure 5.3A). Staining for cadherin-15 protein overlaid on brightfield images revealed protein expression accumulating around the nucleus and in clusters at the periphery of the cells (Figure 5.3A). This was also the case when investigating expression on the ST2 osteoblast cell line (Figure 5.3B). Interestingly, this localisation of cadherin-15 was also seen in the C2C12 muscle cell line, indicating a conservation of expression in stromal cell types (Figure 5.3C). Expression of cadherin-15 in clusters on the cell surface indicated a possible role for cadherin-15 in forming focal adhesions. Therefore, we explored the expression of cadherin-15 in combination with the focal adhesion markers vinculin and talin-1 and the structural protein F-actin. Expression of cadherin-15 protein showed near identical expression patterns to both vinculin (Figure 5.4) and talin-1 (Figure 5.5), suggesting that cadherin-15 is involved in the generation and maintenance of focal adhesions in osteoblasts.

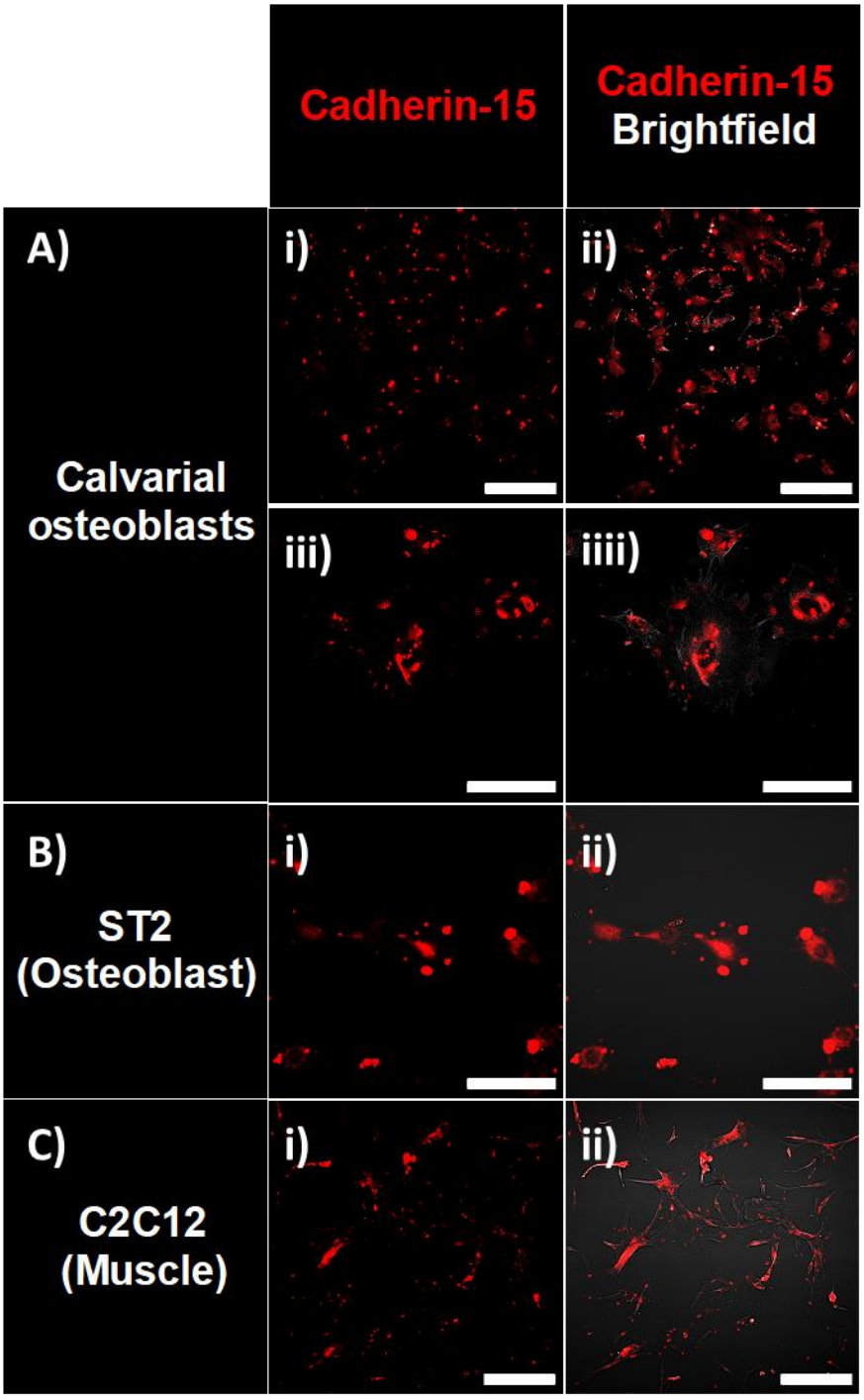

Figure 5.3. Osteoblasts express perinuclear and cell surface cadherin-15

Calvarial osteoblasts **(A)**, ST2 cells **(B)** and C2C12 cells **(C)** were cultured on coverslips and stained for cadherin-15 using a goat anti-mouse cadherin-15 antibody and an anti-goat AF546 secondary (red). Immunofluorescent images were created and overlaid on brightfield images (white) of the same area to explore expression in relation to cell structure. Scale bars = 200μm (Ai, Aii, Ci, Cii) and 100μm (Aiii, Aiiii, Bi, Bii). Data are representative of at least 3 independent experiments.

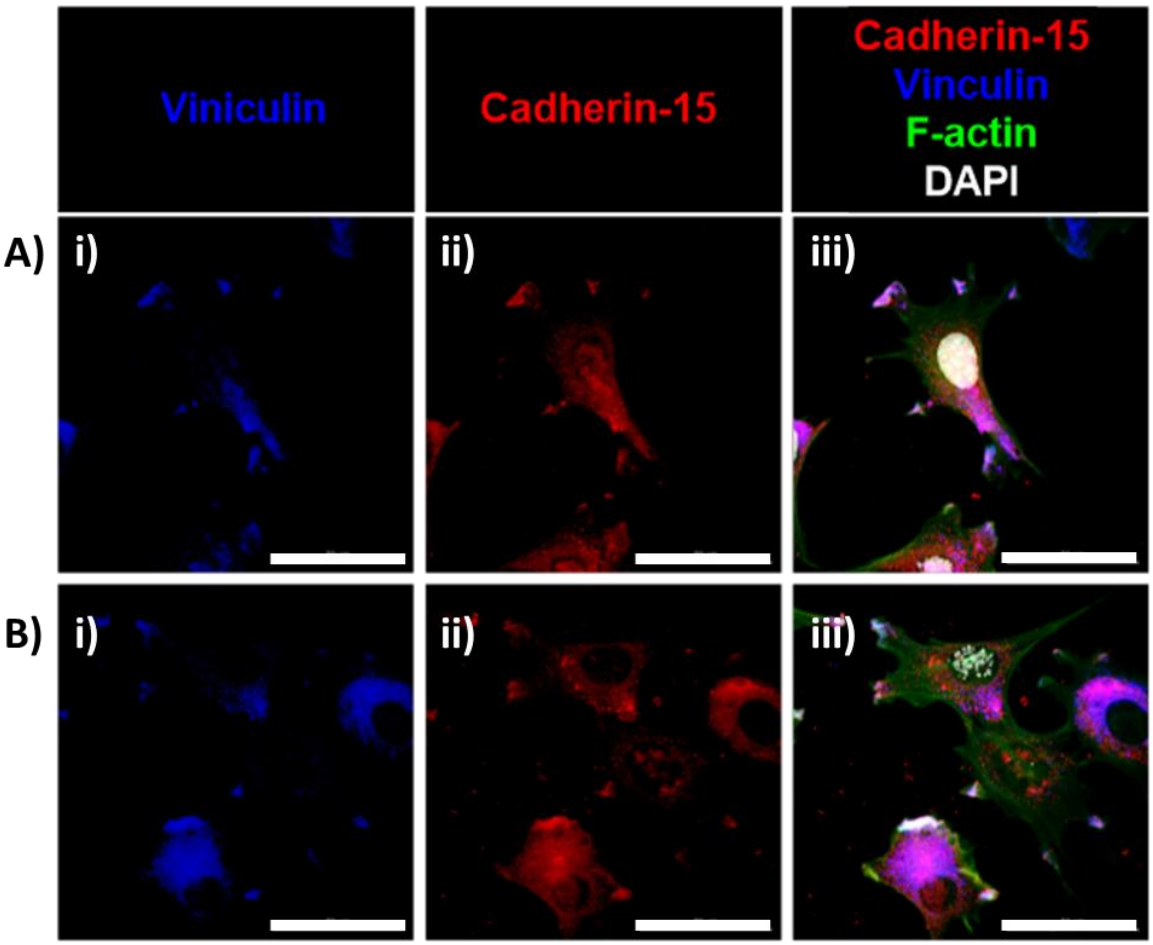

Figure 5.4. Calvarial osteoblasts co-express cadherin-15 and vinculin

Primary calvarial osteoblasts were grown on cover slips for 4 days and fixed with formaldehyde. Vinculin was stained using a rabbit anti-mouse primary and anti-rabbit AF647 secondary (blue). Co-staining for cadherin-15 protein (red) was done using a goat anti-mouse primary and anti-goat AF546 secondary. Areas of co-expression are depicted as Pink. F-actin filaments were stained with Phalloidin (green) to explore cell structure, and nuclei were stained with DAPI (white). Scale bars = 50μm. Data are 2 areas (A,B) representative of 3 independent experiments.

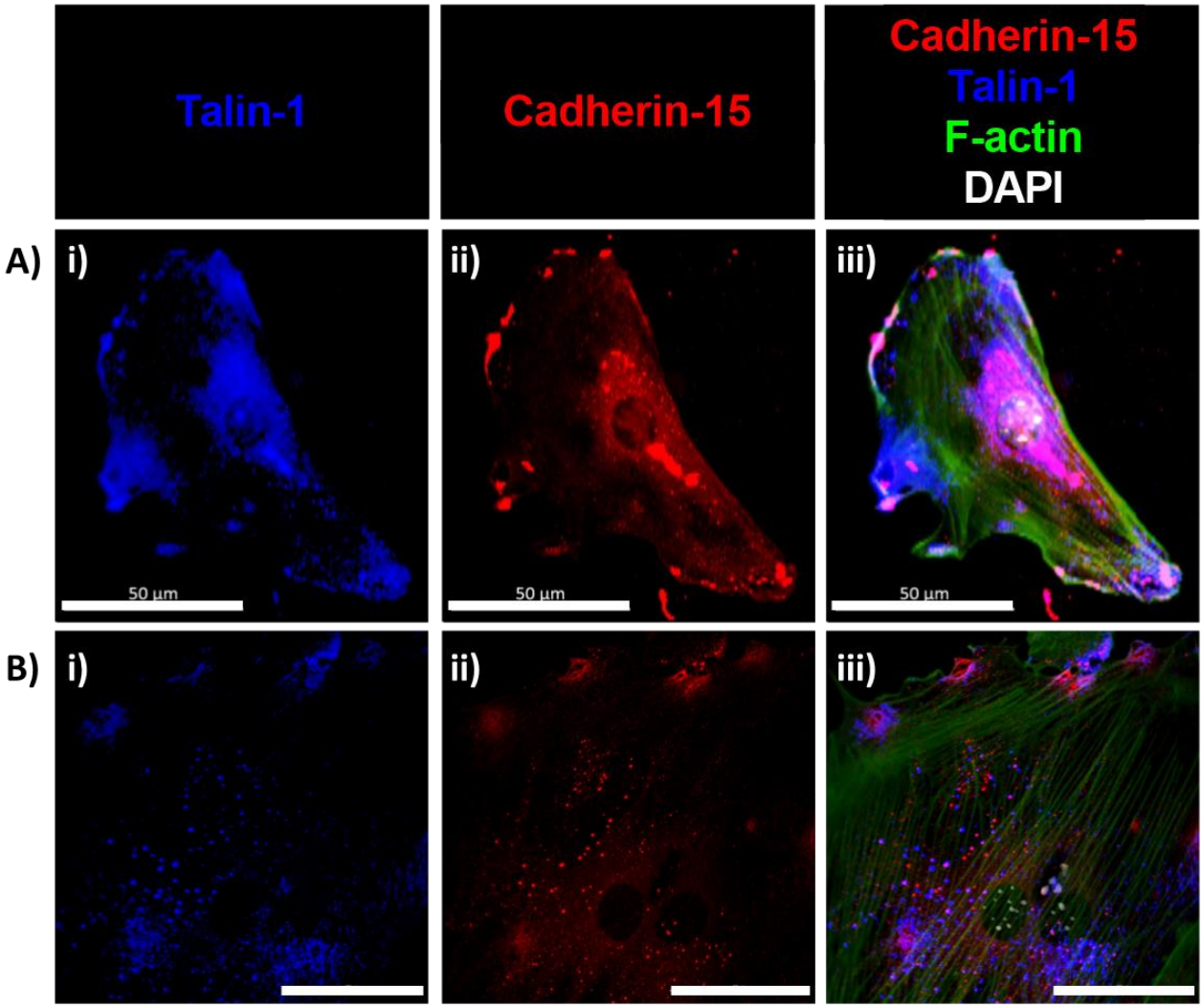

Figure 5.5. Calvarial osteoblasts co-express cadherin-15 and Talin-1

Primary calvarial osteoblasts were grown on cover slips for 4 days and fixed with formaldehyde. Talin-1 was stained using a rabbit anti-mouse primary and anti-rabbit AF647 secondary (blue). Co-staining for cadherin-15 protein (red) was done using a goat anti-mouse primary and anti-goat AF546 secondary. Areas of co-expression are depicted as Pink. F-actin filaments were stained with Phalloidin (green) to explore cell structure and nuclei were stained with DAPI (white). Scale bars = 50µm. Data are 2 areas (A and B) representative of 3 independent experiments.

5.2.3 **Cadherin-15 gene and protein levels do not correspond**

Since cadherin-15 was expressed at both gene and protein levels in human and murine osteoblasts, we explored if loss of cadherin-15 altered osteoblast response to PEPITEM. *Cdh15* gene expression was first knocked down in calvarial osteoblasts using a cocktail of *Cdh15* specific siRNA oligomers (siCdh15). Calvarial osteoblasts showed a sharp significant decrease in *Cdh15* expression when compared to cells treated with control siRNA (siCtrl) or cells only exposed to lipofectamine 24 hours post-treatment (Figure 5.6). Decreased *Cdh15* expression was maintained at all time points (2 and 4 days) post-treatment (Figure 5.6). Since there were no significant differences between lipofectamine treated and siCtrl treated cells, we thus used siCtrl as our control in subsequent analysis. Quantification of protein expression by western blot revealed no change in protein expression between siCdh15 and siCtrl treated cells when analysed 96 hours after knockdown (Figure 5.7). Similarly, no differences in MFI were observed when exploring cadherin-15 expression via flow cytometry (Figure 5.8). We investigated this further by visualising cadherin-15 protein expression following siRNA treatment by fluorescent microscopy. There was very little visual change in surface expression in siCdh15 treated calvarial osteoblasts compared to siCtrl treatment (Figure 5.9). However, a possible decrease in perinuclear expression was observed, suggesting potential cycling of protein from nuclear stores to the surface (Figure 5.9). Unsurprisingly, we observed no change in calvarial osteoblast ALP response to PEPITEM following siCdh15 transfection when compared with siCtrl (Figure 5.10). Since we did not successfully remove cadherin-15 protein expression, no conclusion on the role of cadherin-15 in mediating the effects of PEPITEM in murine cells can be achieved.

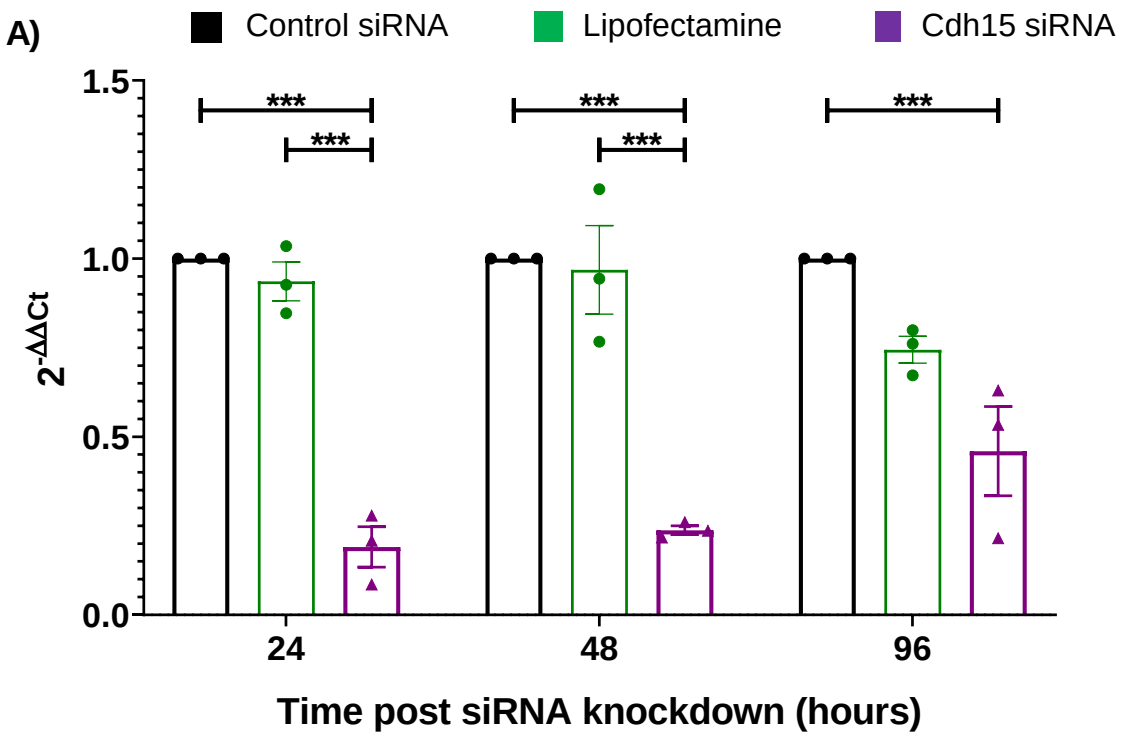

Figure 5.6. siRNA for Cdh15 results in sustained gene knockdown in calvarial osteoblasts.

Calvarial osteoblasts were treated with a cocktail of 4 *Cdh15* siRNA (siCdh15) oligomers (purple, n=3), control scrambled (siCtrl) siRNA (black, n=3) or lipofectamine control (green, n=3). RNA was isolated at 24, 48 and 96 hours post knockdown and analysed for *Cdh15* expression using real-time PCR shown as $2^{-\Delta\Delta Ct}$ where ΔΔCt is the difference between *Cdh15* expression and *B2m* housekeeping gene normalised to siCtrl values. ANOVA showed a significant effect of treatment on *Cdh15* gene expression, p<0.001. Data are mean ± SEM for 3 independent experiments and donors. * = P<0.05 and ***=P<0.001 by Bonferroni multiple comparisons test.

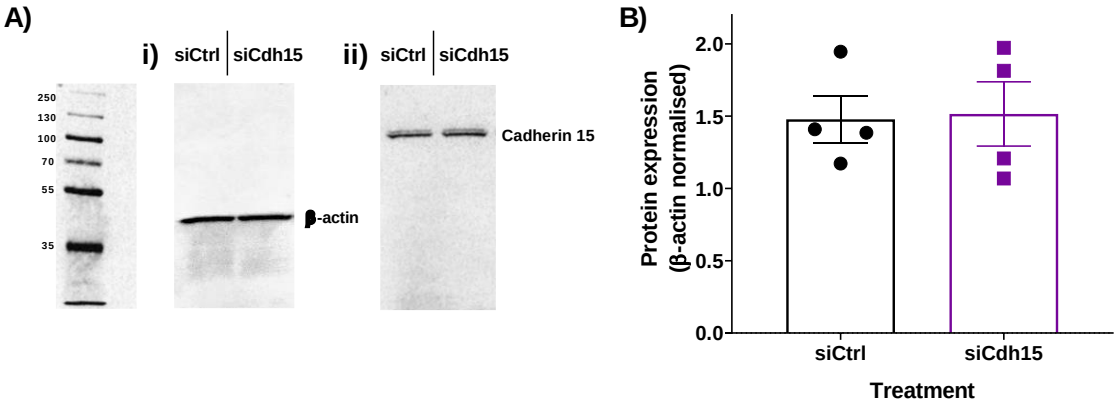

Figure 5.7. siCdh15 treatment did not alter calvarial osteoblast cadherin-15 protein expression.

Calvarial osteoblasts were treated with siCdh15 (n=4, purple) or siCtrl (n=4, black). Ninety-six hours after siRNA knockdown cell lysates were isolated and run via western blot and analysed for cadherin-15 expression and β-actin control expression. **A.** Representative western blot showing expression of β-actin **(i)** and cadherin-15 **(ii)**. **B.** Cadherin-15 protein expression was calculated by analysing band intensity, normalising expression to β-actin (n=4). Data are mean ± SEM.

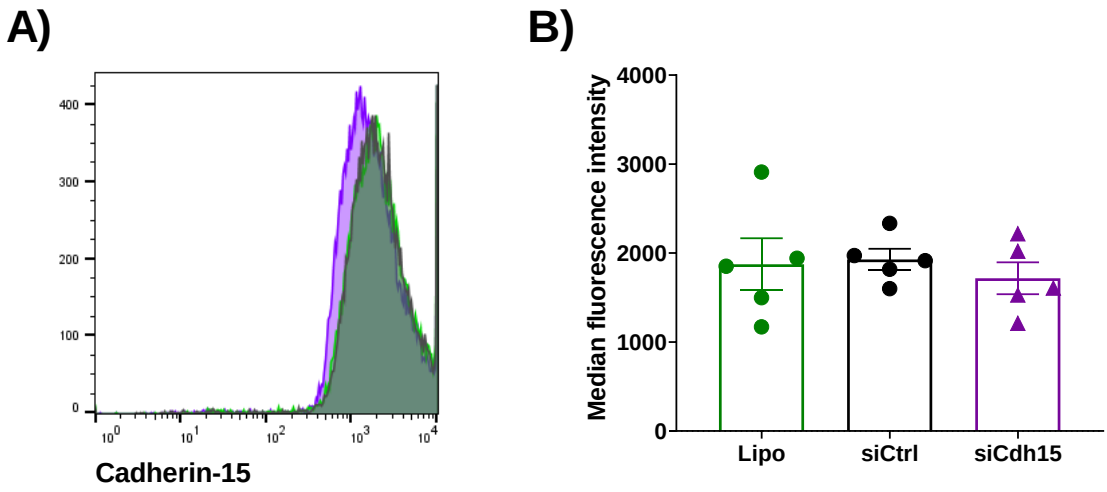

Figure 5.8. Cadherin-15 protein expression by flow cytometry following siCdh15 treatment.

Calvarial osteoblasts were treated with siCdh15 (purple, n=5), siCtrl (black, n=5) or lipofectamine control (green, n=5) and flow cytometry was performed 96 hours later to analyse changes in Cadherin-15 expression. **A.** Live cells in each treatment group were gated and histograms of cadherin-15 expression were produced. **B.** Median fluorescence intensity was calculated in each condition. Data are mean ± SEM for 5 independent donors and experiments.

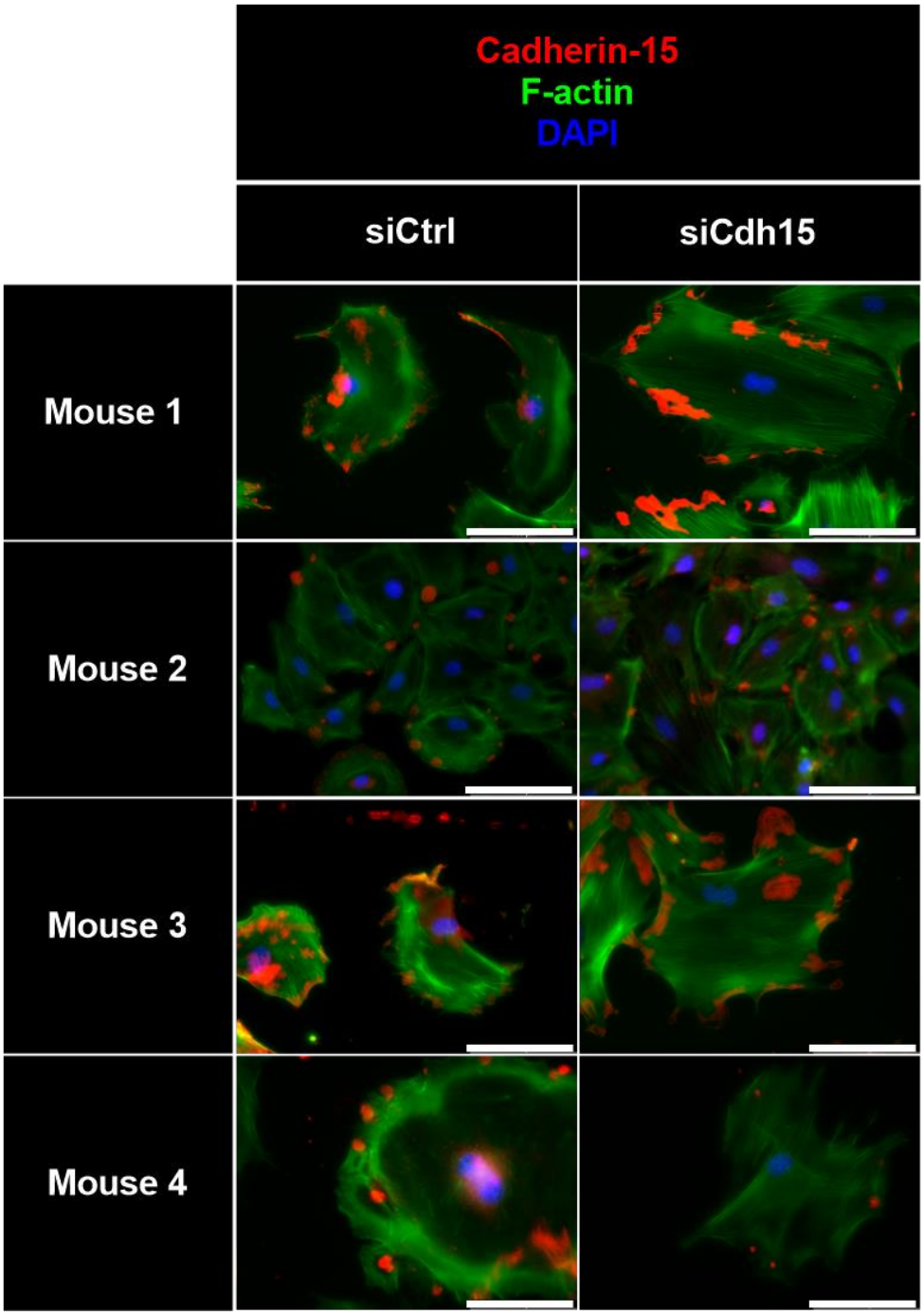

Figure 5.9. siCdh15 treatment of calvarial osteoblasts did not alter protein expression by Immunofluorescence.

Primary calvarial osteoblasts from 4 different donors were treated with siCdh15 (n=4) or siCtrl (n=4). Ninety-six hours after siRNA knockdown cells were fixed with formaldehyde and stained for cadherin-15 protein (red), F-actin filaments (phalloidin, green) and nuclei (DAPI, white) and imaged using immunofluorescence. Scale bars = 100μm. Images show a representative section of 4 individual donors.

A)

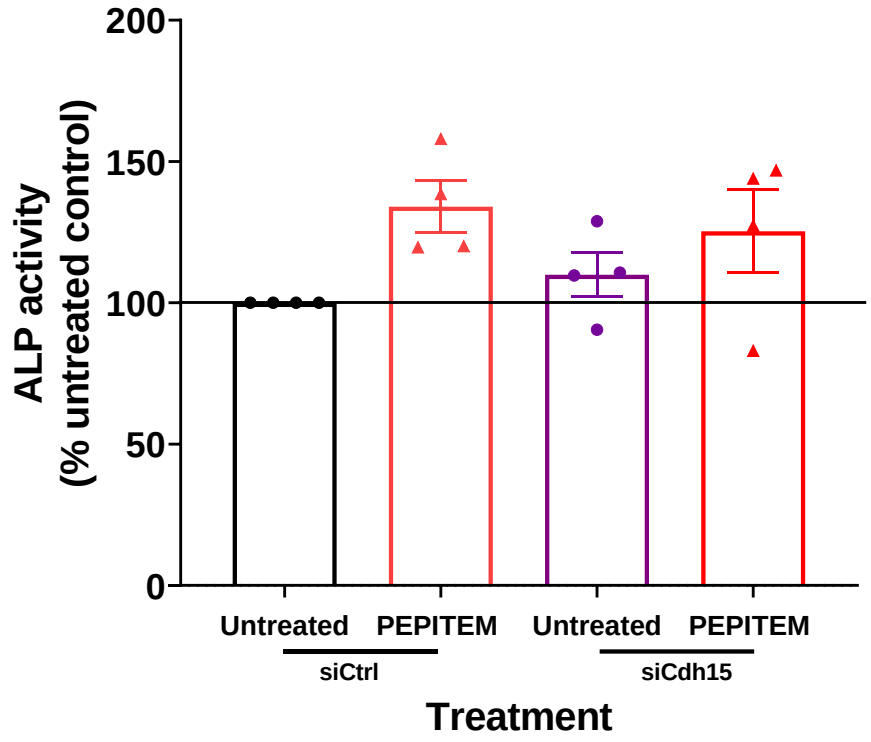

Figure 5.10. siCdh15 treatment of calvarial osteoblasts does not alter ALP activity.

Calvarial osteoblasts were treated with siCtrl and siCdh15 and cultured for 96 hours. Cells from each siRNA group were left untreated (siCtrl, black, n=4; siCdh15, purple, n=4) or treated on days 0 and 2 cells were treated with PEPITEM (siCtrl, red, n=4; siCdh15, red, n=4). ALP activity was measured and presented as activity as a percentage of untreated siCtrl control. Data are mean ± SEM for 4 independent experiments and donors.

5.2.4 Human osteoblasts are dependent on cadherin-15 expression for ALP activity.

We also explored the response of human primary osteoblasts to siRNA knockdown. Similarly, to calvarial osteoblasts, human osteoblasts treated with siCDH15 had significantly lower *CDH15* expression compared to siCTRL treated cells 96 hours following siRNA knockdown (Figure 5.11). We therefore explored the functional response of human primary osteoblasts to PEPITEM following *CDH15* knockdown. Interestingly, treatment of human osteoblasts with siCDH15 led to a significant reduction in the ALP activity of osteoblasts compared to siCTRL cells (Figure 5.12). Similarly, we found that gene expression for alkaline phosphatase, *ALPL*, was significantly downregulated by siRNA treatment, but not other osteoblast markers, *RUNX2* and *SPP1* (Figure 5.13). Increased ALP activity following PEPITEM treatment was lost in siCDH15 cells (Figure 5.12). However, due to the decreased ALP activity in untreated siCDH15 cells, multiple pathways may have been altered. Whilst these results reveal that cadherin-15 is expressed in osteoblasts and is in fact required for effective function, these data are inconclusive on the role of cadherin-15 in the osteoblast response to PEPITEM.

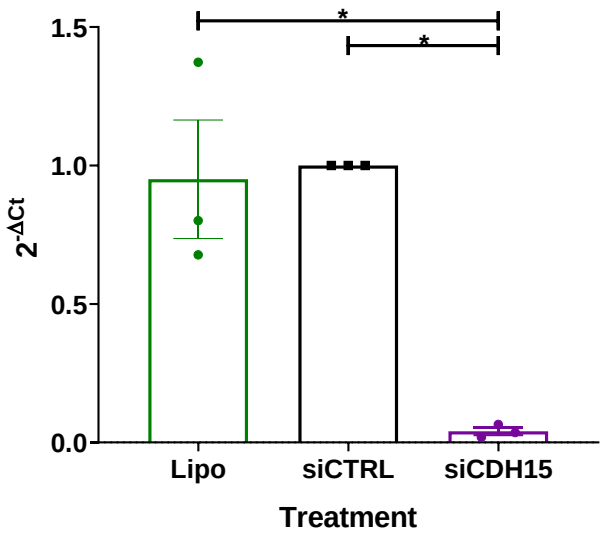

Figure 5.11. siRNA for *CDH15* caused sustained gene knockdown in human osteoblasts.

Primary human osteoblasts were treated with a cocktail of 4 *CDH15* siRNA (siCDH15) oligomers (purple, n=3), control scrambled (siCTRL) siRNA (black, n=3) or lipofectamine control (green, n=3). RNA was isolated at 96 hours post knockdown and analysed for *CDH15* expression using real-time PCR shown as $2^{-\Delta\Delta Ct}$ where ΔΔCt is the difference between *CDH15* expression and *B2M* housekeeping gene normalised to siCTRL values. ANOVA showed a significant effect of treatment on *CDH15* gene expression, $p<0.001$. Data are mean ± SEM for 3 independent experiments. * = $P<0.05$ by Bonferroni multiple comparisons test.

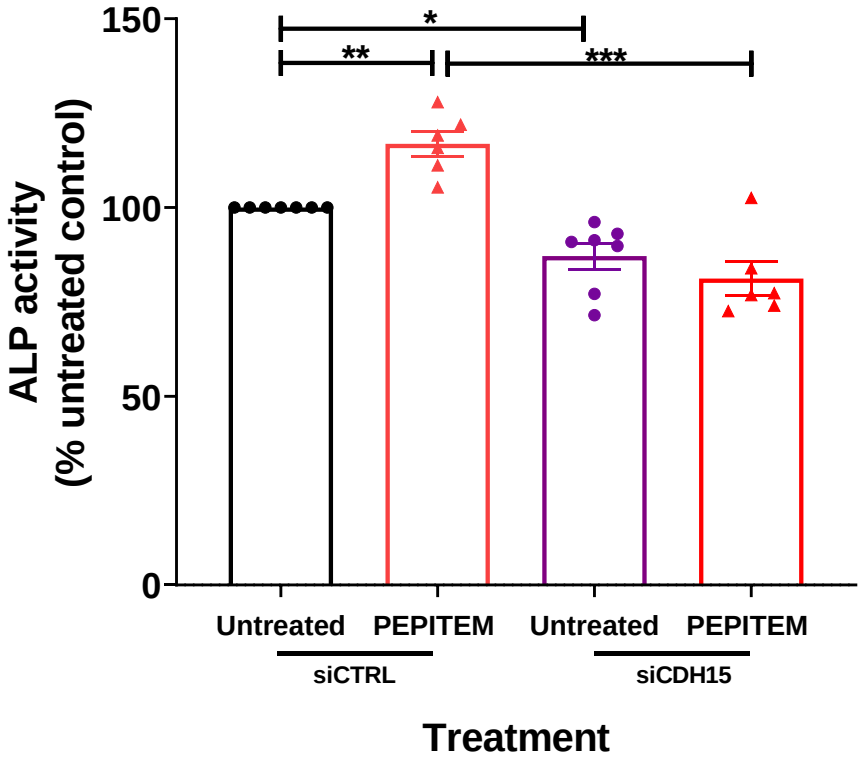

Figure 5.12. Human osteoblasts have decreased ALP activity following siCDH15 treatment.

Primary human osteoblasts were treated with siCDH15 or siCTRL and cultured left untreated (siCtrl, black, n=7; siCdh15, purple, n=6) or treated on days 0 and 2 with PEPITEM (siCtrl, red, n=7; siCdh15, red, n=6). Ninety-six hours after siRNA knockdown ALP activity was analysed in each cell type and presented as activity as a percentage of untreated siCtrl control. ANOVA showed a significant effect of PEPITEM and siRNA treatment on ALP activity, $p<0.01$. Data are mean ± SEM for 4 independent experiments from 6 independent donors. * = $p< 0.05$, ** = $p< 0.01$, *** = $p<0.001$ by Bonferroni multiple comparison test.

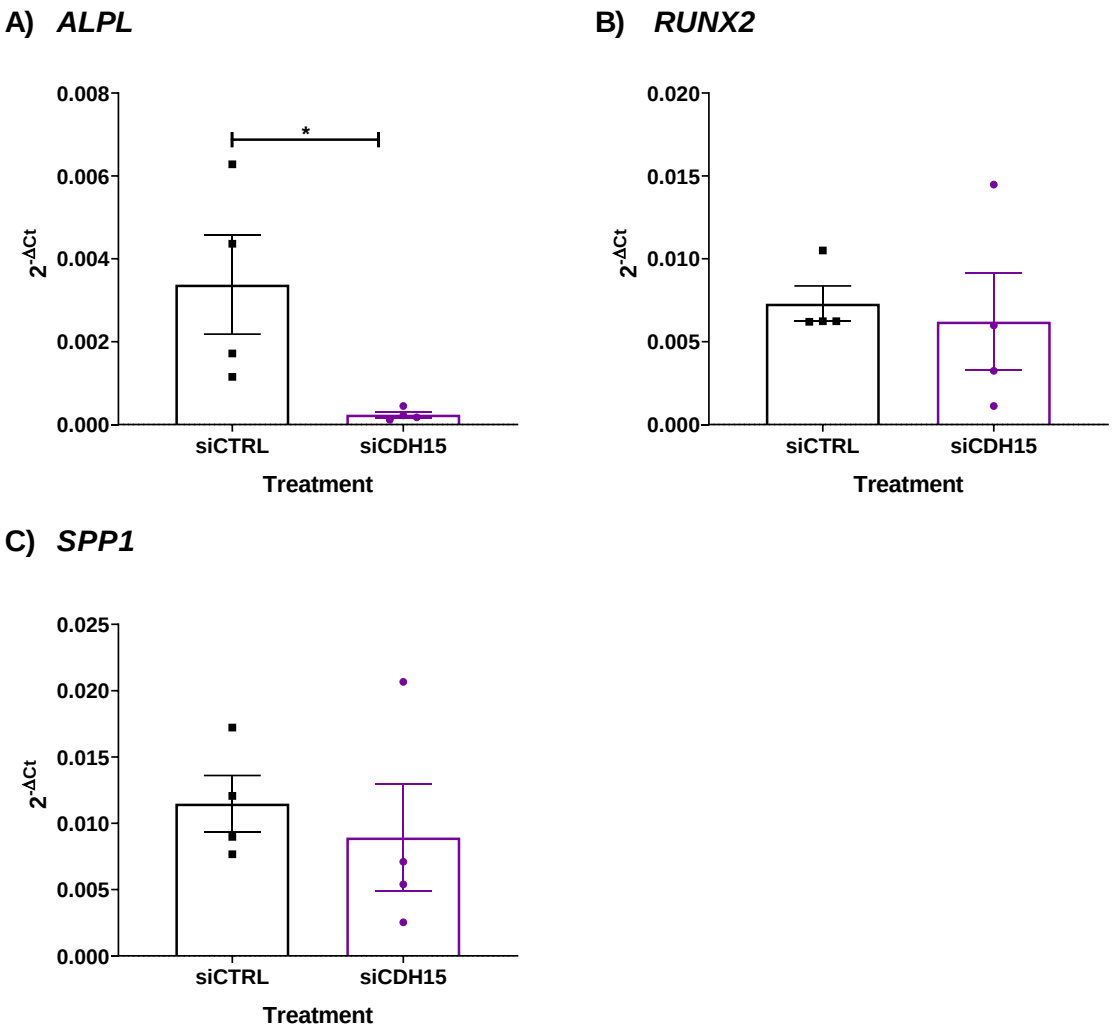

Figure 5.13. *ALP* gene expression was downregulated by siRNA treatment

Primary human osteoblasts had *CDH15* knocked down by siRNA oligomers for *CDH15* (siCDH15, n=4) or were treated with an siRNA control (siCTRL, n=4). Ninety-six hours post siRNA knockdown, mRNA was isolated and analysed for expression of *ALPL* **(A)**, *RUNX2* **(B)** and *SPP1* **(C)** by qPCR displayed as $2^{-\Delta Ct}$ where ΔCt is the difference between *ALPL, RUNX2 or SPP1* expression and *B2M* housekeeping gene. Data are Mean ± SEM for 4 independent experiments. * = P<0.05 by students t-test.

5.3 Discussion

In this chapter, we sought to identify the signalling pathway through which PEPITEM induces its response. We discovered that osteoblasts, but not osteoclasts, express a previously identified signalling molecule in the PEPITEM pathway, cadherin-15, at both gene and protein level. Whilst *Cdh15* gene expression in osteoblasts was significantly lower than that in muscle cells, protein expression was unchanged, indicating either lower degradation or increased storage. Fluorescent imaging showed expression of cadherin-15 protein at a peri-nuclear location and at the cell surface, where expression was coupled to that of focal adhesion and cadherin signalling markers Vinculin and Talin-1, suggesting roles in signalling and structural support. Removing cadherin-15 expression in murine cells using siRNA ultimately proved unsuccessful, due to protein levels being maintained despite significant knockdown of gene expression. This again may point towards high levels of intracellular protein storage, which can be utilised in the case of decreased gene expression. Consistent cadherin-15 protein expression meant PEPITEM – cadherin-15 interactions could not be studied. We also struggled to explore the role of cadherin-15 in the PEPITEM pathway in human osteoblasts, however here this was due to the essential nature of cadherin-15 in ensuring osteoblast maturation. CDH15 siRNA treatment of human osteoblasts led to a decrease in ALP activity, and osteoblast gene expression regardless of PEPITEM treatment. Whilst the effects of PEPITEM were lost in the human osteoblasts following siRNA knockdown, whether this was due to an inability of cells to respond to PEPITEM due to loss of cadherin-15 or due to osteoblast maturation being decreased by cadherin-15 knockdown itself

remains unknown. Overall, we have revealed an essential role for cadherin-15 in osteoblast survival/maturation, where previously it has had little research.

5.3.1 Cadherin-15 expression in osteoblasts

Cadherin-15 has previously been shown to be highly expressed in muscle, hence its alternative name M-cadherin.[640,641] Differentiation of C2C12 and Sol8 (myocyte cell lines) into mature muscle results in an increase in *Cdh15* gene expression with differentiation.[640,641] In addition, this expression has been seen in nuclear/perinuclear regions of the cell as well as in the cytosol and on the cell surface.[642–644] This matches with our observation in C2C12 differentiated cells, where immunofluorescence revealed nuclear and cell surface protein expression. In contrast, whilst many cadherins have been found to be expressed in osteoblasts, there is very little evidence exploring cadherin-15. Using a pan cadherin antibody (MoAb C-1821), general cadherin expression has been observed in MC3T3 cells and human BMSCs.[638,645] However, northern blot and qPCR analysis did not detect *Cdh15* expression in primary calvarial osteoblasts, C3H10T1/2 cells or ST2 cells.[646] In fact, C2C12 cells differentiation into osteoblasts by inducing *Runx2* expression or treating with BMP decreased *Cdh15* expression with differentiation.[647] Whilst this does not completely reflect our data, we did observe a significant reduction (~100-fold) in *Cdh15* gene expression in calvarial osteoblasts compared to C2C12 differentiated muscle cells. In addition, expression of *Cdh15* was very lowly expressed and therefore may not be detected by less powerful detection methods. Other studies have however found slight cadherin-15 expression in osteoblast-like cells. Col1a1 expressing osteoblasts and DMP1 expressing osteocytes analysed by an Illumina microarray showed expression of *Cdh15* in both cells types.[648]

Interestingly, there was a 5.3 fold increase in osteocytes, indicating cadherin-15 is used more in osteocyte signalling.[648] Moreover, expression of *Cdh15* was increased in calvarial osteoblasts compared to non-osteoblast calvarial cells, the majority of which would have been more pre-osteoblasts or stem cell in origin.[648] We also observed an increase in *CDH15* expression in human osteoblasts when compared to MSCs where expression was undetectable by RT-PCR. Thus, whilst cadherin-15 may not be as highly expressed in osteoblasts compared to cells in muscle at a gene level, its upregulation during differentiation from MSCs and higher expression in osteocytes indicates an essential function in cellular activity.

5.3.2 Cadherin-15 function in murine osteoblasts

Of interest, no studies appear to have explored cadherin-15 protein expression in osteoblasts. Herein, we report for the first time similar levels of cadherin-15 protein in osteoblasts and muscle using immunofluorescence and flow cytometry staining. The location of cadherin-15 expression and the molecules it is associated with may provide some insights into its function in osteoblasts and how it could respond to PEPITEM. We observed co-expression of cadherin-15 in osteoblasts with vinculin and talin-1. Vinculin has previously been associated with cadherin signalling.[649] Three-dimensional super-resolution microscopy of vinculin and cadherin junctions revealed a confirmation change in vinculin upon cadherin activation in C2C12 and Madin-Darby Canine Kidney (MDCK) cells.[649] This enabled communication with actomyosin and thus regulation of cellular adherens junctions.[649] Talin-1 is also a marker of cellular adhesion junctions, however, is closely linked to integrin signalling.[304] Removal of Talin-1 in endothelium alters VE-cadherin organisation on the cell surface.[650] Thus, similar mechanisms may organise cadherin-

15 expression in the osteoblasts surface, allowing its interactions with surrounding molecules or cells.

The fact that following significant downregulation of *Cdh15* expression in calvarial osteoblasts there was no protein change may indicate that high levels of cadherin-15 are stored within the cells and degradation of the protein is slow. Our data suggests that cadherin-15 expression occurs in a peri-nuclear location in osteoblasts. This may be used as a cadherin-15 storage site, especially as this localisation of cadherin-15 appeared to decrease fluorescent intensity in siRNA treated cells. This hypothesis is supported by previous studies showing recycling of E-cadherin in MDCK cells. Perinuclear staining of E-cadherin was associated with the golgi complex due to its localisation in the cell or due to overlapping expression with golgi marker GM130.[651,652] Inhibition of cadherin-15 protein production using cycloheximide lost this perinuclear staining despite vesicular staining being maintained.[651] This suggests high levels of protein are produced and stored in the golgi ready for trafficking to the cell surface when required. In addition, surface biotinylation of E-cadherin in MDCK cells showed E-cadherin was re-expressed on the cell surface 15 minutes after internalised.[651] High levels of cadherin recycling may provide another reason why murine cadherin-15 protein levels were not decreased in our study following siRNA treatment. Furthermore, recent research has revealed three-phosphorylation sites on cadherins that can increase the stability of the protein. VE-cadherin mutations of S>A at 840, 846, and 847 resulted in increased lysosomal uptake of VE-cadherin from the cell surface and internalisation.[653] Thus in normal conditions, cadherins are relatively stable at the cell surface and protein degradation is low, allowing long term expression and low levels of replacement. This is also

indicated in our study with high levels of protein expression, but low gene expression. Whilst these studies look at different cell types and different cadherins, the similarities of each of the cadherins may indicate they all respond in similar ways. In fact, in cadherin-15 KO mice, there was upregulation of N-cadherin and E-Cadherin and no defects in myoblast differentiation.[654] This lack of cellular functional change was believed to occur due to N-cadherin being able to replace M-cadherin and perform the same functions,[654] thus indicating functional redundancy within the cadherin family.

5.3.3 Human osteoblast cadherin-15 function

This similarity between cadherins may also be the cause of decreased osteoblastic activity and gene expression in human osteoblasts following treatment with *CDH15* targeting siRNA. Due to the similarities between the nucleotide sequences of each cadherin,[655] there is a possibility of off target effects on cadherin gene expression (which we did not analyse), particularly with the use of a pool of 4 different siRNAs. Other cadherins have previously been shown to be expressed and signal in osteoblasts. MC3T3 cells, calvarial osteoblasts, C3H10T1/2 cells, ST2 cells and Saos2 cells show expression of N-cadherin, E-cadherin and cadherin-11 (otherwise known as Ob-cadherin) by northern blot and RT-PCR.[637–639,646,654,656]

Expression of N-cadherin protein (cadherin-2) has been observed in rat and human bone via in situ hybridisation.[656] Expression increased in Saos-2 cells during differentiation, peaking at later time-points (day 29 and 33).[656] Using an N-cadherin mutation, MC3T3 cells had decreased adhesion to a confluent monolayer of MC3T3 cells.[639] In addition, alkaline phosphatase activity, calcium uptake and expression of *BSP* and *BGLAP* were all decreased.[639] Similar was also observed in primary

osteoblasts treated with a His-Ala-Val adhesion motif which decreases N-cadherin signalling.[656] Nodule creation, ALP activity and cellular adhesion were all decreased and cells with a mutant N-cadherin protein gained an elongated cell phenotype. Thus, if our siRNA had off target effects on N-cadherin, then decreased osteoblast potential would have been observed.

The other major cadherin shown to be expressed in osteoblasts is cadherin-11.[637,638,646] Dot plot hybridisation showed expression of *Cdh11* only in primary osteoblasts and MC3T3 cells, with no expression in the NIH3T3 fibroblasts or in any other organ (thymus, spleen, brain, kidney, lung, liver, testis, heart).[637] In addition, MC3T3 cells increased *Cdh11* expression following 7 days of differentiation in mature osteoblasts.[637] C2C12 cells treated with BMP also increase gene expression of *Cdh11* with concurrent increases in osteoblast related genes.[646] *Cdh11* has been observed to be involved in osteoblast adhesion, and transfection into L-cells results in increased adhesion.[637] Calvarial osteoblasts isolated from $Cdh11^{-/-}$ mice had decreased mineral production and expression of *Runx2, Sp7* and *Bglap*.[657] Furthermore, $Cdh11^{-/-}$ mice had decreased BV/TV in the metaphysis indicating an essential role in bone production.[657] Thus, if our siRNA removed expression of Cdh11 by off target effects, it may explain why osteoblast function was reduced. Expression of each cadherin following siRNA knockdown would have to be analysed to explore if there are altered gene expression.

Altered osteoblast activity may be due to direct effects on cadherin-15 protein expression. As mentioned earlier, cadherin-15 has not been explored at a protein level in osteoblasts. However, its functions in other cell types may be mirrored in osteoblasts and thus are worth exploring. Treatment of C2C12 cells with an siRNA

for CDH15 resulted in increased cellular apoptosis, with increased expression of caspase-9 and decreased phospho-Akt, GSK-3β, survivin and cyclin D.[658] In contrast, treatment with a recombinant cadherin-15 FC led to increased phosphor-Akt, survivin and cyclin D.[658] This not only indicates that cadherin-15 is essential for cell survival, but also that it induces outside-in signalling via the Akt pathway. However, more work is needed to understand Cdh15s exact role in osteoblasts following knockdown.

5.3.4 Signalling between cadherin-15 and PEPITEM

In regard to the direct relationship between cadherin-15 and PEPITEM, our data are inconclusive. Previously, endothelial cells treated with cadherin-15 siRNA, resulting in decreased gene and protein expression, led to loss of the immunomodulatory actions of PEPITEM, showing an essential nature for cadherin-15 in PEPITEM signalling.[473] Calvarial osteoblasts did not lose expression of cadherin-15 following siRNA knockdown, particularly on the cell surface, and thus cells could most likely still respond to PEPITEM (as observed in our study). Prolonged siRNA knockdown or the use of cadherin-15 blocking antibodies will be essential for to completely understand both how osteoblasts use cadherin-15 for general function, but also how it interacts with PEPITEM. On the other hand, human osteoblasts did lose their enhanced anabolic response to PEPITEM, but we are unable to understand if this was due to loss of cadherin-15 – PEPITEM interactions or result from the changes in osteoblast phenotype due to loss of cadherin-15 alone. Increased apoptosis or other changes that occur by cdh15 knockdown may alter any potential signalling pathways activated by PEPITEM regardless of direct interactions with cadherin-15. Regardless, in any context the role of cadherin-15 in the PEPITEM

pathway has not been explored. Understanding if PEPITEM can bind directly to cadherin-15 or other receptors, and the downstream intracellular signalling that follows is needed.

In conclusion, the role of cadherin-15 in the bioactivity of PEPITEM in osteoblasts is still unknown due to issue with changing protein expression or because of its essential nature in osteoblasts. Further studies will need the use of cadherin-15 blocking proteins to fully understand the pathway.

6 Investigating the Role of PEPITEM in Diseased Bone

6.1 Introduction

Bone formation and resorption are highly regulated in healthy individuals, ensuring there is balance and bone mass is maintained. However, this is not always the case. In diseases, such as osteoporosis (both menopause and senile), there is a net loss of bone resulting from increased bone resorption by osteoclasts and decreased bone formation by osteoblasts. There are multiple cellular changes that occur in such diseases, causing alterations in response to treatments and homeostatic signalling pathways. Alternatively, following fracture there is a requirement for net bone formation in order to restore broken bone. As evident above, there is a need to boost bone growth in diseases and fracture to repair bone function. Current treatments, such as PTH, bisphosphonates and novel pathway activators (anti-sclerostin antibodies), have potential to boost bone growth in the short term. However, long-term treatment has reduced efficacy with some patients being non-responsive to treatments, and there are issues with side-effects and treatment delivery mechanisms, resulting in low medication adherence.

In the previous chapters we observed that PEPITEM was able to induce bone growth in homeostatic conditions, with direct actions on osteoblasts. In this chapter we therefore sought to identify if the osteogenic actions of PEPITEM are maintained in murine and human osteoporosis, with age and following fracture. We hypothesise that PEPITEM is able to maintain its pro-anabolic actions in musculoskeletal disease.

6.2 Results

6.2.1 Murine ovariectomy induces an osteoporosis-like phenotype

We have previously seen that PEPITEM causes a pro-anabolic phenotype on homeostatic bone, thus we wanted to explore the effects of PEPITEM in bone diseases. First, we induced an osteoporosis-like phenotype in 12-week old female mice, where bone mass has already peaked, through ovariectomy (OVX, Figure 6.1). Characterisation of the model at 1, 2 and 4-weeks following OVX showed that tibial trabecular bone volume was conserved 1-week post-OVX but had decreased at 2-weeks and further declined by 4-weeks post-OVX (Figure 6.2A/B). The same decrease was also observed in trabecular number (Figure 6.2C). Tibial trabecular thickness was unchanged between baseline and 2 or 4-weeks post-OVX. Interestingly, a small significant increase in trabecular thickness was recorded at 1-week post-OVX (Figure 6.2C). In contrast, we observed a significant increase in trabecular separation and trabecular pattern factor between baseline and 4-weeks post-OVX (Figure 6.2D/E). No changes in cortical bone were observed at any point following induction of OVX (Figure 6.3). Exploring vertebral bone, changes mapped to what we observed in the tibiae, although the decreases in BV/TV and trabecular number, and increases in trabecular separation and trabecular pattern factor were delayed, only becoming significant 4-weeks post-OVX (Figure 6.4A, B, D, E). Furthermore, trabecular thickness was unchanged at all time points (Figure 6.4C). Changes in bone strength were also analysed through 3-point-bend testing, revealing no changes in bone strength or stiffness occurred regardless of time post-OVX (Figure 6.5).

Ageing also induces bone loss, thus we compared the changes in tibial trabecular (Figure 6.6), tibial cortical (Figure 6.6) and vertebral trabecular bone (Figure 6.7) following OVX in 12-week-old mice to age related changes seen in middle aged (30 week) and aged (over 100 week) mice (Table 6.1). Like OVX, ageing significantly decreased tibial and vertebral BV/TV and trabecular number, and increased trabecular separation and pattern factor at both 30 (tibia) and 100 (tibia and vertebra) weeks. However, unlike OVX, trabecular thickness increased with age and was significantly higher in 100-week-old mice. Trabecular BV/TV, trabecular number, and trabecular separation 4 weeks post-OVX were non-significant compared to 30-week-old mice, but were still significantly increased (BV/TV, trabecular number) or decreased (trabecular separation, trabecular pattern factor) compared to 100-week-old mice (Table 6.1). Cortical bone parameters cortical thickness and cortical area are also decreased with ageing, but not following OVX.

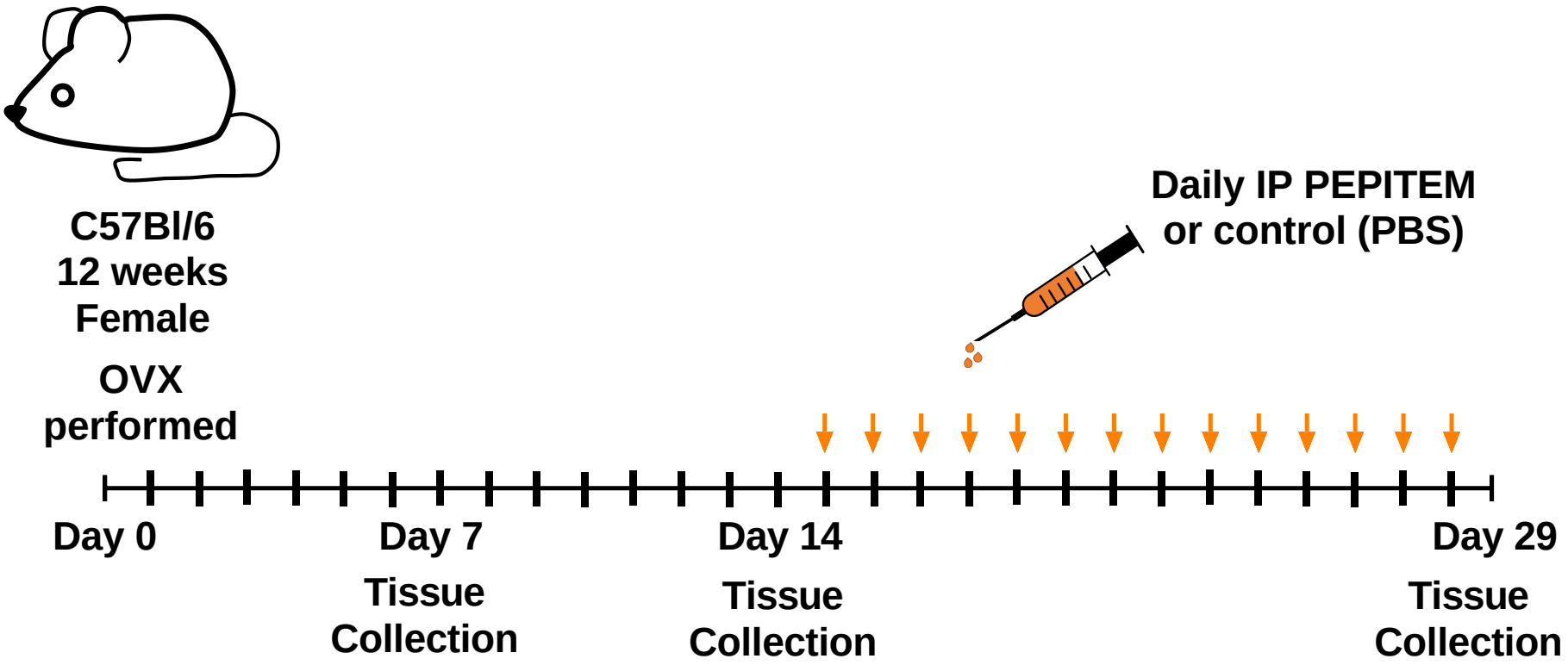

Figure 6.1. *In vivo* model to study PEPITEMs role on ovariectomised bone.

Female, WT mice had ovariectomy (OVX) performed to initiate bone loss. Baseline (day 0) and control tissue was collected 7, 14 and 29 days post-OVX. To explore treatment effect, daily IP PEPITEM (300µg) or control (PBS) was given starting from 2-weeks post-OVX for 14 days. Fifteen days post the onset of daily injections (29 days post-OVX), mice were culled, and tissue was collected for analysis.

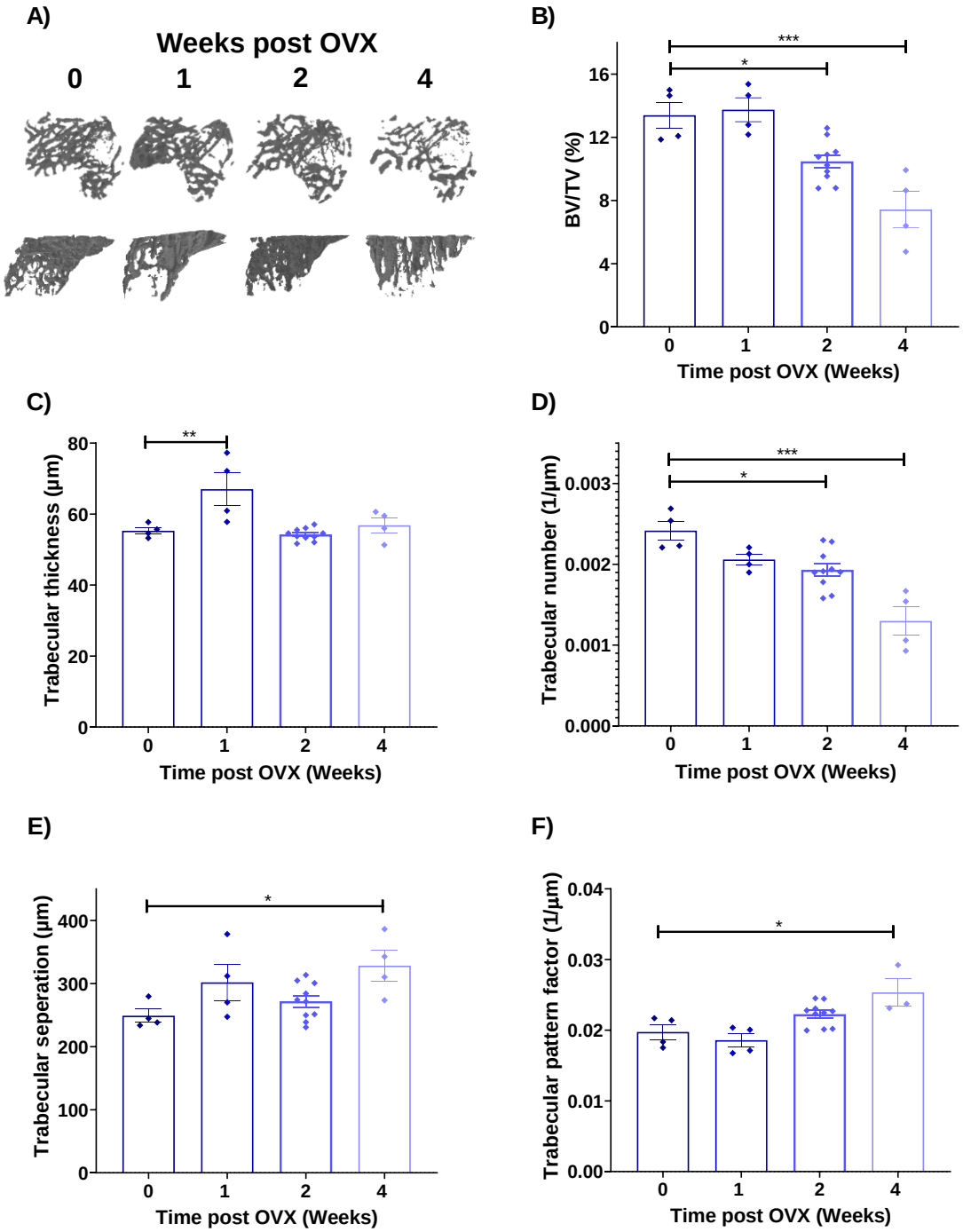

Figure 6.2. OVX induced tibiae trabecular bone loss.
Following OVX, tissue was collected at baseline (n=4), 1-week (n=4), 2-weeks (n=10) and 4-weeks (n=4) post-OVX. Tibiae were scanned by µ-CT and regions of interest were drawn around trabecular bone in the metaphysis to analyse trabecular parameters. **A.** Representative 3D renders of trabecular bone from each time point. **B-F.** Trabecular bone was analysed for **B.** trabecular bone volume (BV/TV, %), **C.** trabecular thickness (µm), **D.** trabecular number (1/µm), **E.** trabecular separation (µm) and **F.** trabecular pattern factor (1/µm). In B-F, ANOVA showed a significant effect of time on bone parameters, P<0.05. Data are mean ± SEM for 3 independent experiments. * = P<0.05, ** = P<0.01 and ***=P<0.001 by Bonferroni multiple comparisons test.

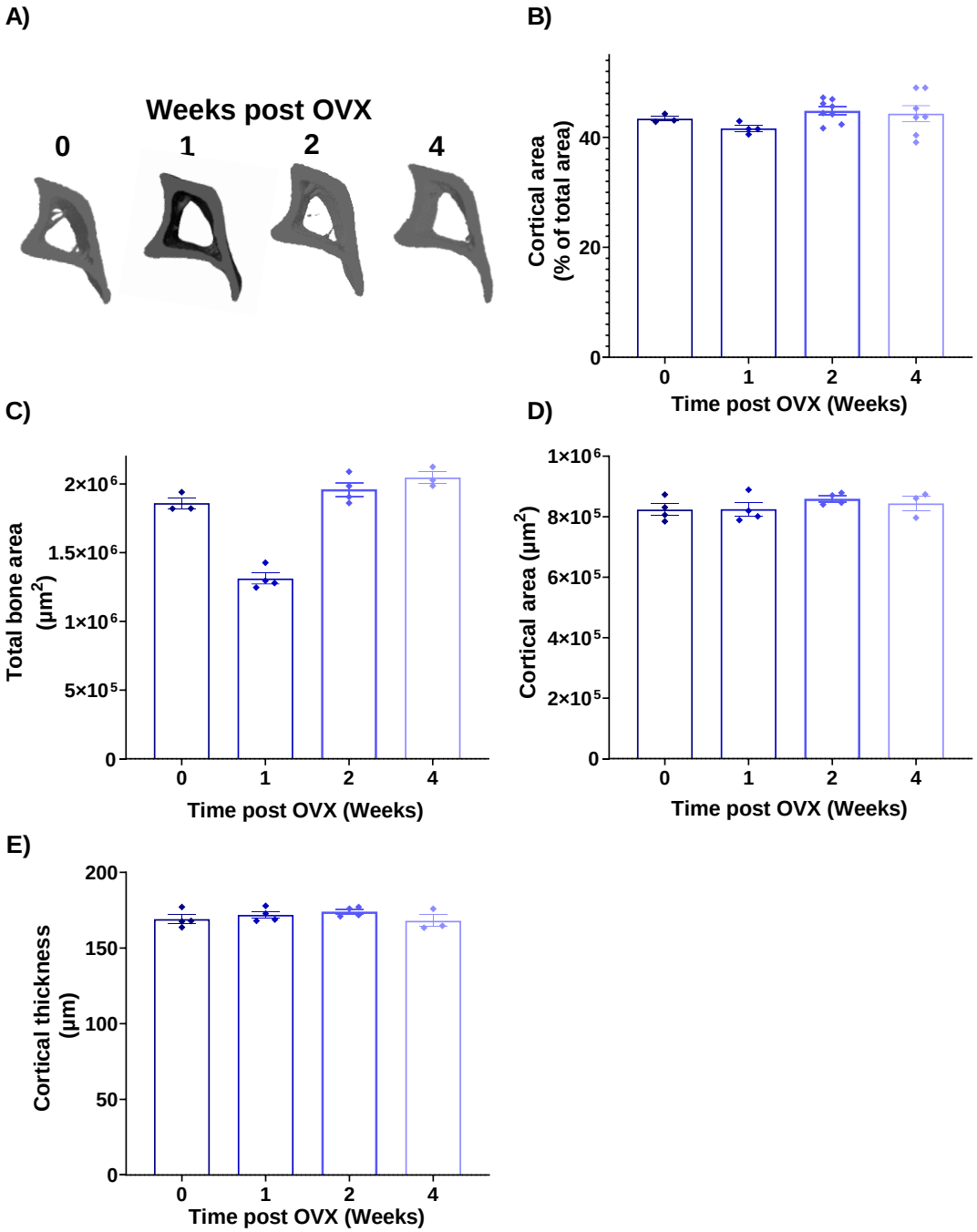

Figure 6.3. OVX did not alter cortical bone.
Following OVX, tissue was collected at baseline (n=4), 1-week (n=4), 2-weeks (n=4) and 4-weeks (n=4) post-OVX. Tibiae were dissected, fixed in paraformaldehyde, and scanned by µ-CT. Regions of interest were drawn around cortical bone, but not trabecular, in the epiphysis and analysed for cortical parameters. **A.** Representative models of cortical bone from each time-point. **B-E.** Cortical bone was analysed for **B.** percentage of cortical area (%), **C.** total bone area (µm^2), **D.** total cortical area (µm^2), and **E.** Cortical thickness (µm). ANOVA showed no significant effect on time on cortical parameters. Data are mean ± SEM for 3 independent experiments.

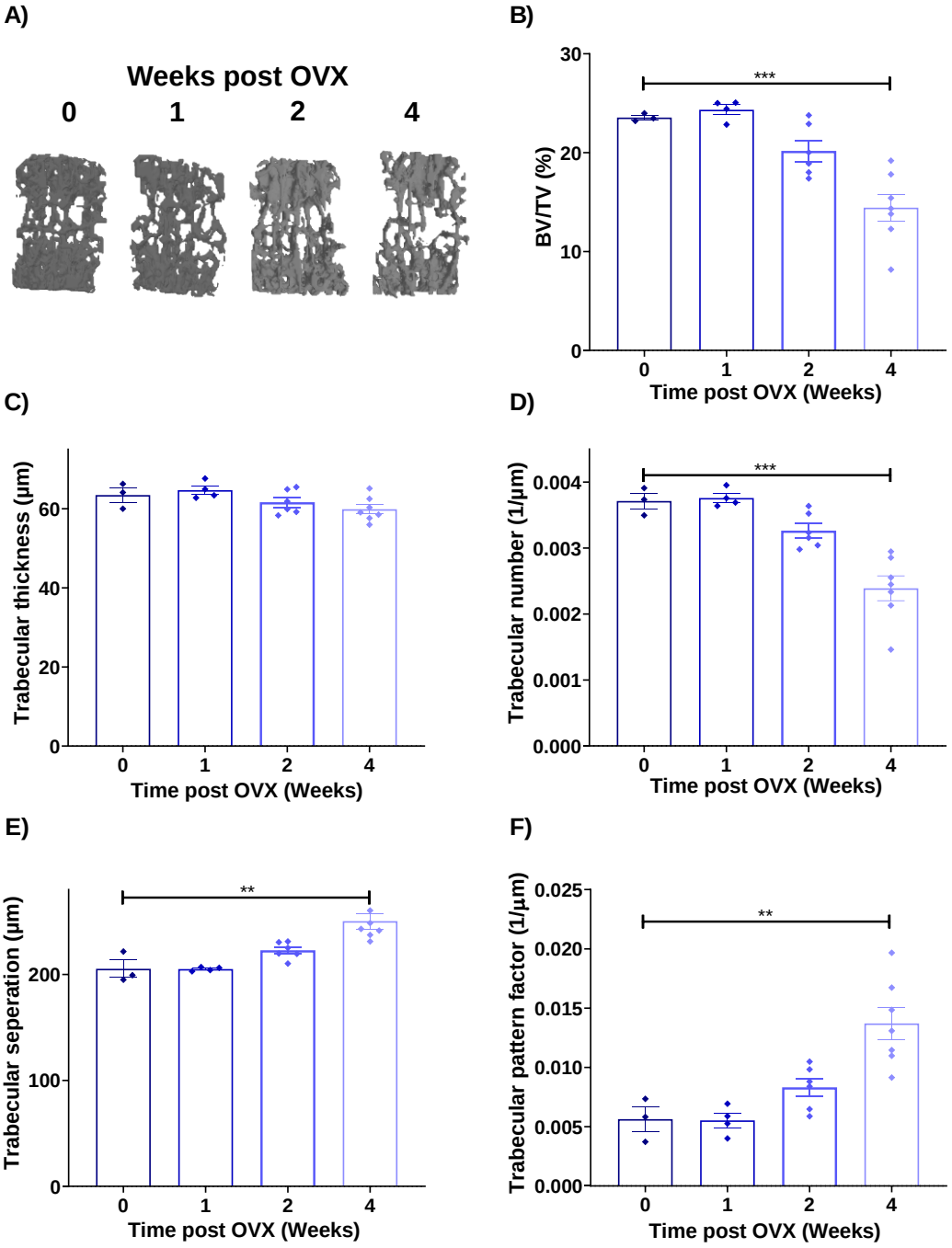

Figure 6.4. OVX induced vertebral trabecular bone loss.
Following induction of OVX, tissue was collected at baseline (n=4), 1-week (n=4), 2-weeks (n=6) and 4-weeks (n=7) post-OVX. . Vertebrae were dissected, fixed in paraformaldehyde, and scanned by µ-CT. Regions of interest were drawn around trabecular bone to analyse trabecular parameters. **A.** Representative 3D renders of trabecular bone from L4 vertebrae at each time point. **B-F.** Trabecular bone was analysed for **B.** trabecular bone volume (BV/TV, %), **C.** trabecular thickness (µm), **D.** trabecular number (1/µm), **E.** trabecular separation (µm) and **F.** trabecular pattern factor (1/µm). In B, D-F, ANOVA showed a significant effect of time on bone parameters, P<0.05. Data are mean ± SEM for 3 independent experiments. ** = P<0.01 and ***=P<0.001 by Bonferroni multiple comparisons test.

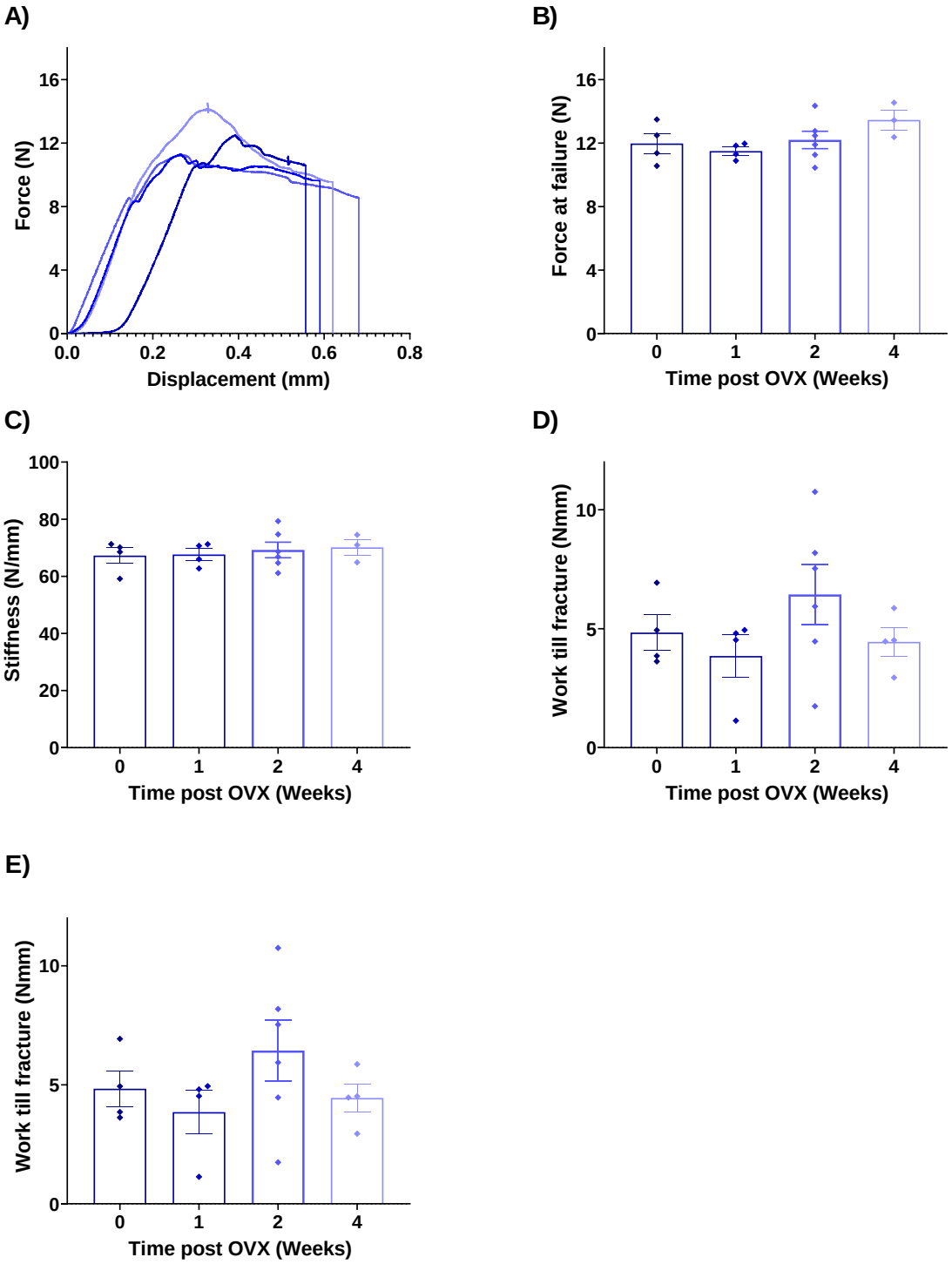

Figure 6.5. Bone strength was not changed by OVX.
Tissue was collected from ovariectomised mice at baseline (n=4), 1-week (n=4), 2-weeks (n=6) and 4-weeks (n=4) post-OVX. Femurs were dissected, fixed in paraformaldehyde, and tested by 3-point-bend. **A.** Representative graphs showing displacement of bone (mm) in relation to force applied (N) from each time point. **B-E.** Force vs displacement plots were analysed for **B.** stiffness (N/mm), **C.** force at failure (N), **D.** force at fracture (N), and **E.** work till fracture (Nmm). Data are mean ± SEM for 3 independent experiments.

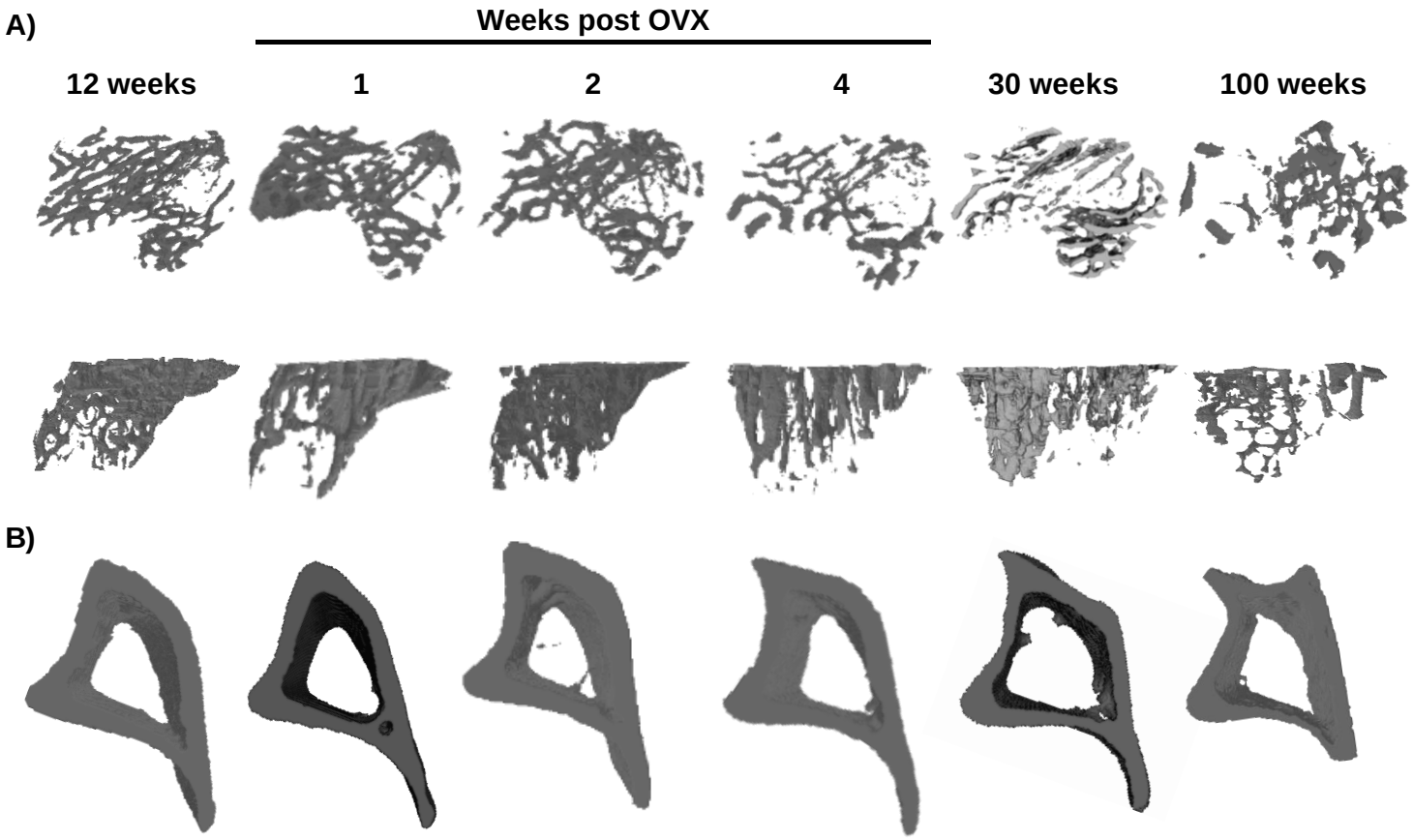

Figure 6.6. 3D models of trabecular and cortical bone from OVX and aged mice tibiae.

Tissue was collected from ovariectomised mice at baseline (n=4), 1-week (n=4), 2-weeks (n=4 for cortical, n = 10 for trabecular) and 4-weeks (n=4) post-OVX, or from WT 30-week-old (n=3) or over 100-week-old (n=3) mice. 3D models were generated and imaged for **A.** trabecular bone and **B.** cortical bone from each time-point/age.

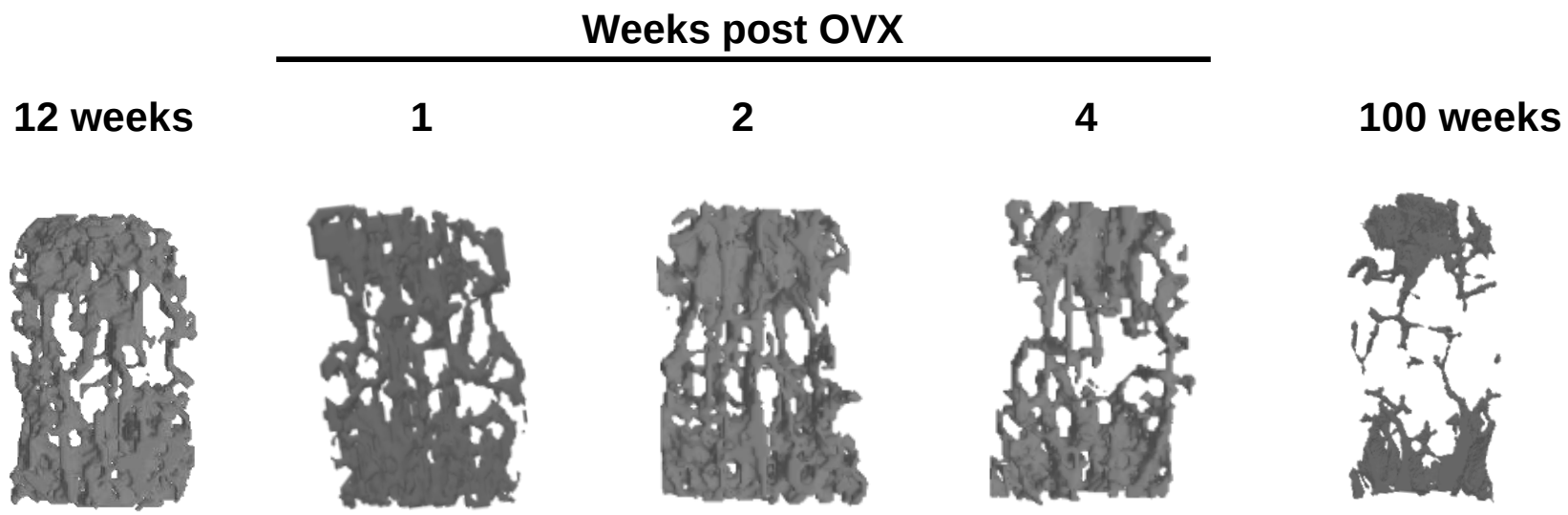

Figure 6.7. 3D models of trabecular and cortical bone from OVX and aged mice L4 vertebrae.

Tissue was collected from ovariectomised mice at baseline (n=4), 1-week (n=4), 2-weeks (n=6 for trabecular) and 4-weeks (n=7) post-OVX, or from WT 100-week-old (n=4) mice. 3D models of trabecular bone were generated from L4 vertebrae.

Table 6.1. Micro-CT results from ovariectomised and aged mice.

Bone	Parameter	12_weeks	30_weeks	Significance	100_weeks	Significance	1_week_OVX	Significance	2_week_OVX	Significance	4_week_OVX	Significance
Trabecular bone	BV/TV (%)	12.34±1.536	7.77±1.11	a,c	2.342±1.091	a,b	13.75±1.509	b,c	10.47±1.293	c	7.43±2.3	a,c
	Tb.N (1/µm)	0.002496±0.0002252	0.001392±0.0001776	a,c	0.0003667±0.000185	a,b	0.00206±0.0001374	b,c	0.001931±0.0002444	a,b,c	0.0013±0.0003601	a,c
	Tb.th (µm)	49.33±2.727	55.75±1.76	c	64.67±4.221	a,b	67.04±9.194	a,b	54.24±1.708	c	56.87±4.192	
	Tb.sp (µm)	205.7±10.45	389.6±27.34	a,c	564.4±148	a,b	302±57.56	c	272±28.9	b,c	328.3±47.95	a,c
	Tb.pf (1/µm)	0.02368±0.002274	0.02211±0.002096	c	0.03018±0.0032	a,b	0.01858±0.001895	a,c	0.02226±0.00167	c	0.02536±0.003359	
	Ct.Ar (%)	43.33±0.8786	34.66±2.051	a	37.21±0.8074	a	41.62±0.9951	b	44.81±2.042	b,c	44.3±3.847	b,c
	B.Ar (µm2)	996516±122126	850219±5416	c	598015±46867	a,b	731970±54443	a,b	858941±18621	c	843834±41649	c
	T.Ar (µm2)	2330606±316598	2425289±191264	c	1605742±92501	a,b	1311960±79361	a,b	1960140±99960		2046053±70844	
	Cs.Th (µm)	175.4±16.21	152.4±8.684	c	122.8±6.108	a	171.9±4.541	c	174±3.053	c	168±6.873	c
Vertebral bone	BV/TV (%)	17.83±3.054	-		12.65±1.917	a	23.33±0.7894	c	19.77±2.08	c	14.29±3.499	a
	Tb.N (1/µm)	0.003051±0.0004983	-		0.001846±0.0003255	a	0.003683±0.0001742	c	0.003206±0.0001838	c	0.002348±0.0004606	a
	Tb.th (µm)	58.4±1.965	-		67.57±2.692	a	63.35±0.9798		61.55±2.979	c	60.32±3.623	c
	Tb.sp (µm)	180.6±10.4	-		332±17.45	a	208.8±4.322	c	224.8±9.756	a,c	257±20.81	a,c
	Tb.pf (1/µm)	0.01225±0.003717	-		0.01069±0.004839		0.0058±0.001404		0.008392±0.001704		0.01372±0.003628	

Data are mean ± SEM. Bone trabecular volume = BV/TV, Tb.N = Trabecular number, Tb.th = Trabecular thickness, Tb.sp = Trabecular separation, Tb.pf = Trabecular pattern factor, % Ct.Ar = % cortical area, B.Ar = Bone area, T.ar = Total area, Cs.Th = Cortical thickness. a = P<0.05 compared to baseline (12_weeks), b = P<0.05 compared to middle aged (30_weeks), c = P<0.05 compared to aged (100_weeks) by Bonferoni's multiple comparison test.

6.2.2 PEPITEM treatment protects mice from OVX-induced bone loss

Since our model demonstrated bone loss at both 2 and 4 weeks post-OVX, we wanted to investigate the therapeutic use of PEPITEM in OVX. We therefore treated mice with PEPITEM or PBS as a control 2-weeks post-OVX surgery (Figure 6.1). Treatment with PBS control still led to decreased BV/TV at 4-weeks post-OVX compared to 2-week untreated OVX controls (Figure 6.8A,B). However, BV/TV was unchanged in PEPITEM treated mice compared to 2-weeks post-OVX and was significantly higher than PBS treated control at 4-weeks (Figure 6.8B). Similar results were observed in trabecular number, trabecular pattern factor and trabecular separation, where significant changes were seen following PBS treatment compared to 2-weeks post-OVX, but parameters were not significantly changed in PEPITEM treated mice compared to 2-weeks post-OVX (Figure 6.8D-E). Interestingly, there was a significant increase in trabecular thickness following PEPITEM treatment compared to both 2-weeks post-OVX and 4-weeks with PBS treatment (Figure 6.8C). As expected, there were no changes in any of the cortical parameters analysed regardless of treatment with PEPITEM or PBS control (Figure 6.9).

Investigating vertebral trabecular bone, PBS control treatment had no influence on loss of bone, with significantly decreased BV/TV and trabecular number, and significantly increased trabecular pattern factor and trabecular separation observed (Figure 6.10). Surprisingly, PEPITEM had little, if any, protective effect. Whilst most of the parameters analysed (BV/TV, trabecular separation, and trabecular pattern factor) were not significantly changed at 4-weeks post-OVX with PEPITEM treatment compared to 2-weeks post-OVX, they were not also not significantly changed when compared to 4-weeks PBS treatment (Figure 6.10).

Additionally, mice had significantly decreased vertebral trabecular number in both PBS and PEPITEM treated mice (Figure 6.10D).

Overall, we observed that PEPITEM was able to protect murine long bones from OVX induced bone loss, however more research is required to understand its potential in vertebrae and other models of bone loss, such as ageing.

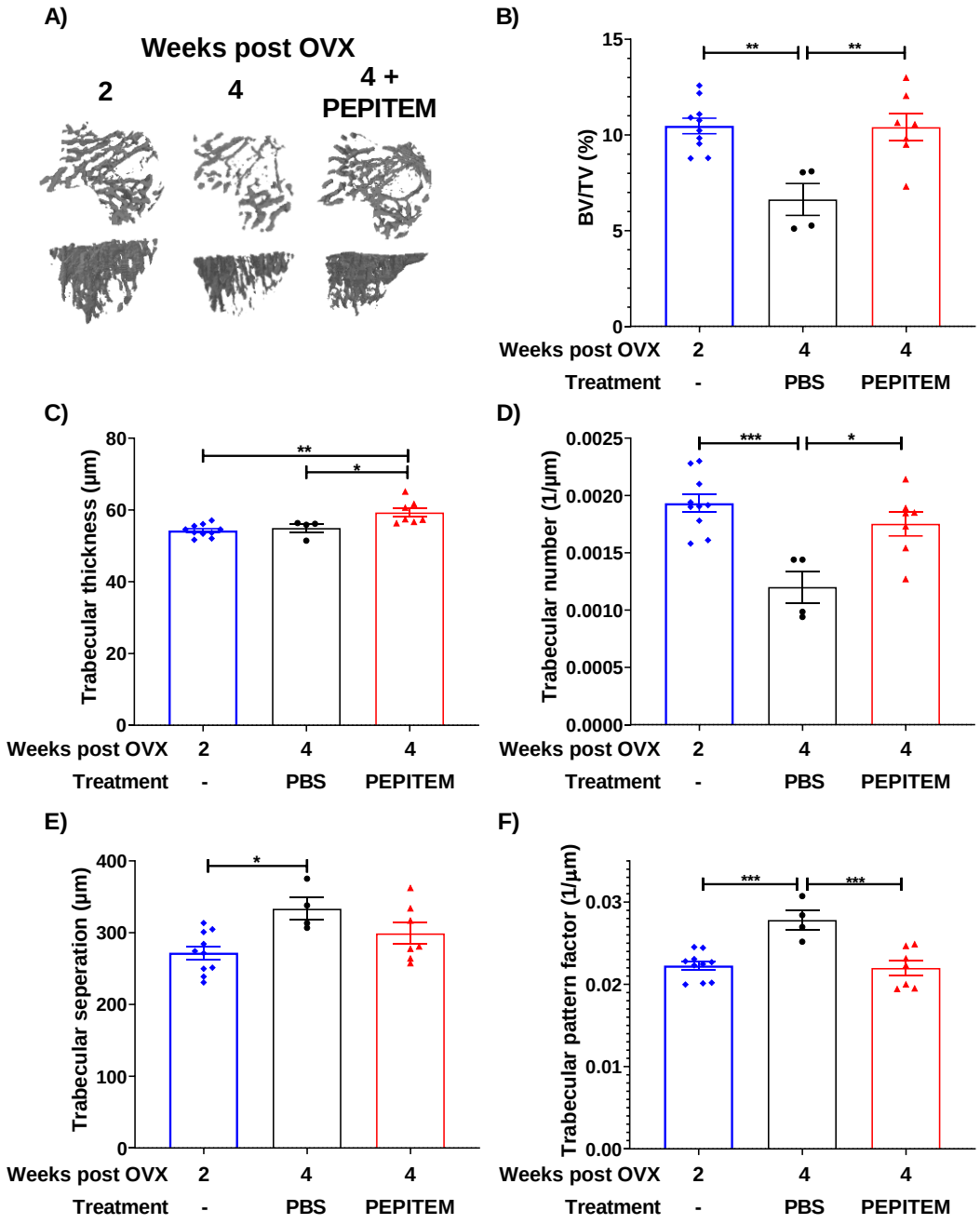

Figure 6.8. PEPITEM protected trabecular bone from OVX induced damage. Two-weeks post-OVX onset mice were treated with daily IP PEPITEM (300µg) or control (PBS) for 14 days. Tissue was collected at baseline (2-weeks post-OVX, Blue, n=10) and 4-weeks post-OVX following PBS (Black, n=4) or PEPITEM (Red, n=8) treatment. Tibiae were scanned by µ-CT and regions of interest were drawn around trabecular bone in the metaphysis to analyse trabecular parameters. **A.** Representative 3D renders of trabecular bone from each time point. **B-F.** Trabecular bone was analysed for **B.** trabecular bone volume (BV/TV, %), **C.** trabecular thickness (µm), **D.** trabecular number (1/µm), **E.** trabecular separation (µm) and **F.** trabecular pattern factor (1/µm). ANOVA showed significant effect of time on bone parameters, $P<0.05$. Data are mean ± SEM for 3 independent experiments. * = $P<0.05$, ** = $P<0.01$ and ***=$P<0.001$ by Bonferroni multiple comparisons test.

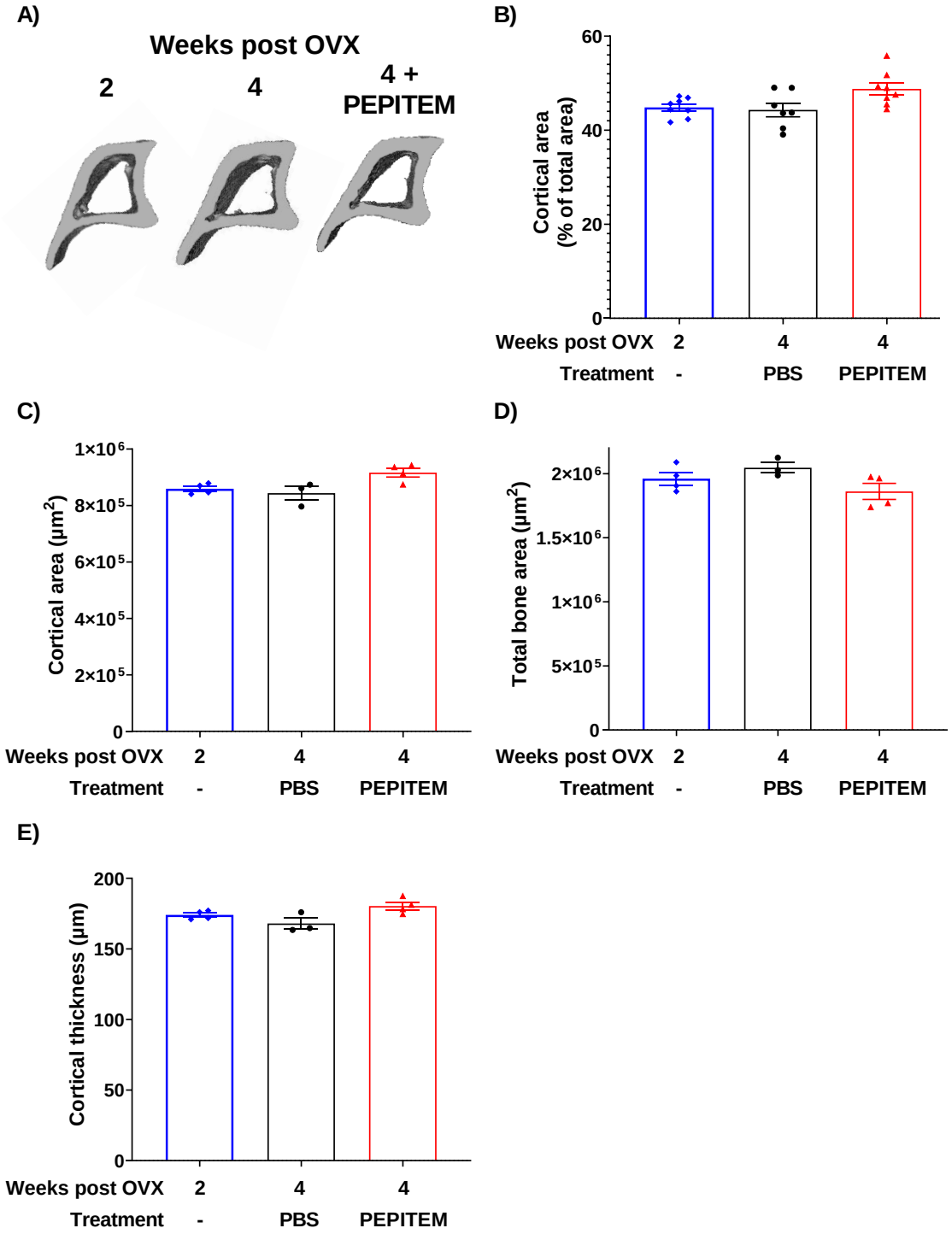

Figure 6.9. Cortical bone was not changed by treatment in OVX mice.
Two-weeks post-OVX onset mice were treated with daily IP PEPITEM (300µg) or control (PBS) for 14 days. Tissue was collected at baseline (2-weeks post-OVX, blue, n=10) and 4-weeks post-OVX following PBS (black, n=3) or PEPITEM (red, n=4) treatment. Regions of interest were drawn around cortical bone, but not trabecular, in the epiphysis and analysed for cortical parameters. **A.** Representative models of cortical bone from each time-point. **B-E.** Cortical bone was analysed for **B.** percentage of cortical area (%), **C.** total bone area (µm^2), **D.** total cortical area (µm^2), and **E.** Cortical thickness (µm). Data are mean ± SEM for 2 independent experiments.

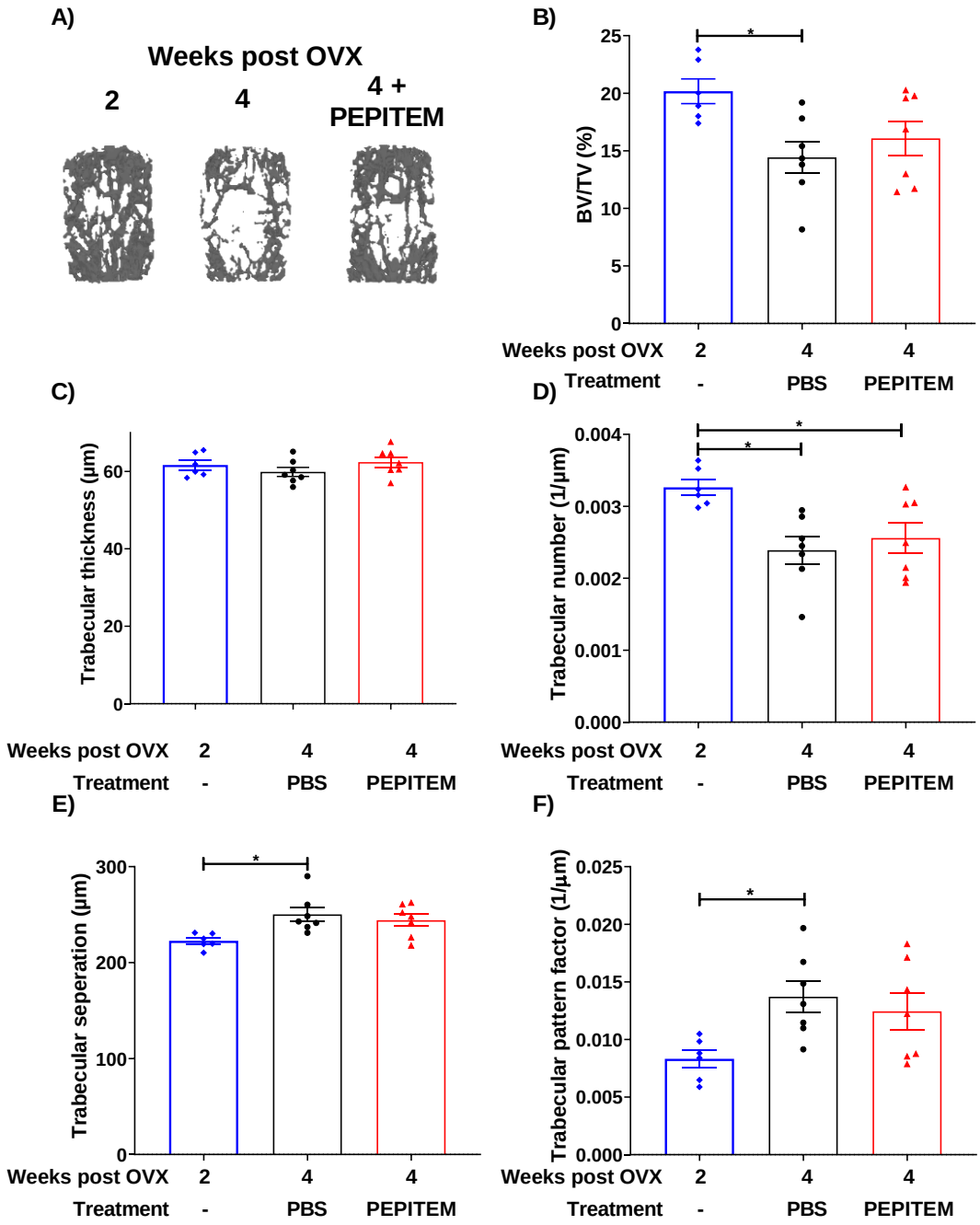

Figure 6.10. PEPITEM did not protect vertebrae from OVX induced trabecular bone loss.

Two-weeks post-OVX onset mice were treated with daily IP PEPITEM (300µg) or control (PBS) for 14 days. Tissue was collected at baseline (2-weeks post-OVX, Blue, n=6) and 4-weeks post-OVX following PBS (Black, n=7) or PEPITEM (Red, n=7) treatment. Regions of interest were drawn around the trabecular bone in vertebrae L4-L6. **A.** Representative 3D renders of trabecular bone in vertebrae L4 from each time point. **B-F.** Trabecular bone was analysed for **B.** trabecular bone volume (BV/TV, %), **C.** trabecular thickness (µm), **D.** trabecular number (1/µm), **E.** trabecular separation (µm) and **F.** trabecular pattern factor (1/µm). In B, D, E and F, ANOVA showed significant effect of time on bone parameters. Data are mean ± SEM for 3 independent experiments. * = P<0.05 by Bonferroni's multiple comparisons test.

6.2.3 PEPITEM activity was decreased with age, but not osteoporosis

Considering that PEPITEM was able to act in some capacity in disease states, we wanted to confirm this in human osteoporosis. Human samples were collected from patients undergoing emergency surgery for fractures (falls/ road accidents) with a mean of age 81 (ranging from 58 to 97, Table 6.2). Additionally, body mass index (BMI), C-reactive protein (CRP) levels and ALP levels were analysed from the patients (Table 6.2). Neither ALP nor CRP levels correlated with age, however some donors had higher than average baseline levels (Figure 6.11A,C,D). Interestingly, BMI of the participants showed a significant negative correlation with age (Figure 6.11B). However, as with the rest of this chapter, participant numbers are low and thus changes observed can be skewed by singular results. Therefore, correlations must be viewed with caution and no full conclusions can be made.

Osteoblasts were isolated from each donor and genes were analysed for expression of osteoblast maturation markers. All cells expressed osteoblast markers with *ALPL*, *SP7* and *SPP1* expression showing no correlation with age (Figure 6.12A-C). However, *RUNX2* expression showed a significant negative correlation with age (Figure 6.12D). We also explored expression of genes related to the PEPITEM pathway including *CDH15, YWHAZ, SPHK1, SPHK2, S1PR1* and *S1PR4*, all of which showed no correlation between age and expression of the gene (Figure 6.13A-F).

We next explored the alkaline phosphatase activity of the cells. ALP activity had a significant negative correlation with donor age (Figure 6.14A), however ALP activity did not correlate with osteoporosis diagnosis (Figure 6.14B). Furthermore, *ALPL* gene expression positively correlated with ALP activity (Figure 6.14C). Since

ALP levels decreased with age, we tested the response of such cells to PEPITEM. Osteoblasts response to PEPITEM also decreased with age, with older patients having a smaller response to PEPITEM than younger (Figure 6.15A). No significance was observed between donors diagnosed with osteoporosis and healthy controls (Figure 6.15B). Furthermore, no correlation occurred between expression of CDH15 gene by the donors and ALP activity of the cells (Figure 6.15C).

We also explored the response of cells to S1P. No correlation was seen between changes in ALP activity in response to S1P and age (Figure 6.16A). Comparing expression of *S1PR1* and *S1PR4* to response to S1P, we found no trend between *S1PR1* concentration and S1P induced ALP activity (Figure 6.16B), by contrast, *S1PR4* expression was positively correlated to ALP activity in responses to S1P (Figure 6.16C).

These data indicate that cells are still able to respond to PEPITEM in disease states, but this response is controlled by patient age and the location of the bone.

Table 6.2. Participant information

Catagory	Control	Osteoporotic
Participants	4	6
Male:Female	1:3	1:5
Age	73.5±16.25	86±5.797
BMI	24.98±5.558	22.25±3.783
CRP	23.5±26.16	52.8±89.42
ALP	169.5±75.66	84.2±14.06

Data are mean ± SEM. Age = years, BMI = kg/m², CRP = mg/L, ALP = IU/L.

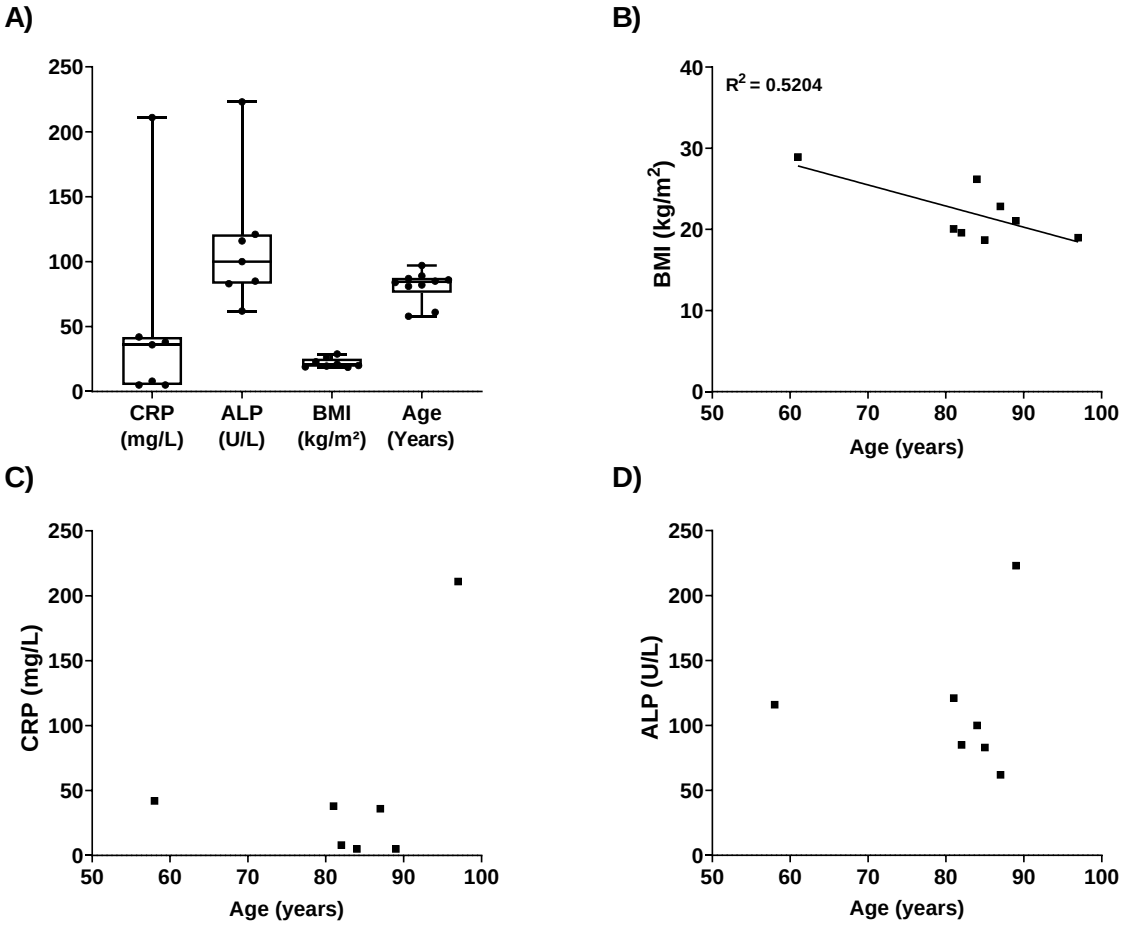

Figure 6.11. Participant information from bone donors.

Blood and bone were collected from patients undergoing emergency surgery for fracture. **A.** Range of values, mean and interquartile ranges for CRP levels (n=7), ALP levels (n=8), BMI (n=8) and Age (n=10) for each donor (where taken). **B-D.** Trend between age and BMI **(B)**, CRP **(C)** and ALP **(D)** for each parameter where both were recorded. Linear regression line of best fit is shown when $p<0.05$.

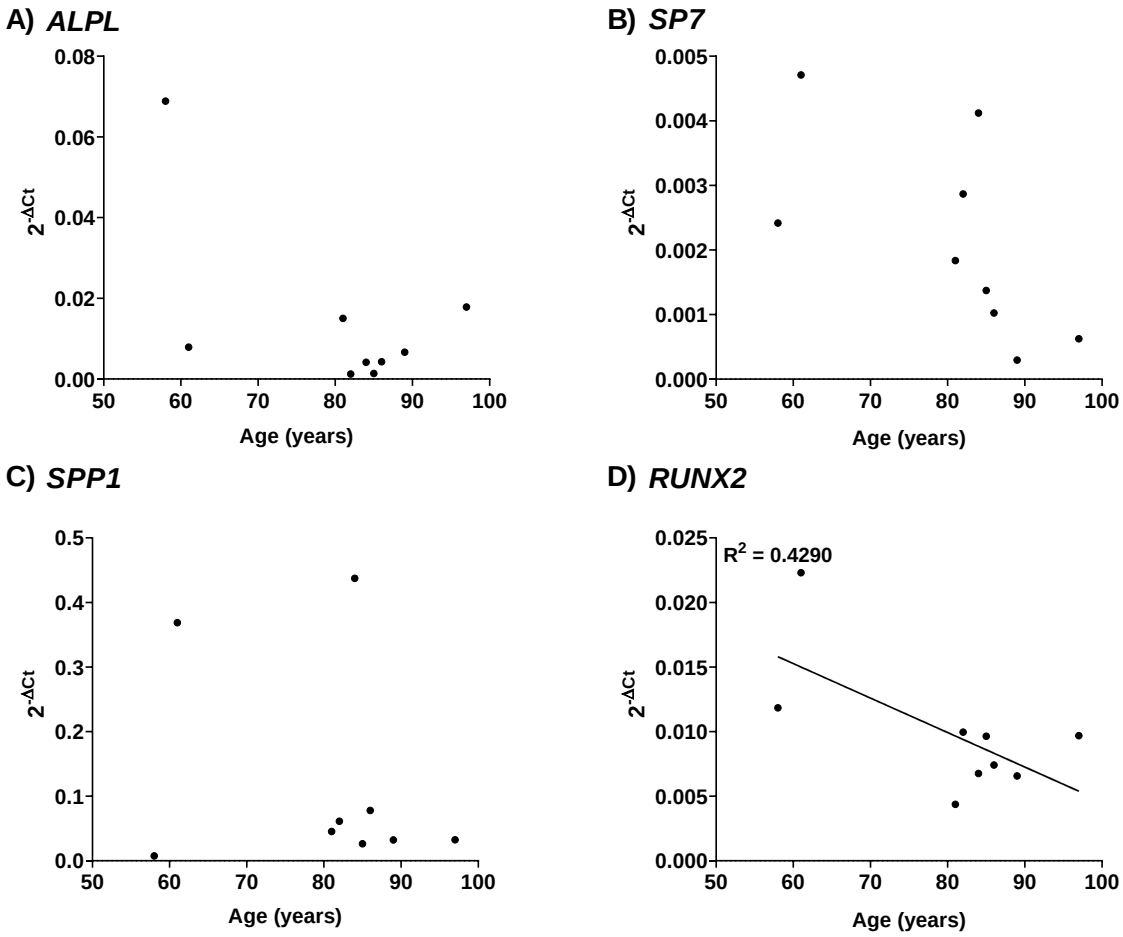

Figure 6.12. RUNX2 expression may decreased in aged osteoblasts.

Primary osteoblasts were isolated from human donors (n=9) undergoing surgery for fractures. RNA was isolated and qPCR was performed to explore expression of osteoblast genes **A.** *ALPL*, **B.** *SP7*, **C.** *SPP1*, **D.** *RUNX2* which were plotted in relation to the donor's age. Linear regression line of best fit is shown when $p<0.05$.

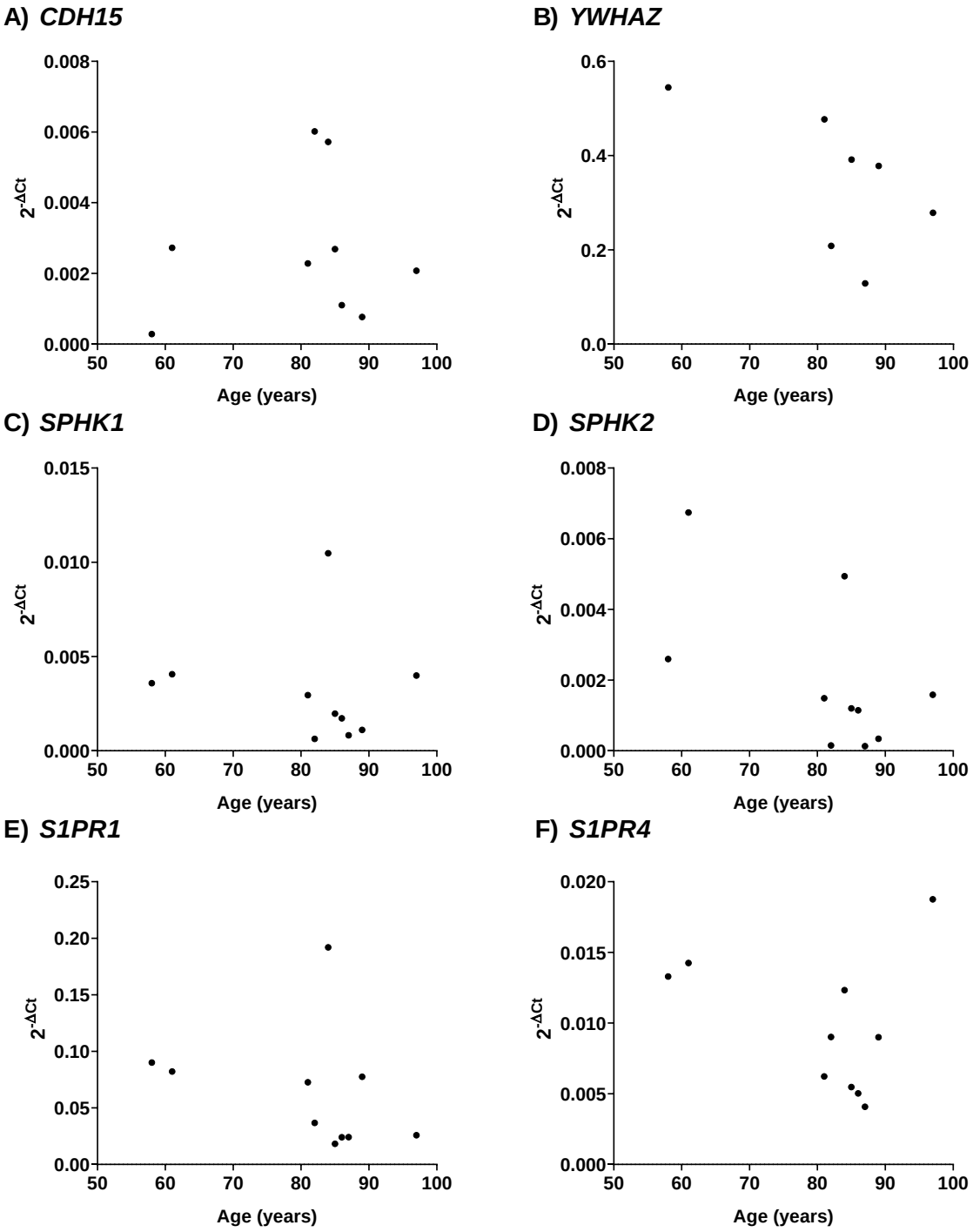

Figure 6.13. Genes relating to the PEPITEM pathway were unaltered by age.

Primary osteoblasts were isolated from human donors (n=7-9) undergoing surgery for fractures. RNA was isolated and qPCR was performed to explore expression of osteoblast genes **A.** *CDH15*, **B.** *YWHAZ*, **C.** *SPHK1*, **D.** *SPHK2*, **E.** *S1PR1* and **F.** *S1PR4* which were plotted in relation to the donor's age.

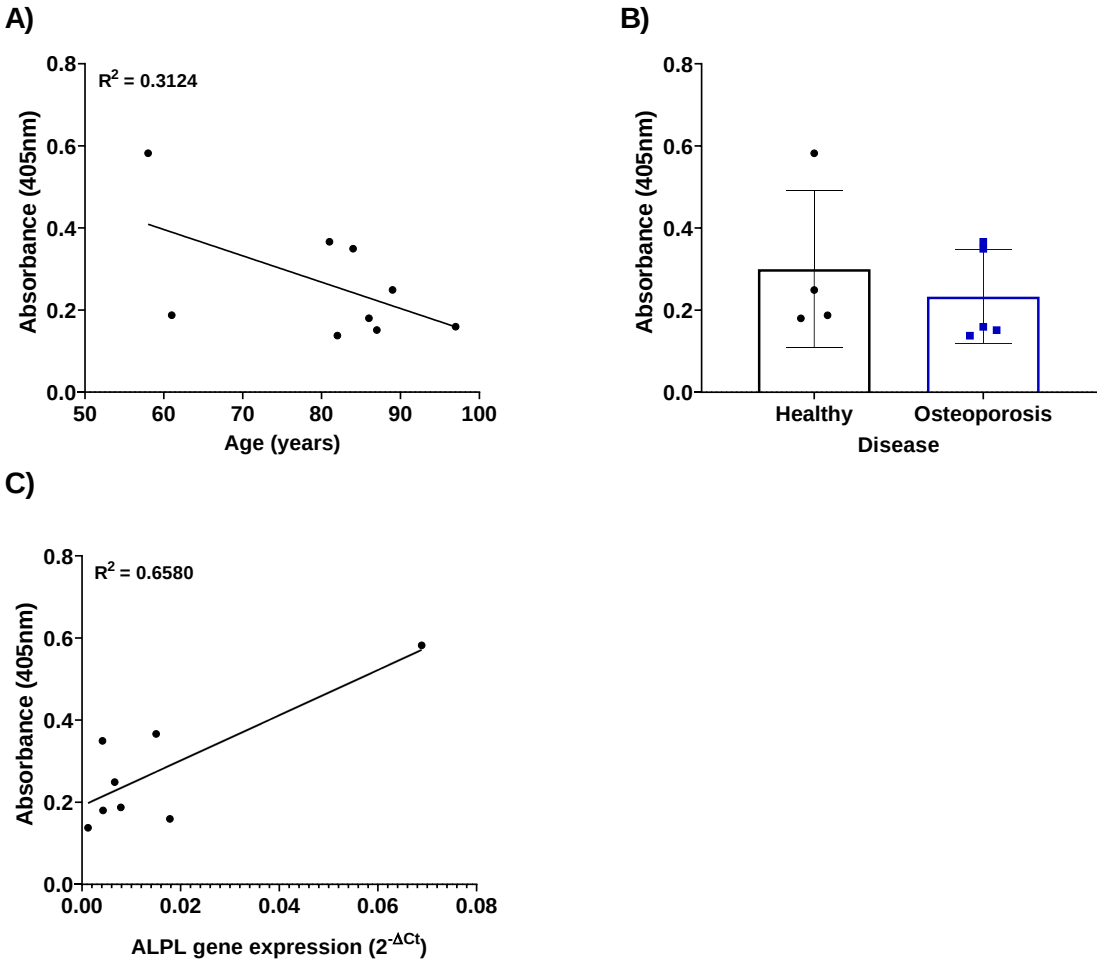

Figure 6.14. ALP activity in osteoblasts negatively trends with age.

Primary osteoblasts were isolated from human donors (n=8-9) undergoing surgery for fractures. Osteoblasts were cultured and analysed for alkaline phosphatase activity by ELISA. **A.** ALP activity shown by absorbance in each donor compared to age. **B.** ALP activity of each donor split by diagnosis of osteoporosis. Data are mean ± SEM. **C.** ALP activity of each donor correlated to *ALPL* gene expression from the same cells. Linear regression line of best fit is shown when $p<0.05$.

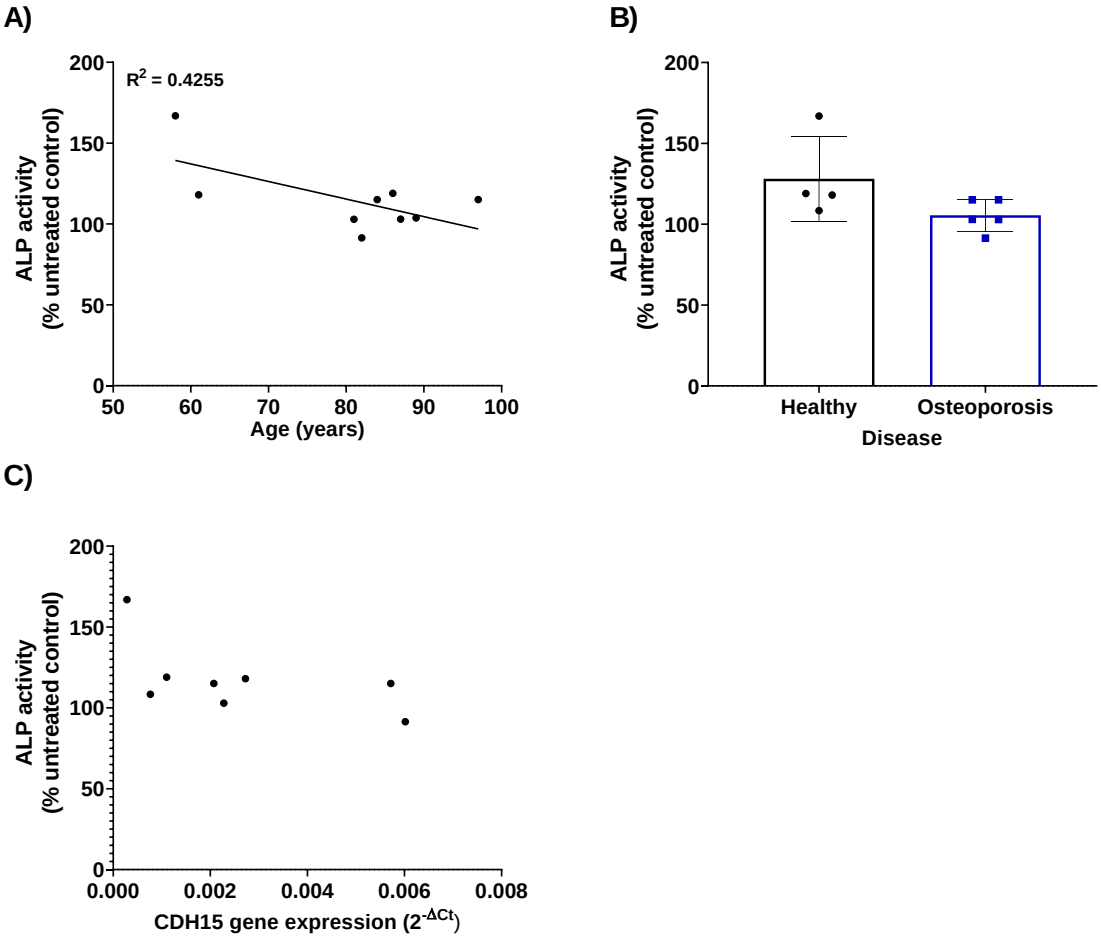

Figure 6.15. Osteoblast response to PEPITEM might negatively correlate age.

Primary osteoblasts were isolated from human donors (n=8-9) undergoing surgery for fractures. Osteoblasts were cultured for 8 days untreated or treated with PEPITEM and analysed for alkaline phosphatase activity by ELISA. ALP activity is presented as a percentage of activity in PEPITEM treated cells compared to untreated cells. **A.** ALP activity of each donor compared to donor age. **B.** ALP activity of each donor split by diagnosis of osteoporosis. Data are mean ± SEM **C.** ALP activity of each donor correlated to *CDH15* gene expression from the same cells. Linear regression line of best fit is shown when $p<0.05$.

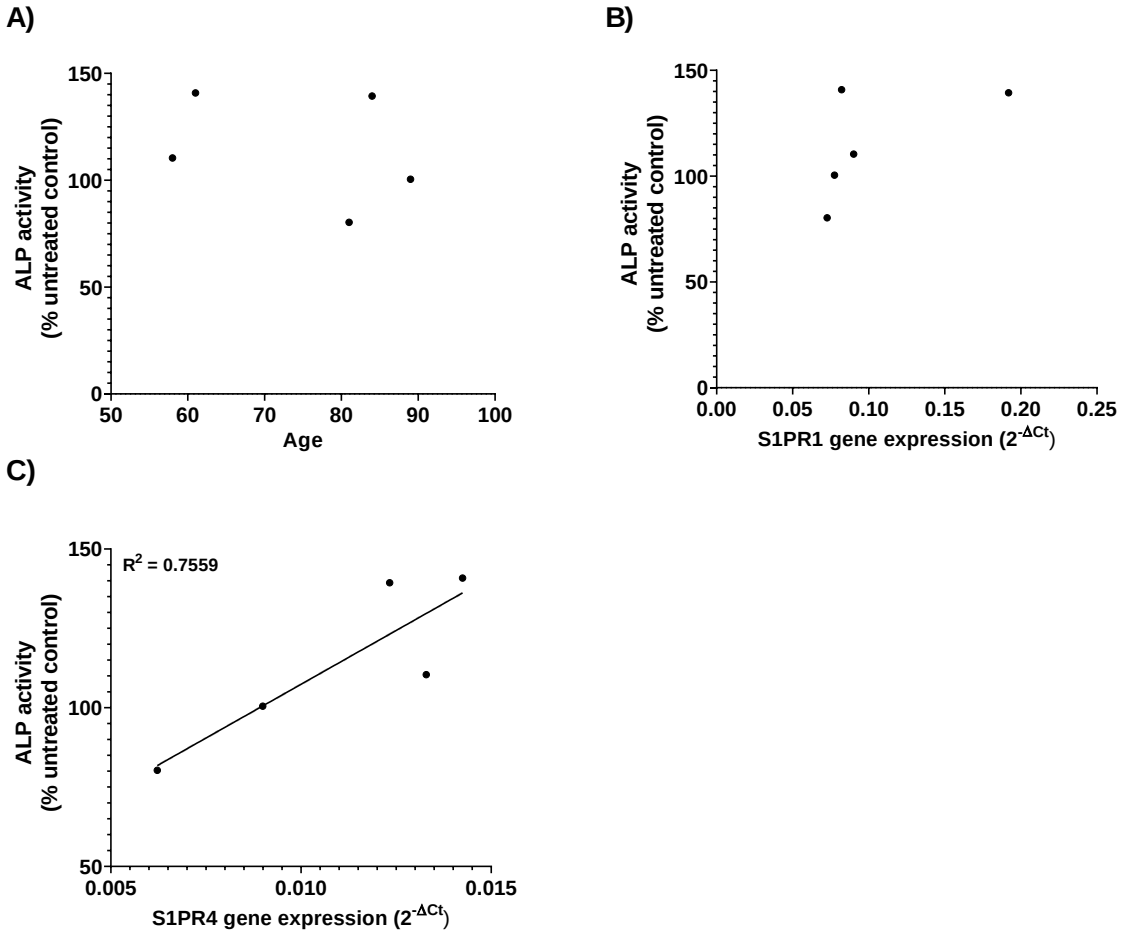

Figure 6.16. Aging did not alter osteoblast response to S1P.

Primary osteoblasts were isolated from human donors (n=5) undergoing surgery for fractures. Osteoblasts were cultured for 8 days untreated or treated with S1P and analysed for alkaline phosphatase activity by ELISA. ALP activity is presented as a percentage of activity in S1P treated cells compared to untreated cells. **A.** ALP activity of each donor as a percentage of S1P vs control compared to donor age. **B.** ALP activity of each donor as a percentage of S1P vs control correlated to *S1PR1* gene expression from the same cells. **C.** ALP activity of each donor as a percentage of S1P vs control correlated to *S1PR4* gene expression from the same cells. Linear regression line of best fit is shown when $p<0.05$.

6.3 Discussion

Here we observed the phenotypic changes that occur in bone during diseases (osteoporosis), with ageing and following fracture. In addition, we analysed the responses of whole bone and bone cells to PEPITEM during such changes to identify its potential for use as a therapy. Characterisation of bone loss in ovariectomised mice revealed trabecular bone loss occurred 2 and 4 weeks post-OVX. However, this was not equivalent to ageing, only reaching trabecular bone loss occurring in 30-week-old mice. PEPITEM treatment over 2-weeks protected OVX mice from bone loss in the tibia, but not the vertebrae, possibly indicating to different mechanisms of action, or altered levels of bone loss.

Exploring the cellular phenotypic changes that occur with age we found that RUNX2 expression and ALP activity was significantly decreased with age, indicating less of an osteoblastic phenotype. However, no differences in ALP activity were observed in patients with osteoporosis compared to controls. Whilst no differences were seen in pathway genes for PEPITEM or S1P signalling, functionally, PEPITEM responses were suppressed in older individuals leading to decreased ALP activity. However, there were no differences in osteoblast response to PEPITEM in healthy controls or patients with osteoporosis. This may suggest that PEPITEM is less effective at protecting bone and boosting bone growth in older patients, but osteoporotic differences alone do not impact its actions. In contrast, response to S1P was not dependent on age, and instead correlated with expression of S1PR4, indicating a possible receptor for downstream signalling. In conclusion, we determined that PEPITEM can act in a protective manner in human and murine osteoporosis, however overall response may be decreased by age.

6.3.1 Characterising changes in age and osteoporotic bone

OVX is known to decrease trabecular bone parameters, however the rate and degree of bone loss are not always maintained between studies. Most studies exploring C57Bl6 mice, showed a decrease in trabecular bone BV/TV, trabecular number and an increase in trabecular separation at 4 weeks following OVX,[213,659–663] matching the results from our study. However, there are contrasting results published regarding changes in trabecular thickness. We observed no changes in this parameter following OVX, which has also been described in mice and rats from 4 weeks to 3 months post-OVX.[660,661,664–666] Yet, other studies find that trabecular thickness decreased as a result of OVX even when the same parameters (C57Bl6 mice and 4 weeks of OVX) are used.[213,659,662] It has been suggested that the reason for trabecular thickness increasing or remaining unchanged is due to thinner trabecular bone being completely resorbed and lost, leaving the larger trabecular, which increases the average trabecular thickness.[659,667,668] The studies that found a decrease in trabecular thickness used *in vivo* micro-CT scanning where lower spatial resolution is used in scans, altering the voxel size measured.[669,670] Higher voxel size micro-CT scanning *in vivo* compared to *in vitro* leads to an overestimate and significantly higher values for trabecular thickness in homeostatic *in vivo* scanned mice.[667] Thus, the smallest trabecular bone may not be detected at any timepoint, so only changes in thicker trabecular can be analysed, leading to the observed decrease compared to controls.

No changes in cortical parameters and bone strength are also commonly seen following OVX,[213,401,671,672] suggesting that the model may not be representative of post-menopausal osteoporosis, since decreases in cortical bone and bone strength

are often observed in human osteoporosis,[673–675] and with age in mice.[239] In addition, some studies use aged mice, where bone loss has already begun, to increase bone loss through OVX,[668,672] which may provide changes that are closer to human osteoporosis. Overall, our results match to the majority of studies exploring the timeline of OVX, suggesting the model has been performed correctly and could be used to analyse murine osteoporosis.

To the best of our knowledge, no other study has explored the response of bone following OVX to the changes that occur with ageing. We found that bone loss following 4-weeks of OVX in 12-week-old mice is representative to the amount of bone lost at 30-weeks-old, equivalent to ~ 40 years old in humans. Longer time points of OVX have indicated that very little bone loss occurs after the initial mass reduction following OVX.[666] The OVX model therefore may not produce large levels of bone loss at any stage that occur in human osteoporosis. Bone loss also occurs faster in younger mice following OVX compared to older mice,[214] most likely due to bone loss having already occurred due to age. Therefore, using aged mice is more likely to represent human bone loss since menopause occurs in older adults, where bone loss has already occurred to some degree.

Looking at ageing directly, significantly decreased BV/TV, trabecular number and increased trabecular separation have been widely reported in mice at 3, 6, 16, 24 and 31 months supplementing our results.[238,676,677] However, differences are again present when exploring trabecular thickness, which some matching our study and finding an increase in aged mice,[238,677] and others publishing a decrease in trabecular thickness with age.[676] We have demonstrated that whilst OVX bone loss is not as great as aged-induced bone loss, there is still rapid bone loss, matching the

initial changes that occur in ageing and allowing this models use to understand the therapeutic potential of treatments in disease.

6.3.2 **Ageing alters the phenotype of bone cells**

In vitro studies on aged and osteoporotic bone have previously uncovered a change in phenotype due to one or both factors. Aged osteoblasts isolated from human and murine bone expressed lower levels of osteoblast specific genes such as *SP7, BGLAP, SPP1, RUNX2* and *ALP* when compared to young, indicating a decrease in osteoblast differentiation and activity in the bone.[243,244,678] In our study we also observed a trend towards decreased *RUNX2* expression, however we did not see changes in expression of *ALPL, SP7* or *SPP1*. This, in part, may be due to sample size since *SP7* has a borderline negative correlation with a p value of 0.067. Low samples sizes may also create correlations where they aren't actually present, due to outliers or differing values skewing the results. Alternatively, the majority of patients in our study were over 80 years of age, with only two donors under the age of 65. In many published studies every one of our donors would be classed as aged, meaning the decrease in expression may already have occurred. In all studies comparing old and young, the young donors average at between 15 and 38 years-old, making a large difference to the aged donors (often aged at least 50+).[244,678] This may indicate that any downregulation in osteoblast ability may have already occurred in all the donors in our study. Despite this, we do observe a tentative negative correlation between ALP activity and age, suggesting even in later life osteoblasts continue to lose bone producing potential. This is also seen in many other studies, with primary osteoblasts from aged donors (human and murine) showing decreased ALP activity, along with mineral production compared to young controls.[115,243,678,679] A

similar finding is also seen change between osteoporotic osteoblasts and non-osteoporotic osteoblasts, with decreased ALP activity,[680,681] and lower proliferation rates.[682–684] However, this is not always the case and some papers show no difference in ALP activity between osteoporotic and non-osteoporotic samples, matching our data. Reasons for the differences could be explained by changes in age between controls and osteoporotic patients, which, whilst not significant, the non-osteoporotic patients mean age is lower than patients.[680,685] In our study, as previously mentioned, most patients are over 80 and there are more female compared to male participants. This makes it highly likely that even the patients recorded as being non-osteoporotic will have entered menopause and thus osteoporosis will have begun,[686] even if it is not phenotypically detectable. Thus, confirming changes in osteoporosis is difficult, particularly since BMD was not measured at the time bone was taken. This may also explain why no changes were observed when comparing the response of osteoporotic and non-osteoporotic cells to PEPITEM, thus no conclusion can be made regarding that data. Alternatively, senile osteoporosis and menopausal osteoporosis have been shown to occur primarily due to changes in osteoblasts and osteoclast respectively,[686] thus in the female osteoporosis patients changes in osteoblasts may be less prominent. Significantly more patients and increased male representation are required to separate the changes in osteoblast activity that occur due to menopausal osteoporosis and senile osteoporosis.

Other changes are also seen in aged and osteoporotic osteoblasts that we did not measure here but may influence bone growth and interfere with PEPITEM responses. For example, osteoblasts isolated from aged bone regardless of

osteoporosis have decreased IL3 and IL6, whereas osteoporotic age-matched bone has decreased IL-1β and increased TNFα, indicating an inflammatory phenotype.[687] Of interest, in the immediate time following fracture, inflammation is highly prevalent in the bone.[279,281,282] It is well known that inflammation alters osteoblast activity,[627] therefore, it is possible osteoblasts isolated from fracture bone in each study display a significantly different phenotype to those *in vivo* due to the presence of inflammation. Osteoporotic osteoblasts also show an increase in many microRNAs which may alter their functional potential and influence with signalling pathways.[685] Of the measured microRNAs, many are involved in downregulation of osteoblast activity,[685] supporting earlier findings. However, their full functions have yet to be fully explored.

6.3.3 **Comparing the current therapeutics for bone loss**

In our study we observed a positive response of ovariectomised bone to PEPITEM over two-weeks, protecting tibial trabecular bone from further loss. Whilst these results were similar to PEPITEM treatment of homeostatic mice, mice in the ovariectomy study were at least 12 weeks of ageing, thus having reached peak bone mass and the rapid bone growth would have slowed. This may alter PEPITEMs actions on osteoclasts and osteoblasts due to decreased cell numbers and localisation, possibly explaining the changes in vertebral response to PEPITEM and levels of bone growth. Due to the short treatment period (2-weeks) and starting treatment at 2-weeks post-OVX, it is difficult to directly compare results from PEPITEM treated mice to mice treated with other therapeutics, since they often treat prophylactically or for significantly longer periods of time (5 weeks to 12 months). Treatment of ovariectomised rodents prior to or from onset of OVX with

bisphosphonates (Ris, Ale, Zol)[659,672] or PTH[666] leads to bone parameters remaining similar to sham operated animals, indicating a protective phenotype. However, in these studies, treatment was given prophylactically, which is often not possible in human osteoporosis due to the inability to detect osteoporosis and no set age of onset. Studies using the above therapeutics and where treatment was started following 2 – 5 weeks of OVX have reported protective responses and bone loss was not significantly decreased compared to sham operated controls.[663,688] However, treatments are given for longer periods than in our study to detect responses. For example, treatment of mice 4-weeks following OVX for 4-weeks with PTH results in no change in BV/TV and other trabecular parameters compared to sham, thus indicating a protective phenotype.[660] This was also the case for C57Bl6 mice 2-weeks weeks post-OVX treated for 12 weeks with PTH and alendronate,[688] 5 weeks with an anti-sclerostin antibody,[665] or for 3 months with a cathepsin K inhibitor,[661] where no change in BV/TV and other parameters were observed compared to sham mice. Whilst we observed no change compared to 2-weeks post-OVX, there was not an increase towards baseline levels. This may be due to the short time frame of treatment, which may only have stopped the immediate bone damage. Therefore, studies exploring PEPITEM for longer treatment times are essential to see if bone levels can be restored to baseline levels following the initial bone loss.

Another interesting finding from our study was that vertebral and tibial bone respond differently to PEPITEM following OVX. It is well known that mechanical stress on bone is an inducer of bone growth through its actions on osteocytes and osteoblasts. In OVX, mechanical stress on tibias in combination with PTH treatment increased the response of bone compared to PTH or stress alone.[660] Tibias are

placed under increased stress compared to the spine in mice due to quadrupedal walking.[689–691] Therefore, it is possible that the combination of stress on the bone and PEPITEM treatment was able to increase bone in the long bones, but not the vertebrae. Additionally, the bone loss observed in the vertebrae from our ovariectomised mice was delayed compared to the tibiae bone loss. This is a well-studied phenomenon and loss of BV/TV and trabecular number has been found to have a delayed decrease and to be less severe, both at short (1-28 days) and long (3 - 9 months) timepoints post-OVX.[668,692–694] Thus, the rate of bone loss occurring between 2-4 weeks may be lower in the vertebrae compared to the long bones, as such leading to PEPITEMs response being suppressed. Alternatively, the differences in localised responses to OVX indicate that distinct bone remodelling may occur in each region, influencing the action of PEPITEM. Differing treatment regimens, such as localised PEPITEM administration or longer treatment duration, are required to fully understand the effects of PEPITEM on vertebral bone loss. Additionally, as indicated above, age induced bone loss and OVX bone loss occur at different rates and involve changes in different cell types, thus exploring the response of older mice to PEPITEM is also essential to explore the response to senile osteoporosis and menopausal osteoporosis in older individuals.

6.3.4 **Treatment responses with ageing**

Response of osteoblasts to PEPITEM decreased with age in our study. However, these results are still inconclusive due to the limited number of participants and the participants ages. The small number of participants means outliers skew the data, possibly creating correlations were there wouldn't be in a larger cohort. Therefore, all conclusions need to be tempered to account for this until a larger study

is conducted. Additionally, since this is the first study to explore PEPITEM and osteoblasts, no direct comparisons can be made. However, the response of PEPITEM has previously been diminished in other diseases. For example, PEPITEM concentration was significantly decreased in the serum of type-1-diabetes patients and aged patients, due to a decrease in expression of adiponectin receptors on B cells.[473] In addition, we do not yet fully understand the mechanistic pathway of PEPITEM in bone, thus this knowledge is needed to fully understand why the actions of PEPITEM are decreased with age. Of note, the previously believed receptor of PEPITEM, cadherin-15 was not decreased with age, and there was no correlation between ALP activity in response to PEPITEM and level of cadherin-15 expression, suggesting another pathway may be prominent in osteoblasts. Whilst not directly related to the bone, CDH15 protein expression has shown to decrease in aged compared to young muscle,[448] indicating it is a protein/ gene that can be controlled by age. Ultimately, upon greater understanding of the mechanism of action of PEPITEM, work should be done to explore how related proteins are altered in disease and with age.

We also observed no changes in response of cells to S1P in our study with age. However, this again may be due to the high mean age of the patients meaning changes in response may already have occurred in all donors. Younger donors are required to fully interpret this result.

In conclusion, we have observed a protective function in osteoporosis, both at a cellular and whole bone level. Whilst the response was reduced with age, menopausal osteoporosis often begins at a much younger age than that of the donors from our study, where higher responses to PEPITEM are observed.

7 General Discussion

7.1 Summary of findings

In this thesis we sought to understand and characterise the effect of PEPITEM on bone homeostasis and in disease. We began by performing observational studies on PEPITEM *in vivo*, from which we understood the main role of PEPITEM in bone growth. The cellular responses and potential signalling pathways were subsequently analysed, exploring direct responses to PEPITEM, the PEPITEM pathway molecule S1P and the supposed PEPITEM receptor cadherin-15. We finished by exploring the alterations in PEPITEM response *in vivo* and *in vitro* following disease onset to understand it's therapeutic value. The main findings of our study were as follows:

- Short term treatment of homeostatic mice with PEPITEM can induce a pro-anabolic phenotype, increasing bone mass and bone strength.
- Increases in bone are due to direct effects on osteoblasts, improving their differentiation with increased mineral production.
- Secondary effects of PEPITEM cause a decrease in osteoclastogenesis, which may be a result of PEPITEM induced osteoblast changes.
- Osteoclast responses are suppressed by S1P treatment, indicating it is a possible signalling molecule between osteoblasts and osteoclasts.
- S1P inhibited murine osteoblast activity and led to the acquisition of an inflammatory phenotype.
- Therapeutic PEPITEM treatment protects mice from OVX induced bone damage.
- PEPITEM still increases osteoblast activity in osteoporotic and aged osteoblasts, however the response may be supressed with age.

7.2 Findings in the context of the literature

This is the first study to explore the direct relationship between PEPITEM and bone, and thus it is difficult to characterise the response in relation to the literature. We have previously shown that in murine models of rheumatoid arthritis, therapeutic treatment of mice with PEPITEM results in a complete loss in bone damage observed.[496] However, due to an inti-inflammatory effect of PEPITEM, and thus a decrease in joint swelling with treatment, it is impossible to dissect if the changes in bone were due to direct actions of PEPITEM on bone or due to a reduction in inflammation induced bone loss.[473] Here we showed that a direct response of bone to PEPITEM can occur, with homeostatic mice showing an increase in trabecular bone parameters following short term treatment, with a direct effect on osteoblasts. In addition, osteoporotic mice were protected from trabecular bone loss, indicating a functional response in diseases. Previous studies exploring PEPITEM precursor protein YWHAZ found it was pro-anabolic, boosting osteoblast production and protecting mice from OVX induced bone loss.[510,511] Whilst this models the changes observed in our study, YWHAZ is known to influence many pathways within the cells, therefore changes observed may not be due to a decrease in PEPITEM production.[502]

7.2.1 How does PEPITEM signal in bone

We predicted the responses seen in osteoblasts and osteoclasts were resultant from signalling between PEPITEM, cadherin-15 and S1P. Whilst human osteoblasts responded positively to S1P and had no response to PEPITEM following cadherin-15 knockdown, murine osteoblasts reduced ALP activity and downregulated expression of osteoblast maturation markers following S1P treatment. This indicates other

pathways may be involved in PEPITEM signalling. The main pathways involved in osteoblast maturation include wnt,[695,696] notch[697–699] and BMP[614,700,701] signalling. Of note, disruption of the interaction between N-cadherin and LRP5/6 in osteoblasts, using a competitive peptide, promoted Wnt/β-catenin signalling, leading to increased ALP activity and mineral formation.[702] In addition, internalisation of E-cadherin resulted in the activation of Wnt signalling in MDCK cells.[703] Therefore PEPITEM binding directly to cadherin-15 may promote internalisation or alter protein interactions, leading to enhanced Wnt signalling and osteoblast mineral production. However, experiments blocking cadherin-15 signalling are required to confirm it as a key molecule in the action of PEPITEM on osteoblasts.

It is also conceivable that PEPITEM signals through a novel pathway not previously explored in regard to PEPITEM. Precursor protein 14-3-3ζ has been shown to bind to and alter the signalling of a large number of proteins.[499] Some of these interactions may occur through binding of the PEPITEM sequence in 14-3-3ζ to the protein. This would allow isolated PEPITEM to also bind to the proteins and induce signalling. These interactions include binding to 3BP2,[508] which is a signalling molecule essential for osteoblast development and mineral produciton.[509] Previous work from out laboratory also found thrombospondin-1 as a potential match for PEPITEM binding, however, it was a significantly lower match for binding than cadherin-15. Constitutive expression of Thrombospondin-1 in human MSCs or MC3T3 cells decreases osteoblast differentiation.[704,705] If PEPITEM was able to bind to thrombospondin-1 and induce protein downregulation or degradation, an increase in osteoblast signalling may be observed. However, binding between PEPITEM and

thrombospondin-1 requires confirmation and the changes in thrombospondin-1 expression following PEPITEM treatment needs to be explored.

PEPITEM also altered the crosstalk between osteoblasts and osteoclasts, decreasing osteoclastogenesis. In human cells, this communication might be explained through S1P release, however murine macrophages had enhanced osteoclastogenesis in response to S1P. Therefore, other signalling molecules may be released from osteoblasts in response to PEPITEM. The major communication molecules between osteoblasts and osteoclasts are RANKL and OPG, which promote and inhibit osteoclastogenesis respectively.[229,706–710] It is possible PEPITEM decreased RANKL release and increased OPG release, overall inhibiting osteoclastogenesis and bone destruction. Exploring RANKL and OPG concentrations in conditioned media from PEPITEM treated osteoblasts is required to fully interpret this hypothesis. Additionally, full mass spectrometry analysis of osteoblast conditioned media following PEPITEM treatment may reveal novel inhibitors of osteoclastogenesis, in addition to providing additional understanding of PEPITEMs mechanism of action.

7.3 Therapeutic potential of our research

We, for the first time, have identified a novel endogenous molecule that had dual responses *in vivo* and *in vitro* on osteoblasts and osteoclasts, leading to protection from disease induced bone loss. Therefore, there is high potential for the use of PEPITEM to promote bone growth and treat bone loss in disease. Whilst this is the first study exploring PEPITEMs effect on bone, our findings can be explored in relation to changes that have been seen with treatments that are currently in use

(both in the UK and externally), with particular interest in bisphosphonates and parathyroid hormone.

Bisphosphonates are the major treatment for osteoporosis, with significant inhibitory effects on osteoclastogenesis.[303,304,313,316,323,326,561,580] In our study they led to a complete absence of osteoclastogenesis. This is also the case in other publications, where osteoclast numbers are reduced both *in vivo* and *in vitro* following any bisphosphonate treatment.[316,590,711] However, very little research has found an increase in bone of homeostatic mice or osteoporotic mice treated with bisphosphonates at shorter time frames, with most studies looking at 4 weeks of treatment onwards. This may therefore suggest PEPITEM has slightly more efficacy and can promote faster bone growth in disease. The complete loss of osteoclasts following bisphosphonate treatment can also lead to off target effects known as frozen bone, where the absence of osteoclast stops the resorption of microfractures or old bone, and thus weakens overall bone strength.[313,346,354] In comparison, treatment of osteoclasts with S1P or media from PEPITEM treated osteoblasts only led to a fractional decrease in osteoclasts, thus allowing resorption to continue, but restoring the balance between bone formation and resorption. In addition, there are limited effects of bisphosphonates on osteoblasts, thus bone formation is not promoted.

When bisphosphonates cannot be taken, teriparatide (PTH) is recommended as a secondary treatment.[712] In both homeostatic and diseased conditions (OVX), treatment with PTH caused similar changes to what is observed with PEPITEM. This includes increased bone parameters and strength in homeostasis, and protection of mice from OVX induced bone loss.[399,401,660,663,713] This indicates PEPITEM may also

be able to be used in osteoporosis and other diseases of bone loss due to the similar response of bone. Interestingly, PTH increased osteoclast numbers *in vitro* by inducing the upregulation of RANKL expression on osteoblasts.[392,589] This may indicate PEPITEM is advantageous during long term treatment through slight downregulation of osteoclasts in combination with increased osteoblast mineral production. Of interest, teriparatide treatment is also primarily given daily,[714] indicating that if PEPITEM were to be used to treat bone diseases, compliance might match teriparatide compliance (82% after 18 months).[715] However, patients are often concerned about daily injections and injection discomfort.[715] Using novel delivery techniques, such as liposome enclosed PEPITEM, modified PEPITEM compounds with a longer half-life, or targeting molecules involved later in the pathway, may improve responses to PEPITEM and reduce the frequency of treatments required. Longer studies with PEPITEM are also required to analyse changes in cortical bone that may occur, but also whether in disease the protection is maintained or in fact if bone can be restored to its resting values following the initial large scale bone loss.

Using combination treatments have also shown potential in treating bone diseases. Combination of intermittent PTH and bone strain leads to enhanced bone protection in OVX mice.[660] This is similar with using PTH followed by bisphosphonates or vice-versa where in osteoporosis and other diseases prolonged bone protection are observed.[716–718] We observed increased bone growth in the long bones (tibias) compared to the vertebrae in OVX mice following PEPITEM treatment, thus indicating combined therapies may be useful in PEPITEM regimes. Furthermore, using PEPITEM as an initial or secondary treatment for bone diseases may also be

useful, particularly in patients who do not respond well to conventional therapeutics.[719,720]

Alternatively, novel delivery mechanisms from bone targeting drugs have been devised. Smart, silica gels have been produced which can slowly release bisphosphonates into the surrounding environment.[721] Injection of such gel directly into a fracture sight or area of high bone loss would allow a concentrated delivery of bisphosphonate, improving bone responses and reducing a need for patient compliance. Due to its simple synthesis, delivery of PEPITEM via a similar mechanism would be possible, potentially improving the response of bone in osteoporosis and maybe protecting vertebrae from bone loss, which is not seen using generalised administration.

Both bisphosphonates and PTH also have side effects when used for longer regimens. These include common symptoms like bone and joint pain, nausea and high calcium levels, and more harmful side effects such as increased fracture risks and osteonecrosis of the jaw.[376,379,403,722] Furthermore, bisphosphonates need to be taken on an empty stomach, with patients being upright for 30 minutes following ingestion to ensure maximal resorption, thus significantly reducing compliance regardless of positive bone related results being observed with the treatment.[343] Currently PEPITEMs side-effects and off-target effects have not been analysed, and thus need exploring to understand if PEPITEM may relieve some of the negative associated with current treatments. In addition, the anti-inflammatory action of PEPITEM may also provide additional help in diseases such as rheumatoid arthritis and osteoarthritis, where both inflammation and bone damage occur.

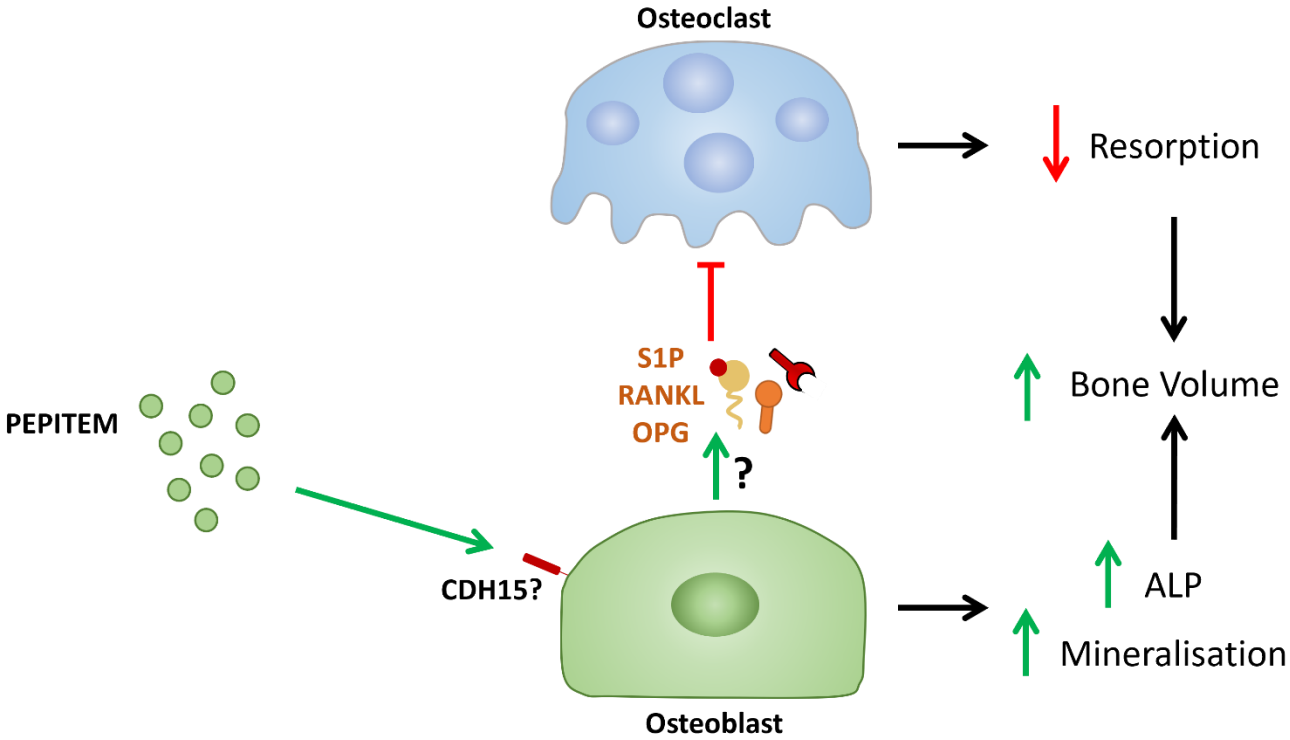

Figure 7.1. Overview of PEPITEMs potential signalling pathways in bone
PEPITEM was shown to promote an increase in bone volume *in vivo*, leading to physiological changes in bone strength and structure. *In vitro* studies revealed a direct effect of PEPITEM on osteoblasts causing increased ALP activity and mineral release. However, the signalling pathways and receptors for PEPITEM on osteoblasts have not yet been fully elucidated. PEPITEM has no direct effect on osteoclasts, however PEPITEM treated mice had decreased osteoclast numbers and treatment of osteoclasts with osteoblast conditioned media reduced resorption. However, the cross-signalling molecules are not yet understood, with potential molecules including RANKL, OPG and S1P. S1P treatment of osteoclasts decreased osteoclastogenesis, however S1Ps release in response to PEPITEM in osteoblasts is so far unknown. Overall, the impact of PEPITEM on bone growth has been revealed, but further work needs to be done on understanding the downstream signalling pathways and PEPITEMs role in other bone diseases.

7.4 Study limitations

All experiments exploring the responses of cells were done *in vitro* monocultures and whilst we used both primary isolated cells and cell lines, *in vitro* culture systems do not reflect the natural environment of bone.[723,724] *In vivo,* there are high levels of both pro-anabolic and pro-catabolic factors surrounding the bone which consistently influence osteoblast and osteoclast phenotypes.[723,724] These molecules also induce different mechanisms of osteoblast differentiation, altering expression profiles and thus maybe their direct response to PEPITEM.

In addition, we did not investigate the changes in osteocytes following PEPITEM treatment and there were no osteocytes present in our cultures. Osteocytes are known to be a key influencer of both osteoblast and osteoclast actions and therefore their removal may alter the responses of cells.[115,725–727] In addition, osteocytes express higher levels of *Cdh15* that osteoblasts and therefore may also respond directly to PEPITEM and alter the phenotypic responses.[648] However, osteocyte are present within murine bone, and therefore the *in vivo* data would indicate they do not inhibit the action of PEPITEM.

Cell cultures were also done using 2D culture systems, which alters the phenotype of cells due to binding to plastic as opposed to cells or bone.[728–731] Therefore, this study is limited in fully understanding the role of PEPITEM on cells in their natural environment, and novel 3D cultures containing mineral and other bone prevalent molecules are required to understand the full effect of PEPITEM.

Our *in vivo* data also has some limitations. Exploring the response to homeostatic bone to PEPITEM was only performed on male mice, whereas

responses in disease (OVX) were only observed in female mice. Male and female mice have differences in bone turnover rate, in addition to response to treatments *in vivo* and *in vitro.*[717,732–736] Therefore, the responses to PEPITEM in homeostasis or in disease may occur at different levels and have distinct outputs. Future experiment should confirm the homeostatic changes in female mice and explore the response of male mice to osteoporosis to ensure the pathway is sustained regardless of sex.

Additionally, all experiments were done in young (8-12-week-old) mice. Bone goes through many changes with ageing,[214,239,247] and diseases such as osteoporosis are much more common in older individuals. Therefore, our study may not depict the full changes in response to PEPITEM that occur in human bone, particularly since we observed reduced osteoblast responses in aged individuals. Additionally, experiments on homeostatic mice were performed on 8-week-old mice, where bone has still yet to reach peak bone mass. Therefore, net bone production will be occurring, which may be promoted further by PEPITEM, an effect which may not be seen in older mice where there is no net formation or resorption.

Our dosing regimens also had limitation, due to the short timeframe and off-target effects of liposome treatment. As previously discussed, liposomes will have some influence on PEPITEM take up, and no *in vitro* studies were performed exploring PEPITEM given in liposomes. This may have completely altered the bioactivity of PEPITEM, which needs exploring further in combination with the liposome formulae used. Furthermore, whilst PBS or an empty liposome accounted for injection control, the lack of a scrambled control or peptide control limits the conclusions that can be formed from the *in vivo* studies. Whilst they still prove that

PEPITEM has a positive effect, a peptide control would allow a comparison against other peptides and provide a more conclusive understanding.

In vivo experiments in mice are the gold standard model for exploring changes in bone in response to a treatment. However, there are large differences between human and mouse bone, with significant variations in trabecular patterns and osteocyte connections.[737,738] These changes may alter the phenotypic response of bone to PEPITEM, which needs to be explored to ensure changes trabecular structure match the increases seen human in osteoblast function.

Unfortunately, conclusions made on the impact of osteoporosis on human bone response to PEPITEM are limited due to the number and age of the patients. Low patient number, high ages, and an increased ratio of females to males suggest our data on osteoporosis may not reflect the full picture as many of the patients would already have gone through menopause and bone loss would have occurred resulting in osteoporosis. In addition, many patients did not have their bone scanned for BMD and thus it was unknown exactly which patients had osteoporosis.

Isolation of human samples may also change the phenotype of the cells. This is particularly the case in the fracture patients, since high levels of inflammation would have been present,[55,277,739] which can alter osteoblast phenotype.[624,740–742] In addition, osteoblasts were isolated from hip and knee joint, and phenotypic responses may change depending on cellular location.

7.5 Future studies

Our studies have provided provisional observational answers into the role of PEPITEM on bone in health and disease. However, many more questions are yet to

be answered and addition experiments are required to fully characterise the response of cells and bone to PEPITEM.

- Using PEPITEM for longer timeframes in mice, such as 4 – 8 weeks in both homeostasis and disease (OVX) may allow understanding of changes that occur in cortical bone, and if the initial increases observed are maintained, enhanced, or lost by longer term treatment.

- Treatment of aged mice, where osteoporosis has occurred, with PEPITEM to understand if PEPITEMs response is maintain with age.

- More studies are required exploring the response of osteoporotic bone to PEPITEM. In particular, attention should be paid to testing osteoporotic bone from younger females (post-menopause) before age related effects have influenced bone.

- Further work is required exploring the response of osteoblasts and osteoclasts to S1P. Inhibitors of S1P production in osteoblasts and S1P receptors in osteoblasts and osteoclasts will reveal the mechanism of S1P signalling. Additional studies using a range of S1P concentrations and other cell types are also needed to test why S1P results differ in murine and human cells.

- The use of transgenic models, such as removing S1P receptors from osteoblasts and osteoclasts, osteoblast specific Cadherin-15 knock out, RANKL/OPG conditional knock out, would allow an understanding of

PEPITEM signalling pathway in bone, indicating if S1P or other co-signalling molecules are involved *in vivo*.

- In murine bone, cadherin-15 blocking antibodies could inhibit cadherin-15 functionality, since siRNA knockdown did not decrease protein expression.

- Human osteoblasts reliance on cadherin-15 could be explored by further analysis of signalling pathways altered by knockdown, in addition to investigating if other cadherins are altered which are more classically shown to influence osteoblasts.

- Signalling pathways require further analysis, such as using phospho-assays to understand the key signalling pathways activated by PEPITEM. Once identified, inhibitors of such pathways will prove their relevance.

In conclusion, we have shown that PEPITEM is able to increase bone growth through direct actions on osteoblasts and indirect actions on osteoclasts. This mechanism is also present in disease, where osteoporotic mice are protected from bone loss in their long bone following PEPITEM treatment. Whilst the signalling mechanisms in bone is still unknown, our results indicate that PEPITEM has potential for use as a therapeutic in bone diseases to protect against bone loss.

8 Bibliography

1. Wagner, D. O. & Aspenberg, P. Where did bone come from? *Acta Orthopaedica* vol. 82 393–398 (2011).
2. Sansom, I. J., Smith, M. P., Armstrong, H. A. & Smith, M. M. Presence of the earliest vertebrate hard tissues in conodonts. *Science (80-.).* **256**, 1308–1311 (1992).
3. Adams, M. E. Development, Hormonal Control of. in *Encyclopedia of Insects* 261–266 (Elsevier Inc., 2009). doi:10.1016/B978-0-12-374144-8.00080-1.
4. Digirolamo, D. J., Kiel, D. P. & Esser, K. A. Bone and skeletal muscle: Neighbors with close ties. *J. Bone Miner. Res.* **28**, 1509–1518 (2013).
5. Lowenstam, H. Minerals formed by organisms. *Science (80-.).* **211**, 1126–1131 (1981).
6. Simkiss, K. Calcium and carbonate metabolism in the frog (Rana temporaria) during respiratory acidosis. *Am. J. Physiol.* **214**, 627–634 (1968).
7. Ruben, J. A. & Bennett, A. A. The evolution of bone. *Evolution (N. Y).* **41**, 1187–1197 (1987).
8. Ruben, J. A. & Bennett, A. F. Antiquity of the vertebrate pattern of activity metabolism and its possible relation to vertebrate origins. *Nature* **286**, 886–888 (1980).
9. Kawasaki, K. & Weiss, K. M. Mineralized tissue and vertebrate evolution: The secretory calcium-binding phosphoprotein gene cluster. *Proc. Natl. Acad. Sci. U. S. A.* **100**, 4060–4065 (2003).
10. Kawasaki, K. & Weiss, K. M. Genetic Basis for the Evolution of Vertebrate Mineralized Tissue. in *Handbook of Biomineralization* vol. 1 330–347 (Wiley-VCH Verlag GmbH, 2008).
11. Burr, D. B., Ruff, C. B. & Thompson, D. D. Patterns of skeletal histologic change through time: Comparison of an archaic native american population with modern populations. *Anat. Rec.* **226**, 307–313 (1990).
12. Liu, Y. *et al.* The Orphan Receptor Tyrosine Kinase Ror2 Promotes Osteoblast Differentiation and Enhances ex Vivo Bone Formation. *Mol. Endocrinol.* **21**, 376–387 (2007).
13. Palmer, L. C., Newcomb, C. J., Kaltz, S. R., Spoerke, E. D. & Stupp, S. I. Biomimetic systems for hydroxyapatite mineralization inspired by bone and enamel. *Chem. Rev.* **108**, 4754–4783 (2008).
14. Veldurthy, V. *et al.* Vitamin D, calcium homeostasis and aging. *Bone Research* vol. 4 1–7 (2016).
15. Mitchell, H. H., Hamilton, T. S., Steggerda, F. R. & Bean, H. W. THE CHEMICAL COMPOSITION OF THE ADULT HUMAN BODY AND ITS BEARING ON THE BIOCHEMISTRY OF GROWTH. *J. Biol. Chem.* **158**, 625–637 (1945).
16. Szent-Györgyi, A. G. Calcium regulation of muscle contraction. *Biophys. J.* **15**, 707–723 (1975).
17. Malaisse, W. J. Role of Calcium in the Regulation of Hormonal Secretion. *Horm. Res.* **20**, 28–37 (1984).
18. Südhof, T. C. Calcium control of neurotransmitter release. *Cold Spring Harb.*

Perspect. Biol. **4**, (2012).
19. Mikaelsson, M. E. The Role of Calcium in Coagulation and Anticoagulation. in *Coagulation and Blood Transfusion* 29–37 (Springer US, 1991). doi:10.1007/978-1-4615-3900-1_3.
20. COPP DH, S. A. Effect of parathyroidectomy on calcium kinetics. in *Use of Radioisotopes in Animal Biology and the Medical Sciences* (ed. International Atomic Energy Agency) 63 (Academic Press, 1962).
21. Erecinska, M., Stubbs, M., Miyata, Y., Ditre, C. M. & Wilson, D. F. Regulation of cellular metabolism by intracellular phosphate. *BBA - Bioenerg.* **462**, 20–35 (1977).
22. Dennis, V. W. *Phosphate metabolism: Contribution of different cellular compartments*. *Kidney International* vol. 49 (1996).
23. Shears, S. B. *et al.* Defining Signal Transduction by Inositol Phosphates. in *Sub-cellular biochemistry* vol. 59 389–412 (NIH Public Access, 2012).
24. Michigami, T., Kawai, M., Yamazaki, M. & Ozono, K. Phosphate as a Signaling Molecule and Its Sensing Mechanism. *Physiol Rev* **98**, 2317–2348 (2018).
25. Van Meer, G., Voelker, D. R. & Feigenson, G. W. Membrane lipids: Where they are and how they behave. *Nature Reviews Molecular Cell Biology* vol. 9 112–124 (2008).
26. Rutkowski, J. M. *et al.* Adiponectin alters renal calcium and phosphate excretion through regulation of klotho expression. *Kidney Int.* **91**, 324–337 (2017).
27. Duckworth, J. & Godden, W. The replenishment of depleted skeletal reserves of magnesium. *Biochem. J.* **37**, 595–598 (1943).
28. Burnell, J. M. Changes in bone sodium and carbonate in metabolic acidosis and alkalosis in the dog. *J. Clin. Invest.* **50**, 327–331 (1971).
29. Romer, A. S. Eurypterid influence on vertebrate history. *Science (80-.).* **78**, 114–117 (1933).
30. Wroe, S. & Milne, N. Convergence and remarkably consistent constraint in the evolution of carnivore skull shape. *Evolution (N. Y).* **61**, 1251–1260 (2007).
31. Paluh, D. J., Stanley, E. L. & Blackburn, D. C. Evolution of hyperossification expands skull diversity in frogs. *Proc. Natl. Acad. Sci. U. S. A.* **117**, 8554–8562 (2020).
32. Brink, O., Vesterby, A. & Jensen, J. Pattern of injuries due to interpersonal violence. *Injury* **29**, 705–709 (1998).
33. Strait, D. S. *et al.* The feeding biomechanics and dietary ecology of Australopithecus africanus. *Proc. Natl. Acad. Sci. U. S. A.* **106**, 2124–2129 (2009).
34. Plavcan, J. M. Taxonomic variation in the patterns of craniofacial dimorphism in primates. *J. Hum. Evol.* **42**, 579–608 (2002).
35. Morris, J. S. & Carrier, D. R. Sexual selection on skeletal shape in Carnivora. *Evolution (N. Y).* **70**, 767–780 (2016).
36. Doran, D. M. Comparative locomotor behavior of chimpanzees and bonobos: The influence of morphology on locomotion. *Am. J. Phys. Anthropol.* **91**, 83–98 (1993).
37. Sockol, M. D., Raichlen, D. A. & Pontzer, H. Chimpanzee locomotor energetics and the origin of human bipedalism. *Proc. Natl. Acad. Sci. U. S. A.* **104**, 12265–12269 (2007).

38. Jungers, W. L. Lucy's limbs: Skeletal allometry and locomotion in Australopithecus afarensis. *Nature* **297**, 676–678 (1982).
39. Bramble, D. M. & Lieberman, D. E. Endurance running and the evolution of Homo. *Nature* vol. 432 345–352 (2004).
40. Keller, T. S. *et al.* Relationship between vertical ground reaction force and speed during walking, slow jogging, and running. *Clin. Biomech.* **11**, 253–259 (1996).
41. Rose, M. D. A hominine hip bone, KNM-ER 3228, from East Lake Turkana, Kenya. *Am. J. Phys. Anthropol.* **63**, 371–378 (1984).
42. Latimer, B. & Lovejoy, C. O. The calcaneus of Australopithecus afarensis and its implications for the evolution of bipedality. *Am. J. Phys. Anthropol.* **78**, 369–386 (1989).
43. Larson, S. G. Evolutionary transformation of the hominin shoulder. *Evol. Anthropol. Issues, News, Rev.* **16**, 172–187 (2007).
44. Werner, S. L., Fleisig, G. S., Dillman, C. J. & Andrews, J. R. Biomechanics of the elbow during baseball pitching. *J. Orthop. Sports Phys. Ther.* **17**, 274–278 (1993).
45. Pieper, H. G. Humeral torsion in the throwing arm of handball players. *Am. J. Sports Med.* **26**, 247–253 (1998).
46. Jin, S. W., Sim, K. B. & Kim, S. D. Development and growth of the normal cranial vault: An embryologic review. *Journal of Korean Neurosurgical Society* vol. 59 192–196 (2016).
47. Farr, J. N. & Khosla, S. Skeletal changes through the lifespan—from growth to senescence. *Nat. Rev. Endocrinol.* **11**, 513 (2015).
48. Gilbert, S. F. Osteogenesis: The Development of Bones. (2000).
49. Berendsen, A. D. & Olsen, B. R. Bone development. *Bone* **80**, 14–18 (2015).
50. Ting, M. C. *et al.* EphA4 as an effector of Twist1 in the guidance of osteogenic precursor cells during calvarial bone growth and in craniosynostosis. *Development* **136**, 855–864 (2009).
51. Caddy, J., Luoma, L. & Berry, F. FOXC1 negatively regulates BMP-SMAD activity and Id1 expression during osteoblast differentiation. *FOXC1 negatively Regul. BMP-SMAD Act. Id1 Expr. Dur. osteoblast Differ.* 673889 (2019) doi:10.1101/673889.
52. Kress, W. *et al.* Saethre–Chotzen syndrome caused by TWIST 1 gene mutations: functional differentiation from Muenke coronal synostosis syndrome. *Eur. J. Hum. Genet.* **14**, 39–48 (2006).
53. Marsell, R. & Einhorn, T. A. The biology of fracture healing. *Injury* **42**, 551–555 (2011).
54. Shapiro, F. Bone development and its relation to fracture repair. The role of mesenchymal osteoblasts and surface osteoblasts. *European Cells and Materials* vol. 15 53–76 (2008).
55. Bahney, C. S. *et al.* Cellular biology of fracture healing. *Journal of Orthopaedic Research* vol. 37 35–50 (2019).
56. Mori-Akiyama, Y., Akiyama, H., Rowitch, D. H. & De Crombrugghe, B. Sox9 is required for determination of the chondrogenic cell lineage in the cranial neural crest. *Proc. Natl. Acad. Sci. U. S. A.* **100**, 9360–9365 (2003).
57. Smits, P., Dy, P., Mitra, S. & Lefebvre, V. Sox5 and Sox6 are needed to develop and maintain source, columnar, and hypertrophic chondrocytes in the

cartilage growth plate. *J. Cell Biol.* **164**, 747–758 (2004).
58. Catheline, S. E. *et al.* Chondrocyte-specific RUNX2 Overexpression Causes Chondrodysplasia During Development, but is Not Sufficient to Induce OA-like Articular Cartilage Degeneration in Adult Mice Without Injury. *bioRxiv* 470005 (2018) doi:10.1101/470005.
59. Qin, X. *et al.* Runx2 is essential for the transdifferentiation of chondrocytes into osteoblasts. *PLOS Genet.* **16**, e1009169 (2020).
60. Yoshida, C. A. *et al.* Runx2 and Runx3 are essential for chondrocyte maturation, and Runx2 regulates limb growth through induction of Indian hedgehog. *Genes Dev.* **18**, 952–963 (2004).
61. Zhou, X. *et al.* Chondrocytes Transdifferentiate into Osteoblasts in Endochondral Bone during Development, Postnatal Growth and Fracture Healing in Mice. *PLoS Genet.* **10**, e1004820 (2014).
62. Zhang, J., Pan, J. & Jing, W. Motivating role of type H vessels in bone regeneration. *Cell Prolif.* **53**, (2020).
63. Percival, C. J. & Richtsmeier, J. T. Angiogenesis and intramembranous osteogenesis. *Dev. Dyn.* **242**, 909–922 (2013).
64. Kusumbe, A. P., Ramasamy, S. K. & Adams, R. H. Coupling of angiogenesis and osteogenesis by a specific vessel subtype in bone. *Nature* **507**, 323–328 (2014).
65. Shore, E. M. Fibrodysplasia ossificans progressiva (FOP): A disorder of extraskeletal endochondral ossification. *Semin. Arthritis Rheum.* **42**, 546 (2013).
66. Liu, X. *et al.* SDF-1 Promotes Endochondral Bone Repair during Fracture Healing at the Traumatic Brain Injury Condition. *PLoS One* **8**, e54077 (2013).
67. Midura, R. J. *et al.* Calcospherulites11Calcospherulites (calco: calcium salt + spherulite: spherical crystalline body); calcium-containing, spherical bodies have also been referred to as calcified microspheres, mineral clusters, crystal ghost aggregates, calcification nodules, calcospherites, and small calcified spheres. isolated from the mineralization front of bone induce the mineralization of type I ... *Bone* **41**, 1005–1016 (2007).
68. James, A. W. Review of Signaling Pathways Governing MSC Osteogenic and Adipogenic Differentiation. *Scientifica (Cairo).* **2013**, 1–17 (2013).
69. Stein, G. S. & Lian, J. B. Molecular mechanisms mediating proliferation/differentiation interrelationships during progressive development of the osteoblast phenotype. *Endocr. Rev.* **14**, 424–442 (1993).
70. Stein, G. S. *et al.* Runx2 control of organization, assembly and activity of the regulatory machinery for skeletal gene expression. *Oncogene* vol. 23 4315–4329 (2004).
71. Beck, J., Zerler, B. & Moran, E. Gene array analysis of osteoblast differentiation. *Cell Growth Differ.* **12**, 61–83 (2001).
72. Henry, J. P. & Bordoni, B. *Histology, Osteoblasts*. *StatPearls* (StatPearls Publishing, 2020).
73. Capulli, M., Paone, R. & Rucci, N. Osteoblast and osteocyte: Games without frontiers. *Archives of Biochemistry and Biophysics* vol. 561 3–12 (2014).
74. Moutier, R., Toyama, K., Cotton, W. R. & Gaines, J. F. Three recessive genes for congenital osteopetrosis in the Norway rat. *J. Hered.* **67**, 189–190 (1976).
75. Shalhoub, V., Jackson, M. E., Lian, J. B., Stein, G. S. & Marks, S. C. Gene

expression during skeletal development in three osteopetrotic rat mutations: Evidence for osteoblast abnormalities. *J. Biol. Chem.* **266**, 9847–9856 (1991).
76. Garnero, P. The Role of Collagen Organization on the Properties of Bone. *Calcif. Tissue Int.* **97**, 229–240 (2015).
77. Weiner, S. & Traub, W. Organization of hydroxyapatite crystals within collagen fibrils. *FEBS Lett.* **206**, 262–266 (1986).
78. SHELDON, H. & ROBINSON, R. A. Electron microscope studies of crystal-collagen relationships in bone. IV. The occurrence of crystals within collagen fibrils. *J. Biophys. Biochem. Cytol.* **3**, 1011–1016 (1957).
79. Paschalis, E. P. *et al.* Distribution of Collagen Cross-Links in Normal Human Trabecular Bone. *J. Bone Miner. Res.* **18**, 1942–1946 (2003).
80. CALVO, M. S., EYRE, D. R. & GUNDBERG, C. M. Molecular Basis and Clinical Application of Biological Markers of Bone Turnover*. *Endocr. Rev.* **17**, 333–368 (1996).
81. Schnieke, A., Harbers, K. & Jaenisch, R. Embryonic lethal mutation in mice induced by retrovirus insertion into the α1(I) collagen gene. *Nature* **304**, 315–320 (1983).
82. Bacon, S. & Crowley, R. Developments in rare bone diseases and mineral disorders. *Ther. Adv. Chronic Dis.* **9**, 51–60 (2018).
83. Boraschi-Diaz, I. *et al.* Metabolic phenotype in the mouse model of osteogenesis imperfecta. *J. Endocrinol.* **234**, 279–289 (2017).
84. Zha, L. *et al.* Collagen1α1 promoter drives the expression of Cre recombinase in osteoblasts of transgenic mice. *J. Genet. Genomics* **35**, 525–530 (2008).
85. Oesper, R. E. The Collected Papers of Carl Wilhelm Scheele. *J. Chem. Educ.* **8**, 2304 (1931).
86. Eliaz, N. & Metoki, N. Calcium phosphate bioceramics: A review of their history, structure, properties, coating technologies and biomedical applications. *Materials (Basel).* **10**, 334 (2017).
87. Fedde, K. N. *et al.* Alkaline phosphatase knock-out mice recapitulate the metabolic and skeletal defects of infantile hypophosphatasia. *J. Bone Miner. Res.* **14**, 2015–2026 (1999).
88. Rezende, L. A., Ciancaglini, P., Pizauro, J. M. & Leone, F. A. Inorganic pyrophosphate-phosphohydrolytic activity associated with rat osseous plate alkaline phosphatase. *Cell. Mol. Biol. (Noisy-le-grand).* **44**, 293–302 (1998).
89. Majeska, R. J. & Wuthier, R. E. Studies on matrix vesicles isolated from chick epiphyseal cartilage Association of pyrophosphatase and ATPase activities with alkaline phosphatase. *BBA - Enzymol.* **391**, 51–60 (1975).
90. Moss, D. W., Eaton, R. H., Smith, J. K. & Whitby, L. G. Association of inorganic-pyrophosphatase activity with human alkaline-phosphatase preparations. *Biochem. J.* **102**, 53–57 (1967).
91. Luo, X. H. *et al.* Adiponectin stimulates human osteoblasts proliferation and differentiation via the MAPK signaling pathway. *Exp. Cell Res.* **309**, 99–109 (2005).
92. Isogai, Y. *et al.* Parathyroid hormone regulates osteoblast differentiation positively or negatively depending on the differentiation stages. *J. Bone Miner. Res.* **11**, 1384–93 (1996).
93. Wada, Y. *et al.* Changes in osteoblast phenotype during differentiation of enzymatically isolated rat calvaria cells. *Bone* **22**, 479–485 (1998).

94. Li, Y., Su, J., Sun, W., Cai, L. & Deng, Z. AMP-activated protein kinase stimulates osteoblast differentiation and mineralization through autophagy induction. *Int. J. Mol. Med.* **41**, 2535–2544 (2018).
95. Choudhary, S., Huang, H., Raisz, L. & Pilbeam, C. Anabolic effects of PTH in cyclooxygenase-2 knockout osteoblasts in vitro. *Biochem. Biophys. Res. Commun.* **372**, 536–541 (2008).
96. Lee, M. S. *et al.* GM-CSF Regulates Fusion of Mononuclear Osteoclasts into Bone-Resorbing Osteoclasts by Activating the Ras/ERK Pathway. *J. Immunol.* **183**, 3390–3399 (2009).
97. Massey, H. M. & Flanagan, A. M. Human osteoclasts derive from CD14-positive monocytes. *Br. J. Haematol.* **106**, 167–170 (1999).
98. Dougall, W. C. *et al.* RANK is essential for osteoclast and lymph node development. *Genes Dev.* **13**, 2412–2424 (1999).
99. Jacome-Galarza, C. E., Lee, S. K., Lorenzo, J. A. & Aguila, H. L. Identification, characterization, and isolation of a common progenitor for osteoclasts, macrophages, and dendritic cells from murine bone marrow and periphery. *J. Bone Miner. Res.* **28**, 1203–1213 (2013).
100. Jacquin, C., Gran, D. E., Lee, S. K., Lorenzo, J. A. & Aguila, H. L. Identification of multiple osteoclast precursor populations in murine bone marrow. *J. Bone Miner. Res.* **21**, 67–77 (2006).
101. Jacome-Galarza, C. E. *et al.* Developmental origin, functional maintenance and genetic rescue of osteoclasts. doi:10.1038/s41586-019-1105-7.
102. Parfitt, A. M. Osteonal and hemi-osteonal remodeling: The spatial and temporal framework for signal traffic in adult human bone. *J. Cell. Biochem.* **55**, 273–286 (1994).
103. Jacome-Galarza, C. E., Lee, S. K., Lorenzo, J. A. & Aguila, H. L. Identification, characterization, and isolation of a common progenitor for osteoclasts, macrophages, and dendritic cells from murine bone marrow and periphery. *J. Bone Miner. Res.* **28**, 1203–1213 (2013).
104. Azuma, Y., Kaji, K., Katogi, R., Takeshita, S. & Kudo, A. Tumor necrosis factor-α induces differentiation of and bone resorption by osteoclasts. *J. Biol. Chem.* **275**, 4858–4864 (2000).
105. Hodge, J. M., Collier, F. M., Pavlos, N. J., Kirkland, M. A. & Nicholson, G. C. M-csf potently augments rankl-induced resorption activation in mature human osteoclasts. *PLoS One* **6**, e21462 (2011).
106. Nakamura, I. *et al.* Role of α(v)β3 integrin in osteoclast migration and formation of the sealing zone. *J. Cell Sci.* **112**, 3985–3993 (1999).
107. Faccio, R. *et al.* Localization and possible role of two different alpha v beta 3 integrin conformations in resting and resorbing osteoclasts. *J. Cell Sci.* **115**, 2919–2929 (2002).
108. Nakamura, I., Duong, L. T., Rodan, S. B. & Rodan, G. A. Involvement of αvβ3 integrins in osteoclast function. *J. Bone Miner. Metab.* **25**, 337–344 (2007).
109. Feng, S. *et al.* Atp6v1c1 is an essential component of the osteoclast proton pump and in F-actin ring formation in osteoclasts. *Biochem. J.* **417**, 195–203 (2009).
110. TROEN, B. R. The Regulation of Cathepsin K Gene Expression. *Ann. N. Y. Acad. Sci.* **1068**, 165–172 (2006).
111. Gauthier, J. Y. *et al.* The discovery of odanacatib (MK-0822), a selective

inhibitor of cathepsin K. *Bioorganic Med. Chem. Lett.* **18**, 923–928 (2008).
112. Andersen, T. L. *et al.* A scrutiny of matrix metalloproteinases in osteoclasts: Evidence for heterogeneity and for the presence of MMPs synthesized by other cells. *Bone* **35**, 1107–1119 (2004).
113. Franz-Odendaal, T. A., Hall, B. K. & Witten, P. E. Buried alive: How osteoblasts become osteocytes. *Developmental Dynamics* vol. 235 176–190 (2006).
114. Manolagas, S. C. Birth and Death of Bone Cells: Basic Regulatory Mechanisms and Implications for the Pathogenesis and Treatment of Osteoporosis*. *Endocr. Rev.* **21**, 115–137 (2000).
115. Stern, A. R. *et al.* Isolation and culture of primary osteocytes from the long bones of skeletally mature and aged mice. *Biotechniques* **52**, 361–373 (2012).
116. Zhang, K. *et al.* E11/gp38 Selective Expression in Osteocytes: Regulation by Mechanical Strain and Role in Dendrite Elongation. *Mol. Cell. Biol.* **26**, 4539–4552 (2006).
117. Ubaidus, S. *et al.* FGF23 is mainly synthesized by osteocytes in the regularly distributed osteocytic lacunar canalicular system established after physiological bone remodeling. *J. Electron Microsc. (Tokyo).* **58**, 381–392 (2009).
118. Blair, H. C. *et al.* Osteoblast differentiation and bone matrix formation in vivo and in vitro. *Tissue Engineering - Part B: Reviews* vol. 23 268–280 (2017).
119. Veverka, V. *et al.* Characterization of the structural features and interactions of sclerostin. Molecular insight into a key regulator of Wnt-mediated bone formation. *J. Biol. Chem.* **284**, 10890–10900 (2009).
120. Atkins, G. J. *et al.* Sclerostin is a locally acting regulator of late-osteoblast/preosteocyte differentiation and regulates mineralization through a MEPE-ASARM-dependent mechanism. *J. Bone Miner. Res.* **26**, 1425–1436 (2011).
121. McDonald, M. M. *et al.* Inhibiting the osteocyte-specific protein sclerostin increases bone mass and fracture resistance in multiple myeloma. *Blood* **129**, 3452–3464 (2017).
122. Palumbo, C., Palazzini, S. & Marotti, G. Morphological study of intercellular junctions during osteocyte differentiation. *Bone* **11**, 401–406 (1990).
123. Doty, S. B. Morphological evidence of gap junctions between bone cells. *Calcif. Tissue Int.* **33**, 509–512 (1981).
124. Knothe Tate, M. L., Niederer, P. & Knothe, U. In vivo tracer transport through the lacunocanalicular system of rat bone in an environment devoid of mechanical loading. *Bone* **22**, 107–117 (1998).
125. Tatsumi, S. *et al.* Targeted Ablation of Osteocytes Induces Osteoporosis with Defective Mechanotransduction. *Cell Metab.* **5**, 464–475 (2007).
126. Nakashima, T. *et al.* Evidence for osteocyte regulation of bone homeostasis through RANKL expression. *Nat. Med.* **17**, 1231–1234 (2011).
127. Pitsillides, A. A. *et al.* Mechanical strain-induced NO production by bone cells: a possible role in adaptive bone (re)modeling? *FASEB J.* **9**, 1614–1622 (1995).
128. Komiya, Y. & Habas, R. Wnt signal transduction pathways. *Organogenesis* vol. 4 68–75 (2008).
129. Tu, X. *et al.* Noncanonical Wnt Signaling through G Protein-Linked PKCδ Activation Promotes Bone Formation. *Dev. Cell* **12**, 113–127 (2007).
130. Chang, J. *et al.* Noncanonical Wnt-4 signaling enhances bone regeneration of mesenchymal stem cells in craniofacial defects through activation of p38

MAPK. *J. Biol. Chem.* **282**, 30938–30948 (2007).
131. Prowse, P. D. H., Elliott, C. G., Hutter, J. & Hamilton, D. W. Inhibition of Rac and ROCK Signalling Influence Osteoblast Adhesion, Differentiation and Mineralization on Titanium Topographies. *PLoS One* **8**, 58898 (2013).
132. Orriss, I. R. *et al.* Spina bifida-predisposing heterozygous mutations in Planar Cell Polarity genes and Zic2 reduce bone mass in young mice. *Sci. Rep.* **8**, 1–14 (2018).
133. Takada, I. *et al.* A histone lysine methyltransferase activated by non-canonical Wnt signalling suppresses PPAR-gamma transactivation. *Nat. Cell Biol.* **9**, 1273–1285 (2007).
134. Carroll, T. J., Park, J. S., Hayashi, S., Majumdar, A. & McMahon, A. P. Wnt9b plays a central role in the regulation of mesenchymal to epithelial transitions underlying organogenesis of the mammalian urogenital system. *Dev. Cell* **9**, 283–292 (2005).
135. Später, D. *et al.* Wnt9a signaling is required for joint integrity and regulation of Ihh during chondrogenesis. *Development* **133**, 3039–3049 (2006).
136. Jin, Y. R., Han, X. H., Taketo, M. M. & Yoon, J. K. Wnt9b-dependent FGF signaling is crucial for outgrowth of the nasal and maxillary processes during upper jaw and lip development. *Development* **139**, 1821–1830 (2012).
137. Zheng, H. F. *et al.* WNT16 influences bone mineral density, cortical bone thickness, bone strength, and osteoporotic fracture risk. *PLoS Genet.* **8**, (2012).
138. Bennett, C. N. *et al.* Regulation of osteoblastogenesis and bone mass by Wnt10b. *Proc. Natl. Acad. Sci. U. S. A.* **102**, 3324–3329 (2005).
139. Tu, X. *et al.* Noncanonical Wnt Signaling through G Protein-Linked PKCδ Activation Promotes Bone Formation. *Dev. Cell* **12**, 113 (2007).
140. Boyden, L. M. *et al.* High Bone Density Due to a Mutation in LDL-Receptor–Related Protein 5. *N. Engl. J. Med.* **346**, 1513–1521 (2002).
141. Johnson, M. L. & Johnson, M. L. *The high bone mass family-the role of Wnt/Lrp5 signaling in the regulation of bone mass*. *J Musculoskel Neuron Interact* vol. 4 (2004).
142. Niziolek, P. J., Bullock, W., Warman, M. L. & Robling, A. G. Missense Mutations in LRP5 associated with high bone mass protect the mouse skeleton from disuse-and ovariectomy-induced osteopenia. *PLoS One* **10**, (2015).
143. Gong, Y. *et al.* LDL receptor-related protein 5 (LRP5) affects bone accrual and eye development. *Cell* **107**, 513–523 (2001).
144. Little, R. D. *et al.* A mutation in the LDL receptor-related protein 5 gene results in the autosomal dominant high-bone-mass trait. *Am. J. Hum. Genet.* **70**, 11–19 (2002).
145. Holmen, S. L. *et al.* Essential role of β-catenin in postnatal bone acquisition. *J. Biol. Chem.* **280**, 21162–21168 (2005).
146. Day, T. F., Guo, X., Garrett-Beal, L. & Yang, Y. Wnt/β-catenin signaling in mesenchymal progenitors controls osteoblast and chondrocyte differentiation during vertebrate skeletogenesis. *Dev. Cell* **8**, 739–750 (2005).
147. Yao, G. Q., Wu, J. J., Troiano, N. & Insogna, K. Targeted overexpression of Dkk1 in osteoblasts reduces bone mass but does not impair the anabolic response to intermittent PTH treatment in mice. *J. Bone Miner. Metab.* **29**, 141–148 (2011).

148. Balemans, W. *et al.* Increased bone density in sclerosteosis is due to the deficiency of a novel secreted protein (SOST). *Hum. Mol. Genet.* **10**, 537–543 (2001).
149. Brunkow, M. E. *et al.* Bone dysplasia sclerosteosis results from loss of the SOST gene product, a novel cystine knot-containing protein. *Am. J. Hum. Genet.* **68**, 577–589 (2001).
150. Balemans, W. *et al.* Identification of a 52 kb deletion downstream of the SOST gene in patients with van Buchem disease. *J. Med. Genet.* **39**, 91–97 (2002).
151. Kopan, R. Notch signaling. *Cold Spring Harb. Perspect. Biol.* **4**, (2012).
152. Hilton, M. J. *et al.* Notch signaling maintains bone marrow mesenchymal progenitors by suppressing osteoblast differentiation. *Nat. Med.* **14**, 306–314 (2008).
153. Kalajzic, I. *et al.* Use of type I collagen green fluorescent protein transgenes to identify subpopulations of cells at different stages of the osteoblast lineage. *J. Bone Miner. Res.* **17**, 15–25 (2002).
154. Mizutani, K., Ikeda, K., Kawai, Y. & Yamori, Y. Resveratrol stimulates the proliferation and differentiation of osteoblastic MC3T3-E1 cells. *Biochem. Biophys. Res. Commun.* **253**, 859–863 (1998).
155. Ornstrup, M. J., Harsløf, T., Kjær, T. N., Langdahl, B. L. & Pedersen, S. B. Resveratrol increases bone mineral density and bone alkaline phosphatase in obese men: A randomized placebo-controlled trial. *J. Clin. Endocrinol. Metab.* **99**, 4720–4729 (2014).
156. Cottart, C. H., Nivet-Antoine, V. & Beaudeux, J. L. Review of recent data on the metabolism, biological effects, and toxicity of resveratrol in humans. *Molecular Nutrition and Food Research* vol. 58 7–21 (2014).
157. Ji, Y., Ke, Y. & Gao, S. Intermittent activation of notch signaling promotes bone formation. *Am. J. Transl. Res.* **9**, 2933–2944 (2017).
158. Lowery, J. W., Brookshire, B. & Rosen, V. A survey of strategies to modulate the bone morphogenetic protein signaling pathway: Current and future perspectives. *Stem Cells International* vol. 2016 (2016).
159. Wang, R. N. *et al.* Bone Morphogenetic Protein (BMP) signaling in development and human diseases. *Genes and Diseases* vol. 1 87–105 (2014).
160. Lee, K.-S. *et al.* Runx2 Is a Common Target of Transforming Growth Factor β1 and Bone Morphogenetic Protein 2, and Cooperation between Runx2 and Smad5 Induces Osteoblast-Specific Gene Expression in the Pluripotent Mesenchymal Precursor Cell Line C2C12. *Mol. Cell. Biol.* **20**, 8783–8792 (2000).
161. Lee, M. H., Kwon, T. G., Park, H. S., Wozney, J. M. & Ryoo, H. M. BMP-2-induced Osterix expression is mediated by Dlx5 but is independent of Runx2. *Biochem. Biophys. Res. Commun.* **309**, 689–694 (2003).
162. Zhang, M. *et al.* BMP-2 modulates β-catenin signaling through stimulation of Lrp5 expression and inhibition of β-TrCP expression in osteoblasts. *J. Cell. Biochem.* **108**, 896–905 (2009).
163. Turgeman, G. *et al.* Systemically administered rhBMP-2 promotes MSC activity and reverses bone and cartilage loss in osteopenic mice. *J. Cell. Biochem.* **86**, 461–474 (2002).
164. Moon, Y. J. *et al.* Smad4 controls bone homeostasis through regulation of osteoblast/osteocyte viability. *Exp. Mol. Med.* **48**, e256 (2016).

165. Wu, X. Bin *et al.* Impaired osteoblastic differentiation, reduced bone formation, and severe osteoporosis in noggin-overexpressing mice. *J. Clin. Invest.* **112**, 924–934 (2003).
166. Gazzerro, E. *et al.* Skeletal overexpression of gremlin impairs bone formation and causes osteopenia. *Endocrinology* **146**, 655–665 (2005).
167. Gazzerro, E., Gangji, V. & Canalis, E. Bone morphogenetic proteins induce the expression of noggin, which limits their activity in cultured rat osteoblasts. *J. Clin. Invest.* **102**, 2106–2114 (1998).
168. Pereira, R. C., Economides, A. N. & Canalis, E. Bone Morphogenetic Proteins Induce Gremlin, a Protein That Limits Their Activity in Osteoblasts [1]. *Endocrinology* **141**, 4558–4563 (2000).
169. Laursen, M. *et al.* Recombinant bone morphogenetic protein-7 as an intracorporal bone growth stimulator in unstable thoracolumbar burst fractures in humans: Preliminary results. *Eur. Spine J.* **8**, 485–490 (1999).
170. Garrison, K. *et al.* Bone morphogenetic protein (BMP) for fracture healing in adults. *Cochrane Database of Systematic Reviews* vol. 2010 (2008).
171. Govender, S. *et al.* Recombinant human bone morphogenetic protein-2 for treatment of open tibial fractures a prospective, controlled, randomized study of four hundred and fifty patients. *J. Bone Jt. Surg. - Ser. A* **84**, 2123–2134 (2002).
172. Van Der Horst, G., Farih-Sips, H., Löwik, C. W. G. M. & Karperien, M. Hedgehog stimulates only osteoblastic differentiation of undifferentiated KS483 cells. *Bone* **33**, 899–910 (2003).
173. Yuasa, T. *et al.* Sonic hedgehog is involved in osteoblast differentiation by cooperating with BMP-2. *J. Cell. Physiol.* **193**, 225–232 (2002).
174. Nakashima, K. *et al.* The novel zinc finger-containing transcription factor Osterix is required for osteoblast differentiation and bone formation. *Cell* **108**, 17–29 (2002).
175. Tu, Q., Valverde, P. & Chen, J. Osterix enhances proliferation and osteogenic potential of bone marrow stromal cells. *Biochem. Biophys. Res. Commun.* **341**, 1257–1265 (2006).
176. Tu, Q. *et al.* Osterix overexpression in mesenchymal stem cells stimulates healing of critical-sized defects in murine calvarial bone. *Tissue Eng.* **13**, 2431–2440 (2007).
177. Yoshida, C. A. *et al.* Sp7 inhibits osteoblast differentiation at a late stage in mice. *PLoS One* **7**, 32364 (2012).
178. Kobayashi, H., Gao, Y. H., Ueta, C., Yamaguchi, A. & Komori, T. Multilineage differentiation of Cbfa1-deficient calvarial cells in vitro. *Biochem. Biophys. Res. Commun.* **273**, 630–636 (2000).
179. Takarada, T. *et al.* An analysis of skeletal development in osteoblast-specific and chondrocyte-specific runt-related transcription factor-2 (Runx2) knockout mice. *J. Bone Miner. Res.* **28**, 2064–2069 (2013).
180. Ueta, C. *et al.* Skeletal malformations caused by overexpression of Cbfa1 or its dominant negative form in chondrocytes. *J. Cell Biol.* **153**, 87–99 (2001).
181. Adhami, M. D. *et al.* Loss of Runx2 in Committed Osteoblasts Impairs Postnatal Skeletogenesis. *J. Bone Miner. Res.* **30**, 71–82 (2015).
182. Galindo, M. *et al.* The bone-specific expression of Runx2 oscillates during the cell cycle to support a G1-related antiproliferative function in osteoblasts. *J.*

Biol. Chem. **280**, 20274–20285 (2005).
183. Kido, S. *et al.* Expression of RANK is dependent upon differentiation into the macrophage/osteoclast lineage: Induction by 1α,25-dihydroxyvitamin D 3 and TPA in a human myelomonocytic cell line, HL60. *Bone* **32**, 621–629 (2003).
184. Atkins, G. J. *et al.* RANKL Expression Is Related to the Differentiation State of Human Osteoblasts. *J. Bone Miner. Res.* **18**, 1088–1098 (2003).
185. Kawai, T. *et al.* B and T lymphocytes are the primary sources of RANKL in the bone resorptive lesion of periodontal disease. *Am. J. Pathol.* **169**, 987–998 (2006).
186. Wei, X. *et al.* Fibroblasts express RANKL and support osteoclastogenesis in a COX-2-dependent manner after stimulation with titanium particles. *J. Bone Miner. Res.* **20**, 1136–1148 (2005).
187. Kapur, R. P. *et al.* Malignant Autosomal Recessive Osteopetrosis Caused by Spontaneous Mutation of Murine Rank. *J. Bone Miner. Res.* **19**, 1689–1697 (2004).
188. Lamothe, B. *et al.* TRAF6 ubiquitin ligase is essential for RANKL signaling and osteoclast differentiation. *Biochem. Biophys. Res. Commun.* **359**, 1044–1049 (2007).
189. Guo, J. *et al.* An Allosteric-Probe for Detection of Alkaline Phosphatase Activity and Its Application in Immunoassay. *Front. Chem.* **6**, 618 (2018).
190. Lee, S. E. *et al. The Phosphatidylinositol 3-Kinase, p38, and Extracellular Signal-regulated Kinase Pathways Are Involved in Osteoclast Differentiation*. (2002) doi:10.1016/S8756-3282(01)00657-3.
191. Huang, H. *et al.* Induction of c-Fos and NFATc1 during RANKL-stimulated osteoclast differentiation is mediated by the p38 signaling pathway. *Biochem. Biophys. Res. Commun.* **351**, 99–105 (2006).
192. Wang, Z. Q. *et al.* Bone and haematopoietic defects in mice lacking c-fos. *Nature* **360**, 741–745 (1992).
193. Rüther, U., Garber, C., Komitowski, D., Müller, R. & Wagner, E. F. Deregulated c-fos expression interferes with normal bone development in transgenic mice. *Nature* **325**, 412–416 (1987).
194. Nelson, C. A., Warren, J. T., Wang, M. W. H., Teitelbaum, S. L. & Fremont, D. H. RANKL employs distinct binding modes to engage RANK and the osteoprotegerin decoy receptor. *Structure* **20**, 1971–1982 (2012).
195. Simonet, W. S. *et al. Osteoprotegerin: A Novel Secreted Protein Involved in the Regulation of Bone Density*. *Cell* vol. 89 309–319 (Cell Press, 1997).
196. Bucay, N. *et al.* Osteoprotegerin-deficient mice develop early onset osteoporosis and arterial calcification. *Genes Dev.* **12**, 1260–1268 (1998).
197. Mizuno, A. *et al.* Severe osteoporosis in mice lacking osteoclastogenesis inhibitory factor/osteoprotegerin. *Biochem. Biophys. Res. Commun.* **247**, 610–615 (1998).
198. Tondravi, M. M. *et al.* Osteopetrosis in mice lacking haematopoietic transcription factor PU.1. *Nature* **386**, 81–84 (1997).
199. Carey, H. A. *et al.* Enhancer variants reveal a conserved transcription factor network governed by PU.1 during osteoclast differentiation. *Bone Res.* **6**, 1–12 (2018).
200. Anderson, G. *et al.* Thalidomide derivative CC-4047 inhibits osteoclast formation by down-regulation of PU.1. *Blood* **107**, 3098–3105 (2006).

201. Johnell, O. *et al.* Mortality after osteoporotic fractures. *Osteoporos. Int.* **15**, 38–42 (2004).
202. Johansson, C., Black, D., Johnell, O., Odén, A. & Mellström, D. Bone mineral density is a predictor of survival. *Calcif. Tissue Int.* **63**, 190–196 (1998).
203. Browner, W. S., Seeley, D. G., Vogt, T. M. & Cummings, S. R. Non-trauma mortality in elderly women with low bone mineral density. Study of Osteoporotic Fractures Research Group. *Lancet (London, England)* **338**, 355–8 (1991).
204. Hernlund, E. *et al.* Osteoporosis in the European Union: medical management, epidemiology and economic burden. *Arch. Osteoporos.* **8**, 136 (2013).
205. Talbot, L. A., Musiol, R. J., Witham, E. K. & Metter, E. J. Falls in young, middle-aged and older community dwelling adults: Perceived cause, environmental factors and injury. *BMC Public Health* **5**, 86 (2005).
206. Johnell, O. & Kanis, J. A. An estimate of the worldwide prevalence and disability associated with osteoporotic fractures. *Osteoporos. Int.* **17**, 1726–1733 (2006).
207. Looker, A. C., Melton, L. J., Harris, T. B. & Shepherd, J. A. Prevalence and trends in low femur bone density among older US adults: NHANES 2005-2006 compared with NHANES III. *J. Bone Miner. Res.* **25**, 64–71 (2010).
208. Akkawi, I. & Zmerly, H. Osteoporosis: Current concepts. *Joints* vol. 6 122–127 (2018).
209. McKinlay, S. M., Brambilla, D. J. & Posner, J. G. The normal menopause transition. *Am. J. Hum. Biol.* **4**, 37–46 (1992).
210. Finkelstein, J. S. *et al.* Bone Mineral Density Changes during the Menopause Transition in a Multiethnic Cohort of Women. *J. Clin. Endocrinol. Metab.* **93**, 861–868 (2008).
211. Bjørnerem, Å. *et al.* Menopause-Related Appendicular Bone Loss is Mainly Cortical and Results in Increased Cortical Porosity. *J. Bone Miner. Res.* **33**, 598–605 (2018).
212. Koebele, S. V. & Bimonte-Nelson, H. A. Modeling menopause: The utility of rodents in translational behavioral endocrinology research. *Maturitas* vol. 87 5–17 (2016).
213. Roberts, B. C. *et al.* The longitudinal effects of ovariectomy on the morphometric, densitometric and mechanical properties in the murine tibia: A comparison between two mouse strains. *Bone* **127**, 260–270 (2019).
214. Zhou, S. *et al.* Age-dependent variations of cancellous bone in response to ovariectomy in C57BL/6J mice. *Exp. Ther. Med.* **15**, 3623–3632 (2018).
215. Rosales Rocabado, J. M. *et al.* A multi-factorial analysis of bone morphology and fracture strength of rat femur in response to ovariectomy. *J. Orthop. Surg. Res.* **13**, 318 (2018).
216. Rissanen, J. P. *et al.* Short-term changes in serum PINP predict long-term changes in trabecular bone in the rat ovariectomy model. *Calcif. Tissue Int.* **82**, 155–161 (2008).
217. Lei, Z., Xiaoying, Z. & Xingguo, L. Ovariectomy-associated changes in bone mineral density and bone marrow haematopoiesis in rats. *Int. J. Exp. Pathol.* **90**, 512–519 (2009).
218. Jerome, C. P., Turner, C. H. & Lees, C. J. Decreased bone mass and strength in ovariectomized cynomolgus monkeys (Macaca fascicularis). *Calcif. Tissue Int.* **60**, 265–270 (1997).

219. Jayo, M. J., Jerome, C. P., Lees, C. J., Rankin, S. E. & Weaver, D. S. Bone mass in female cynomolgus macaques: A cross-sectional and longitudinal study by age. *Calcif. Tissue Int.* **54**, 231–236 (1994).
220. Liu, C. -C & Howard, G. A. Bone-cell changes in estrogen-induced bone-mass increase in mice: Dissociation of osteoclasts from bone surfaces. *Anat. Rec.* **229**, 240–250 (1991).
221. Chen, F. P., Wang, K. C. & Huang, J. D. Effect of Estrogen on the Activity and Growth of Human Osteoclasts In Vitro. *Taiwan. J. Obstet. Gynecol.* **48**, 350–355 (2009).
222. Shevde, N. K., Bendixen, A. C., Dienger, K. M. & Pike, J. W. Estrogens suppress RANK ligand-induced osteoclast differentiation via a stromal cell independent mechanism involving c-Jun repression. *Proc. Natl. Acad. Sci. U. S. A.* **97**, 7829–7834 (2000).
223. Kameda, T. *et al.* Estrogen inhibits bone resorption by directly inducing apoptosis of the bone-resorbing osteoclasts. *J. Exp. Med.* **186**, 489–495 (1997).
224. Streicher, C. *et al.* Estrogen Regulates Bone Turnover by Targeting RANKL Expression in Bone Lining Cells. *Sci. Rep.* **7**, (2017).
225. Krum, S. A. *et al.* Estrogen protects bone by inducing Fas ligand in osteoblasts to regulate osteoclast survival. *EMBO J.* **27**, 535–545 (2008).
226. Wang, L. *et al.* Osteoblast-induced osteoclast apoptosis by fas ligand/FAS pathway is required for maintenance of bone mass. *Cell Death Differ.* **22**, 1654–1664 (2015).
227. Zhu, S. *et al.* Ovariectomy-induced bone loss in TNFα and IL6 gene knockout mice is regulated by different mechanisms. *J. Mol. Endocrinol.* **60**, 185–198 (2018).
228. Cenci, S. *et al.* Estrogen deficiency induces bone loss by enhancing T-cell production of TNF-α. *J. Clin. Invest.* **106**, 1229–1237 (2000).
229. Zhang, Y. H., Heulsmann, A., Tondravi, M. M., Mukherjee, A. & Abu-Amer, Y. Tumor necrosis factor-α (TNF) stimulates RANKL-induced osteoclastogenesis via coupling of TNF type 1 receptor and RANK signaling pathways. *J. Biol. Chem.* **276**, 563–568 (2001).
230. Roggia, C. *et al.* Up-regulation of TNF-producing T cells in the bone marrow: A key mechanism by which estrogen deficiency induces bone loss in vivo. *Proc. Natl. Acad. Sci. U. S. A.* **98**, 13960–13965 (2001).
231. Pacifici, R. *et al.* Spontaneous release of interleukin 1 from human blood monocytes reflects bone formation in idiopathic osteoporosis. *Proc. Natl. Acad. Sci. U. S. A.* **84**, 4616–4620 (1987).
232. Kim, J. H. *et al.* The Mechanism of Osteoclast Differentiation Induced by IL-1. *J. Immunol.* **183**, 1862–1870 (2009).
233. Pantschenko, A. G. *et al.* Effect of osteoblast-targeted expression of Bcl-2 in bone: Differential response in male and female mice. *J. Bone Miner. Res.* **20**, 1414–1429 (2005).
234. Raisz, L. G. & Seeman, E. Causes of Age-Related Bone Loss and Bone Fragility: An Alternative View. *J. Bone Miner. Res.* **16**, 1948–1952 (2001).
235. Berger, C. *et al.* Peak bone mass from longitudinal data: Implications for the prevalence, pathophysiology, and diagnosis of osteoporosis. *J. Bone Miner. Res.* **25**, 1948–1957 (2010).

236. Papaioannou, A. *et al.* Risk factors for low BMD in healthy men age 50 years or older: A systematic review. *Osteoporos. Int.* **20**, 507–518 (2009).
237. Daly, R. M. *et al.* Gender specific age-related changes in bone density, muscle strength and functional performance in the elderly: A-10 year prospective population-based study. *BMC Geriatrics* vol. 13 71 (2013).
238. Halloran, B. P. *et al.* Changes in bone structure and mass with advancing age in the male C57BL/6J mouse. *J. Bone Miner. Res.* **17**, 1044–1050 (2002).
239. Ferguson, V. L., Ayers, R. A., Bateman, T. A. & Simske, S. J. Bone development and age-related bone loss in male C57BL/6J mice. *Bone* **33**, 387–398 (2003).
240. Smit, T. H., Odgaard, A. & Schneider, E. Structure and function of vertebral trabecular bone. *Spine (Phila. Pa. 1976).* **22**, 2823–2833 (1997).
241. Haden, S. T., Brown, E. M., Hurwitz, S., Scott, J. & Fuleihan, G. E. H. The effects of age and gender on parathyroid hormone dynamics. *Clin. Endocrinol. (Oxf).* **52**, 329–338 (2000).
242. Marcocci, C., Cianferotti, L. & Cetani, F. Bone disease in primary hyperparathyrodism. *Therapeutic Advances in Musculoskeletal Disease* vol. 4 357–368 (2012).
243. Rauner, M., Sipos, W. & Pietschmann, P. Age-dependent Wnt gene expression in bone and during the course of osteoblast differentiation. *Age (Omaha).* **30**, 273–282 (2008).
244. Becerikli, M. *et al.* Age-dependent alterations in osteoblast and osteoclast activity in human cancellous bone. *J. Cell. Mol. Med.* **21**, 2773–2781 (2017).
245. Almeida, M., Han, L., Martin-Millan, M., O'Brien, C. A. & Manolagas, S. C. Oxidative stress antagonizes Wnt signaling in osteoblast precursors by diverting β-catenin from T cell factor- to forkhead box O-mediated transcription. *J. Biol. Chem.* **282**, 27298–27305 (2007).
246. Monteiro, R. & Azevedo, I. Chronic Inflammation in Obesity and the Metabolic Syndrome. *Mediators Inflamm.* **2010**, 1–10 (2010).
247. Ueda, Y. *et al.* Induction of Senile Osteoporosis in Normal Mice by Intra-Bone Marrow-Bone Marrow Transplantation from Osteoporosis-Prone Mice. *Stem Cells* **25**, 1356–1363 (2007).
248. Kveiborg, M., Rattan, S. I. S., Clark, B. F. C., Eriksen, E. F. & Kassem, M. Treatment with 1,25-dihydroxyvitamin D3 reduces impairment of human osteoblast functions during cellular aging in culture. *J. Cell. Physiol.* **186**, 298–306 (2001).
249. Baxter, M. A. Study of Telomere Length Reveals Rapid Aging of Human Marrow Stromal Cells following In Vitro Expansion. *Stem Cells* **22**, 675–682 (2004).
250. Saeed, H. *et al.* Telomerase-deficient mice exhibit bone loss owing to defects in osteoblasts and increased osteoclastogenesis by inflammatory microenvironment. *J. Bone Miner. Res.* **26**, 1494–1505 (2011).
251. Pignolo, R. J. *et al.* Defects in telomere maintenance molecules impair osteoblast differentiation and promote osteoporosis. *Aging Cell* **7**, 23–31 (2008).
252. Kim, H. N. *et al.* DNA damage and senescence in osteoprogenitors expressing Osx1 may cause their decrease with age. *Aging Cell* **16**, 693–703 (2017).
253. Chen, Q. *et al.* DNA damage drives accelerated bone aging via an NF- κ B-

dependent mechanism. *J. Bone Miner. Res.* **28**, 1214–1228 (2013).
254. Clunie, G. & Horwood, N. Loss and gain of bone in spondyloarthritis: what drives theseopposing clinical features? *Ther. Adv. Musculoskelet. Dis.* **12**, (2020).
255. Briot, K. & Roux, C. Inflammation, bone loss and fracture risk in spondyloarthritis. *RMD Open* **1**, e000052 (2015).
256. Goldring, S. R. & Gravallese, E. M. Mechanisms of bone loss in inflammatory arthritis: Diagnosis and therapeutic implications. *Arthritis Res.* **2**, 33–37 (2000).
257. Llorente, I., García-Castañeda, N., Valero, C., González-Álvaro, I. & Castañeda, S. Osteoporosis in Rheumatoid Arthritis: Dangerous Liaisons. *Front. Med.* **7**, 802 (2020).
258. Coury, F., Peyruchaud, O. & Machuca-Gayet, I. Osteoimmunology of bone loss in inflammatory rheumatic diseases. *Front. Immunol.* **10**, 679 (2019).
259. Polzer, K. *et al.* Interleukin-1 is essential for systemic inflammatory bone loss. *Ann. Rheum. Dis.* **69**, 284–290 (2010).
260. Lee, Y. M., Fujikado, N., Manaka, H., Yasuda, H. & Iwakura, Y. IL-1 plays an important role in the bone metabolism under physiological conditions. *Int. Immunol.* **22**, 805–816 (2010).
261. Li, X., Zhou, Z. Y., Zhang, Y. Y. & Yang, H. L. IL-6 Contributes to the Defective Osteogenesis of Bone Marrow Stromal Cells from the Vertebral Body of the Glucocorticoid-Induced Osteoporotic Mouse. *PLoS One* **11**, 154677 (2016).
262. Harmer, D., Falank, C. & Reagan, M. R. Interleukin-6 Interweaves the Bone Marrow Microenvironment, Bone Loss, and Multiple Myeloma. *Front. Endocrinol. (Lausanne).* **9**, (2018).
263. Zhao, B., Grimes, S. N., Li, S., Hu, X. & Ivashkiv, L. B. TNF-induced osteoclastogenesis and inflammatory bone resorption are inhibited by transcription factor RBP-J. *J. Exp. Med.* **209**, 319–334 (2012).
264. Zhao, B. Does TNF Promote or Restrain Osteoclastogenesis and Inflammatory Bone Resorption? *Crit. Rev. Immunol.* **38**, 253 (2018).
265. Steffen, U., Schett, G. & Bozec, A. How autoantibodies regulate osteoclast induced bone loss in rheumatoid arthritis. *Front. Immunol.* **10**, 1483 (2019).
266. Titanji, K. Beyond Antibodies: B Cells and the OPG/RANK-RANKL Pathway in Health, Non-HIV Disease and HIV-Induced Bone Loss. *Front. Immunol.* **8**, 1 (2017).
267. Takayanagi, H. *et al.* T-cell-mediated regulation of osteoclastogenesis by signalling cross-talk between RANKL and IFN-gamma. *Nature* **408**, 600–605 (2000).
268. Kawai, T. *et al.* B and T Lymphocytes Are the Primary Sources of RANKL in the Bone Resorptive Lesion of Periodontal Disease. *Am. J. Pathol.* **169**, 987 (2006).
269. Lencel, P. & Magne, D. Inflammaging: The driving force in osteoporosis? *Med. Hypotheses* **76**, 317–321 (2011).
270. Josephson, A. M. *et al.* Age-related inflammation triggers skeletal stem/ progenitor cell dysfunction. *Proc. Natl. Acad. Sci. U. S. A.* **116**, 6995–7004 (2019).
271. Liang, W. & Chikritzhs, T. The Effect of Age on Fracture Risk: A Population-Based Cohort Study. *J. Aging Res.* **2016**, (2016).
272. Franic, D. & Verdenik, I. Risk factors for osteoporosis in postmenopausal

women -from the point of view of primary care gynecologist. *Zdr. Varst.* **57**, 33–38 (2018).
273. Mayer, S. W., Joyner, P. W., Almekinders, L. C. & Parekh, S. G. Stress Fractures of the Foot and Ankle in Athletes. *Sports Health* **6**, 481–491 (2014).
274. Astur, D. C. *et al.* Stress fractures: definition, diagnosis and treatment. *Rev. Bras. Ortop. (English Ed.* **51**, 3–10 (2016).
275. Oryan, A., Monazzah, S. & Bigham-Sadegh, A. Bone injury and fracture healing biology. *Biomedical and Environmental Sciences* vol. 28 57–71 (2015).
276. Kolar, P. *et al.* The early fracture hematoma and its potential role in fracture healing. *Tissue Engineering - Part B: Reviews* vol. 16 427–434 (2010).
277. Kolar, P., Gaber, T., Perka, C., Duda, G. N. & Buttgereit, F. Human early fracture hematoma is characterized by inflammation and hypoxia. in *Clinical Orthopaedics and Related Research* vol. 469 3118–3126 (Springer New York LLC, 2011).
278. Schell, H. *et al.* The haematoma and its role in bone healing. *J. Exp. Orthop.* **4**, (2017).
279. Stefanowski, J. *et al.* Spatial Distribution of Macrophages During Callus Formation and Maturation Reveals Close Crosstalk Between Macrophages and Newly Forming Vessels. *Front. Immunol.* **10**, (2019).
280. Vi, L. *et al.* Macrophages Promote Osteoblastic Differentiation In Vivo: Implications in Fracture Repair and Bone Homeostasis. *J. Bone Miner. Res.* **30**, 1090–1102 (2015).
281. Kon, T. *et al.* Expression of osteoprotegerin, receptor activator of NF-κB ligand (osteoprotegerin ligand) and related proinflammatory cytokines during fracture healing. *J. Bone Miner. Res.* **16**, 1004–1014 (2001).
282. Currie, H. N., Loos, M. S., Vrana, J. A., Dragan, K. & Boyd, J. W. Spatial cytokine distribution following traumatic injury. *Cytokine* **66**, 112–118 (2014).
283. Gerstenfeld, L. *et al.* Impaired Fracture Healing in the Absence of TNF-α Signaling: The Role of TNF-α in Endochondral Cartilage Resorption. *J. Bone Miner. Res.* **18**, 1584–1592 (2003).
284. Glass, G. E. *et al.* TNF-α promotes fracture repair by augmenting the recruitment and differentiation of muscle-derived stromal cells. *Proc. Natl. Acad. Sci. U. S. A.* **108**, 1585–1590 (2011).
285. Kobayashi, K. *et al.* Tumor necrosis factor alpha stimulates osteoclast differentiation by a mechanism independent of the ODF/RANKL-RANK interaction. *J. Exp. Med.* **191**, 275–86 (2000).
286. Karnes, J. M., Daffner, S. D. & Watkins, C. M. Multiple roles of tumor necrosis factor-alpha in fracture healing. *Bone* vol. 78 87–93 (2015).
287. Könnecke, I. *et al.* T and B cells participate in bone repair by infiltrating the fracture callus in a two-wave fashion. *Bone* **64**, 155–165 (2014).
288. Street, J. *et al.* Vascular endothelial growth factor stimulates bone repair by promoting angiogenesis and bone turnover. *Proc. Natl. Acad. Sci. U. S. A.* **99**, 9656–9661 (2002).
289. Komatsu, D. E. & Hadjiargyrou, M. Activation of the transcription factor HIF-1 and its target genes, VEGF, HO-1, iNOS, during fracture repair. *Bone* **34**, 680–688 (2004).
290. Street, J. & Lenehan, B. Vascular endothelial growth factor regulates osteoblast survival - Evidence for an autocrine feedback mechanism. *J. Orthop.*

Surg. Res. **4**, 1–13 (2009).
291. Tsuji, K. *et al.* BMP2 activity, although dispensable for bone formation, is required for the initiation of fracture healing. *Nat. Genet.* **38**, 1424–1429 (2006).
292. United States. Congress. Office of Technology Assessment. *Hip fracture outcomes in people age fifty and over*. *Background paper / Office of Technology Assessment* (1994).
293. Cooper, C. *et al.* The crippling consequences of fractures and their impact on quality of life. in *American Journal of Medicine* vol. 103 (Elsevier Inc., 1997).
294. Panula, J. *et al.* Mortality and cause of death in hip fracture patients aged 65 or older - A population-based study. *BMC Musculoskelet. Disord.* **12**, 105 (2011).
295. Birkhäuser, M. Selektive Östrogen-Rezeptormodulatoren (SERMs) zur prävention und therapie der postmenopausalen osteoporose. *Ther. Umschau* **69**, 163–172 (2012).
296. Gambacciani, M. & Levancini, M. Hormone replacement therapy and the prevention of postmenopausal osteoporosis. *Przeglad Menopauzalny* vol. 13 213–220 (2014).
297. de Villiers, T. J. Selective estrogen receptor modulators in the treatment of osteoporosis: a review of the clinical evidence. *Clin. Investig. (Lond).* **1**, 719–724 (2011).
298. Hu, L. *et al.* Comparison of intramedullary nailing and plate fixation in distal tibial fractures with metaphyseal damage: A meta-analysis of randomized controlled trials. *Journal of Orthopaedic Surgery and Research* vol. 14 30 (2019).
299. Achten, J. *et al.* UK Fixation of Distal Tibia Fractures (UK FixDT): Protocol for a randomised controlled trial of 'locking' plate fixation versus intramedullary nail fixation in the treatment of adult patients with a displaced fracture of the distal tibia. *BMJ Open* **5**, e009162 (2015).
300. Giannoudis, P. V., Papakostidis, C. & Roberts, C. A review of the management of open fractures of the tibia and femur. *Journal of Bone and Joint Surgery - Series B* vol. 88 281–289 (2006).
301. National Institute of Health and Care Excellence. Overview | Bisphosphonates for treating osteoporosis | Guidance | NICE. *NICE Guidelines* https://www.nice.org.uk/guidance/TA464 (2019).
302. Russell, R. G. G., Mühlbauer, R. C., Bisaz, S., Williams, D. A. & Fleisch, H. The influence of pyrophosphate, condensed phosphates, phosphonates and other phosphate compounds on the dissolution of hydroxyapatite in vitro and on bone resorption induced by parathyroid hormone in tissue culture and in thyroparathyroidectomised rats. *Calcif. Tissue Res.* **6**, 183–196 (1970).
303. Rogers, M. J., Crockett, J. C., Coxon, F. P. & Mönkkönen, J. Biochemical and molecular mechanisms of action of bisphosphonates. *Bone* vol. 49 34–41 (2011).
304. Lin, J. H. Bisphosphonates: A review of their pharmacokinetic properties. *Bone* vol. 18 75–85 (1996).
305. Lin, J. H., Chen, I. W. & Duggan, D. E. Effects of dose, sex, and age on the disposition of alendronate, a potent antiosteolytic bisphosphonate, in rats. *Drug Metab. Dispos.* **20**, 473–8 (1992).
306. Lin, J. H., Duggan, D. E., Chen, I. W. & Ellsworth, R. L. Physiological disposition of alendronate, a potent anti-osteolytic bisphosphonate, in

laboratory animals. *Drug Metab. Dispos.* **19**, (1991).
307. Lin, J. H., Los, L. E., Ulm, E. H. & Duggan, D. E. Kinetic studies on the competition between famotidine and cimetidine in rats. Evidence of multiple renal secretory systems for organic cations. *Drug Metab. Dispos.* **16**, (1988).
308. Gertz, B. J., Holland, S. D., Kline, W. F., Matuszewski, B. K. & Porras, A. G. Clinical pharmacology of alendronate sodium. *Osteoporos. Int.* **3**, 13–16 (1993).
309. Khan, S. A. *et al.* Elimination and biochemical responses to intravenous alendronate in postmenopausal osteoporosis. *J. Bone Miner. Res.* **12**, 1700–1707 (1997).
310. Roelofs, A. J. *et al.* Influence of bone affinity on the skeletal distribution of fluorescently labeled bisphosphonates in vivo. *J. Bone Miner. Res.* **27**, 835–847 (2012).
311. Sato, M. *et al.* Bisphosphonate action. Alendronate localization in rat bone and effects on osteoclast ultrastructure. Bisphosphonate Action Alendronate Localization in Rat Bone and Effects on Osteoclast Ultrastructure. *J Clin Invest* **88**, 2095–2105 (1991).
312. Thompson, K., Rogers, M. J., Coxon, F. P. & Crockett, J. C. Cytosolic entry of bisphosphonate drugs requires acidification of vesicles after fluid-phase endocytosis. *Mol. Pharmacol.* **69**, 1624–1632 (2006).
313. Drake, M. T., Clarke, B. L. & Khosla, S. Bisphosphonates: Mechanism of action and role in clinical practice. *Mayo Clinic Proceedings* vol. 83 1032–1045 (2008).
314. Malwal, S. R. *et al.* Bisphosphonate-Generated ATP-Analogs Inhibit Cell Signaling Pathways. *J. Am. Chem. Soc.* **140**, 7568–7578 (2018).
315. Bégault, B., Anagnostopoulos, T. & Edelman, A. ATP-regulated chloride conductance in endoplasmic reticulum (ER)-enriched pig pancreas microsomes. *BBA - Biomembr.* **1152**, 319–327 (1993).
316. Abe, K. *et al.* Effects of bisphosphonates on osteoclastogenesis in RAW264.7 cells. *Int. J. Mol. Med.* **29**, 1007–1015 (2012).
317. Kaczmarczyk-Sedlak, I. *et al.* Effect of administration of etidronate and retinol on bone mechanical properties in ovariectomized rats. *Pharmacol. Reports* **57**, 203–211 (2005).
318. Lepola, V. T. *et al.* Bisphosphonates clodronate and etidronate in the prevention of ovariectomy-induced osteopenia in growing rats. *J. Bone Miner. Res.* **11**, 1508–1517 (1996).
319. Itoh, F. *et al.* Treatment effects of bisphosphonates on ovariectomy-induced osteopenia in rats: Comparison between clodronate and etidronate. *J. Bone Miner. Metab.* **17**, 252–258 (1999).
320. Campbell, I. A., Douglas, J. G., Francis, R. M., Prescott, R. J. & Reid, D. M. Five year study of etidronate and/or calcium as prevention and treatment for osteoporosis and fractures in patients with asthma receiving long term oral and/or inhaled glucocorticoids. *Thorax* **59**, 761–768 (2004).
321. Beauchesne, M. F. & Miller, P. F. Etidronate and alendronate in the treatment of postmenopausal osteoporosis. *Annals of Pharmacotherapy* vol. 33 587–599 (1999).
322. Herbert Fleisch. *Bisphosphonates in bone disease*. (The Parthenon Publishing Group, New York, 1997).

323. Fleisch, H. Bisphosphonates: Mechanisms of action. *Endocrine Reviews* vol. 19 80–100 (1998).
324. Ballantyne, E. “Bisphosphonates: Possible Modes of Action and Implications for Dental Implant Treatment. A Review of the Literature”. *J. Gen. Pract.* **03**, (2016).
325. Dunford, J. E. *et al.* Structure-activity relationships for inhibition of farnesyl diphosphate synthase in vitro and inhibition of bone resorption in vivo by nitrogen-containing bisphosphonates. *J. Pharmacol. Exp. Ther.* **296**, 235–242 (2001).
326. Kavanagh, K. L. *et al.* The molecular mechanism of nitrogen-containing bisphosphonates as antiosteoporosis drugs. *Proc. Natl. Acad. Sci. U. S. A.* **103**, 7829–7834 (2006).
327. Dunford, J. E., Rogers, M. J., Ebetino, F. H., Phipps, R. J. & Coxon, F. P. Inhibition of protein prenylation by bisphosphonates causes sustained activation of Rac, Cdc42, and Rho GTPases. *J. Bone Miner. Res.* **21**, 684–694 (2006).
328. Halasy-Nagy, J. M., Rodan, G. A. & Reszka, A. A. Inhibition of bone resorption by alendronate and risedronate does not require osteoclast apoptosis. *Bone* **29**, 553–559 (2001).
329. Liberman, U. A. *et al.* Effect of Oral Alendronate on Bone Mineral Density and the Incidence of Fractures in Postmenopausal Osteoporosis. *N. Engl. J. Med.* **333**, 1437–1444 (1995).
330. Harris, S. T. *et al.* Effects of risedronate treatment on vertebral and nonvertebral fractures in women with postmenopausal osteoporosis: A randomized controlled trial. *J. Am. Med. Assoc.* **282**, 1344–1352 (1999).
331. Black, D. M. *et al.* Randomised trial of effect of alendronate on risk of fracture in women with existing vertebral fractures. *Lancet* **348**, 1535–1541 (1996).
332. Black, D. M. *et al.* Fracture risk reduction with alendronate in women with osteoporosis: The fractureintervention trial. *J. Clin. Endocrinol. Metab.* **85**, 4118–4124 (2000).
333. Black, D. M. *et al.* Once-Yearly Zoledronic Acid for Treatment of Postmenopausal Osteoporosis. *N. Engl. J. Med.* **356**, 1809–1822 (2007).
334. Wells, G. A. *et al.* Risedronate for the primary and secondary prevention of osteoporotic fractures in postmenopausal women. *Cochrane Database Syst. Rev.* (2008) doi:10.1002/14651858.cd004523.pub3.
335. Allen, C. S., Yeung, J. H., Vandermeer, B. & Homik, J. Bisphosphonates for steroid-induced osteoporosis. *Cochrane Database of Systematic Reviews* vol. 2016 (2016).
336. Lyles, K. W. *et al.* Zoledronic Acid and Clinical Fractures and Mortality after Hip Fracture. *N. Engl. J. Med.* **357**, 1799–1809 (2007).
337. Rizzoli, R. Two-year results of once-weekly administration of alendronate 70 mg for the treatment of postmenopausal osteoporosis. *J. Bone Miner. Res.* **17**, 1988–1996 (2002).
338. Brown, J. P. *et al.* The efficacy and tolerability of risedronate once a week for the treatment of postmenopausal osteoporosis. *Calcif. Tissue Int.* **71**, 103–111 (2002).
339. Black, D. M. *et al.* Effects of continuing or stopping alendronate after 5 years of treatment: The Fracture Intervention Trial long-term extension (FLEX): A

randomized trial. *J. Am. Med. Assoc.* **296**, 2927–2938 (2006).
340. Rauch, F., Travers, R., Plotkin, H. & Glorieux, F. H. The effects of intravenous pamidronate on the bone tissue of children and adolescents with osteogenesis imperfecta. *J. Clin. Invest.* **110**, 1293–1299 (2002).
341. LeBlanc, A. *et al.* Bisphosphonates as a supplement to exercise to protect bone during long-duration spaceflight. *Osteoporos. Int.* **24**, 2105–2114 (2013).
342. Penning-van Beest, F. J. A., Goettsch, W. G., Erkens, J. A. & Herings, R. M. C. Determinants of persistence with bisphosphonates: A study in women with postmenopausal osteoporosis. *Clin. Ther.* **28**, 236–242 (2006).
343. Ettinger, B. Alendronate Use Among 812 Women: Prevalence of Gastrointestinal Complaints, Noncompliance with Patient Instructions, and Discontinuation. *J. Manag. Care Pharm.* **4**, 488–492 (1998).
344. Lin, J. H., Chen, I. -W & Deluna, F. A. On the absorption of alendronate in rats. *J. Pharm. Sci.* **83**, 1741–1746 (1994).
345. Park-Wyllie, L. Y. *et al.* Bisphosphonate use and the risk of subtrochanteric or femoral shaft fractures in older women. *JAMA - J. Am. Med. Assoc.* **305**, 783–789 (2011).
346. Alwahhabi, B. K. S. & Alsuwaine, B. A. Long-Term use of bisphosphonates in osteoporosis. *Saudi Med. J.* **38**, 604–608 (2017).
347. Kostenuik, P. J. *et al.* Denosumab, a Fully Human Monoclonal Antibody to RANKL, Inhibits Bone Resorption and Increases BMD in Knock-In Mice That Express Chimeric (Murine/Human) RANKL*. *J. Bone Miner. Res.* **24**, 182–195 (2009).
348. Overview | Denosumab for the prevention of osteoporotic fractures in postmenopausal women | Guidance | NICE.
349. Cummings, S. R. *et al.* Denosumab for Prevention of Fractures in Postmenopausal Women with Osteoporosis. *N. Engl. J. Med.* **361**, 756–765 (2009).
350. Yasuda, H. RANKL, a necessary chance for clinical application to osteoporosis and cancer-related bone diseases. *World J. Orthop.* **4**, 207–217 (2013).
351. Ominsky, M. S. *et al.* Denosumab, a fully human RANKL antibody, reduced bone turnover markers and increased trabecular and cortical bone mass, density, and strength in ovariectomized cynomolgus monkeys. *Bone* **49**, 162–173 (2011).
352. McClung, M. R. *et al.* Effect of denosumab on bone mineral density and biochemical markers of bone turnover: 8-year results of a phase 2 clinical trial. *Osteoporos. Int.* **24**, 227–235 (2013).
353. Stopeck, A. T. *et al.* Denosumab compared with zoledronic acid for the treatment of bone metastases in patients with advanced breast cancer: A randomized, double-blind study. *J. Clin. Oncol.* **28**, 5132–5139 (2010).
354. Anastasilakis, A. D., Toulis, K. A., Polyzos, S. A., Anastasilakis, C. D. & Makras, P. Long-term treatment of osteoporosis: Safety and efficacy appraisal of denosumab. *Therapeutics and Clinical Risk Management* vol. 8 295–306 (2012).
355. Morizio, P., Burkhart, J. I. & Ozawa, S. Denosumab: A Unique Perspective on Adherence and Cost-effectiveness Compared With Oral Bisphosphonates in Osteoporosis Patients. *Annals of Pharmacotherapy* vol. 52 1031–1041 (2018).
356. Freemantle, N. *et al.* Final results of the DAPS (Denosumab Adherence

Preference Satisfaction) study: a 24-month, randomized, crossover comparison with alendronate in postmenopausal women. *Osteoporos. Int.* **23**, 317–326 (2012).
357. Xie, J. *et al.* Calcitonin and Bone Physiology: In Vitro, in Vivo, and Clinical Investigations. *Int. J. Endocrinol.* **2020**, (2020).
358. Keller, J. *et al.* Calcitonin controls bone formation by inhibiting the release of sphingosine 1-phosphate from osteoclasts. *Nat. Commun.* **5**, 1–13 (2014).
359. Arvinte, T. & Drake, A. F. Comparative study of human and salmon calcitonin secondary structure in solutions with low dielectric constants. *J. Biol. Chem.* **268**, 6408–6414 (1993).
360. Bhandari, K. H., Newa, M., Chapman, J. & Doschak, M. R. Synthesis, characterization and evaluation of bone targeting salmon calcitonin analogs in normal and osteoporotic rats. *J. Control. Release* **158**, 44–52 (2012).
361. Mochizuki, K. & Inoue, T. Effect of salmon calcitonin on experimental osteoporosis induced by ovariectomy and low-calcium diet in the rat. *J. Bone Miner. Metab.* **18**, 194–207 (2000).
362. Wei, J., Wang, J., Gong, Y. & Zeng, R. Effectiveness of combined salmon calcitonin and aspirin therapy for osteoporosis in ovariectomized rats. *Mol. Med. Rep.* **12**, 1717–1726 (2015).
363. Geusens, P. *et al.* Effect of salmon calcitonin on femoral bone quality in adult ovariectomized ewes. *Calcif. Tissue Int.* **59**, 315–320 (1996).
364. Reginster, J. Y. *et al.* Long-term (3 years) prevention of trabecular postmenopausal bone loss with low-dose intermittent nasal salmon calcitonin. *J. Bone Miner. Res.* **9**, 69–73 (2009).
365. Reginster, J. Y., Neuprez, A., Hiligsmann, M. & Bruyère, O. Oral calcitonin in the management of osteoarthritis: Hope or fantasy? *International Journal of Clinical Rheumatology* vol. 5 53–58 (2010).
366. Plosker, G. L. & McTavish, D. Intranasal Salcatonin (Salmon Calcitonin): A Review of its Pharmacological Properties and Role in the Management of Postmenopausal Osteoporosis. *Drugs and Aging* vol. 8 378–400 (1996).
367. Overman, R. A., Borse, M. & Gourlay, M. L. *Salmon Calcitonin Use and Associated Cancer Risk*. *Annals of Pharmacotherapy* vol. 47 1675–1684 (2013).
368. Masarachia, P. J. *et al.* Odanacatib reduces bone turnover and increases bone mass in the lumbar spine of skeletally mature ovariectomized rhesus monkeys. *J. Bone Miner. Res.* **27**, 509–523 (2012).
369. Chapurlat, R. D. Odanacatib: A review of its potential in the management of osteoporosis in postmenopausal women. *Therapeutic Advances in Musculoskeletal Disease* vol. 7 103–109 (2015).
370. Eisman, J. A. *et al.* Odanacatib in the treatment of postmenopausal women with low bone mineral density: Three-year continued therapy and resolution of effect. *J. Bone Miner. Res.* **26**, 242–251 (2011).
371. Bone, H. G. *et al.* Odanacatib, a cathepsin-K inhibitor for osteoporosis: A two-year study in postmenopausal women with low bone density. *J. Bone Miner. Res.* **25**, 937–947 (2010).
372. Mullard, A. Merck & Co. drops osteoporosis drug odanacatib. *Nat. Rev. Drug Discov.* **15**, 669–670 (2016).
373. Niikura, K., Takeshita, N. & Takano, M. A Vacuolar ATPase Inhibitor,

FR167356, Prevents Bone Resorption in Ovariectomized Rats With High Potency and Specificity: Potential for Clinical Application. *J. Bone Miner. Res.* **20**, 1579–1588 (2005).
374. Visentin, L. *et al.* A selective inhibitor of the osteoclastic V-H+-ATPase prevents bone loss in both thyroparathyroidectomized and ovariectomized rats. *J. Clin. Invest.* **106**, 309–318 (2000).
375. Ominsky, M. S. *et al.* Romosozumab Improves Bone Mass and Strength While Maintaining Bone Quality in Ovariectomized Cynomolgus Monkeys. *J. Bone Miner. Res.* **32**, 788–801 (2017).
376. Cosman, F. *et al.* Romosozumab Treatment in Postmenopausal Women with Osteoporosis. *N. Engl. J. Med.* **375**, 1532–1543 (2016).
377. Miyauchi, A. *et al.* Increased bone mineral density for 1 year of romosozumab, vs placebo, followed by 2 years of denosumab in the Japanese subgroup of the pivotal FRAME trial and extension. *Arch. Osteoporos.* **14**, 59 (2019).
378. Didangelos, A. *et al.* Proteomics characterization of extracellular space components in the human aorta. *Mol. Cell. Proteomics* **9**, 2048–2062 (2010).
379. Saag, K. G. *et al.* Romosozumab or Alendronate for Fracture Prevention in Women with Osteoporosis. *N. Engl. J. Med.* **377**, 1417–1427 (2017).
380. Bonnelye, E., Chabadel, A., Saltel, F. & Jurdic, P. Dual effect of strontium ranelate: Stimulation of osteoblast differentiation and inhibition of osteoclast formation and resorption in vitro. *Bone* **42**, 129–138 (2008).
381. Rybchyn, M. S., Slater, M., Conigrave, A. D. & Mason, R. S. An Akt-dependent increase in canonical Wnt signaling and a decrease in sclerostin protein levels are involved in strontium ranelate-induced osteogenic effects in human osteoblasts. *J. Biol. Chem.* **286**, 23771–23779 (2011).
382. Delannoy, P., Bazot, D. & Marie, P. J. Long-term treatment with strontium ranelate increases vertebral bone mass without deleterious effect in mice. *Metabolism.* **51**, 906–911 (2002).
383. Lavet, C., Mabilleau, G., Chappard, D., Rizzoli, R. & Ammann, P. Strontium ranelate stimulates trabecular bone formation in a rat tibial bone defect healing process. *Osteoporos. Int.* **28**, 3475–3487 (2017).
384. Bain, S. D., Jerome, C., Shen, V., Dupin-Roger, I. & Ammann, P. Strontium ranelate improves bone strength in ovariectomized rat by positively influencing bone resistance determinants. *Osteoporos. Int.* **20**, 1417–1428 (2009).
385. Meunier, P., Aaron, J., Edouard, C. & Vignon, G. Osteoporosis and the replacement of cell populations of the marrow by adipose tissue. A quantitative study of 84 iliac bone biopsies. *Clin. Orthop. Relat. Res.* **80**, 147–154 (1971).
386. Kaufman, J.-M. *et al.* Efficacy and Safety of Strontium Ranelate in the Treatment of Osteoporosis in Men. *J. Clin. Endocrinol. Metab.* **98**, 592–601 (2013).
387. Reginster, J. Y. *et al.* Maintenance of antifracture efficacy over 10 years with strontium ranelate in postmenopausal osteoporosis. *Osteoporos. Int.* **23**, 1115–1122 (2012).
388. O'Donnell, S., Cranney, A., Wells, G., Adachi, J. & Reginster, J. Strontium ranelate for preventing and treating postmenopausal osteoporosis. in *Cochrane Database of Systematic Reviews* (ed. Cranney, A.) (John Wiley & Sons, Ltd, 2006).
389. Boivin, G. *et al.* In osteoporotic women treated with strontium ranelate,

strontium is located in bone formed during treatment with a maintained degree of mineralization. *Osteoporos. Int.* **21**, 667–677 (2010).
390. Pors Nielsen, S. *et al.* Influence of strontium on bone mineral density and bone mineral content measurements by dual X-ray absorptiometry. *J. Clin. Densitom.* **2**, 371–379 (1999).
391. Osagie-Clouard, L. *et al.* Parathyroid hormone 1-34 and skeletal anabolic action. *Bone Joint Res.* **6**, 14–21 (2017).
392. Silva, B. C. & Bilezikian, J. P. Parathyroid hormone: anabolic and catabolic actions on the skeleton. *Curr. Opin. Pharmacol.* **22**, 41 (2015).
393. Ishizuya, T. *et al.* Parathyroid hormone exerts disparate effects on osteoblast differentiation depending on exposure time in rat osteoblastic cells. *J. Clin. Invest.* **99**, 2961–2970 (1997).
394. Schiller, P. C., D'Ippolito, G., Roos, B. A. & Howard, G. A. Anabolic or Catabolic Responses of MC3T3-E1 Osteoblastic Cells to Parathyroid Hormone Depend on Time and Duration of Treatment. *J. Bone Miner. Res.* **14**, 1504–1512 (1999).
395. Yamashita, J. & McCauley, L. K. Effects of Intermittent Administration of Parathyroid Hormone and Parathyroid Hormone-Related Protein on Fracture Healing: A Narrative Review of Animal and Human Studies. *JBMR Plus* **3**, (2019).
396. Iida-Klein, A. *et al.* Short-term continuous infusion of human parathyroid hormone 1-34 fragment is catabolic with decreased trabecular connectivity density accompanied by hypercalcemia in C57BL/J6 mice. *J. Endocrinol.* **186**, 549–557 (2005).
397. Dobnig, H. & Turner, R. T. The effects of programmed administration of human parathyroid hormone fragment (1-34) on bone histomorphometry and serum chemistry in rats. *Endocrinology* **138**, 4607–4612 (1997).
398. Watanabe, A. *et al.* Effect of dosing frequency of teriparatide (PTH 1-34) on bone formation in rats: Comparison of bone metabolism marker levels. *J. Toxicol. Sci.* **43**, 435–442 (2018).
399. Andersson, N., Lindberg, M. K., Ohlsson, C., Andersson, K. & Ryberg, B. Repeated in vivo determinations of bone mineral density during parathyroid hormone treatment in ovariectomized mice. *J. Endocrinol.* **170**, 529–537 (2001).
400. Burr, D. B. *et al.* Intermittently administered human parathyroid hormone(1-34) treatment increases intracortical bone turnover and porosity without reducing bone strength in the humerus of ovariectomized cynomolgus monkeys. *J. Bone Miner. Res.* **16**, 157–165 (2001).
401. Brouwers, J. E. M., Van Rietbergen, B., Huiskes, R. & Ito, K. Effects of PTH treatment on tibial bone of ovariectomized rats assessed by in vivo micro-CT. *Osteoporos. Int.* **20**, 1823–1835 (2009).
402. Takakura, A. *et al.* Administration frequency as well as dosage of PTH are associated with development of cortical porosity in ovariectomized rats. *Bone Res.* **5**, 1–14 (2017).
403. Neer, R. M. *et al.* Effect of Parathyroid Hormone (1-34) on Fractures and Bone Mineral Density in Postmenopausal Women with Osteoporosis. *N. Engl. J. Med.* **344**, 1434–1441 (2001).
404. Barbehenn, E. K. & Lurie, P. D. Osteosarcoma risk in rats using PTH 1-34.

Trends in endocrinology and metabolism: TEM vol. 12 383 (2001).
405. Karatoprak, C. *et al.* Severe hypercalcemia due to teriparatide. *Indian J. Pharmacol.* **44**, 270–271 (2012).
406. Leder, B. Z. Optimizing Sequential and Combined Anabolic and Antiresorptive Osteoporosis Therapy. *JBMR Plus* **2**, 62–68 (2018).
407. Black, D. M. *et al.* One Year of Alendronate after One Year of Parathyroid Hormone (1–84) for Osteoporosis. *N. Engl. J. Med.* **353**, 555–565 (2005).
408. Arita, Y. *et al.* Paradoxical decrease of an adipose-specific protein, adiponectin, in obesity. *Biochem. Biophys. Res. Commun.* **257**, 79–83 (1999).
409. Hotta, K. *et al.* Plasma concentrations of a novel, adipose-specific protein, adiponectin, in type 2 diabetic patients. *Arterioscler. Thromb. Vasc. Biol.* **20**, 1595–1599 (2000).
410. Scherer, P. E., Williams, S., Fogliano, M., Baldini, G. & Lodish, H. F. A novel serum protein similar to C1q, produced exclusively in adipocytes. *J. Biol. Chem.* **270**, 26746–26749 (1995).
411. Fruebis, J. *et al.* Proteolytic cleavage product of 30-kDa adipocyte complement-related protein increases fatty acid oxidation in muscle and causes weight loss in mice. *Proc. Natl. Acad. Sci.* **98**, 2005–2010 (2012).
412. Mangge, H. *et al.* Preatherosclerosis and adiponectin subfractions in obese adolescents. *Obesity* **16**, 2578–2584 (2008).
413. Waki, H. *et al.* Impaired multimerization of human adiponectin mutants associated with diabetes. Molecular structure and multimer formation of adiponectin. *J. Biol. Chem.* **278**, 40352–40363 (2003).
414. Hada, Y. *et al.* Selective purification and characterization of adiponectin multimer species from human plasma. *Biochem. Biophys. Res. Commun.* **356**, 487–493 (2007).
415. Cawthorn, W. P. *et al.* Bone marrow adipose tissue is an endocrine organ that contributes to increased circulating adiponectin during caloric restriction. *Cell Metab.* **20**, 368–375 (2014).
416. Suchacki, K. J. *et al.* Bone marrow adipose tissue is a unique adipose subtype with distinct roles in glucose homeostasis. *Nat. Commun.* **11**, (2020).
417. L Newton, A., J Hanks, L., Davis, M. & Casazza, K. The relationships among total body fat, bone mineral content and bone marrow adipose tissue in early-pubertal girls. *Bonekey Rep.* **2**, (2013).
418. Yamauchi, T. *et al.* Cloning of adiponectin receptors that mediate antidiabetic metabolic effects. *Nature* **423**, 762–769 (2003).
419. Yamauchi, T., Iwabu, M., Okada-Iwabu, M. & Kadowaki, T. Adiponectin receptors: A review of their structure, function and how they work. *Best Pract. Res. Clin. Endocrinol. Metab.* **28**, 15–23 (2014).
420. Kadowaki, T. & Yamauchi, T. Adiponectin Receptor Signaling: A New Layer to the Current Model. *Cell Metab.* **13**, 123–124 (2011).
421. Holland, W. L. *et al.* Receptor-mediated activation of ceramidase activity initiates the pleiotropic actions of adiponectin. *Nat. Med.* **17**, 55–63 (2011).
422. Obeid, S. & Hebbard, L. Role of adiponectin and its receptors in cancer. *Cancer Biol. Med.* **9**, 213–220 (2012).
423. Wu, Y. *et al.* Genome-wide association study for adiponectin levels in filipino women identifies CDH13 and a novel uncommon haplotype at KNG1-ADIPOQ. *Hum. Mol. Genet.* **19**, 4955–4964 (2010).

424. Hug, C. *et al.* T-cadherin is a receptor for hexameric and high-molecular-weight forms of Acrp30/adiponectin. *Proc. Natl. Acad. Sci. U. S. A.* **101**, 10308–10313 (2004).
425. Yamauchi, T. *et al.* Targeted disruption of AdipoR1 and AdipoR2 causes abrogation of adiponectin binding and metabolic actions. *Nat. Med.* **13**, 332–339 (2007).
426. Ramasamy, S. K. Structure and Functions of Blood Vessels and Vascular Niches in Bone. *Stem Cells Int.* **2017**, 1–10 (2017).
427. Kamada, A. *et al.* Gene Expression of Adiponectin Receptors during Osteoblastic Differentiation. *J Oral Tissue Engin* **15**, 102–108 (2017).
428. Hyun, W. L. *et al.* Adiponectin stimulates osteoblast differentiation through induction of COX2 in mesenchymal progenitor cells. *Stem Cells* **27**, 2254–2262 (2009).
429. Pacheco-Pantoja, E. L., Fraser, W. D., Wilson, P. J. M. & Gallagher, J. A. Differential effects of adiponectin in osteoblast-like cells. *J. Recept. Signal Transduct.* **34**, 351–360 (2014).
430. Pang, T. T. L. *et al.* Inhibition of Islet Immunoreactivity by Adiponectin Is Attenuated in Human Type 1 Diabetes. *J. Clin. Endocrinol. Metab.* **98**, E418–E428 (2013).
431. Pacheco-Pantoja, E. L., Waring, V. J., Wilson, P. J. M., Fraser, W. D. & Gallagher, J. A. Adiponectin receptors are present in RANK-L-induced multinucleated osteoclast-like cells. *J. Recept. Signal Transduct.* **33**, 291–297 (2013).
432. Berner, H. S. *et al.* Adiponectin and its receptors are expressed in bone-forming cells. *Bone* **35**, 842–849 (2004).
433. Fazeli, P. K. *et al.* Marrow fat and bone-new perspectives. *J. Clin. Endocrinol. Metab.* **98**, 935–945 (2013).
434. DiMascio, L. *et al.* Identification of adiponectin as a novel hemopoietic stem cell growth factor. *J. Immunol.* **178**, 3511–20 (2007).
435. Wu, X., Huang, L. & Liu, J. Effects of adiponectin on osteoclastogenesis from mouse bone marrow-derived monocytes. *Exp. Ther. Med.* **17**, 1228 (2018).
436. Lin, Y. Y. *et al.* Adiponectin receptor 1 regulates bone formation and osteoblast differentiation by GSK-3β/β-Catenin signaling in mice. *Bone* **64**, 147–154 (2014).
437. Kajimura, D. *et al.* Adiponectin regulates bone mass via opposite central and peripheral mechanisms through foxo1. *Cell Metab.* **17**, 901–915 (2013).
438. Oshima, K. *et al.* Adiponectin increases bone mass by suppressing osteoclast and activating osteoblast. *Biochem. Biophys. Res. Commun.* **331**, 520–526 (2005).
439. Chen, T., Wu, Y. W., Lu, H., Guo, Y. & Tang, Z. H. Adiponectin enhances osteogenic differentiation in human adipose-derived stem cells by activating the APPL1-AMPK signaling pathway. *Biochem. Biophys. Res. Commun.* **461**, 237–242 (2015).
440. Wu, Y. *et al.* Central adiponectin administration reveals new regulatory mechanisms of bone metabolism in mice. *Am. J. Physiol. Metab.* **306**, E1418–E1430 (2014).
441. Ye, L. *et al.* Histone demethylases KDM4B and KDM6B promotes osteogenic differentiation of human MSCs. *Cell Stem Cell* **11**, 50–61 (2012).

442. Tu, Q. *et al.* Adiponectin inhibits osteoclastogenesis and bone resorption via APPL1-mediated suppression of Akt1. *J. Biol. Chem.* **286**, 12542–12553 (2011).
443. Yu, L. *et al.* Adiponectin Regulates Bone Marrow Mesenchymal Stem Cell Niche Through a Unique Signal Transduction Pathway: An Approach for Treating Bone Disease in Diabetes. *Stem Cells* **33**, 240–252 (2015).
444. Park, D. *et al.* Endogenous bone marrow MSCs are dynamic, fate-restricted participants in bone maintenance and regeneration. *Cell Stem Cell* **10**, 259–272 (2012).
445. Döring, Y., Pawig, L., Weber, C. & Noels, H. The CXCL12/CXCR4 chemokine ligand/receptor axis in cardiovascular disease. *Front. Physiol.* **5 JUN**, (2014).
446. Colnot, C. Skeletal cell fate decisions within periosteum and bone marrow during bone regeneration. *J. Bone Miner. Res.* **24**, 274–282 (2009).
447. Michaud, J., Im, D.-S. & Hla, T. Inhibitory Role of Sphingosine 1-Phosphate Receptor 2 in Macrophage Recruitment during Inflammation. *J. Immunol.* **184**, 1475–1483 (2010).
448. Sartawi, Z., Schipani, E., Ryan, K. B. & Waeber, C. Sphingosine 1-phosphate (S1P) signalling: Role in bone biology and potential therapeutic target for bone repair. *Pharmacol. Res.* **125**, 232–245 (2017).
449. Meshcheryakova, A., Mechtcheriakova, D. & Pietschmann, P. Sphingosine 1-phosphate signaling in bone remodeling: multifaceted roles and therapeutic potential. *Expert Opin. Ther. Targets* **21**, 725–737 (2017).
450. Aneka Sowman, Sam Olechnowicz & James Edwards. OC9: Sarcopenia is negatively related to osteogenic impacts achieved through habitual physical activity: findings from a population-based cohort of older females,Bone Research Society, Annual Meeting 2017 Proceedings. 25-27 June 2017, Bristol, UK. in *Journal of musculoskeletal & neuronal interactions* vol. 18 108–151 (NLM (Medline), 2018).
451. Justesen, J. *et al. Adipocyte tissue volume in bone marrow is increased with aging and in patients with osteoporosis*. *Biogerontology* vol. 2 165–171 (2001).
452. Li, G. W. *et al.* Quantitative evaluation of vertebral marrow adipose tissue in postmenopausal female using MRI chemical shift-based water-fat separation. *Clin. Radiol.* **69**, 254–262 (2014).
453. Syed, F. A. *et al.* Effects of estrogen therapy on bone marrow adipocytes in postmenopausal osteoporotic women. *Osteoporos. Int.* **19**, 1323–1330 (2008).
454. Jürimäe, J. & Jürimäe, T. Adiponectin is a predictor of bone mineral density in middle-aged premenopausal women. *Osteoporos. Int.* **18**, 1253–1259 (2007).
455. Wang, F. *et al.* Deficiency of Adiponectin Protects against Ovariectomy-Induced Osteoporosis in Mice. *PLoS One* **8**, e68497 (2013).
456. Luo, E. *et al.* Sustained release of adiponectin improves osteogenesis around hydroxyapatite implants by suppressing osteoclast activity in ovariectomized rabbits. *Acta Biomater.* **8**, 734–743 (2012).
457. Rinotas, V. & Douni, E. Molecular Interaction of BMAT with Bone. *Curr. Mol. Biol. Reports* **4**, 34–40 (2018).
458. Mauro, L. *et al.* Estrogen receptor-α drives adiponectin effects on cyclin D1 expression in breast cancer cells. *FASEB J.* **29**, 2150–2160 (2015).
459. Mohamed, M. K. & Abdel-Rahman, A. A. Effect of long-term ovariectomy and estrogen replacement on the expression of estrogen receptor gene in female

rats. *Eur. J. Endocrinol.* **142**, 307–314 (2000).
460. Wong, S. Y. P., Kariks, J., Evans, R. A., Dunstan, C. R. & Hills, E. The effect of age on bone composition and viability in the femoral head. *J. Bone Jt. Surg.* **67**, 274–283 (1985).
461. Tan, C. O. *et al.* Adiponectin is associated with bone strength and fracture history in paralyzed men with spinal cord injury. *Osteoporos. Int.* **25**, 2599–2607 (2014).
462. Bacchetta, J. *et al.* The relationship between adipokines, osteocalcin and bone quality in chronic kidney disease. *Nephrol. Dial. Transplant.* **24**, 3120–3125 (2009).
463. Haugen, S. *et al.* Adiponectin reduces bone stiffness: Verified in a three-dimensional artificial human bone model In Vitro. *Front. Endocrinol. (Lausanne).* **9**, 236 (2018).
464. Lewis, J. W., Edwards, J. R., Naylor, A. J. & McGettrick, H. M. Adiponectin signalling in bone homeostasis, with age and in disease. *Bone Research* vol. 9 1–11 (2021).
465. Li, C. *et al.* Homing of bone marrow mesenchymal stem cells mediated by sphingosine 1-phosphate contributes to liver fibrosis. *J. Hepatol.* **50**, 1174–1183 (2009).
466. Granero-Moltó, F. *et al.* Regenerative effects of transplanted mesenchymal stem cells in fracture healing. *Stem Cells* **27**, 1887–1898 (2009).
467. Asiedu, K. O. *et al.* Bone marrow cell homing to sites of acute tibial fracture: 89 Zr-oxine cell labeling with positron emission tomographic imaging in a mouse model. *EJNMMI Res.* **8**, 1–11 (2018).
468. Yang, L. *et al.* Sphingosine 1-Phosphate Receptor 2 and 3 Mediate Bone Marrow-Derived Monocyte/Macrophage Motility in Cholestatic Liver Injury in Mice. *Sci. Rep.* **5**, 13423 (2015).
469. Xiao, L., Zhou, Y., Friis, T., Beagley, K. & Xiao, Y. S1p-S1PR1 signaling: The "Sphinx" in osteoimmunology. *Frontiers in Immunology* vol. 10 1409 (2019).
470. Daum, G. *et al.* Determinants of Serum- and Plasma Sphingosine-1-Phosphate Concentrations in a Healthy Study Group. *TH Open* **04**, e12–e19 (2020).
471. Murata, N. *et al.* Interaction of sphingosine 1-phosphate with plasma components, including lipoproteins, regulates the lipid receptor-mediated actions. *Biochem. J.* **352**, 809–815 (2000).
472. Swan, D. J., Kirby, J. A. & Ali, S. Vascular biology: the role of sphingosine 1-phosphate in both the resting state and inflammation. *J. Cell. Mol. Med.* **14**, 2211–2222 (2010).
473. Chimen, M. *et al.* Homeostatic regulation of T cell trafficking by a B cell-derived peptide is impaired in autoimmune and chronic inflammatory disease. *Nat. Med.* **21**, 467–475 (2015).
474. Mendelson, K., Evans, T. & Hla, T. Sphingosine 1-phosphate signalling. *Dev.* **141**, 5–9 (2014).
475. Hait, N. C. & Maiti, A. The Role of Sphingosine-1-Phosphate and Ceramide-1-Phosphate in Inflammation and Cancer. *Mediators Inflamm.* **2017**, 1–17 (2017).
476. Hisano, Y., Nishi, T. & Kawahara, A. The functional roles of S1P in immunity. *J. Biochem.* **152**, 305–311 (2012).
477. Van Brocklyn, J. R. *et al.* Dual actions of sphingosine-1-phosphate: Extracellular through the G(i)- coupled receptor Edg-1 and intracellular to

regulate proliferation and survival. *J. Cell Biol.* **142**, 229–240 (1998).
478. Yamazaki, Y. *et al.* Edg-6 as a putative sphingosine 1-phosphate receptor coupling to Ca(2+) signaling pathway. *Biochem. Biophys. Res. Commun.* **268**, 583–589 (2000).
479. Malek, R. L. *et al.* Nrg-1 belongs to the endothelial differentiation gene family of G protein-coupled sphingosine-1-phosphate receptors. *J. Biol. Chem.* **276**, 5692–5699 (2001).
480. Im, D. S. *et al.* Characterization of a novel sphingosine 1-phosphate receptor, Edg-8. *J. Biol. Chem.* **275**, 14281–14286 (2000).
481. Tantikanlayaporn, D. *et al.* Sphingosine-1-Phosphate Modulates the Effect of Estrogen in Human Osteoblasts. *JBMR Plus* **2**, 217–226 (2018).
482. Ishii, M. & Kikuta, J. Sphingosine-1-phosphate signaling controlling osteoclasts and bone homeostasis. *Biochimica et Biophysica Acta - Molecular and Cell Biology of Lipids* vol. 1831 223–227 (2013).
483. Ishii, M. *et al.* Sphingosine-1-phosphate mobilizes osteoclast precursors and regulates bone homeostasis. *Nature* **458**, 524–528 (2009).
484. Ishii, M., Kikuta, J., Shimazu, Y., Meier-Schellersheim, M. & Germain, R. N. Chemorepulsion by blood S1P regulates osteoclast precursor mobilization and bone remodeling in vivo. *J. Exp. Med.* **207**, 2793–2798 (2010).
485. Higashi, K. *et al.* Sphingosine-1-phosphate/S1PR2-mediated signaling triggers Smad1/5/8 phosphorylation and thereby induces Runx2 expression in osteoblasts. *Bone* **93**, 1–11 (2016).
486. Roelofsen, T. *et al.* Sphingosine-1-phosphate acts as a developmental stage specific inhibitor of platelet-derived growth factor-induced chemotaxis of osteoblasts. *J. Cell. Biochem.* **105**, 1128–1138 (2008).
487. Brizuela, L. *et al.* Osteoblast-derived sphingosine 1-phosphate to induce proliferation and confer resistance to therapeutics to bone metastasis-derived prostate cancer cells. *Mol. Oncol.* **8**, 1181–1195 (2014).
488. Ryu, J. *et al.* Sphingosine 1-phosphate as a regulator of osteoclast differentiation and osteoclast-osteoblast coupling. *EMBO J.* **25**, 5840–5851 (2006).
489. Grey, A. *et al.* Osteoblastic cells express phospholipid receptors and phosphatases and proliferate in response to sphingosine-1-phosphate. *Calcif. Tissue Int.* **74**, 542–550 (2004).
490. Hashimoto, Y. *et al.* Sphingosine-1-phosphate inhibits differentiation of C3H10T1/2 cells into adipocyte. *Mol. Cell. Biochem.* **401**, 39–47 (2014).
491. Ota, K. *et al.* Sclerostin Is Expressed in Osteoclasts From Aged Mice and Reduces Osteoclast-Mediated Stimulation of Mineralization. *J. Cell. Biochem.* **114**, 1901 (2013).
492. Sato, C., Iwasaki, T., Kitano, S., Tsunemi, S. & Sano, H. Sphingosine 1-phosphate receptor activation enhances BMP-2-induced osteoblast differentiation. *Biochem. Biophys. Res. Commun.* **423**, 200–205 (2012).
493. Matsuzaki, E. *et al.* Sphingosine-1-phosphate promotes the nuclear translocation of β-catenin and thereby induces osteoprotegerin gene expression in osteoblast-like cell lines. *Bone* **55**, 315–324 (2013).
494. Kikuta, J. *et al.* Sphingosine-1-phosphate-mediated osteoclast precursor monocyte migration is a critical point of control in antibone-resorptive action of active vitamin D. *Proc. Natl. Acad. Sci. U. S. A.* **110**, 7009–7013 (2013).

495. Wei, S. H. *et al.* Sphingosine 1-phosphate type 1 receptor agonism inhibits transendothelial migration of medullary T cells to lymphatic sinuses. *Nat. Immunol.* **6**, 1228–1235 (2005).
496. Kemble, S., Harford, L. & McGettrick, H. O013 New therapeutic avenues in rheumatoid arthritis: exploring the role of the adiponectin-pepitem axis. in *Oral presentations* vol. 77 A7.1-A7 (BMJ Publishing Group Ltd and European League Against Rheumatism, 2018).
497. Matsubara, H. *et al.* PEPITEM/Cadherin 15 Axis Inhibits T Lymphocyte Infiltration and Glomerulonephritis in a Mouse Model of Systemic Lupus Erythematosus. *J. Immunol.* **204**, 2043–2052 (2020).
498. Gardino, A. K., Smerdon, S. J. & Yaffe, M. B. Structural determinants of 14-3-3 binding specificities and regulation of subcellular localization of 14-3-3-ligand complexes: A comparison of the X-ray crystal structures of all human 14-3-3 isoforms. *Seminars in Cancer Biology* vol. 16 173–182 (2006).
499. Jin, J. *et al.* Proteomic, functional, and domain-based analysis of in vivo 14-3-3 binding proteins involved in cytoskeletal regulation and cellular organization. *Curr. Biol.* **14**, 1436–1450 (2004).
500. Peng, C. Y. *et al.* Mitotic and G2 checkpoint control: Regulation of 14-3-3 protein binding by phosphorylation of Cdc25c on serine-216. *Science (80-.).* **277**, 1501–1505 (1997).
501. Zha, J., Harada, H., Yang, E., Jockel, J. & Korsmeyer, S. J. Serine phosphorylation of death agonist BAD in response to survival factor results in binding to 14-3-3 not BCL-X(L). *Cell* **87**, 619–628 (1996).
502. Kleppe, R., Martinez, A., Døskeland, S. O. & Haavik, J. The 14-3-3 proteins in regulation of cellular metabolism. *Semin. Cell Dev. Biol.* **22**, 713–719 (2011).
503. Liu, Y., Ross, J. F., Bodine, P. V. N. & Billiard, J. Homodimerization of Ror2 tyrosine kinase receptor induces 14-3-3β phosphorylation and promotes osteoblast differentiation and bone formation. *Mol. Endocrinol.* **21**, 3050–3061 (2007).
504. Priam, S. *et al.* Identification of Soluble 14-3-3∈ as a Novel Subchondral Bone Mediator Involved in Cartilage Degradation in Osteoarthritis. *Arthritis Rheum.* **65**, 1831–1842 (2013).
505. Bronisz, A. *et al.* Microphthalmia-associated transcription factor interactions with 14-3-3 modulate differentiation of committed myeloid precursors. *Mol. Biol. Cell* **17**, 3897–3906 (2006).
506. Schmidt, J. R. *et al.* Osteoblast-released matrix vesicles, regulation of activity and composition by sulfated and non-sulfated glycosaminoglycans. *Mol. Cell. Proteomics* **15**, 558–572 (2016).
507. Sanchez, C. *et al.* Comparison of secretome from osteoblasts derived from sclerotic versus non-sclerotic subchondral bone in OA: A pilot study. *PLoS One* **13**, (2018).
508. Foucault, I., Liu, Y. C., Bernard, A. & Deckert, M. The chaperone protein 14-3-3 interacts with 3BP2/SH3BP2 and regulates its adapter function. *J. Biol. Chem.* **278**, 7146–7153 (2003).
509. Mukherjee, P. M. *et al.* Cherubism gene Sh3bp2 is important for optimal bone formation, osteoblast differentiation, and function. *Am. J. Orthod. Dentofac. Orthop.* **138**, 140.e1-140.e11 (2010).
510. Pan, J., Huang, C., Chen, G., Cai, Z. & Zhang, Z. MicroRNA-451 blockade

promotes osteoblastic differentiation and skeletal anabolic effects by promoting YWHAZ-mediated RUNX2 protein stabilization. *Medchemcomm* **9**, 1359–1368 (2018).
511. Yin, P. *et al.* Inhibition of miR-22 promotes differentiation of osteoblasts and improves bone formation via the YWHAZ pathway in experimental mice. *Arch. Med. Sci.* **16**, 1419–1431 (2020).
512. Naylor, A. J. *et al.* A differential role for CD248 (Endosialin) in PDGF-mediated skeletal muscle angiogenesis. *PLoS One* **9**, e107146 (2014).
513. Ranzoni, A. M., Corcelli, M., Arnett, T. R. & Guillot, P. V. Data Descriptor: Micro-computed tomography reconstructions of tibiae of stem cell transplanted osteogenesis imperfecta mice. *Sci. Data* **5**, (2018).
514. Hardy, R. S. *et al.* 11 Beta-hydroxysteroid dehydrogenase type 1 regulates synovitis, joint destruction, and systemic bone loss in chronic polyarthritis. *J. Autoimmun.* **92**, 104–113 (2018).
515. Faulwetter, S., Dailianis, T., Vasileiadou, A. & Arvanitidis, C. X-ray micro-computed tomography Contrast enhancing techniques for the application of micro-CT in marine biodiversity studies. *Microsc. Anal.* **27**, S4–S7 (2013).
516. Hemmatian, H. *et al.* Accuracy and reproducibility of mouse cortical bone microporosity as quantified by desktop microcomputed tomography. *PLoS One* **12**, (2017).
517. Feldkamp, L. A., Davis, L. C. & Kress, J. W. Practical cone-beam algorithm. *J. Opt. Soc. Am. A* **1**, 612 (1984).
518. Hulley, P. A. *et al.* Hypoxia-inducible factor 1-alpha does not regulate osteoclastogenesis but enhances bone resorption activity via prolyl-4-hydroxylase 2. *J. Pathol.* **242**, 322–333 (2017).
519. Campbell, G. M. & Sophocleous, A. Quantitative analysis of bone and soft tissue by micro-computed tomography: applications to ex vivo and in vivo studies. *Bonekey Rep.* **3**, 564 (2014).
520. Oliviero, S., Giorgi, M., Laud, P. J. & Dall'Ara, E. Effect of repeated in vivo microCT imaging on the properties of the mouse tibia. *PLoS One* **14**, e0225127 (2019).
521. Chernyaev, E. V. *1 Introduction 2 Terminology Positive and negative nodes*. *Elements*.
522. Cignoni, P. *et al.* MeshLab: An open-source mesh processing tool. in *6th Eurographics Italian Chapter Conference 2008 - Proceedings* 129–136 (2008).
523. Savi, F. M., Brierly, G. I., Baldwin, J., Theodoropoulos, C. & Woodruff, M. A. Comparison of Different Decalcification Methods Using Rat Mandibles as a Model. *J. Histochem. Cytochem.* **65**, 705–722 (2017).
524. Rajfer, R. A. *et al.* Prevention of Osteoporosis in the Ovariectomized Rat by Oral Administration of a Nutraceutical Combination That Stimulates Nitric Oxide Production. *J. Osteoporos.* **2019**, (2019).
525. Heath, D. J. *et al.* An osteoprotegerin-like peptidomimetic inhibits osteoclastic bone resorption and osteolytic bone disease in myeloma. *Cancer Res.* **67**, 202–208 (2007).
526. Esapa, C. T. *et al.* Bone Mineral Content and Density. in *Current Protocols in Mouse Biology* (John Wiley & Sons, Inc., 2012). doi:10.1002/9780470942390.mo120124.
527. Ng, C. K.-Y., Carr, K., McAinsh, M. R., Powell, B. & Hetherington, A. M.

Drought-induced guard cell signal transduction involves sphingosine-1-phosphate. *Nature* **410**, 596–599 (2001).
528. Sullards, M. C. & Merrill, A. H. Analysis of Sphingosine 1-Phosphate, Ceramides, and Other Bioactive Sphingolipids by High-Performance Liquid Chromatography-Tandem Mass Spectrometry. *Sci. STKE* **2001**, (2001).
529. Orriss, I. R., HAJJAWI, M. O. R., Huesa, C., Macrae, V. E. & Arnett, T. R. Optimisation of the differing conditions required for bone formation in vitro by primary osteoblasts from mice and rats. *Int. J. Mol. Med.* **34**, 1201–1208 (2014).
530. Bakker, A. D. & Klein-Nulend, J. Osteoblast isolation from murine calvaria and long bones. *Methods Mol. Biol.* **816**, 19–29 (2012).
531. Davies, O. G. *et al.* Osteoblast-Derived Vesicle Protein Content Is Temporally Regulated During Osteogenesis: Implications for Regenerative Therapies. *Front. Bioeng. Biotechnol.* **7**, 92 (2019).
532. Kim, I. S. *et al.* Novel effect of biphasic electric current on in vitro osteogenesis and cytokine production in human mesenchymal stromal cells. *Tissue Eng. Part A* **15**, 2411–2422 (2009).
533. Maridas, D. E., Rendina-Ruedy, E., Le, P. T. & Rosen, C. J. Isolation, culture, and differentiation of bone marrow stromal cells and osteoclast progenitors from mice. *J. Vis. Exp.* **2018**, (2018).
534. Rao, H., Tan, J., Faruqi, F., Beltzer, J. & Park, S. Corning ® Osteo Assay Surface : A New Tool to Study Osteoclast and Osteoblast Differentiation and Function Sn APPS hots. *SnAPPShots* (2010).
535. Marton, N. *et al.* Extracellular vesicles regulate the human osteoclastogenesis: divergent roles in discrete inflammatory arthropathies. *Cell. Mol. Life Sci.* **74**, 3599–3611 (2017).
536. Goel, P. N. *et al.* Suppression of Notch Signaling in Osteoclasts Improves Bone Regeneration and Healing. *J. Orthop. Res.* **37**, 2089–2103 (2019).
537. Bradley, E. W. & Oursler, M. J. Osteoclast culture and resorption assays. *Methods Mol. Biol.* **455**, 19–35 (2008).
538. Uzarski, J. S., DiVito, M. D., Wertheim, J. A. & Miller, W. M. Essential Design Considerations for the Resazurin Reduction Assay to Noninvasively Quantify Cell Expansion within Perfused Extracellular Matrix Scaffolds. *Biomaterials* **129**, 163 (2017).
539. Huang Liu, M. *et al.* Automated RNA Sample QC Using the Agilent 2200 TapeStation System. in *International Plant and Animal Genome Conference XXII* (2014).
540. Jahn, C. E., Charkowski, A. O. & Willis, D. K. Evaluation of isolation methods and RNA integrity for bacterial RNA quantitation. *J. Microbiol. Methods* **75**, 318–324 (2008).
541. Elbrecht, V. *et al.* Testing the potential of a ribosomal 16S marker for DNA metabarcoding of insects. *PeerJ* **2016**, (2016).
542. Kastanis, G. J. *et al.* In-depth comparative analysis of Illumina® MiSeq run metrics: Development of a wet-lab quality assessment tool. *Mol. Ecol. Resour.* **19**, 377 (2019).
543. Andrews, S. FastQC: a quality control tool for high throughput sequence data. http://www.bioinformatics.babraham.ac.uk/projects/fastqc.
544. Bushnell B. *BBMap: A Fast, Accurate, Splice-Aware Aligner (Conference)* |

OSTI.GOV. *Lawrence Berkeley National Lab.(LBNL), Berkeley, CA (United States)* (2014).
545. Howe, K. L. *et al.* Ensembl 2021. *Nucleic Acids Res.* **49**, D884–D891 (2021).
546. Dobin, A. *et al.* STAR: ultrafast universal RNA-seq aligner. *Bioinformatics* **29**, 15 (2013).
547. Liao, Y., Smyth, G. K. & Shi, W. featureCounts: an efficient general purpose program for assigning sequence reads to genomic features. *Bioinformatics* **30**, 923–930 (2014).
548. Liao, Y., Smyth, G. K. & Shi, W. The Subread aligner: fast, accurate and scalable read mapping by seed-and-vote. *Nucleic Acids Res.* **41**, e108 (2013).
549. Love, M. I., Huber, W. & Anders, S. Moderated estimation of fold change and dispersion for RNA-seq data with DESeq2. *Genome Biol.* **15**, 1–21 (2014).
550. Yu, G., Wang, L. G., Han, Y. & He, Q. Y. ClusterProfiler: An R package for comparing biological themes among gene clusters. *Omi. A J. Integr. Biol.* **16**, 284–287 (2012).
551. Luo, W. & Brouwer, C. Pathview: an R/Bioconductor package for pathway-based data integration and visualization. *Bioinformatics* **29**, 1830–1831 (2013).
552. Tsukasaki, M. *et al.* Stepwise cell fate decision pathways during osteoclastogenesis at single-cell resolution. *Nat. Metab. 2020 212* **2**, 1382–1390 (2020).
553. Baryawno, N. *et al.* A cellular taxonomy of the bone marrow stroma in homeostasis and leukemia. *Cell* **177**, 1915 (2019).
554. Stuart, T. *et al.* Comprehensive Integration of Single-Cell Data. *Cell* **177**, 1888-1902.e21 (2019).
555. Hao, Y. *et al.* Integrated analysis of multimodal single-cell data. *Cell* **184**, 3573-3587.e29 (2021).
556. Satija, R., Farrell, J. A., Gennert, D., Schier, A. F. & Regev, A. Spatial reconstruction of single-cell gene expression data. *Nat. Biotechnol. 2015 335* **33**, 495–502 (2015).
557. Butler, A., Hoffman, P., Smibert, P., Papalexi, E. & Satija, R. Integrating single-cell transcriptomic data across different conditions, technologies, and species. *Nat. Biotechnol.* **36**, 411–420 (2018).
558. Cai, L. *et al.* Effects of parathyroid hormone (1-34) on the regulation of the lysyl oxidase family in ovariectomized mice. *RSC Adv.* **8**, 30629–30641 (2018).
559. Datta, N. S., Pettway, G. J., Chen, C., Koh, A. J. & McCauley, L. K. Cyclin D1 as a target for the proliferative effects of PTH and PTHrP in early osteoblastic cells. *J. Bone Miner. Res.* **22**, 951–964 (2007).
560. Qin, L. *et al.* Gene expression profiles and transcription factors involved in parathyroid hormone signaling in osteoblasts revealed by microarray and bioinformatics. *J. Biol. Chem.* **278**, 19723–19731 (2003).
561. Kinakis, I., Kousidou, O. C. & Karamanos, N. K. In vitro and in vivo antiresorptive effects of bisphosphonates in metastatic bone disease. *In Vivo* vol. 19 311–318 (2005).
562. McSheehy, P. M. J. & Chambers, T. J. Osteoblastic cells mediate osteoclastic responsiveness to parathyroid hormone. *Endocrinology* **118**, 824–828 (1986).
563. Hahn, M., Vogel, M., Pompesius-Kempa, M. & Delling, G. Trabecular bone pattern factor—a new parameter for simple quantification of bone microarchitecture. *Bone* **13**, 327–330 (1992).

564. Serguienko, A., Wang, M. Y. & Myklebost, O. Real-Time Vital Mineralization Detection and Quantification during In Vitro Osteoblast Differentiation. *Biol. Proced. Online* **20**, 14 (2018).
565. Yang, D., Yoon, S.-J. & Lee, D.-W. Preparation and Evaluation of Dexamethasone (DEX)/Growth and Differentiation Factor-5 (GDF-5) Surface-Modified Titanium Using β-Cyclodextrin-Conjugated Heparin (CD-Hep) for Enhanced Osteogenic Activity In Vitro and In Vivo. *Int. J. Mol. Sci.* **18**, 1695 (2017).
566. Taylor, S. E. B., Shah, M. & Orriss, I. R. Generation of rodent and human osteoblasts. *Bonekey Rep.* **3**, (2014).
567. Ahmad, M. *et al.* Cell-based RNAi screening and high-content analysis in primary calvarian osteoblasts applied to identification of osteoblast differentiation regulators. *Sci. Rep.* **8**, (2018).
568. Sims, N. A. *et al.* Human and murine osteocalcin gene expression: conserved tissue restricted expression and divergent responses to 1,25-dihydroxyvitamin D3 in vivo. *Mol. Endocrinol.* **11**, 1695–708 (1997).
569. Lam, J. *et al.* TNF-α induces osteoclastogenesis by direct stimulation of macrophages exposed to permissive levels of RANK ligand. *J. Clin. Invest.* **106**, 1481–1488 (2000).
570. Neal, C. L. & Yu, D. 14-3-3ζ as a prognostic marker and therapeutic target for cancer. *Expert Opin. Ther. Targets* **14**, 1343–1354 (2010).
571. Ferguson, V. L., Ayers, R. A., Bateman, T. A. & Simske, S. J. Bone development and age-related bone loss in male C57BL/6J mice. *Bone* **33**, 387–398 (2003).
572. Oussoren, C. *et al.* Lymphatic uptake and biodistribution of liposomes after subcutaneous injection: IV. Fate of liposomes in regional lymph nodes. *Biochim. Biophys. Acta - Biomembr.* **1370**, 259–272 (1998).
573. Oussoren, C., Zuidema, J., Crommelin, D. J. A. & Storm, G. Lymphatic uptake and biodistribution of liposomes after subcutaneous injection.: II. Influence of liposomal size, lipid composition and lipid dose. *Biochim. Biophys. Acta - Biomembr.* **1328**, 261–272 (1997).
574. Oussoren, C., Zuidema, J., Croramelin, D. J. A. & Storm, G. Lymphatic Uptake and Biodistribution of Liposomes after Subcutaneous Injection I. Influence of the Anatomical Site of Injection. *http://dx.doi.org/10.3109/08982109709035487* **7**, 85–99 (2008).
575. Oussoren, C. & Storm, G. Role of macrophages in the localisation of liposomes in lymph nodes after subcutaneous administration. *Int. J. Pharm.* **183**, 37–41 (1999).
576. Zweifler, L. E., Koh, A. J., Daignault-Newton, S. & McCauley, L. K. Anabolic actions of PTH in murine models: two decades of insights. *J. Bone Miner. Res.* **36**, 1979–1998 (2021).
577. Childress, P. *et al.* Nmp4/CIZ suppresses the response of bone to anabolic parathyroid hormone by regulating both osteoblasts and osteoclasts. *Calcif. Tissue Int.* **89**, 74 (2011).
578. Yao, W. *et al.* Overexpression of secreted frizzled-related protein 1 inhibits bone formation and attenuates parathyroid hormone bone anabolic effects. *J. Bone Miner. Res.* **25**, 190–199 (2010).
579. Essex, A. L. *et al.* Bisphosphonate Treatment Ameliorates Chemotherapy-

Induced Bone and Muscle Abnormalities in Young Mice. *Front. Endocrinol. (Lausanne).* **10**, 809 (2019).
580. Zhu, E. D., Louis, L., Brooks, D. J., Bouxsein, M. L. & Demay, M. B. Effect of Bisphosphonates on the Rapidly Growing Male Murine Skeleton. *Endocrinology* **155**, 1188 (2014).
581. Jongen, J. W. J. M., Bos, M. P., Van Der Meer, J. M. & Herrmann-Erlee, M. P. M. Parathyroid hormone-induced changes in alkaline phosphatase expression in fetal calvarial osteoblasts: Differences between rat and mouse. *J. Cell. Physiol.* **155**, 36–43 (1993).
582. Rey, A., Manen, D., Rizzoli, R., Ferrari, S. L. & Caverzasio, J. Evidences for a role of p38 MAP kinase in the stimulation of alkaline phosphatase and matrix mineralization induced by parathyroid hormone in osteoblastic cells. *Bone* **41**, 59–67 (2007).
583. Yu, B. *et al.* PTH Induces Differentiation of Mesenchymal Stem Cells by Enhancing BMP Signaling. *J. Bone Miner. Res.* **27**, 2001 (2012).
584. Sinha, P. *et al.* Loss of Gsα in the postnatal skeleton leads to low bone mass and a blunted response to anabolic parathyroid hormone therapy. *J. Biol. Chem.* **291**, 1631–1642 (2016).
585. Siddiqui, J. A. *et al.* Catabolic Effects of Human PTH (1–34) on Bone: Requirement of Monocyte Chemoattractant Protein-1 in Murine Model of Hyperparathyroidism. *Sci. Reports 2017 71* **7**, 1–14 (2017).
586. Kawano, T. *et al.* The Anabolic Response to Parathyroid Hormone Is Augmented in Rac2 Knockout Mice. *Endocrinology* **149**, 4009–4015 (2008).
587. Lee, S. K. & Lorenzo, J. A. Regulation of receptor activator of nuclear factor-kappa B ligand and osteoprotegerin mRNA expression by parathyroid hormone is predominantly mediated by the protein kinase a pathway in murine bone marrow cultures. *Bone* **31**, 252–259 (2002).
588. Kondo, H., Guo, J. & Bringhurst, F. R. Cyclic adenosine monophosphate/protein kinase A mediates parathyroid hormone/parathyroid hormone-related protein receptor regulation of osteoclastogenesis and expression of RANKL and osteoprotegerin mRNAs by marrow stromal cells. *J. Bone Miner. Res.* **17**, 1667–1679 (2002).
589. Fu, Q., Jilka, R. L., Manolagas, S. C. & O'Brien, C. A. Parathyroid hormone stimulates receptor activator of NFkappa B ligand and inhibits osteoprotegerin expression via protein kinase A activation of cAMP-response element-binding protein. *J. Biol. Chem.* **277**, 48868–48875 (2002).
590. Van Beek, E. R., Löwik, C. W. G. M. & Papapoulos, S. E. Bisphosphonates suppress bone resorption by a direct effect on early osteoclast precursors without affecting the osteoclastogenic capacity of osteogenic cells: the role of protein geranylgeranylation in the action of nitrogen-containing bisphosphonates on osteoclast precursors. *Bone* **30**, 64–70 (2002).
591. Armamento-Villareal, R., Napoli, N., Panwar, V. & Novack, D. Suppressed bone turnover during alendronate therapy for high-turnover osteoporosis. *N. Engl. J. Med.* **355**, 2048–2050 (2006).
592. Odvina, C. V. *et al.* Severely suppressed bone turnover: a potential complication of alendronate therapy. *J. Clin. Endocrinol. Metab.* **90**, 1294–1301 (2005).
593. Burr, D. B. *et al.* Tissue mineralization is increased following 1-year treatment

with high doses of bisphosphonates in dogs. *Bone* **33**, 960–969 (2003).
594. Parfitt, A. M. Misconceptions (2): turnover is always higher in cancellous than in cortical bone. *Bone* **30**, 807–809 (2002).
595. Kim, M. Y., Lee, K., Shin, H.-I., Lee, K.-J. & Jeong, D. Metabolic activities affect femur and lumbar vertebrae remodeling, and anti-resorptive risedronate disturbs femoral cortical bone remodeling. *Exp. Mol. Med.* **53**, 103–114 (2021).
596. Hwang, P. W. & Horton, J. A. Variable osteogenic performance of MC3T3-E1 subclones impacts their utility as models of osteoblast biology. *Sci. Rep.* **9**, 8299 (2019).
597. Neve, A., Corrado, A. & Cantatore, F. P. Osteoblast physiology in normal and pathological conditions. *Cell Tissue Res.* **343**, 289–302 (2011).
598. Li, H. *et al.* Immature osteoblast lineage cells increase osteoclastogenesis in osteogenesis imperfecta murine. *Am. J. Pathol.* **176**, 2405–2413 (2010).
599. Weigert, A., Olesch, C. & Brüne, B. Sphingosine-1-Phosphate and Macrophage Biology—How the Sphinx Tames the Big Eater. *Front. Immunol.* **10**, 1706 (2019).
600. Hammad, S. M. *et al.* Dual and distinct roles for sphingosine kinase 1 and sphingosine 1 phosphate in the response to inflammatory stimuli in RAW macrophages. *Prostaglandins Other Lipid Mediat.* **85**, 107–114 (2008).
601. Patra, D., Mueller, J., DeLassus, E. & Sandell, L. J. Characterization of skeletal defects in mice with OSX-CRE-directed ablation of site-1 protease. *Osteoarthr. Cartil.* **24**, S131–S132 (2016).
602. Duong, C. Q. *et al.* Expression of the lysophospholipid receptor family and investigation of lysophospholipid-mediated responses in human macrophages. *Biochim. Biophys. Acta - Mol. Cell Biol. Lipids* **1682**, 112–119 (2004).
603. Geng, Y. J., Kodama, T. & Hansson, G. K. Differential expression of scavenger receptor isoforms during monocyte- macrophage differentiation and foam cell formation. *Arterioscler. Thromb.* **14**, 798–806 (1994).
604. Martino, A. *et al.* Sphingosine 1-Phosphate Interferes on the Differentiation of Human Monocytes into Competent Dendritic Cells. *Scand. J. Immunol.* **65**, 84–91 (2007).
605. Ryu, J. *et al.* Sphingosine 1-phosphate as a regulator of osteoclast differentiation and osteoclast–osteoblast coupling. *EMBO J.* **25**, 5840–5851 (2006).
606. Moon, S. J. *et al.* Temporal differential effects of proinflammatory cytokines on osteoclastogenesis. *Int. J. Mol. Med.* **31**, 769–777 (2013).
607. Hicks, S. C., Townes, F. W., Teng, M. & Irizarry, R. A. Missing data and technical variability in single-cell RNA-sequencing experiments. *Biostatistics* **19**, 562–578 (2018).
608. Feuerborn, R. *et al.* High density lipoprotein (HDL)-associated sphingosine 1-phosphate (S1P) inhibits macrophage apoptosis by stimulating STAT3 activity and survivin expression. *Atherosclerosis* **257**, 29–37 (2017).
609. Nguyen, J. & Nohe, A. Factors that Affect the Osteoclastogenesis of RAW264.7 Cells. *J. Biochem. Anal. Stud.* **2**, (2017).
610. Carpio, L. C. *Sphingolipids stimulate cell growth via MAP kinase activation in osteoblastic cells*. (1999).
611. Lucki, N. C., Li, D. & Sewer, M. B. Sphingosine-1-Phosphate Rapidly Increases Cortisol Biosynthesis and the Expression of Genes Involved in Cholesterol

Uptake and Transport in H295R Adrenocortical Cells. *Mol. Cell. Endocrinol.* **348**, 165 (2012).
612. Koch, A. *et al.* Downregulation of sphingosine 1-phosphate (S1P) receptor 1 by dexamethasone inhibits S1P-induced mesangial cell migration. *Biol. Chem.* **396**, 803–812 (2015).
613. Hashimoto, Y. *et al.* Sphingosine-1-phosphate-enhanced Wnt5a promotes osteogenic differentiation in C3H10T1/2 cells. *Cell Biol. Int.* **40**, 1129–1136 (2016).
614. Yamaguchi, A., Sakamoto, K., Minamizato, T., Katsube, K. & Nakanishi, S. Regulation of osteoblast differentiation mediated by BMP, Notch, and CCN3/NOV. *Jpn. Dent. Sci. Rev.* **44**, 48–56 (2008).
615. Cruz, A. C. C., Silva, M. L., Caon, T. & Simões, C. M. O. Addition of bone morphogenetic protein type 2 to ascorbate andβ-glycerophosphate supplementation did not enhance osteogenic differentiationof human adipose-derived stem cells. *J. Appl. Oral Sci.* **20**, 628 (2012).
616. Golan, K., Kollet, O. & Lapidot, T. Dynamic cross talk between S1P and CXCL12 regulates hematopoietic stem cells migration, development and bone remodeling. *Pharmaceuticals* **6**, 1145–1169 (2013).
617. Shahnazari, M., Chu, V., Wronski, T. J., Nissenson, R. A. & Halloran, B. P. CXCL12/CXCR4 signaling in the osteoblast regulates the mesenchymal stem cell and osteoclast lineage populations. *FASEB J.* **27**, 3505–3513 (2013).
618. Hu, S.-L. *et al.* S1P promotes IL-6 expression in osteoblasts through the PI3K, MEK/ERK and NF-κB signaling pathways. *Int. J. Med. Sci.* **17**, 1207–1214 (2020).
619. Kozawa, O., Tokuda, H., Matsuno, H. & Uematsu, T. Activation of mitogen-activated protein kinase is involved in sphingosine 1-phosphate-stimulated interleukin-6 synthesis in osteoblasts. *FEBS Lett.* **418**, 149–151 (1997).
620. Huang, R. L. *et al.* IL-6 potentiates BMP-2-induced osteogenesis and adipogenesis via two different BMPR1A-mediated pathways. *Cell Death Dis. 2018 92* **9**, 1–15 (2018).
621. Hughes, F. J. & Howells, G. L. Interleukin-6 inhibits bone formation in vitro. *Bone Miner.* **21**, 21–28 (1993).
622. Sullivan, C. B. *et al.* TNFα and IL-1β influence the differentiation and migration of murine MSCs independently of the NF-κB pathway. *Stem Cell Res. Ther.* **5**, 1–13 (2014).
623. Mao, C. Y. *et al.* Double-edged-sword effect of IL-1β on the osteogenesis of periodontal ligament stem cells via crosstalk between the NF-κB, MAPK and BMP/Smad signaling pathways. *Cell Death Dis.* **7**, (2016).
624. Sonomoto, K. *et al.* Interleukin-1β induces differentiation of human mesenchymal stem cells into osteoblasts via the Wnt-5a/receptor tyrosine kinase-like orphan receptor 2 pathway. *Arthritis Rheum.* **64**, 3355–3363 (2012).
625. Croes, M. *et al.* Proinflammatory Mediators Enhance the Osteogenesis of Human Mesenchymal Stem Cells after Lineage Commitment. *PLoS One* **10**, e0132781 (2015).
626. Danks, L. *et al.* RANKL expressed on synovial fibroblasts is primarily responsible for bone erosions during joint inflammation. *Ann. Rheum. Dis.* **75**, 1187–1195 (2016).
627. Baum, R. & Gravallese, E. M. Impact of inflammation on the osteoblast in

rheumatic diseases. *Current Osteoporosis Reports* vol. 12 9–16 (2014).
628. Croft, A. P. *et al.* Distinct fibroblast subsets drive inflammation and damage in arthritis. *Nature* vol. 570 246–251 (2019).
629. McGettrick, H. M., Butler, L. M., Buckley, C. D., Ed Rainger, G. & Nash, G. B. Tissue stroma as a regulator of leukocyte recruitment in inflammation. *J. Leukoc. Biol.* **91**, 385–400 (2012).
630. Shepherd, S., Shapland, M., Pearce, N. X. & Scully, S. Pattern, severity and aetiology of injuries in victims of assault. *J. R. Soc. Med.* **83**, 75–78 (1990).
631. Huang, C. C. *et al.* S1p increases vegf production in osteoblasts and facilitates endothelial progenitor cell angiogenesis by inhibiting mir-16-5p expression via the c-src/fak signaling pathway in rheumatoid arthritis. *Cells* **10**, (2021).
632. Peng, Y., Wu, S., Li, Y. & Crane, J. L. *Type H blood vessels in bone modeling and remodeling*. *Theranostics* vol. 10 (Ivyspring International Publisher, 2020).
633. Zhang, Y. *et al.* Angiogenesis Changes in Ovariectomized Rats with Osteoporosis Treated with Estrogen Replacement Therapy. *Biomed Res. Int.* **2019**, (2019).
634. Shen, Q. *et al.* Inhibiting expression of Cxcl9 promotes angiogenesis in MSCs-HUVECs co-culture. *Arch. Biochem. Biophys.* **675**, 108108 (2019).
635. Huang, B. *et al.* Osteoblasts secrete Cxcl9 to regulate angiogenesis in bone. *Nat. Commun.* **7**, (2016).
636. Czekanska, E. M., Stoddart, M. J., Richards, R. G. & Hayes, J. S. In search of an osteoblast cell model for in vitro research. *European Cells and Materials* vol. 24 1–17 (2012).
637. Okazaki, M. *et al.* Molecular cloning and characterization of OB-cadherin, a new member of cadherin family expressed in osteoblasts. *J. Biol. Chem.* **269**, 12092–12098 (1994).
638. Tsutsumimoto, T., Kawasaki, S., Ebara, S. & Takaoka, K. TNF-α and IL-1β suppress N-cadherin expression in MC3T3-E1 cells. *J. Bone Miner. Res.* **14**, 1751–1760 (1999).
639. Cheng, S. L., Shin, C. S., Towler, D. A. & Civitelli, R. A dominant negative cadherin inhibits osteoblast differentiation. *J. Bone Miner. Res.* **15**, 2362–2370 (2000).
640. Hsiao, S. P. & Chen, S. L. Myogenic regulatory factors regulate M-cadherin expression by targeting its proximal promoter elements. *Biochem. J.* **428**, 223–233 (2010).
641. Liu, C., Gersch, R. P., Hawke, T. J. & Hadjiargyrou, M. Silencing of Mustn1 inhibits myogenic fusion and differentiation. *Am. J. Physiol. - Cell Physiol.* **298**, 1100–1108 (2010).
642. Maier, A. & Bornemann, A. M-cadherin transcription in satellite cells from normal and denervated muscle. *Am. J. Physiol. Physiol.* **286**, C708–C712 (2004).
643. McClure, M. J., Ramey, A. N., Rashid, M., Boyan, B. D. & Schwartz, Z. Integrin-α7 signaling regulates connexin 43, M-cadherin, and myoblast fusion. *Am. J. Physiol. - Cell Physiol.* **316**, C876–C887 (2019).
644. Yeghiazaryan, M. *et al.* Fine-structural distribution of MMP-2 and MMP-9 activities in the rat skeletal muscle upon training: A study by high-resolution in situ zymography. *Histochem. Cell Biol.* **138**, 75–87 (2012).
645. Liu, P., Lin, J. H. & Zhang, B. Differential regulation of cadherin expression by

osteotropic hormones and growth factors in vitro in human osteoprogenitor cells. *Acta Pharmacol. Sin.* **26**, 705–713 (2005).
646. Kawaguchi, J., Kii, I., Sugiyama, Y., Takeshita, S. & Kudo, A. The transition of cadherin expression in osteoblast differentiation from mesenchymal cells: Consistent expression of cadherin-11 in osteoblast lineage. *J. Bone Miner. Res.* **16**, 260–269 (2001).
647. Yu, S. *et al.* Heparin-binding EGF-like growth factor and miR-1192 exert opposite effect on Runx2-induced osteogenic differentiation. *Cell Death Dis.* **4**, 1–11 (2013).
648. Paic, F. *et al.* Identification of differentially expressed genes between osteoblasts and osteocytes. *Bone* **45**, 682–692 (2009).
649. Bertocchi, C. *et al.* Nanoscale architecture of cadherin-based cell adhesions. *Nat. Cell Biol.* **19**, 28–37 (2017).
650. Pulous, F. E., Grimsley-Myers, C. M., Kansal, S., Kowalczyk, A. P. & Petrich, B. G. Talin-Dependent Integrin Activation Regulates VE-Cadherin Localization and Endothelial Cell Barrier Function. *Circ. Res.* **124**, 891 (2019).
651. Le, T. L., Yap, A. S. & Stow, J. L. Recycling of E-Cadherin: A Potential Mechanism for Regulating Cadherin Dynamics. *J. Cell Biol.* **146**, 219 (1999).
652. Woichansky, I., Beretta, C. A., Berns, N. & Riechmann, V. Three mechanisms control E-cadherin localization to the zonula adherens. *Nat. Commun. 2016 71* **7**, 1–11 (2016).
653. McEwen, A. E., Maher, M. T., Mo, R. & Gottardi, C. J. E-cadherin phosphorylation occurs during its biosynthesis to promote its cell surface stability and adhesion. *Mol. Biol. Cell* **25**, 2365–2374 (2014).
654. Hollnagel, A., Grund, C., Franke, W. W. & Arnold, H.-H. The Cell Adhesion Molecule M-Cadherin Is Not Essential for Muscle Development and Regeneration. *Mol. Cell. Biol.* **22**, 4760–4770 (2002).
655. Kister, A. E., Roytberg, M. A., Chothia, C., Vasiliev, J. M. & Gelfand, I. M. The sequence determinants of cadherin molecules. *Protein Sci.* **10**, 1801 (2001).
656. Ferrari, S. L. *et al.* Role for N-cadherin in the development of the differentiated osteoblastic phenotype. *J. Bone Miner. Res.* **15**, 198–208 (2000).
657. Di Benedetto, A. *et al.* N-cadherin and cadherin 11 modulate postnatal bone growth and osteoblast differentiation by distinct mechanisms. *J. Cell Sci.* **123**, 2640 (2010).
658. Wang, Y., Mohamed, J. S. & Alway, S. E. M-cadherin-inhibited phosphorylation of ß-catenin augments differentiation of mouse myoblasts. *Cell Tissue Res.* **351**, 183–200 (2013).
659. Brouwers, J. E. M., Lambers, F. M., Gasser, J. A., Van Rietbergen, B. & Huiskes, R. Bone degeneration and recovery after early and late bisphosphonate treatment of ovariectomized wistar rats assessed by in vivo micro-computed tomography. *Calcif. Tissue Int.* **82**, 202–211 (2008).
660. Roberts, B. C. *et al.* PTH(1–34) treatment and/or mechanical loading have different osteogenic effects on the trabecular and cortical bone in the ovariectomized C57BL/6 mouse. *Sci. Rep.* **10**, 1–16 (2020).
661. Panwar, P. *et al.* An Ectosteric Inhibitor of Cathepsin K Inhibits Bone Resorption in Ovariectomized Mice. *J. Bone Miner. Res.* **32**, 2415–2430 (2017).
662. Onoe, Y. *et al.* Comparative Effects of Estrogen and Raloxifene on B

Lymphopoiesis and Bone Loss Induced by Sex Steroid Deficiency in Mice. *J. Bone Miner. Res.* **15**, 541–549 (2000).
663. Alexander, J. M. *et al.* Human Parathyroid Hormone 1–34 Reverses Bone Loss in Ovariectomized Mice. *J. Bone Miner. Res.* **16**, 1665–1673 (2001).
664. Kim, J. Y., Jang, H. W., Kim, J. I. & Cha, I. H. Effects of pre-extraction intermittent PTH administration on extraction socket healing in bisphosphonate administered ovariectomized rats. *Sci. Rep.* **11**, 1–8 (2021).
665. Zhang. Sclerostin Antibody Prevented Progressive Bone Loss in Combined Ovariectomized and Concurrent Functional Disuse. *Physiol. Behav.* **176**, 139–148 (2017).
666. Shen, V., Birchman, R., Wu, D. D. & Lindsay, R. Skeletal effects of parathyroid hormone infusion in ovariectomized rats with or without estrogen repletion. *J. Bone Miner. Res.* **15**, 740–746 (2000).
667. Longo, A. B., Salmon, P. L. & Ward, W. E. Comparison of ex vivo and in vivo micro-computed tomography of rat tibia at different scanning settings. *J. Orthop. Res.* **35**, 1690–1698 (2017).
668. Francisco, J. I., Yu, Y., Oliver, R. A. & Walsh, W. R. Relationship between age, skeletal site, and time post-ovariectomy on bone mineral and trabecular microarchitecture in rats. *J. Orthop. Res.* **29**, 189–196 (2011).
669. Holdsworth, D. W. & Thornton, M. M. Micro-CT in small animal and specimen imaging. *Trends Biotechnol.* **20**, 34–39 (2002).
670. Badea, C. T., Drangova, M., Holdsworth, D. W. & Johnson, G. A. In Vivo Small Animal Imaging using Micro-CT and Digital Subtraction Angiography. *Phys. Med. Biol.* **53**, R319 (2008).
671. Li, Z., Kuhn, G., Schirmer, M., Müller, R. & Ruffoni, D. Impaired bone formation in ovariectomized mice reduces implant integration as indicated by longitudinal in vivo micro-computed tomography. *PLoS One* **12**, e0184835 (2017).
672. Watkins, M. P. *et al.* Bisphosphonates improve trabecular bone mass and normalize cortical thickness in ovariectomized, osteoblast connexin43 deficient mice. *Bone* **51**, 787–794 (2012).
673. Dash, A. S. *et al.* Abnormal microarchitecture and stiffness in postmenopausal women with isolated osteoporosis at the 1/3 radius. *Bone* **132**, 115211 (2020).
674. Cheung, A. M., Frame, H., Ho, M., Mackinnon, E. S. & Brown, J. P. Bone strength and management of postmenopausal fracture risk with antiresorptive therapies: considerations for women’s health practice. *Int. J. Womens. Health* **8**, 537–547 (2016).
675. Seeman, E. Age- and menopause-related bone loss compromise cortical and trabecular microstructure. *Journals Gerontol. - Ser. A Biol. Sci. Med. Sci.* **68**, 1218–1225 (2013).
676. Almeida, M. *et al.* Skeletal Involution by Age-associated Oxidative Stress and Its Acceleration by Loss of Sex Steroids. *J. Biol. Chem.* **282**, 27285 (2007).
677. Glatt, V., Canalis, E., Stadmeyer, L. & Bouxsein, M. L. Age-Related Changes in Trabecular Architecture Differ in Female and Male C57BL/6J Mice. *J. Bone Miner. Res.* **22**, 1197–1207 (2007).
678. Zhang, H., Lewis, C. G., Aronow, M. S. & Gronowicz, G. A. The effects of patient age on human osteoblasts' response to Ti-6A1-4V implants in vitro. *J. Orthop. Res.* **22**, 30–38 (2004).
679. Zhou, S. *et al.* Age-Related Intrinsic Changes in Human Bone Marrow-Derived

Mesenchymal Stem Cells and Their Differentiation to Osteoblasts. *Aging Cell* **7**, 335 (2008).
680. Trošt, Z. *et al.* A microarray based identification of osteoporosis-related genes in primary culture of human osteoblasts. *Bone* **46**, 72–80 (2010).
681. Smith, P. N. *et al.* Heparanase in primary human osteoblasts. *J. Orthop. Res.* **28**, 1315–1322 (2010).
682. Perinpanayagam, H. *et al.* Early cell adhesion events differ between osteoporotic and non-osteoporotic osteoblasts. *J. Orthop. Res.* **19**, 993–1000 (2001).
683. Kassem, M. *et al.* Demonstration of Cellular Aging and Senescence in Serially Passaged Long-Term Cultures of Human Trabecular Osteoblasts. *Osteoporos Int* **7**, 514–524 (1997).
684. Byers, R. J., Denton, J., Hoyland, J. A. & Freemont, A. J. Differential patterns of osteoblast dysfunction in trabecular bone in patients with established osteoporosis. *J. Clin. Pathol.* **50**, 760–764 (1997).
685. Kelch, S. *et al.* MiRNAs in bone tissue correlate to bone mineral density and circulating miRNAs are gender independent in osteoporotic patients. *Sci. Rep.* **7**, 1–12 (2017).
686. Gold, E. B. The Timing of the Age at Which Natural Menopause Occurs. *Obstet. Gynecol. Clin. North Am.* **38**, 425–440 (2011).
687. Walsh, C. A., Birch, M. A., Fraser, W. D., Ginty, A. F. & Gallagher, J. A. Cytokine expression by cultured osteoblasts from patients with osteoporotic fractures. *Int. J. Exp. Pathol.* **81**, 159–163 (2000).
688. Yao, W. *et al.* Reversing bone loss by directing mesenchymal stem cells to bone. *Stem Cells* **31**, 2003–2014 (2013).
689. Hosoido, T. *et al.* Qualitative Comparison between Rats and Humans in Quadrupedal and Bipedal Locomotion. *J. Behav. Brain Sci.* **03**, 137–149 (2013).
690. Larson, S. G. & Demes, B. Weight Support Distribution During Quadrupedal Walking in Ateles and Cebus. *Am. J. Phys. Anthropol.* **144**, 633–642 (2011).
691. Son, K. M., Jung, H. A., Hong, J. I., Park, I. Y. & Kim, H. A. Development of a Mouse Model of Knee Osteoarthritis Based on Obesity and Bipedal Walking. *J. Orthop. Res.* **37**, 2411–2419 (2019).
692. Yousefzadeh, N., Kashfi, K., Jeddi, S. & Ghasemi, A. Ovariectomized rat model of osteoporosis: A practical guide. *EXCLI J.* **19**, 89–107 (2020).
693. Yamaura, M. *et al.* Local bone turnover in the metaphysis of the proximal tibia and the lumbar vertebra during the early periods after ovariectomy in rats. *Calcif. Tissue Int.* **58**, 52–59 (1996).
694. Wronski, T. J., Dann, L. M. & Horner, S. L. Time course of vertebral osteopenia in ovariectomized rats. *Bone* **10**, 295–301 (1989).
695. Liu, X. *et al.* Wnt signaling in bone formation and its therapeutic potential for bone diseases. *Therapeutic Advances in Musculoskeletal Disease* vol. 5 13–31 (2013).
696. Zhong, Z., Ethen, N. J. & Williams, B. O. WNT signaling in bone development and homeostasis. *Wiley Interdiscip. Rev. Dev. Biol.* **3**, 489–500 (2014).
697. Regan, J. & Long, F. Notch signaling and bone remodeling. *Curr. Osteoporos. Rep.* **11**, 126–129 (2013).
698. Canalis, E. Notch signaling in osteoblasts. *Sci. Signal.* **1**, pe17–pe17 (2008).

699. Luo, Z. *et al.* Notch Signaling in Osteogenesis, Osteoclastogenesis, and Angiogenesis. *American Journal of Pathology* vol. 189 1495–1500 (2019).
700. Behr, B. *et al.* A comparative analysis of the osteogenic effects of BMP-2, FGF-2, and VEGFA in a calvarial defect model. *Tissue Eng. - Part A* **18**, 1079–1086 (2012).
701. Valcourt, U. & Moustakas, A. BMP signaling in osteogenesis, bone remodeling and repair. *European Journal of Trauma* vol. 31 464–479 (2005).
702. Haÿ, E. *et al.* Peptide-based mediated disruption of N-cadherin-LRP5/6 interaction promotes Wnt signaling and bone formation. *J. Bone Miner. Res.* **27**, 1852–1863 (2012).
703. Howard, S., Deroo, T., Fujita, Y. & Itasaki, N. A Positive Role of Cadherin in Wnt/β-Catenin Signalling during Epithelial-Mesenchymal Transition. *PLoS One* **6**, e23899 (2011).
704. Ueno, A. *et al.* Constitutive expression of thrombospondin 1 in MC3T3-E1 osteoblastic cells inhibits mineralization. *J. Cell. Physiol.* **209**, 322–332 (2006).
705. Bailey DuBose, K., Zayzafoon, M. & Murphy-Ullrich, J. E. Thrombospondin-1 inhibits osteogenic differentiation of human mesenchymal stem cells through latent TGF-β activation. *Biochem. Biophys. Res. Commun.* **422**, 488–493 (2012).
706. Luo, G., Li, F., Li, X., Wang, Z. G. & Zhang, B. TNF-α and RANKL promote osteoclastogenesis by upregulating RANK via the NF-κB pathway. *Mol. Med. Rep.* **17**, 6605–6611 (2018).
707. Jurado, S. *et al.* Effect of IL-1β, PGE2, and TGF-β1 on the expression of OPG and RANKL in normal and osteoporotic primary human osteoblasts. *J. Cell. Biochem.* **110**, 304–310 (2010).
708. Huang, J. C. *et al.* PTH differentially regulates expression of RANKL and OPG. *J. Bone Miner. Res.* **19**, 235–244 (2004).
709. Thomas, G. P., Baker, S. U. K., Eisman, J. A. & Gardiner, E. M. Changing RANKL/OPG mRNA expression in differentiating murine primary osteoblasts. *J. Endocrinol.* **170**, 451–460 (2001).
710. Giner, M. *et al.* RANKL/OPG in primary cultures of osteoblasts from post-menopausal women. Differences between osteoporotic hip fractures and osteoarthritis. *J. Steroid Biochem. Mol. Biol.* **113**, 46–51 (2009).
711. Tsubaki, M. *et al.* Nitrogen-containing bisphosphonates inhibit RANKL- and M-CSF-induced osteoclast formation through the inhibition of ERK1/2 and Akt activation. *J. Biomed. Sci.* **21**, (2014).
712. Nice. Alendronate, etidronate, residronate, raloxifene, strontium ranelate and teriparatide for the secondary prevention of osteoporotic fragility fractures in postmenopausal women (amended). **2008**, 1–99 (2011).
713. Chen, Y. J. *et al.* Intermittent parathyroid hormone improve bone microarchitecture of the mandible and femoral head in ovariectomized rats. *BMC Musculoskelet. Disord.* **18**, 1–8 (2017).
714. Lindsay, R., Krege, J. H., Marin, F., Jin, L. & Stepan, J. J. Teriparatide for osteoporosis: Importance of the full course. *Osteoporos. Int.* **27**, 2395–2410 (2016).
715. Adachi, J. D., Hanley, D. A., Lorraine, J. K. & Yu, M. Assessing compliance, acceptance, and tolerability of teriparatide in patients with osteoporosis who fractured while on antiresorptive treatment or were intolerant to previous

antiresorptive treatment: An 18-month, multicenter, open-label, prospective study. *Clin. Ther.* **29**, 2055–2067 (2007).
716. Zhang, C. & Song, C. Combination Therapy of PTH and Antiresorptive Drugs on Osteoporosis: A Review of Treatment Alternatives. *Front. Pharmacol.* **11**, (2020).
717. Meier, C. *et al.* The role of teriparatide in sequential and combination therapy of osteoporosis. *Swiss Med. Wkly. 2014 23* **144**, (2014).
718. Finkelstein, J. S. *et al.* The Effects of Parathyroid Hormone, Alendronate, or Both in Men with Osteoporosis. *http://dx.doi.org/10.1056/NEJMoa035725* **349**, 1216–1226 (2009).
719. Compston, J. Bone-forming agents in non-responders to bisphosphonates. *Lancet* **390**, 1565–1566 (2017).
720. Siddique, N., Fallon, N., Steen, G., Walsh, J. B. & Casey, M. C. Treatment of osteoporosis with recombinant parathyroid hormone, utilisation of total body DXA to observe treatment effects on total body composition and factors determining response to therapy. *Ir. J. Med. Sci.* **188**, 505–515 (2019).
721. Papathanasiou, K. E., Turhanen, P., Brückner, S. I., Brunner, E. & Demadis, K. D. Smart, programmable and responsive injectable hydrogels for controlled release of cargo osteoporosis drugs. *Sci. Reports 2017 71* **7**, 1–9 (2017).
722. Pozzi, S. *et al.* High-Dose Zoledronic Acid Impacts Bone Remodeling with Effects on Osteoblastic Lineage and Bone Mechanical Properties. *Clin. Cancer Res.* **15**, 5829–5839 (2009).
723. Hulsart-Billström, G. *et al.* A surprisingly poor correlation between in vitro and in vivo testing of biomaterials for bone regeneration: results of a multicentre analysis. *Eur. Cells Mater.* **31**, 312–322 (2016).
724. Sieberath, A. *et al.* A Comparison of Osteoblast and Osteoclast In Vitro Co-Culture Models and Their Translation for Preclinical Drug Testing Applications. *Int. J. Mol. Sci.* **21**, 912 (2020).
725. Klein-Nulend, J. *et al.* Sensitivity of osteocytes to biomechanical stress in vitro. *FASEB J.* **9**, 441–445 (1995).
726. Zimmerman, S. M. *et al.* Loss of RANKL in osteocytes dramatically increases cancellous bone mass in the osteogenesis imperfecta mouse (oim). *Bone Reports* **9**, 61–73 (2018).
727. Canalis, E. *et al.* Notch Signaling in Osteocytes Differentially Regulates Cancellous and Cortical Bone Remodeling. *J. Biol. Chem.* **288**, 25614–25625 (2013).
728. Payr, S. *et al.* Direct comparison of 3D and 2D cultivation reveals higher osteogenic capacity of elderly osteoblasts in 3D. *J. Orthop. Surg. Res.* **16**, 1–7 (2021).
729. Sawa, N., Fujimoto, H., Sawa, Y. & Yamashita, J. Alternating Differentiation and Dedifferentiation between Mature Osteoblasts and Osteocytes. *Sci. Reports 2019 91* **9**, 1–9 (2019).
730. Naqvi, S. M., Panadero Pérez, J. A., Kumar, V., Verbruggen, A. S. K. & McNamara, L. M. A Novel 3D Osteoblast and Osteocyte Model Revealing Changes in Mineralization and Pro-osteoclastogenic Paracrine Signaling During Estrogen Deficiency. *Front. Bioeng. Biotechnol.* **8**, 601 (2020).
731. Bellido, T. & Delgado-Calle, J. Ex Vivo Organ Cultures as Models to Study Bone Biology. *JBMR Plus* **4**, (2020).

732. Haffner-Luntzer, M., Fischer, V. & Ignatius, A. Differences in Fracture Healing Between Female and Male C57BL/6J Mice. *Front. Physiol.* **12**, (2021).
733. Wang, Y. *et al.* Gender differences in the response of CD-1 mouse bone to parathyroid hormone: potential role of IGF-I. *J. Endocrinol.* **189**, 279–287 (2006).
734. Babey, M. *et al.* Gender-Specific Differences in the Skeletal Response to Continuous PTH in Mice Lacking the IGF1 Receptor in Mature Osteoblasts. *J. Bone Miner. Res.* **30**, 1064–1076 (2015).
735. Abe, K. & Aoki, Y. Sex differences in bone resorption in the mouse femur. *Cell Tissue Res. 1989 2551* **255**, 15–21 (1989).
736. DeMambro, V. E. *et al.* Gender-Specific Changes in Bone Turnover and Skeletal Architecture in Igfbp-2-Null Mice. *Endocrinology* **149**, 2051–2061 (2008).
737. Bonewald, L. F. The amazing osteocyte. *J. Bone Miner. Res.* **26**, 229–238 (2011).
738. Kerschnitzki, M. *et al.* The organization of the osteocyte network mirrors the extracellular matrix orientation in bone. *J. Struct. Biol.* **173**, 303–311 (2011).
739. Schmidt-Bleek, K. *et al.* Cellular composition of the initial fracture hematoma compared to a muscle hematoma: A study in sheep. *J. Orthop. Res.* **27**, 1147–1151 (2009).
740. Marie, P. J. Osteoblast dysfunctions in bone diseases: From cellular and molecular mechanisms to therapeutic strategies. *Cell. Mol. Life Sci.* **72**, 1347–1361 (2015).
741. Hengartner, N.-E., Fiedler, J., Ignatius, A. & Brenner, R. E. IL-1β Inhibits Human Osteoblast Migration. *Mol. Med.* **19**, 36–42 (2013).
742. Chang, J. *et al.* Inhibition of Osteoblast Functions by IKK/NF-kB in Osteoporosis. *Nat. Med.* **15**, 682 (2009).

9 Appendix

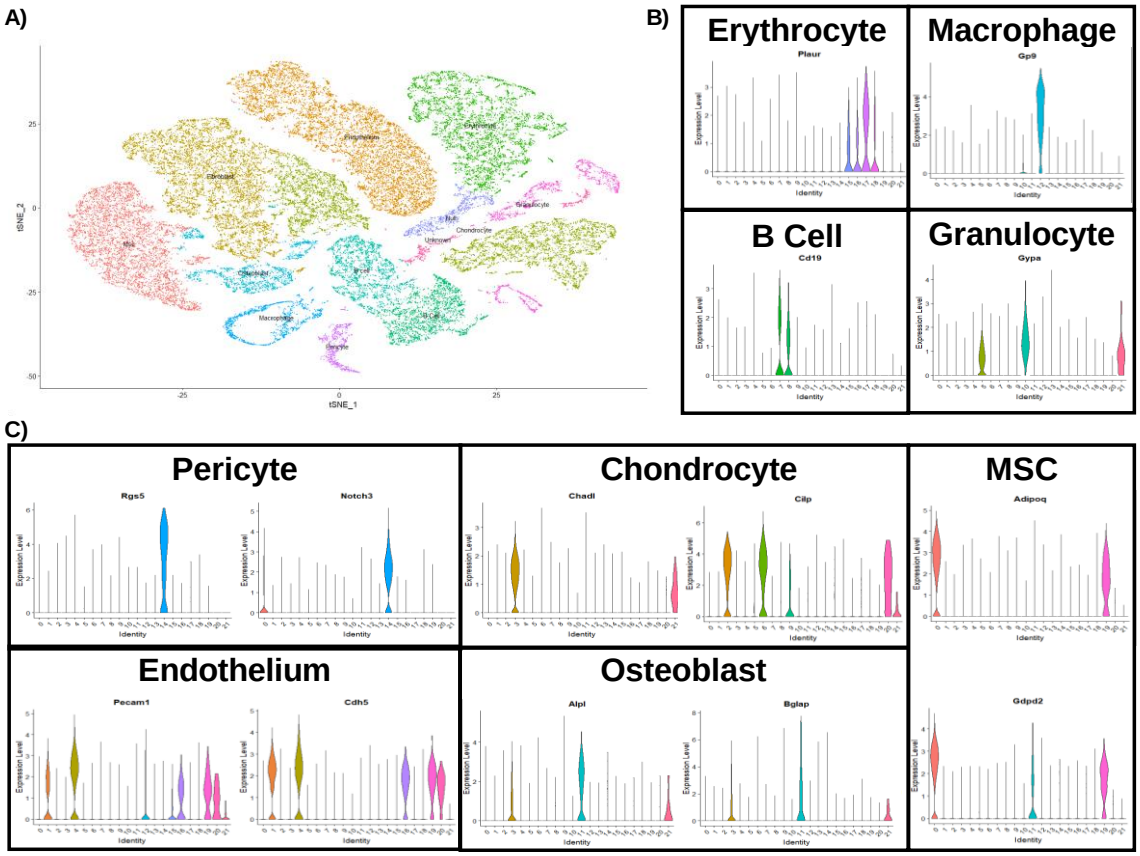

Figure 9.1. Identification of osteoblasts from dataset GSE128423.

Single-cell RNA sequencing of stromal cells from murine bone marrow from pre-published dataset GSE128423 was analysed using the Seurat package. **A.** Following pre-processing, cells were clustered and identifying genes for specific cell types were analysed. **B-C.** This allowed identification of immune cells **(B)**, pericytes, chondrocytes, endothelium, MSCs and osteoblasts **(C)**. The osteoblast cluster was isolated and used in subsequent analysis.

9.1 Script for pre-processing bulk RNAseq samples

```
#Combine multiple reads
set -e
module purge; module load bluebear
cat JLCobDIFWT2_S1*fastq.gz > JLCobDIFWT2_S1.fastq.gz
cat JLCobDIFWT3_S4*fastq.gz > JLCobDIFWT3_S4.fastq.gz
cat JLCobDIFWT3-1_S10*fastq.gz > JLCobDIFWT3-1.fastq.gz
cat JLCobDIFWT4_S7*fastq.gz > JLCobDIFWT4.fastq.gz
cat JLCobDIFWT4-1_S12*fastq.gz > JLCobDIFWT4-1.fastq.gz
cat JLCobS1PWT2*fastq.gz > JLCobS1PWT2.fastq.gz
cat JLCobS1PWT3*fastq.gz > JLCobS1PWT3.fastq.gz
cat JLCobS1PWT3-1*fastq.gz > JLCobS1PWT3-1.fastq.gz
cat JLCobS1PWT4*fastq.gz > JLCobS1PWT4.fastq.gz
cat JLCobS1PWT4-1*fastq.gz > JLCobS1PWT4-1.fastq.gz; done

# Remove adapter contamination, polyA read through, and low-quality reads
set -e
module purge; module load bluebear
module load BBMap/38.87-GCC-8.3.0
for i in *.fastq.gz; do bbduk.sh in=$i out=trimmed_clean_$i \
ref=truseq_rna.fa.gz literal=AAAAAAAAAAAAAAAAAA \
k=13 \
ktrim=r \
useshortkmers=t \
mink=5 \
qtrim=r \
trimq=10 \
minlength=20; done

# Run FastQC
set -e
module load FastQC/0.11.9-Java-11
fastqc `find -name '*fastq*' -print` --outdir=fastqc

# Run MultiQC
set -e
module purge; module load bluebear
module load MultiQC/1.9-foss-2019b-Python-3.7.4
MultiQC
BB_WORKDIR=$(mktemp -d /scratch/${USER}_${SLURM_JOBID}.XXXXXX)
export TMPDIR=${BB_WORKDIR}

# Align sequences with STAR
set -e
module purge; module load bluebear
module load STAR/2.7.2b-GCC-8.3.0
for i in *.fastq.gz; do STAR --runThreadN ${SLURM_NTASKS} \
```

```
--genomeDir /RNAseq/Genomebuild \
--readFilesIn $i \
--readFilesCommand zcat \
--outFileNamePrefix aligned_$i \
--outSAMtype BAM SortedByCoordinate \
--outSAMunmapped Within \
--outSAMattributes Standard
test -d ${BB_WORKDIR} && /bin/cp -r ${BB_WORKDIR} ./
test -d ${BB_WORKDIR} && /bin/rm -rf ${BB_WORKDIR};
done

#STAR aligner

set -e
module purge; module load bluebear
module load STAR/2.7.2b-GCC-8.3.0
module load SAMtools/1.9-foss-2018b
for i in *.fastq.gz; do STAR --runThreadN ${SLURM_NTASKS} \
--genomeDir /RNAseq/Genomebuild \
--readFilesIn $i \
--readFilesCommand zcat \
--outFilterType BySJout \
--outFilterMultimapNmax 20 \
--alignSJoverhangMin 8 \
--alignSJDBoverhangMin 1 \
--outFilterMismatchNmax 999 \
--outFilterMismatchNoverLmax 0.1 \
--alignIntronMin 20 \
--alignIntronMax 1000000 \
--alignMatesGapMax 1000000 \
--limitBAMsortRAM 16000000000 \
--outSAMattributes NH HI NM MD \
--outSAMtype BAM SortedByCoordinate \
--outFileNamePrefix Juliacode_$i ; done

#Sam tools statistics and index
for bamfile in *.sortedByCoord.out.bam ; do samtools index ${bamfile} ; done
for bamfile in *.sortedByCoord.out.bam ; do samtools flagstat ${bamfile}; done
#for i in *sortedByCoord.out.bam; do samtools index
$iAligned.sortedByCoord.out.bam; done
BB_WORKDIR=$(mktemp -d /scratch/${USER}_${SLURM_JOBID}.XXXXXX)
export TMPDIR=${BB_WORKDIR}

# Run feature counts
set -e
module purge; module load bluebear
mkdir counts
module load Subread/2.0.1-GCC-8.3.0
```

```
featureCounts \
    -t exon \
     -g gene_id \
     --primary \
     -a /rds/projects/m/mcgetthm-bone
pepitem/RNAseq/Genomebuild/Mus_musculus.GRCm39.104.gtf \
     -o counts/$i.featureCounts \
     *bam
```

9.2 Script to build genome

```
# Download genome from ensembl

set -e
module purge; module load bluebear
module load wget/1.20.1-GCCcore-8.3.0
wget ftp://ftp.ensembl.org/pub/release-
104/fasta/mus_musculus/dna/Mus_musculus.GRCm39.dna.primary_assembly.fa.gz
wget ftp://ftp.ensembl.org/pub/release-
104/gtf/mus_musculus/Mus_musculus.GRCm39.104.gtf.gz
set -e

# unzip files to run genome build script
module purge; module load bluebear
gunzip Mus_musculus.GRCm39.dna.primary_assembly.fa.gz
gunzip Mus_musculus.GRCm39.104.gtf.gz
BB_WORKDIR=$(mktemp -d /scratch/${USER}_${SLURM_JOBID}.XXXXXX)
export TMPDIR=${BB_WORKDIR}

# Generate genome in STAR
set -e
module purge; module load bluebear
module load STAR/2.7.2b-GCC-8.3.0
STAR --runThreadN ${SLURM_NTASKS} \
--runMode genomeGenerate \
--genomeDir /RNAseq/Genomebuild \
--genomeFastaFiles
/RNAseq/Genomebuild/Mus_musculus.GRCm39.dna.primary_assembly.fa \
--sjdbGTFfile /RNAseq/Genomebuild/Mus_musculus.GRCm39.104.gtf \
--sjdbOverhang 75

test -d ${BB_WORKDIR} && /bin/cp -r ${BB_WORKDIR} ./
test -d ${BB_WORKDIR} && /bin/rm -rf ${BB_WORKDIR}
```

9.3 R-script for analysing S1P treated osteoblast bulk data

```
# Load packages
```

```
library(GOSemSim)
library(ggupset)
library(DESeq2)
library(ggfortify)
library (ggrepel)
library (DESeq2)
library (PCAtools)
library(limma)
library(EnhancedVolcano)
library(edgeR)
library(dplyr)
library(readr)
library(tidyverse)
library(ggnewscale)
library(pathview)

# Load sample information matrix
sampleinfo <- read.delim("SampleInfo.txt")
View(sampleinfo)
sampleinfo

sampleinfo2 <- read.delim("SampleInfoS1P.txt")
View(sampleinfo)
sampleinfo

# Read the data into R
seqdata <- read_tsv("All.featureCounts", comment="#")
head(seqdata)

# Tidy up file names
countdata <- seqdata %>%
  column_to_rownames("Geneid") %>% # turn the geneid column into rownames
  rename_all(str_remove, ".fastq.gzAligned.sortedByCoord.out.bam") %>% # remove
the ".bam" from the column names
  rename_all(str_remove, "Juliacode_trimmed_clean_JLCob") %>%
  select(sampleinfo$Sample) %>%
  as.matrix()
countdata
colSums(countdata)
countdata <- countdata[,c(-6, -7, -8, -9, -10)]

# Obtain CPMs
myCPM <- cpm(countdata)

# Visualise CPM
plot(myCPM[,1],countdata[,1], xlab="CPM", ylab="Raw Count",
main=colnames(myCPM)[1],
     ylim=c(0,50), xlim=c(0,3))
```

```
# Add a vertical line at 0.25 CPM
abline(v=0.25)

# Process data
thresh <- myCPM > 0.3
head(thresh)
rowSums(head(thresh))
table(rowSums(thresh))
keep <- rowSums(thresh) >= 2
summary(keep)
counts.keep <- countdata[keep,]
dim(countdata)
dim(counts.keep)

# Generate PCA

vstcounts <- vst(counts.keep)
vst_pcDat <- prcomp(t(vstcounts))
StatusCol <- match(sampleinfo$Status, c("WT", "S1P")) + 1
autoplot(vst_pcDat,
        data = sampleinfo2,
        colour = 'Batch',
        shape = "Status",
        main = 'VST transform PCA',
        max.overlaps = 10,
        size = 10)

# Design matrix exploring S1P vs WT normalised to batch
design <- as.formula(~ Status + Batch)
modelMatrix <- model.matrix(design, data = sampleinfo)
modelMatrix
sampleinfo2$Status <- factor(sampleinfo2$Status, levels = c("WT", "S1P"))
modelMatrix <- model.matrix(design, data = sampleinfo2)
modelMatrix

# Generation of DESeq dataset
dds <- DESeqDataSetFromMatrix(countData = counts.keep,
                              colData = sampleinfo2,
                              design = design)
dds <- DESeq(dds)
plotDispEsts(dds)
rld <- rlog(dds)

# Comparing treatment groups

WT_vs_S1P <- results(dds,contrast=c("Status", "WT", "S1P"), alpha=0.05)
summary(WT_vs_S1P)
DESeq2::plotMA(WT_vs_S1P, ylim = c(-10,10))
```

```
# Generating p value histogram
hist(WT_vs_S1P$pvalue, breaks=20, col="grey" )


# Finding the top differentially regulated gene and naming samples using ENSEMBL
library( "biomaRt" )
ensembl = useMart( "ensembl", dataset = "mmusculus_gene_ensembl" )
Attributes <- listAttributes(ensembl)
Attributes
head(keytypes(ensembl), n=3)
sum(WT_vs_S1P $padj < 0.05, na.rm = TRUE)
topGeneWT_vs_S1P <- as.data.frame(WT_vs_S1P) %>%
  rownames_to_column("GeneID") %>%
  arrange(padj) %>%
  head(100)
WT_vs_S1P$ensembl
rownames(rld)
WT_vs_S1P$ensembl <- sapply(strsplit( rownames(WT_vs_S1P), split="\\+" ), "[", 1 )
genemap <- getBM( attributes = c("ensembl_gene_id", "entrezgene_id",
"mgi_symbol"),
                  filters = "ensembl_gene_id",
                  values = WT_vs_S1P$ensembl,
                  mart = ensembl )
idx <- match( WT_vs_S1P$ensembl, genemap$ensembl_gene_id )
WT_vs_S1P$entrez <- genemap$entrezgene[ idx ]
WT_vs_S1P$mgi_symbol <- genemap$mgi_symbol[ idx ]
head(WT_vs_S1P, 4)

# Generate table of up and down differentially expressed genes
write.csv(as.data.frame(WT_vs_S1P), file="WT_vs_S1P.csv")
UpWT_vs_S1P <- WT_vs_S1P[WT_vs_S1P$log2FoldChange < 0 &
!is.na(WT_vs_S1P$log2FoldChange), ]
DownWT_vs_S1P <- WT_vs_S1P[WT_vs_S1P$log2FoldChange > 0 &
!is.na(WT_vs_S1P$log2FoldChange), ]
write.csv(as.data.frame(UpWT_vs_S1P), file="UpWT_vs_S1P.csv")
write.csv(as.data.frame(DownWT_vs_S1P), file="DownWT_vs_S1P.csv")

# Creation of a volcano plot
WT_vs_S1P_FC <- lfcShrink(dds,
                          contrast = c('Status','WT','S1P'), res=WT_vs_S1P, type = 'normal')
EnhancedVolcano(WT_vs_S1P_FC,
                lab = WT_vs_S1P$mgi_symbol,
                x = 'log2FoldChange',
                y = 'pvalue',
                title = "WT_vs_S1P",
                xlim = c(-10,10))
library("genefilter")
```

```
topVarGenes <- head(order(-rowVars(assay(rld))),500)
mat <- assay(rld)[ topVarGenes, ]
mat <- mat - rowMeans(mat)
df <- as.data.frame(colData(rld)[,c("Status","Batch")])
pheatmap(mat, annotation_col=df, show_colnames = F, show_rownames = F)
mart <- useMart("ensembl","mmusculus_gene_ensembl")
gns <- getBM(c("mgi_symbol","ensembl_gene_id"), "ensembl_gene_id",
row.names(mat), mart)
row.names(mat)[match(gns[,2], row.names(mat))] <- gns[,1]


# Visualising differentially upregulated or downregulated genes and pathway analysis

library(pheatmap)
library(clusterProfiler)
library(enrichplot)
library(ggplot2)
organism = "org.Mm.eg.db"
library(organism, character.only = TRUE)
df = read.csv("WT_vs_S1P.csv", header = TRUE)
up = read.csv("UpWT_vs_S1P.csv", header=TRUE)
down = read.csv("DownWT_vs_S1P.csv", header=TRUE)
original_gene_listup <- up$log2FoldChange
original_gene_listdown <- down$log2FoldChange
original_gene_list <- df$log2FoldChange
names(original_gene_listup) <- up$X
names(original_gene_listdown) <- down$X
names(original_gene_list) <- df$X
gene_listup<-na.omit(original_gene_listup)
gene_listdown<-na.omit(original_gene_listdown)
gene_list<-na.omit(original_gene_list)
gene_listup = sort(gene_listup, decreasing = TRUE)
gene_listdown = sort(gene_listdown, decreasing = TRUE)
gene_list = sort(gene_list, decreasing = TRUE)

# GSE Go analysis
gseup <- gseGO(geneList=gene_listup,
           ont ="ALL",
           keyType = "ENSEMBL",
           nPerm = 10000,
           minGSSize = 3,
           maxGSSize = 800,
           pvalueCutoff = 0.05,
           verbose = TRUE,
           OrgDb = org.Mm.eg.db,
           pAdjustMethod = "none")
gsedown <- gseGO(geneList=gene_listdown,
             ont ="ALL",
```

```
            keyType = "ENSEMBL",
            nPerm = 10000,
            minGSSize = 3,
            maxGSSize = 800,
            pvalueCutoff = 0.05,
            verbose = TRUE,
            OrgDb = org.Mm.eg.db,
            pAdjustMethod = "none")
gse <- gseGO(geneList=gene_list,
            ont ="ALL",
            keyType = "ENSEMBL",
            nPerm = 10000,
            minGSSize = 3,
            maxGSSize = 800,
            pvalueCutoff = 0.05,
            verbose = TRUE,
            OrgDb = org.Mm.eg.db,
            pAdjustMethod = "none")

#Dotplot
require(DOSE)
dotplot(gseup, showCategory=10, split=".sign") + facet_grid(.~.sign)
dotplot(gsedown, showCategory=10, split=".sign") + facet_grid(.~.sign)
dotplot(gse, showCategory=15) + facet_grid(.~.sign)

# Enrich Go analysis
all_genesup <- as.character(up$ensembl)
all_genesdown <- as.character(down$ensembl)
signif_up <- up[up$padj < 0.05 & !is.na(up$padj), ]
signif_down <- down[down$padj < 0.05 & !is.na(down$padj), ]
signif_df <- df[df$padj < 0.05 & !is.na(df$padj), ]
signif_genesup <- as.character(signif_up$ensembl)
signif_genesdown <- as.character(signif_down$ensembl)
signif_genes <- as.character(signif_df$ensembl)
egoup <- enrichGO(gene = signif_genesup,
            universe = all_genesup,
            keyType = "ENSEMBL",
            OrgDb = org.Mm.eg.db,
            ont = "BP",
            pAdjustMethod = "BH",
            qvalueCutoff = 0.05,
            readable = TRUE)
egodown <- enrichGO(gene = signif_genesdown,
            universe = all_genesdown,
            keyType = "ENSEMBL",
            OrgDb = org.Mm.eg.db,
            ont = "BP",
            pAdjustMethod = "BH",
```

```
            qvalueCutoff = 0.05,
            readable = TRUE)
cluster_summary <- data.frame(egoup)
cluster_summary <- data.frame(egodown)
x2up <- pairwise_termsim(egoup)
x2down <- pairwise_termsim(egodown)
x2up2 <- pairwise_termsim(egoup2)
x2down2 <- pairwise_termsim(egodown2)

# Generation of Emap plot
png(filename="emapup.png", width = 1000, height = 1000)
emapplot(x2up, showCategory=10, color = "p.adjust", layout = "nicely")
dev.off()
png(filename="emapdown.png", width = 1000, height = 1000)
emapplot(x2down, showCategory=10, color = "p.adjust", layout = "nicely")
dev.off()
png(filename="emapup2.png", width = 1000, height = 1000)
emapplot(x2up2, showCategory=30, color = "p.adjust", layout = "nicely")
dev.off()
png(filename="emapdown2.png", width = 1000, height = 1000)
emapplot(x2down2, showCategory=30, color = "p.adjust", layout = "nicely")
dev.off()

# Generation of go, cnet and tree plot
goplot(egoup)
goplot(egodown)
treeplot(x2up)
treeplot(x2down)
png(filename="cnetup.png", width = 2000, height = 1200)
cnetplot(egoup,
        categorySize="pvalue",
        showCategory = 9,
        foldChange= signif_df_lFCup,
        vertex.label.font=6,
        max.overlaps = Inf,
        cex_category = 1,
        cex_gene = 1,
        node_label_size = 1,
        cex_label_category = 1,
        cex_label_gene = 1)
dev.off()
png(filename="cnetdown.png", width = 2000, height = 1200)
cnetplot(egodown,
        categorySize="pvalue",
        showCategory = 9,
        foldChange= signif_df_lFCdown,
        vertex.label.font=6,
        max.overlaps = Inf,
```

```
        cex_category = 1,
        cex_gene = 1,
        node_label_size = 1,
        cex_label_category = 1,
        cex_label_gene = 1)
dev.off()
png(filename="upsetup.png", width = 1000, height = 1000)
upsetplot(x2up)
dev.off()
png(filename="upsetdown.png", width = 1000, height = 1000)
upsetplot(x2down)
dev.off()


# Table of differentially expressed pathways
write.csv(egoup, "EnrichGoWTS1Pup.csv")
write.csv(egodown, "EnrichGoWTS1Pdown.csv")
egoup2 <- clusterProfiler::simplify(egoup, cutoff=0.5, by="p.adjust", select_fun=min)
egodown2 <- clusterProfiler::simplify(egodown, cutoff=0.5, by="p.adjust",
select_fun=min)
write.csv(egoup2, "EnrichGoWTS1Pup2.csv")
write.csv(egodown2, "EnrichGoWTS1Pdown2.csv")



# gseKEGG analysis
ids<-bitr(names(original_gene_list), fromType = "ENSEMBL", toType = "ENTREZID",
OrgDb=organism)
dedup_ids = ids[!duplicated(ids[c("ENSEMBL")]),]
df2 = df[df$X %in% dedup_ids$ENSEMBL,]
df2$Y = dedup_ids$ENTREZID
kegg_gene_list <- df2$log2FoldChange
names(kegg_gene_list) <- df2$Y
kegg_gene_list<-na.omit(kegg_gene_list)
kegg_gene_list = sort(kegg_gene_list, decreasing = TRUE)
kegg_organism = "mmu"
kk2 <- gseKEGG(geneList     = kegg_gene_list,
               organism     = kegg_organism,
               nPerm        = 10000,
               minGSSize    = 3,
               maxGSSize    = 800,
               pvalueCutoff = 0.05,
               pAdjustMethod = "none",
               keyType       = "ncbi-geneid")
View(kk2)
write.csv(kk2, "PathwayWTS1P.csv")

# Visualisation of KEGG pathways
```

```
dotplot(kk2, showCategory = 10, title = "Enriched Pathways" , split=".sign") +
facet_grid(.~.sign)
cnetplot(kk2, categorySize="pvalue", foldChange=gene_list)
dme <- pathview(gene.data=kegg_gene_list, pathway.id="mmu04974", species =
kegg_organism)
knitr::include_graphics("mmu04974.pathview.png")

# Generation of table for differentially expressed genes and pathways

library("formattable")
df <- read.csv("WT_vs_S1P.csv")
df <- df[,c("mgi_symbol", "log2FoldChange", "padj")]
view(df)
signif_df <- df[df$padj < 0.05 & !is.na(df$padj), ]
signif_df <- signif_df %>% arrange(log2FoldChange)
signif_df2 <- signif_df %>% arrange(padj)
view(signif_df2)
view(signif_df)
formattable(df)
plain_formatter <- formatter("span")
width_formatter <- formatter("span",
                         style = x ~ style(width = suffix(x, "px")))
sign_formatter <- formatter("span",
                        style = x ~ style(color = ifelse(x > 0.01, "lightgreen",
                                                 ifelse(x < 0.01, "green", "black"))))
pm_color_bar <- function(color1 = "pink", color2 = "lightgreen"){
  formatter("span",
          style = function(x) style(
            display = "inline-block",
            float = ifelse(x >= 0, "right", "left"),
            "text-align" = ifelse(x >= 0, "right", "left"),
            "margin-left" = ifelse(x >= 0, "0%", "50%"),
            "margin-right" = ifelse(x >= 0,"50%", "0%"),
            "border-radius" = "4px",
            "background-color" = ifelse(x >= 0, color1, color2),
            width = percent(0.5*proportion(abs(as.numeric(x))))
          ))
}
Top50up <- top_n(signif_df, 50, log2FoldChange)
Top50up <- Top50up %>% arrange(-log2FoldChange)
view(Top50up)
Top50bot <- top_n(signif_df, -50, log2FoldChange)
view(Top50bot)
color_bar <- formattable(signif_df, align='c',
          list(padj = color_tile('lightblue', 'white'),
               log2FoldChange = pm_color_bar(c("pink"))))
color_top <- formattable(Top50up, align='c',
                     list(padj = color_tile('lightblue', 'white'),
```

```
                        log2FoldChange = pm_color_bar(c("pink"))))
color_bot <- formattable(Top50bot, align='c',
                    list(padj = color_tile('lightblue', 'white'),
                        log2FoldChange = pm_color_bar(c("pink"))))

html_header="
<head>
<meta charset=\"utf-8\">
<meta name=\"viewport\" content=\"width=device-width, initial-scale=1\">
<link rel=\"stylesheet\"
href=\"https://maxcdn.bootstrapcdn.com/bootstrap/3.3.7/css/bootstrap.min.css\">
</head>
<body>
"
write(paste(html_header, color_top, sep=""), "./Top50.html")
write(paste(html_header, color_bot, sep=""), "./Bottom50.html")
library(htmltools)
library(webshot)
webshot::install_phantomjs(version = "2.1.1",
                        baseURL =
"https://github.com/wch/webshot/releases/download/v0.3.1/",
                        force = TRUE)
export_formattable <- function(f, file, width = "120%", height = NULL,
                           background = "white", delay = 0.2)
{
  w <- as.htmlwidget(f, width = width, height = height)
  path <- html_print(w, background = background, viewer = NULL)
  url <- paste0("file:///", gsub("\\\\", "/", normalizePath(path)))
  webshot(url,
          file = file,
          selector = ".formattable_widget",
          delay = delay)
}
export_formattable(color_top,"top50.png")
export_formattable(color_bot,"bot50.png")
Path <- read.csv("PathwayWTS1P.csv")
Path <- Path[,c("ID", "Description", "NES", "p.adjust")]
view(Path)
Path <- Path %>% arrange(NES)
view(Path)
color_Path <- formattable(Path, align='c',
                    list(p.adjust = color_tile('lightblue', 'white'),
                        NES = pm_color_bar(c("pink"))))
write(paste(html_header, color_Path, sep=""), "./Pathways.html")
export_formattable(color_Path,"Pathways.png", width = "2000")
Pathup <- read.csv("EnrichGoWTS1Pup2.csv")
Pathup <- Pathup[,c("ID", "Description", "GeneRatio", "p.adjust")]
view(Pathup)
```

```
color_up <- formattable(Pathup, align='c',
                        list(p.adjust = color_tile('lightblue', 'white'),
                             GeneRatio = color_tile("Pink", "white")))
write(paste(html_header, color_up, sep=""), "./upPathways.html")
export_formattable(color_up,"UpPathways.png", width = "2000")
Pathdown <- read.csv("EnrichGoWTS1Pdown2.csv")
Pathdown <- Pathdown[,c("ID", "Description", "GeneRatio", "p.adjust")]
view(Pathdown)
color_down <- formattable(Pathdown, align='c',
                        list(p.adjust = color_tile('lightblue', 'white'),
                           GeneRatio = color_tile("Pink", "white")))
write(paste(html_header, color_down, sep=""), "./downPathways.html")
export_formattable(color_down,"downPathways.png", width = "2000")
```

9.4 R-script for analysing data set GSE147174

```
# Load packages
library(Seurat)
library(dplyr)
library(Seurat)
library(patchwork)
library(cowplot)
library(ggplot2)

#Create a merge Seruat objects
data_dir <- '\\GSE147174_RAW\\Day0'
list.files(data_dir) # Should show barcodes.tsv, genes.tsv, and matrix.mtx
expression_matrix <- Read10X(data.dir = data_dir)
Day0 = CreateSeuratObject(counts = expression_matrix, project = "Day0")
colnames(Day0)
expression_matrix
data_dir <- '\\GSE147174_RAW\\Day1'
list.files(data_dir) # Should show barcodes.tsv, genes.tsv, and matrix.mtx
expression_matrix <- Read10X(data.dir = data_dir)
Day1 = CreateSeuratObject(counts = expression_matrix, project = "Day1")
data_dir <- '\\GSE147174_RAW\\Day3'
list.files(data_dir) # Should show barcodes.tsv, genes.tsv, and matrix.mtx
expression_matrix <- Read10X(data.dir = data_dir)
Day3 = CreateSeuratObject(counts = expression_matrix, project = "Day3")
Clast <- readRDS(file = "clast.rds")
Day0
Day1
Day3
Clast <- merge(Day0, y = c(Day1, Day3), add.cell.ids = c("Day0", "Day1", "Day3"),
project = "combined")
dim(Clast)
rownames(Clast)
```

```
head(colnames(expression_matrix))
tail(colnames(expression_matrix))
head(Clast@meta.data)

# Process samples
Clast[["percent.mt"]] <- PercentageFeatureSet(Clast, pattern = "^mt-")
Clast <- subset(Clast, subset = nFeature_RNA > 200 & nFeature_RNA < 6000)
Clast.list <- SplitObject(Clast, split.by = "orig.ident")
Clast.list <- Clast.list[c("Day0", "Day1", "Day3")]
Clast.list

# Find differentially expressed gene
DefaultAssay(Data.combined) <- "integrated"
Data.combined <- ScaleData(Data.combined, verbose = FALSE)
for (i in 1:length(Clast.list)) {
  Clast.list[[i]] <- NormalizeData(Clast.list[[i]], verbose = FALSE)
  Clast.list[[i]] <- FindVariableFeatures(Clast.list[[i]], selection.method = "vst",
                                          nfeatures = 6000, verbose = FALSE)}
reference.list <- Clast.list[c("Day0", "Day1", "Day3")]
Data.anchors <- FindIntegrationAnchors(object.list = reference.list, dims = 1:20)
Data.combined <- IntegrateData(anchorset = Data.anchors, dims = 1:20)
Data.combined <- RunPCA(Data.combined, features = VariableFeatures(object =
Data.combined))
Data.combined <- RunTSNE(Data.combined, reduction = "pca", dims = 1:10)
Data.combined <- FindNeighbors(Data.combined, reduction = "pca", dims = 1:20)
Data.combined <- FindClusters(Data.combined, resolution = 0.5)
p1 <- DimPlot(Data.combined, reduction = "tsne", group.by = "orig.ident", label =
TRUE) + NoLegend()
p2 <- DimPlot(Data.combined, reduction = "tsne", label = TRUE, split.by =
"orig.ident")
plot_grid(p2)
markers <- FindAllMarkers(Data.combined, only.pos = TRUE, min.pct = 0.25,
logfc.threshold = 0.25)
markers
markers %>% group_by(cluster) %>% top_n(n = 2, wt = avg_log2FC)
top10 <- markers %>% group_by(cluster) %>% top_n(n = 10, wt = avg_log2FC)
write.table(top10$gene, file = '\\GSE147174_RAW\\top12.csv')
pdf(file = "\\GSE147174_RAW\\Differences.pdf", width=20, height=9)
DoHeatmap(Data.combined, features = top10$gene) + NoLegend()
dev.off()

# Visualise expression of genes in each cluster
VlnPlot(Data.combined, features = c("ENSMUSG00000023274",
"ENSMUSG00000053977", "ENSMUSG00000030724", "ENSMUSG00000026395"),
pt.size = 0)
FeaturePlot(Data.combined, features = c("ENSMUSG00000051439",
"ENSMUSG00000059498", "ENSMUSG00000028111"))
saveRDS(Data.combined, file = "Osteoclastnew.rds")
```

```
top10$gene <- paste0("'", top10$gene, "'")
top10$gene

# Name new cluster IDs
new.cluster.ids <- c("NA", "Pre-osteoclast", "NA", "Macrophage", "Mature
Osteoclast", "NA", "Macrophage", "Monocyte", "NA", "NA", "Macrophage",
"Monocyte", "Macrophage", "NA")
names(new.cluster.ids) <- levels(Data.combined)
Remaned.Data.combined <- RenameIdents(Data.combined, new.cluster.ids)
DimPlot(Remaned.Data.combined, reduction = "tsne", label = TRUE, split.by =
"orig.ident")

# Isolate cells for further analysis
new.cluster.ids <- c("Macrophage", "Pre-osteoclast", "Macrophage", "Monocyte",
"Osteoclast", "Macrophage", "Monocyte", "Macrophage")
names(new.cluster.ids) <- levels(Renamed.Data.combined)
Renamed.Data.combined <- RenameIdents(Renamed.Data.combined,
new.cluster.ids)
DimPlot(Renamed.Data.combined, reduction = "tsne", label = TRUE, split.by =
"orig.ident")

# Visualisation of gene expression changes
FeaturePlot(Renamed.Data.combined, features = c( "ENSMUSG00000028111"),
label = TRUE)
VlnPlot(Renamed.Data.combined, features = c( "ENSMUSG00000028111",
"ENSMUSG00000022295", "ENSMUSG00000054594", "ENSMUSG00000030669"))
levels(Renamed.Data.combined) <- c("Monocyte", "Macrophage", "Pre-osteoclast",
"Osteoclast")
DefaultAssay(Renamed.Data.combined) <- "RNA"
saveRDS(Renamed.Data.combined, file = "Labelledall.rds")
DotPlot(Renamed.Data.combined, features = c("ENSMUSG00000028111"), cols =
c("blue", "red", "Green"), dot.scale = 20,
      ) + RotatedAxis()
FeaturePlot(Renamed.Data.combined, features = c( "ENSMUSG00000028111"),
label = TRUE, split.by = "orig.ident")
```

9.5 R-script for analysing GSE128423

```
# Load packages
library(dplyr)
library(Seurat)
library(patchwork)

# Create Seurat objects
data_dir <- '\\GSE128423_RAW\\std1'
list.files(data_dir) # Should show barcodes.tsv, genes.tsv, and matrix.mtx
expression_matrix <- Read10X(data.dir = data_dir)
std1 = CreateSeuratObject(counts = expression_matrix)
```

```
data_dir <- '\\GSE128423_RAW\\std2'
list.files(data_dir) # Should show barcodes.tsv, genes.tsv, and matrix.mtx
expression_matrix <- Read10X(data.dir = data_dir)
std2 = CreateSeuratObject(counts = expression_matrix)
data_dir <- '\\GSE128423_RAW\\std3'
list.files(data_dir) # Should show barcodes.tsv, genes.tsv, and matrix.mtx
expression_matrix <- Read10X(data.dir = data_dir)
std3 = CreateSeuratObject(counts = expression_matrix)
data_dir <- '\\GSE128423_RAW\\std4'
list.files(data_dir) # Should show barcodes.tsv, genes.tsv, and matrix.mtx
expression_matrix <- Read10X(data.dir = data_dir)
std4 = CreateSeuratObject(counts = expression_matrix)
data_dir <- '\\GSE128423_RAW\\std5'
list.files(data_dir) # Should show barcodes.tsv, genes.tsv, and matrix.mtx
expression_matrix <- Read10X(data.dir = data_dir)
std5 = CreateSeuratObject(counts = expression_matrix)
data_dir <- '\\GSE128423_RAW\\std6'
list.files(data_dir) # Should show barcodes.tsv, genes.tsv, and matrix.mtx
expression_matrix <- Read10X(data.dir = data_dir)
std6 = CreateSeuratObject(counts = expression_matrix)
Scadden <- merge(std1, y = c(std2, std3, std4, std5, std6), add.cell.ids = c("1", "2",
"3", "4", "5", "6"), project = "Scadden")
Scadden
head(colnames(Scadden))
tail(colnames(Scadden))

# Process RNA sequencing data
Scadden[["percent.mt"]] <- PercentageFeatureSet(Scadden, pattern = "^Mt-")
VlnPlot(Scadden, features = c("nFeature_RNA", "nCount_RNA", "percent.mt"), ncol =
3)
plot1 <- FeatureScatter(Scadden, feature1 = "nCount_RNA", feature2 = "percent.mt")
plot2 <- FeatureScatter(Scadden, feature1 = "nCount_RNA", feature2 =
"nFeature_RNA")
plot1 + plot2
Scadden <- subset(Scadden, subset = nFeature_RNA > 200 & nFeature_RNA <
6000 & percent.mt < 5)
# Find variable genes and clusters
Scadden <- NormalizeData(Scadden, normalization.method = "LogNormalize",
scale.factor = 10000)
Scadden <- FindVariableFeatures(Scadden, selection.method = "vst", nfeatures =
2000)
top10 <- head(VariableFeatures(Scadden), 10)
plot1 <- VariableFeaturePlot(Scadden)
plot2 <- LabelPoints(plot = plot1, points = top10, repel = TRUE)
plot1 + plot2
all.genes <- rownames(Scadden)
Scadden <- ScaleData(Scadden, features = all.genes)
Scadden <- RunPCA(Scadden, features = VariableFeatures(object = Scadden))
```

```
print(Scadden[["pca"]], dims = 1:5, nfeatures = 5)
DimHeatmap(Scadden, dims = 1:15, cells = 500, balanced = TRUE)
Scadden <- JackStraw(Scadden, num.replicate = 100)
Scadden <- ScoreJackStraw(Scadden, dims = 1:20)
JackStrawPlot(Scadden, dims = 1:15)
Scadden <- FindNeighbors(Scadden, dims = 1:10)
Scadden <- FindClusters(Scadden, resolution = 0.5)
head(Idents(Scadden), 5)
Scadden <- RunUMAP(Scadden, dims = 1:10)
DimPlot(Scadden, reduction = "umap")
Scadden <- RunTSNE(Scadden, dims = 1:10)
DimPlot(Scadden, reduction = "tsne")
saveRDS(Scadden, file = "\\GSE128423_RAW\\Scadden.rds")

# Identify and name clusters
Scadden.markers <- FindAllMarkers(Scadden, only.pos = TRUE, min.pct = 0.25,
logfc.threshold = 0.25)
Scadden.markers %>% group_by(cluster) %>% top_n(n = 2, wt = avg_logFC)
pdf(file = "\\GSE128423_RAW\\Raw.Osteoblast.pdf", width=20, height=9)
VlnPlot(Scadden, features = c("Alpl", "Bglap", "Bglap2", "Omd", "Runx2", "Sp7",
"Ostn"), pt.size = 0) #Osteoblast
dev.off()
pdf(file = "GSE128423_RAW\\Raw.Pericyte.pdf", width=20, height=9)
VlnPlot(Scadden, features = c("Acta2", "Rgs5", "Notch3"), pt.size = 0) #Pericyte
dev.off()
pdf(file = "\\GSE128423_RAW\\Raw.Muscle.pdf", width=20, height=9)
VlnPlot(Scadden, features = c("Actn3", "Aldoa", "Tnnt3"), pt.size = 0) #Muscle
dev.off()
pdf(file = "\\GSE128423_RAW\\Raw.Fibro.pdf", width=20, height=9)
VlnPlot(Scadden, features = c("Cd248", "Cd34", "Cdh11", "Col1a1", "Thy1", "Pdgfra",
"Pdpn"), pt.size = 0) #fibroblast
dev.off()
pdf(file = "\\GSE128423_RAW\\Raw.lining.pdf", width=20, height=9)
VlnPlot(Scadden, features = c("Cd55", "Clic5", "Col22a1"), pt.size = 0) #lininglayer
dev.off()
pdf(file = "\\GSE128423_RAW\\Raw.Chondrocyte.pdf", width=20, height=9)
VlnPlot(Scadden, features = c("Sox6", "Cd14", "Chad", "Chadl", "Cilp", "Clu", "Sox9",
"Matn3"), pt.size = 0) #Chondrocyte
dev.off()
pdf(file = "\\GSE128423_RAW\\Raw.0.sino.pdf", width=20, height=9)
VlnPlot(Scadden, features = c("Tfpi", "Ubd", "Lrg1", "Stab2", "Fabp2", "Cldn5",
"Gpm6a", "Rgs4"), pt.size = 0) #EC-sinusoidal
dev.off()
pdf(file = "\\GSE128423_RAW\\Raw.6.arteriolar.pdf", width=20, height=9)
VlnPlot(Scadden, features = c("Egfl7", "Flt1", "Ramp3", "Cdh5", "Icam2", "Emcn",
"Pecam1", "Tie1"), pt.size = 0) #EC-arteriolar
dev.off()
pdf(file = "\\GSE128423_RAW\\Raw.11.arterial.pdf", width=20, height=9)
```

```
VlnPlot(Scadden, features = c("C1qtnf9", "Pecam1", "Vwf", "Cd34", "Egfl7",
"Tspan13", "Sparcl1", "Sdpr"), pt.size = 0) #EC-arterial
dev.off()
pdf(file = "\\GSE128423_RAW\\Raw.1Msc.pdf", width=20, height=9)
VlnPlot(Scadden, features = c("Cxcl12", "Hp", "Adipoq", "Lpl", "Esm1", "Gdpd2",
"Cxcl14", "Kitl"), pt.size = 0) #MSC
dev.off()
pdf(file = "\\GSE128423_RAW\\Raw.Bcell.pdf", width=20, height=9)
VlnPlot(Scadden, features = c("Cd19", "Bcl6", "Blnk", "Ebf1", "Cd79a", "Cd79b"),
pt.size = 0) #B cell
dev.off()
pdf(file = "\\GSE128423_RAW\\Raw.Erythro.pdf", width=20, height=9)
VlnPlot(Scadden, features = c("Gypa", "Rhag", "Tfrc", "Rhd"), pt.size = 0)
dev.off()
 pdf(file = "\\GSE128423_RAW\\Raw.Granulo.pdf", width=20, height=9)
VlnPlot(Scadden, features = c("Cd52", "Cd177", "Clec4a2", "Plaur"), pt.size = 0)
dev.off()
pdf(file = "\\GSE128423_RAW\\Raw.Macro.pdf", width=20, height=9)
VlnPlot(Scadden, features = c("Gp9", "Itga2b", "Cd9", "Gp1bb"), pt.size = 0)
dev.off()
top10 <- Scadden.markers %>% group_by(cluster) %>% top_n(n = 10, wt =
avg_logFC)
DoHeatmap(Scadden, features = top10$gene) + NoLegend()

# Rename cluster IDs
new.cluster.ids <- c("Msc", "Endothelium", "Fibroblast", "Chondrocyte",
"Endothelium", "Erythrocyte", "Chondrocyte",
    "B Cell", "B cell", "Fibroblast", "Erythrocyte", "Osteoblast", "Macrophage", "Null",
"Pericyte", "Granulocyte", "Unknown", "Granulocyte", "Granulocyte",
"Msc", "Chondrocyte", "Erythrocyte")
names(new.cluster.ids) <- levels(Scadden)
Scadden <- RenameIdents(Scadden, new.cluster.ids)
DimPlot(Scadden, reduction = "umap", label = TRUE, pt.size = 0.5) + NoLegend()
saveRDS(Scadden, file = "\\GSE128423_RAW\\Scadden_New.rds") *Takes ages

# Isolate osteoblast populations
Scadden <- readRDS(file = "\\GSE128423_RAW\\Scadden.rds")
VlnPlot(Scadden, features = c("Rgs5", "Notch3", "Chadl", "Cilp", "Pecam1", "Cdh5"),
pt.size = 0)
VlnPlot(Scadden, features = c("Alpl", "Bglap", "Adipoq", "Gdpd2", Pecam1", "Cdh5"),
pt.size = 0)
VlnPlot(Scadden, features = c("Cd19", "Gypa", "Gp9", "Plaur", Pecam1", "Cdh5"),
pt.size = 0)
Stromal <- subset(Scadden, idents = c("Osteoblast", "Endothelium", "Fibroblast",
"Chondrocyte", "Pericyte", "Msc"))
DimPlot(Stromal, reduction = "tsne", label = TRUE, pt.size = 0.5) + NoLegend()
saveRDS(Stromal, file = "\\GSE128423_RAW\\ScaddenStromal.rds")
```

```
# Further cluster osteoblasts
osteo <- subset(Stromal, idents = "Osteoblast")
osteo <- FindNeighbors(osteo, dims = 1:10)
osteo <- FindClusters(osteo, resolution = 0.5)
head(Idents(osteo), 5)
osteo <- RunTSNE(osteo, dims = 1:10)
DimPlot(osteo, reduction = "tsne")
VlnPlot(osteo, features = c("Runx2", "Sp7", "Lepr", "Cxcl12", "Kitl", "Cd200", "Spp1",
"Bglap", "Col1a1"), pt.size = 0)
osteo.markers <- FindAllMarkers(osteo, only.pos = TRUE, min.pct = 0.25,
logfc.threshold = 0.25)
osteo.markers %>% group_by(cluster) %>% top_n(n = 2, wt = avg_logFC)
top10 <- osteo.markers %>% group_by(cluster) %>% top_n(n = 10, wt = avg_logFC)
DoHeatmap(osteo, features = top10$gene) + NoLegend()
new.cluster.ids <- c("Pre-Osteoblasts", "Early Osteoprogenitors", "Mature
Osteoblasts", "Muscle", "Early Osteoprogenitors", "Pre-Osteoblasts", "Pre-
Osteoblasts", "Mature Osteoblasts")
names(new.cluster.ids) <- levels(osteo)
osteo <- RenameIdents(osteo, new.cluster.ids)
DimPlot(osteo, reduction = "tsne", label = TRUE, pt.size = 1) + NoLegend()
osteo <- subset(osteo, idents = c("Pre-Osteoblasts", "Early Osteoprogenitors",
"Mature Osteoblasts"))
my_levels <- c("Early Osteoprogenitors", "Pre-Osteoblasts", "Mature Osteoblasts")
Idents(osteo) <- factor(Idents(osteo), levels= my_levels)

#Visualise gene expression in new osteoblast clusters
VlnPlot(osteo, features = c("Cxcl12", "Kitl", "Runx2", "Col1a1", "Alpl", "Ptch1", "Sp7"),
pt.size = 0.5)
DotPlot(Scadden, features = c("Ywhaz")) + ggtitle("") + theme(legend.position =
'none') & theme(axis.title.x = element_blank(), axis.text.x = element_blank())
FeaturePlot(Scadden, features = c("S1pr1"), reduction = "tsne", label=TRUE) +
ggtitle("") + theme(legend.position = 'none')
```

9.6 Published review

Bone Research www.nature.com/boneres

REVIEW ARTICLE OPEN

Adiponectin signalling in bone homeostasis, with age and in disease

Jonathan W. Lewis[1], James R. Edwards[2], Amy J. Naylor[1] and Helen M. McGettrick[1]

Adiponectin is the most abundant circulating adipokine and is primarily involved in glucose metabolism and insulin resistance. Within the bone, osteoblasts and osteoclasts express the adiponectin receptors, however, there are conflicting reports on the effects of adiponectin on bone formation and turnover. Many studies have shown a pro-osteogenic role for adiponectin in in vivo murine models and in vitro: with increased osteoblast differentiation and activity, alongside lower levels of osteoclastogenesis. However, human studies often demonstrate an inverse relationship between adiponectin concentration and bone activity. Moreover, the presence of multiple isoforms of adiponectin and multiple receptor subtypes has the potential to lead to more complex signalling and functional consequences. As such, we still do not fully understand the importance of the adiponectin signalling pathway in regulating bone homeostasis and repair in health, with age and in disease. In this review, we explore our current understanding of adiponectin bioactivity in the bone; the significance of its different isoforms; and how adiponectin biology is altered in disease. Ultimately, furthering our understanding of adiponectin regulation of bone biology is key to developing pharmacological and non-pharmacological (lifestyle) interventions that target adiponectin signalling to boost bone growth and repair in healthy ageing, following injury or in disease.

Bone Research (2021)9:1 ; https://doi.org/10.1038/s41413-020-00122-0

The principal cellular constituents of bone (primarily osteoblasts and osteoclasts) rapidly respond to circulating signals, altering global levels of bone formation and resorption respectively, and thus impacting bone homeostasis.[1–3] The effects of adiponectin in bone have been researched in multiple conditions; however, these studies report variable outcomes with little explanation. Further exploration of adiponectin signalling is essential to fully understand the possibility of promoting or inhibiting its actions during ageing or disease. Of note, very few studies have examined the effect of adiponectin on osteoclasts, so we understand much less about its role in bone turnover. Here we explore the current literature on adiponectin in bone, looking in depth at the comparison between human and murine in vivo and in vitro data in health, with age and in disease, with reference (where possible) to the adiponectin isoform described.

ADIPONECTIN

Adiponectin is the most abundant circulating adipocyte-secreted adipokine found in blood serum (5–15 μg/mL).[4,5] The full-length protein (244 amino acids[6]) can be cleaved into smaller active components,[7] which circulate either as it's globular domain[7] or as full-length homo-complexes referred to by their differing molecular weights (MW): a trimer (low MW; LMW); a hexamer (medium MW; MMW) or an oligomer (high MW; HMW) (Fig. 1).[8–10] At a cellular level, adipocytes within the bone marrow adipose tissue (BMAT) and white adipose tissue (WAT) produce all of these adiponectin isoforms.[11] For example, similar levels of adiponectin gene expression were observed in murine adipocytes isolated from WAT or BMAT.[11] Yet protein expression was reportedly lower in rat total BMAT lysates[12] and higher in adipocytes isolated from BMAT from rabbits and healthy 30-year old humans,[11] compared to WAT. As such adipocytes from both tissues can contribute to the local levels of adiponectin within the bone (and bone marrow), as well as the circulating levels of adiponectin that are more commonly reported in studies. Indeed, BMAT levels positively correlate with total serum adiponectin levels in humans.[13] Whilst, the relative contribution of each adipose tissue to the levels of adiponectin in the bone is unclear, and may change with age and disease (as discussed in the later sections), many studies speculate that due to its proximity BMAT acts as the largest contributor of adiponectin to the local bone levels.

Adiponectin mediates its effects through adiponectin receptors 1 and 2 (AdipoR1 and AdipoR2)[14,15] leading to downstream signalling through several pathways including AMP kinase (AMPK), PI3K/protein kinase B, MAP kinase (MAPK), STAT3 (signalling transducer and activator of transcription 3) and ceramidase activation (Fig. 1).[16–18] In addition to the classical adiponectin receptors, HMW and MMW adiponectin can also interact with T-cadherin (cadherin-13; CDH13).[19,20] However, AdipoR1 and R2 knockout mice have a near-complete lack of adiponectin signalling,[21] thus the functional relevance of T-cadherin in mediating the effects of adiponectin is currently unclear. Moreover, potential signalling mechanisms downstream of adiponectin–T-cadherin interactions have not yet been fully explored. Crucially, evidence suggests that the individual adiponectin receptors have differing binding efficacies for the different isoforms of adiponectin; with a murine myocyte cell line

[1]Rheumatology Research Group, Institute of Inflammation and Ageing, University of Birmingham, Birmingham B15 2TT, UK and [2]Ageing & Regeneration Research Group, Botnar Research Centre, University of Oxford, Oxford OX3 7LD, UK
Correspondence: Helen M. McGettrick (h.m.mcgettrick@bham.ac.uk)

Received: 24 April 2020 Revised: 28 August 2020 Accepted: 14 October 2020
Published online: 07 January 2021

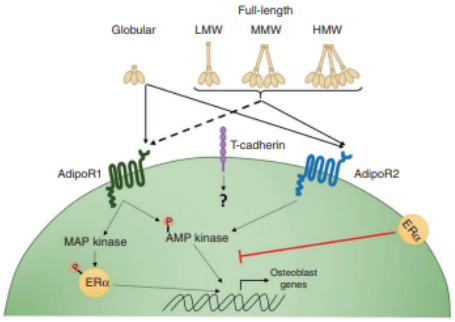

Fig. 1 Adiponectin signalling. The full-length adiponectin protein can be cleaved into smaller active components, which circulate either as it's globular domain[7] or as full-length homo-complexes—low molecular weight (LMW) trimers, medium molecular weight (MMW) hexamers or high molecular weight (HMW) oligomers.[8–10] Adiponectin can bind to two classical adiponectin receptors 1 and 2 (AdipoR1 and AdipoR2)[14,15] leading to downstream signalling through several pathways, primarily driving AMP kinase (AMPK) and to a lesser extent activating MAP kinase (MAPK).[16–18] Expression of the oestrogen receptor (ERα) appears to skew adiponectin receptor signalling to primarily trigger the MAPK pathway,[61] which in turn phosphorylates both ERα and transcription factor SP1, altering downstream signalling. AdipoR1 has a higher affinity for the globular domain of adiponectin, whilst AdipoR2 displays an intermediate affinity for all adiponectin isoforms.[21] In addition to the classical adiponectin receptors, HMW and MMW adiponectin can also interact with T-cadherin (cadherin-13; CDH13),[19,20] although the downstream signalling and functional outcomes from these interactions are currently unknown

demonstrating higher affinity of AdipoR1 for globular adiponectin, whilst AdipoR2 displays an intermediate affinity for all adiponectin isoforms.[14] Thus, it is likely that these differing protein–receptor interactions results in divergent cellular responses to adiponectin, even within the same cell. In addition, many studies explore serum levels rather than the tissue-level expression of adiponectin, and whilst the bone is well vascularised,[22] understanding the link between serum levels and local tissue effects has proved challenging.

ADIPONECTIN RECEPTOR EXPRESSION IN CELLS OF THE BONE

Within the bone, precursor bone cells, osteoblasts and osteoclasts have all been reported to express the adiponectin receptors, although conflicting findings exist that are important to consider when interpreting adiponectin-signalling responses from in vitro studies. For instance, AdipoR1 and R2 mRNA and protein are detectable in murine osteoblasts,[23] human osteoblast precursors (bone marrow stromal cell- BMSC and osteoblast-like cell lines)[24,25] and osteoclast precursors (human peripheral blood monocytes, PBMC).[26,27] In all cases, adiponectin receptor 1 was detected at significantly higher levels (up to 100-fold) than adiponectin receptor 2. Indeed in some studies expression of AdipoR2 was below the limits of detection—e.g. no AdipoR2 protein was detected in healthy human tibial osteoblasts[28] nor gene expression observed in the MC3T3 murine osteoblast precursor cell line.[29] The absence or lower expression of adiponectin receptor 2 on bone cells suggests that they preferentially response to globular adiponectin, which has a higher affinity for adiponectin receptor 1 than the other forms of adiponectin.[14] Moreover, the majority of in vitro osteoblast models display increased expression of AdipoR1, but not AdipoR2, following differentiation, including Saos-2[25] and C3H10T1/2,[24] a response not seen when MC3T3 were used.[23] In contrast, MC3T3 cells up-regulated AdipoR2 expression and down-regulated AdipoR1 expression upon differentiation.[23] This difference in the expression pattern by MC3T3 cells upon differentiation may help to explain some of the confounding results observed between studies exploring osteoblast response to adiponectin. By contrast, in vitro osteoclastogenesis does not appear to affect the expression of adiponectin receptors at either the mRNA or protein level.[27]

The expression of adiponectin receptors by the main precursors and mature bone cells demonstrates that all have the potential to interact with and respond to adiponectin during the different stages of bone homeostasis. However, key questions remain: What is the impact of adiponectin signalling on bone formation and turnover? How are these adiponectin-mediated effects influenced by bone damage, with age and by inflammatory diseases? Can a greater understanding of adiponectin regulation of bone homeostasis lead to novel strategies to repair injured and damaged bone?

IMPACT OF ADIPONECTIN ON OSTEOBLASTOGENESIS AND ACTIVITY

Bone marrow adipocytes continuously release adipokines into the bone niche, bathing all cells including osteoblast and osteoclast progenitors in adiponectin.[30,31] Indeed, the limited available data indicates that within the bone marrow niche adiponectin acts to promote osteoblastogenesis, whilst simultaneously inhibiting osteoclastogenesis (Table 1).[24,32–35] Addition of full-length[24,35] or globular[36] adiponectin induces the expression of the osteogenic-related genes osteopontin[24,36] and alkaline phosphatase[24,35,36] in the murine mesenchymal progenitor cell line, C3H10T1/2,[24] the pre-osteoblast MC3T3-E1 murine cell-line,[35] and in human adipose-derived stem cells (ADSC) in vitro.[36] Moreover, BMSCs from 5 week old adiponectin knockout mice exhibited reduced gene expression of key osteoblast promoting lysine specific histone demethylases (KDM4B and KDM6B) when compared to wildtype mice infused with either globular or full-length adiponectin.[37] Absence of KDM4B and KDM6B reportedly increased gene expression of PPARG in human BMSC and thus switched the differentiation fate from osteogenic to adipogenic in vitro.[38] Indeed, the presence of fatty bone marrow in adiponectin knockout mice was attributed to reduced KDM4B and KDM6B expression in BMSCs, triggering adipogenesis and ultimately causing a reduction in osteoblasts and increase in adipocytes on the trabecular surfaces.[37] Furthermore, siRNA knockdown of AdipoR1 in C3H10T1/2 cells significantly reduced adiponectin-induced osteoblast differentiation in vitro.[24] Supporting this, enhanced matrix mineralisation was observed in human ADSCs cultured in the presence of globular adiponectin compared to untreated controls.[36] Of note, one study disagrees with the above literature: Kajimura et al., demonstrated that 6 week old adiponectin knockout mice have increased bone mass and osteoblast numbers, suggesting adiponectin inhibits bone mass accrual in young mice.[34] However, no changes were observed in the gene expression of the osteoblast differentiation markers runx2 and osterix in 12-week-old bones from adiponectin knockout mice compared to the wildtype controls—suggesting that by this time point adiponectin was no longer able to limit bone formation.[34] Importantly the mineralisation capacity of cells from these bones was not assessed. Bones from 10-day old adiponectin knockout mice exhibited increased cellular proliferation and reduced apoptosis.[34] Indeed, treating serum-starved wildtype calvarial osteoblasts with either full-length or global adiponectin reduced proliferation and increased apoptosis rate over 24 h.[34] Importantly, no changes in proliferation or apoptosis have been reported in the aforementioned studies, where various osteoblasts were cultured in the presence of

Table 1. In vitro effects of adiponectin on bone cells

Adiponectin Type	Species	Cell type	Effect	Ref
Full-length	Mouse	C3H10T1/2	↑ OPN mRNA ↑ ALP mRNA	24
	Mouse	MC3T3	↑ Mineralisation	35
	Mouse	RAW624	↓ Differentiation ↑ Apoptosis	32
	Human	Mononuclear osteoclast precursor	↓ Differentiation ↑ Apoptosis	35
	Mouse	$CD14^+$ PBMC	↓ Resorption	35
Globular	Human	Adipogenic stem cells	↑ RUNX2, OPN, ALP mRNA ↑ Mineralisation	36
	Mouse	RAW264.7	↓ Resorption ↓ Osteoclast number ↑ Apoptosis	39
All	Mouse	Adiponectin KO BMSC	↓ Adipogenic differentiation	37
	Mouse	AdipoR1 siRNA KD C3H10T1/2	↓ Osteoblast differentiation	24

AdipoR adiponectin receptor 1, *ALP* alkaline phosphatase, *BMSC* bone marrow stem cells, *KD* knock down, *KO* knockout, *OPN* osteopontin, *PBMC* peripheral blood monocytic cells, *RUNX2* RUNX family transcription factor 2, *siRNA* short interfering RNA

serum.[24,35,36] Serum starvation, therefore, may account for the discrepancies in proliferation and apoptosis observed between these studies and the Kajimura et al. Overall, adiponectin appears to have a predominantly positive role in boosting pre-osteoblast differentiation and mineralisation capacity, potentially protecting the bone by inducing formation and repair.

IMPACT OF ADIPONECTIN ON OSTEOCLASTOGENESIS AND ACTIVITY

By contrast, few groups have analysed the effect of adiponectin on osteoclastogenesis to date (Table 1). Addition of full-length adiponectin significantly inhibited the ability of human mononuclear cells and murine macrophage progenitors to differentiate into mature osteoclasts when cultured in vitro in the presence of osteoclastogenic stimulating factors [macrophage colony-stimulating factor and receptor activator of nuclear factor kappa-B ligand (RANKL)].[39] Similarly, globular adiponectin blocked RANKL-induced osteoclastogenesis of the murine monocyte cell line RAW264.7.[39] Importantly these studies indicate that adiponectin reduces the ability of osteoclast precursors to mature. Akin to data on osteoblast precursors, global adiponectin treatment reduced the proliferation rate of RAW264.7 osteoclast precursors and increased their apoptosis through APPL1-mediated down-regulation of Akt1 activity.[39] As such it is unclear whether adiponectin mediates a direct effect on osteoclastogenesis or an indirect effect by reducing overall precursor numbers. Additional studies are urgently required to reproduce these findings and clarify the supposed anti-osteoclastogenic role of adiponectin.

REGULATOR OF OSTEOBLAST AND OSTEOCLAST PROGENITOR MIGRATION

Osteoblast progenitors must exit the bone marrow niche to migrate towards the sites of resorption and/or damage (Fig. 2).[40] Indeed fate mapping experiments have revealed that 70% of the osteoblasts found replenishing the endosteal surface during homeostasis originated from the bone marrow-derived osteoblast precursors.[41] In addition, YFP-positive osteoblast precursors migrated from the neighbouring bone marrow to the site of calvarial microfracture, accounting for the majority of the cells at the site of injury after 7 days when compared to the bone resident pre- and mature osteoblast.[41] This process can be controlled by the CXCR4-CXCL12 axis, where high levels of CXCL12 attract CXCR4 expressing cells and retain them.[42] Globular adiponectin significantly reduces expression of CXCR4 mRNA in cultured murine BMSCs,[40] therefore reducing the attraction of these cells to CXCL12 in the bone marrow. Similarly, adiponectin-deficient mice have higher numbers of CXCL12 positive cells within the bone marrow compared to wildtype mice,[40] indicating that adiponectin regulates the exit of BMSCs from the bone marrow into the local bone environment where they can differentiate into osteoblasts.[40,43] In addition, globular adiponectin enhanced BMSC migration across a Matrigel-coated Boyden chamber over 16h in vitro, which was coupled with an increase in MMP9 mRNA expression.[40] Moreover, systemic globular adiponectin infusion increased serum CXCL12 levels and promoted $nestin^+$ BMSC exit the bone marrow niche into the peripheral blood.[40] Furthermore, therapeutic infusion of globular adiponectin significantly increased new bone formation at the site of calvarial injury, to a higher degree than seen in wildtype and adiponectin-deficient mice.[40] This was attributed to enhanced migration of osteoblasts from the periphery to the injury site following adiponectin treatment, resulting in increased bone regeneration. Collectively these studies indicate that adiponectin regulates the CXCR4–CXCL12 axis within the bone marrow niche, facilitating the migratory exit of bone progenitor cells from this niche into the periphery in health and in response to injury. Comparably, osteoclast precursors such as PBMCs, express CXCR4[44] and therefore osteoclast migration out the bone may mirror the mechanisms described for osteoblasts. Yet, few studies have examined the functional consequence of adiponectin on osteoclast migration, which are required to fully understand the overall impact of adiponectin on bone.

In addition to the CXCR4-CXCL12 axis, the bioactive lipid — sphingosine-1-phosphate (S1P)— has also been reported to influence the migration of osteoblast and osteoclast precursors (Fig. 2).[45,46] S1P is synthesised intracellularly through the phosphorylation of sphingosine by the sphingosine kinases 1 and 2, and then trafficked out of the cell via sphingosine transporters where it interacts with S1P receptors to mediate its effects.[47] Elevated levels of circulating S1P are observed in adiponectin-overexpressing transgenic mice.[17] However, very little is known about the possible consequence of adiponectin on S1P-regulated migration. Both osteoblast and osteoclast precursors express S1P receptors (S1PR1, S1PR2).[48–50] In addition, BMSC

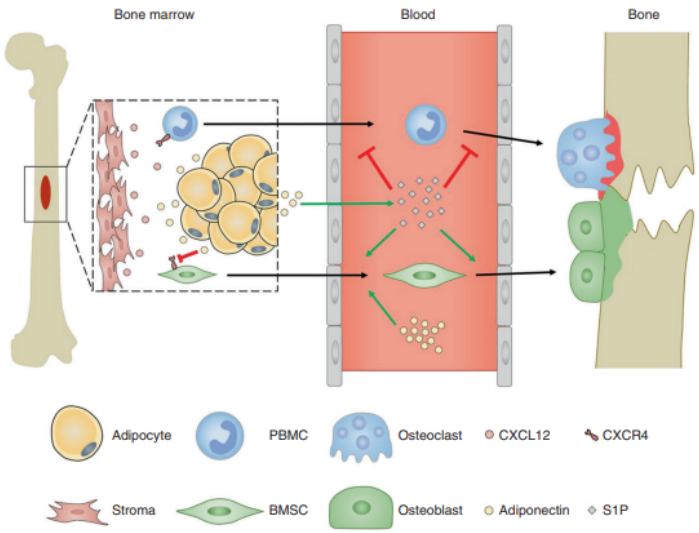

Fig. 2 Adiponectin regulation of osteoblast and osteoclast migration. Osteoblast progenitors must exit the bone marrow niche to migrate towards the sites of resorption and/or damage. In fate mapping experiments, YFP expressing bone marrow-derived osteoblast precursors migrated to the endosteal surface to replenish osteoblast populations in healthy conditions and also in response to calvarial microfracture.[41] Osteoblast and osteoclast progenitors express CXCR4 and migrate towards high levels of CXCL12 causing them to be retained in the bone marrow.[42] Adiponectin directly[40] and through increasing S1P in the serum,[17] leads to increased osteoblast progenitor migration into the circulation and to bone in health,[48] which is enhanced during injury.[41,116,117] In contrast, S1P chemorepels osteoclast progenitors and osteoclasts,[51] leading to decreased migration to damaged sites. This ultimately maintains the balance between resorption (red) and formation (green) to ensure structured bone repair

migrate towards S1P in vitro.[48] However, osteoclast precursors chemorepel from S1P, either through S1PR1/2[50] or S1PR2/3.[51] In addition, sphingosine kinase 1 activity was upregulated in osteoclasts upon differentiation,[52] indicating a role for osteoclast S1P release in maintaining the osteoclast-osteoblast balance. However, the impact of adiponectin in these responses remains unknown. One could postulate that direct effects of adiponectin signalling and adiponectin-induced increases in serum S1P cause the recruitment of the earliest bone precursors into the periphery, whilst simultaneously retaining pre-osteoblasts and mature osteoclasts within the bone to enable bone homeostasis and repair. Overall, these studies indicate that adiponectin increases osteoblast precursor migration, in part through CXCR4–CXCL12 axis and S1P, to favour bone formation. However, further work is required to fully understand these interactions and their functional consequences, as well as other potential molecular mechanisms underpinning adiponectin regulation of osteoblast and osteoclast migration.

ROLE OF ADIPONECTIN IN THE REGULATION OF BONE HOMEOSTASIS

In health and ageing

The actions of adiponectin in homeostatic bone turnover have been extensively explored in human and murine in vivo and in vitro studies in order to understand how it can be targeted in disease states (Tables 2 and 3). Of note, these studies overwhelmingly focus on juvenile or adult models, where BMAT and WAT are fully developed, and can both contribute to bone adiponectin levels. No studies to date have examined the role of adiponectin in foetal and neonatal bone development.

Global overproduction of full-length adiponectin significantly increases trabecular bone mass and reduces bone resorption (as measured by plasma cross-linked N-telopeptides of type I collagen (nTx) levels) over a 2-week period in young 8 week old mice.[35] Similarly, higher bone mineral density (BMD) and reduced number of TRAP5b-positive osteoclasts were observed in aged (56 weeks) AdipoR1-overexpressing transgenic mice, but not in younger mice aged 8 or 32 weeks.[33] Likewise, AdipoR1-deficient mice have decreased trabecular bone volume, thickness, number and spacing, along with reduced osteoblast numbers.[53] Similarly, 36 week old adiponectin knockout mice also display severe low bone mass affecting all skeletal elements, yet this was linked to decreased number and proliferation ability of osteoblasts rather than effects on osteoclasts.[34] Interestingly osteoclast numbers were unaffected by loss of AdipoR1 in young mice aged 4 and 30 weeks.[53] Collectively, these studies suggest that age may significantly alter the effects of adiponectin on osteoclasts. Moreover, they suggest that adiponectin-signalling through AdipoR1 is critical for maintaining osteoblast survival and activity with age and may also regulate osteoclast apoptosis.

Mirroring the in vivo findings described above, bone explants from 3-day old wildtype mice implanted subcutaneously into the flank of adiponectin knockout mice had reduced trabecular volume and cortical bone parameters 2–4 weeks after implantation when compared to those implanted into wildtype mice,[39] indicating that systemic levels of adiponectin were sufficient to impact normal bone remodelling. In vitro studies support these findings, with full-length adiponectin stimulating bone matrix deposition and hydroxyapatite formation by MC3T3-E1 cells, and reducing its resorption by $CD14^+$ PBMC osteoclast precursors.[35] Collectively these data indicate that adiponectin promotes bone

Table 2. In vivo effect of adiponectin in health, ageing and obesity

Condition	Species	Model	Adiponectin Type	Effect	Ref
Health	Mouse	homeostasis	AdipoR1 overexpression	↑ BMD ↓ TRAP5b	33
	Mouse	Adenovirus induced adiponectin overproduction	Full-length	↑ Bone mass, ↓ NTx	35
	Mouse	Bone explants	Adiponectin KO	↓ Trabecular/Cortical bone	39
	Mouse	homeostasis	AdipoR1 KO	↓ Trabecular bone ↓ Osteoblast number	53
Ageing	Human	67.2 ± 13.9[a]	–	Serum adiponectin ≠ Bone Strength	65
	Human	Post menopause	–	↑ Serum adiponectin ↓ BMD	57
	Mouse	OVX	Adiponectin KO	↓ Bone damage	58
	Rabbit	OVX with HA implant	Full-length	↓ Bone loss	59
	Human	40 ± 11.5[a]	–	↑ Serum adiponectin = ↓Bone Strength	64
	Mouse	5 months	Adiponectin-Tg overexpression	↑ Serum adiponectin = ↓Bone Strength	66
Obesity	Human	Weight loss	–	↑ Serum adiponectin ↓ β-CTX collagen	71

AdipoR1 adiponectin receptor 1, *β-CTX collagen* collagen β c-terminal telopeptide; *BMD* bone mineral density, *HA* hydroxyapatite, *KO* knockout, *NTx* cross-linked N-telopeptides of type I collagen, *OVX* ovariectomy, *Tg* transgenic
[a]Years as mean ± SD

Table 3. In vivo effect of adiponectin in disease

Disease	Species	Model	Adiponectin Type	Cell	Effect	Ref
OA	Human	–	–	–	↑ Serum adiponectin in erosive OA	86
	Mouse	STR/Ort	–	–	↑ Serum adiponectin = ↓ Severity	87,118
Periodontitis	Mouse	Experimental periodontitis	Adiponectin KO	–	↑ Osteoclast number, ↓ Bone strength	89
			Globular	–	↑ Osteoclast number, ↓ Bone loss	89
	Mouse	In vitro LPS inflammation	Globular	RAW624	↓ TNF-α and IL1β ↑ IL10	90
RA	Human	–	Full-length	–	↑ Serum adiponectin	91
	Human	–	Full-length	–	↑ Plasma adiponectin	91,92
	Human	Ex vivo culture	Unknown	Osteoblast	↓ Osterix mRNA ↑ OPG mRNA	94
	Human	Ex vivo culture	Unknown	Osteoclast	↑ MMP9 & TRAP mRNA	94
	Mouse	CIA	Full-length	–	↑ Damage, ↓ BMD, ↑ Osteoclast number	98
	Mouse	CIA	Globular	–	↓ BMD	99
	Mouse	CIA	Unknown	–	↓ Score	101
	Mouse	CIA	Full-length	–	↓ Score, ↓ MMP3	102
Osteosarcoma	Human	16-year-old patient	–	–	↑ Adiponectin mRNA in diseased bone	105
	Mouse	In vitro	Globular	Saos-2	↑ Viability	106
	Mouse	In vitro	AdipoR inhibitor	Saos-2	↓ Proliferation	108
Cancer metastasis	Mouse	5TGMI cell cancer	Adiponectin KO	–	↑ Bone damage	111
			L-4F (HMW adiponectin)	–	↓ Bone damage	111
OI	Murine	*Col1a1* mutation	–	–	↓ Body fat	113
Osteopetrosis	Murine	Obesity induced	–	–	Exercise = ↓ Aberrant bone growth	114
	Human	Infantile osteopetrosis	Full-length	BMMC	↓ Adiponectin release ↓ Adipogenic differentiation	115

AdipoR adiponectin receptor, *BMMC* bone marrow mononuclear cells, *BMD* bone mineral density, *CIA* collagen induced arthritis, *HMW* high molecular weightb, *LPS* lipopolysaccharide, *MMP* matrix metalloproteinase, *KO* knockout, *OA* osteoarthritis, *OI* osteogenesis imperfecta, *OPG* osteoprotegerin, *RA* rheumatoid arthritis, *Score* clinical score, *SRT/Ort* murine strain prone to OA

formation and limits bone resorption in healthy young and old mice (Fig. 3A), where exogenous adiponectin may serve to maintain bone mass during age-related bone loss. Moreover, therapeutically adjusting the circulating levels of adiponectin may result in beneficial effects on the bone, avoiding the need to develop drugs that specifically target the bone. Importantly, no studies have yet explored the role of adiponectin in the development and maturation of healthy human bones either in vivo or ex vivo.

signalling through the MAPK pathway in these tissues and potentially contributes to menopause-induced bone loss.

Age-related decline in BMD is associated with increased susceptibility to microfractures in humans,[63] however very few studies have directly examined the effect of adiponectin on bone strength. High circulating levels of adiponectin negatively correlate with bone strength and reduced maximal load in middle-aged overweight men (mean ± S.D.—age 40 ± 11.5 years, BMI 25 ± 6.2).[64] By contrast, no link has been found between circulating adiponectin levels and the frequency of fracture in the men over the age of 70 with an average BMI ~26 in this correlative study.[65] These limited data appear to suggest that circulating levels of adiponectin influences bone strength and risk of fracture at least in overweight middle-aged men. However, more detailed longitudinal human studies, in which confounders such as BMI are carefully controlled for, are required to fully dissect the interaction of circulating adiponectin levels with BMD and fracture rates across different age groups.

Even fewer in vivo and in vitro studies exist that have directly assessed bone strength in response to adiponectin. Agreeing with the human data, adiponectin-overexpressing transgenic mice exhibited lower bone mass and lower strength at 2, 4[33] and 5[66] months compared to age matched wild-type controls. In addition treating 3-D cultures of human osteoblasts and osteoclast precursors in mineral forming spheres (known as osteospheres) with an unknown adiponectin isoform significantly reduced their strength, as assessed using nano-indentation; indicating weaker, more breakable bone.[67] Mechanistic studies are required to elucidate the how the ageing process alters adiponectin signalling within the bone, but also systemically, to modulate BMD and strength.

In obesity and obesity-related diseases

Circulating adiponectin levels are decreased in obesity in both adults and children (young and adolescent).[68,69] This is in-part due to adipocytes in the WAT acquiring a pro-inflammatory phenotype, which alters their production of various adipokines including adiponectin.[70] Whether adipocytes in BMAT acquire the same obesity-linked phenotype remains unclear. Interestingly, weight loss in obese adolescents was associated with increased serum adiponectin levels coupled to lower levels of the bone resorption marker, collagen β c-terminal telopeptide.[71] Moreover, caloric restriction in mice[11,72] or humans with anorexia nervosa[73–76] has also been associated with an increase in bone marrow adiposity, coupled with increased adiponectin and a decrease in bone mass. Despite the link between obesity and reduced BMD (Table 2),[69,77,78] most studies overlook adiponectin measurements in their analyses. Therefore, further research is needed to explore the impact of obesity in humans on adiponectin signalling in bone.

Whilst murine models can provide a more in-depth study of the effects of obesity on the bone, again none of the available literature explores the importance of adiponectin in the changes they describe. For instance, 12-weeks of high fat diet significantly reduced trabecular bone volume and number,[79] and decreased the amount of cancellous bone, as well as collagen and osteoid expression observed after 23-weeks of the diet[80] in wildtype mice — where these changes were linked to increases in adipocyte volume, and thus BMAT, rather than reduction in osteoblast or osteoclast numbers. Moreover, obesity significantly limited fracture repair, with no callus or connected bone observed in obese mice days after fracture unlike control animals.[81] High levels of limb fractures are also observed in obese children,[82–84] where abnormal BMAT and adiponectin levels may be contributing to reduced bone strengthen and delayed repair.

Obesity increases the risk of patients developing osteoarthritis (OA) and therefore, it is possible that changes in adiponectin may have detrimental effects on the bones of patients with OA (Table 3).[77,78,85] Human studies have revealed higher levels of adiponectin in a meta-analysis of patients with more advanced OA compared to BMI matched patients with new onset OA;[78] and in the serum of women with erosive OA in the hand compared to non-erosive disease.[86] In contrast, serum adiponectin concentrations negatively correlated with cartilage lesions and OA severity in adolescent (26 weeks old) STR/Ort mice, suggesting adiponectin has a protective role in a human-like murine OA model.[87] It is difficult to make any definitive conclusions based on the currently available data on whether changes in adiponectin levels represent part of the molecular mechanism driving pathology of OA, or are part of the protective response to the on-going joint damage. As such these concepts need to be explored further taking into account the aforementioned confounding factors.

In inflammatory disease

Periodontitis. Periodontitis is the most common inflammatory bone disease worldwide, affecting 60% of >75-year olds.[88] Despite this, we have a limited understanding of the importance of adiponectin in periodontal bone damage; with most of the evidence to date generated using murine models (Table 3). For instance, following induction of experimental periodontitis by coating molars with a bacterial broth, adiponectin knockout mice have increased osteoclast numbers in palatal bone compared to wildtype control mice.[89] Moreover, globular adiponectin therapy reduced the number of $TRAP^+$ osteoclasts in the inflamed palatal bone in adiponectin knockout mice, leading to a concomitant reduction in alveolar bone loss.[89] In vitro, RAW264 osteoclast precursors treated with lipopolysaccharide (LPS) and globular adiponectin showed reduced pro-inflammatory cytokine secretion (TNF-α and IL-1β) and increased anti-inflammatory IL-10 release, compared to LPS treatment alone.[90] Clearly further studies are required, but the data available suggest that adiponectin exerts a direct anti-osteoclastogenic role during periodontitis.

Rheumatoid arthritis. Patients with rheumatoid arthritis (RA) have elevated levels of adiponectin in plasma[91,92] and synovial fluid,[93] compared to sex, age and BMI-matched control samples. These findings correlate with radiographic erosions suggesting a role for adiponectin in disease pathology (Table 3).[92,93] Moreover, adiponectin stimulated MMP9 and TRAP expression in cultured human osteoclasts from RA patients[94]—unlike what has been reported for healthy osteoblasts (see above). Importantly these data suggest that the chronic inflammatory environment in RA switches the adiponectin response in osteoclasts from being anti-osteoclastogenic to a pathological pro-resorptive response. However, osteoblasts isolated from trabecular bone of RA patients cultured with adiponectin showed reduced mRNA expression of osteoblast differentiation marker osterix and increased osteoprotegerin (RANKL competitive inhibitor).[94] Overall these data indicate that adiponectin contributes to bone damage in rheumatoid arthritis: where it directly reduces osteoblast differentiation, whilst stimulating osteoclastogenesis leading to enhanced bone resorption (Fig. 3B). It is unclear what specific factors linked to the chronic conditions of rheumatoid arthritis are responsible for the reversal of the effects of adiponectin on osteoblasts and osteoclasts. It is highly likely to be a consequence of the multi-factorial pathological changes that occur within the joint, such as reduced adiposity within the synovium and BMAT,[95] the chronic production of pro-osteoclastogenic cytokines (TNFα and RANKL[96]) and pro-inflammatory cytokines (e.g. IL-1β) that influence expression of AdipoR1 in the synovium,[97] which act in concert to either mask the anti-osteoclastogenic effects of adiponectin or to alter adiponectin receptor-mediated signalling in an as yet unknown manner.

Despite this, preclinical animal studies have been inconclusive (Table 3). Therapeutic treatment with full length[98] or globular adiponectin[99] exacerbated juxta-articular bone erosions in

collagen induced arthritis models, with a concomitant reduction in BMD,[98,99] bone volume to trabecular volume ratio,[98] and trabecular number[98] seen when compared to untreated mice[99] or to mice treated with osteopontin short hairpin RNA.[98] These pathological effects of adiponectin therapy have been attributed to an increase in osteoclast number and osteoclast activity — as measured by enhanced levels of RANKL mRNA expression.[99] Moreover, therapeutic administration of functional blocking antibodies against MMW (KH7-33), or both MMW and HMW (KH4-8) isoforms of adiponectin, after disease onset significantly decreased arthritic clinical score and degradation in the joint cavities, when compared to arthritic mice treated with PBS.[100] Whilst no specific bone parameters were measured, KH4-8 treatment also led to a reduction in serum RANKL concentrations when compared to controls,[100] suggesting reduced osteoclast numbers and activity, and potentially bone damage in these animals. By contrast, therapeutic treatment of arthritic mice with an unknown isoform of adiponectin[101] or full-length adiponectin[102] at first signs of inflammation reduced the histopathological score (a composite measure of inflammatory cell infiltration, synovial hyperplasia, and bone destruction) when compared to untreated controls. Of note, these studies did not directly measure changes in bone anatomy following adiponectin therapy, therefore it is unclear whether the reduction in histopathological score observed equated to reduced bone damage. Supporting this possibility, the collagen-matrix degrading metalloproteinase, MMP3, was expressed at significantly lower levels in arthritic joints treated with adiponectin than the contralateral PBS treated joints.[102] There are clear experimental differences between the studies cited above, which might account for the discrepancies in the reported effects. For example, the studies reporting pro-arthritic effects administered adiponectin a maximum of 3 times a week, whereas mice displaying anti-arthritic responses were given daily injections of adiponectin. Such different treatment regimens will alter the absolute concentration of adiponectin experienced by cells at a given time and thus their responses, which in turn will impact the pathological responses observed. Further research is urgently needed to clarify the role of adiponectin therapy on bone damage in murine models of inflammatory arthritis.

CANCER AND RARE BONE DISEASES

Cancer

Tumour growth within the skeleton can occur through multiple mechanisms, including the inappropriate expansion and activity of osteoblasts (osteosarcoma)[103] or more commonly as a result of tumour metastasis, often seen in advanced breast cancers.[104] Assessing the impact of adiponectin in osteosarcoma is very challenging: primary tumours are extremely rare (1 in 100,000) and osteosarcoma cell lines (e.g. Saos-2 and MG-63) are frequently used as "normal" immortalised osteoblasts in in vitro studies.[105] As such limited data exists on adiponectin effects on bone cancer development and progression (Table 3). RNA-sequencing analysis revealed higher adiponectin gene expression in the bone from a single patient with primary osteosarcoma compared to the patient's own healthy bone tissue,[105] although analysis of more patient samples is required to make any definitive conclusions. In vitro, globular adiponectin increased the viability of the human Saos2 osteosarcoma cell line, but reduced the activity of the pro-mineralisation enzyme, alkaline phosphatase, in supernatants.[105] By contrast, the adiponectin receptor agonist, AdipoRon, decreased the proliferation of Saos-2 cells in vitro.[106] Given that AdipoR1 has a higher affinity for globular adiponectin, it is possible that increased signalling through AdipoR1 compared to AdipoR2 may promote abnormal osteoblast proliferation contributing to osteosarcoma, whilst equal signalling through both receptors may be important to control normal proliferative responses in healthy bone. Indeed, the loss of AdipoR1 has been linked to reduced osteoblast survival in vitro,[24] and absolute number in vivo[53] under healthy conditions (as described — *In health and ageing*) and may represent a novel therapeutic strategy to treat osteosarcoma. It is important to note that no data are currently available on the bone phenotype in AdipoR2 deficient mice or cells. These concepts require further investigation.

Tumour metastasis to the bone results in bone damage, increased pain and is a leading cause of death in breast cancer patients.[61,103,107] Divergent adiponectin responses have been reported for tumour lines in vitro based on their expression of the oestrogen receptor (ER). The non-invasive ER^+ MCF-7 breast cancer cell line demonstrated increased proliferation response to globular adiponectin.[61] By contrast, treatment with full-length[108,109] or globular[61] adiponectin reduced cell proliferation,[61,108,109] and increased apoptosis[109] of the invasive ER^- MDA-MB-231 breast cancer cell line. Of note, adiponectin-induced signalling through the AMPK pathway in ER^- MDA-MB-231 cells, whilst MAPK pathway was triggered in ER^+ MCF-7 cells.[61] However, the effects of adiponectin on the migratory capacity of ER- cells and their ability to metastasise to the bone remains unclear; with studies reporting an increased migration of ER- cells using globular adiponectin, but no effect upon full-length adiponectin treatment.[110] Moreover, inoculation of normal mice with established multiple myeloma (5TGM1) cells intravenously induced bone damage in wildtype mice, which was further exacerbated in adiponectin knockout mice.[111] Furthermore, increasing HMW adiponectin levels by administering an apolipoprotein memetic peptide, L-4F, dramatically reduced bone lesions and damage, and concomitantly increased trabecular bone volume in myeloma-bearing mice compared to vehicle treated controls.[111] Collectively, these data indicate that adiponectin can protect against multiple-myeloma-induced bone damage, potentially by acting directly on the tumour cell (5TGM1 cell) to induce apoptotsis.[111] Clearly additional research is required to dissect the importance of oestrogen signalling and adiponectin-mediated tumour migration, as well as the contribution of different adiponectin isoforms to these responses and whether particular isoforms may be therapeutically beneficial to patients with osteosarcoma.

Osteopetrosis and osteogenesis imperfecta

Patients with rare bone diseases, such as osteogenesis imperfecta (OI) and osteopetrosis, have unorganised bone structure and increased bone frailty,[112] which can severely reduce the quality of life of those affected. The role of adiponectin in these diseases has been sparsely researched (Table 3) and requires further investigation. In patients with OI, mutations in COL1A1 or COL1A2 result in increased bone fragility.[113] Moreover, *Col1a1* mutant mouse have reduced overall body fat content,[113] suggesting that these mice have lower levels of adiponectin — although this was not explicitly measured. Similarly, an osteopetrosis-like phenotype is induced in mice maintained on the obesity-inducing high carbohydrate diet,[114] and where adiponectin concentrations are presumably much lower (as discussed above in the obesity section). Conversely, exercise-induced weight loss significantly reduced aberrant bone growth in osteopetrotic mice and re-established bone homeostasis,[114] indicating that increasing adiponectin levels may have therapeutic benefit in osteopetrosis. Additionally, BMSC from infantile osteopetrosis patients were unable to differentiate into adipocytes, secreting lower levels of adiponectin compared to BMSC isolated from healthy age-matched donors.[115] Neither study actually measured adiponectin, yet it seems highly probable that fluctuations in its concentrations may contribute to changes in the bone. A greater understanding of adiponectin signalling and regulation of normal bone structure and strength in these rare diseases is urgently needed-based on our current knowledge treatment with adiponectin may alleviate some of the symptoms that patient's experience.

CONCLUSION

Under healthy conditions, adiponectin supports the proliferation, migration, mineralisation and survival of osteoblasts, whilst concomitantly limiting proliferation, migration and survival in osteoclasts. On balance, this allows adiponectin to promote bone formation and limit bone resorption. By contrast, these traits are broadly dysregulated in bones following menopause and in patients with obesity or diseases such as chronic inflammation and cancer, where the loss of adiponectin, or changes in environmental cues that impact the downstream signalling pathways triggered by adiponectin (e.g. MAPK vs AMPK) pathologically tip the balance in favour of bone resorption and damage (Fig. 3). However, inconsistencies in study design and outcome measures, along with discrepancies in the observations made in animals and humans make it difficult to draw definitive conclusions that can be utilised clinically. Indeed, in-depth, large-scale studies exploring adiponectin levels in multiple bone diseases, accounting for confounding factors such as age and BMI, are needed to fully understand how adiponectin interacts with bone. Furthermore, more detailed mechanistic studies are required to understand the interaction of the different adiponectin isoforms with each of the receptors, and the impact which oestrogen receptors and other unknown molecules have on downstream signalling and the functional consequences of these. These studies are critical to further our understanding of the beneficial and pathological roles of adiponectin for a specific context, and the efficacy of targeting adiponectin or its signalling therapeutically to treat bone abnormalities and induce repair.

ACKNOWLEDGEMENTS

JWL was supported by a MRC-Versus Arthritis Centre for Musculoskeletal Ageing Research PhD studentship (MR/R502364/1). AJN was supported by an Arthritis Research UK Career Development Fellowship (21743).

AUTHOR CONTRIBUTIONS

All authors contributed to the drafting, editing and writing of the manuscript.

ADDITIONAL INFORMATION

Competing interests: The authors declare no competing interests.

REFERENCES

1. Khammissa, R. A. G. et al. The biological activities of vitamin d and its receptor in relation to calcium and bone homeostasis, cancer, immune and cardiovascular systems, skin biology, and oral health. *Biomed. Res. Int.* **2018**, 1–9 (2018).
2. Balogh, E., Paragh, G. & Jeney, V. Influence of iron on bone homeostasis. *Pharmaceuticals* **11**, 107 (2018).
3. Penido, M. G. M. G. & Alon, U. S. Phosphate homeostasis and its role in bone health. *Pediatr. Nephrol.* **27**, 2039–2048 (2012).
4. Arita, Y. et al. Paradoxical decrease of an adipose-specific protein, adiponectin, in obesity. *Biochem. Biophys. Res. Commun.* **257**, 79–83 (1999).
5. Hotta, K. et al. Plasma concentrations of a novel, adipose-specific protein, adiponectin, in type 2 diabetic patients. *Arterioscler. Thromb. Vasc. Biol.* **20**, 1595–1599 (2000).
6. Scherer, P. E., Williams, S., Fogliano, M., Baldini, G. & Lodish, H. F. A novel serum protein similar to C1q, produced exclusively in adipocytes. *J. Biol. Chem.* **270**, 26746–26749 (1995).
7. Fruebis, J. et al. Proteolytic cleavage product of 30-kDa adipocyte complement-related protein increases fatty acid oxidation in muscle and causes weight loss in mice. *Proc. Natl. Acad. Sci. U.S.A.* **98**, 2005–2010 (2012).
8. Mangge, H. et al. Preatherosclerosis and adiponectin subfractions in obese adolescents. *Obesity* **16**, 2578–2584 (2008).
9. Waki, H. et al. Impaired multimerization of human adiponectin mutants associated with diabetes. Molecular structure and multimer formation of adiponectin. *J. Biol. Chem.* **278**, 40352–40363 (2003).
10. Hada, Y. et al. Selective purification and characterization of adiponectin multimer species from human plasma. *Biochem. Biophys. Res. Commun.* **356**, 487–493 (2007).
11. Cawthorn, W. P. et al. Bone marrow adipose tissue is an endocrine organ that contributes to increased circulating adiponectin during caloric restriction. *Cell Metab.* **20**, 368–375 (2014).
12. Suchacki, K. J. et al. Bone marrow adipose tissue is a unique adipose subtype with distinct roles in glucose homeostasis. *Nat. Commun.* **11**, 3097 (2020).
13. L Newton, A. J., Hanks, L., Davis, M. & Casazza, K. The relationships among total body fat, bone mineral content and bone marrow adipose tissue in early-pubertal girls. *Bonekey Rep.* **2**, 315 (2013).
14. Yamauchi, T. et al. Cloning of adiponectin receptors that mediate antidiabetic metabolic effects. *Nature* **423**, 762–769 (2003).
15. Yamauchi, T., Iwabu, M., Okada-Iwabu, M. & Kadowaki, T. Adiponectin receptors: a review of their structure, function and how they work. *Best Pract. Res. Clin. Endocrinol. Metab.* **28**, 15–23 (2014).
16. Kadowaki, T. & Yamauchi, T. Adiponectin receptor signaling: a new layer to the current model. *Cell Metab.* **13**, 123–124 (2011).
17. Holland, W. L. et al. Receptor-mediated activation of ceramidase activity initiates the pleiotropic actions of adiponectin. *Nat. Med.* **17**, 55–63 (2011).
18. Obeid, S. & Hebbard, L. Role of adiponectin and its receptors in cancer. *Cancer Biol. Med.* **9**, 213–220 (2012).
19. Wu, Y. et al. Genome-wide association study for adiponectin levels in filipino women identifies CDH13 and a novel uncommon haplotype at KNG1-ADIPOQ. *Hum. Mol. Genet.* **19**, 4955–4964 (2010).
20. Hug, C. et al. T-cadherin is a receptor for hexameric and high-molecular-weight forms of Acrp30/adiponectin. *Proc. Natl. Acad. Sci. U.S.A.* **101**, 10308–10313 (2004).
21. Yamauchi, T. et al. Targeted disruption of AdipoR1 and AdipoR2 causes abrogation of adiponectin binding and metabolic actions. *Nat. Med.* **13**, 332–339 (2007).
22. Ramasamy, S. K. Structure and functions of blood vessels and vascular niches in bone. *Stem Cells Int.* **2017**, 1–10 (2017).
23. KAMADA, A. et al. Gene expression of adiponectin receptors during osteoblastic differentiation. *J. Oral. Tissue Eng.* **15**, 102–108 (2017).
24. Hyun, W. L. et al. Adiponectin stimulates osteoblast differentiation through induction of COX2 in mesenchymal progenitor cells. *Stem Cells* **27**, 2254–2262 (2009).
25. Pacheco-Pantoja, E. L., Fraser, W. D., Wilson, P. J. M. & Gallagher, J. A. Differential effects of adiponectin in osteoblast-like cells. *J. Recept. Signal Transduct.* **34**, 351–360 (2014).
26. Pang, T. T. L. et al. Inhibition of islet immunoreactivity by adiponectin is attenuated in human type 1 diabetes. *J. Clin. Endocrinol. Metab.* **98**, E418–E428 (2013).
27. Pacheco-Pantoja, E. L., Waring, V. J., Wilson, P. J. M., Fraser, W. D. & Gallagher, J. A. Adiponectin receptors are present in RANK-L-induced multinucleated osteoclast-like cells. *J. Recept. Signal Transduct.* **33**, 291–297 (2013).
28. Luo, X. H. et al. Adiponectin stimulates human osteoblasts proliferation and differentiation via the MAPK signaling pathway. *Exp. Cell Res.* **309**, 99–109 (2005).
29. Berner, H. S. et al. Adiponectin and its receptors are expressed in bone-forming cells. *Bone* **35**, 842–849 (2004).
30. Fazeli, P. K. et al. Marrow fat and bone-new perspectives. *J. Clin. Endocrinol. Metab.* **98**, 935–945 (2013).
31. DiMascio, L. et al. Identification of adiponectin as a novel hemopoietic stem cell growth factor. *J. Immunol.* **178**, 3511–3520 (2007).
32. Wu, X., Huang, L. & Liu, J. Effects of adiponectin on osteoclastogenesis from mouse bone marrow-derived monocytes. *Exp. Ther. Med.* **17**, 1228–1233 (2019).
33. Lin, Y. Y. et al. Adiponectin receptor 1 regulates bone formation and osteoblast differentiation by GSK-3β/β-Catenin signaling in mice. *Bone* **64**, 147–154 (2014).
34. Kajimura, D. et al. Adiponectin regulates bone mass via opposite central and peripheral mechanisms through foxo1. *Cell Metab.* **17**, 901–915 (2013).
35. Oshima, K. et al. Adiponectin increases bone mass by suppressing osteoclast and activating osteoblast. *Biochem. Biophys. Res. Commun.* **331**, 520–526 (2005).
36. Chen, T., Wu, Y. W., Lu, H., Guo, Y. & Tang, Z. H. Adiponectin enhances osteogenic differentiation in human adipose-derived stem cells by activating the APPL1-AMPK signaling pathway. *Biochem. Biophys. Res. Commun.* **461**, 237–242 (2015).
37. Wu, Y. et al. Central adiponectin administration reveals new regulatory mechanisms of bone metabolism in mice. *Am. J. Physiol. Metab.* **306**, E1418–E1430 (2014).
38. Ye, L. et al. Histone demethylases KDM4B and KDM6B promotes osteogenic differentiation of human MSCs. *Cell Stem Cell* **11**, 50–61 (2012).
39. Tu, Q. et al. Adiponectin inhibits osteoclastogenesis and bone resorption via APPL1-mediated suppression of Akt1. *J. Biol. Chem.* **286**, 12542–12553 (2011).
40. Yu, L. et al. Adiponectin regulates bone marrow mesenchymal stem cell niche through a unique signal transduction pathway: an approach for treating bone disease in diabetes. *Stem Cells* **33**, 240–252 (2015).

41. Park, D. et al. Endogenous bone marrow MSCs are dynamic, fate-restricted participants in bone maintenance and regeneration. *Cell Stem Cell* **10**, 259–272 (2012).
42. Döring, Y., Pawig, L., Weber, C. & Noels, H. The CXCL12/CXCR4 chemokine ligand/receptor axis in cardiovascular disease. *Front. Physiol* **5**, 212 (2014).
43. Colnot, C. Skeletal cell fate decisions within periosteum and bone marrow during bone regeneration. *J. Bone Miner. Res.* **24**, 274–282 (2009).
44. Michaud, J., Im, D.-S. & Hla, T. Inhibitory role of sphingosine 1-phosphate receptor 2 in macrophage recruitment during Inflammation. *J. Immunol.* **184**, 1475–1483 (2010).
45. Sartawi, Z., Schipani, E., Ryan, K. B. & Waeber, C. Sphingosine 1-phosphate (S1P) signalling: Role in bone biology and potential therapeutic target for bone repair. *Pharmacol. Res.* **125**, 232–245 (2017).
46. Meshcheryakova, A., Mechtcheriakova, D. & Pietschmann, P. Sphingosine 1-phosphate signaling in bone remodeling: multifaceted roles and therapeutic potential. *Exp. Opin. Ther. Targets* **21**, 725–737 (2017).
47. Mendelson, K., Evans, T. & Hla, T. Sphingosine 1-phosphate signalling. *Development* **141**, 5–9 (2014).
48. Li, C. et al. Homing of bone marrow mesenchymal stem cells mediated by sphingosine 1-phosphate contributes to liver fibrosis. *J. Hepatol.* **50**, 1174–1183 (2009).
49. Ishii, M. et al. Sphingosine-1-phosphate mobilizes osteoclast precursors and regulates bone homeostasis. *Nature* **458**, 524–528 (2009).
50. Ishii, M., Kikuta, J., Shimazu, Y., Meier-Schellersheim, M. & Germain, R. N. Chemorepulsion by blood S1P regulates osteoclast precursor mobilization and bone remodeling in vivo. *J. Exp. Med* **207**, 2793–2798 (2010).
51. Yang, L. et al. Sphingosine 1-phosphate receptor 2 and 3 mediate bone marrow-derived monocyte/macrophage motility in cholestatic liver injury in mice. *Sci. Rep.* **5**, 13423 (2015).
52. Ryu, J. et al. Sphingosine 1-phosphate as a regulator of osteoclast differentiation and osteoclast-osteoblast coupling. *EMBO J.* **25**, 5840–5851 (2006).
53. Aneka Sowman, Sam Olechnowicz & James Edwards. OC9: sarcopenia is negatively related to osteogenic impacts achieved through habitual physical activity: findings from a population-based cohort of older females, Bone Research Society, Annual Meeting 2017 Proceedings. 25–27 June 2017, Bristol, UK. J Musculoskeletal Neuronal Interactions. **18**, 108–151 (2018)..
54. Justesen, J. et al. Adipocyte tissue volume in bone marrow is increased with aging and in patients with osteoporosis. *Biogerontology* **2**, 165–171 (2001).
55. Li, G. W. et al. Quantitative evaluation of vertebral marrow adipose tissue in postmenopausal female using MRI chemical shift-based water-fat separation. *Clin. Radiol.* **69**, 254–262 (2014).
56. Syed, F. A. et al. Effects of estrogen therapy on bone marrow adipocytes in postmenopausal osteoporotic women. *Osteoporos. Int.* **19**, 1323–1330 (2008).
57. Jürimäe, J. & Jürimäe, T. Adiponectin is a predictor of bone mineral density in middle-aged premenopausal women. *Osteoporos. Int.* **18**, 1253–1259 (2007).
58. Wang, F. et al. Deficiency of adiponectin protects against ovariectomy-induced osteoporosis in mice. *PLoS One* **8**, e68497 (2013).
59. Luo, E. et al. Sustained release of adiponectin improves osteogenesis around hydroxyapatite implants by suppressing osteoclast activity in ovariectomized rabbits. *Acta Biomater.* **8**, 734–743 (2012).
60. Rinotas, V. & Douni, E. Molecular interaction of BMAT with bone. *Curr. Mol. Biol. Rep.* **4**, 34–40 (2018).
61. Mauro, L. et al. Estrogen receptor-α drives adiponectin effects on cyclin D1 expression in breast cancer cells. *FASEB J.* **29**, 2150–2160 (2015).
62. Mohamed, M. K. & Abdel-Rahman, A. A. Effect of long-term ovariectomy and estrogen replacement on the expression of estrogen receptor gene in female rats. *Eur. J. Endocrinol.* **142**, 307–314 (2000).
63. Wong, S. Y. P., Kariks, J., Evans, R. A., Dunstan, C. R. & Hills, E. The effect of age on bone composition and viability in the femoral head. *J. Bone Jt. Surg.* **67**, 274–283 (1985).
64. Tan, C. O. et al. Adiponectin is associated with bone strength and fracture history in paralyzed men with spinal cord injury. *Osteoporos. Int.* **25**, 2599–2607 (2014).
65. Bacchetta, J. et al. The relationship between adipokines, osteocalcin and bone quality in chronic kidney disease. *Nephrol. Dial. Transpl.* **24**, 3120–3125 (2009).
66. Rutkowski, J. M. et al. Adiponectin alters renal calcium and phosphate excretion through regulation of klotho expression. *Kidney Int.* **91**, 324–337 (2017).
67. Haugen, S. et al. Adiponectin reduces bone stiffness: verified in a three-dimensional artificial human bone model In Vitro. *Front. Endocrinol.* **9**, 236 (2018).
68. Panagopoulou, P. et al. Adiponectin and insulin resistance in childhood obesity. *J. Pediatr. Gastroenterol. Nutr.* **47**, 356–362 (2008).
69. Landrier, J. F. et al. Reduced adiponectin expression after high-fat diet is associated with selective up-regulation of ALDH1A1 and further retinoic acid receptor signaling in adipose tissue. *FASEB J.* **31**, 203–211 (2017).
70. Greenberg, A. S. & Obin, M. S. Obesity and the role of adipose tissue in inflammation and metabolism. *Am J Clin Nutr* **83**, 461S–465S (2006).
71. Campos, R. M. et al. Relationship between adiponectin and leptin on osteocalcin in obese adolescents during weight loss therapy. *Arch. Endocrinol. Metab.* **62**, 275–284 (2018).
72. Devlin, M. J. et al. Caloric restriction leads to high marrow adiposity and low bone mass in growing mice. *J. Bone Miner. Res.* **25**, 2078–2088 (2010).
73. Abella, E. et al. Bone marrow changes in anorexia nervosa are correlated with the amount of weight loss and not with other clinical findings NERVOSA 582. Am. *J. Clin. Pathol.* **118**, 582–588 (2002).
74. Tagami, T. et al. Adiponectin in anorexia nervosa and bulimia nervosa. *J. Clin. Endocrinol. Metab.* **89**, 1833–1837 (2004).
75. Bredella, M. A. et al. Increased bone marrow fat in anorexia nervosa. *J. Clin. Endocrinol. Metab.* **94**, 2129–2136 (2009).
76. Iwahashi, H. et al. Plasma adiponectin levels in women with Anorexia Nervosa. *Horm. Metab. Res.* **35**, 537–540 (2003).
77. Spector, T. D., Hart, D. J. & Doyle, D. V. Incidence and progression of osteoarthritis in women with unilateral knee disease in the general population: the effect of obesity. *Ann. Rheum. Dis.* **53**, 565–568 (1994).
78. Tang, Q. et al. Association of osteoarthritis and circulating adiponectin levels: a systematic review and meta-analysis. *Lipids Health Dis.* **17**, 189 (2018).
79. Doucette, C. R. et al. A high fat diet increases bone marrow adipose tissue (MAT) but does not alter trabecular or cortical bone mass in C57BL/6J mice. *J. Cell. Physiol.* **230**, 2032–2037 (2015).
80. Fehrendt, H. et al. Negative influence of a long-term high-fat diet on murine bone architecture. *Int. J. Endocrinol.* **2014**, 318924 (2014).
81. Gao, F., Lv, T. R., Zhou, J. C. & Qin, X. D. Effects of obesity on the healing of bone fracture in mice. *J. Orthop. Surg. Res.* **13**, 145 (2018).
82. Kim, S.-J., Ahn, J., Kim, H. K. & Kim, J. H. Obese children experience more extremity fractures than nonobese children and are significantly more likely to die from traumatic injuries. *Acta Paediatr.* **105**, 1152–1157 (2016).
83. Valerio, G. et al. Prevalence of overweight in children with bone fractures: a case control study. *BMC Pediatr.* **12**, 166 (2012).
84. Lane, J. C. et al. Preschool obesity is associated with an increased risk of childhood fracture: a longitudinal cohort study of 466,997 children and up to 11 years of follow-up in Catalonia, Spain. *J. Bone Miner. Res.* **35**, 1022–1030 (2020).
85. Anandacoomarasamy, A., Caterson, I., Sambrook, P., Fransen, M. & March, L. The impact of obesity on the musculoskeletal system. *Int. J. Obes.* **32**, 211–222 (2008).
86. Filkova, M. et al. Increased serum adiponectin levels in female patients with erosive compared with non-erosive osteoarthritis. *Ann. Rheum. Dis.* **68**, 295–296 (2009).
87. Giambelli, R. et al. Adiponectin serum levels and disease severity in the STR/Ort mouse model of osteoarthritis. *Osteoarthr. Cartil.* **24**, S85 (2016).
88. AIHW. Australia's dental generations: The National Survey of Adult Oral Health *2004-2006* (AIHW) (2004).
89. Zhang, L. et al. Adiponectin ameliorates experimental periodontitis in diet-induced obesity mice. *PLoS One* **9**, e97824 (2014).
90. Kamio, N., Akifusa, S., Yamaguchi, N., Nonaka, K. & Yamashita, Y. Anti-inflammatory activity of a globular adiponectin function on RAW 264 cells stimulated by lipopolysaccharide from Aggregatibacter actinomycetemcomitans. *FEMS Immunol. Med. Microbiol.* **56**, 241–247 (2009).
91. Šenolt, L., Pavelka, K., Housa, D. & Haluzík, M. Increased adiponectin is negatively linked to the local inflammatory process in patients with rheumatoid arthritis. *Cytokine* **35**, 247–252 (2006).
92. Ebina, K. et al. Serum adiponectin concentrations correlate with severity of rheumatoid arthritis evaluated by extent of joint destruction. *Clin. Rheumatol.* **28**, 445–451 (2009).
93. Giles, J. T., Allison, M., Bingham, C. O., Scott, W. M. & Bathon, J. M. Adiponectin is a mediator of the inverse association of adiposity with radiographic damage in rheumatoid arthritis. *Arthritis Care Res.* **61**, 1248–1256 (2009).
94. Krumbholz, G. et al. Response of human rheumatoid arthritis osteoblasts and osteoclasts to adiponectin. *Clin. Exp. Rheumatol.* **35**, 406–414 (2017).
95. Sudoł-Szopińska, I. et al. Significance of bone marrow edema in pathogenesis of rheumatoid arthritis. *Pol. J. Radiol.* **78**, 57–63 (2013).
96. Shiratori, T. et al. IL-1β induces pathologically activated osteoclasts bearing extremely high levels of resorbing activity: a possible pathological subpopulation of osteoclasts, accompanied by suppressed expression of Kindlin-3 and Talin-1. *J. Immunol.* **200**, 218–228 (2018).
97. Lee, Y. A. et al. Synergy between adiponectin and interleukin-1β on the expression of interleukin-6, interleukin-8, and cyclooxygenase-2 in fibroblast-like synoviocytes. *Exp. Mol. Med.* **44**, 440–447 (2012).
98. Qian, J. et al. Adiponectin aggravates bone erosion by promoting osteopontin production in synovial tissue of rheumatoid arthritis. *Arthritis Res. Ther.* **20**, 76 (2018).

99. Sun, X. et al. Adiponectin exacerbates collagen-induced arthritis via enhancing Th17 response and prompting RANKL expression. *Sci. Rep.* **5**, 11296 (2015).
100. Lee, Y. A. et al. Potential therapeutic antibodies targeting specific adiponectin isoforms in rheumatoid arthritis. *Arthritis Res. Ther.* **20**, 245 (2018).
101. Wu, D. et al. Adiponectin exerts a potent anti-arthritic effect and insulin resistance in collagen-induced arthritic rats. *Int. J. Rheum. Dis.* **21**, 1496–1503 (2018).
102. Lee, S. W., Kim, J. H., Park, M. C., Park, Y. B. & Lee, S. K. Adiponectin mitigates the severity of arthritis in mice with collagen-induced arthritis. *Scand. J. Rheumatol.* **37**, 260–268 (2008).
103. Franchi, A. Epidemiology and classification of bone tumors. *Clin. Cases Miner. Bone Metab.* **9**, 92–95 (2012).
104. Coleman, R. E. Metastatic bone disease: clinical features, pathophysiology and treatment strategies. *Cancer Treat. Rev.* **27**, 165–176 (2001).
105. Märtson, A. et al. Transcriptome analysis of osteosarcoma identifies suppression of wnt pathway and up-regulation of adiponectin as potential biomarker. *Genomics Discov.* **1**, 3 (2013).
106. Sapio, L. et al. AdipoRon affects cell cycle progression and inhibits proliferation in human osteosarcoma cells. *J. Oncol.* **2020**, 1–12 (2020).
107. Cetin, K., Christiansen, C. F., Sværke, C., Jacobsen, J. B. & Sørensen, H. T. Survival in patients with breast cancer with bone metastasis: a Danish population-based cohort study on the prognostic impact of initial stage of disease at breast cancer diagnosis and length of the bone metastasis-free interval. *BMJ Open* **5**, e007702 (2015).
108. Dos Santos, E. et al. Adiponectin mediates an antiproliferative response in human MDA-MB 231 breast cancer cells. *Oncol. Rep.* **20**, 971–977 (2008).
109. Kang, J. H. et al. Adiponectin induces growth arrest and apoptosis of MDA-MB-231 breast cancer cell. *Arch. Pharm. Res.* **28**, 1263–1269 (2005).
110. Libby, E. F. et al. Globular adiponectin enhances invasion in human breast cancer cells. *Oncol. Lett.* **11**, 633–641 (2016).
111. Fowler, J. A. et al. Host-derived adiponectin is tumor-suppressive and a novel therapeutic target for multiple myeloma and the associated bone disease. *Blood* **118**, 5872–5882 (2011).
112. Bacon, S. & Crowley, R. Developments in rare bone diseases and mineral disorders. *Ther. Adv. Chronic Dis.* **9**, 51–60 (2018).
113. Boraschi-Diaz, I. et al. Metabolic phenotype in the mouse model of osteogenesis imperfecta. *J. Endocrinol.* **234**, 279–289 (2017).
114. Lacerda, D. R. et al. Osteopetrosis in obese female rats is site-specifically inhibited by physical training. *Exp. Physiol.* **100**, 44–56 (2015).
115. Uckan, D. et al. Adipocyte differentiation defect in mesenchymal stromal cells of patients with malignant infantile osteopetrosis. *Cytotherapy* **11**, 392–402 (2009).
116. Granero-Moltó, F. et al. Regenerative effects of transplanted mesenchymal stem cells in fracture healing. *Stem Cells* **27**, 1887–1898 (2009).
117. Asiedu, K. O. et al. Bone marrow cell homing to sites of acute tibial fracture: ^{89}Zr-oxine cell labeling with positron emission tomographic imaging in a mouse model. *EJNMMI Res.* **8**, 109 (2018).
118. Walton, M. Degenerative joint disease in the mouse knee; histological observations. *J. Pathol.* **123**, 109–122 (1977).